Design, Synthesis and Studies on the Photophysical Properties of Unnatural Triazolyl and Tetrazolyl Nucleosides and the Applications of Triazolyl Nucleosides Thereof

A Dissertation Submitted to the
Indian Institute of Technology Guwahati
As Partial Fulfillment for the Award of Degree of

Doctor of Philosophy
in Chemistry
by

Sangita Talukdar
Roll No. 10612246

Department of Chemistry
Indian Institute of Technology Guwahati
Guwahati 781039

June 2014

Dedicated to

My
Parents
&
Brother
And
Those who have helped me

INDIAN INSTITUTE OF TECHNOLOGY, GUWAHATI
Department of Chemistry

DECLARATION

I do hereby declare that the research work embodied in this thesis entitled "***Design, Synthesis and Studies on the Photophysical Properties of Unnatural Triazolyl and Tetrazolyl Nucleosides and the Applications of Triazolyl Nucleosides Thereof***" has been carried out by me under the supervision of **Dr. Subhendu Sekhar Bag** in the Department of Chemistry, Indian Institute of Technology Guwahati, India.

In keeping with the general practice of reporting scientific observations, due acknowledgements have been made wherever the work described is based on the findings of other investigators.

IIT Guwahati
June, 2014.

Sangita Talukdar

Dr. Subhendu Sekhar Bag, Ph.D.
Associate Professor
Department of Chemistry
Indian Institute of Technology
Guwahati -781039
Assam, INDIA

Ph: +91-361-258-2324 (O)
Ph: +91-361-258-4324 (R)
Fax: +91-361-258-2349

E-mail: ssbag75@yahoo.co.in
ssbag75@iitg.ernet.in

CERTIFICATE

This is to certify that the research work presented in this thesis entitled "***Design, Synthesis and Studies on the Photophysical Properties of Unnatural Triazolyl and Tetrazolyl Nucleosides and the Applications of Triazolyl Nucleosides Thereof***" is an authentic record of the results obtained from the research work carried out by **Ms. Sangita Talukdar** under my supervision in the Department of Chemistry, Indian Institute of technology Guwahati, India. This work is original and has not been submitted elsewhere for a degree or award.

IIT Guwahati
June, 2014

Dr. Subhendu Sekhar Bag
(Thesis Supervisor)

ACKNOWLODGEMENT

It is with high regards and profound respect that I express a deep sense of sincere gratitude to my supervisor **Dr. Subhendu Sekhar Bag** for his stimulating guidance, precious constructive suggestions and decisive insights during the entire course of my research work.

I would like to thank my Doctoral Committee members, **Prof. T. Punniyamurthy** (chairman), **Dr. Chandan Mukherjee** (member) and **Dr. Anil Mukund Limaye** (member) for their intellectual input, encouragement, valuable suggestions and comments during the entire course of my research work.

I wish to thank my lab mates Rajen da, Subhashis, Hiranya, Suranjan, Manoj, Suman and Afsana for their cooperation, support and pleasant company throughout my research work. Without their help it would have been impossible to complete my research work. I would also like to acknowledge summer trainee students Soumen, Narayani, Sudeshna, Mampi and Saikat for their help, support and pleasant company in the laboratory during their summer project work.

Sincere thanks go to my other lab mates, Zia da, Dipankar, Momina, Tridip, Anindya, Gaurangi, Abhishek, Shaad for their cooperation and sharing some happy moments inside and outside the laboratory.

I would like to acknowledge my seniors Dev da, Chaitanya da, Narashimha and Santosh da who have indirectly helped me during the entire course of my research work. Special thanks to Babulal da for his help in collecting XRD data. Thanks to my batch mates Chandani, Sengoden, Ashim, Ganesh and Muruagavel for their support and suggestions. Thanks to Samir, Bhaskar, Kamali, Rituparna, Daramdev, Wajid and Jyoti for their help and support. Thanks to all of my friends, juniors and seniors whom I met during my past four years of life for their help.

My special thanks go to my senior Sagar da for his help and valuable suggestions.

My honest regards to all the faculty members of our department for their encouragement and help. I want to express my thanks to Kesho Singh for his help in

collecting Mass Spectra data and our technical and official staffs as well as Subal da for their help and support.

Finally, I owe success to my parents (Mr. Gopesh Talukdar and Mrs. Hiran Talukdar) who have been a constant source of inspiration to carry out my career. I wish to thank them for giving me the freedom to pursue a career path of my choice and their constant support and encouragement in realizing my dreams.

I want to express my thanks to my brother Rahul and all the family members for their support.

I would like to acknowledge the Department of Chemistry, IIT Guwahati for giving me the opportunity and fellowship to carry out my research work.

Sangita Talukdar

Sangita Talukdar

Present Address:

C/O: Dr. SubhenduSekhar Bag
Department of Chemistry
Indian Institute of Technology Guwahati
Guwahati – 781039, Assam, India
Phone: +91 361 2582324
E mail:sgt@iitg.ernet.in
sgt.chem@gmail.com

Permanent Address:

City – Guwahati
P. O. – Basistha
Dist. – Kamrup
Pin – 781028
Assam, India
Mobile**:** +91 9085292053

Area of Interest

Design and synthesis of unnatural fluorescent nucleosides for chemical and biochemical application.

Education:

2014	**Ph. D.** [Thesis submitted (June)]
2008	**Master of Science**(*in Organic Chemistry*)
	Guahati University, Guwahati
2006	**Bachelor of Science** *(Chemistry Hons.)*
	Cotton College
	Gauhati University

Honors/Awards:

- Junior Research Fellowship and Eligibility for Lectureship (**UGC-JRF-NET**), June– 2010, awarded by Council of Scientific & Industrial Research and University Grants Commission, India.
- Qualified **GATE–2010**(Graduate Admission Test in Engineering) examination organizedby Ministry of Human Resource Development, Government of India.

List of Publications

1. ●Triazolyl-Donor/Acceptor Chromophore Decorated Unnatural Nucleosides and Oligonucleotides with Duplex Stability Comparable to that of Natural A/T Pair ● Bag, S. S.; Talukdar, S.; Matsumoto, K.; Kundu, R. *J. Org. Chem.* **2013**, *78*, 278.
2. ●Dual Door Entry to Exciplex Emission in A Chimeric DNA Duplex Containing Non-nucleoside-Nucleoside Pair ● Bag, S. S.; Talukdar, S.; Kundu, R.; Saito, I.; Jana, S. *Chem. Commun.* **2013**, *50,* 829.
3. ●Unnatural triazolyl nucleoside stabilizes an abasic site containing DNA duplex equally as the stabilization of a natural A-T pair ● Bag, S. S.; Kundu, R.; Talukdar, S. *RSC Advances* **2013**, *3, 21352*.
4. ●Fluorometric Sensing of Cu^{2+} Ion with Fluorescent Light-up Probe, Triazolylpyrene (^{TNDMB}Py) ● Bag, S. S.; Kundu R.; Talukdar S. *Tetrahedron Lett.* **2012**, *53,* 5875.
5. Chapter in a Book Series ●Design and Synthesis of Triazolyl-Donor/Acceptor Unnatural Nucleotides and Oligonucleotides ● Bag, S. S.; Talukdar, S. *In Current Protocols in Nucleic Acid Chemistry*, Wiely Online Library, (ISBN: 9780471142706, DOI: 10.1002/0471142700).

Article 4 is not included in the thesis.

Communicated

1. ●Triazolyl-Donor/Acceptor Chomophores Decorated Unnatural Nucleosides: Synthesis, and Photophysical Properties● Bag, S. S.; Talukdar, S.; Mukherjee, S.●
2. ●Tetrazolyl-Donor/Acceptor Chomophores Decorated Unnatural Nucleosides: Synthesis, and Photophysical Properties ● Bag, S. S.; Talukdar, S.●

List of Conferences/Symposiums

1. National Conference on Frontiers in Chemical Sciences (FICS) – 2012, Organized by *Department of Chemistry, IIT Guwahati, India*.
2. Junior National Organic Symposium Trust (J-NOST-2012), Organized by *Department of Chemistry, IIT Guwahati, India*.

ABSTRACT

This dissertation entitled **"DESIGN, SYNTHESIS AND STUDIES ON THE PHOTOPHYSICAL PROPERTIES OF UNNATURAL TRIAZOLYL AND TETRAZOLYL NUCLEOSIDES AND THE APPLICATIONS OF TRIAZOLYL NUCLEOSIDES THEREOF"** is an embodiment of research aimed towards: the synthesis and photophysical studies of (a) triazolyl and (b) tetrazolyl donor/acceptor aromatic nucleosides, (c) the study of charge transfer complexation (among triazolyl donor/acceptor aromatic nucleosides) mediated DNA duplex stabilization, (d) the study of abasic site stabilization by a triazolyl donor/acceptor aromatic nucleoside and (e) the studies on the dual mechanism to exciplex formation in a chimeric DNA duplex containing an unnatural triazolyl nucleoside paired against a non-nucleoside base surrogate, oxopyrenyl-serinol. Towards this journey several novel unnatural fluorescent/non-fluorescent triazolyl and tetrazolyl donor/acceptor aromatic nucleosides were synthesized, their photophysical properties were evaluated and the biophysical properties of two triazolyl nucleosides were investigated.

The thesis contains a total of **6 Chapters** including one Review Chapter (**Chapter 1**). Each chapter contains their individual experimental and reference sections. In short, **Chapter 1** is a review of some important unnatural nucleoside base surrogates and their applications. **Chapter 2** deals with the synthesis and photophysical properties of some new unnatural triazolyl donor-acceptor nucleosides generated *via* "click" chemistry. Our design concept was based on the hypothesis that a pair of such donor/acceptor nucleoside might involve in π-stacking as well as in photophysical interaction leading to stabilization of DNA duplex if such nucleosides can be incorporated into short oligonucleotide sequences. Synthesis and studies on the photophysical property of donor-acceptor unnatural tetrazolyl nucleosides are the contents of **Chapter 3. Chapter 4** deals with the application of a pair of dono-acceptor triazolyl nucleoside to the stabilization of DNA duplexes *via* charge transfer/π-π stacking interaction. We have shown that ground state charge transfer complexation force among triazolyl unnatural donor-acceptor nucleobase pair ($^{TPhen}\mathbf{B}_{Do}$: $^{TNB}\mathbf{B}_{Ac}$) is good enough to stabilize a DNA duplex.

The large surface area, polarizability and strong stacking propensity of triazolylphenanthrene ($^{TPhen}\mathbf{B}_{Do}$) play a major role to offer higher thermal stabilization of an abasic site compared to a natural **A:T** pair *via* strong intercalative stacking

interaction which is discussed in **Chapter 5**. Finally, **Chapter 6** introduced a novel chemeric DNA duplex, wherein a non-nucleosidic base surrogate ^{OxoPy}**S** selectively paired against an unnatural triazolylphenanthrene nucleoside (^{TPhen}**B**$_{Do}$), which represents a very interesting dual door entry system for exciplex emission.

CHAPTER 1: UNNATURAL NUCLEOSIDE BASE SURROGATES AND THEIR APPLICATIONS: A REVIEW

This chapter highlights some of the DNA base analogues and a set of emissive RNA alphabet, their duplex stabilizing property, abilities of probing abasic DNA, involvement in FRET or exciplex emission events in the context of DNA (**Figure A1**).

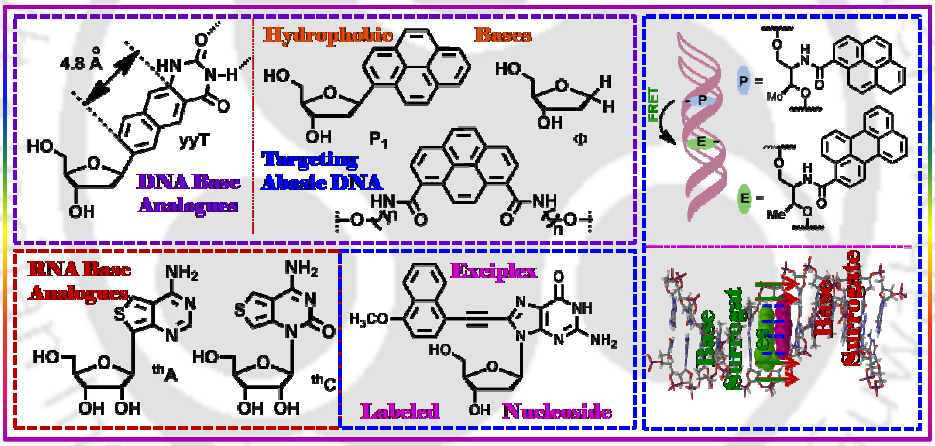

Figure A1: Schematic presentation of synthesis of fluorophores *via* "click" reaction and Sonogashira coupling.

The lack of significant fluorescence in naturally occurring nucleobases has prompted the design of fluorescent nucleobase analogues with improved photophysical properties for nucleic acids research. Thus, much effort has been devoted to develop non-natural, stable, H-bonded as well as hydrophobic base pairs of orthogonal recognition properties. Beside the H-bonding force, the role of other attractive forces like, hydrophobic, π-stacking, CH-π interaction, dipole moment,

polarizability and electrostatic interaction between a pair of designed unnatural nucleobase analogues, either in a self-pair or in a heteropair, has been established in the context of DNA duplex stabilization and enzymatic recognition *via* the generation of several nonfluorescent/fluorescent base analogues. Several fluorescent DNA base analogues (nucleosidic and/or non-nucleosidic base surrogates) have been exploited in various applications, such as in DNA analysis, monitoring hybridization events, in delineating structure and dynamics of DNA, in probing DNA lesion, in search of light harvesting DNA based materials and in other biotechnological and material science applications. Various photophysical properties, such as FRET, exciplex and excimer emission, have also been studied with the multichromophoric DNA containing multiple unnatural fluorescent base analogues exploiting the rigid DNA conformation as the organizing scaffold. Some of the environmentally sensitive fluorescent oligonucleotide probes containing microenvironment sensitive fluorescence have been used as a molecular signaling device in DNA detection.

CHAPTER 2: STUDIES ON THE SYNTHESIS AND PHOTOPHYSICAL PROPERTIES OF TRIAZOLYL NUCLEOSIDES

This chapter describes the design and synthesis of triazolyl donor/acceptor aromatic nucleosides and the study of their photophysical properties. Till the date, the charge transfer interaction among the designed unnatural nucleobases was not considered. As a part of our ongoing research effort toward generation of molecules with tuned photophysical properties *via* click reaction, we thought that it would be worthwhile to synthesize triazolyl nucleosides containing donor/acceptor aromatics to produce modulated photophysical response into the unnatural nucleosides (UNNs) and to showcase the possible π-stacking as well as charge transfer interaction ability among donor and acceptor triazolyl aromatic nucleosides. Utilizing this concept we have designed and synthesized few unnatural triazolyl nucleosides *via* azide-alkyne cycloaddition chemistry and studied the photophysical properties of some of them in details particularly in the context of their ability to show ground state charge transfer interaction property (**Figure A2**).

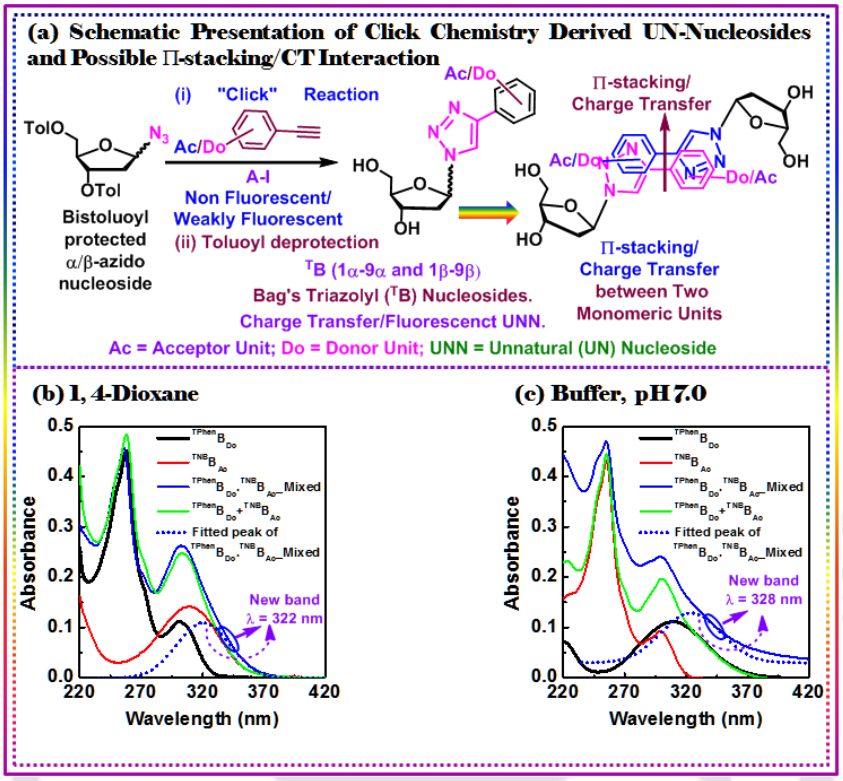

Figure A2: (a) Schematic presentation of synthesis of triazolyl unnatural nucleosides (UNN) and (b-c) the spectroscopic evidence of ground state charge transfer complexation.

The π-π stacking propensity among the donor and/or acceptor nucleosides was evident from crystal arrangement of three individual nucleosides. The UV-visible spectra of a 1:1 mixture in low polar dioxane solvent and in polar phosphate buffer of donor triazolylphenanthrene nucleoside ($^{TPhen}\mathbf{B_{Do}}$) and acceptor triazolylnitrobenzene nucleoside ($^{TNB}\mathbf{B_{Ac}}$) showed the possibility of ground state association property which is reflected in the appearance of a new absorption band at longer wavelength region, longer than any of the parent nucleosides (**Figure A2**). Analysis of the UV-visible spectra of the mixture and the combined spectra of the individual nucleosides both in dioxane and in buffer revealed a possible formation of ground state charge transfer complexation (**Figure A2b-c**). All experimental results are presented in this chapter.

CHAPTER 3: STUDIES ON THE SYNTHESIS AND PHOTOPHYSICAL PROPERTIES OF TETRAZOLYL NUCLEOSIDES

This chapter describes the design and synthesis of tetrazolyl donor/acceptor aromatic nucleobase surrogates and the study of their photophysical properties in various organic solvents. A literature study revealed that there exist only a few tetrazole-based *C*-nucleosides which have been synthesized for medicinal chemistry application. However, tetrazole-based *N*-nucleosides have not been explored much till date. Therefore, as a part of our journey for the synthesis of fluorescent unnatural nucleosides capable of showing π-π stacking and/or charge transfer interaction property in a donor/acceptor pair, we thought that it would be worthwhile to synthesise donor/acceptor aromatics containing tetrazolyl nucleosides and study their photophysical properties.

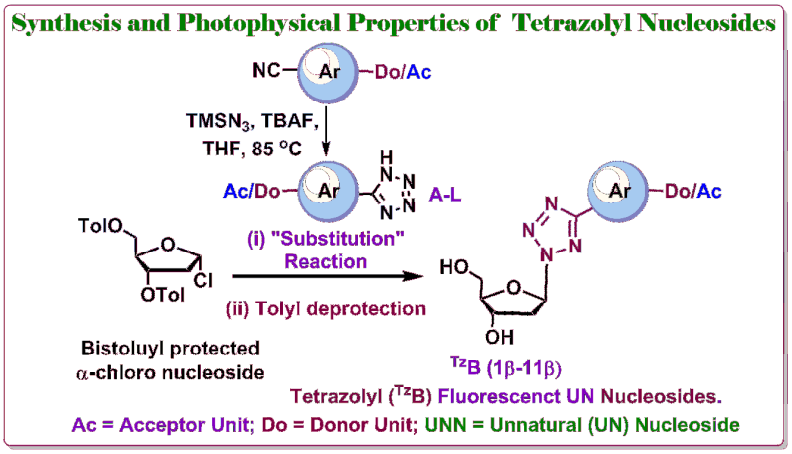

Figure A3: Schematic presentation of synthesis of donor/acceptor unnatural tetrazolyl nucleosides (UNN).

With this background and aim we have synthesized few unnatural tetrazolyl aromatic donor/acceptor nucleosides *via* stereospecific substitution reaction and studied their photophysical properties (**Figure A3**). Investigation of photophysical property of few of the tetrazolyl nucleosides revealed that linking of fluorescent/non-fluorescent aromatic unit with a tetrazole moiety could lead to the modulation of the emission property of some of the fluorescent aromatics. All experimental results are presented in this chapter.

CHAPTER 4: STUDIES ON THE STABILIZATION OF A DNA DUPLEX DECORATED WITH UNNATURAL TRIAZOLYL DONOR/ACCEPTOR NUCLEOSIDES: ROLE OF π-STACKING AND CHARGE TRANSFER INTERACTIONS

This chapter describes the studies on the charge transfer complexation /π-stacking interaction mediated stabilization of a DNA duplex containing triazolyl donor ($^{TPhen}\mathbf{B}_{Do}$) nucleoside paired against it in a self-pair duplex or paired against a triazolyl acceptor ($^{TNB}\mathbf{B}_{Ac}$) nucleoside forming a hetero-pair duplex. In the design of non-hydrogen bonding base pairs, researchers have concentrated mainly on factors like, π-stacking, hydrophobicity, steric shape mimicry and in few cases the dipole moment *etc.*, in the stabilization of the DNA duplex. However, the idea of charge transfer complexation among a donor/acceptor pair of nucleobases paired against each other in a hetero-pair duplex and the DNA duplex stabilization by charge transfer complexation was not considered. Therefore, we explored this possibility by utilizing our newly designed triazolyl donor/acceptor nucleosides.

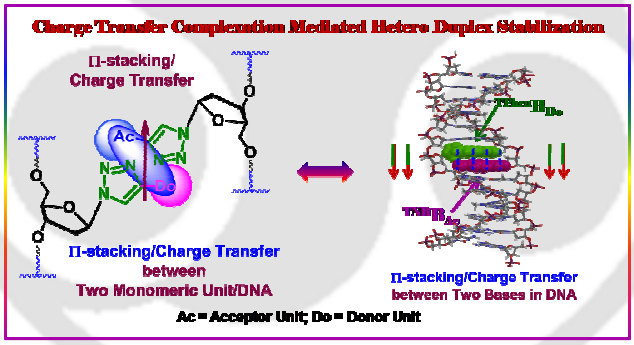

Figure A4: Schematic presentation of charge transfer complex formation between a donor and acceptor triazolyl unnatural nucleotides (UNN) inside a DNA duplex.

With this aim we have incorporated two triazolyl aromatic nucleosides ($^{T}\mathbf{B}$s) into short 13-mer oligonucleotide sequences to evaluate the stable duplex formation abilities. Thus, we have shown that our new and novel triazolyl unnatural donor/acceptor nucleobases offer a good stabilization of the heteropair ($^{TNB}\mathbf{B}_{Ac}$ **:** $^{TPhen}\mathbf{B}_{Do}$ /self pair ($^{TPhen}\mathbf{B}_{Do}$**:** $^{TPhen}\mathbf{B}_{Do}$) duplexes that are comparable to that of a natural A-T pair (**Figure A4**). The stabilization of the duplexes was explained on the

basis of possible involvement of charge transfer complexation (in a hetero-pair) and/or π-stacking interactions (in both the self-pair and hetero-pair) supported by spectroscopic evidences. All experimental results are presented in this chapter.

CHAPTER 5: STUDIES ON THE STABILIZATION OF AN ABASIC SITE PAIRED AGAINST AN UNNATURAL TRIAZOLYL NUCLEOSIDE

In this chapter, we report the stabilization of a DNA duplex containing an abasic site paired against a novel unnatural nucleoside, triazolylphenanthrene ($^{TPhen}\mathbf{B_{Do}}$). Inspired by the large surface area (248 $Å^2$ against natural A-T pair surface area 273 $Å^2$, calculated from macromodel), high polarizability, high stacking propensity (higher than adenine) and our recent observation on strong self-pair/hetero-pair stabilization, we thought that it would be worthwhile to study abasic DNA stabilization using our unnatural triazolylphenanthrene nucleoside $^{TPhen}\mathbf{B_{Do}}$ (**1**, **Figure A5**). Therefore, we planned to study the thermal as well as thermodynamic origin of abasic DNA stabilization by our synthesized oligonucleotide probe containing $^{TPhen}\mathbf{B_{Do}}$ nucleoside.

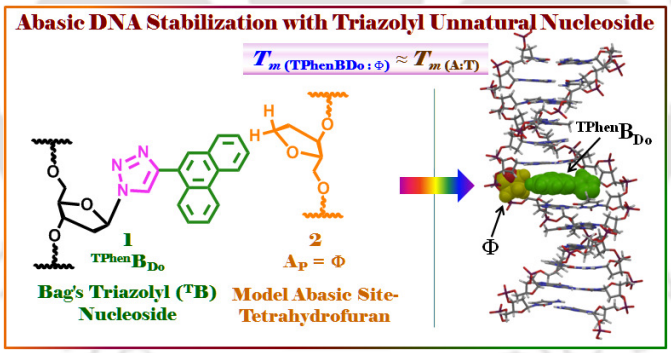

Figure A5: Schematic presentation of intercalative stacking interaction and abasic site stabilization by triazolyl unnatural nucleoside, $^{TPhen}\mathbf{B_{Do}}$.

We observed that the nucleoside $^{TPhen}\mathbf{B_{Do}}$ offered comparable thermal stabilization of a $^{TPhen}\mathbf{B_{Do}}$ **-*Φ*** duplex to that of a natural A-T pair *via* strong intercalative stacking interaction along an abasic site. Moreover, this stabilization is better than any of the reported abasic duplex stabilization by nucleosidic base surrogate. The UV-visible,

CD, and fluorescence spectroscopic studies supported the intercalative stacking interaction. The high stabilization of $^{Tphen}\mathbf{B_{Do}}$:**Φ** duplex represents a remarkable improvement in stability and selectivity over previously reported non-hydrogen-bonded base pairs.

CHAPTER 6: STUDIES ON THE DUAL MECHANISM OF EXCIPLEX EMISSION IN A CHIMERIC DNA DUPLEX CONTAINING NON-NUCLEOSIDE-NUCLEOSIDE BASE PAIR

In this chapter, the establishment on the dual mechanism to the exciplex emission has been presented in a conceptual chimeric DNA duplex wherein a fluorescent non-nucleosidic base surrogate ($^{OxoPy}\mathbf{S}$) paired against a fluorescent nucleosidic base surrogate ($^{TPhen}\mathbf{B_{Do}}$).

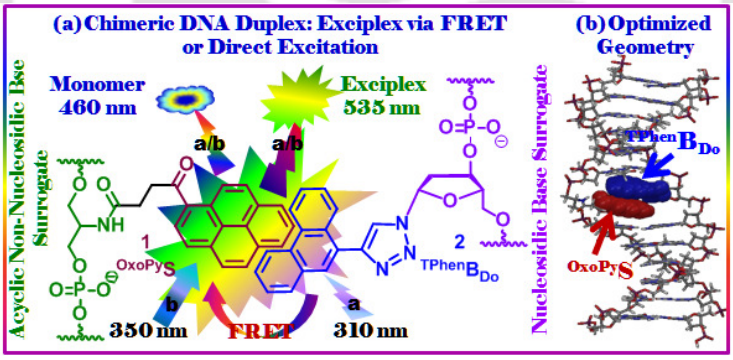

Figure A6: (a) Schematics of exciplex formation and structures of the acyclic non-nucleosidic base surrogate $^{OxoPy}\mathbf{S}$ and nucleosidic base surrogate $^{TPhen}\mathbf{B_{Do}}$. (b) Amber* optimized geometry of the chimeric base pair ($^{OxoPy}\mathbf{S}$:$^{TPhen}\mathbf{B_{Do}}$) held by intercalative inter-strand π-stacking interaction showing the possibility of exciplex formation.

Recently there has been a growing interest to search for DNA based materials. Towards this end several multiple chromophore labeled oligonucleotide probes have been developed for possible application in optical devices, light harvesting materials. However, all the design depends either on the fluorescent nucleoside or on the fluorescent non-nucleosidic base surrogates. Moreover, the DNA duplex wherein a fluorescent nucleosidic base surrogate paired against a non-nucleosidic base surrogate

involved in FRET or exciplex formation is not known. Inspired by the DNA duplex stabilizing property by our designed fluorescent unnatural nucleoside, triazolylphenanthrene ($^{TPhen}\mathbf{B}_{\mathbf{Do}}$), we thought that it would be worthwhile if we could design a fluorescently labeled flexible non-nucleosidic base surrogate and allow it to pair with our unnatural nucleoside, $^{TPhen}\mathbf{B}_{\mathbf{Do}}$ in a duplex, we could end up with chimeric DNA duplex with exciplex or FRET emission property (**Figure A6**).

The non-nucleosidic base surrogate $^{OxoPy}\mathbf{S}$ showed significant selectivity for the nucleosidic base surrogate $^{TPhen}\mathbf{B}_{\mathbf{Do}}$ over all four natural bases. Interestingly, these nucleobases were packed inside the duplex *via* intercalative stacking interaction. All the spectroscopic evidences suggested that both the process of excitation of oxopyrene chromophore of $^{OxoPy}\mathbf{S}$-either energy transfer from excited triazolylphenanthrene to oxopyrene *via* FRET or direct excitation of $^{OxoPy}\mathbf{S}$ at its absorbance maximum-led to the exciplex emission. The mechanism of exciplex formation *via* FRET which we have shown would become possible further by judicious designing and proper positioning of the donor/acceptor pair in a probe wherein the pair involves in strong intercalative π-π stacking interaction. To the best of our knowledge this is the start of a new generation of probes which could find wide applications in the field of chemical biology and in designing light harvesting DNA materials. We also hope that the design of such systems would have great impact in devising optoelectronics and might find application in chemistry, biology, material sciences and in diagnostic technology.

List of Abbreviations

A	Adenine
Ac	Acyl
Ar	Aryl
Abs	Absorbance
AMP	Adenosine monophosphate
ATP	Adenosine triphosphate
Ap	Aminopurine
AIDS	Acquired Immuno Deficiency Syndrome
AZT	Azidothymidine
Bn	Benzyl
B3LYP	Becke, three-parameter, Lee-Yang-Parr
BDF	Base-discriminating fluorescent
t-BuOH	Tertiary butanol
$^{TPhen}B_{Do}$	Triazolyl Phenantherene donor nucleoside
$^{TBN}B_{Ac}$	Triazolyl nitrobenzene acceptor nucleoside
$^{Tz}B_{Ac}$	Tetrazolyl acceptor nucleosidic base
$^{Tz}B_{Do}$	Tetrazolyl donor nucleosidic base
C	Cytosine
CD	Circular Dichrosim
CT	Charge Transfer
Cu	Copper
CuAAC	Copper Catalysed Azide Alkyne Click Reaction
CuCl	Copper chloride
CuI	Copper iodide
Cyhex	Cyclohexane
$CHCl_3$	Chloroform

$CuSO_4$	Copper sulfate
CH_3CN	Acetonitrile
D-A	Acceptor
Diox	1,4-Dioxane
DMF	Dimethyl formamide
DMSO	Dimethyl sulfoxide
DNA	Deoxyribonucleic acid
DFT	Density functional theory
DCM	Dichloromethane
DIPEA	N,N-Diisopropyl ethyl amine
DMAP	N, N-Dimethylamino pyridine
DMTr	4,4′-dimethoxytrityl chloride
Et_3N	Triethylamine
EtOAc	Ethylacetate
EtOH	Ethanol
eV	Electron volt
EDC.HCl	1-(3-Dimethylaminopropyl)-3-ethylcarbodiimide-hydrochloride
Eqv.	Equivalent
Fl	Fluorescence
FISH	Fluorescence In Situ Hybridization
FRET	Fluorescence Resonance Energy Transfer
G	Guanine
GNP	Gold nanoparticle
HOBT	1-hydroxy-benzotriazole
HRMS	High Resolution Mass Spectroscopy
HOMO	Highest Occupied Molecular Orbital

ICT	Intramolecular Charge Transfer
IR	Infrared Spectroscopy
KOH	Potassium hydroxide
K_2CO_3	Potassium carbonate
k	Rate Constant
LUMO	Lowest Unoccupied Molecular Orbital
Max	Maxima
MeOH	Methanol
mM	Mili molar
m.p.	Melting point
MALDI-ToF	Matrix Assisted Laser Desorption Ionization-Time of Flight
NMR	Nuclear Magnetic Resonance
nM	Nano molar
nm	Nanometer
ODN	Oligodeoxyribonucleotide
ODF	Oligodeoxyfluorisides
ORTEP	Oak Ridge Thermal Ellipsoid Plot
OLED	Organic light emitting diodes
O_2	Oxygen
OxoPy	Oxopyrene
$^{OxoPy}S$	Oxopyrene serinol
Py	Pyrene
Per	Perylene
PNA	Protein nucleic acid
PCR	Polymerase chain reaction
PET	Photoinduced electron transfer
Ph	Phenyl

ppm	Parts per million
r.t.	Room temperature
RNA	Ribonucleic acid
SNP	Single Nucleotide Polymorphism
ss	Single strand
T	Thymine
TBAF	Tetrabutylammonium fluoride
TFE	Trifluoroethanol
TLC	Thin layer chromatography
THF	Tetrahydrofuran
TDDFT	Time dependent density functional theory
TEA	Triethyl amine
TFA	Trifluoroacetic Acid
T_m	Thermal melting temperature of DNA
TMS	Trimethylsilyl
TPhen	Triazolylphenantherene
TLC	Thin Layer Chromatography
TO	Thiazole Orange
UV	Ultra violate
Zn	Zinc
μM	Micro molar
Φ	Quantum Yield
ε	Molar extinction co-efficient
τ	Decay time
Å	Angstrom (10^{-8}cm)
$\tilde{\nu}$	Wave Number
λ	Wave Length

λ_{max}^{abs}	Absorption maxima
λ_{max}^{fl}	Fluorescence maxima

NMR Data

δ	Chemical shift in NMR
s	singlet
d	doublet
t	triplet
q	quartet
m	multiplet
bs	broad singlet
dd	double doublet
dt	doublet of triplet
ddd	doublet of doublet of doublet
J	coupling constant in Hz

CONTENTS Page No.

Chapter 1

UNNATURAL NUCLEOSIDE BASE SURROGATES AND THEIR APPLICATIONS: A REVIEW

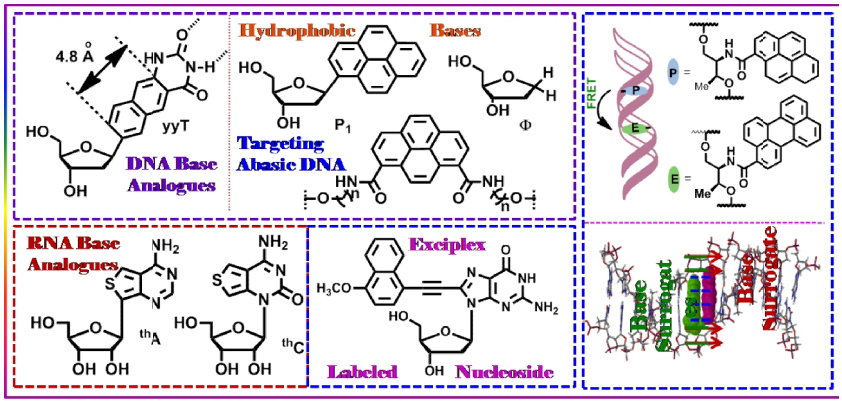

1.1 Introduction

DNA is an essential biomolecule which is responsible for encoding the complex information necessary for life. The specific pairing of dA with dT and dC with dG in duplex DNA (**Figure 1.1**) and during polymerase-mediated replication is the basis of the genetic alphabet, ultimately leading to the basis of genetic code.[1] However, there is no reason to limit the genetic alphabets and hence the information stored in them to only two base pairs. It was a logical thought among the scientific community that an expanded genetic alphabet would not only enable the encoding of additional information for both *in vitro* and *in vivo* applications but also enable a wide variety of biotechnology applications. Expansion of the genetic alphabet to include a third base pair, formed between two identical or different unnatural nucleotides, referred to as self-pairs and hetero pairs, respectively, would expand the informational and functional potential of DNA such as site directed oligonucleotide labeling and *in vitro* selections with oligonucleotides bearing increased chemical diversity.[2] Thus, not only the design and synthesis of efficient new base pair/pairs is an exciting research area but also the application of these artificial base-pairs to drive the synthesis of unnatural proteins is currently an attractive field of research with a hope to translate an expanded genetic alphabet into an expanded genetic code creating a synthetic organism one day with ability to encode proteins with new physico-chemical properties.[3]

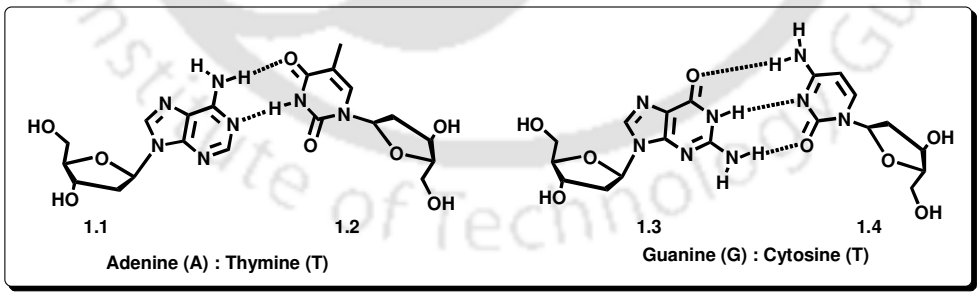

Figure 1.1: Presentation of hydrogen bonding between the DNA bases.

The idea of expansion of genetic alphabet for generating DNA and RNA with enhanced functional abilities was pioneered by Alex Rich[4] in 1962 to propose the concept of orthogonal base pairing between *iso*-G and *iso*-C and inspired Prof. Steven A. Benner in the late 1980's to expand the genetic alphabet from four to six letters.[5]

Benner's early research work focused on the development of new base pairs based on hydrogen bonding patterns orthogonal to those in canonical Watson-Crick base pairs.[6] Following Benner's work, many researchers have contributed to the field of expansion of genetic alphabets. As for example, a modified version of Rich's proposed *iso*-G/*iso*-C base pair has been demonstrated in RNA by Dervan in 1993.[7] As a result of tremendous research efforts, a large number of non-natural nucleosides capable of showing H-bonding/π-stacking interaction properties have been developed and their biophysical properties in the context of DNA have vigorously been investigated. As for example, a number of base analogues with orthogonal H-bonding complementarities[8] in relation to the natural Watson-Crick H-bonding have been exploited to examine the importance of hydrogen bonding interactions in the stabilization of nucleic acids structure, in the study of interbiomolecular interactions,[9a-b] and in the base recognition ability of enzymes.[9c-g] Several modified nucleosides with reporter functionalities have also been synthesized for monitoring the local microenvironmental change around the nucleic acids associated with interbiomolecular interactions.[10] Latter on in 1994, creation of non-H-bonding unnatural nucleobase surrogates by Kool *et al.* has opened a new dimension in the design of hydrophobic unnatural DNA base analogues.[11] Thus, they have explored the possible aromatic stacking, hydrophobic or CH-π interactions between the bases and shown that these attractive forces are good enough to stabilize a DNA duplex and are well recognized by DNA polymerases. Triggered by Kool's work, much efforts have been put forth to develop non-natural, stable, hydrophobic base pairs of orthogonal recognition properties towards expanding the genetic alphabets.[11] Recently, the design of unnatural DNA base pairs with tuned charge transfer/photophysical properties is a rapidly growing research field towards the development of nucleic acid based diagnostics and sensing materials.[12] While the development of bases with improved charge transfer characteristic would lead to oligonucleotides with novel electronic properties,[12] the fluorescent nucleobases could offer opportunity for in vivo imaging as well as for the development of nucleic acid based sensors.[13] Toward this end, several unnatural nucleobases have been designed for the development of functional nucleic acids.[10h,14] However, the rational design of non-hydrogen bonding base pairs

remains a challenge. In most of the design of non-hydrogen bonding base pairs, researchers have concentrated mainly on the factors like, π-stacking, hydrophobicity, steric shape mimicry and in few cases the dipole moment, *etc.*, in the stabilization of DNA duplex.[11`]

Thus, the efforts toward developing a third base pair have focused on the design of nucleobase analogues to pair *via* orthogonal hydrogen bonding (H-bonding, **Figure 1.2**), based on the work of the Benner group and more recently, on predominantly non-H-bonding (**Figure 1.3**) analogues that pair *via* hydrophobic interactions, based on the work of the Kool group.

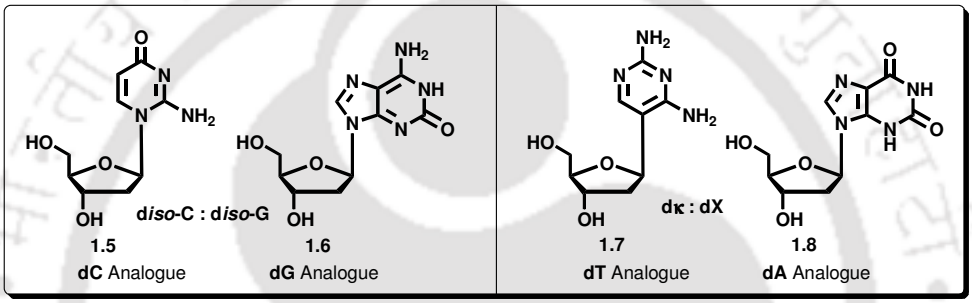

Figure 1.2: Presentation of H-bonding base pairs among unnatural nucleosides.

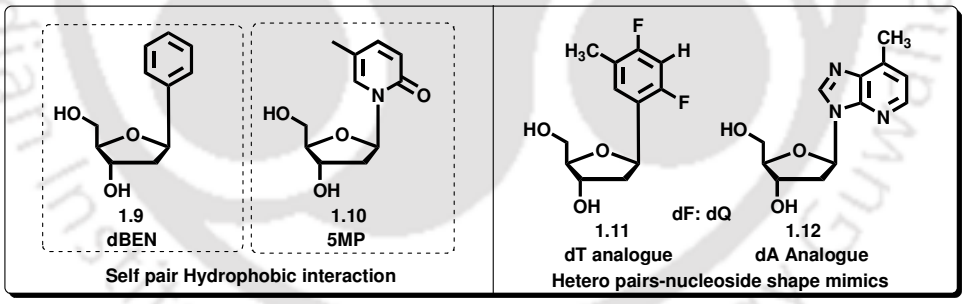

Figure 1.3: Presentation of non H-bonding base pairs among nucleoside base analogues.

However, the unnatural base pairs so far have been reported have several shortcomings, including tautomerization of *iso*-G and poor recognition of *iso*-C by RNA polymerases. These shortcomings pose difficulties for mRNA preparation. Since, all modern molecular biology techniques require the amplification of DNA by PCR, therefore, it would be worthwhile to design such unnatural pair for which both PCR amplification and transcription by RNA polymerase would be efficient.

Increasing diversity of these modified DNA and RNA molecules promises their enhanced widespread potential applications in biomedical sciences such as drug candidates. Novel, hydrophobic base pairs have been thus developed recently, but their use in transcription is still under investigation. Thus, there is a need to develop conceptually new and novel base analogues which will be recognized by DNA polymerases for both replication and transcription process with high efficiency.

1.2 Need for Unnatural Nucleotide Bases

The natural bases although differ in their organic structure and functional groups, belong to two major heterocyclic families. They do not differ much in their properties, like stacking ability, size, sensitivity in protonation in neutral pH etc. They only absorb light in ultraviolet region and are not responsive to the visible light. The intrinsic fluorescence of the naturally occurring nucleotide bases in DNA and RNA is extremely weak with very short fluorescence decay times, generally in the range of a few picoseconds. So, they can't be detected by highly sensitive fluorescence detection techniques and hence do not provide much structural information. The rarity of the fluorescent natural bases like wyosine (Yt) which is found in the anticodon region of $tRNA^{Phe}$, has limited their use in fluorescence studies. Thus, RNA and DNA, in general, lack naturally occurring intrinsic fluorescence reporters in contrast to proteins, which may contain one or more naturally occurring tryptophan or tyrosine residues that can be exploited for fluorescence measurements.

Therefore, the lack of naturally occurring fluorescent bases has spurred the development of artificial nucleosides with interesting photophysical properties which can be used as probes for DNA analysis. These nucleosides can be designed in such a way so as to get desired fluorescence properties and which can be incorporated into oligonucleotides using the standard automated synthetic methods. The fluorescence properties, from DNA and RNA molecules, thus can be observed without any competing background signals mainly by two ways: (a) incorporation of unnatural nucleotide base analogues into the oligonucleotide sequence and/or (b) incorporation of fluorophore into the natural bases *i.e.* by synthesizing labeled bases. We will focus

only to the unnatural deoxyribonucleotide base analogues and some of their applications.

1.3. Design of Unnatural Base Pairs

Expanding the genetic alphabet requires an unnatural base pair with inter base interactions, of whatever sort, that confer stability on a DNA duplex and that is replicated by a DNA polymerase. Specifically, each unnatural triphosphate must be efficiently and selectively incorporated opposite its partner in the template to form a stable base pair. Conversely, no natural substrate should be inserted opposite the unnatural nucleotide in the template with high efficiency. Also, continued synthesis past the unnatural base pair must be efficient. Moreover, (a) the synthetic nucleosides should be amenable to phosphoramidite synthesis for incorporation into oligo-nucleotides by solid-phase synthesis. (b) should not disrupt B-form duplex DNA. Thus, the efforts toward developing a third base pair have focused on nucleobase analogues designed to pair *via* orthogonal hydrogen bonding (H-bonding, **Figure 1.2**), or on predominantly non-H-bonding (**Figure 1.3**) analogues that pair *via* hydrophobic interactions. (c) Furthermore, the designed nucleosides should behave as a regular nucleoside in its interaction with proteins and enzymes; and should be capable of being converted to the triphosphate and be incorporated into DNA with high efficiency by current commercial polymerases. (d) For probing DNA structure, and for the application of DNA based materials, the ideal fluorescent nucleoside base analogues should (i) maintain the structural similarity i.e. should be steric shape mimic of the natural nucleobases as well as hybridization and recognition properties, (ii) exhibit a red shifted absorption spectra, (iii) must possess efficient fluorescence property such as adequate emission quantum efficiency, long fluorescence life time, microenvironment sensitivity and long wavelength emission, preferably in the visible range.

Therefore, the major efforts are focused on the development of a stable third base-pair that would not only provide stability to the DNA duplex like the natural base-pairs but would be replicated efficiently with high fidelity. Recent efforts have resulted in designing and construction of a number of such base-pairs that are stable

within the DNA duplex. However, to date, because of the challenging problem of enzymatic replication of such base pairs, only very few of these artificial base-pairs have been efficiently and selectively replicated. The base-pairs formed are of following categories: (a) unnatural hydrogen-bonding pattern as well as upon the shape complementarity, (b) hydrophobic forces, (c) non-nucleosidic base surrogate, (d) and even covalent cross-linking. We will focus on discussing the first three base analogues.

1.4. Artificial Base-Pairs Based on Hydrogen Bonding Interaction

Specific base-pairing in nucleic acids is essential to the accurate replication and expression of genetic information. It is made possible, in part, by unique hydrogen bonding complementarity, which depends critically on the tautomeric states of the bases. Tautomerisation reverses the polarity by interconverting H-bond donors and acceptors. The different electronegativities of oxygen and nitrogen exocyclic substituents are consistent with observed equilibrium constants of 10^4 in favour of the amino tautomers of A and C, and the keto forms of G and T. Modification of these groups though, perturbs the equilibrium, it is made possible by suitable design and with the help of synthetic chemistry. Thus, the compounds, which are mutagenic *in vivo*, can function as analogues of both A, G, C and T depending on the opportunities for H-bonding available in a given environment. The concept of hydrogen-bonding patterns and shape complementarity was pioneered by Alex Rich in 1962 (e.g., isoguanosine, *iso*-G; isocytidine, *iso*-C; **Figure 1.2**) and later by Prof. Steven A. Benner in the late 1980's. Further development has led to the introduction of other donor-acceptor (D-A) purine-pyrimidine pairs and finally to a generalization of the Watson-Crick nucleobase pairs (**Figure 1.4**).[6]

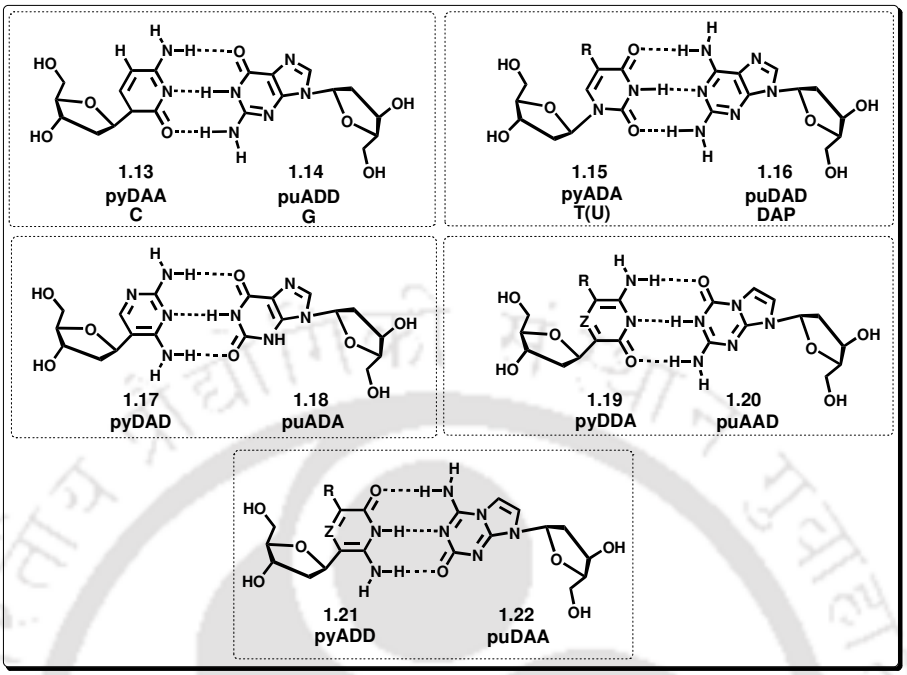

Figure 1.4: Several base pairs with hydrogen bonds.[6]

A number of DNA base analogues are now available, some even commercially, for incorporation into oligonucleotides for biophysical and biochemical studies. These nucleotide base probes share common chemical features, like faithful mimicry of native base structure and optimization of fluorescence quantum yields and lifetimes. Each base analogue also exhibits some unique fluorescence, structural or chemical properties, which should be considered when deciding on the optimal probe for use in studies of a particular nucleic acid system. We will summarize below some of the important deoxyribonucleotide base analogues reported till the date.

1.4.1. Purine Base Analogues

***2-Aminopurine (2-AP) as Adenine Base Analogue*:** 2-aminopurine (2-AP) (**1.23**), a structural isomer of adenine which is highly fluorescent was first demonstrated by Stryer and colleagues.[15] As it is structurally similar to adenine (6-aminopurine), 2-AP is a non-perturbing substitution of adenine and also forms thermodynamically stable base pairs with thymine and uracil through hydrogen bonds in DNA and RNA helices respectively (**Figure 1.5**). 2-AP is also forms a base pair

with cytosine, in contrast to adenine, which is the basis for 2-AP's mutagenicity. 2-AP can be incorporated into both DNA and RNA oligonucleotide sequences in a site-specific manner. The quantum yield of 2-AP is highly sensitive to its microenvironment and insensitive to base pairing and other H-bonding interactions. Hence, it serves as an efficient reporter nucleoside analogue in an oligonucleotide probe to detect subtle conformational changes in nucleic acids.

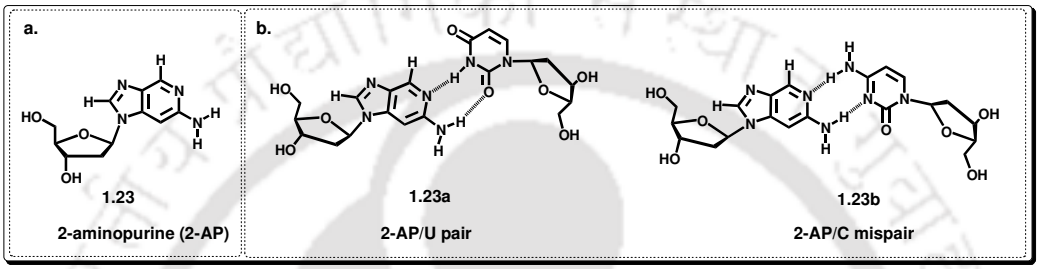

Figure 1.5: (a) Structure of 2-Aminopurine and its (b) Hydrogen bonding pattern with uracil and cytosine.

Other base analogues of adenine include 2-aminoadenine (2,6-diaminopurine) and 7-aminopropargyl-7-deaza-2,6-diaminopurine. 2-aminoadenine was synthesized and introduced into oligonucleotides by Chollet *et al.*,[16] which pairs up with thymine through additional hydrogen bonds and also introduces subtle changes in the minor groove of DNA. Oligonucleotide hybridization probes containing 2-aminoadenine have shown increased selectivity and hybridization strength during DNA-DNA hybridization to phage or genomic target DNA. 2-Aminoadenine has been used to probe minor groove detection during the treatment of DNA by 12 restriction endonucleases wherein inhibition of cleavage is the result for several restriction enzymes. 7-aminopropargyl-7-deaza-2,6-diaminopurine has been synthesized and incorporated into oligonucleotides by Brown *et al.*, and its pairing property has been studied. When paired up opposite to thymine, it was found to have similar thermodynamic stability as that of C:G pair.[17]

ATP/AMP Analogues: Other fluorescent analogues of adenine have been developed and used primarily as probes of AMP/ATP binding by enzymes (**Figure 1.6**). These other base analogues include etheno-ATP[18a-c] and lin-benzo-AMP[18d], which are analogues of ATP and AMP, respectively. Another ATP analogue,

formycin 5'-triphosphate[18e], has been used as a substrate analogue for adenylate cyclase. These analogues have been used primarily in studies of nucleotide cofactor binding to enzymes.

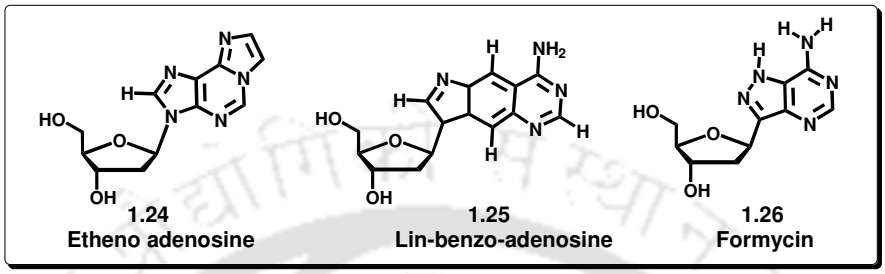

Figure 1.6: Structures of adenine base analogues used to construct fluorescent nucleoside and nucleotide analogues- Etheno-adenosine, lin-benzo-adenosine and formycin.

Pteridine Analogues of Adenine and Guanine: Pteridine is a class of heterocyclic compounds composed of fused pyrimidine and pyrazine rings.[19] Pteridine analogues of adenine and guanine have also been synthesized. Reported pteridine adenine analogues include 4-amino-6-methyl-8-(2-deoxy-β-D-ribofuranosyl)-7(8*H*)-pteridone (6-MAP) (**1.27**, **Figure 1.7a**) and 4-amino-2,6-dimethyl-8-(2'-deoxy-β-D-ribofuranosyl)-7(8*H*)-pteridone (6-DMAP) [20a] (**1.28**, **Figure 1.7a**). They have been synthesized and incorporated into short stretches of oligonucleotides in order to study their pairing and fluorescence properties. The pteridine-containing oligonucleotides have melting temperatures similar to that of the unmodified control oligonucleotides thus showing that they induce minimal changes in DNA when incorporated as an adenine analogue. Two pteridine guanine analogues, 3- methyl isoxanthopteridine (3-MI) (**1.29**, **Figure 1.7b**) and 6- methyl isoxanthopteridine(6-MI) [20b,c] (**1.30**, **Figure 1.7b**) have been synthesized and incorporated into DNA. After incorporation into DNA, both the pteridine adenine and guanine analogues display significant quenching of fluorescence intensity, increased complexity of fluorescence decay curve and decreased mean fluorescence lifetime. The degree of quenching of fluorescence intensity of pteridine adenine and guanine analogues correlate with the number and proximity of purines in the oligonucleotide. The degree of quenching did not increase

upon formation of double stranded oligonucleotides but the complexity of decay curves increased and mean fluorescence lifetimes decreased.

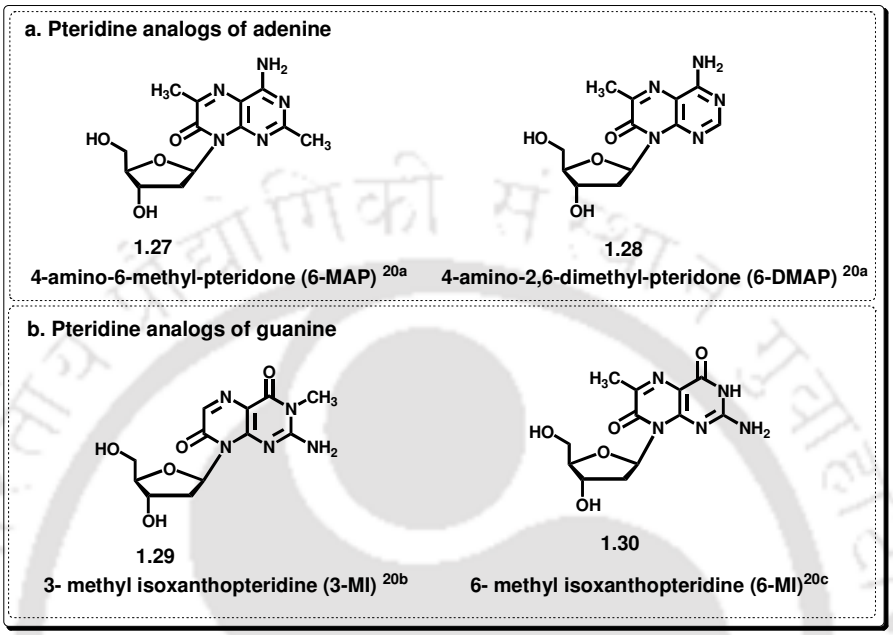

Figure 1.7: Structure of Pteridine analogues of (a) adenine and (b) guanine

1.4.2. Pyrimidine Base Analogues

Benzo[g]quinazoline Based Thymine Base Analog: Godde and colleagues have synthesized bases with extended aromatic domains that increase third strand binding through stacking interactions.[21] One of the polycyclic aromatic base analogues of thymine, benzo[*g*]quinazoline-2,4-(*1H,3H*)-dione(**1.31**, **Figure 1.8**), is found to display strong fluorescence emission centered at 434 nm (Φ_F ~ 0.82) and two major excitation maxima (260 and 360 nm).[21] Formation of the triple helical structure using a third oligopyrimidine Hoogsteen strand that contain this fluorescent thymine analogue, results in a shift of the fluorescence emission maximum to shorter wavelengths and a decrease in fluorescence intensity.[21] In a duplex, it does not produce any significant changes in fluorescence properties.[21] Thus, the sensitivity of this base analogue to the helical conformation allows selective detection of triplex over duplex formation.

***Thymine Analogue**:* Another thymine analogue 5-methyl-2-pyrimidinone (**1.33**, **Figure 1.8**) has been synthesized and used in early studies of DNA duplexes. This base analogue does not pair well with adenine, however, using time-resolved fluorescence decay measurements it has been shown that the predominant state of the base in the context of a DNA oligonucleotide is stacked so that its fluorescence is efficiently quenched.[22]

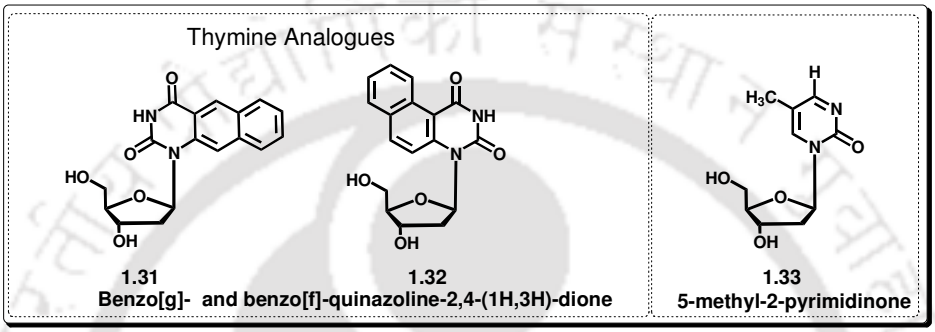

Figure 1.8: benzo*[g]/[f]*quinazoline-2,4-(1H,3H)-dione and 5-methyl-2-pyrimidinone as thymine analogue.

Benzo[g]quinazoline Based Cytosine Base Analogue: A 2'-O-Me ribonucleoside derivative of 4-amino-1*H*benzo[*g*]quinazoline-2-one (**1.34**, **Figure 1.9**) has also been synthesized based on the same heterocyclic benzo[*g*]quinazoline (**1.35**, **Figure 1.9**) design and used as a novel fluorescent cytosine base analogue probe.[23] This cytosine base analogue exhibits a fluorescence emission centered at 456 nm, characterized by four major excitation maxima (250, 300, 320 and 370 nm) and a fluorescence quantum yield of Φ_F = 0.62 at pH = 7.1. The fluorescence emission of this probe shifts from 456 to 492 nm when pH is decreased from 7.1 to 2.1. The pKa (4.0) of the probe is close to that of cytosine (4.17). This probe has been used to detect the protonation state of base triplets in triple stranded structures.

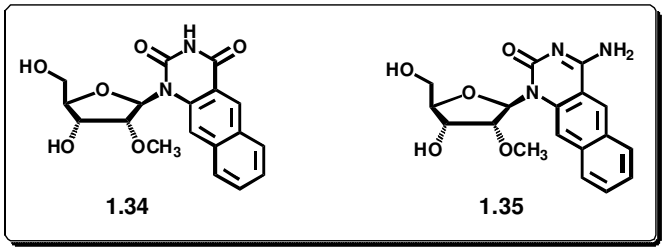

Figure 1.9: Structures of 1-(2-O-methyl-β-D-ribofuranosyl)- benzo[*g*]quinazoline and 1-(2-O-methyl-β-D-ribofuranosyl)-4-amino-1*H* benzo[*g*]quinazoline-2-one.

Tricyclic Cytosine (tC): Norden and colleagues have described a new cytosine base analogue, 3,5-diaza-4-oxophenothiazine or tricyclic cytosine (tC) (**1.36**), which can form a specific base pair with guanine (**Figure 1.10**). Like the benzo[*g*]quinazoline base analogues, this base maintains its relatively high quantum yield (Φ_F = 0.20) even after incorporation into single and double stranded oligonucleotides, like artificial peptide nucleic acid (PNA) biopolymers and RNA-DNA duplexes.[24]

Elaboration of the tC(O) scaffold can yield a nitroxide spin labeled compound (**1.31**) that may be used for EPR measurements[25a] and the "G-clamp" which has increased binding affinity to guanine (**A**, **C**, **D**)[25b-e] (**Figure 1.10**).

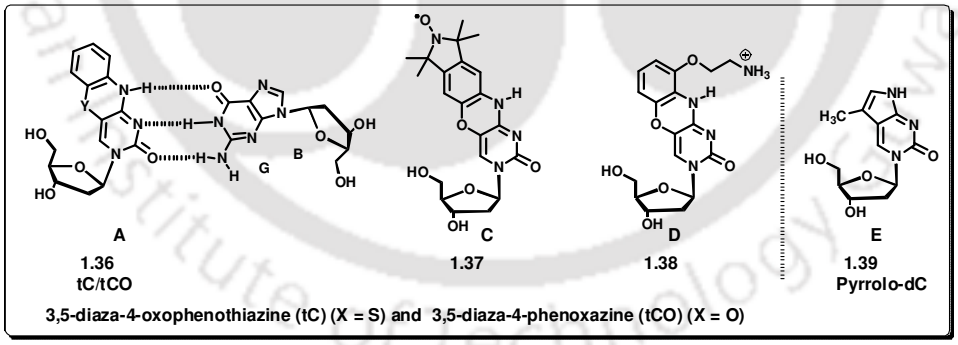

Figure 1.10: 3,5-diaza-4-oxophenothiazine (tC) (X = S) and 3,5-diaza-4-phenoxazine (tCO) (X = O) in hybridization with guanine (A, C, D). The structure of pyrrolo-dC (E).

Pyrrolo-dC as Cytosine Analogue*:* In another study, a new highly fluorescent base analogue of cytosine, pyrrolo-dC (**1.39**), (**Figure 1.10**) has been introduced to characterize the transcription bubble in elongation complexes of T7 RNA

polymerase.[26a-b] Pyrrolo-dC has excitation and emission maxima at 350 nm and 460 nm, respectively, which, like the previously described analogues, allows selective excitation in the presence of native nucleic acid bases and proteins. This base analogue can pair with guanine and like 2-AP, pteridine and hydrocarbon base analogues, shows significant quenching of fluorescence when incorporated into single and double stranded DNA. The quenching can be used to monitor local melting of the **G:C** base pairs in a DNA helix and can serve as a complementary probe to 2-AP, which reports on melting of AT base pairs.[26c]

Xanthosine Analogue: The base analogue of the rare base xanthosine (5-aza-7-deazaxanthine) (**1.38**) has been synthesized and reported by Benner *et al.* (**Figure 1.11**).[27] This base was designed based on the supposition that the rare tRNA constituent wyosine carries the 5-aza-7-deazapurine substructure, and it is this structure that makes the base fluorescent. When excited at 250 nm, this base analogue displays two emission maxima at 410 nm and 580 nm.

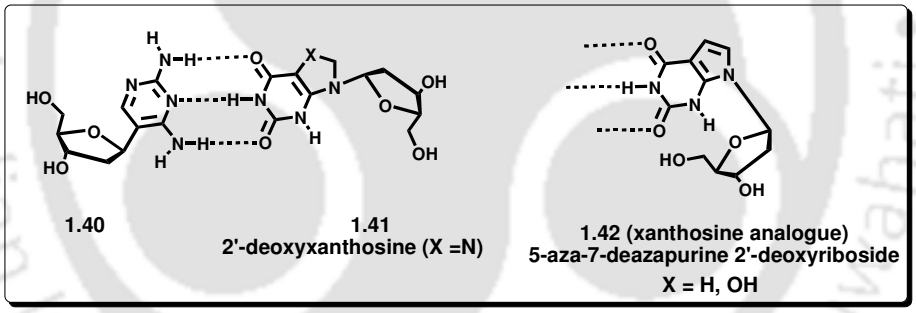

Figure 1.11: Structure and hydrogen bonding property of xanthosine analogue.

1.4.3. Size Expanded Base Pairs

The concept of nucleosides having increased size originated three decades ago when Leonardo *et al.* synthesized an adenine ribonucleoside analogue in which the base was stretched out by the insertion of a benzene ring in between two rings of adenine.[28a] This ribonucleoside was used as a substrate for many ATP-dependent enzymes, in order to probe the active sites of the enzymes. Later on, the 2'-deoxy variant of benzo A was prepared from the ribonucleoside.[28b] However, the analogue was never incorporated into oligonucleotide as automated DNA synthesizers were not

invented during that time. Leonard predicted that the stretched out adenine base would destabilize a natural DNA as it is too large as compared to natural DNA bases.

The synthesis and study of expanded DNA bases was done with the motive of expansion of genetic alphabets which is orthogonal to the natural one, to develop bases with greater electronic conjugation which can endow the nucleosides with fluorescence properties, to probe the steric effects of the active sites of polymerase enzymes and finally to develop a new helix that is thermodynamically more stable than the natural DNA due to the stacking interactions between the bases.[29]

Benzo Fused Molecular Designs: With the aim of generating size expanded DNA molecules the expanded analogues of the purines and pyrimidines containing the fused benzene ring have been synthesized by Kool *et al.* and their properties studied. The benzo fused analogues of purines and pyrimidines paired with natural DNA bases could potentially yield a regular helix with expanded diameter (**Figure 1.11**).[30] The fusion of the benzo ring increases the size of the natural nucleoside by 2.4 Å, with similar vectors of extension. Modeling studies as well as experimental studies have shown that the DNA backbone with benzo-fused nucleosides required only small adjustments of bond angles with no large change to sugar conformations in order to adjust the expanded nucleosides inside the helix duplex. However, the expanded DNA differs from the natural B- DNA in one respect: that it generates greater number of base pairs per turn creating larger outer circumference than that of the natural DNA. Modeling studies have suggested that there are 14 base pairs per turn as compared to the 10.5 base pairs in natural B-DNA.

While natural DNA is composed of four components with two types of ring systems, the purine and the pyrimidine rings, there are eight components of size expanded DNA, known as x-DNA with four types of ring systems. In x-DNA, the *benzo*purines are paired against pyrimidines and the *benzo*pyrimidines are paired against purines. While the pairing selectivity in natural DNA comes from the complementary hydrogen bonding but in x-DNA, complementary hydrogen bonding as well as complementary size are the determining factors of pairing selectivity (**Figure 1.12**).[30 c]

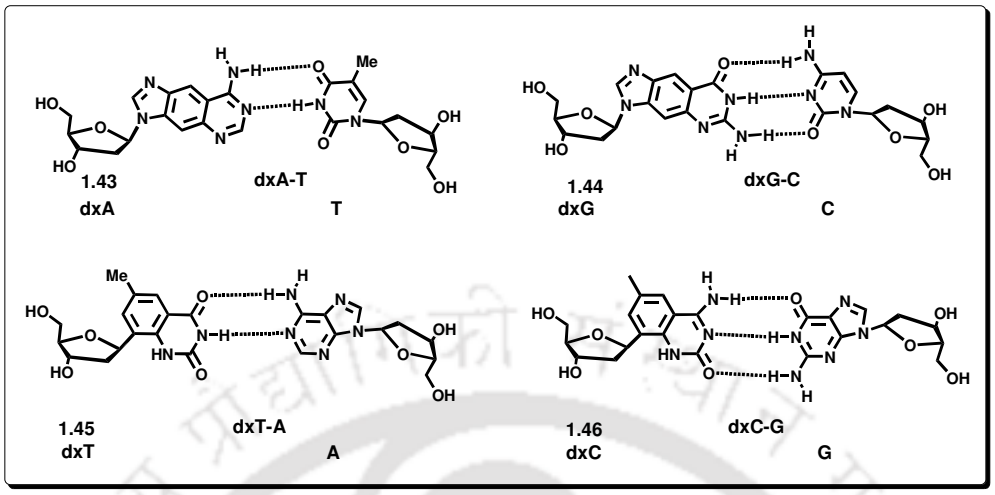

Figure 1.12: Structures and H-bonding pattern of x-DNA bases.

The x-DNA involved a linear extension of purine and pyrimidine by the addition of a benzene ring to the natural bases, a similar benzo-homologation with a different extension vector yielded the y-DNA which Kool *et al.* named as "wide DNA" (**Figure 1.13**).[31] The extended conjugation of the expanded DNA bases due to the added benzo fusion rendered it fluorescent with a large Stokes shift of 50-80 nm in contrast to the naturally occurring bases. They are efficient fluorophores and fluoresce in the visible wavelength region with quantum yields between 0.30 and 0.6.[31 a, c]

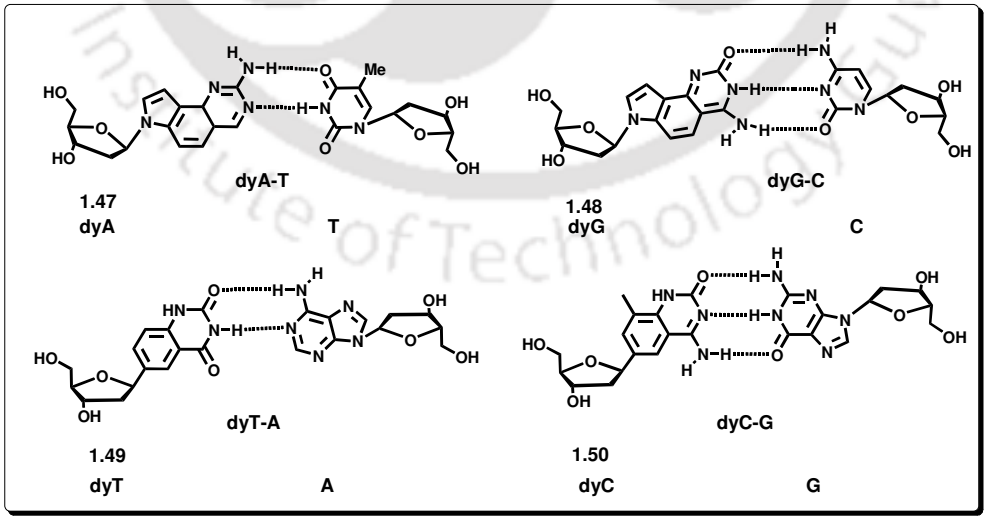

Figure 1.13: Structures and H-bonding pattern of y-DNA bases.

The designed expanded bases that are singly substituted into natural DNA have been found to destabilize the DNA helix as the benzo-expanded base pair is too large which induces strain leading to backbone distortions. For the xDNA analogues, the destabilization penalty ranged from 0.3 to 1.7 kcal/mol relative to the stability of natural base pairs and for yDNA pairs, the range has been found to be 0.6-2.2 kcal/mol. However, replacement of natural bases with all unnatural size expanded base pairs the x-DNA and y-DNA have been found to form highly stable, sequence selective double helices. It is reported that the size-expanded bases form the components of artificial genetic system with eight components as compared to the four components in the natural genetic system.[32] The high binding selectivity, affinity in base pairing and fluorescence property of expanded DNA bases might be useful in detection of nucleic acid sequences.

Naptho Fused Molecular Designs: Latter on, Kool *et al.* has developed more widened DNA by synthesizing expanded DNA base pairs via naptho-homologation. Two naptho-homologated deoxyribonucleosides dyyT and dyyC which are expanded analogues of thymidine and cytosine thus have been synthesized and incorporated into oligonucleotides (**Figure 1.14**)[33] and found that the inclusion of two benzene rings widened the dyyT and dyyC by about 4.8 Å as compared to their natural counterparts. Such type of DNA was named as "double wide DNA" by Kool *et al.* The extra conjugation rendered by the additional benzene ring makes the DNA bases fluorescent with red-shifted absorption and emission property.[33] The fluorescence of yy-DNA bases suggests that such type of widened bases might find applications in detection and imaging of natural nucleic acids. However, in contrast to the standard nucleic acid probes, the yy DNAs do not give simple denaturation behaviour. The complex melting behavior indicates that the strong single-stranded stacking of the component bases might prevent the measurement of the affinity of yyDNAs for their complements using standard thermal denaturation methods.

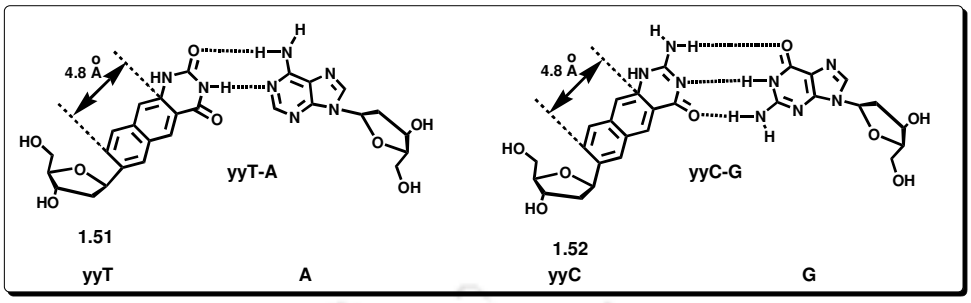

Figure 1.14: Structures and H-bonding pattern of doublewide DNA.

1.4.4. Alkynyl Extended Base Pairs

Inouye *et al.*[34] have reported another type of acetylene-linked extended DNA bases bearing pyrimidine heterocycles. These C-nucleosides have been found to form Watson-Crick like H-bonds (**Figure 1.15**) like the natural bases. These bases have shown to form a right handed duplex of comparable stability to that of a natural DNA.

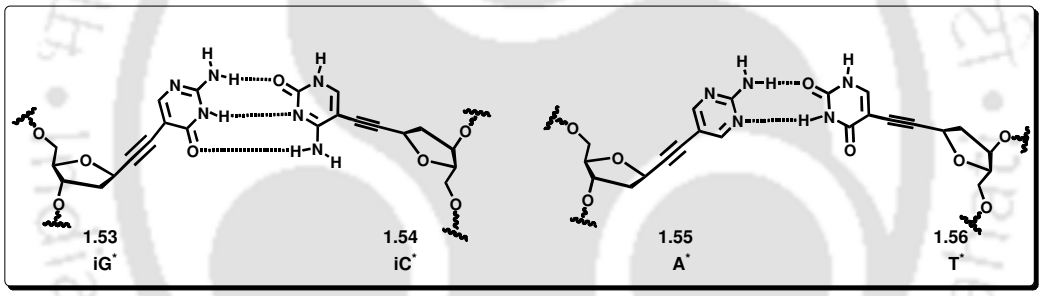

Figure 1.15: Structures and H-bonding pattern of Inouye's extended base pairs.

1.4.5. Four Hydrogen Bonded Base Pair

Minakawa and Matsuda *et al.*,[35] have reported two pairs of extended DNA base pairs capable of forming four hydrogen bonds (**Figure 1.16**). These imidazolopyridopyrimidine and napthyridine base C-nucleosides provides extra stablility to the duplex by +8-9^{o}C due to four H-bonds. These base-pairs have been found to be recognized by Klenow fragment polymerase and have successfully been incorporated against their non-natural complememtary bases.[36]

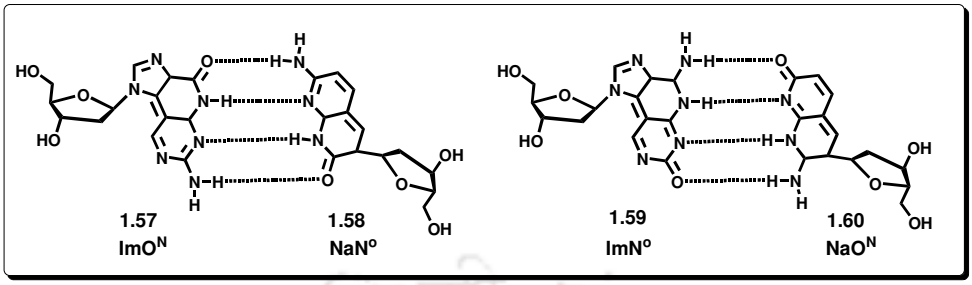

Figure 1.16: Structures and H-bonding pattern of Minakawa and Mastuda four H-bonded base pairs.

1.4.6. Pyridone Based Base-Pairs

The most fascinating pyridone based nucleobases, **y**[37a] (**1.61**, **Figure 1.17**) and **v**[37b] (**1.65**, **Figure 1.16**) have been designed by Hirao *et al.* [38] **dyTP** has been incorporated into DNA opposite to **dx** more efficiently than any of the natural nucleobases. The **dyTP** has also been found to be incorporated into the template opposite to designed **"ds"** base with higher efficiency than any natural base[39] and a 3-fold higher selectivity than its incorporation opposite to **dx**.[40] The efficiency and fidelity of **y-v** pairing have been found as high as in natural base-pairs. The **y**-**s** pair has been utilized for in vitro incorporation of chlorotyrosine into a protein.[41] Thus, **y-s** pair serves as a new genetic codon system.

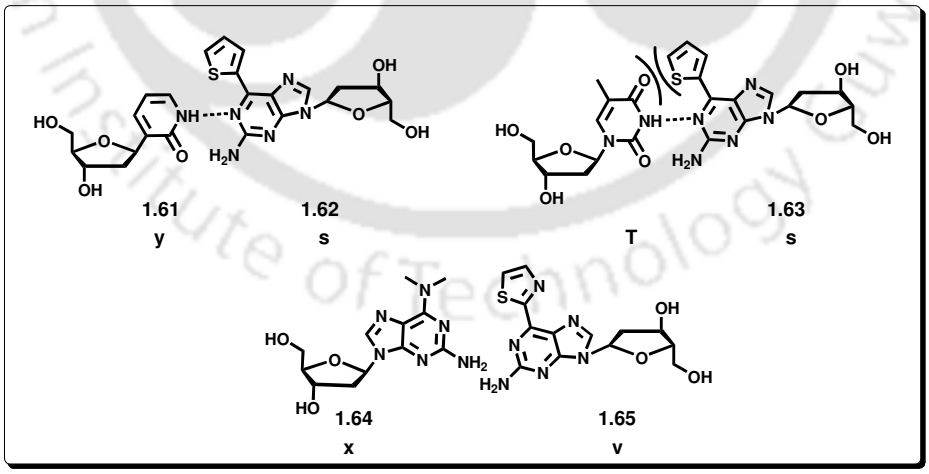

Figure 1.17: Hirao's pyridone base-pairs.

1.4.7. Halogen Bonded Base Pair

Sekine *et al.*,[42] have proposed conceptual halogen bonding as an alternative to H-bonds for specific base-pairing of artificial nucleosides. Several halogenated benzene and pyridine pairs have been studied but the most stable and selective binding has been found for difluoroiodobenzene (**2FI**) and pyridine (**3Py**) pair (**1.66** and **1.67**, **Figure 1.18**).

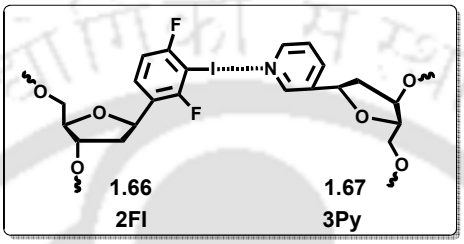

Figure 1.18: Proposed Sekine's Halogen bonded base pair.

1.5. A Complete Set of Emissive RNA Alphabet

It is clear from the above discussion that several nucleoside analogues including the several emissive nucleosides have been reported over the years.[43] Describing the H-bonded/non-H-bonded RNA base analogues, though, is beyond the scope of the thesis, we found one highly inspiring and interesting report by Tor *et al.* who have described for the first time the isomorphic design[43a, 44] of emissive DNA and RNA alphabets and a complete set of RNA alphabets with novel fluorescent and biophysical property.[45]

Previously, Kool *et al.* have reported a complete set of emissive expanded RNA nucleoside analogues and studied their fluorescence photophysical properties (**Figure 1.19**). They have found that the benzo-expanded ribonucleosides (xRNA), analogues to A, G, C, and U RNA monomers, are efficient fluorophores with emission maxima ranging from 369-411 nm.[46]

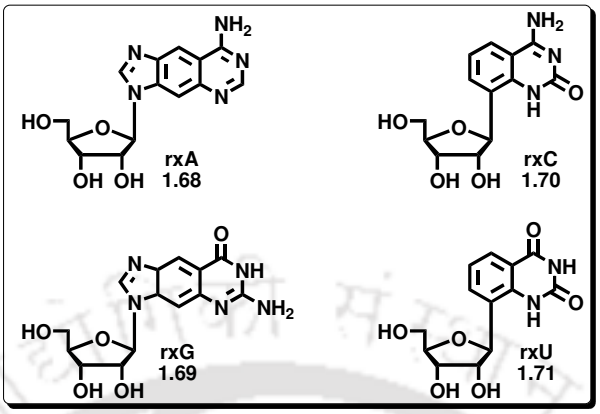

Figure 1.19: The size expanded emissive xRNA genetic set develoed by Kool *et al.*

Later on, they have described the use of size-expanded versions of adenosine (**rxA**) and uridine (**rxU**) as a novel set of steric probes to investigate the RNAi mechanism. For that purpose they have incorporated these two bases into biologically active siRNAs and use in biophysical studies. Their studies demonstrate the utility of xRNA nucleobases as mechanistic tools in biologically functioning siRNAs.[47]

In continuation of the isomorphic base design Tor *et al.* have taken very interesting and challenging task to offer a complete set of emissive RNA-alphabets derived from a single heterocyclic core that has not been addressed previously. In their design they emphasized on the structural similarity with the native counterparts which ultimately would lead to minimize structural and functional perturbation which is an inevitable consequence of replacing any native residue with a synthetic probe. Therefore, they have reported the design and synthesis of isomorphic base analogues, a complete set of ribonucleoside alphabets, consisting of highly emissive purine (th**A**, th**G**) and pyrimidine (th**U**, th**C**) analogues (**Figure 1.20**). All are derived from thieno[3,4-*d*]pyrimidine as the heterocyclic nucleus (**1.33**, **Figure 1.20**). The beauty of this parent heterocycle is that it can be viewed as a precursor to 5,6-modified emissive pyrimidines as well as a purine mimic with thiophene substituted for the imidazole moiety.

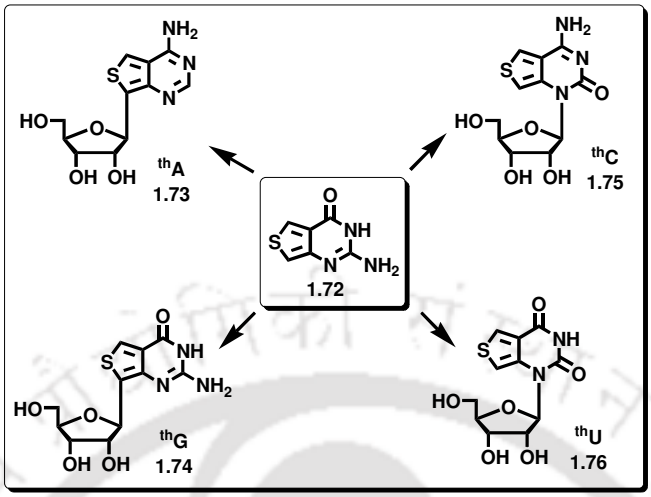

Figure 1.20: Isomorphic and emissive RNA alphabet designed by Tor *et al*. derived from a single from thieno[3,4-*d*]pyrimidine as the heterocyclic nucleus.

They have investigated the conformation of all the nucleoside analogues in solid state. Thus, the crystal structures of the modified ribonucleosides showed that they all display an anti orientation at their glycosidic linkages which is similar to the preference seen with the native counterparts. However, while the pyrimidine analogues **thU** and **thC**, possess partial C2′-endo conformation of sugar, the purine analogues **thG** and **thA** exhibit C2′-endo and C3′-endo ribose pucker, respectively, in the solid state, which are the predominant conformations adopted by the natural ribonucleosides. However, overlayed crystal structure of **thG** and **thA** with their native counterparts reflects minimal distortion of the ribose conformation.[45] The fundamental spectroscopic properties of the modified nucleosides **thU**, **thC**, **thA**, and **thG** have also been investigated which showed good solvatochromicity along with a long wave length absorption longer than their native counterparts and highly fluorescence characteristics better that their natural counterparts. They have also incorporated **thG** into 17-mer RNA and tested the duplex stability and found the results comparable to that offered by natural G base. It is a fact that many emissive nucleoside analogues, including the classical 2-aminopurine get quenched upon incorporation into oligonucleotides.[43a, 48] However, it is highly interesting to note that the oligonucleotide containing the emissive **thG** "sandwiched" between two potentially quenching G residues displayed strong visible emission with good

quantum yield which is of 0.10.[45] Therefore, this set of emissive RNA nucleosides designed by Tor *et al.* represents a novel class of fluorescent base analogues having properties like native Watson–Crick faces, unparalleled structural isomorphicity with respect to native nucleosides, minimal perturbation in duplexes and intense visible emission.

Later on, Tor *et al.* have exploited the isomorphic fluorescent analogue of adenosine (th**A**) as Adenosine deaminase (ADA) inhibitor, a major enzyme involved in purine metabolism. They have found that this enzyme converts th**A** into an isomorphic inosine analogue (th**I**), which possesses distinct photophysical properties as compared to th**A**. They have demonstrated the utility of this sensitive fluorescence-monitored transformation for the high-throughput detection and analysis of ADA inhibitors which are of particular importance for the treatment of certain leukemias. The conversion of th**A** (**1.73**, **Scheme 1.1**) to th**I** (**1.79**, **Scheme 1.1**) has led to an emission enhancement and is feasible even at low nM concentrations. This high-throughput method for identifying inhibitors via the detection of enhanced fluorescence signal is superior to the currently avail methods which rely on either absorption spectroscopy or chromatographic methods, which require relatively large concentrations and are not normally amenable for high-throughput formats.[49]

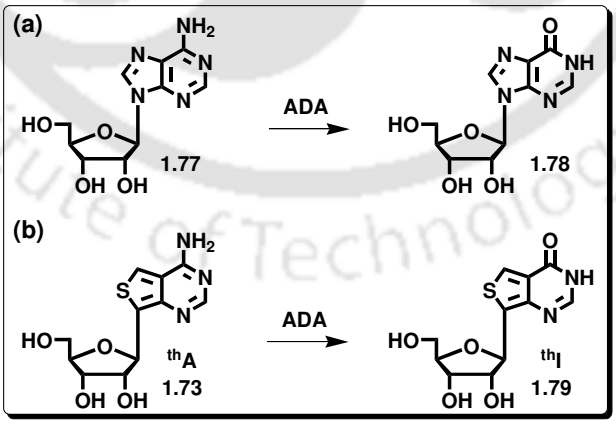

Scheme 1.1: ADA-catalyzed interconversion of (a) A to I and (b) th**A** to th**I**.

1.6. Non-Hydrogen-Bonded Nucleosides

The concept of hydrophobic interactions[50] was first introduced by Kool *et al.* after observing that hydrogen bonds were not necessary for efficient base-pairing. The first non-hydrogen bonding artificial base pair of this type reported by Kool *et al.* in 1995 was difluorotoluene/adenine pair (**F:A**, **Figure 1.21**), wherein the difluorotoluene was an isostere of thymine.[51] In 1999, they described the aqueous solution structure of DNA duplex containing the base pair **F:A**. Because of the lack of hydrogen bonding interaction, the base pair was destabilizing as compared to the natural **A:T** base pair by 9.6 ^{o}C when incorporated in the middle of DNA duplex. However, the d**F** triphosphate (d**FTP**) was efficiently replicated by the DNA polymerase enzyme.[52] Later on, it has been shown that the non-H-bonding **F** formed stable base pair with another adenine mimic **Z** and the **F:Z** pair was found to code for each other by DNA polymerases.[53a] A similar analogue of adenine **Q**, was synthesized and incorporated into DNA by them in order to study the minor groove interactions.[53b] The study indicated that without H-bonding, the shape complementarity is sufficient enough for selective replication of a base. However, it has been observed that the minor-groove interactions are important for further extension of the growing chain since a template containing **Q** is more efficiently extended to form a **Q:T** or **Q:F** base-pair than a template containing **Z**.

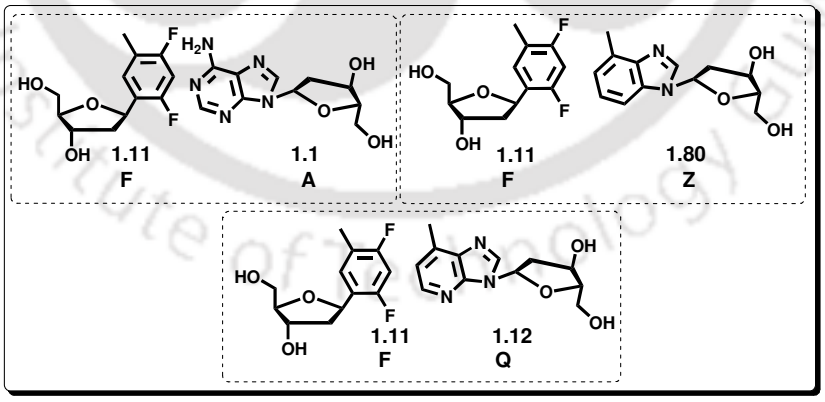

Figure 1.21: Hydrophobic hetero-pairs developed by Kool *et al*.

The concept of hydrophobic nucleobase-pairs capable of forming stable duplexes was further elaborated by Romesberg group. Thus, they have shown that methylated

or fluorinated benzenes (i.e., **DM5**, **TM**, **2MN**, **3MN**, or **3FB**) also form stable duplexes where the self-pair is held together by hydrophobic and stacking interactions inside the DNA duplex (**Figure 1.22**).[54] The self-pairs of **DM5, TM, 2MN, 3MN**, **3FB** have been found to be efficiently replicated by DNA polymerases but due to lack of minor-groove interactions, the chain extension is failed. The self- pair of isocarbostyril (**1.83**) when incorporated in DNA has been found to be stabilize the duplex more than that of an A:T pair by 3.4°C and has almost equal stability as that of a G:C pair.[55]

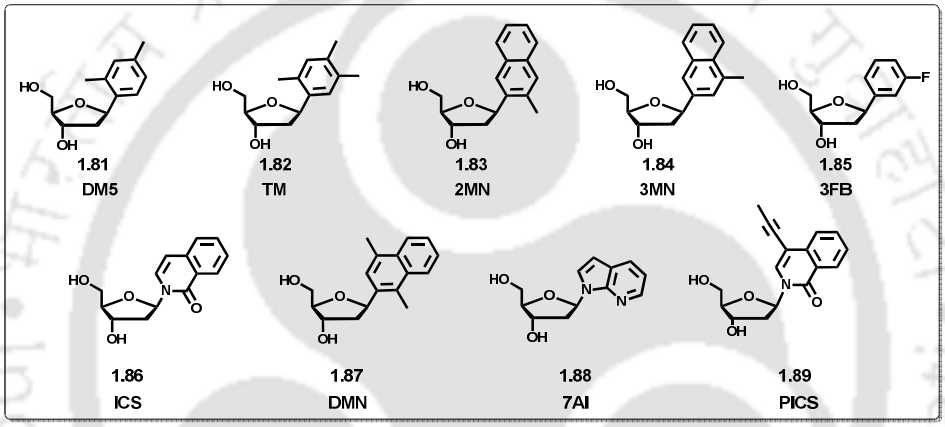

Figure 1.22: Artificial nucleobaes forming selective self-pairs and efficiently incorporated by DNA polymerases.

The hetero base pair consisting of isocarbostyril and 7-azaindole (**1.89**) developed by Romesberg *et al.,*[56] has been found to be only slightly less stable than the natural A:T pair (T_m = 57.2 °C and 59.2 °C for 7**AI**:**ICS** and dA:dT, respectively). Several heteropairs have parallely been designed and investigated, out of which few successful combinations of base pairs are as follows e.g., benzofuran (**BFr**), benzothiophene (**BTp**), and indole (**IN**) with pyridone (**4MP**);[57a] bromobenzene (**4Br**) with benzonitrile (**2CN**); [57b] methylthiophene (**MTp**) with isocarbostyril (**4MICS**);[57c] and methoxytoluene (**MMO2**) with **TM** (**Figure 1.23**).[57d] All of them are efficiently replicated with high fidelity but are less efficiently extended. The **MMO2:5SICS** pair,[58] is efficiently replicated and extended with high fidelity. The **5FM:5SICS** or **NaM:5SICS** are identified by them as the best heteropairs, showing efficient replication and transcription like their natural counterparts.[59]

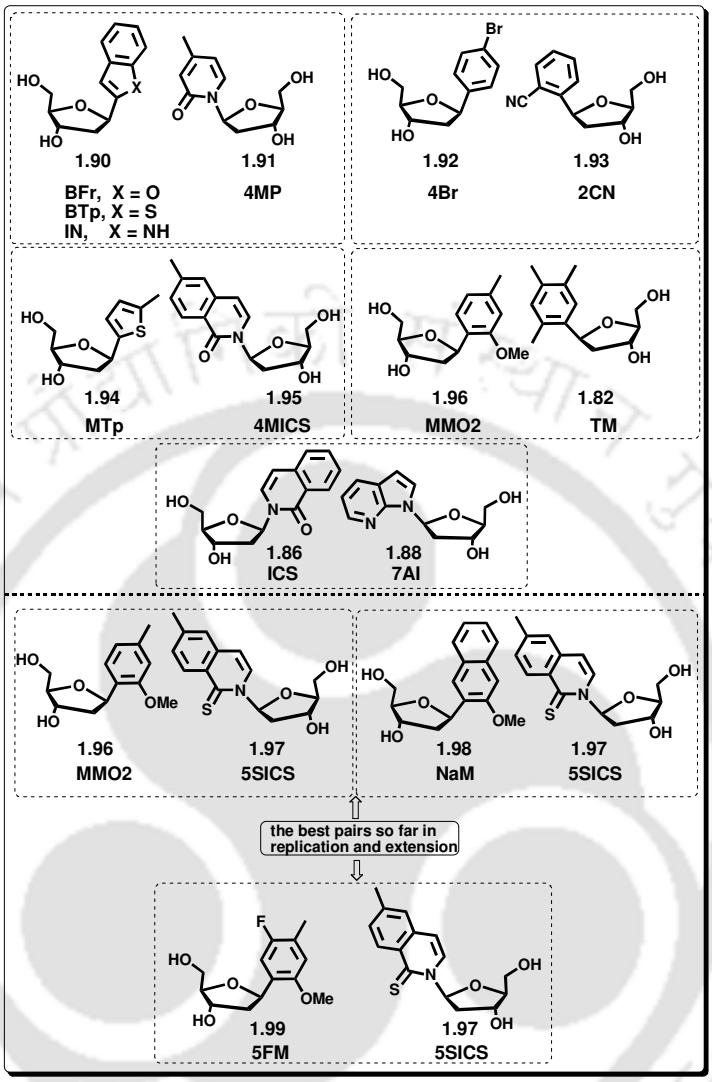

Figure 1.23: Hetero-pairs efficiently replicated and extended by DNA polymerases.

Leumann *et al.* have studied the non-hydrogen bonding and non-shape complementary self-pair 2, 2′ bipyridyl (**2BP**) in connection with DNA duplex stabilization.[60a] The thermal denaturation experiments revealed that the base pair d**BP**:d**BP** (**1.100**) is more stable than a dA:dT base pair by 3.4 K, and of similar stability to a dG:dC base-pair[60a] (**Figure 1.24**). A similar observation was made for the biphenyl base pair (**1.101**) by Leumann *et al.*[60b] When incorporated in DNA, the duplex stability is more than that of A:T pair and similar to that of G:C pair. The study of the base-pairs **1.100** and **1.101** by Leumann *et al.*[60] has led to the conclusion

that interstrand stacking interaction is the governing force for the duplex stability in these two base pairs. They have also studied self-pairs of cyclohexylphenyl *C*-nucleosides (**1.102**) and found it to stabilize the DNA duplex even more strongly[60c] than the biphenyl moieties. Their study demonstrates that the hydrophobic forces also contribute to the stability of the duplex as efficiently as the stacking interactions. Thus, they successfully have designed and developed a few stable base pairs not relying on hydrogen bonds. The stability of the base pairs has been explained on the basis of interstrand stacking interactions as well as hydrophobic interactions.

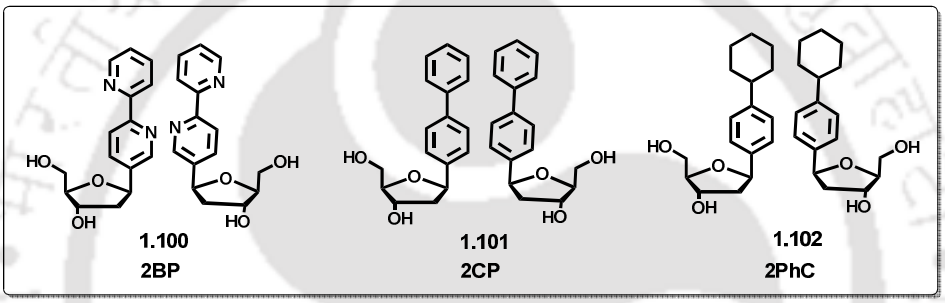

Figure 1.24: Artificial nucleobaes forming stable self-pairs based on aromatic π-stacking interactions.

Yokoyama and Hirao *et al.* have developed an unnatural hydrophobic base pyrrole-2-carbaldehyde which was paired up with 9-methylimidazol[(4,5)-b]pyridine to form an artificial base-pair (**1.103**).[61] The pyrrole-2-carbaldehyde pairs up efficiently with 9-methylimidazol[(4,5)-b]pyridine and shows its specificity in replication (**Figure 1.25**).

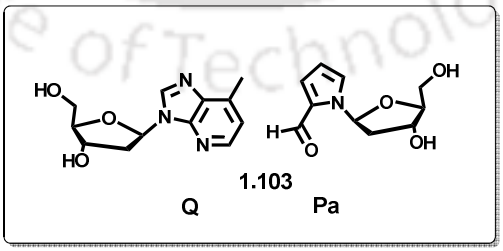

Figure 1.25: Artificial hetero-pair reported by Hirao *et al*.

The base pair (**1.104**) comprising of pentafluorophenyl and phenyl units have been developed by Hunziker *et al.*[62] It was based on the idea that the inverse quadrupolar moments of benzene and hexafluorobenzene leading to edge-to-edge attractive intermolecular forces could provide stable non-hydrogen bonded base pairs. However, it has been observed that the base pair (**1.104**) destabilize the duplex by 15 ^{o}C as compared to the natural A:T base pair (**Figure 1.26**).

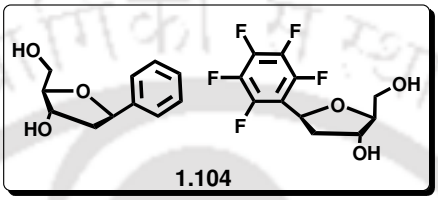

Figure 1.26: Artificial hetero-pair reported by Hunziker *et al*.

A large number of nucleosides with aromatic polycyclic hydrocarbons (**Figure 1.27**) have been designed and synthesized out of which some of them have been incorporated in oligonucleotides in order to study the non-hydrogen bonding or hydrophobic interactions between the artificial base pairs and the DNA duplex stabilization. Few important aromatic nucleoside base analogues are presented in **Figure 1.27**.

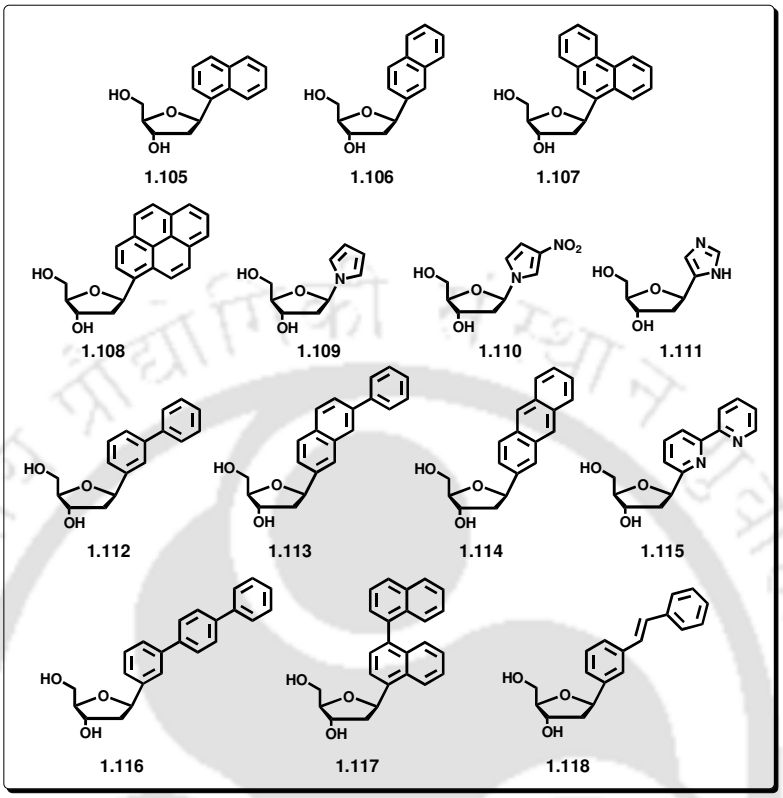

Figure 1.27: Simple hydrocarbon aromatic base replacements. Some of them have been incorporated into DNA to study the stacking interactions.[63]

In order to address the DNA damage of tumor cell and thus to search for chemical agents that increase DNA damage by ionizing radiation under anaerobic conditions, Greenberg *et al.*[64] have recently incorporated aryl halide C-nucleotides in DNA that produce highly reactive σ-radicals for application as radiosensitizing agents. They observed that the duplex DNA containing the bases, **1.119-1.121** form interstrand cross-links upon γ-radiolysis under anaerobic conditions (**Figure 1.28**). Among the three nucleosides, **1.121** has been found to be recognized by Deep Vent (exo^-) DNA polymerase as a substrate and preferentially incorporated it opposite pyrimidines, but no further extension has been detected. Therefore, the aryl halide nucleotide analogues that produce DNA interstrand cross-links under anaerobic conditions upon irradiation would find potential application as radiosensitizing agents.

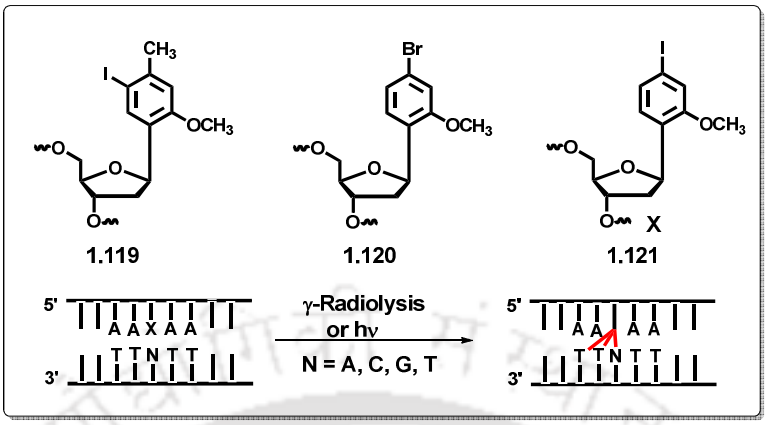

Figure 1.28: Structures of *C*-nucleosides and formation of interstrand cross-links under anaerobic conditions.

1.7. Non-Nucleosidic Base Surrogates

. Although modification of the sugar, base or phosphate backbone of DNA has been thoroughly studied in order to understand biological and chemical properties of nucleic acids but the flexible backbones in combination with non-hydrogen bonding bases were not explored much. A flexible backbone in comparison with the rigid phosphate backbone imparts higher degree of flexibility and also opens up an easy way of synthesis for incorporating a large variety of different building blocks. There exist a few cases in literature where the development of non-nucleosidic DNA building blocks has been investigated. Early reports indicate their synthesis solely for diagnostic purposes but later on they were incorporated inside DNA in order to investigate the photophysical and biophysical property of the non-nucleosidic building blocks inside the DNA duplex.

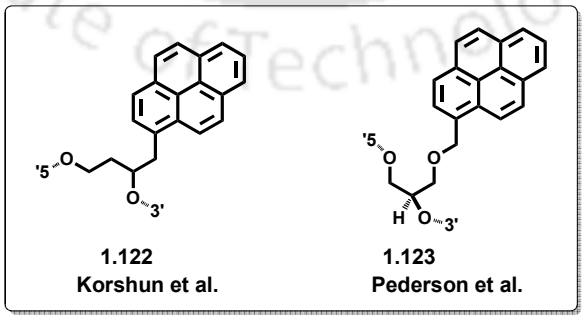

Figure 1.29: Non- nucleosidic base pairs with flexible backbone.

The first example of non-nucleosidic base surrogate was provided by Korshun *et al.*[65] who studied the fluorescence properties of the racemic mixture of 4-(1-pyrenyl)-1,3-butandiol (**1.122**) in DNA (**Figure 1.29**) and concluded that such oligonucleotides with polyaromatic fluorophores are promising DNA probes. However, they did not measure the thermodynamic stability of the duplexes containing these non-nucleosidic base surrogates. In 2002, Pedersen *et al.* developed 1-*O*-(1-pyrenylmethyl)glycerol (**1.123**, **Figure 1.29**) mainly for diagnostic purpose.[66a] In 2004, they incorporated 1-*O*-(1 pyrenylmethyl)glycerols opposite to each other in a DNA duplex and studied their thermodynamic stability.[66b] The modified DNA was found to be 0.7 ^{o}C less stable than the unmodified duplexes. The structure elucidation study showed that the two pyrenyl units were held together by strong π-π stacking interaction.

Oligonucleotides containing non-nucleosidic phenantherene building blocks have been synthesized by Häner *et al.* for studying the DNA duplex stabilization property.[67] The thermal denaturation experiment of the duplex containing the non-nucleosidic phenantherene building blocks revealed that the phenantherene of probe ODN when paired against thymine or adenine of target ODNs destabilize the duplex DNA. On the other hand, when the two phenantherene of two complementary ODNs were paired against each other the duplex become stabilized (**1.124**, **Figure 1.30**). Thus, the non-nucleosidic phenantherene derived building block could serve as a base surrogate which can stabilize a DNA duplex without sacrificing much the B-form conformation of DNA duplex.[67] Following these observations, they have synthesized non-nucleosidic phenanthroline derivatives (**1.125**, **Figure 1.30**) which have been incorporated into oligonucleotides to test their duplex stabilizing properties.[68] The thermal denaturation experiments revealed that phenanthroline derivatives stabilized the DNA duplex more than the corresponding phenantherene derivatives. The greater dipole moment of the hetero-aromatic phenanthroline as compared to phenantherene was considered as the responsible factor for the greater stabilization of phenanthroline derivatives resulting in stronger interstrand stacking interactions. H□ner and co-workers studied the effect of the linker length on the stability of the DNA hybrids containing phenanthroline and pyrene building blocks opposite to an abasic site (**1.125-1.126**, **Figure 1.30**). The study of thermal melting stability showed that the

stabilization of the hybrids was dependent on the length of the linkers which seemed to decrease if the length of the linkers is too short. The phenanthroline derivatives led to the stabilization of the duplex containing the abasic site as the linker length increased. On the other hand, in case of pyrene derivatives T_m was found to be rather independent of the linker length.

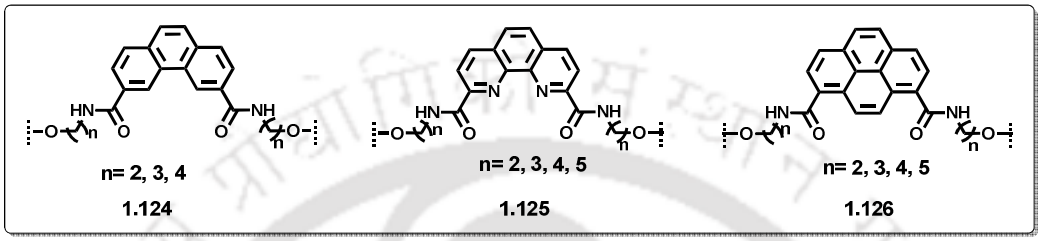

Figure 1.30: Structures of the phenantherene-, phenanthroline-, pyrene-, derived non-nucleosidic base surrogates.

The work accomplished by Häner and coworkers emphasizes that stacking interactions play a significant role in stabilizing a DNA double helix. In order to study such kind of stacking interactions Wagenknecht *et al.*[69] have synthesized the phosphoramidite of the perylene bisimide dye (**Figure 1.31**) and incorporated it as an artificial nucleoside base surrogate at 5′- terminal and at the internal positions of the designed DNA duplexes. The thermal denaturation experiments suggested that the internally modified oligonucleotides exhibited strong stacking interactions between the perylene bisimide chromophore and the DNA bases. It was also concluded that the internally modified oligonucleotides could be applied for charge transport studies in DNA. The 5′-terminally attached perylene bisimide chromophore induced dimerization of the duplexes via stacking of the two perylene bisimide chromophores. Such kind of dimerization indicated the potential application for the formation of ordered and thermally stable supramolecular DNA based architectures for nanotechnological applications.

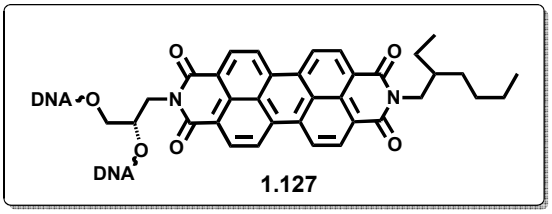

Figure 1.31: Structure of the perylene bisimide non-nucleosidic base surrogate.

1.8. Applications of Unnatural Nucleobase Analogues

1.8.1. Applications in Studying the Duplex Stability

The modified nucleosides designed and synthesized so far have been incorporated into short stretches of oligonucleotide in order to study their thermal melting and/or thermodynamic stabilities with respect to the natural nucleobases. The idea of synthesizing artificial bases was to mimic the natural ones in order to study the role of hydrogen bonding, π-π stacking or hydrophobic interactions on the stabilization of the duplexes. In this respect many self-pair and hetreo-pair hydrophobic base surrogates have been designed which has already been discussed. Few more examples are discussed below. Rappaport *et al.* have synthesized a base pair comprising of 5-methyl-2-pyrimidinone ($\mathbf{dT_h}$) that pair against 6-thioguanine ($\mathbf{dG_s}$) (**Figure 1.32)** similar to that of dC:dG natural base pair with two interbase H-bonds.[70a] The base pair has been incorporated into DNA which is found to stabilize the formed duplex without affecting much the B-form conformation of DNA double helix. Interestingly, this base pair is recognized and extended by Klenow polymerases with similar efficiency like the natural pairs.[70b]

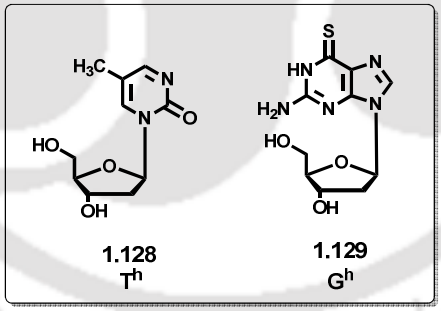

Figure 1.32: Hydrogen bonding base-pair developed by Rappaport *et al*.

Hirao *et al.*[71] have reported a **Dss** base which when paired against another artificial base pair, the duplex formed is found to be highly stable (**Figure 1.33a)**. The **Dss** base slightly destabilizes the duplexes when paired against any of the natural bases. Most importantly, enzymatic incorporation of the **Dss** base into DNA or RNA opposite to **Pa** is found to be highly selective.

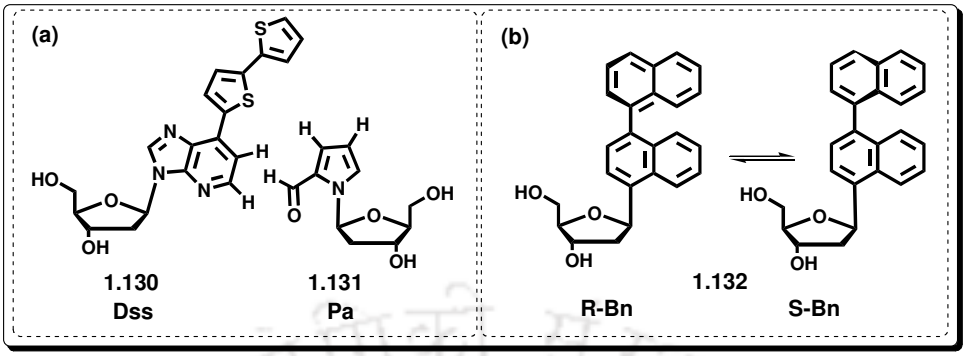

Figure 1.33: Non-natural base-pairs based on (a) hydrophobic and shape complementary interactions (b) hydrophobic and π-stacking interactions.

Seitz and co-workers have synthesized a binaphthyl (**Bn**) nucleoside as a new non-planar base-surrogate (**Figure 1.33b**) and incorporated it into oligonucleotide and studied the stability of the duplex.[72] It has been observed that multiple **Bn** bases when incorporated into a DNA duplex impart slightly more stability to the duplexes as compared to a natural A:T base pair through both intra- and extra-helical stacking interactions.

1.8.2. Applications in Studying the Abasic Duplex Stability

An abasic site (Ap ≡ ϕ) is one of the most common forms of DNA lesions created by the loss of a nucleosidic base leaving behind the deoxyribose sugar in DNA.[73] An abasic site is generally repaired by base excision repair machinery which when left unrepaired can lead to deleterious consequences to the cell as well as the organism. Therefore, in order to probe and stabilize abasic site, several modified nucleosidic/non-nucleosidic base surrogates have been designed and investigated. As for example, non-nucleosidic pyrene dicarboxamide derivatives and phenanthroline dicarboxamide derivatives have been designed by Häner *et al.* and used to study the stabilities of the DNA containing the abasic site.[74] It has been observed from the thermal denaturation experiments that both the phenanthroline and pyrene derived base surrogates (**Figure 1.30**) have led to significant stabilization of the abasic DNA duplex. In case of non-nucleosidic pyrene, the degree of stabilization is found to be independent of the linker length while a strong influence of the linker length on the thermal melting behavior of the abasic duplexes is observed in case of phenanthroline

paired against an abasic site. It has been concluded that the stabilization of the abasic site by both the types of polyaromatic hydrocarbons as non-nucleosidic base surrogates results from the stacking interactions between the polyaromatic residues and base pairs adjacent to the abasic site.[74] Shimidzu *et al.* have studied the abasic site stabilization with the oligodeoxynucleotide probe containing 2-methoxy-6-chloro-9-aminoacridine (**Acr**) (**1.133, Figure 1.34**). The thermal denaturation experiment has shown that the base surrogate acridine when paired against an abasic site stabilizes the abasic duplex by 11.2 ^{o}C more than any of the duplexes wherein the abasic site is paired against any of the natural bases.[75]

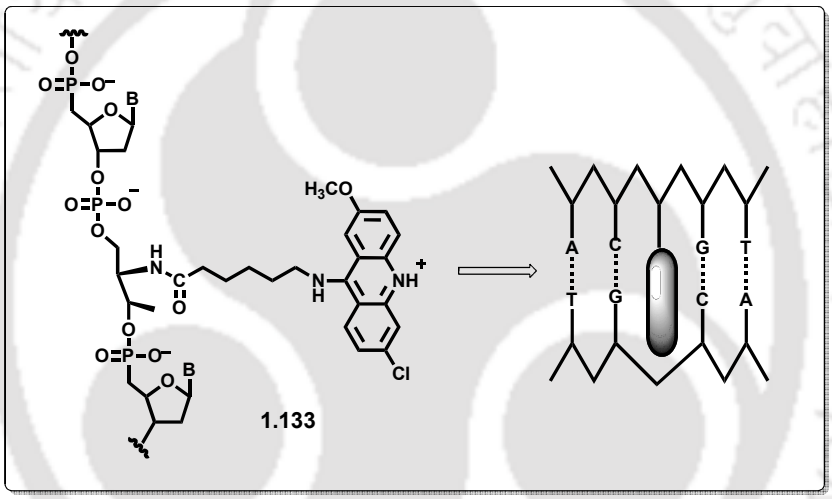

Figure 1.34: Oligodeoxynucleotide (ODN) modified with 2-methoxy-6-chloro-9-aminoacridine (**Acr**) which can stabilize an abasic site.

Complementary nucleobases with extended aromatic systems have been designed for probing of abasic sites in damaged DNA. As for example, 1-pyrenyl C-nucleoside (**1.108**, **Figure 1.35**) facing an abasic site was developed by Kool *et al.*[76] The pyrene shows selectivity for the abasic site over the natural bases. The 1-pyrene/abasic site is only 1.6-2.2 ^{o}C less stable than that of natural A:T pair. A similar type of base pair has been developed by Leumann *et al.*[76d] in 2012 which has also been incorporated into DNA. It was found that the 2-pyrene/abasic site destabilized the duplex by about 2.0 to 2.7 ^{o}C as compared to the natural A:T pair (**1.134, Figure 1.35**). Similarly, porphyrin C-nucleoside (**1.135, Figure 1.35**)[77a] and substituted indole *N*-nucleosides[77b] were found to stabilize an abasic DNA when paired against abasic site by stacking

interactions with the neighbouring bases. The ODN probes containing these extended artificial nucleobases can be employed as probes for sensing of damaged DNA strands.

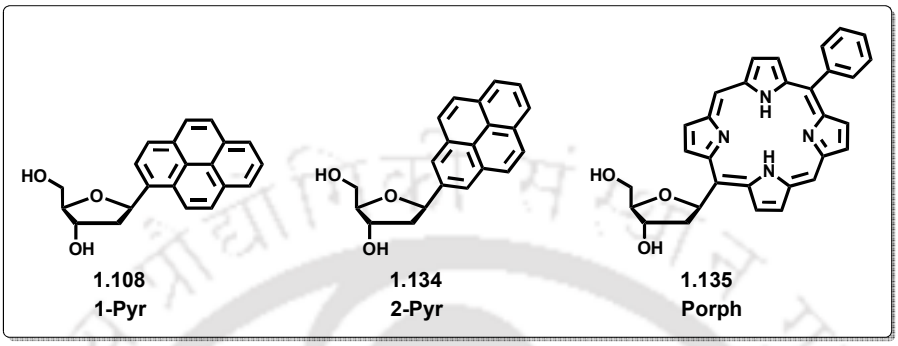

Figure 1.35: Structure of extended aryl-nucleosides complementary to abasic sites of damaged DNA.

1.8.3. Applications in Studying the Photophysical Processes in Fluorescent Unnatural DNA

Fluorescence techniques, now a days, find widespread application in biochemical and biophysical studies of macromolecules, specially, in studies of nucleic acids, fluorescence spectroscopy provides an important tool for the detection and probing of structure, dynamics and interbiomolecular interactions. Highly fluorescent dyes or nucleotide base analogues or fluorescently labeled nucleobases can serve as extremely sensitive probes in nucleic acid systems and enable experiments to be carried out in solution. Therefore, the lack of naturally occurring fluorescent bases has spurred the development of new modified nucleosides over the years with bright fluorescence properties which will be the probe for DNA analysis and can vastly be used in biological chemistry, biotechnology, biophysics and in light harvesting DNA based materials. Now a days, fluorescence based gene detection schemes are used routinely in numerous applications, such as DNA sequencing,[78] in situ genetic analysis, SNP typing through techniques like fluorescence in situ hybridization (FISH),[79] and highthroughput screening (HTS)[80]. Therefore, a major fraction of laboratories in the chemical, biological, and biomedical sciences make use of fluorescence methods and of fluorophores as reporters for elucidating the structure, functions and dynamics of biomolecules and biomolecular interactions.

Despite the large amount of research efforts undertaken at making new classes of fluorescent labels, commonly available organic fluorophores still suffer from a number of limitations such as the fluorophores often possess widely varied absorption maxima.[81] Therefore, to address the limitations of the available fluorophores for practical applications, a number of significant approaches including the development of quantum dots[82] and FRET dye pairs[83] have been undertaken by several research groups. Moreover, as a result of tremendous research efforts a large number of fluorescent nucleosides/nucleoside base surrogates as novel intrinsically fluorescent nucleosides/base surrogates have been designed and exploited for the applications in fluorescence based techniques. As for example, a number of donor-acceptor labeled fluorescent oligonucleotide probes have been designed to study the photophysical phenomena like Förster resonance energy transfer (FRET) process, exciplex emission etc. during the course of hybridization event. Kool *et al.* have designed DNA probe containing an assembly of ~3−5 fluorescent nucleosides decorated with aromatic hydrocarbons and heterocycles as nucleobases. The fluorophores are arranged in a DNA-like chain, which they called as an "oligodeoxyfluoroside" (ODF).[63a, 84] These fluorophores are found to engaged in efficient electronic communication of excitation energy leading to the occurrence of multiple forms of energy transfer, including FRET, exciplex, excimer, H-dimer, and other mechanisms via close interactions of such flat aromatic fluorophores.[84b]

Förster resonance energy transfer (FRET) is a process in which energy is transferred non-radiatively from an excited donor molecule to an unexcited acceptor molecule over distances longer than their collisional diameters. FRET being a distance dependent process is used as a 'spectroscopic ruler' for determining the distance between a donor and an acceptor leading to the investigation of structure/dynamics of DNA. Towards this end, several donor-acceptor labelled fluorescent DNA probes have been designed for DNA analysis via generation of FRET signal. As for an example, dual labeled DNA containing pyrene as donor and perylene as an acceptor chromophore has been utilized by Shimadzu *et al.*[85] for investigating nucleic acid hybridization assay (**Figure 1.36**). Thus, in this system, FRET with 100% efficiency has been observed upon hybridization of a target 32-mer

and its complementary two 16-mer deoxyribonucleotides whose neighboring terminals are labeled with a pyrene and perylene residues, respectively. Upon excitation at the absorption maximum of donor chromophore pyrene (λ_{ex}=347nm), FRET emission from perylene is observed at 459 nm.

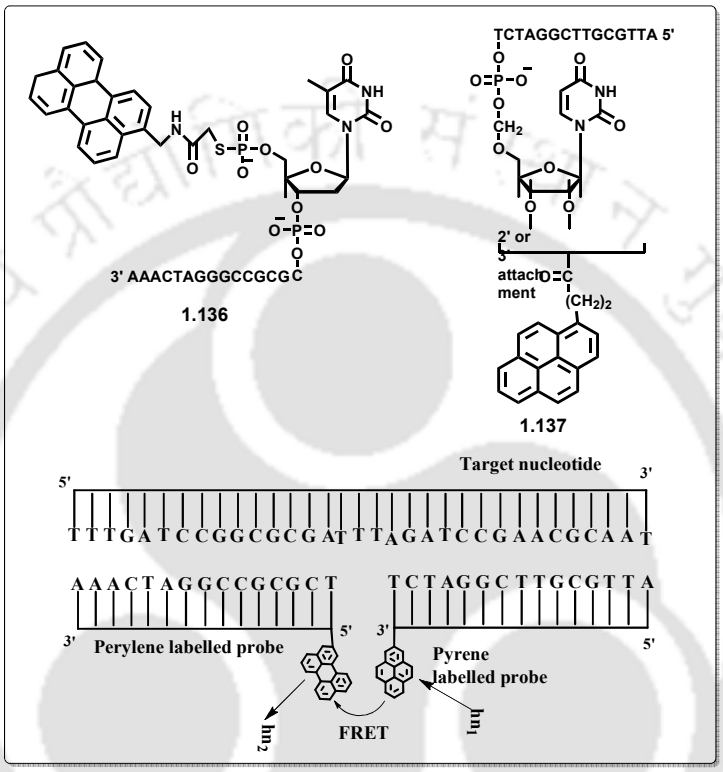

Figure 1.36: FRET from pyrene (donor) to perylene (acceptor) in nucleic acid

Polyfluorophores labelled DNA have been designed by Kool *et al.* to study the photophysical aspects of labelled DNA. In the design of polyflorous DNA, Kool *et al.* have shown that oligomeric exciplex and excimer forming fluorophores conjugated to DNA have the potential to act as donors for Förster resonance energy transfer process (**Figure 1.37**).[86] The Kool's designed oligodeoxyfluorosides (ODFs) contained stacked, electronically interacting fluorophores replacing the nucleobases on a DNA scaffold. They have designed twenty tetrameric ODNs containing a combination of monomer chromophores which includes pyrene, benzopyrene, perylene, dimethylaminostilbene, and a nonfluorescent spacer. These chromophores are conjugated in varied combinations at the 3′-end of a 14-mer DNA probe sequence. They observed characteristic excimer and exciplex emission in the absence of an

acceptor chromophore in many of their designed ODF-DNAs.[86] They also have investigated the ability of the twenty ODFs to donate energy to Cy5 and TAMRA dyes conjugated to a complementary strand of a target DNA. The acceptor dyes have been placed either at the near or far end of the ODF-conjugated probes in their design to test the possibility of a FRET process. Thus they are the first to establish the fact that the excimer/exciplex bands can act as donor from where the energy is transferred to the acceptor chromophores Cy5 and/or TAMRA leading to an FRET emission from the acceptor at very long wavelength region (**Figure 1.37**). This phenomenon has been observed for few of their designed multichromophore labeled probe DNA (ODF). They have concluded that ODFs may be candidates of "universal FRET donors" which could allow multicolor FRET of multiple species using only one excitation.

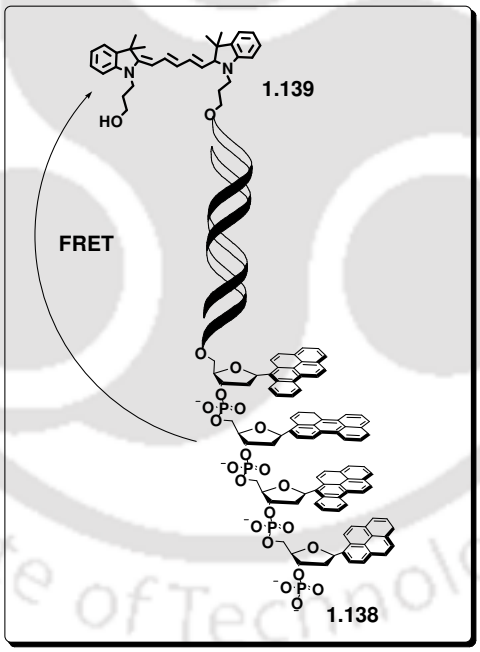

Figure 1.37: Schematic illustration of FRET in oligodeoxyfluorisides ODFs.

Excimer is the complexation between the ground state and excited state of the same chromophore while exciplex is the comlexation between excited state of a donor/acceptor and the ground state of an acceptor/donor chromophore. The excimer and exciplex formation has rigorously been studied in context of DNA in order to

probe the inter-biomolecular interaction and in fluorescence based detection of biomolecules.

As for example, excimer fluorescence emission have been applied for the detection of insertion/deletion (indel) polymorphisms that occupy approximately 10% of all the polymorphisms in the human genome[87a-c], and lead to serious gene expression errors because they often cause a translational frame shift and create premature proteins. Saito *et al.*, have designed a ^{Py2}**Lys**-containing (**1.139**, **Figure 1.38**) ODN, 5'-d(GTGTTAAGCC^{Py2}**Lys**GCCAATATGT)-3'.[87d-e] With excitation at 350 nm, the fluorescence of the single-stranded ODN has been found negligible. When ^{Py2}**Lys**-containing ODN is hybridized with 5'-d(ACATATTGGCGGCTTAACAC)-3', which does not possess the base opposite to ^{Py2}**Lys**, the fluorescence still remains weak . In contrast, the fluorescence spectrum of the duplex with 5'-d(ACATATTGGC**A**GGCTTAACAC)-3', where A is the base opposite to ^{Py2}**Lys** exhibits a strong fluorescence peak at 495 nm that is corresponding to the fluorescence wavelength from a pyrene excimer (**Figure 1.34**). The clear change in the fluorescence that depends on the presence or absence of the inserted base opposite to ^{Py2}**Lys** (**A** bulge) is useful for the detection of insertion polymorphisms. They have tested the detection of an insertion mutation by hybridization of ^{Py2}**Lys**-containing probe using the coding sequence of the epithelial sodium channel *b* subunit (*b*ENaC) gene associated with Liddle's syndrome, which is an autosomal dominant form of hypertension with variable clinical expression. ^{Py2}**Lys**-containing probe, 5'-d(CTCACTGGGGTAGGGCCCAGT^{Py2}**Lys**GTTGGGGCT)-3', has been prepared and hybridized with *b*ENaC gene sequences, 5'-d(AGCCCCAAC(G)$_n$ ACTGGGCCCTACCCCAGTGAG)-3' (wild type, n = 0; G-inserted mutant, n = 1). It has been observed that the fluorescence emission from the duplex with a G-inserted strand is very strong and clearly distinguishable from the poor fluorescence of the duplex with a wild type strand. The hybridization of ^{Py2}**Lys**-containing ODN with a target DNA facilitates the determination of the presence/absence of insertion polymorphisms located at a specific site on the target DNA by a simply mixing.[87 d-e]

The exciplex emission in modified nucleoside containing DNA has been exploited by Saito *et al.* for the detection of target DNA in their designed oligonucleotide probe

containing methoxy-substituted fluorescent guanosine derivarive, $^{8\text{-MPE}}$**G** (**1.140**, **Figure 1.39**) These methoxy-substituted fluorescent guanosine derivarives have an intriguing property, *i.e*., they possess lower oxidation potentials than native guanosine and emit strong fluorescence at more than 380 nm.

It has been observed that the fluorescence of single stranded ODN **1** (X = $^{8\text{-MPE}}$**G)** is relatively weak and appeared at around 380 nm. When the opposite base of a complementary strand is adenine (**N** = A) in a duplex ODN **1** (X = $^{8\text{-MPE}}$**G**, **1.140**) /ODN **2** (N = A), a new and strong emission is observed at a longer wavelength around 440 nm (**Figure 1.39**). The emission at 435 nm is not observed when the opposite bases of complementary strands are G, C and T, suggesting that the new emission is an exciplex emission from a complex formed between $^{8\text{-MPE}}$**G** and adenine (A).[88] The stacking interaction between electron donating guanosine $^{8\text{-MPE}}$**G** of the probe DNA and adenine base of target DNA is the responsible factor for the formation of an exciplex upon photoexcitation of $^{8\text{-MPE}}$**G**.

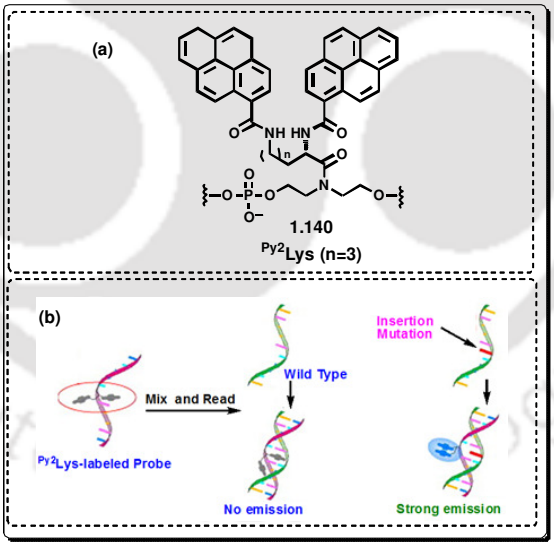

Figure 1.38: (a) Schematic representation of the structure of ^{Py2}**Lys** (**1.139**) and hybridization of ^{Py2}**Lys**-containing probe an ODN with and without A bulge. "

A more prominent example of exciplex formation is observed from methoxy-substituted naphthalene derivative $^{8\text{-MNE}}$**G** (**1.141**, **Figure 1.39**). Thus, a characteristic fluorescence from the naphthalene chromophore appeared at 390~430 nm for single stranded ODN **1** (X = $^{8\text{-MNE}}$**G**). However, in a duplex [ODN **1** (**X =** $^{8\text{-MNE}}$**G**) /ODN **2**

(N = A)], a new exciplex emission at 470 nm emerges together with the appearance of original naphthalene fluorescence, suggesting a partial formation of excited state complex (**Figure 1.38**). The formation of ground state complex between the naphthalene chromophore and A is indicated by the appearance of a new absorption band in the UV-visible spectrum of the duplex ODN **1** (X = $^{8\text{-MNE}}$**G**) /ODN **2** (N = A). The fluorescence color change is also observable by naked eye upon illumination with 365 nm transilluminator. The fluorescence lifetime of double stranded ODN **1** (**X =** $^{8\text{-MNE}}$**G**) /ODN **2** (N = A) with a biexponential decay has been measured. The longer lifetime component (τ = 2.2 nsec) is ascribable to the formation of an exciplex between $^{8\text{-MNE}}$**G** and A, whereas the shorter lifetime component (τ = 1.1 nsec) resulted from the naphthalene chromophore of $^{8\text{-MNE}}$**G**. The study of fluorescence lifetime indicated the existence of two species that are responsible for the fluorescence emission and suggest that longer lifetime component with a strong emission at 470 nm is due to the formation of an exciplex between $^{8\text{-MNE}}$**G** and adenosine (A).[88]

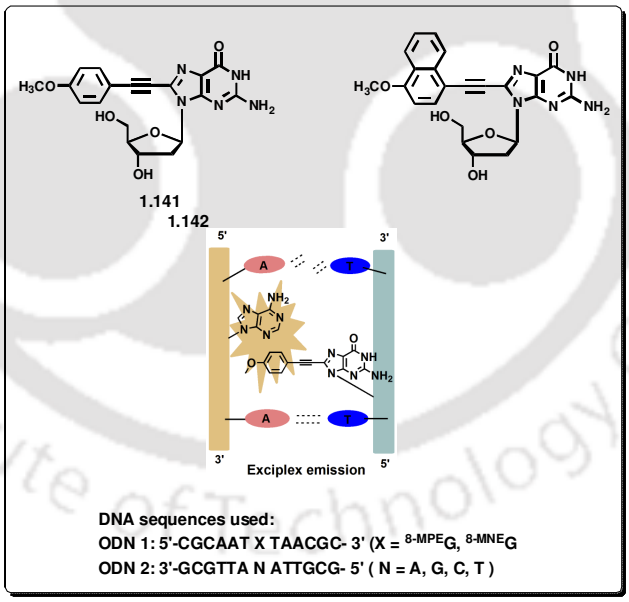

Figure 1.39: Exciplex formation between adenine and guanine derivative.

1.9. Summary and Future Prospect

The lack of significant fluorescence in naturally occurring nucleobases has prompted the design of fluorescent nucleobase analogues with improved photophysical properties for nucleic acids research. As a result of tremendous research efforts, from various scientific corners out of inspiration from nature or a rational designing approach, an enormous number of such emissive DNA base analogues appear in the literature. Many of them are also commercially available for incorporation into DNA and many others form the examples of expanded genetic alphabet.

Much effort has been devoted to develop non-natural, stable, H-bonded as well as hydrophobic base pairs of orthogonal recognition properties. Besides the H-bonding force, the role of other attractive forces like, hydrophobic, π-stacking, CH-π interaction, dipole moment, polarizability and electrostatic interaction between a pair of designed unnatural nucleobase analogues, either in a self-pair or in a heteropair, has been established in the context of DNA duplex stabilization and enzymatic recognition via the generation of several nonfluorescent/fluorescent base analogues. Several fluorescent DNA base analogues (nucleosidic and/or non-nucleosidic base surrogates) have been exploited in various applications, such as in DNA analysis, monitoring hybridization events, in delineating structure and dynamics of DNA, in probing DNA lesion, in search of light harvesting DNA based materials and in other biotechnological and material science applications. Various photophysical properties, such as FRET, exciplex and excimer emission, have also been studied with the multichromophoric DNA containing multiple unnatural fluorescent base analogues exploiting the rigid DNA conformation as the organizing scaffold. Some of the environmentally sensitive fluorescent oligonucleotide probes containing microenvironment sensitive fluorescence have been used as a molecular signaling device in DNA detection.

This chapter has highlighted some of these DNA base analogues and a set of emissive RNA alphabet, their duplex stabilizing property, abilities of probing abasic DNA, involvement in FRET or exciplex emission events in the context of DNA.

The concept for designing various types of fluorescence nucleoside base analogues and the application of such fluorescent oligonucleotide probe containing fluorescence nucleoside base analogues might find special attention in future of gene detection technology. The field of designing fluorescent nucleoside base analogues of high solvofluorochromicity is also flourishing, and many more advancements towards this end are expected in near future. It is expected that tuning the chromospheres' structure to achieve predictable photophysical property might allow one to create fluorescent nucleoside analogues to be applicable for bioimaging as well as for gene detection technology. The rapidly growing research toward the expansion of genetic alphabet as well as growing demand of nucleic acid based diagnostics and sensing materials necessitates the design and incorporation of unnatural base pairs with high duplex stability as well as tuned charge transfer/photophysical properties. Many more advancements in the field of expanding the genetic alphabet and the application of same to drive the synthesis of unnatural proteins are expected in near future with a hope to translate an expanded genetic alphabet into an expanded genetic code creating a synthetic organism one day with ability to encode proteins with new physicochemical properties.

1.10. References

1. (a) Watson, J. D.; Crick, F. H. *Nature* **1953**, *171*, 737. (b) Saenger, W.; *Principles of Nucleic Acid Structure, Springer, NewYork*, **1984**.
2. (a) Henry, A. A.; Romesberg, F. E. *Curr. Opin. Chem. Biol.* **2003**, *7*, 727. (b) Kool, E. T. *Acc. Chem. Res.* **2002**, *35*, 936. (c) Kool, E. T.; Morales, J. C.; Guckian, K. M. *Angew. Chem., Int. Ed.* **2000**, *39*, 990.
3. Sismour, A. M.; Benner, S. A. *Nucleic Acids Res.* **2005**, *33*, 5640. (b) Leconte, A. M.; Chen, L.; Romesberg, F. E. *J. Am. Chem. Soc.* **2005**, *127*, 12470. (c) Hirao, I.; Kimoto, M.; Mitsui, T.; Fujiwara, T.; Kawai, R.; Sato, A.; Harada, Y.; Yokoyama, S. *Nat. Methods* **2006**, *3*,729.
4. Rich, A.; Kasha, M.; Pullmann, B. *Horizons in Biochem.* **1962**, 103.
5. (a) Switzer, C.; Moroney, S. E.; Benner, S. A. *J. Am. Chem. Soc.* **1989**, *111*, 8322. (b) Switzer, C.Y.; Moroney, S. E.; Benner, S. A. *Biochemistry* **1993**, *32*, 10489.

6. (a) Hutter, D.; Benner, S. A. *J. Org. Chem.* **2003**, *68*, 9839. (b) Krosigk, U. v., Benner, S. A. *Helv. Chim. Acta.* **2004**, *87*, 1299. (c) Yang, Z.; Hutter, D.; Sheng, P.; Sismour, A. M.; Benner, S. A. *Nucleic Acids Res.* **2006**, *34*, 6095. (d) Martinot, T. A.; Benner, S. A. *J. Org. Chem.* **2004**, *69*, 3972. (e) Vogell, J. J.; von Krosigk, U.; Benner, S. A. *J. Org. Chem.* **1993**, *58*, 7542. (f) Benner, S. A. *Acc. Chem. Res.* **2004**, *37*, 784. (g) Voegel, J. J.; Benner, S. A. *J. Am. Chem. Soc.* **1994**, *116*, 6929.

7. Tor, Y.; Devran, P. B. *J. Am. Chem. Soc.* **1993**, *115*, 4461.

8. (a) Piccirilli J. A.; Krauch, T.; Moroney, S. E.; Benner, S. A. *Nature* **1990**, *343*, 33. (b) Yang, Z.; Hutter, D.; Sheng, P.; Sismour, A. M.; Benner, S. A. *Nucleic Acids Res.* **2006**, *34*, 6095. (c) Hirao, I.; Kimoto, M.; Mitsui, T.; Fujiwara, T.; Kawai, R.; Sato, A.; Harada, Y.; Yokoyama, S. *Nat. Methods* **2006**, *3*, 729. (d) Doi, Y.; Chiba, J.; Morikawa, T.; Inouye, M. *J. Am. Chem. Soc.* **2008**, *130*, 8762. (e) Delaney, J. C.; Gao, J.; Liu, H.; Shrivastav, N.; Essigmann, J. M.; Kool, E. T. *Angew. Chem., Int. Ed.* **2009**, *48*, 4524.

9. (a) Smith, S. A.; Rajur, S. B.; McLaughlin, L. W. *Nature Struct. Biol.* **1994**, *1*, 198. (b) Lesser, D. R.; Kurpiewski, M. R.; Jen-Jacobson, L. *Science* **1990**, *250*, 776. (c) Kornberg, A.; Baker, T. A. *DNA Replication*, 2nd ed.; W. H.Freeman: New York, 1992. (d) Echols, H.; Goodman, M. F. *Annu. Rev. Biochem.* **1991**, *60*, 477. (e) Strazewski, P.; Tamm, C. *Angew. Chem., Int. Ed. Engl.* **1990**, *29*, 36.(f) Seo, Y. J.; Matsuda, S.; Romesberg, F. E. *J. Am. Chem. Soc.***2009**, *131*, 5046. (g) Teo, Y. N.; Wilson, J. N.; Kool, E. T. *J. Am. Chem. Soc.* **2009**, *131*, 3923.

10. (a) Kempe, T.; Sundquist, W. I.; Chow, F.; Hu, S. L. *Nucleic Acids Res.* **1985**, *13*, 45. (b) Zischler, H.; Nanda, I.; Schafer, R.; Schmid, M.; Epplen, J. T. *Hum. Genet.* **1989**, *82*, 227 (c) Hustedt, E. J.; Spaltenstein, A.; Kirchner, J. J.; Hopkins, P.B.; Robinson, B. H. *Biochemistry* **1993**, *32*, 1774. (d) Haugland, R. P. *The Handbook: A Guide to Fluorescent Probes and Labeling Technologies*; Molecular Probes. **2005**. (e) Okamoto, A.; Saito, Y.; Saito, I. *J. Photochem. Photobiol. C* **2005**, *6*, 108. (f) Bag, S. S.; Kundu, R.; Matsumoto, K; Saito, Y.; Saito, I. *Bioorg. Med.*

Chem. Lett. **2010**, *20*, 3227. (g) Teo, Y. N.; Kool, E. T. *Chem. Rev.* **2012**, *112*, 4221.

11. (a) Schweitzer, B. A.; Kool, E. T. *J. Am. Chem. Soc.* **1995**, *117*, 1863. (b) Kool, E. T. *Annu. Rev. Biochem.* **2002**, *71*, 191. (c) Seo, Y. J.; Matsuda, S.; Romesberg, F. E. *J. Am. Chem. Soc.* **2009**, *131*, 5046. (d) Jarchow-Choy, S. K.; Sjuvarsson, E.; Sintim, H. O.; Eriksson, S.; Kool, E. T. *J. Am. Chem. Soc.* **2009**, *131*, 5488.

12. (a) Wojciechowski, F.; Leumann, C. J. *Chem. Soc. Rev.* **2011**, *40*, 5669. (b) Grigorenko, N. A.; Leumann, C. J. *Chem.-Eur. J.* **2009**, *15*, 639. (c) Wilson, J. N.; Teo, Y. N.; Kool, E. T. *J. Am. Chem. Soc.* **2007**, *129*, 15426. (d) Robertson, N.; McGowan, C. A. *Chem. Soc. Rev.* **2003**, *32*, 96. (e) Keren, K.; Krueger, M.; Gilad, R.; Ben-Yoseph, G.; Sivan, U.; Braun, E. *Science* **2002**, *297*, 72. (f) Hall, D. B.; Holmlin, R. E.; Barton, J. K. *Nature* **1996**, *382*, 731.

13. (a) Liu, J.; Cao, Z.; Lu, Y. *Chem. Rev.* **2009**, *109*, 1948. (b) Drummond, T.G.; Hill, M.G.; Barton, J. K. *Nat. Biotechnol.* **2003**, *21,* 1192. (c) Kolpashchikov, D. M.; Gerasimova, Y. V.; Khan M. S. *ChemBioChem* **2011**, *12,* 2564. (d) Liu, L.; Li,Y.; Liotta, D.; Lutz, S. *Nucleic Acids Res.* **2009**, *37,* 4472.

14. (a) Stambasky, J.; Hocek, M.; Kouovsky, P. *Chem. Rev.* **2009**, *109*, 6729 and references therein. (b) Kool, E. T. *Acc. Chem. Res.* **2002**, *35*, 936. (c) Tor, Y.; Dervan, P. B. *J. Am. Chem. Soc.* **1993**, *115*, 4461. (d) Clever, G. H.; Kaul, C.; Carell, T. *Angew. Chem., Int. Ed.* **2007**, *46*, 6226.

15. Ward, D. C.; Reich, E.; Stryer, L. *J. Biol. Chem.* **1969**, *244*, 1228.

16. Chollet, A.; Kawashima, E.; *Nucleic Acids Res.* **1988**, *16*, 305.

17. Booth, J.; Cummins, W. J.; Brown, T; *Chem. Commun.* **2004** , 2208.

18. (a) Secrist, J. A. III; Bario, J. R.; Leonard, N. J.; Villar-Polasi, C.; Gilman, A. G. *Science*, **1972**, *176*, 279. (b) Secrist, J. A. III; Bario, J. R.; Leonard, N. J.; Weber, G. *Biochemistry* **1972**, *11*, 3499. (c) Bario, J. R.; Secrist, J. A. III; Leonard, N. J. *Biochem. Biophys. Res. Commun.* **1972**, *45*, 597. (d) Lessor, R. A.; Gibson, K. J.; Leonard, N. J. *Biochemistry* **1984**, *23*, 3868. (e) Rossomando, E. F.; Jahngen, J. H.; Eccleston, J. F. *Proc. Natl. Acad. Sci. USA* **1981**, *78*, 2278.

19. (a) Hurley, D. J.; Tor, Y. *J. Am. Chem. Soc.* **2002**, *124*, 3749. (b) Voet, D.; Voet, J.G. *Biochemistry* (3rd ed.) **2004**, John Wiley & Sons.

20. (a) Hawkins, M. E.; Pfleiderer, W.; Jungmann, O.; Balis, F. M. *Analytical Biochemistry* **2001**, *298*, 231. (b) Datta, K.; Johnson, N. P.; Villani, G.; Marcus, A. H.; Hippel, P. H. *Nucleic Acids Res.* **2012**, *40*, 1191.(c) Myers, J. C.; Moore, S. A.; Shamoo, Y. *J. Biol. Chem.* **2003**, *278,* 42300.

21. Godde, F.; Tolume, J. J.; Moreau, S. *Biochemistry* **1998**, *37*, 13765.

22. Hawkins, M.E.; Pfleiderer, W.; Mazurmder, A.; Pommier, Y. G.; Falls, F. M. *Nucl. Acids Res.* **1995**, *23*, 2872.

23. Godde, F.; Tolume, J. J.; Moreau, S. *Nucleic Acids Res.* **2000**, *28*, 2977.

24. (a) Wilhelmsson, L. M.; Holmen, A.; Lincoln, P.; Nielsen, P. E.; Norden B. *J. Am. Chem. Soc.* **2001**, *123*, 2434. (b) Wilhelmsson, L. M.; Sandin, P.; Holmen, A.; Albinsson, B.; Lincoln, P.; Norden, B. *J. Phys. Chem. B* **2003**, *107*, 9094.

25. (a) Barhate, N.; Cekan, P.; Massey, A.P.; Sigurdsson, S.N. *Angew. Chem., Int. Ed.* **2007**, *46*, 2655. (b) Cekan, P.; Sigurdsson, S.Th. *Chem. Commun.* **2008**, 3393. (c) Lin, K.-Y.; Matteucci, M. *J. Am. Chem. Soc*. **1998**, *120*, 8531. (d) Holmes, S.C.; Arzumanov, A. A.; Gait, M. J. *Nucleic Acids Res.* **2003**, *31*, 2759. (e) Ortega, J.A.; Blas, J.R.; Orozco, M.; Grandas, A.; Pedroso, E.; Robles, J. *Org. Lett.* **2007**, *9*, 4503.

26. (a) Lui, C.; Martin, C. T. *J. Mol. Biol*. **2001**, *308*, 465. (b) Lui, C.; Martin, C. T. *J. Biol. Chem*. **2002**, *277*, 2725. (c) Berry, D. A.; Jung, K. Y.; Wise, D. S.; Sercel, A. D.; Pearson, W. H.; Mackie, H.; Randolph, J. B.; Somers, R. L. *Tetrahedron Lett*. **2004**, *45*, 2457.

27. Rao, P.; Benner, S. A. *J. Org. Chem.* **2001,** *66,* 5012.

28. (a) Scopes, D. I.; Barrio, J. R.; Leonard, N. J. *Science* **1977**, *195*, 296. (b) Lessor, R. A; Gibson, K. J.; Leonard, N. J. *Biochemistry* **1984**, *23*, 3868.

29. Krueger, A. T.; Lu, H.; Lee, A. H. F.; Kool, E. T. *Acc. Chem. Res.* **2007**, *40*, 141.

30. (a) Liu, H.; Gao, J.; Maynard, L.; Saito, Y. D; Kool, E. T. *J. Am. Chem. Soc.* **2004**, *126*, 1102. (b)) Fuentes-Cabrera, M.; Sumpter, B. G.; Wells, J. C. *J. Phys. Chem. B* **2005**, *109*, 21135.

31. (a) Lu, H.; He, K.; Kool, E. T. *Angew. Chem., Int. Ed.* **2004**, *43*, 5834.(b) Lee, A. H. F.; Kool, E. T. *J. Am.Chem. Soc.* **2005**, *127*, 3332. (c) Lee, A. H. F.; Kool, E. T. *J. Org. Chem.* **2005**, *70*, 132.

32. Gao, J.; Liu, H.; Kool, E. T. *Angew. Chem., Int. Ed.* **2005**, *44*, 3118.

33. Lee, A. H. F.; Kool, E. T. *J. Am. Chem. Soc.* **2006**, *128*, 9219.

34. Doi, Y.; Chiba, J.; Morikawa, T.; Inouye, M. *J. Am. Chem. Soc.* **2008**, *130*, 8762.

35. (a) Minakawa, N.; Kojima, N.; Hikishima, S.; Sasaki, T.; Kiyosue, A.; Atsumi, N.; Ueno, Y.; Matsuda, A. *J. Am. Chem. Soc.* **2003**, *125*, 9970. (b) Hikishima, S.; Minakawa, N.; Kuramoto, K.; Ogata, S.; Matsuda, A. *ChemBioChem* **2006**, *7*, 1970.

36. Minakawa, N.; Ogata, S.; Takahashi, M.; Matsuda, A. *J. Am. Chem. Soc.* **2009**, *131*, 1644.

37. (a) Ishikawa, M.; Hirao, I.; Yokoyama, S. *Tetrahedron Lett.* **2000**, *41*, 3931. (b) Mitsui, T.; Kimoto, M.; Harada, Y.; Yokoyama, S.; Hirao, I. *J. Am.Chem. Soc.* **2005**, *127*, 8652.

38. (a) Hirao, I. *Curr. Opin. Chem. Biol.* **2006**, *10*, 622. (b) Hirao, I.; Kimoto, M.; Mitsui, T.; Fujiwara, T.; Kawai, R.; Sato, A.; Harada,Y.; Yokoyama, S. *Nat. Methods* **2006**, *3*, 729.

39. (a) Ishikawa, M.; Hirao, I.; Yokoyama, S. *Nucleic Acids Symp. Ser.* **1999**, *42*, 125. (b) Fujiwara, T.; Kimoto, M.; Sugiyama, H.; Hirao, I.; Yokoyama, S. *Bioorg. Med. Chem. Lett.* **2001**, *11*, 2221.

40. (a) Hirao, I.; Fujiwara, T.; Kimoto, M.; Mitsui, T.; Okuni, T.; Ohtsuki, T.; Yokoyama, S. *Nucleic Acids Symp. Ser.* **2000**, *44*, 261. (b) Fujiwara, T.; Sugiyama, H.; Hirao, I.; Yokoyama, S. *Nucleic Acids Symp. Ser.* **2000**, *44*, 43. (c) Mitsui, T.; Kimoto, K.; Sato, A.;Yokoyama, S.; Hirao, I. *Bioorg. Med. Chem. Lett.* **2003**, *13*, 4515.

41. Hirao, I.; Ohtsuki, T.; Fujiwara, T.; Mitsui, T.; Yokogawa, T.; Okuni, T.; Nakayama, H.; Takio, K.; Yabuki, T.; Kigawa, T.; Kodama, K.; Yokogawa, T.; Nishikawa, K.; Yokoyama, S. *Nat. Biotechnol.* **2002**, *20*, 177.

42. Tawarada, R.; Seio, K.; Sekine, M. *J. Org. Chem.* **2008**, *73*, 383.

43. (a) Sinkeldam, R. W.; Greco, N. J.; Tor, Y. *Chem. Rev.* **2010**, *110*, 2579. (b) Rios, A. C.; Tor, Y. *Astrobiology* **2012**, *12*, 884. (c) Winnacker, M.; Kool, E. T. *Angew. Chem., Int. Ed. Engl.* **2013**, *52,* 12498.

44. (a) Greco, N. J.; Tor, Y. *J. Am. Chem. Soc.* **2005**, *127*, 10784. (b) Tor, Y.; Del Valle, S.; Jaramillo, D.; Srivatsan, S. G.; Rios, A.; Weizman, H. *Tetrahedron* **2007**, *63*, 3608. (c) Tor, Y. *Pure Appl. Chem.* **2009**, *81*, 263. (d) Noe, M.; Sinkeldam, R.W.; Tor, Y. *J. Org. Chem.* **2013**, *78*, 8123. (e) Lane, R.S.K.; Jones, R.; Sinkeldam, R.W.; Tor, Y.; Magennis, S.W. *ChemPhysChem* **2014**, *15*, 867.

45. Shin, D.; Sinkeldam, R. W.; Tor, Y. *J. Am. Chem. Soc.* **2011**, *133*, 14912.

46. Hernández, A. R.; Kool, E. T. *Org. Lett.* **2011**, *13*, 676.

47. Hernández, A. R.; Peterson, L. W.; Kool, E. T. *ACS Chem. Biol.* **2012**, *7*, 1454.

48. (a) Ward, D. C.; Reich, E.; Stryer, L. *J. Biol. Chem.* **1969**, *244*, 1228. (b) Jean, J. M.; Hall, K. B. *Proc. Natl. Acad. Sci. U.S.A.* **2001**, *98*, 37. (c) Jean, J. M.; Hall, K. B. *Biochemistry* **2002**, *41*, 13152.

49. Sinkeldam, R. W.; McCoy, L. S.; Shin, D.; Tor, Y. *Angew. Chem., Int. Ed.* **2013**, *52*, 14026.

50. (a) Kool, E. T. *Annu. Rev. Biophys. Biomol. Struct.* **2001**, *30*, 1. (b) Kool, E. T. *Annu. Rev. Biochem.* **2002**, *71*, 191.

51. (a) Schweitzer, B. A.; Kool, E. T. *J. Org. Chem.* **1994**, *59*, 7238. (b) Schweitzer, B. A.; Kool, E. T. *J. Am. Chem. Soc.* **1995**, *117*, 737.

52. (a) Moran, S.; Ren, R. X. F.; Rumney, S. I. V.; Kool, E. T. *J. Am. Chem. Soc.* **1997**, *119*, 2056. (b) Moran, S.; Ren, R. X. F.; Kool, E. T. *Proc. Natl. Acad. Sci. U.S.A.* **1997**, *94*, 10506.

53. (a) Morales, J. C.; Kool, E. T. *Nat. Struct. Biol.* **1998**, *5*, 950. (b) Morales, J. C.; Kool, E. T. *J. Am. Chem. Soc.* **1999**, *121*, 2323.

54. (a) Ogawa, A. K.; Wu, Y.; Berger, M.; Schultz, P. G.; Romesberg, F. E. *J. Am. Chem. Soc.* **2000**, *122*, 8803. (b) Matsuda, S.; Romesberg, F. E. *J. Am. Chem. Soc.* **2004**, *126*, 14419. (c) Matsuda, S.; Henry, A. A.; Romesberg, F. E. *J. Am. Chem. Soc.* **2006**, *128*, 6369. (d) Henry, A. A.; Olsen, A. G.; Matsuda, S.; Yu, C.; Geierstanger, B. H.; Romseberg, F. E. *J. Am. Chem. Soc.* **2004**, *126*, 6923.

55. (a) Ogawa, A. K.; Wu, Y.; McMinn, D. L.; Liu, J.; Schultz, P. G.; Romesberg, F. E. *J. Am. Chem. Soc.* **2000**, *122*, 3274. (b) Wu, Y.; Ogawa, A. K.; Berger, M.; McMinn, D. L.; Schultz, P. G.; Romesberg, F. E. *J. Am. Chem. Soc.* **2000**, *122*, 7621. (c) Berger, M.; Ogawa, A. K.; McMinn, D. L.; Wu, Y.; Schultz, P. G.; Romesberg, F. E. *Angew. Chem., Int. Ed.* **2000**, *39*, 2940.

56. Berger, M.; Ogawa, A. K.; McMinn, D. L.; Wu, Y.; Schultz, P. G.; Romesberg, F. E. *Angew. Chem., Int. Ed.* **2000**, *122*, 3069.

57. (a) Matsuda, S.; Henry, A. A.; Schultz, P. G.; Romesberg, F. E. *J. Am.Chem. Soc.* **2003**, *125*, 6134. (b) Hwang, G. T.; Romesberg, F. E. *Nucleic Acids Res.* **2006**, *34*, 2037. (c) Berger, M.; Luzzi, S. D.; Henry, A. A.; Romesberg, F. E. *J. Am.Chem. Soc.* **2002**, *124*, 1222. (d) Matsuda, S.; Leconte, A. M.; Romesberg, F. E. *J. Am. Chem. Soc.* **2007**, *129*, 5551.

58. Leconte, A. M.; Hwang, G. T.; Matsuda, S.; Capek, P.; Hari, Y.; Romesberg, F. E. *J. Am. Chem. Soc.* **2008**, *130*, 2336.

59. (a) Seo, Y. J.; Hwang, G. T.; Ordoukhanian, P.; Romesberg, F. E. *J. Am. Chem. Soc.* **2009**, *131*, 3246. (b) Seo, Y. J.; Matsuda, S.;Romesberg, F. E. *J. Am. Chem. Soc.* **2009**, *131*, 5046.

60. (a) Brotschi, C.; Häberli, A.; Leumann, C. J. *Angew. Chem. Int., Ed.* **2001**, *40*, 3012; (b) Brotschi, C.; Leumann, C. J. *Angew. Chem. Int., Ed.* **2003**, *42*, 1655. (c) Kaufmann, M.; Gisler, M.; Leumann, C. J. *Angew. Chem., Int. Ed.* **2009**, *48*, 3810.

61. Mitsui, T.; Kitamura, A.; Kimoto, M.; To, T.; Sato, A.; Hirao, I.; Yokoyama, S. *J. Am. Chem. Soc.* **2003**, *125*, 5298.

62. Mathis, G.; Hunziker, J.; *Angew. Chem. Int. Ed.* **2002**, *41*, 3203.

63. (a) Ren, R. X.-F.; Chaudhuri, N. C.; Paris, P. L.; Rumney IV, S.; Kool, E. T. *J. Am. Chem. Soc.* **1996**, *118*, 7671. (b) Guckian, K. M.; Schweitzer, B. A.; Rex X.-F. R.; Sheils, R. C. J.; Paris, P. L. ; Tahmassebi, D. C.; Kool E.T. *J. Am. Chem. Soc.* **1996**, *118,* 8182. (c) Guckian, K. M.; Schweitzer, B. A.; Rex X.-F. R.; Sheils, R. C.; Tahmassebi, D. C.; Kool, E. T. *J. Am. Chem. Soc.* **2000**, *122*, 2213. (d) Hainke, S.; Singh, I; Hemmings, J.; Seitz, O. *J. Org. Chem.* **2007**, *72*, 8811.

64. Hou, D.; Greenberg, M. M. *J. Org. Chem.* **2014**, *79*, 1877.

65. Balakin, K. V.; Korshun, V. A.; Mikhalev, I. I.; Maleev, G. V.; Malakhov, A. D.; Prokhorenko, I. A.; Berlin, Yu. A. *Biosens. Bioelectron.* **1998**, *13*, 771.

66. (a) Christensen, U. B.; Pedersen, E. B. *Nucleic Acid Res.* **2002**, *30*, 4918. (b) Nielsen, C. B.; Petersen, M.; Pedersen, E. B.; Hansen, P. E.; Christensen, U. B. *Bioconjugate Chem.* **2004**, *15*, 260.

67. Langenegger, S. M.; Häner, R. *Helv. Chim. Acta.* **2002**, *85*, 3414.

68. Langenegger, S. M.; Häner, R. *Tetrahedron Lett*. **2004**, *45*, 9273.

69. Wagner, C; Wagenknecht, H-A. *Org. Lett.* **2006**, *8*, 4191.

70. Rappaport, H. P.; *Nucleic Acids Res*. **1988**, *16*, 7253. (b) Rappaport, H. P. *Biochemistry* **1993**, *32*, 3047.

71. Kimoto,M.; Mitsui, T.; Yokoyama, S.; Hirao, I. *J. Am. Chem. Soc.* **2010**, *132*, 4988.

72. Hainke, S.; Seitz, O. *Angew. Chem., Int. Ed.* **2009**, *48*, 8250.

73. (a) Vesnaver, G; Chang, C-N; Eisenberg, M.; Grollmann, A. P.;Breslaur, K.G.; *Proc. Natl. Acad. Sci. USA* **1989**, *86*, 3614. (b) Scharer, O. D. *Angew. Chem., Int. Ed.* **2003**, *42*, 2946.

74. Langenegger, S. M.; Häner, R. *ChemBioChem* **2005**, *6*, 848.

75. Fukui, K.; Morimoto, M.; Segawa, H.; Tanaka, K.; Shimidzu, T. *Bioconjugate Chem.* **1996**, *7*, 349.

76. (a) Matray, T. J.; Kool, E.T. *J. Am. Chem. Soc*. **1998**, *120*, 6191. (b) Matray, T. J.; Kool, E. T. *Nature* **1999**, *399*, 704. (c) Smirnov, S.; Matray, T. J.; Kool, E. T.; de los Santos, C. *Nucleic Acids Res.* **2002**, *30*, 5561. (d) Wojciechowski, F.; Lietard, J.; Leumann, C. J. *Org. Lett.* **2012**, *14*, 5176.

77. (a) Morales, H.; Kool, E. T. *Org. Lett.* **2002**, *12*, 4377. (b) Zhang, X.; Lee, I.; Berdis, A. J. *Biochemistry* **2005**, *44*, 13101.

78. Fakhrai-Rad, H.; Pourmand, N.; Ronaghi, M. *Hum. Mutat.* **2002**, *19*, 479. (b) Nazarenko, I.; Pires, R.; Lowe, B.; Obaidy, M.; Rashtchian, A. *Nucleic Acids Res.* **2002**, *30*, 2089. (c) Marras, S. A. E.; Kramer, F. R.; Tyagi, S. *Nucleic Acids Res.* **2002**, *30*, e122. (d) Ward, D. C.; Reich, E.; Stryer, L. *J. Biol. Chem.* **1969**, *244*, 1228. (e) Menger, M.; Tuschl, T.; Eckstein, F.; Porschke, D. *Biochemistry* **1996**,

35, 14710. (f) Lacourciere, K. A.; Stivers, J. T.; Marino, J. P. *Biochemistry* **2000**, *39*, 5630. (g) Secrist III, J. A.; Barrio, J. R.; Leonard, N. J. *Science* **1972**, *175*, 646. (h) Holmen, A.; Albinsson, B.; Norden, B. *J. Phys. Chem.* **1994**, *98,* 13460. (i) Seela, F.; Zulauf, M.; Sauer, M.; Deimel, M. *Helv. Chim. Acta.* **2000**, *83*, 910.

79. (a) Hurley, D. J.; Seaman, S. E.; Mazura, J. C.; Tor, Y. *Org. Lett.* **2002**, *4*, 2305. (b) Fauth, C.; Speicher, M. R. *Cytogenet. Cell Genet.* **2001**, *93*,1. (c) Pernthaler, J.; Glockner, F. O.; Schonhuber, W.; Amann, R. *Meth. Microbiol.* **2001**, *30*, 207. (d) Amann, R.; Fuchs, B. M. ; Behrens, S. *Curr. Opin. Biotech.* **2001**, *12*, 231. (e) Sieben, V. J.; Debes-Marun, C. S.; Pilarski, P. M.; Kaigala, G. V.; Pilarski, L. M.; Backhouse, C. *IET Nanobiotechnol.* **2007**, *1*, 27.

80. (a) Pernthaler, A.; Pernthaler, J.; Amann R. *Appl. Environ. Microbiol.* **2002**, *68*, 3094. (b) Wagner, M.; Horny, M.; Daimsz, H. *Curr. Opin. Microbiol.* **2003**, *6*, 302. (c) Hertzberg, R. P.; Pope, A. J. *Curr. Opin. Chem. Biol.* **2000**, *4*, 445. (d) Matsumoto, C.; Hamasaki, K.; Mihara, H.; Ueno, A. *Bioorg. Med. Chem. Lett.* **2000**, *10*, 1857. (e) Venkatesan, A.; Dasgupta, A. *Mol. Cell. Biol.* **2001**, *21*, 2826. (f) Burbaum, J. J.; Sigal, N. H. *Curr. Opin. Chem. Biol.* **1997**, *1*, 72. (g) Hann, M. M.; Oprea, T. I. *Curr. Opin. Chem. Biol.* **2004**, *8*, 255. (h) Liu, B.; Li, S.; J. Hu, *Am. J. Pharmacog.* **2004**, *4*, 263.

81. Steyer, J. A.; Almers, W. *Nat. Rev. Mol. Cell Biol.* **2001**, *2*, 268.

82. (a) Alivisatos, P. *Pure Appl. Chem.* **2000**, *72*, 3. (b) Empedocles, S.; Bawendi, M. *Acc. Chem. Res.* **1999**, *32*, 389. (c) Du, W., Wang, Y., Luo, Q., and Liu, B. F. *Anal. Bioanal. Chem.* **2006**, *386*, 444. (d) Fuller, J. E., Zugates, G. T., Ferreira, L. S., Ow, H. S., Nguyen, N. N., Wiesner, U. B., and Langer, R. S. *Biomaterials* **2008**, *10*, 1526. (e) Empedocles, S. and Bawendi, M. *Acc. Chem. Res.* **1999**, *32*, 389. (f) Cady, N. C., Strickland, A. D., and Batt, C. A. *Mol. Cell. Probes.* **2007**, *2*, 116.

83. (a) Ju, J.; Ruan, C.; Fuller, C. W.; Glazer, A. N.; Mathies, R. A. *Proc. Natl. Acad. Sci. U.S.A.* **1995**, *92*, 4347. (b) Jiao, G. S.; Thoresen, L. H.; Kim, T. G.; Haaland, W. C.; Gao, F.; Topp, M. R.; Hochstrasser, R. M.; Metzker, M. L.; Burgess, K. *Chemistry* **2006**, *30*, 7816.

84. (a) Gao, J.; Strassler, C.; Tahmassebi, D.; Kool, E. T. *J. Am. Chem. Soc.* **2002**, *124*, 11590. (b) Cuppoletti, A.; Cho, Y.; Park, J. S.; Strässler, S.; Kool, E. T. *Bioconjugate Chem*. **2005**, *16*, 528. (c) Ren, R. X.-F.; Chaudhuri, N. C.; Paris, P. L.; Rumney, S. IV; Kool, E. T. *J. Am. Chem. Soc.* **1996**, *118*, 7671. (d) Strässler, C.; Davis, N. E.; Kool, E. T. *Helv. Chim. Acta.* **1999**, *82*, 2160.

85. Masuko, M.; Ohuchi, S.; Sode, K.; Ohtani, H.; Shimadzu, A. *Nucleic Acid Res.* **2000**, *28*, e34.

86. Teo, Y. N.; Kool, E. T. *Bioconjugate Chem.* **2009,** *20,* 2371.

87. (a) Haga, H.; Yamada, Y.; Ohnishi, Y.; Nakamura, Y.; Tanaka, T. *J. Hum. Genet*. **2002**, *47*, 605. (b) Tabara, Y.; Kohara, K.; Miki, T. et al. *Hypertens. Res.* **2012**, *34*, 567. (c) Thompson, E. R.; Gorringe, K. L.; Choong, D. Y. H.; Eccles, D. M.; ConFab, K.; Mitchell, G.; Campbell, I. G. *Breast Cancer Res. Treat.* **2012**, *134*, 543. (d) Okamoto, A.; Ichiba, T.; Saito. I. *J. Am. Chem. Soc*. **2004**, *126*, 8364. (e) Okamoto, A.; Ochi, Y.; Saito, I. *Bioorg. Med. Chem. Lett*. **2005**, *15*, 4279.

88. Saito, Y.; Kugenuma, K.; Tanaka, M.; Suzuki, A.; Saito, I. *Bioorg. Med. Chem. Lett*. **2012**, *22*, 3723.

Chapter 2

STUDIES ON THE SYNTHESIS AND PHOTOPHYSICAL PROPERTIES OF TRIAZOLYL NUCLEOSIDES

Synthesis and Photophysical Properties of Triazolyl UN-Nucleosides

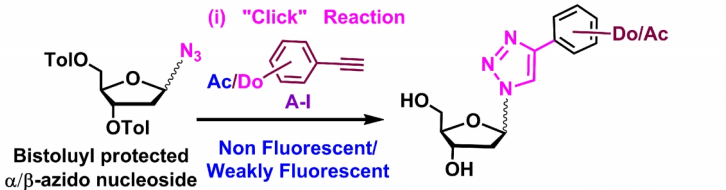

^{T}B (1α-9α and 1β-9β)

Bag's Triazolyl (^{T}B) Nucleosides.

Charge Transfer/Fluorescenct UNN.

R = Protective groups; Ac = Acceptor Unit;
Do = Donor Unit; UNN = Unnatural (UN) Nucleoside

2.1. Introduction

The design and synthesis of non natural nucleosides that are stable to enzymatic and acid hydrolysis is a rapidly growing field of DNA research.[1-2] Apart from being the new building blocks of genome, suitably designed unnatural nucleosides are widely being exploited for the study of interactions involving DNA.[3] These nucleosides have also attracted much attention due to their high potential value as therapeutic agents, biochemical probes, and in the field of expansion of genetic alphabets.[4] Expansion of the genetic alphabet to include a third base pair, formed between two identical (self-pair) or different (hetero-pair) unnatural nucleotides, would expand the informational and functional potential of DNA.[5-6] It was the question, "why DNA and RNA each use only four genetic alphabet" coupled with the exciting possibility of generating DNA and RNA with enhanced functional abilities that led Alex Rich in 1962 to propose the concept of orthogonal base pairing between *iso*-G and *iso*-C and inspired Prof. Steven A. Benner in the late 1980's to expand the genetic alphabet from four to six letters. Benner's idea quickly spread, resulting in increasing amounts of research aimed at expanding the genetic alphabet. Benner's early research focused on the development of new base pairs having hydrogen bonding patterns orthogonal to those in canonical Watson-Crick base pairs. In 1994, Prof. Eric T. Kool opened a new functional dimension with the creation of non-hydrogen bonded unnatural nucleobase surrogates. Inspired by Kool's work, much effort has been devoted to the development of hydrophobic base pairs having orthogonal recognition properties, many of which can even be recognized and incorporated by polymerases. Several groups, including those of Hirao, Romesberg, and Schultz, have contributed towards this end some of which have already been exemplified in **Chapter 1**. It is now clear that expansion of the genetic alphabet has increased the functional potential of DNA, for example by enabling site directed oligonucleotide labeling and *in vitro* selections with oligonucleotides having increased chemical diversity. Translation of an expanded DNA alphabet into RNA is a challenging task, but one which has potential to give rise to semi-synthetic organisms and increased biodiversity.

The major efforts and the first step in the field of expansion of genetic alphabet is the design and synthesis of new nucleoside base surrogates capable of forming stable third base-pair (self-pair or heteropair) of DNA or RNA *via* H-bonding or hydrophobic or other force of attraction and the pair would be efficiently replicated by enzyme with high fidelity.[4,7] Recent efforts have resulted in designing and construction of a number of such base-pairs that includes stable H-bonded pairs[8] and non-natural, stable, hydrophobic base pairs.[9] The non-H-bonded base pairs are found to stabilize DNA *via* π-stacking and hydrophobic interactions among self-/hetero-pair. Considerable efforts have thus been invested in delineating the impact of incorporation of non-H-bonded base pairs such as C-aryl and/or N-aryl unnatural nucleosides into short oligonucleotide sequences either *via* enzymatic or chemical means on the structure, stability of DNA duplex and on the efficiency and specificity in replication by DNA polymerases.[4]

Moreover, the conductive, excessive charge transfer in DNA *via* the base-stack as well as the sensing property of natural DNA is limited to the restricted redox potential and non-fluorescent nature of four natural bases. Therefore, growing demand of nucleic acid based diagnostics and sensing materials needs to design and incorporate unnatural nucleobases with tuned photophysical properties.[10-11] While the development of bases with tuned photophysical properties may lead to oligonucleotides with novel electronic or magnetic properties, fluorescent nucleobases can be used for the development of nucleic acid based sensor.[10-12] Towards this end, several unnatural nucleobases have appeared in the literature for the development of functional nucleic acids.[13] However, the rational design of non-hydrogen bonding base pairs remains a challenge.

In the design of non-hydrogen bonding base pairs, researchers have concentrated mainly on the factors like, π-stacking, hydrophobicity, steric shape mimicry, and in few cases the dipole moment, *etc.*, in the stabilization of DNA duplex.[14] Moreover, to generate such new and interesting nucleobase pairs usable for various DNA based applications, several methodologies have evolved. As for example, Cu(I)-catalyzed azide-alkyne cycloaddition reaction[15a] has got attention only in recent years in the field of nucleic acid chemistry for the design of artificial nucleobases with interesting

properties, functional nucleic acids of potential value in biology, medicine, material sciences, and in nanotechnology.[15] The 1,3-dipolar cycloaddition reaction between a terminal acetylene and an azide was pioneered by Huisgen and later on modified by Tornoe and Meldel in 2001 by the introduction of Cu(I) catalyst.[16] Sharpless and co-workers[17] introduced the concept of "click" reaction for the Cu(I) catalysed 1,3-dipolar cycloaddition reaction between a terminal acetylene and an azide. The original Huisgen 1,3-dipolar cycloaddition reaction suffered from certain disadvantages like poor regioselectivity leading to a mixture of 1,4- and 1,5- disubstituted triazoles and the requirement of elevated temperatures. However, the discovery of Cu(I) salts as a catalyst for the reaction by Meldel and then by Sharpless endowed the reaction with regioselectivity (1,4- regioisomers only) which could be accomplished under mild reaction conditions. The use of Cu(I) catalyst is advantageous as it is inexpensive and easy to handle. Most of the reported protocols involve the use of CuI or the reduction of stable sources of Cu(II), such as $CuSO_4$, with sodium salts or the comproportionation of Cu(II)/Cu(0) species to generate active Cu(I)-catalyst which catalyses the click reaction. **Scheme 2.1** represents the basic click chemistry protocol.

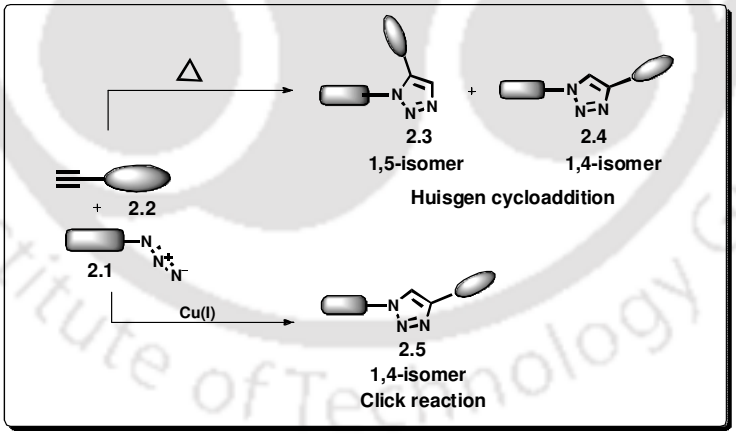

Scheme 2.1: Schematic representation of 1,3-dipolar cycloaddition between an azide and an alkyne.

2.2. Applications of Click Reaction in Nucleic Acids Chemistry

Click chemistry was developed aiming at providing a simple method to join together organic molecules in high yields under mild reaction conditions and in the

presence of a diverse range of functional groups.[18] Ever since the discovery, click chemistry has led to an influx of new ideas in the field of nucleic acids research. There is a great deal of interest in developing new synthetic methods to construct chemically modified DNA oligonucleotides (ODNs) for biological and nanotechnological applications. The copper catalysed alkyne–azide cycloaddition (CuAAC) [16b, 17a-b] reaction, the best example of this new class of extremely efficient chemical reactions, has become a method of choice for decorating DNA in various ways due to its remarkable efficiency. Click chemistry is now used routinely in labelling DNA oligonucleotides with different functionalities, such as, biologically active moieties and fluorescent dyes, labeling of sugar, in geneting cyclic DNA, in joining oligonucleotides to PNA, and to produce analogues of DNA with modified nucleobases and backbones. More recently, click chemistry has found an exciting range of applications in the synthesis of longer oligonucleotides. The features of the click reaction that are potentially useful in such applications are:

(a) Azides and alkynes can be attached to nucleic acids without greatly disturbing their biophysical properties.

(b) The reaction of azides and unactivated alkynes is tolerant to other functional groups.

(c) The triazole unit is extremely stable, and is not toxic. The basic CuAAC click reaction is shown in **Scheme 2.1**.

Few important applications of click chemistry in the field of nucleic acids have been described below which includes:

(a) Click oligonucleotide labelling.

(b) Oligonucleotide ligation and cyclization.

(c) Modification of the sugar-phosphate backbone of DNA with triazolyl backbone.

(d) Modification of naturally occurring bases or replacement of the natural nucleobases with triazolyl derivatives.

2.2.1. Click Oligonucleotide Labelling

One of the most common methods of post-synthetic oligonucleotide labelling involves amide bond formation from an amino-modified oligonucleotide and the N-hydroxysuccinimide ester of a dye (**Scheme 2.2a**). Although, the product is obtained in quantitative yield, one disadvantage of this method is that N-hydroxysuccinimide esters are readily hydrolysed in aqueous media.

The copper-catalysed azide alkyne click reaction *i.e.* CuAAC reaction provides a better method of choice today for labelling oligonucleotides with an array of functional groups, including chimeric molecules, epigenetic modifications and moieties that might be unstable to enzymatic ligation reactions (**Scheme 2.2b**, **c**). The CuAAC reaction is orthogonal to standard amino-link labeling and usually gives high yields of product under mild reaction conditions. Now a day, the CuAAC reaction is being utilized routinely for post-synthetic labeling of oligonucleotide probes suitable for use in DNA analysis.

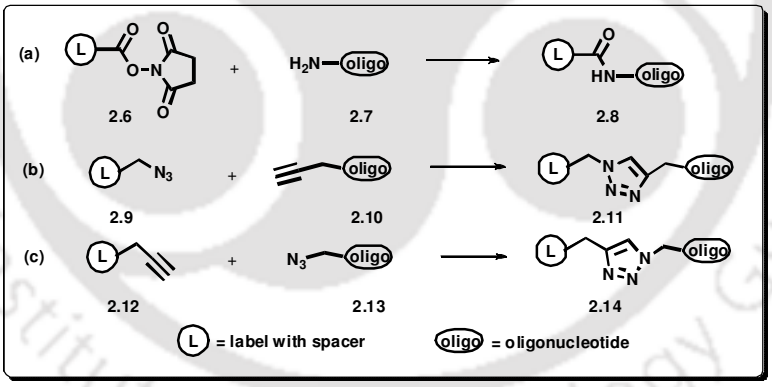

Scheme 2.2: Different methods of labeling of oligonucleotides.

In order to decorate the oligonucleotide with fluorescent label or fluorescent nucleoside, click chemistry has found significant importance. Therefore, utilizing click chemistry, various research groups are involved in designing fluorescent labelled nucleoside and oligonucleotide probes usable for DNA analysis, monitoring the hybridization event and in many other biophysical nanotechnological applications.[15b] As for example, 7-(octa-1,7-diynyl) derivatives of 7-deaza-2′-deoxyguanosine have been conjugated to 3-azido-7-hydroxycoumarin *via* click

reaction to generate fluorescent oligonucleotide probes (**Figure 2.1**).[19] Thus, pyrazolo[3,4-d]pyrimidine nucleoside derivative **2.15** is found to be more fluorescent than pyrrolo[2,3-d]pyrimidine derivative. It has also been found that the quenching of fluorescence in pyrrolo[2,3-d]pyrimidine derivative is stronger with monomeric nucleoside conjugates than the quenching in single-stranded or duplex DNA containing the coumarin labelled nucleoside. The interaction between the nucleobase and dye is more favourable in the monomeric state than in the DNA chain resulting in efficient quenching in the monomeric state *via* electron transfer process than in the DNA where the nucleobase is a part of the stack and is therefore held away from the coumarin. It was observed that the duplex with the bulky dye conjugate was more stable than canonical DNA.

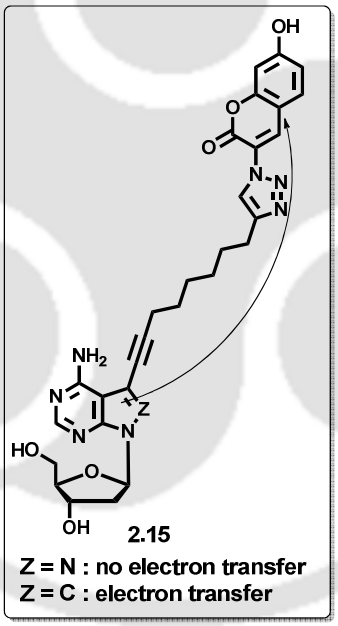

Figure 2.1: Electron transfer studies with pyrrolo/pyrazolopyrimidines and attached triazole coumarin.

Seela *et al.* have also synthesized tripropargylamine-dU from deoxyuridine which has been incorporated into an oligonucleotide. Post synthetic reaction with two, nonfluorescent 3-azido-7 hydroxycoumarin *via* click reaction yielded the bis-coumaryl labelled ODN probe (**Scheme 2.3**). The tripropargyl dU was found to slightly stabilize DNA duplexes and a strongly fluorescent oligonucleotide bis-dye

conjugate was generated from the nonfluorescent 3-azido-7-hydroxycoumarin *via* click reaction.[20]

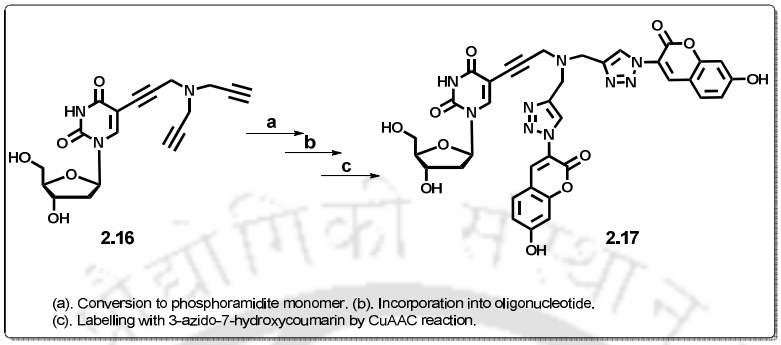

Scheme 2.3: Post synthetic labelling of bis-propargyl DNA with coumarin derivative *via* click reaction.

Multiple labelling of oligonucleotides with sugars was reported by microwave assisted click chemistry by Morvan *et al.*[21] The galactosyl azide was conjugated to the solid supported tri-alkyne-modified T_{12} oligonucleotide in a microwave-assisted CuAAC reaction. The cycloaddition reaction was performed by using 3.3 molar equivalents of azide per alkyne residue in the presence of $CuSO_4$ and sodium ascorbate in water–methanol to yield the solid-supported protected trigalactosyl oligonucleotide product (**Scheme 2.4**). Subsequent deprotection of the carbohydrate-labelled oligonucleotide with aqueous ammonia afforded the fully deprotected trigalactosylated T_{12} oligonucleotide. This methodology can be adopted for the generation of multiple labelled oligonucleotide probes for potential use in biological, therapeutic and diagnostic applications.

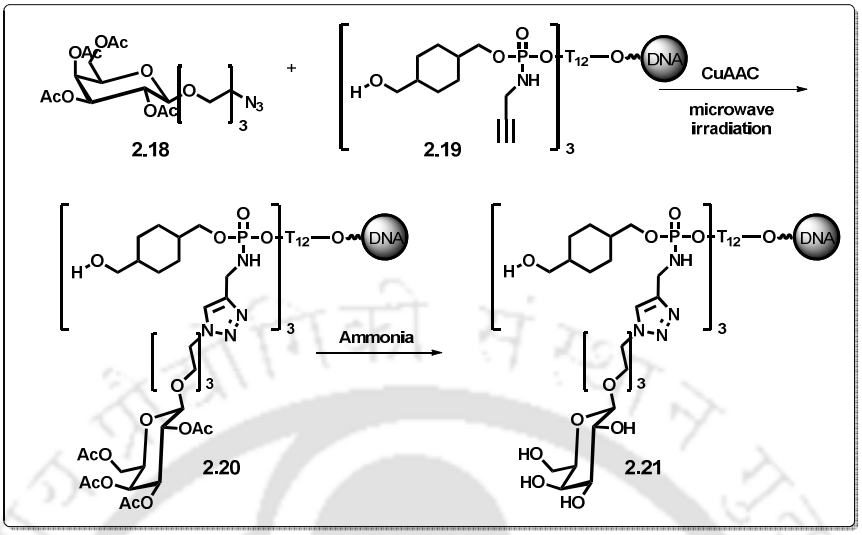

Scheme 2.4: Labelling of oligonucleotides with carbohydrates *via* click chemistry.

2.2.2. Oligonucleotide Ligation and Cyclization

Although there has been great interest in the preparation of synthetic oligonucleotides over the last 30 years, the chemical synthesis of long strands of DNA suffers from problems such as low overall reaction yields, imperfect coupling efficiency and side reactions. Consequently, shorter sequences are usually subjected to multiple enzymatic ligation reactions, using large excess of primers which is an expensive process. The CuAAC reaction has been exploited for this application, since, not only is it a reliable reaction which can be performed using cheap, commercially available reagents, but also the azide and alkyne functionalities can be easily introduced.

Unlike the cycloaddition reaction with small, simple organic molecules, the azide-alkyne cycloaddition with DNA molecules normally require a template to bring the cycloaddition partners in close proximity to improve the efficiency of the reaction. This template is simply a short length of DNA, called a splint which has a complementary sequence in the region where the cycloaddition will take place (**Scheme 2.5**)

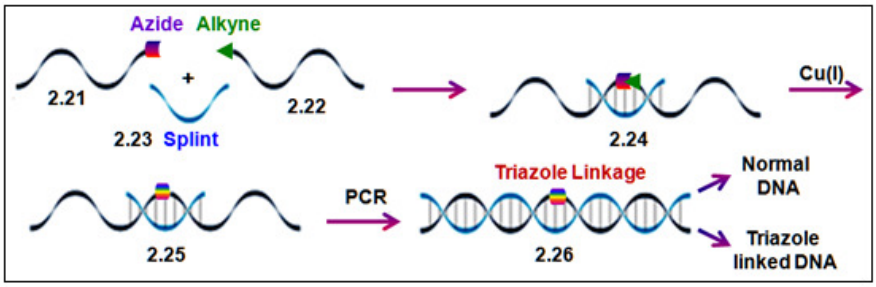

Scheme 2.5: Schematic representation of oligonucleotide ligation.

Click ligation of DNA strands has many potential uses, such as strand ligation, covalently cross-linked duplexes across the nucleobases,[22] the synthesis of cyclic DNA catenanes that is a synthetic mimic of mini-plasmids,[23] and very stable mini-DNA duplexes.[24] As for an example, Brown *et al.* have used the copper-catalyzed azide–alkyne cycloaddition reaction for the template-mediated chemical ligation of two oligonucleotide strands, one with a 50-alkyne and the other with a 30-azide (**Scheme 2.6**) to produce a DNA strand with a continuous 50- to 30- backbone and a lengthy triazole linkage 2.29 at the ligation point.[23]

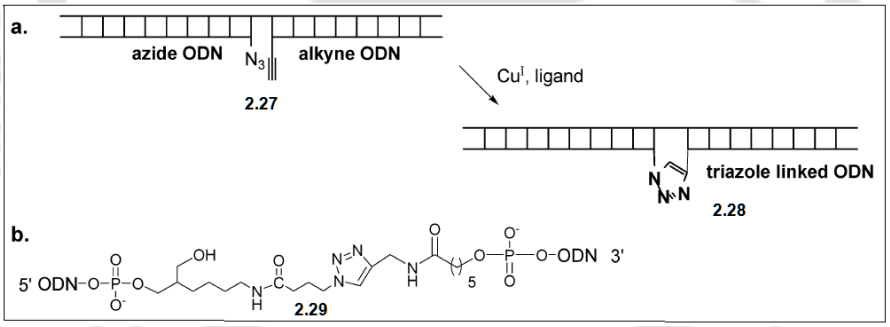

Scheme 2.6: (a) Schematic of template-mediated click-ligation of two oligonucleotides and the (b) chemical structure at ligation point.

In an attempt to produce PCR compatible chemical linkage, a ligated DNA strand containing an unnatural T-triazole-T linkage has been synthesized by click ligation between a 30-mer oligonucleotide with AZT (**2.30**) and 50-mer oligonucleotide with propargylamido dT (**2.31**) (**Scheme 2.7**). During the ligation reaction, the two oligonucleotides were held together by a complementary template oligonucleotide. The resulting click-ligated DNA strand (**2.32**) was used as a template in PCR, and found that the amplification was successful with several different thermostable

polymerases. The PCR amplicon produced contained a single thymine at the ligation site (**2.33**) instead of the two thymine bases that were present in the original template.[25] This is the first report of highly efficient non-enzymatic DNA strand ligation that has been combined with reproducible amplification.

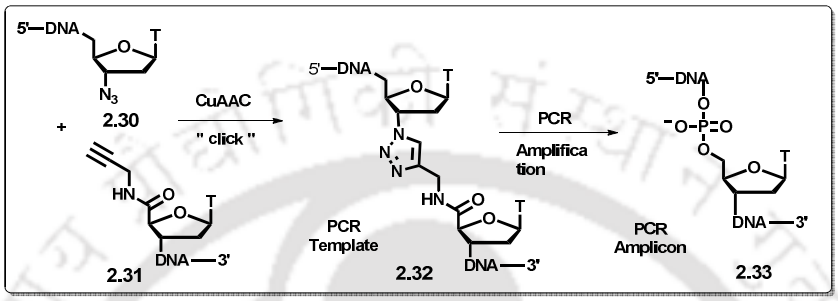

Scheme 2.7: Click ligation strategy to the synthesis and PCR amplification of an unnatural triazole-based DNA backbone.

2.2.3. Modification of Sugar-Phosphate Backbone with Click Triazole Unit

The click chemistry has not only been utilized to modify the natural nucleobases but also used to modify the phosphodiester linkage between the nucleosides. The search for other alternatives for the replacement of the phosphodiester linkage was to eliminate the negative charge in order to improve the uptake by the cells and increase the biological half life.[26] In this context, few examples have been reported in literature where the 1,2,3-triazole ring has been used as a replacement of the phosphodiester linkages. The first example of insertion of 1,2,3-triazole as a linker in place of phosphodiester linkage was reported by Matt *et al.* who have synthesized thymidine dinucleotide analogues by replacing the phosphodiester linkage with triazolyl modified backbone (**Figure 2.2**).[27] However, the replacement of the phosphodiester backbone with a triazole linker with two methylene groups destabilized the DNA duplex.[28]

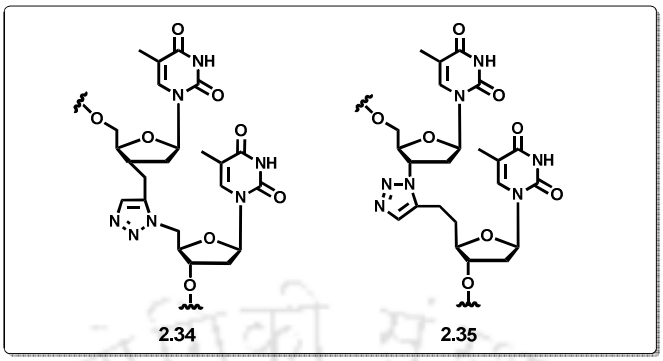

Figure 2.2: Structures of the thymidine dinucleotide linked *via* a triazole unit.

Nuzzi *et al.*[29] have developed an approach based on the repetitive Cu(I)-catalyzed azide-alkyne 1,3-dipolar cycloaddition reaction as a key ligation process of suitably functionalized thymidine building blocks which led to the formation of thymidine trinucleotide (**Figure 2.3**).

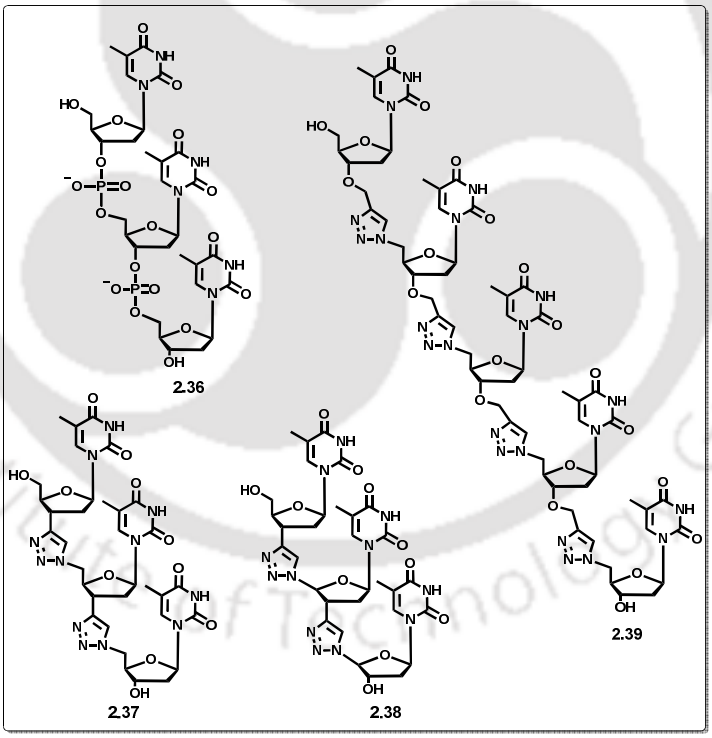

Figure 2.3: Structure of natural oligonucleotide **2.36** and it's triazole backbone analogues **2.37-2.39**.

Lucas *et al.*[30] have reported the synthesis of a triazole-linked 3′–5′ dithymidine using click chemistry under microwave conditions. The work was then extended with

sequential azidation and Cu-catalyzed [3+2] azide-alkyne 1,3-dipolar cycloaddition which led to the formation of a 3′,5′-pentathymidine **2.39** in high yield **(Figure 2.3).** The replacement of the phosphate backbone by triazole linkers in these two reported methodologies was done only for synthetic interest.

Isobe *et al.*[31] have reported the design and synthesis of 10-mer triazole-linked analogue of DNA (^{TL}DNA) using click chemistry (**Scheme 2.8**). The chain elongation reaction was done by using microwave assisted copper-catalyzed Huisgen cycloaddition and the artificial 10-mer ^{TL}DNA so formed was able to form a stable double strand with the complementary strand of natural DNA. The thermal melting temperatures was found to be 20 ^{o}C higher than that of control natural DNA which was explained on the basis of absence of any repulsive interactions between the neutral triazolyl backbone and the anionic phosphate backbone of the natural target.

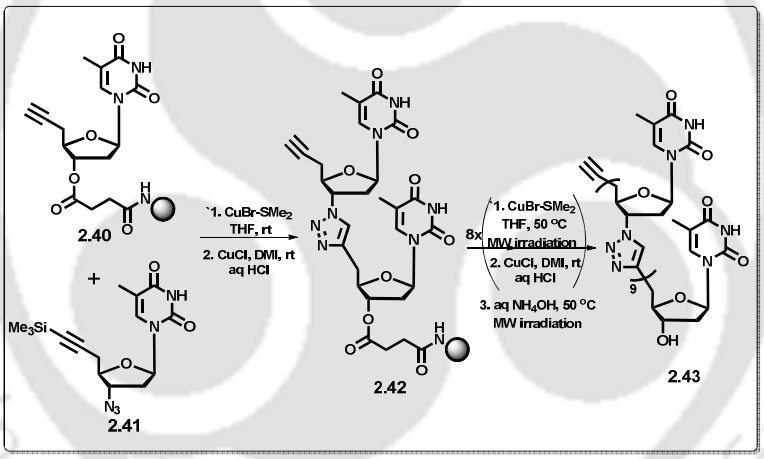

Scheme 2.8: Synthesis of 10-Mer ^{TL}DNA using solid phase synthesis

2.2.4. Modification of Naturally Occurring Bases

Frank Seela *et al.* have reported a series of 1,2,3-triazolyl nucleosides which were synthesized *via* copper(I)- catalyzed 1,3-dipolar cycloaddition of N-9 propargylpurines or N-1 propargylpyrimidines with the tolouyl protected 1-azido-2-deoxyribofuranose (**Scheme 2.9**).[32] When incorporated into oligonucleotides, the 1, 2, 3-triazolyl nucleosides were found to destabilize the duplex DNA when placed opposite to the canonical bases or an abasic site. It was observed that the triazole ring of the nucleosides disrupt the base pair formation with the opposite bases when the

modified nucleosides were incorporated into the middle of the oligonucleotides but retained the stability of the DNA duplexes when positioned at the end of the oligonucleotides.

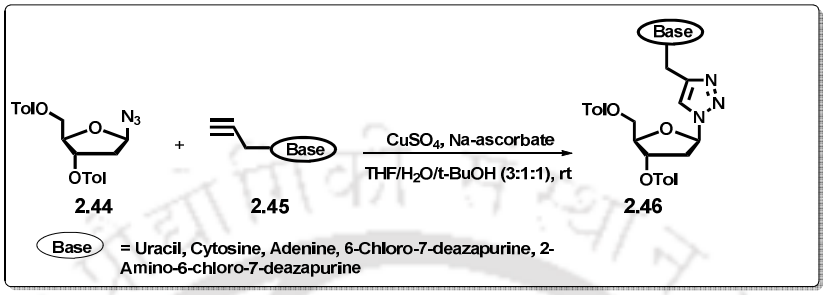

Scheme 2.9: Cu(I)-catalyzed 'click' reaction between propargylated bases and the azido sugar

Cosyn *et al.*[33] have synthesized two series of 2-(1,2,3-triazolyl)adenosine derivatives using Cu(I) catalysed "click" chemistry starting from the common intermediate **2.47**. It was known that the azide substituted π-deficient nitrogen heterocycles spontaneously cyclize to the corresponding fused tetrazole. Despite the equilibrium, the cycloaddition proceeded smoothly but lower yields were observed for the formation of compounds **2.49** probably due to a shift of the equilibrium towards tetrazole (**Scheme 2.10**). The N^6-substituted 2-(1,2,3-triazolyl)- adenosine analogues constituted a new class of selective A3 adenosine receptor agonists, partial agonists, and antagonists.

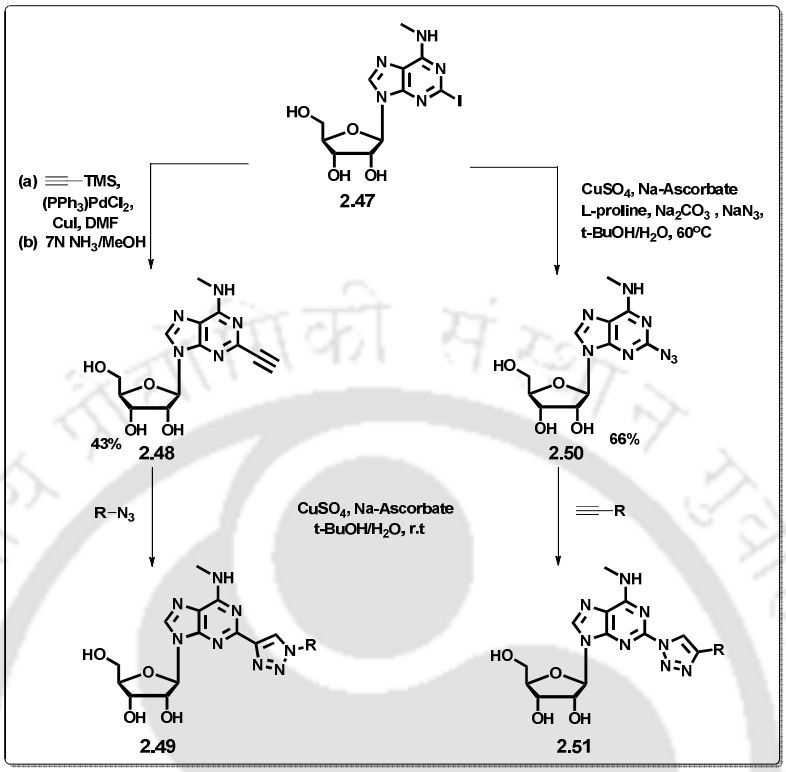

Scheme 2.10: Synthesis of 2-(1,2,3-triazolyl)adenosine derivatives **2.49** and **2.51.**

Laksman *et al.*[34] have investigated the effect of solvent polarity on the azide-tetrazole equilibrium of the C-6 azidopurine nucleosides and subsequently investigated the Cu-catalyzed azide-alkyne ligation reaction of C-6 azidopurine nucleoside (**Scheme 2.11**). The Cu-catalyzed click reaction in biphasic CH_2Cl_2/H_2O medium was found to proceed efficiently as compared to the thermal reactions, which were slow.

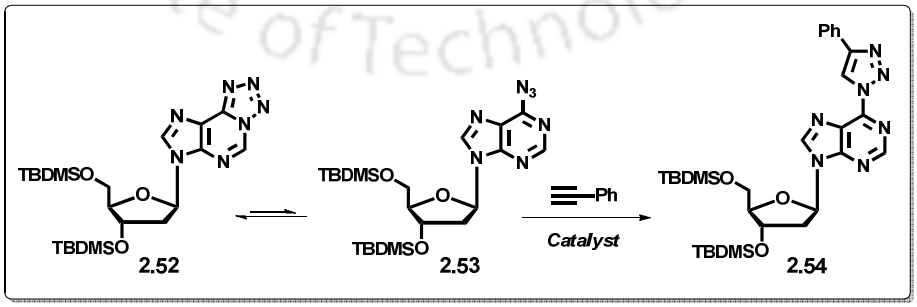

Scheme 2.11: Synthesis of 6-(1,2,3-triazolyl)adenosine derivative **2.54**.

The synthesis and biological properties of C-2 triazolylinosine derivatives have been demonstrated by Lakshman *et al.*[35] (**Scheme 2.12**). The cycloaddition reaction of the azido nucleosides with alkynes was optimized with CuCl in t-BuOH/H_2O with yield of C-2 1,2,3-triazolyl nucleosides around 70–82%. The two C-2 triazolyl adenosine analogues when tested for biological activity demonstrated pronounced antiproliferative activity in human ovarian and colorectal carcinoma cell cultures.

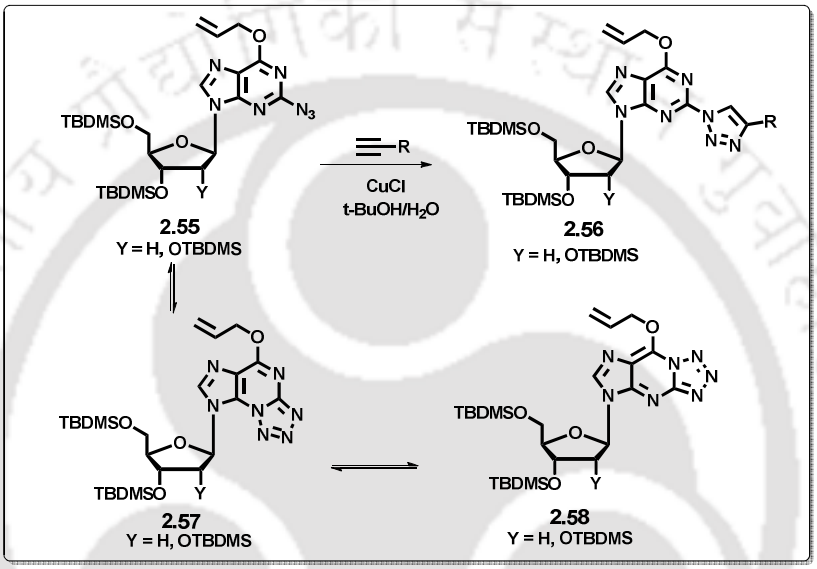

Scheme 2.12: Synthesis of C-2 triazolylinosine derivatives using the Cu(I) catalysed click reaction.

Seela *et al.*[36] have synthesized fluorescent nucleosides (**Figure 2.4**) by click conjugation between 7-deazapurine and 8-aza-7-deazapurine nucleosides related to dA and dG bearing 7-octadiynyl or 7-tripropargylamine side chains with 1-azidomethyl pyrene and studied the fluorescence property. Octadiynyl derivative showed only monomer fluorescence, while the tripropargylamine derivatives caused excimer emission due to the proximal alignment of pyrene residues. 8-Aza-7-deazapurine pyrene "click" conjugates exhibited fluorescence emission much higher than that of 7-deazapurine derivatives because in the later case the fluorescence was quenched by intramolecular charge transfer between the nucleobase and the dye.

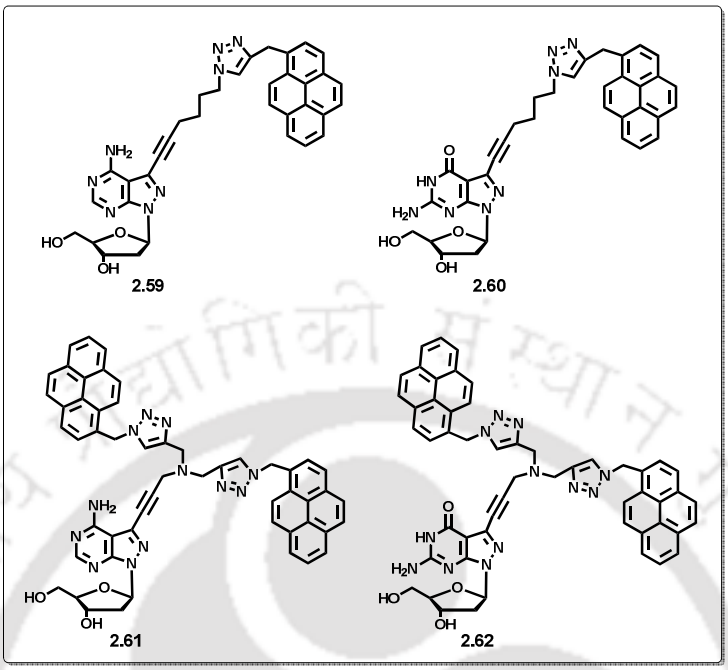

Figure 2.4: Fluorescent pyrene "click" conjugate nucleosides of different linker length.

A novel three step approach for the synthesis of N^6-substituted-2-(1,2,3-triazol-1-yl)-adenine nucleosides have been described by Maris Turks *et al.*[37a] The second step of their synthesis involved the Cu(I) catalysed cycloaddition reaction of 2,6-diazidopurine nucleosides resulting in the formation of 2,6-bis-(1,2,3-triazol-1-yl) purine nucleosides which was undergone regioselective nucleophilic aromatic substitution with amines at C(6) position (**Scheme 2.13**). The resulting compounds exhibited interesting levels of fluorescence with quantum yields of up to 53%. Later on, they have synthesized 2,6-bis-(triazolyl)purine analogues by double azide–alkyne 1,3-dipolar cycloaddition (CuAAC) reactions of 2,6-diazidopurine derivatives which underwent selective nucleophilic aromatic substitution with various thiols at C(6) position to afford thiopurine nucleosides (**Scheme 2.13**).[37b] These 2,6-bis-(triazolyl) nucleosides were prepared for synthetic interest so that it can be used as substrate for further reactions and/or application in DNA.

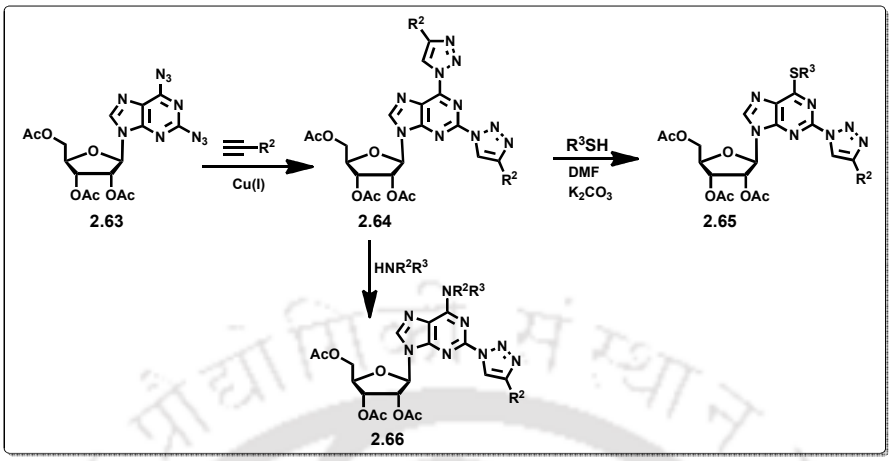

Scheme 2.13: Cu(I) catalyzed cycloaddition reaction of 2,6-diazidopurine ribonucleosides.

Triazolyl-*N*-methylpyrene decorated 7-deazapurines have been synthesized by Seela *et al.* to test the photophysical properties and duplex stability.[38] The pyrene was connected to C-7 of 7-deaza-2′-deoxyguanosine or to the 2′-deoxyribofuranose moiety through triazolyl linkers of different length (**Figure 2.5**). These modified bases were tested for their ability to stabilize the DNA duplex. Thus, it was observed that the nucleoside **2.68** with rigid triazolyl N-methyl pyrene moiety destabilized DNA while the nucleoside **2.67** containing the same fluorophore *via* a flexible acetylenic linker stabilized the DNA.

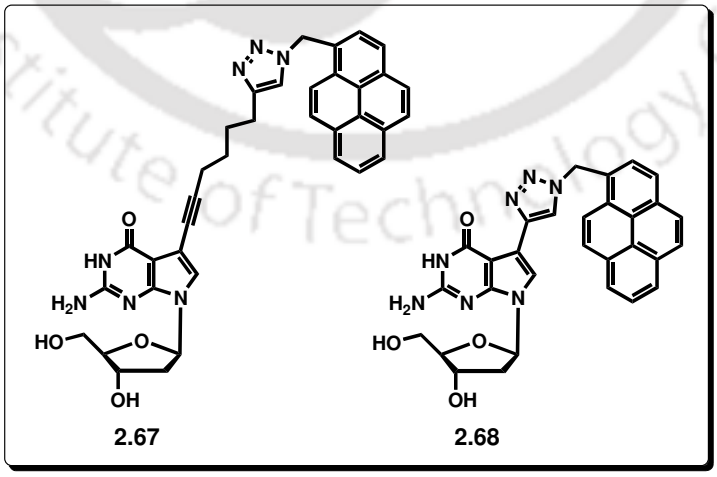

Figure 2.5: Fluorescent nucleosides decorated with pyrene using click chemistrty.

2.2.5. Modification of the Nucleobases

Recently click chemistry is being adopted to replace the natural DNA bases and thus, to generate a set of new nucleoside analogues usable in biological and biophysical applications. As for an example, Nakahara *et al.*,[39] reported the synthesis of triazolyl DNA using click chemistry. Thus, the oligonucleotides containing 1-ethynyl-2- deoxy-β-D-ribofuranose were reacted with a series of azides using the Cu(I)-catalyzed click reaction to produce ODNs containing artificial triazole nucleobases (**Scheme 2.14**). The thermal denaturation study of the post synthetically modified DNAs was done and the T_m values were compared with ethynyl modified ODN and the natural ones. It was observed that the oligonucleotide bearing a (phenylthio)methyl group was more favourable for duplex formation as compared to its benzyl counterpart because of the hydrophobicity induced by an additional sulfur atom to the nucleobase. The oligonucleotide **2.71** formed equally stable duplexes with all the ssDNA containing the natural bases which makes it a non-discriminatory nucleobase, namely a universal base.

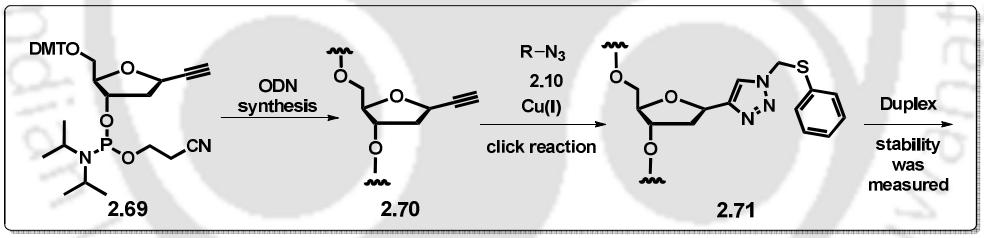

Scheme 2.14: Synthetic scheme of triazolyl DNA by postsynthetic modification of DNA *via* click reaction.

Benhida *et al.* reported a highly efficient microwave-assisted solvent-free synthesis of α- and ß-2′deoxy-1,2,3-triazolyl nucleosides.[40] This methodology comprising of microwave activation coupled with Cu(I) catalysis dramatically increased the rate of the 1,3-dipolar cycloaddition reaction between the azido-2′-deoxyribose and terminal alkynes (**Scheme 2.15**). In the same manner, Ermolat'ev *et al.*[41](**Scheme 2.16**) and Broggi *et al.*[42](**Scheme 2.17**) reported that the 1,3-cycloaddition can be accomplished in high yield within few minutes using microwave irradiation. These nucleosides have been generated out of synthetic interest mainly with the aim of conducting the reactions under neat conditions within a short time.

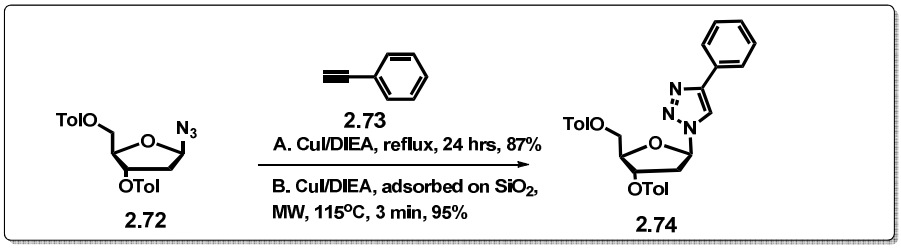

Scheme 2.15: Synthesis of 1,2,3-triazolo nucleoside analogues by microwave irradiation.

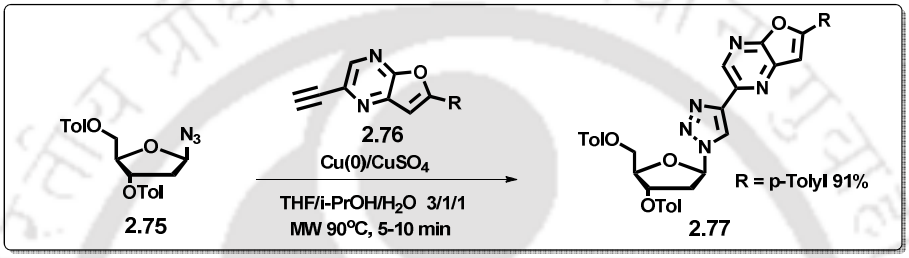

Scheme 2.16: Synthesis of 1,2,3-triazolo nucleoside analogues using microwave irradiation.

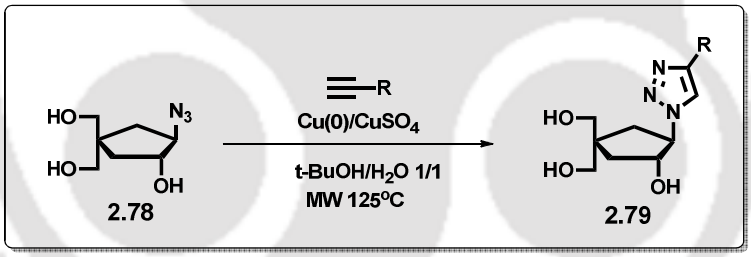

Scheme 2.17: Synthesis of 1,2,3-triazolo carbanucleoside analogues using microwave irradiation.

Driowya *et al.*[43] have developed a clean and efficient one-pot procedure involving a cooperative effect of iron-copper catalysis and ultrasound activation to generate triazolyl nucleosides. This one-pot procedure is simple to operate, gives high yield, is a safe and environment friendly protocol. The anticancer activity of the resulting substituted nucleosides were evaluated against K562 chronic myelogenous leukemia (CML) cell line and some of the synthesized compounds were found to be more active than 5-amino-1-β-D-ribofuranosyl-imidazole-4-carboxamide(AICAR) to kill CML cancer in K562 cell line. Pradere *et al.* reported the preparation of ribavirin analogues by copper- and ruthenium-catalyzed azide-alkyne 1,3-dipolar cycloaddition as a part

of the drug discovery program.[44] The synthesis of 1,4- and 1,5-disubstituted-1,2,3-triazolo-nucleosides from various alkynes with 1′-azido-2′,3′,5′-tri-O-acetylribose using either copper-catalyzed azide-alkyne cycloaddition (CuAAC) or ruthenium-catalyzed azide-alkyne cycloaddition (RuAAC), respectively was described (**Scheme 2.18**). The commercially available [Cp*RuCl(PPh$_3$)$_2$] was used for the ruthenium-catalysed reaction under microwave assisted conditions which led to significant enhancement of the reaction rate.

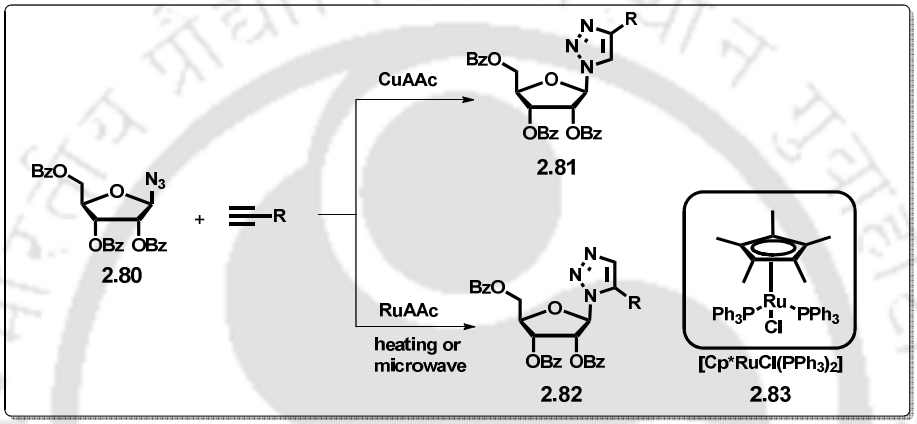

Scheme 2.18: Synthesis of 1,2,3-Triazolo Nucleoside Analogues by (CuAAC) and (RuAAC)

Benhida *et al.*[45] have reported the efficient synthesis and in vitro cytostatic activity of 4-substituted triazolyl-nucleosides. The nucleosides were synthesized by Cu(I) catalysed 1,3-dipolar cycloaddition between 1-azido-ribose 2 and terminal alkynes under a cooperative effect of microwave conditions. Structure–activity relationship study showed that the nucleosides bearing a C8 alkyl chain or *p*-methoxyphenyl on the triazolyl ring are the most active compounds and can be used as lead compounds in cancer chemotherapy.

2.3. Background

From the above discussion it is clear that there exist numerous examples of natural/unnatural nucleosides decorated with triazole moiety and generated *via* click chemistry. Moreover, the design of unnatural nucleobases/nucleobase analogues considered mostly the base pairing ability of those nucleobase in the context of DNA

either *via* H-bonding or π-π stacking or hydrophobic interactions. Furthermore, in many of the examples, the triazole moiety has been utilized as a linker either to link the fluorophore with the natural bases or as a replacement of phosphodiester linkage. However, there exist a few examples of triazolyl nucleoside bases wherein the nucleobases have been replaced by the triazole units. The focus of the synthesis of these triazolyl nucleobases was mainly of synthetic interest or to generate a set of biologically active nucleosides.

While in the design of unnatural nucleobases, a great deal of efforts have been paid in considering H-bonding mimicry or force like π-π stacking/hydrophobic interaction, the force like charge transfer complexation has not been considered in the context of DNA base design. Interactions among the unnatural donor-acceptor nucleobases *via* charge transfer complexation have not been considered which might have potential impact on DNA duplex stabilization.

2.4. Objective

The literature search revealed that donor and/or acceptor aromatic linked click triazoles as unnatural nucleobase surrogates has not been explored.[46] Moreover, till the date, in the development of unnatural bases, the charge transfer interaction among the hetero-pair is not considered. About sixty years ago, Mulliken suggested that the charge-transfer (CT) complexes "may afford new possibilities for understanding intermolecular interactions in biological systems".[47] Since then several biochemical phenomena are being explained based on CT interactions.[48] The charge-transfer along with the π-stacked complexes between the base pairs may afford new possibilities for understanding intermolecular interactions in biological systems, for stabilizing the unnatural base pairs, for developing DNA diagonostic and sensing materials.[49-50] Therefore, it would be of great importance if one can explore the charge transfer interaction force *via* the design of unnatural aromatic base analogues and exploit their efficient charge transfer complexation property which ultimately may lead to an efficient base pair with tuned photophysical properties applicable for the design of DNA diagnostic and sensing materials.[47-50]

Therefore, as a part of our ongoing research effort towards generation of molecules with tuned photophysical properties *via* click reaction,[51] we thought that it would be worthwhile to synthesize triazolyl nucleosides containing donor/acceptor aromatics to produce modulated photophysical response into the unnatural nucleosides (UNNs) to showcase the possible π-stacking as well as charge transfer interaction ability among donor/acceptor triazolyl aromatic nucleosides.

The logic behind our choice of triazole linked with donor/acceptor aromatics to be the nucleobases are:

(a) triazoles are metabolically inert;

(b) the triazole units are more than just passive linkers. They readily associate with biological targets, through hydrogen bonding and dipole interactions.

(c) We envisaged that the pseudoaromatic 1,2,3-triazole can modulate the electronic characteristics of the bases and endow new properties to the unnatural nucleosides.

(d) In addition, if incorporated into a DNA sequence, the triazole as well as aromatic units may play an important role in stabilizing a DNA duplex *via* π-stacking interaction.

(e) Strategically placed triazolyl isosteres can also improve charge transfer interaction properties if incorporated into a DNA.

Utilizing this concept and aim we framed our objective as below:

(a) Design and synthesis of unnatural triazolyl nucleosides with donor-acceptor property *via* azide-alkyne cycloaddition chemistry (**Scheme 2.19**)

(b) Study of photophysical properties of some of them.

(c) Evaluation of their ability to show ground state charge transfer interaction property in a donor-acceptor pair nucleosides.

The idea of our design of unnatural triazolyl nucleobases linked with donor/acceptor aromatic units capable of showing possible charge transfer interaction mainly to uncover the charge transfer (CT) complexation property in solution of a designed pair of nucleoside. This pair might be a candidate base pair of a DNA duplex stabilized by the charge transfer (CT) interaction between the pairing bases.

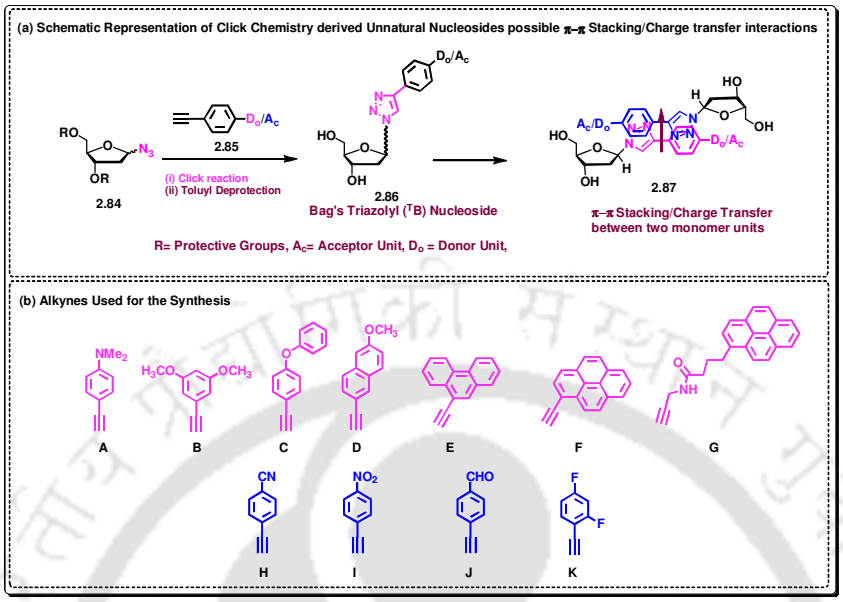

Scheme 2.19: (a) Schematic representation of triazolyl unnatural nucleosides (UNN) and (b) the alkynes used in this study.

2.5. RESULTS and DISCUSSION

2.5.1. Synthesis of Triazolyl Donor/Acceptor Nucleosides

The synthesis of the new class of donor/acceptor triazolyl nucleosides involves the popular 1, 3-dipolar azide-alkyne cyclization pathway as a key step which is shown in **Scheme 2.20**. The synthesis started with 2-deoxy ribose sugar **2.88** which was converted to its 1-*O*-methyl derivative. Subsequent treatment of 1-*O*-methyl-2-deoxy **2.89** ribose with *p*-toluoyl-chloride in pyridine afforded the bis-toluoyl protected sugar **2.90** with very good yield (70%). The treatment of dry HCl gas in a moderately dilute etherial solution of 1-*O*-methyl-3, 5-di-O-p-toluoyl-2-deoxy ribose sugar **2.90** yielded corresponding Hoffer's chlorosugar **2.91** with good yield (59%). Two different methods for the synthesis of starting azidosugar, 2-deoxy-3,5-bis[*O*-(*p*-toluoyl)]-β-D-ribofuranosyl azide, have been described[52a-c] till date. In **method A**, we have used trimethylsilyl azide (TMS-azide) and in second **method B**, cesium azide (CsN_3) has been used to react with Hoffer's chlorosugar to afford azidosugar.[52d] The former one gives 21% as the overall yield while the latter one gives 90% as the

overall yield of the bis-toluoyl protected β-azido nucleoside. The bis-toluoyl protected triazolyl nucleosides are prepared *via* click reaction between the azidosugar, 2-deoxy-3,5-bis[*O*-(*p*-toluoyl)]-β-D-ribofuranosyl azide and aromatic alkynes. The bis-toluoyl protected triazolyl nucleosides are then deprotected using a standard deprotection reaction (**Scheme 2.23**). We utilized method A and method B, respectively, for the preparation of precursor α- and ß- azido nucleoside. Thus, both the epimers were reacted separately with various aromatic alkynes (**2.85A-K**, **Scheme 2.22b**) containing donor/ acceptor substituents in presence of click reagents at 60 ^{o}C in THF to afford our desired triazolyl donor/acceptor nucleosides in good yields (80-90%, **Table 2.1**). All the products were characterized by NMR, mass, IR, melting temperatures and in three cases by single crystal X-ray analysis. The α-epimers were synthesized aiming to incorporate into short oligonucleotide sequences to check the thermal stability of the α-DNA[53] as well with β-DNA context. β-epimers are the building blocks of natural DNA.

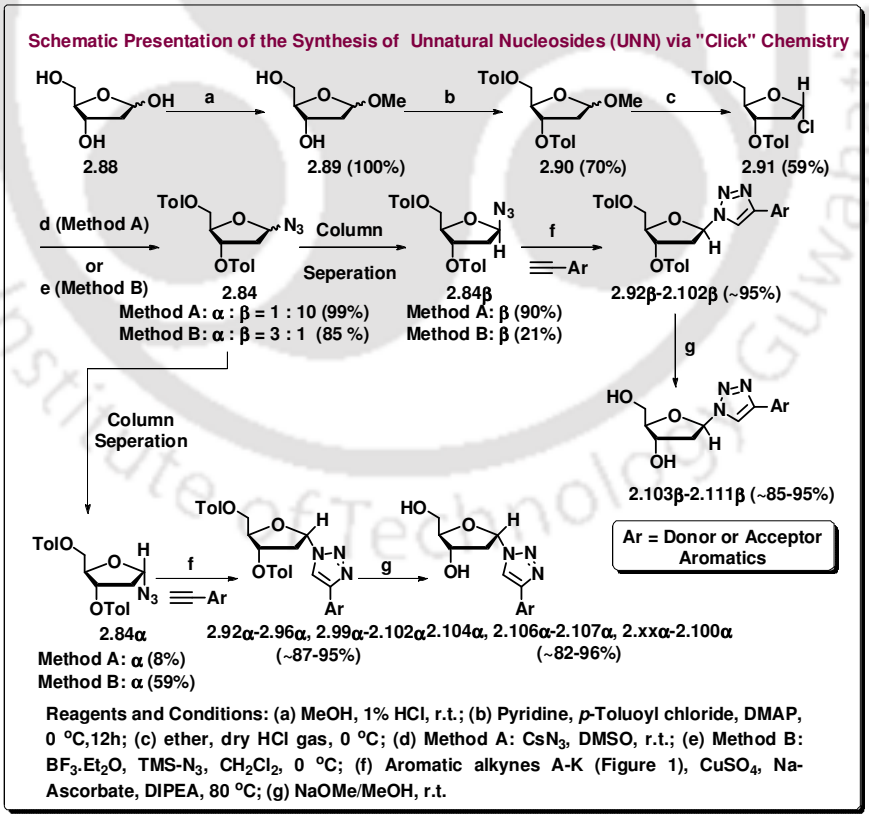

Scheme 2.20: Synthesis of triazolyl UNNs.

Table 2.1: Summary of yield of toluoyl protected and deprotected alpha- and beta-triazolyl donor/acceptor nucleosides.

Entry	Alkynes	Nucleosides [R = toluoyl or H]	Yield %[a]	
			α-isomer (Nucleoside No.)	β-isomer (Nucleoside No.)
1	**A**	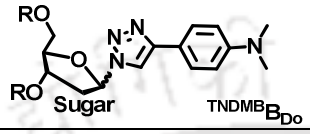 $^{TNDMB}B_{Do}$	**87** (2.92α)	**97** (2.92β)
			---	**91**(2.103β)
2[b]	**B**	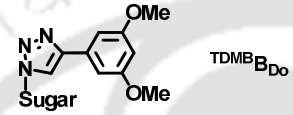 $^{TDMB}B_{Do}$	**95** (2.93α)	**99** (2.93β)
			95 (2.104α)	**95** (2.104β)
3	**C**	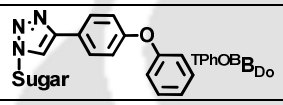 $^{TPhOB}B_{Do}$	**52** (2.94α)	**90** (2.94β)
			---	**91** (2.105β)
4	**D**	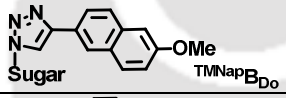 $^{TMNap}B_{Do}$	**98** (2.95α)	**99** (2.95β)
			86 (2.106α)	**88** (2.106β)
5[b]	**E**	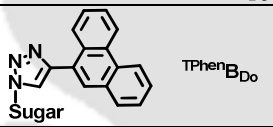 $^{TPhen}B_{Do}$	**96** (2.96α)	**95** (2.96β)
			86 (2.107α)	**92** (2.107β)
6	**F**	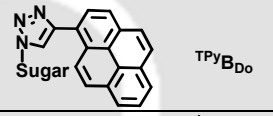 $^{TPy}B_{Do}$	---	**85** (2.97β)
			---	**81** (2.108β)
7	**G**	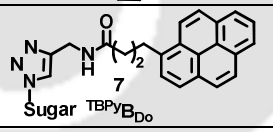 $^{TBPy}B_{Do}$	---	**95** (2.98β)
			---	**83** (2.109β)
8[b]	**H**	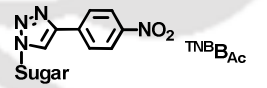 $^{TNB}B_{Ac}$	**98** (2.99α)	**93** (2.99β)
			82 (2.110α)	**91**(2.110β)
9[b]	**I**	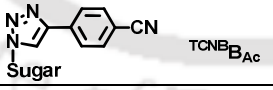 $^{TCNB}B_{Ac}$	**95** (2.100α)	**90** (2.100β)
			94 (2.111α)	**91**(2.111β)
10	***J***	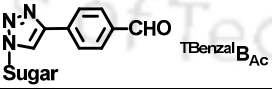 $^{TBenzal}B_{Ac}$	**79** (2.101α)	**97** (2.101β)
			---	---
11	**K**	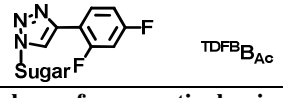 $^{TDFB}B_{Ac}$	**99** (2.102α)	**86** (2.102β)
			---	---

[a]Yields of each top column for a particular isomer are for R = toluoyl and for bottom column R = H. [b]See ref. 16 for the β-isomers of entry 2, 5, 8 and 9.

2.5.2. Structural Characterization

The nucleosides β-conformation was established *via* NOESY spectra as well as *via* single crystal X-ray structure of $^{TPhen}\mathbf{B}_{Do}$ and $^{TNB}\mathbf{B}_{Ac}$. The NOESY spectra of the representative nucleoside **2.107β** (**Figure 2.6a**) showed the presence of cross peak between H1'- H4', H1'- H2'α, H1'- HTriazole and HTriazole - HAryl. The nucleosides α-conformation was also established *via* NOESY spectra of $^{TPhen}\mathbf{B}_{Do}$ as well as *via* single crystal X-ray structure of $^{TMNap}\mathbf{B}_{Ac}$. The NOESY spectra of the representative nucleoside **2.107α** (**Figure 2.6b**) showed the presence of cross peak between H1'- H2'β, H1'-HTriazole and HTriazole - HAryl but the absence of any cross peak between H1'- H4' which was present in the β-isomer.

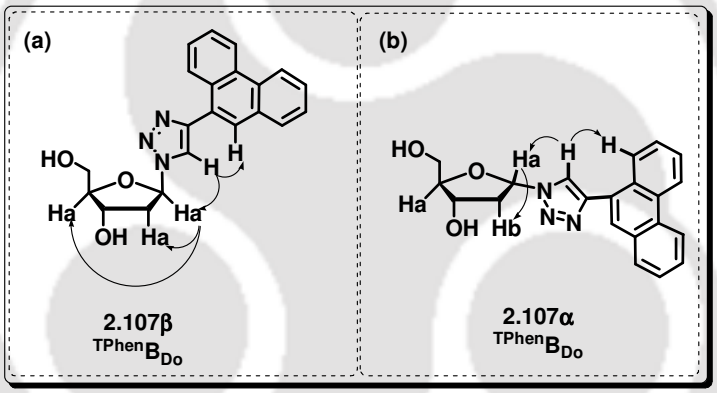

Figure 2.6: Presentation of NOESY cross peak in the two representative β-and α-nucleoside $^{TPhen}\mathbf{B}_{Do}$.

The crystal structure of $^{TPhen}\mathbf{B}_{Do}$ shows an intermolecular π-stacked and H-bonded helical layer network.[52d] The crystal packing shows that the intermolecular π-stacked and H-bonded helical layer network. Phenanthrene units are held by π-π stacking interaction among themselves and aromatic C-H--N bonding with triazole. The polar sugar parts are held together by strong H-bonding interaction among themselves and O-H--N bonding with triazole N-2 and N-3 (2.667 and 1.905 Å respectively). This suggests that the triazolyl phenanthrene nucleoside can indeed engage in H-bonding as well π-stacking interaction (**Figure 2.7**). The crystal structure of the $^{TPhen}\mathbf{B}_{Do}$ nucleoside shows a twist between the triazole and the phenanthrene. Therefore, all rings of the phenanthrene unit may be unable to engage fully in stacking interaction

upon incorporation into a DNA. However, it is possible that the third ring of phenanthrene can involve in groove binding stabilization event leaving other rings for stacking interaction with the bases in a duplex DNA. The crystal parameters of the compound $^{TPhen}\mathbf{B_{Do}}$ (**2.107β**) are given below in **Table 2.2**.

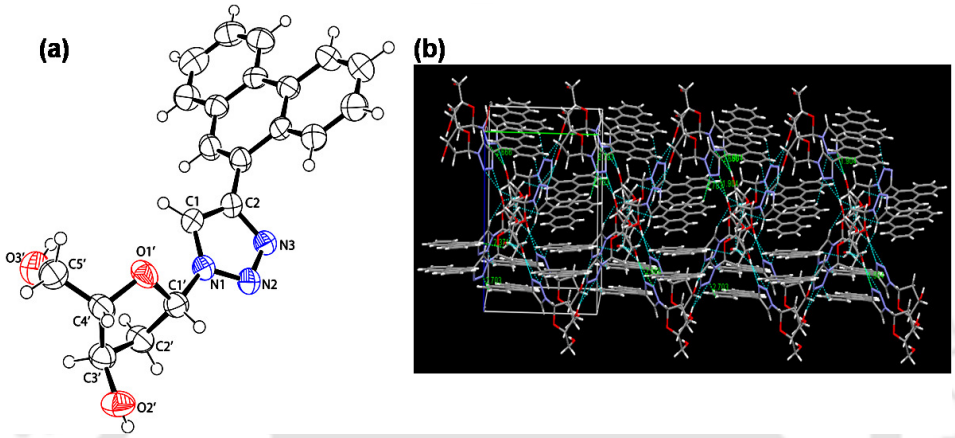

Figure 2.7: (a) ORTEP molecular diagram with thermal ellipsoid at 50% probability, and (b) of $^{TPhen}\mathbf{B_{Do}}$. The crystal structure showing π-π/CH….π and Ar-CH…N/OH…N hydrogen-bonded network with stacked layer of $^{TPhen}\mathbf{B_{Do}}$.

On the other hand, both the packing diagram and crystal arrangement of $^{TNB}\mathbf{B_{Ac}}$ shows H-bonded helical layer chain like structure. Molecules of a single layer are held by H-bonding between sugar CH_2OH….ONO-of nitrobenzene. Another ONO- of one layer involve in H-bonding with sugar CH_2OH of second layer. The two adjacent layers are also involved in stabilized π-stacking interaction between phenyl ring of π-nitrobenzene of one layer and closely spaced triazole ring of another layer (**Figure 2.8**). The nitrobenzene and the triazole moiety of $^{TNB}\mathbf{B_{Ac}}$ are in the same plane that would allow the triazolylnitrobenzene unit to take part in intercalation/or in full stacking interaction within the nucleobases inside a DNA duplex after incorporation into DNA. These all suggested that the triazolyl phenanthrene/nitrobenzene nucleoside can indeed engage in H-bonding as well π-stacking interaction if incorporated in DNA. The crystal parameters of the compound $^{TNB}\mathbf{B_{Ac}}$ (**2.110β**) are given below in **Table 2.2**.

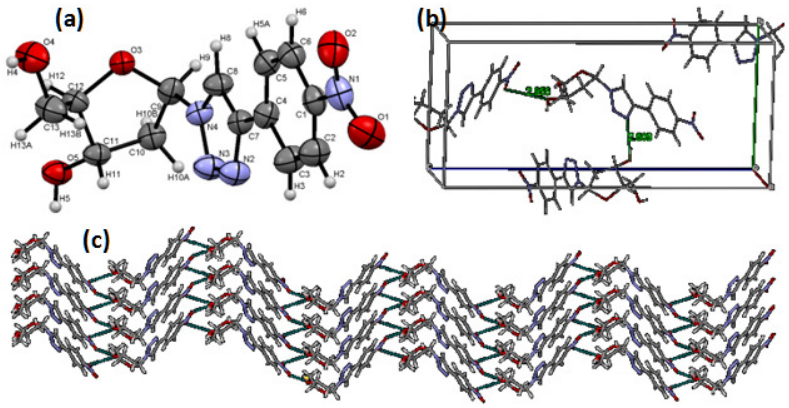

Figure 2.8: (a) ORTEP (50% thermal ellipsoid) diagram, (b) crystal packing and (c) π-stacked and H-bonded helicallayer network of $^{TNB}\mathbf{B}_{Ac}$ nucleoside.

The nucleosides α-configuration has also been established *via* single crystal X-ray structure of α-$^{TMNap}\mathbf{B}_{Do}$. The crystal packing and arrangements of α-$^{TMNap}\mathbf{B}_{Do}$ shows H-bonded corrugated sheet like layer structure. The two corrugated planes (each plane containing two layers making a sheet) are held together *via* Van-der Waals and H-bonding interactions. First layers of each plane are held by Van-der Waals (2.387 Å) interaction between naphthylmethoxy-H of first plane and 5'-CH_2-H of sugar unit of second plane. Similarly, second layers of each plane are held by weak H-bonding (2.657 Å) interaction between naphthylmethoxy-O of first plane and 3'-CH-H of sugar unit of second plane. Each layer of a plane is held together *via* both intramolecular H-bonding (2.030 Å, between triazolyl N_2- and 3'-OH-H) and intermolecular H-bonding (2.714 Å, between triazolyl 3'-OH and 5'-OH of sugar units). The two layers of a plane are held *via* π-π stacking interaction in T-shaped fashion between two aromatic units of each layer *via* aromatic CH-π-interaction and weak H-bonding interaction (2.836 Å and 2.826 Å, respectively) between 2'-OH of sugar of one layer and pyranose ring -O- of sugar of second layer. Interestingly, each plane runs anti-parallel with respect to pyranose sugar unit. Most importantly, the crystal arrangement follows unidirectional growth along c-axis (**Figure 2.9**). The crystal parameters of the compound α-$^{TMNap}\mathbf{B}_{Do}$ (**2.106α**) are given below in **Table 2.2**.

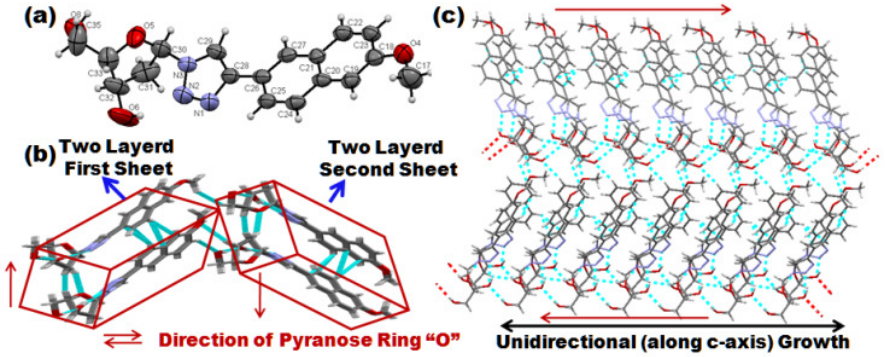

Figure 2.9: (a) ORTEP (50% thermal ellipsoid) diagram, (b) crystal packing and various interactions and (c) π-stacked and H-bonded corrugated sheet like network of α-$^{TMNap}\mathbf{B}_{Do}$ nucleoside.

Table 2.2: The crystal parameters of compounds **2.106α**, **2.107β**, **2.110β**.

Data	**2.106α**	**2.107β**	**2.110β**
Z	4	4	4
Molecular Formula	$C_{18}H_{19}N_3O_4$	$C_{21}H_{19}N_3O_3$	$C_{13}H_{14}N_4O_5$
Temperature (K)	296	296	296
Space Group	P 21 Monoclinic	P 21 21 21 Orthorhombic	P 21 21 21 Orthorhombic
a (Å)	5.808(7)	10.054(3)	6.4456(7)
b (Å)	29.856(4)	12.268(3)	9.8102(8)
c (Å)	9.539(11)	12.268(3)	21.8210(19)
α (degree)	90	90	90
β degree)	90.185	90	90
γ (degree)	90	90	90
M_r	341.36	361.39	306.28
V (Å^3)	1654.2(4)	1732.4(8)	1379.8(2)
μ (mm^{-1})	0.099	0.095	0.116
F(000)	720.0	760.00	640.0
R(reflections)	0.0478(2923)	0.0522(1789)	0.0509(1701)
wR2(reflections)	0.1066(4410)	0.1184(3116)	0.1143(3180)
Correction method	Multi Scan	Multi Scan	Multi Scan

2.5.3. Study of Photophysical Properties

After getting all the nucleosides in hand, we have studied their UV-visible and fluorescence photophysical properties. Previously we and subsequently others have shown that linking of fluorescent/non-fluorescent unit with a triazole moiety could lead to the installation of fluorescence emission properties to the non-fluorescent molecules and/or modulation of the same to a fluorescent molecule.[51] The synthesized nucleic acid building blocks (2'-deoxyribosides) also behaved in a similar way with respect to their photophysical properties. We studied the photophysical properties of few of our synthesized β-nucleosides in various solvents. The nucleoside **2.103β** ($^{TNDMB}\mathbf{B}_{\mathbf{Do}}$) containing a *N,N*-dimethylaminobenzene exhibits very strong absorption maxima at around 270-280 nm in various organic solvents with ~5 nm solvatochromicity. Excitation at absorption maxima of each solvent shows emission at around 365 nm with a red shift of 10 nm as the solvent polarity increases. While the nucleoside exhibits a long wavelength emission, most probably an intramolecular charge transfer (ICT) band,[54-55] at 485 nm in polar solvents like DMF, DMSO and in acetonitrile, the fluorescence intensity become negligible in polar protic solvents like EtOH and MeOH. The quenched incidence of fluorescence can be attributed to the H-bonding mediated radiationless decay of the chromophore in polar protic solvents (**Figure 2.10a-b**).[56] The nucleoside **2.104β** ($^{TDMB}\mathbf{B}_{\mathbf{Do}}$) containing a 3,5-dimethoxybenzene exhibits very strong absorption maxima at around 252-270 nm and weak band at around 290 nm in various organic solvents. Excitation at absorption maxima of each solvent shows emission at around 320 nm with irregular trend in intensity as the solvent polarity increases (**Figure 2.10c-d**).

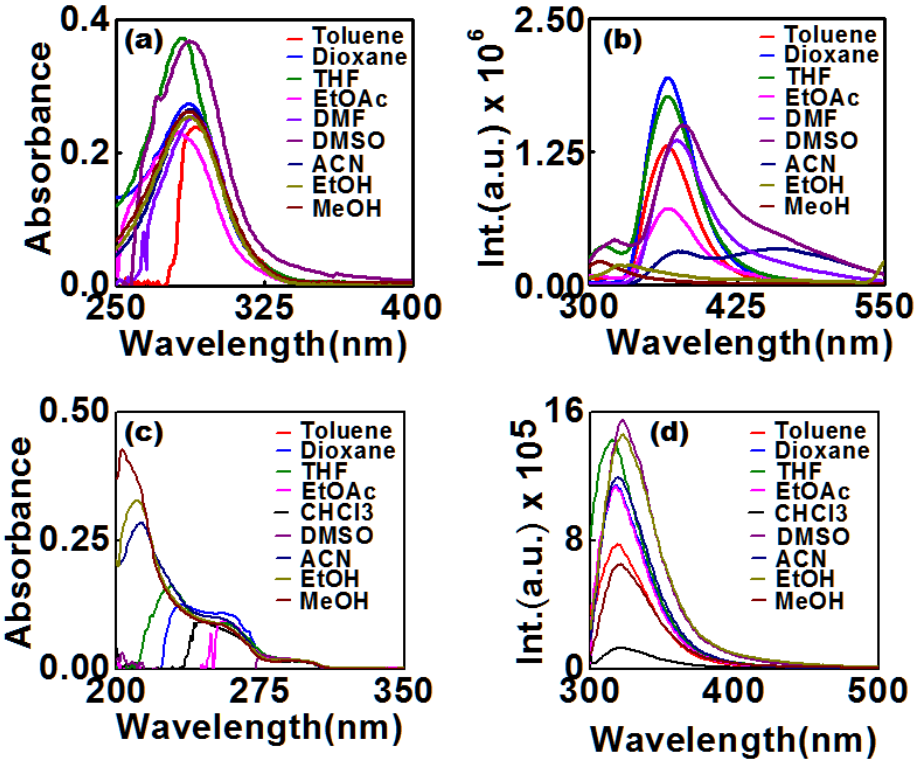

Figure 2.10: UV-visible and fluorescence spectra of nucleoside **2.103β** (a-b) and nucleoside **2.104β** (c-d) in various organic solvents (concentration of each nucleoside was 10 μM). Negative absorbances are due to solvent cut off.

The nucleoside **2.105β** ($^{TPhOB}B_{Do}$) which is a phenoxyphenyltriazole nucleobase possess structureless absorption maxima at around 257-260 nm with little or no solvatochromicity or change in absorbance in all organic solvents tested. Excitation at absorption maxima of each solvent shows structureless emission at around 333 nm with a quenched incidence of fluorescence as the polarity of the solvent increases (**Figure 2.11a-b**).

The nucleoside **2.106β** ($^{TMNap}B_{Do}$) containing a methoxynapthalene aromatic unit exhibits very strong absorption with vibronic structures at 285, 290 and 302 nm in lowest polar solvent toluene. The absorbance is characterized by a hypsochromic shift (2-5 nm) and little hyperchromism as the polarity of the solvent increases. Excitation at absorption maxima (290-300 nm) of each solvent shows emission at around 365 nm with increase in intensity as the solvent polarity increases (**Figure 2.11c-d**).

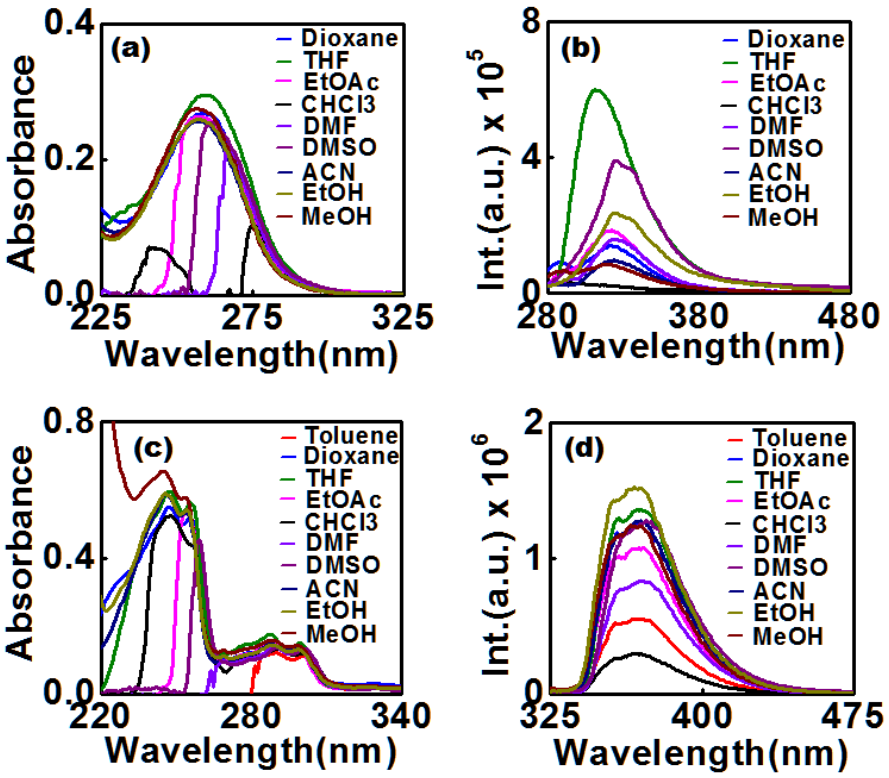

Figure 2.11: UV-visible and fluorescence spectra of nucleoside **2.105β** (a-b) and Nucleoside **2.106β** (c-d) in various organic solvents (concentration of each nucleoside was 10 μM).

The $^{TPhen}\mathbf{B}_{Do}$ (**2.107β**) nucleoside shows blue shifted absorbance as the polarity of the solvent increases (λ_{max} = 302 nm in dioxane → 298 nm in MeOH). Upon excitation at 300 nm, $^{TPhen}\mathbf{B}_{Do}$ shows structured bands at 363 and 380 nm with similar intensities and low quantum yields in all solvents (**Figure 2.12a-b, Table 2.2**). Triazolylpyrene nucleoside $^{TPy}\mathbf{B}_{Do}$ (**2.108β**) shows structureless absorption at 355 nm in toluene which is blue shifted to 348 nm with increase in absorbance as the solvent polarity increases showing an electronic coupling of pyrenyl π-electron cloud with triazole unit. However, it shows a structure emission when excited at 350 nm with appearance of prominent maxima at 387 and 408 nm of similar intensities and quantum yields as the polarity of the solvent increases (**Figure 2.12c-d, Table 2.2**). The fluorescence life time data also supports this observation. On the other hand, the nucleoside $^{TBPy}\mathbf{B}_{Do}$ (**2.109β**) containing a butylpyrene triazole exhibits very strong

absorption with vibronic structures characteristic of butylpyrene at 314, 329 and 346 nm in all solvents tested. The absorbance is characterized by a hypsochromic shift (2-5 nm) and little hyperchromism as the polarity of the solvent increases. Excitation at absorption maxima (~350 nm) in each solvent shows structure emissions at 380, 401, and 421 nm with increase in intensity as the solvent polarity increases. The fluorescence life time data also supports this observation (**Figure 2.13a-b, Table 2.2**).

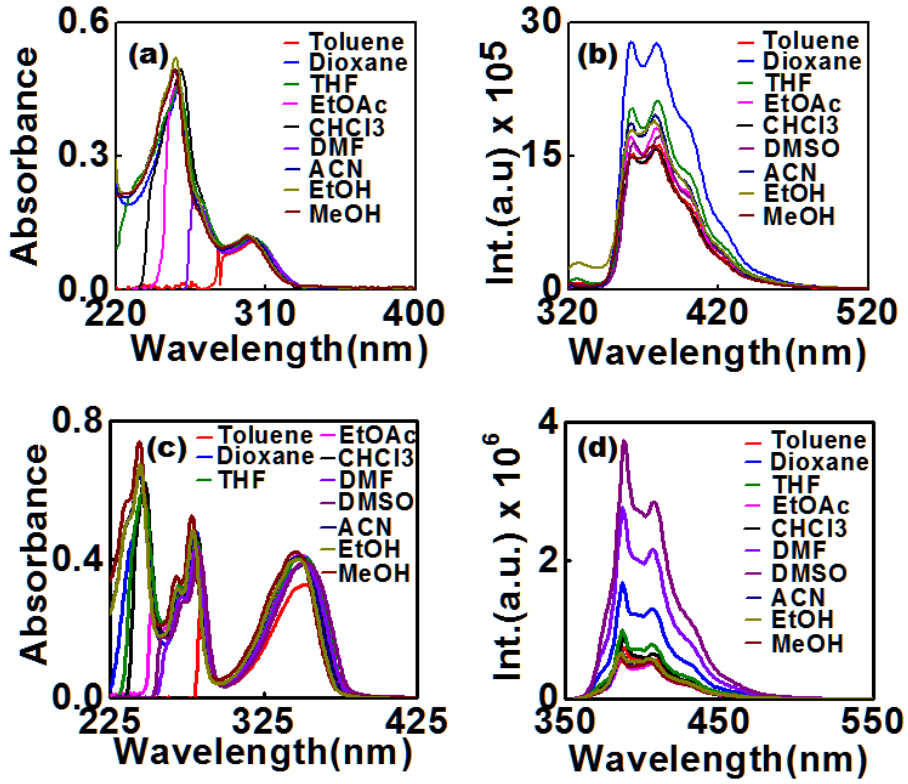

Figure 2.12: UV-visible and fluorescence spectra of nucleoside **2.107β** (a-b) and nucleoside **2.108β** (c-d) in various organic solvents (concentration of each nucleoside was 10 µM).

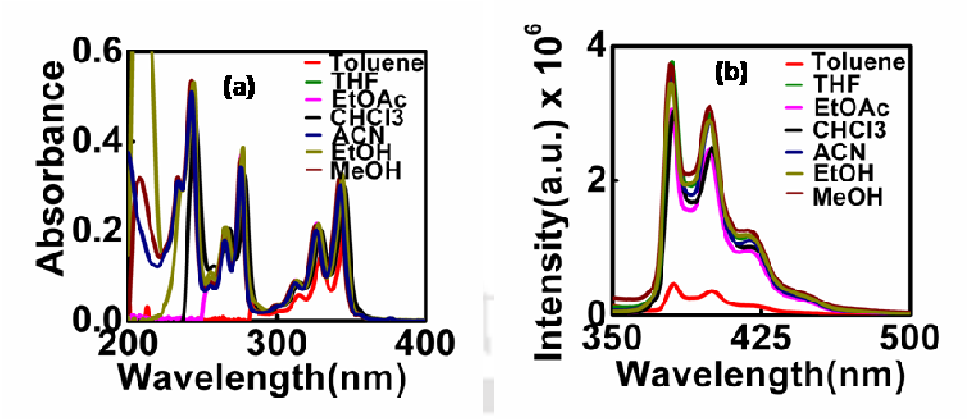

Figure 2.13: UV-visible and fluorescence spectra of nucleoside **2.109β** (a-b) various organic solvents (concentration of each nucleoside was 10 μM).

The nucleoside **2.111β** ($^{TCNB}\mathbf{B}_{Ac}$) containing a cyanobenzene acceptor aromatic unit possess very strong structureless absorption at 287 nm in lowest polar solvent toluene. The absorbance is characterized by a hypsochromic shift (2-5 nm) and hyperchromism as the polarity of the solvent increases. Excitation at 280 nm shows emission at around 315 nm in toluene which becomes broad with an appearance of a red shifted hump (at 335 nm in EtOAc→353 in MeOH) of increased intensity as the solvent polarity increases. This broaden band is most probably the ICT emission (**Figure 2.14c-d**). In summary all the triazolyl aromatic nucleosides shows a significantly red-shifted absorption and emission properties from those of the parent aromatics. It is also obvious that the emission intensity, wavelength and quantum yields are higher than any of the natural nucleosides.

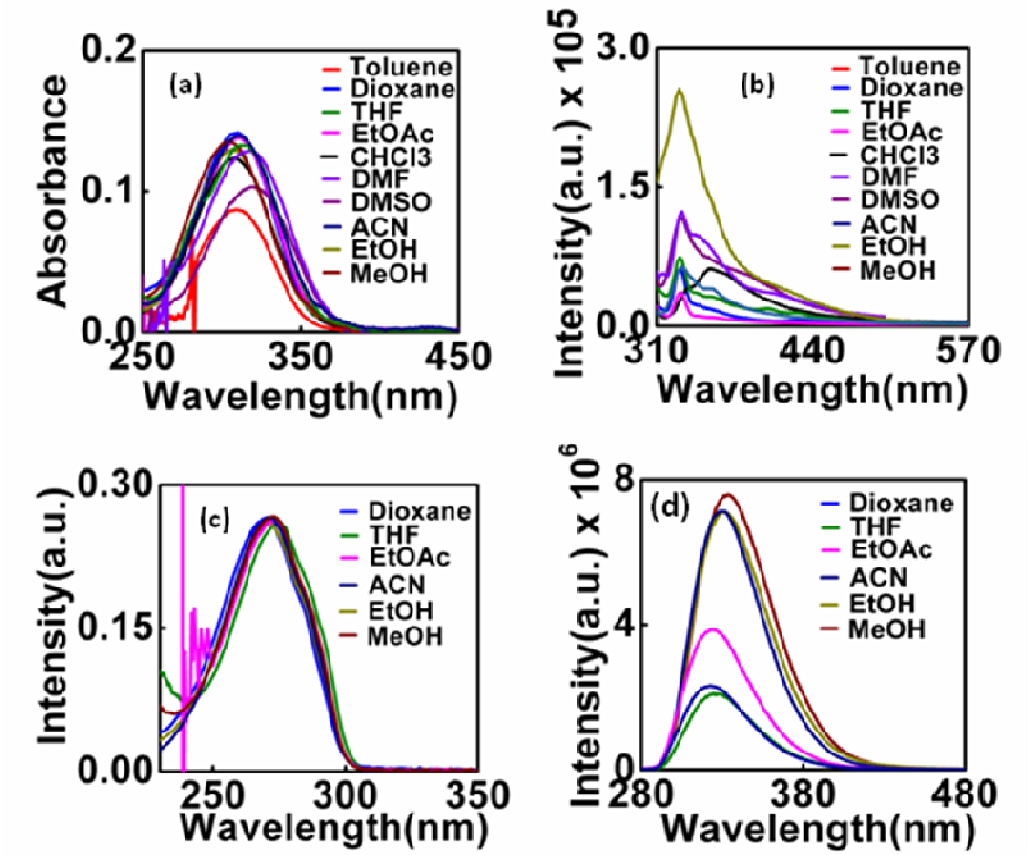

Figure 2.14: UV-visible and fluorescence spectra of nucleoside **2.110β** (a-b) and nucleoside **2.111β** (c-d) in various organic solvents (Concentration of each nucleoside was 10 μM).

Table 2.3: Summary of UV and Fluorescence of $^{TNDMB}B_{Do}$(**2.103β**), $^{TDMB}B_{Do}$(**2.104β**), $^{TPhOB}B_{Do}$(**2.105β**).

Entry	Solvents	Δf	UV-Vis & Fluorescence		
			λ_{abs} *(nm)*	ε_{max}	λ_{fl} *(nm)*
$^{TNDMB}B_{Do}$ **(2.103β)**	Toluene	0.013	290.5	23900	366
	Dioxane	0.021	287	27400	366
	THF	0.21	283	27300	366
	EtOAc	0.201	281	23140	367
	DMF		289	25450	374
	DMSO	0.265	287	36900	380
	ACN	0.305	288	26560	376
	MeOH	0.309	287	26240	309
$^{TDMB}B_{Do}$ **(2.104β)**	Dioxane	0.021	295, 258	1550, 10610	318
	THF	0.21	295, 257	1440, 7370	315
	EtOAc	0.21	295, 257	1670, 9190	317
	CHCl3	0.148	295, 257	1380, 8740	320
	DMSO	0.265	295	1620	322
	ACN	0.305	295, 256	1620, 9640	320
	EtOH	0.29	294, 256	1670, 8460	323
	MeOH	0.309	294, 256	1470, 8350	321
$^{TPhOB}B_{Do}$ **(2.105β)**	Dioxane	0.021	259	26730	323
	THF	0.21	259	29430	312
	EtOAc	0.201	257	26260	321
	DMF		267	21740	325
	DMSO	0.265	262	25290	329
	ACN	0.305	257	25630	324
	MeOH	0.309	257.5	27320	319
	EtOH	0.29	257.5	25830	329

Table 2.4: Summary of UV and Fluorescence of $^{TMNap}B_{Do}$(**2.106β**), $^{TPhen}B_{Do}$(**2.107β**) and $^{TPy}B_{Do}$(**2.108β**)

Entry	Solvents	UV-Vis and Fluorescence			
		λ_{abs} (nm)	ε_{max}	λ_{fl} (nm)	Φ_f
$^{TMNap}B_{Do}$ (**2.106β**)	Toluene	301	11232	369	---
	Dioxane	300	14060	369	---
	THF	299.5	14920	370	---
	EtOAc	298.5	14440	370	---
	DMF	300	13180	371	---
	DMSO	301.5	13340	373	---
	ACN	298.5	13670	369	---
	EtOH	299	12930	368	---
$^{TPhen}B_{Do}$ (**2.107β**)	Toluene	300	10330	378	0.095
	Dioxane	299	11020	376	0.167
	THF	299	11600	378	0.113
	EtOAc	298	11480	377	0.093
	CHCl3	299	11140	377	0.087
	ACN	297	11650	376	0.098
	EtOH	297	12090	375	0.097
	MeOH	295	11200	374	0.080
$^{TPy}B_{Do}$ (**2.108β**)	Toluene	353	32610	408	0.129
	Dioxane	351	41020	407	0.224
	THF	351	40680	407	0.134
	EtOAc	349	41220	407	0.084
	CHCl3	351	38590	407	0.122
	DMF	351	38710	407	0.393
	DMSO	351	39140	408	0.578
	ACN	348	40810	406	0.093
	EtOH	347	39610	406	0.103
	MeOH	346	40790	405	0.089

Table 2.5: Summary of UV and Fluorescence of $^{TOxoPy}\mathbf{B}_{Do}$(**2.109β**), $^{TNB}\mathbf{B}_{Ac}$(**2.110β**) and $^{TCNB}\mathbf{B}_{Ac}$(**2.111β**)

Entry	Solvents	UV-Vis and Fluorescence			
		λ_{abs} (nm)	ε_{max}	λ_{fl} (nm)	Φ_f
$^{TOxoPy}\mathbf{B}_{Do}$ (**2.109β**)	Toluene	345	34230	417	0.077
	THF	344	45200	417	0.093
	EtOAc	343	42770	417	0.064
	$CHCl_3$	345	38840	417	0.086
	ACN	343	40300	417	0.078
	EtOH	342	45650	417	0.087
	MeOH	342	41350	417	0.078
$^{TNB}\mathbf{B}_{Ac}$ (**2.110β**)	Toluene	312	8620	---	---
	Dioxane	312	14010	---	---
	$CHCl_3$	311	12220	---	---
	EtOAc	314	13600	---	---
	THF	316	13200	---	---
	EtOH	310	12820	---	---
	ACN	314	13770	---	---
	MeOH	308	13350	---	---
$^{TCNB}\mathbf{B}_{Ac}$ (**2.111β**)	Dioxane	270	26300	322	---
	THF	275	25800	326	---
	EtOAc	272	26180	324	---
	ACN	271	26600	330	---
	EtOH	271	25910	331	---
	MeOH	273	25710	333	---

After recording the UV-visible and fluorescence spectra of the monomers in different solvents we moved forward to see if there is any ground-state complexation of donor and acceptor triazolyl ($^{TPhen}\mathbf{B}_{Do}$ and $^{TNB}\mathbf{B}_{Ac}$) nucleosides. For that purpose we have chosen various possible combinations of triazolyl-donor/acceptor nucleosides and tested the possibility of forming CT complexation between them.

We observed that a ground-state charge transfer complexation phenomenon is taking place by observing the difference and or addition UV-visible spectra in case of nucleosides ($^{TPhen}\mathbf{B}_{Do}$ and $^{TNB}\mathbf{B}_{Ac}$) in both the non-polar and polar media. From the resolution of the UV-visible spectra of each nucleosides [$^{TPhen}\mathbf{B}_{Do}$ (**2.107β**), $^{TNB}\mathbf{B}_{Ac}$

(**2.110β**)] and their equimolar mixture it was observed that the spectra of eqimolar mixture (blue line) contains new bands (blue dotted line) at around 322 nm and 328 nm in 1,4-dioxane and in phosphate buffer, respectively. This indicated the possible formation of ground state charge transfer complexation between donor ($^{TPhen}\mathbf{B_{Do}}$) and the acceptor ($^{TNB}\mathbf{B_{Ac}}$) nucleosides. This band is also red shifted by about 6 nm when compared between less polar dioxane and highly polar buffer (**Figure 2.18**).

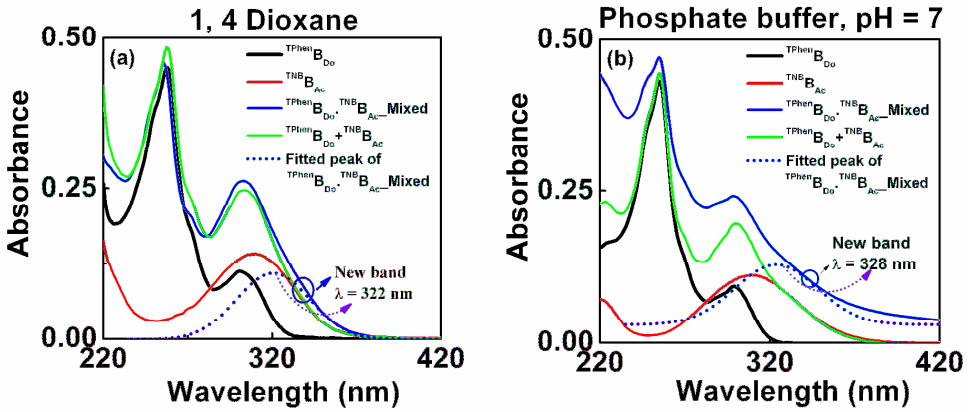

Figure 2.15: UV-visible spectra of each nucleosides [$^{TPhen}\mathbf{B_{Do}}$ (**2.107β**), $^{TNB}\mathbf{B_{Ac}}$ (**2.110β**)] and their equimolar mixture showing appearance of new red shifted bands at 322 nm and 328 nm in 1,4-dioxane and in phosphate buffer, respectively. This indicates the possible formation of ground state charge transfer complexation between donor ($^{TPhen}\mathbf{B_{Do}}$) and the acceptor ($^{TNB}\mathbf{B_{Ac}}$) nucleosides. The dotted line is a gauss fitted curve to resolve the bands for clear distinction. (Nucleoside concentration = 10 μM; 50 mM sodium phosphate, 100 mM NaCl, pH 7.0.).

2.6. CONCLUSION

We have synthesized few new triazolylnucleosides *via* azide-alkyne cycloaddition reaction as a key step of the synthesis with very good yield and their photophysical properties in various organic solvents have been evaluated. The alkynes are commercially available and cheap and the azides can easily be accessed from the chloro sugar. These nucleosides particularly donor-acceptor pairs in DNA are expected to show interesting π-π stacking and photophysical properties. A ground-state charge transfer complexation phenomenon was observed from difference and or addition UV-visible spectra in case of nucleosides ($^{TPhen}\mathbf{B_{Do}}$ and $^{TNB}\mathbf{B_{Ac}}$) in both the

non-polar and polar media. The noncovalent interactions of pyrenyl and butylpyrenyl nucleosides, in particular, with proteins can be studied and the biophysical studies in the context of DNA can be explored with the bases $^{TPhen}\mathbf{B}_{Do}$ and $^{TNB}\mathbf{B}_{Ac}$.

2.7. EXPERIMENTAL SECTION

2.7.1. General Experimental

All reactions were carried out under a nitrogen atmosphere. Organic extracts were dried over anhydrous sodium sulphate. Solvents were removed in a rotary evaporator under reduced pressure. Silica gel (60-120 mesh size) was used for the column chromatography. Reactions were monitored by TLC on silica gel 60 F254 (0.25mm). ^{1}H NMR spectra were measured with Varian 400 (400 MHz) and ^{13}C NMR spectra were measured with Varian 400 (100 MHz) spectrometer. Coupling constant (*J* value) was reported in hertz. The chemical shifts were shown in ppm downfield from tetramethylsilane, using residual chloroform (δ = 7.24 in ^{1}H NMR, δ = 77.23 in ^{13}C NMR), methanol (δ = 3.34 in ^{1}H NMR, δ = 49.2 in ^{13}C NMR), dimethyl sulfoxide (δ = 2.48 in ^{1}H NMR, δ = 39.5 in ^{13}C NMR), as an internal standard. Mass spectra were recorded using WATERS MS system, Q-tof premier and data analyzed using Mass Lynx 4.1. IR spectra were recorded in KBr or neat on a Perkin Elmer Spectrum one FT-IR spectrometer.

2.7.2. Crystallographic Description and ORTEP Diagram

Crystal data were collected with Bruker Smart Apex-II CCD diffractometer using graphite monochromated MoKα radiation (λ = 0.71073 Å) at 298 K. Cell parameters were retrieved using SMART [a] software and refined with SAINT[a] on all observed reflections. Data reduction was performed with the SAINT software and corrected for Lorentz and polarization effects. Absorption corrections were applied with the program SADABS[b]. The structure was solved by direct methods implemented in SHELX-97[c] program and refined by full-matrix least-squares methods on F2. All non-hydrogen atomic positions were located in difference Fourier maps and refined anisotropically. The hydrogen atoms were placed in their geometrically generated

positions. Crystals were isolated in from acetonitrile/chloroform mixture at room temperature.

a. SMART V 4.043 Software for the CCD Detector System; Siemens Analytical Instruments Division: Madison, WI, 1995.

b. SAINT V 4.035 Software for the CCD Detector System; Siemens Analytical Instruments Division: Madison, WI, 1995.

c. Sheldrick, G. M. SHELXL-97, Program for the Refinement of Crystal Structures; University of Göttingen: Göttingen (Germany), **1997**.

2.7.3. Synthesis and Characterization

Synthesis of 1-O-methyl-2-deoxy-α/β-D-ribofuranose (2.89): 2-deoxy ribose sugar (**2.88**, 4 g, 29.8mmol) taken in a round bottom flask was dissolved in methanol and 1% HCl solution was added to it (a solution of 50 ml of dry methanol and 0.85 ml

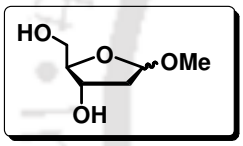

of acetyl chloride was stirred for 1.5 hr at room temperature to prepare 1% HCl solution). The solution was stirred for 2 h at room temperature under N_2 atmosphere. The reaction mixture was neutralized after 2 hours by addition of $NaHCO_3$ and again stirred for 40 min. The reaction mixture was filtered through Whatman-41 filter paper and the filtrate was evaporated to dryness in vaccumn to yield a honey-like product **11** with 100% yield.

Synthesis of 1-O-methyl-2-deoxy-3,5-bis[O-(p-toluoyl)]-α/β-D-ribofuranose (2.90): 1-methoxy-2-deoxy ribose sugar (**2.89**, 4.41 g, 29.78 mol) was dissolved in dry pyridine and 0.488 g (3.99 mmol) of DMAP was added to it. The solution was

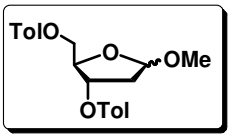

stirred for 5 minutes and then it was cooled to 0 ^{o}C. *p*-Toluoylchloride (8.5 ml, 60.784 mmol) was added to it drop wise and the solution was stirred for 12 hours at 0 ^{o}C. The reaction mixture was then extracted with DCM and washed with $NaHCO_3$ and co-evaporated with toluene 3 times to remove the pyridine. The product **2.90** was separated by column chromatography (silica gel 60-120, hexane: EtOAc = 10:1) and the overall yield was 7.5 g (70%, 0.02 mol) and the material was fully used for the next step. R_f is 0.3 in 7% EtOAc in hexane; ^{1}H NMR ($CDCl_3$, 400 MHz) δ 2.40 (3H,

s), 2.41 (3H, s), 2.51-2.58 (2H, m), 3.40 (3H, s), 4.51-4.55 (2H, m), 4.61-4.65 (1H, m), 5.19 (1H, d, *J* = 4.8 Hz), 5.40-5.43 (1H, m), 7.21-7.26 (4H, m), 7.90-7.95 (4H, m); ^{13}C NMR ($CDCl_3$, 100 MHz) δ 21.6, 39.2, 55.0, 64.3, 74.7, 81.0, 105.0 and 105.1 (C-1), 127.1, 127.2, 129.1, 129.7, 129.8, 143.7, 143.9, 166.2, 166.4; ESI-TOF-MS m/z 407 $[M+Na]^+$.

Synthesis of 2-deoxy-3, 5-di-O-p-toluoyl-α-D-ribofuranosyl chloride (2.91): Dry HCl gas was passed through an ethereal solution of 1-*O*-methyl-3, 5-di-*O*-*p*-toluoyl-2-deoxy ribose sugar (**2.90**, 7.5 g, 0.02 mol) at 0 ^{o}C. The white solid product obtained was filtered and washed with dry ether. The product **2.91** was then dried in vacuum and the overall yield was 4.48 g (59%, 0.01 mol).R_f= 0.3 in 20 % EtOAc in hexane;

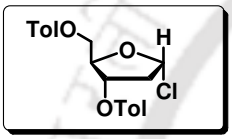

^{1}H NMR ($CDCl_3$, 400 MHz) δ 2.41 (3H, s), 2.42 (3H, s), 2.75 (1H, d, *J* = 14.8 Hz), 2.84-2.91 (1H, m), 4.6 (1H, dd, *J* = 4.4, 12.4 Hz), 4.68 (1H, dd, *J* = 3.2, 12.0 Hz), 4.86 (1H, q, *J* = 3.2 Hz), 5.56 (1H, dd, *J* = 2.8, 6.4 Hz), 6.48 (1H, d, *J* = 5.2 Hz), 7.21-7.28 (4H, m), 7.9 (2H, d, *J* = 8.0 Hz), 7.99 (2H, d, *J* = 8.0 Hz); ^{13}C NMR ($CDCl_3$, 100 MHz) δ 21.9, 44.7, 63.7, 64.5, 73.8, 84.2, 84.9, 95.5, 126.9, 129.4, 129.9, 130.1, 144.3, 144.5, 166.3, 166.6; ESI-TOF-MS m/z 389 $[M+H]^+$.

Synthesis of 2-deoxy-3,5-bis[O-(p-toluoyl)]-α-/β-D-ribofuranosylazide (2.84β, Method A): To a solution of cesium azide (CsN_3) (1.2 eq., 4.63 mmol, 0.81 g) in dry DMSO toluoyl protected chloro-deoxyribose sugar (**2.91**, 1eq., 1.5 g, 3.86 mmol) was added at room temperature. The solution was stirred vigorously for 6 hours. After completion of the reaction monitored by TLC the reaction mixture was partitioned between water and EtOAc. The organic layer was washed with water followed by brine solution, dried over Na_2SO_4, and then concentrated. The crude azide**14** obtained was found to be 1.51 g (99%, 3.82 mmol). The mixture of α- and *β*-isomers produced in 1 : 10 ratio was then separated by silica gel column chromatography (230-400 mesh) using hexane/EtOAc (20 : 1) mixture as eluting solvent system to isolate both the α- (***2.84α***) and β-epimer (***2.84β***) in 8% (0.122 g) and 90% yield (1.37 g), respectively and characterized by IR, NMR spectroscopy and mass spectrometry. TLC $(R_f)_{\alpha\text{-epimer}}$ = 0.3 and TLC $(R_f)_{\beta\text{-epimer}}$ = 0.35 in 20% EtOAc in hexane.

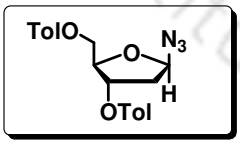

2.7.4. General Procedure for the synthesis of 2-deoxy-3,5-bis[O-(p-toluoyl)]-α-/β-D-ribofuranosylazide (2.84 α/β, Method B):

To a solution of toluoyl protected chloro-deoxyribose sugar (***2.84α***, 1.5 g, 3.86 mmol) in dry DCM, $BF_3.Et_2O$ (0.1 eq., 0.386 mmol, 4.76 ml) and trimethylsilylazide (TMS-N_3) (1.2 eq., 4.63 mmol, 0.61 ml) were added at 0°C. The solution was stirred vigorously for 6 hours. The reaction mixture was partitioned between water and DCM. The organic layer was washed with water followed by brine solution, dried over Na_2SO_4, and then concentrated. The azide **2.84** obtained was found to be 1.29 g (85 %, 3.26mmol). The mixture of α- and β-isomers produced in 3 : 1 ratio (**2.84**) was then separated by column chromatography using 230-400 mesh size silica gel (Solvent system Hexane : EtOAc = 20 : 1) to isolate both the α- (**2.84α**) and β-epimer (**2.84β**) in are 59% (0.9 g) and 21% yield (0.32 g),respectively and were characterized. TLC $(R_f)_{\alpha\text{-epimer}}$ = 0.3 and TLC $(R_f)_{\beta\text{-epimer}}$ = 0.35 in 20% EtOAc in hexane.

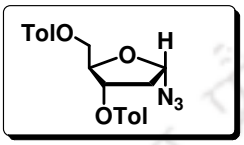

2-Deoxy-3,5-bis[O-(p-toluoyl)]-β-D-ribofuranosylazide (2.84β): IR (KBr) 2110, 1715 cm^{-1} ; ^1H NMR ($CDCl_3$, 400 MHz) δ 2.41 (3H, s), 2.42 (3H, s), 4.52-4.61 (5H, m), 5.52-5.59 (1H, m), 5.72 (1H, t, *J* = 4.8 Hz), 7.22-7.26 (4H, m), 7.90 (2H, d, *J* = 8.4 Hz), 7.98 (2H, d, *J* = 8.4 Hz); ^{13}C NMR ($CDCl_3$, 100 MHz) δ 21.7, 38.9, 64.1, 74.7, 83.7, 92.1, 126.8, 126.9, 129.3, 129.7, 129.9, 144.0, 144.3, 166.2, 166.3; ESI-TOF-MS m/z 418 $[M + Na]^+$.

2-Deoxy-3,5-bis[O-(p-toluoyl)]-α-D-ribofuranosylazide (2.84α): IR (KBr) 2110, 1715 cm^{-1} ; ^1H NMR ($CDCl_3$, 400 MHz) δ 2.23 (1H, d, *J* = 14.4 Hz.), 2.41 (3H, s), 2.42 (3H, s), 2.52-2.59 (1H, m), 4.50-4.64 (2H, m), 4.71 (1H, q, *J* = 3.6, 3.2 Hz.), 5.48-5.51 (1H, m), 5.70 (1H, d, *J* = 5.6 Hz), 7.23-7.27 (4H, m), 7.91 (2H, d, *J* = 8.4, Hz), 7.96 (2H, d, *J* = 8.4, Hz) ; ^{13}C NMR ($CDCl_3$, 100 MHz) δ 21.7, 38.8, 64.1, 74.7, 83.7, 92.1, 126.7, 126.9, 129.3, 129.7, 129.9, 144.0, 144.3, 166.2, 166.3; ESI-TOF-MS m/z 418 $[M + Na]^+$.

2.7.5. General procedure for the synthesis of triazolyl donor/acceptor aromatic nucleosides *via* "Click" reaction

In a round bottomed flask fitted with a septum, α- and/or β-azido–deoxy ribose sugar (1.0 equiv) was dissolved in dry THF and degassed for 10 min with N_2. Then, the aromatic alkyne (1.5 equiv) was added and both stirring and degassing were continued for next 5 min. After that, 6 mol% of sodium ascorbate dissolved in small quantity of water was added to it and the solution was degassed for another 5 min. Then 1 mol% of copper sulphate dissolved in small quantity of water was added to it followed by degassing. The final ratio of THF : H_2O in the reaction mixture should be 3:1. Finally, DIPEA was added to the reaction mixture. The solution was refluxed at 75-80 ^oC with overnight stirring. After consumption of the starting azide, the reaction mixture was evaporated and partitioned between water and ethyl acetate. The organic layer was washed with water followed by brine solution, dried over Na_2SO_4, and then concentrated. The products were then separated by column chromatography and characterized. The average isolated yields were between 90-99%.

Synthesis of 3′, 5′-bis{O-(p-toluoyl)}-2′-deoxy-1′-β-triazolyl-N,N-dimethyl amino benzene nucleoside (2.92β, bis-toluoyl-β-$^{TNDMB}B_{Do}$): Using the general procedure, starting from 60 mg of β-azido–deoxy ribose sugar (**2.84β**, 0.15 mmol) and 26.14 mg of 1-ethynyl-N,N-dimethylaniline (**2.85A**, 0.18 mmol), 78.26 mg (0.145 mmol) of the title compound **2.92β** was isolated as a yellow solid. Yield 96.6%; mp 185-188 ^oC; IR (KBr) 1721, 1612, 1508, 1296, 1279, 1109 cm^{-1}; ^1H NMR ($CDCl_3$, 400 MHz) δ 2.38 (3H, s), 2.44 (3H, s), 2.99 (6H, s), 3.12-3.18 (2H, m), 4.57 (1H, dd, *J* = 3.6, 11.6 Hz), 4.65-4.72 (2H ,m), 5.77-5.79 (1H, m), 6.54 (1H, t, *J* = 6.8 Hz), 6.7 (2H, d, *J* = 8.8 Hz), 7.2 (2H, d, *J* = 7.6 Hz), 7.28 (2H, d, *J* = 8.0 Hz), 7.54 (2H, d, *J* = 8.8 Hz), 7.79 (1H, s), 7.89 (2H, d, *J* = 8.0 Hz), 7.96 (2H, d, *J* = 8.4 Hz); ^{13}C NMR ($CDCl_3$, 100 MHz) δ 21.8, 38.6, 40.52, 64.0, 74.9, 83.6, 88.9, 112.5, 116.6, 118.6, 126.6, 126.8, 129.4, 129.8, 129.9, 144.2, 144.6, 148.8, 150.6, 166.0, 166.3; HRMS calcd for $C_{31}H_{33}N_4O_5$ $[M + H]^+$ 541.2445, found 541.2485.

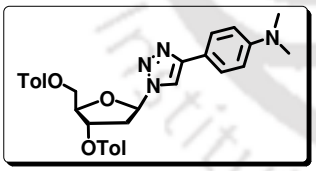

Synthesis of 3′, 5′-bis{O-(p-toluoyl)}-2′-deoxy-1′-α-triazolyl-N,N-dimethyl amino benzene nucleoside (2.92α, bis-toluoyl-α-$^{TNDMB}B_{Do}$): Using the general procedure, starting from 50 mg of α-azido–deoxy ribose sugar (**2.84α**, 0.126 mmol) and 22.071 mg of 1-ethynyl N,N-dimethylaniline (**2.85A**, 0.607 mmol), 58.9 mg (0.109mmol) of the title compound **2.92α** was isolated as a yellow solid. Yield

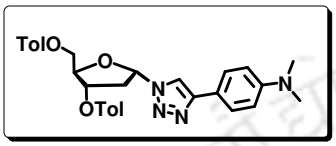

86.5%; mp158-160 ^{o}C; IR (KBr) 1718, 1611, 1377, 1309, 1102 cm^{-1} ; ^{1}H NMR ($CDCl_3$, 400 MHz) δ 2.33 (3H, s), 2.4 (3H, s), 2.96 (6H, s), 2.99-3.14 (2H, m), 4.55-4.64 (2H, m), 4.8- 4.84 (1H, m), 5.65 (1H, d, *J* = 5.6 Hz.), 6.53 (1H, d, *J* = 6.4 Hz), 6.73 (2H, d, *J* = 8.8 Hz.), 7.09 (2H,d, *J* = 7.6 Hz), 7.24 (2H, d, *J* = 8 Hz.), 7.66 (2H, d, *J* = 8 Hz), 7.7 (2H, d, *J* = 8 Hz.), 7.94 (2H, d, *J* = 8.0 Hz), 7.98 (1H, s); ^{13}C NMR ($CDCl_3$, 100 MHz) δ 21.7, 38.7, 40.5, 64.1, 74.7, 84.8, 89.9, 112.5, 116.5, 118.9, 126.3, 126.8, 129.4, 129.8, 144.2, 144.3, 148.4, 150.5, 165.9, 166.2. HRMS calcd for $C_{31}H_{33}N_4O_5$ $[M + H]^+$ 541.2445, found 541.2440.

Synthesis of 3′, 5′-bis{O-(p-toluoyl)}-2′-deoxy-1′-β-triazolyldimethoxyphenyl nucleoside (2.93β, bis-toluoyl-β-$^{TDMB}B_{Do}$): Using the general procedure, starting from 200 mg (0.506 mmol) of azido–deoxy ribose sugar **2.84β** and 98.45 mg (0.607 mmol) of 1-ethynyl 3,5 dimethoxy benzene **2.85B**, 290.9 mg (0.522 mmol) of the title compound **2.93β** was isolated as a white solid. Yield 99%; mp155-158 ^{o}C; IR (KBr) 1715, 1611, 1276, 1204, 1156 cm^{-1}; ^{1}H NMR ($CDCl_3$, 400 MHz) *δ* 2.35 (3H, s), 2.44

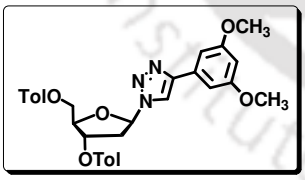

(3H, s), 2.88-2.93 (1H, m), 3.12-3.17 (1H, m), 3.49 (1H, s), 3.82 (6H, s), 4.57-4.61 (1H, m), 4.69-4.72 (2H, m), 5.78-5.79 (1H, m), 6.44 (1H, s), 6.54-6.57 (1H, t, *J* = 6.4 Hz), 6.88 (1H, s), 7.19 (2H, d, *J* = 8.0 Hz), 7.28 (2H, d, *J* = 8.0 Hz), 7.87 (2H, d, *J* = 8.0 Hz), 7.96 (2H, d, *J* = 7.6 Hz), 7.97 (1H, s); ^{13}C NMR ($CDCl_3$, 100 MHz) *δ* 21.9, 38.9, 55.7, 64.1, 75.0, 83.9, 89.3, 101.0, 103.9, 118.5, 126.6, 126.8, 129.6, 129.8, 130.0, 144.5, 144.8, 148.3, 161.3, 166.1, 166.1; ESI-TOF-MS m/z 580 $[M + Na]^+$; HRMS calcd. for $C_{31}H_{32}N_3O_7$ ($[M+H]^+$) 558.2240, found 558.2233.

Synthesis of 3′, 5′-bis{O-(p-toluoyl)}-2′-deoxy-1′-α-triazolyldimethoxyphenyl nucleoside (2.82α, bis-toluoyl-α-$^{TDMB}B_{Do}$):Using the general procedure, starting from

200 mg (**2.84α**, 0.506 mmol) of *α*-azido–deoxy ribose sugar and 98.45 mg (**2.85B**, 0.607 mmol) of 1-ethynyl 3,5 dimethoxy benzene, 267.6 mg (0.480mmol) of the title compound **2.93α** was isolated as colourless gel. Yield 95%; IR (KBr) 3145, 1720, 1611, 1269 cm^{-1} .^{1}H NMR ($CDCl_3$, 400 MHz) δ 2.21 (3H, s), 2.29 (3H, s), 2.9-3.01

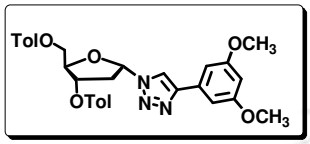

(2H, m), 3.68 (6H, s), 4.45-4.52 (2H, m), 4.71-4.74 (1H, m), 5.54-5.55 (1H, m), 6.33 (1H, t, *J* = 2.4 Hz), 6.45-6.47(1H, m), 6.86 (2H , d, *J* = 2.4 Hz), 6.98 (2H, d, *J* = 8 Hz), 7.13 (2H, d, *J* = 8 Hz), 7.56 (2H, d, *J* = 8 Hz), 7.83 (2H, d, *J* = 8 Hz), 8.01 (1H, s); ^{13}C NMR ($CDCl_3$, 100 MHz) δ 21.6, 21.7, 38.8, 55.4, 64.0, 74.7, 85.1, 90.2, 100.7, 103.7, 118.4, 126.2, 126.7, 129.3, 129.4, 129.6, 129.7, 132.3, 144.3, 144.5, 147.7, 161.2, 165.9, 166.2. HRMS calcd for $C_{31}H_{32}N_3O_7$ $[M+H]^+$ 558.2235, found 558.2232.

Synthesis of 3′, 5′-bis{O-(p-toluoyl)}-2′-deoxy-1′-β-triazolylphenoxyphenyl nucleoside (2.94β, bis-toluoyl-β-$^{TPhOB}B_{Do}$): Using the general procedure, starting from 60 mg (**2.84β**, 0.152mmol) of *β*-azido–deoxy ribose sugar and 35.4 mg (**2.85C**, 0.182 mmol) of 1-ethynyl phenoxy benzene, 80.60 mg (0.137 mmol) of the title compound **2.94β** was isolated as a white solid. Yield 90%; IR (KBr) 1721, 1612, 1508, 1296, 1279, 1109 cm^{-1}; ^{1}H NMR ($CDCl_3$, 400 MHz) δ 2.36 (3H, s), 2.44 (3H,

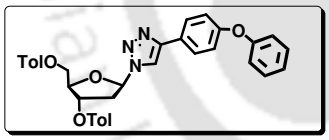

s), 2.89-2.93 (1H, m), 3.13-3.19 (1H, m), 4.56 (1H, dd, *J* = 4, 12 Hz), 4.68-4.78 (2H, m), 5.79-5.80 (1H, m), 6.56 (1H, t, *J* = 6.2), 6.99 (2H, d, *J* = 8.4 Hz), 7.04 (2H, d, *J* = 8.4 Hz), 7.13-7.15 (1H, m), 7.19 (2H, d, *J* = 8 Hz), 7.26-7.29 (3H, m), 7.34-7.38 (2H, m), 7.59 (2H, d, *J* = 8.8 Hz),7.86-7.88 (2H, m), 7.96 (2H, d, *J* = 8 Hz); ^{13}C NMR ($CDCl_3$, 400 MHz) δ 21.81, 38.8, 63.9, 74.9, 83.8, 89.2, 117.7, 119.1, 119.2, 123.7, 125.5, 126.6, 126.8, 127.4, 129.1, 129.5, 129.8, 129.9, 144.4, 144.7, 147.9, 157.1, 157.5, 166.1, 166.3; HRMS calcd for $C_{35}H_{32}N_3O_6$ $[M+H]^+$ 590.2286, found 558.2287.

Synthesis of 3′, 5′-bis{O-(p-toluoyl)}-2′-deoxy-1′-α-triazolylphenoxyphenyl nucleoside (2.94α, bis-toluoyl-α-$^{TPhOB}B_{Do}$): Using the general procedure, starting

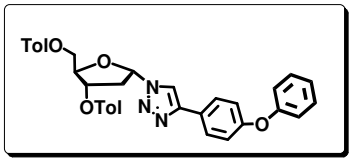

from 50 mg (**2.84α**, 0.126 mmol) of *α*-azido–deoxy ribose sugar and 29.3 mg (**2.85C**, 0.152mmol) of ethynylphenoxybenzene, 38.5 mg (0.065 mmol) of the the title compound **2.94α** was isolated as a white solid. Yield 51.85%; mp129-

130 °C; IR (KBr) 1718, 1699, 1278, 1244, 1178, 1109 cm^{-1} ; ^1H NMR ($CDCl_3$, 400 MHz) δ 2.26 (3H, s), 2.35 (3H, s), 2.93-3.10 (2H, m), 4.49-4.59 (2H, m), 4.74-4.77 (1H, m), 5.59 (1H, d, *J* = 6.4 Hz), 6.49 (1H, d, *J* = 6 Hz), 6.95-7.07 (7H, m), 7.19 (2H, d, *J* = 8 Hz), 7.28 (2H, t, *J* = 8 Hz), 7.59 (2H, d, *J* = 8 Hz), 7.68 (2H, d, *J* = 8.8 Hz.), 7.87 (2H, d, *J* = 8.4 Hz), 7.99 (1H, s); ^{13}C NMR ($CDCl_3$, 100 MHz) δ 21.9, 38.9, 64.1, 74.8, 74.8, 85.2, 90.3, 117.7, 119.2, 123.7, 125.9, 126.4, 126.9, 127.5, 129.4, 129.5, 129.8, 129.9, 130.0, 144.5, 144.6, 147.6, 157.2, 157.6, 166.1, 166.3. HRMS calcd for $C_{34}H_{32}N_3O_6$ $[M+H]^+$ 590.2283, found 590.2287.

Synthesis of 3′, 5′-bis{O-(p-toluoyl)}-2′-deoxy-1′-β-triazolylmethoxynapthalene nucleoside (2.95β, bis-toluoyl-β-$^{TMNap}B_{Do}$): Using the general procedure, starting from 60 mg (0.152 mmol) of β-azidodeoxyribose sugar (**2.84β**) and 33.16 mg (**2.85D**, 0.182 mmol) of 2-ethynyl-6-methoxy napthalene , 87.04 mg (0.151 mmol) of the title compound **2.95β** was isolated as a brown solid. Yield 99.3%; mp 197-200 °C; R_f = 0.45 in 2:1 (v/v) hexane/ethylacetate; IR (KBr) 1711, 1611, 1273, 1124 cm^{-1}; ^1H NMR

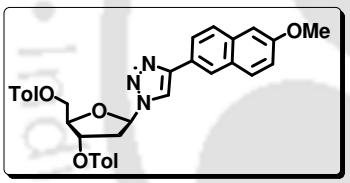

($CDCl_3$, 400 MHz) δ 2.31 (3H, s), 2.45 (3H, s), 2.92-2.95 (1H, m), 3.17-3.21 (1H, m), 3.94 (3H, s), 4.57-4.60 (1H, m), 4.70-4.78 (2H, m), 5.81-5.82 (1H, m), 6.59-6.62 (1H, t, *J* = 5.2 Hz), 7.14-7.18 (4H, m), 7.29 (2H, d, *J* = 6.8 Hz), 7.69-7.72 (3H, m), 7.89 (2H, d, *J* = 6.4 Hz), 7.97 (2H, d, *J* = 6.8 Hz), 8.02 (1H, s), 8.08 (1H, s); ^{13}C NMR ($CDCl_3$, 400 MHz) δ 21.8, 21.9, 38.9, 55.5, 64.0, 74.9, 83.9, 89.3, 105.9, 117.9, 119.4, 124.6, 125.7, 126.6, 126.8, 127.4, 129.1, 129.5, 129.8, 130.0, 134.6, 144.4, 144.7, 148.6, 158.2, 166.1, 166.4; HRMS calcd. for $C_{34}H_{32}N_3O_6$ $[M + H]^+$ 578.2286, found 578.2365.

Synthesis of 3′, 5′-bis{O-(p-toluoyl)}-2′-deoxy-1′-α-triazolylmethoxynapthalene nucleoside (2.95α, bis-toluoyl-α-$^{TMNap}B_{Do}$): Using the general procedure, starting from 50 mg (**2.84α**, 0.126 mmol) of α-azido–deoxy ribose sugar and 27.52 mg

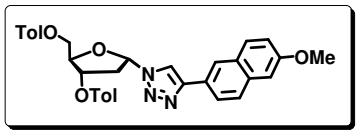

(**2.85D**, 0.151 mmol) of 2-ethynyl-6-methoxy napthalene, 71.3 mg (0.123mmol) of the title compound **2.95α** was isolated as a white solid. Yield 98 %; mp144-148 °C; IR (KBr) 3154, 1717, 1611, 1270, 851, 819, 750, 690 cm^{-1} ; ^1H NMR ($CDCl_3$, 400 MHz) δ 2.27 (3H, s), 2.41 (3H, s), 3.03-3.16 (2H, m), 3.94 (3H, s),

4.59-4.68 (2H, m), 4.87-4.88 (1H, m), 5.69 (1H, d, *J* = 6.4 Hz), 6.62 (1H, d, *J* = 6.8 Hz.), 7.05 (2H, d, *J* = 8 Hz), 7.13-7.17 (2H,m), 7.26 (2H, d, *J* = 8 Hz), 7.68-7.71 (3H, m), 7.75 (1H, d, *J* = 8.4 Hz), 7.86-7.88 (1H, m), 7.96 (2H, d, *J* = 8 Hz), 8.17 (1H, s), 8.19 (1H, s); ^{13}C NMR ($CDCl_3$, 100 MHz) δ 21.7, 21.8, 38.9, 55.4, 64.1, 74.9, 85.1, 90.3, 105.9, 117.9, 119.4, 124.5, 125.9, 126.3, 126.8, 127.4, 129.1, 129.5, 129.7, 129.8, 134.5, 144.4, 144.6, 148.2, 158.1, 165.9, 166.3. HRMS calcd for $C_{34}H_{32}N_3O_6$ $[M+H]^+$ 578.2286, found 578.2296.

Synthesis of 3′, 5′-bis{O-(p-toluoyl)}-2′-deoxy-1′-β-triazolylphenanthrene nucleoside (2.96 β, bis-toluoyl-β-$^{TPhen}B_{Do}$): Using the general procedure, starting from 200 mg (0.506 mmol) of azido–deoxy ribose sugar **2.84β** and 122.77 mg (0.607 mmol) of 9-ethynylphenantherene (**2.85E**), 288.7 mg (0.484 mmol) of the title compound **2.96 β** was isolated as a yellow solid. Yield 95.6%; mp 148-151 ^{o}C; IR

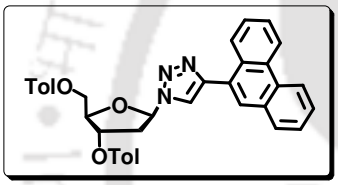

(KBr) 1714, 1610, 1281, 1123, 1020 cm^{-1} ; ^{1}H NMR ($CDCl_3$, 400 MHz) *δ* 2.22 (3H, s), 2.45 (3H, s), 2.98-3.01 (1H, m), 3.29-3.33 (1H, m), 4.62-4.65 (1H, m), 4.73 (2H, s), 5.83-5.84 (1H, m), 6.66 (1H, t, *J* = 8.0 Hz), 7.06 (2H, d, *J* = 7.6 Hz), 7.29 (2H, d, *J* = 7.6 Hz), 7.57-7.61 (2H, m), 7.69 (2H, t, *J* = 6.8, 7.2 Hz), 7.84 (4H, d, *J* = 6.8 Hz), 7.98 (2H, d, *J* = 7.6 Hz), 8.08 (1H, s), 8.33 (1H, d, *J* = 8.4 Hz), 8.71 (1H, d, *J* = 8.4 Hz), 8.77 (1H, d, *J* = 8.0 Hz); ^{13}C NMR ($CDCl_3$, 100 MHz) *δ* 21.5, 21.7, 29.7, 38.5, 63.9, 74.8, 83.7, 89.1, 121.7, 122.6, 122.9, 126.3, 126.5, 126.6, 126.8, 126.9, 127.0, 127.2, 128.5, 128.9, 129.3, 129.4, 129.6, 129.9, 130.0, 130.5, 130.7, 131.2, 144.1, 144.5, 147.3, 165.9, 166.3; ESI-TOF-MS m/z 598 $[M + H]^+$; HRMS calcd. for $C_{37}H_{32}N_3O_5$ ($[M+H]^+$) 598.2342, found 598.2322.

Synthesis of 3′, 5′-bis{O-(p-toluoyl)}-2′-deoxy-1′-α-triazolylphenanthrene nucleoside (2.96α, bis-toluoyl-α-$^{TPhen}B_{Do}$): Using the general procedure, starting

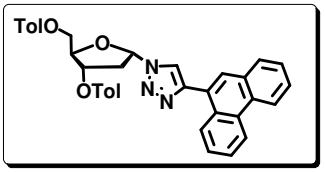

from 200 mg (0.506 mmol) of *α*-azido–deoxy ribose sugar **2.84α** and 122.77 mg (**2.85E**, 0.607 mmol) of 9-ethynylphenantherene, 288.7 mg (0.483mmol) of the title compound **2.96α** was isolated as a yellow gel. Yield 95.5%; IR (KBr) 1719, 1611, 1270, 1100, 752, 728 cm^{-1}; ^{1}H NMR ($CDCl_3$, 400 MHz)

δ ^{1}H NMR ($CDCl_3$, 400 MHz) δ 2.24 (3H, s), 2.44 (3H, s), 3.07-3.14 (1H, m), 3.29-3.3 (1H, m), 4.61-4.71 (2H, m), 4.9-4.91 (1H, m), 5.70 (1H, d, *J* = 6.8 Hz), 6.69 (1H, d, *J* = 6 Hz), 7.00 (2H, d, *J* = 8 Hz), 7.29 (2H, d, *J* = 7.6 Hz), 7.51-7.55 (1H, m), 7.59-7.71 (5H, m), 7.81 (1H, d, *J* = 7.6 Hz), 7.88 (1H, s), 7.97 (2H, d, *J* = 8 Hz), 8.22 (1H, s), 8.38 (1H, d, *J* = 8 Hz), 8.71 (1H, d, *J* = 8 Hz), 8.77 (1H, d, *J* = 8 Hz); ^{13}C NMR ($CDCl_3$, 100 MHz) δ 21.6, 21.7, 39.1, 64.1, 74.8, 85.2, 90.4, 121.2, 122.6, 122.9, 126.2, 126.4, 126.8, 126.9, 126.9, 127.2, 128.5, 128.8, 129.4, 129.7, 129.8, 130.1, 130.5, 130.7, 131.3, 144.3, 144.4, 146.9, 165.9, 166.2. ; HRMS calcd for $C_{37}H_{32}N_3O_5$ $[M+H]^+$ 598.2336, found 598.2333.

Synthesis of 3′, 5′-bis{O-(p-toluoyl)}-2′-deoxy-1′-α-triazolylpyrene nucleoside (2.97β, bis-toluoyl-β-$^{TPy}B_{Do}$): Using the general procedure, starting from 100 mg (0.253 mmol) of *β*-azido–deoxy ribose sugar **2.84β** and 68.59 mg (**2.85F**, 0.304 mmol) of 1-ethynyl pyrene, 133.63 mg (0.215 mmol) of the title compound **2.97β** was isolated as a yellow solid. Yield 85%; IR (KBr) 2926, 1719, 1610, 1278 cm^{-1}; ^{1}H NMR

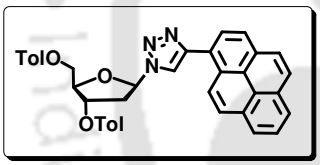

($CDCl_3$, 400 MHz) δ 2.16 (3H, s), 2.45 (3H, s), 2.98-3.04 (1H, m), 3.29-3.36 (1H, m), 4.63 (1H, dd, *J* = 3.2, 11.2 Hz), 4.74-4.79 (2H, m), 5.86-5.87 (1H, m), 6.69 (1H, t, *J* = 6.4 Hz), 7.03 (1H, d, *J* = 8 Hz), 7.29 (2H, d, *J* = 7.6 Hz), 7.89 (2H, d, *J* = 8 Hz), 7.98-8.11 (8H, m), 8.16-8.22 (4H, m), 8.63 (1H, d, *J* = 8 Hz) ; ^{13}C NMR ($CDCl_3$, 100 MHz) δ 21.9, 38.9, 64.0, 74.9, 83.9, 89.3, 121.6, 124.9, 125.3, 125.6, 126.3, 126.6, 127.3, 127.5, 128.1, 128.4, 128.8, 129.4, 129.5, 129.8, 130.0, 144.3, 144.7, 148.1, 166.1, 166.4. ; HRMS calcd for $C_{39}H_{33}N_3O_5$ $[M]^+$ 623.2420, found 623.2454.

Synthesis of 3′, 5′-bis{O-(p-toluoyl)}-2′-deoxy-1′-α-triazolyl butylpyrene nucleoside (2.98β, bis-toluoyl-β-$^{TBPy}B_{Do}$): Using the general procedure, starting from 50 mg (0.126 mmol) of *β*-azido–deoxy ribose sugar **2.84β** and 47.06 mg (**2.85G**,

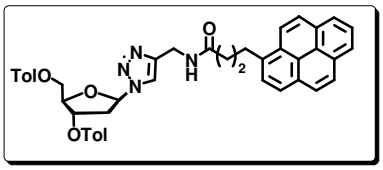

0.151 mmol) of pyrene butyric acid *N*- propynyl amide, 86.00 mg (0.122 mmol) of the triazolyl butylpyrene nucleoside **2.98β** was isolated as a dirty white solid. Yield 94.58%; IR (KBr) 3334.6, 2942.2, 1726.1, 1650.5, 1610, 1278 cm^{-1}; ^{1}H NMR ($CDCl_3$, 400 MHz) δ 2.16-2.22 (2H, m), 2.27 (1H, d, *J* = 8 Hz), 2.33

(3H, s), 2.42 (3H, s), 2.76-2.82 (1H, m), 3.17-3.24 (1H, m), 3.35 (1H, t, *J* = 8 Hz), 4.43-4.63 (5H, m), 4.53-4.55 (1H, m), 5.71-5.74 (1H, m), 6.14-6.16 (1H, m), 6.38 (1H, t, *J* = 6 Hz), 7.15 (2H, d, *J* = 8 Hz), 7.25 (2H, d, *J* = 8 Hz), 7.69 (1H, s), 7.79-7.83 (3H, m), 7.91-8.00 (6H, m), 8.08 (2H, d, *J* = 8 Hz), 8.13-8.16 (2H, m), 8.26 (1H, d, *J* = 8.8 Hz); ^{13}C NMR ($CDCl_3$, 100 MHz) δ 21., 27.4, 32.89, 34.9, 35.9, 38.09, 64.1, 74.9, 83.8, 88.9, 121.4, 123.5, 124.9, 125.9, 126.5, 126.8, 127.5, 127.7, 128.9, 129.4, 129.5, 129.8, 129.9, 131.1, 131.6, 135.9, 144.3, 144.7, 145.2, 166.0, 166.3, 172.9. HRMS calcd for $C_{44}H_{42}N_4O_6$ $[M]^+$ 722.3104, found 722.3107.

Synthesis of 3′, 5′-bis{O-(p-toluoyl)}-2′-deoxy-1′-β-triazolyl nitrophenyl nucleoside (2.99β, bis-toluoyl-β-$^{TNB}B_{Ac}$): Using the general procedure, starting from 200 mg (0.506 mmol) of azido–deoxy ribose sugar **2.84β** and 89.31 mg (0.607 mmol) of 1-ethynyl 4-nitro benzene (**2.85I**), 255.6 mg (0.472 mmol) of the compound **2.99β** was isolated as a yellow solid. Yield 93.23%; mp 185-190 ^{o}C; IR (KBr) 1715, 1610,

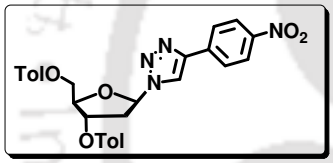

1514, 1343, 1278, 1102 cm^{-1}; ^{1}H NMR ($CDCl_3$, 400 MHz) *δ* 2.36 (3H, s), 2.44 (3H, s), 2.95-2.98 (1H, m), 3.17-3.22 (1H, m), 4.55 (1H, dd, *J* = 1.6, 11.6 Hz), 4.63-4.71 (1H, m), 4.78-4.87 (1H, m), 5.68-5.81 (1H, m), 6.58-6.59 (1H, m), 7.18 (2H, d, *J* = 7.2 Hz), 8.09 (1H, s), 8.20 (2H, d, *J* = 8.0 Hz); ^{13}C NMR ($CDCl_3$, 100 MHz) *δ* 21.8, 21.9, 38.9, 63.9, 74.6, 84.0, 89.4, 111.63, 118.88, 119.5, 126.2, 126.4, 126.7, 129.5, 129.8, 129.9, 132.7, 134.8, 144.5, 144.8, 146.4, 166.1, 166.2; ESI-TOF-MS m/z 565 $[M + Na]^+$; HRMS calcd. for $C_{29}H_{26}N_4O_7Na$ ($[M+Na]^+$) 565.1699, found 565.1677.

Synthesis of 3′, 5′-bis{O-(p-toluoyl)}-2′-deoxy-1′-α-triazolyl nitrophenyl nucleoside (2.99α, bis-toluoyl-α-$^{TNB}B_{Ac}$): Using the general procedure, starting from 200 mg (0.506 mmol) of azido–deoxy ribose sugar **2.84α** and 89.31 mg (0.607 mmol)

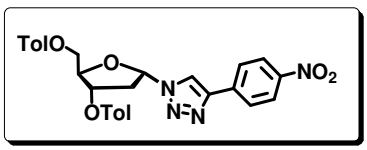

of 1-ethynyl 4-nitro benzene (**2.85I**), 268.8 mg (0.496mmol) of the title compound **2.99α** was isolated as a yellow solid. Yield 98%; mp180-182 ^{o}C; IR (KBr) 1716, 1610, 1514, 1339 cm^{-1} ; ^{1}H NMR ($CDCl_3$, 400 MHz) δ 2.34 (3H, s), 2.43 (3H, s), 3.04-3.23 (2H, m), 4.59-4.69 (2H, m), 4.86-4.89 (1H, m), 5.68 (1H, d, *J* = 6 Hz), 6.6 (1H, d, *J* = 5.6), 7.07 (2H, d, *J* = 8 Hz), 7.28 (2H, d, *J* = 8 Hz), 7.63

(2H, d, *J* = 8.0 Hz), 7.95 (4H, d, *J* = 8.4), 8.24 (1H, s), 8.26 (1H, s), 8.27 (1H, s); ^{13}C NMR ($CDCl_3$, 100 MHz) δ 21.9, 38.9, 64.0, 74.8, 85.4, 90.5, 119.7, 124.4, 126.3, 126.8, 129.4, 129.5, 129.7, 129.9, 136.9, 144.5, 144.8, 145.8, 147.5, 165.9, 166.3. HRMS calcd for $C_{29}H_{27}N_4O_7$ $[M+H]^+$ 543.1874, found 543.1879.

Synthesis of 3′, 5′-bis{O-(p-toluoyl)}-2′-deoxy-1′-β-triazolyl cyanophenyl nucleoside (2.100β, bis-toluoyl-β-$^{TCNB}B_{Ac}$): Using the general procedure, starting from 200 mg (0.506 mmol) of azido–deoxy ribose sugar **2.84β** and 77.199 mg (0.607 mmol) of 4-ethynylbenzonitrile (**2.85H**), 237.84 mg (0.46 mmol) of the title compound **2.100β** was isolated as a white solid. Yield 90%; mp175-180 ^{o}C; IR (KBr) 2228, 1719, 1613, 1277, 1122 cm^{-1} ; ^{1}H NMR ($CDCl_3$, 400 MHz) *δ* 2.28 (3H, s), 2.35 (3H, s), 2.83-2.89 (1H, m), 3.07-3.14 (1H, m), 4.46 (1H, dd, *J* = 4.0, 12.0 Hz), 4.61-4.63 (1H, m), 4.66 (1H, dd, *J* = 3.6, 12.0 Hz), 5.71-5.74 (m, 1H), 6.48 (1H, t, *J* = 6.4 Hz), 7.08 (2H, d, *J* = 8.0 Hz), 7.19 (2H, d, *J* = 7.6 Hz), 7.53 (2H, d, *J* = 8.4 Hz), 7.63 (2H, d, *J* = 8.4 Hz), 7.75 (2H, d, *J* = 8.0 Hz), 7.87 (2H, d, *J* = 8.0 Hz), 7.89 (1H, s); ^{13}C NMR ($CDCl_3$, 100 MHz) *δ* 21.8, 21.9, 38.9, 63.9, 74.6, 84.0, 89.4, 111.6, 118.9, 119.5, 126.2, 126.4, 126.7, 129.8, 130.0, 132.7, 134.8, 144.5, 144.8, 146.4, 166.1, 166.2; ESI-TOF-MS m/z 523 $[M + H]^+$; HRMS calcd. for $C_{30}H_{26}N_4O_5Na$ ($[M+Na]^+$) 545.1801, found 545.1782.

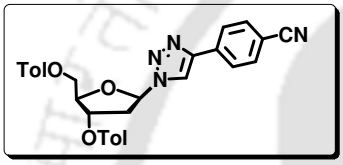

Synthesis of 3′, 5′-bis{O-(p-toluoyl)}-2′-deoxy-1′-α-triazolyl cyanophenyl nucleoside (2.100α, bis-toluoyl-α-$^{TCNB}B_{Ac}$): Using the general procedure, starting from 200 mg (0.506 mmol) of azido–deoxy ribose sugar **2.84α** and 77.199 mg (0.607 mmol) of 4-ethynylbenzonitrile (**2.85H**), 250.65mg (0.480mmol) of the compound **2.100α** was isolated as a white solid. Yield 95%; mp160-163 ^{o}C; IR (KBr) 2226, 1717, 1611,1104 cm^{-1} ; ^{1}H NMR ($CDCl_3$, 400 MHz) δ 2.35 (3H, s), 2.43 (3H, s), 3.03-3.1 (1H, m), 3.17-3.2 (1H, m), 4.58-4.68(2H, m), 4.84-4.86 (1H, m), 5.67 (1H, d, *J* = 8 Hz), 6.59 (1H, d, *J* = 6.8 Hz), 7.06 (2H, d, *J* = 8 Hz), 7.28 (2H, d *J* = 8.4 Hz), 7.62 (2H, d, *J* = 8 Hz), 7.69 (2H, d, *J* = 8.8 Hz), 7.9 (2H, d, *J* = 8.6 Hz), 7.95 (2H, d, *J* = 8 Hz), 8.21 (1H, s); ^{13}C NMR ($CDCl_3$, 100 MHz) δ 21.9, 39.0, 64.0, 74.8, 85.4, 90.5, 118.9, 119.4, 126.2, 129.4, 129.5, 129.7, 129.9, 132.9, 144.5, 144.8,

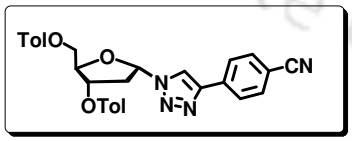

146.1, 165.9, 166.3. HRMS calcd. for $C_{30}H_{27}N_4O_5$ $[M+H]^+$ 523.1976, found 543.1974.

Synthesis of 3′, 5′-bis{O-(p-toluoyl)}-2′-deoxy-1′-β-triazolyl formylbenzene nucleoside (2.101β, bis-toluoyl-β-$^{TBenzal}B_{Ac}$): Using the general procedure, starting from 60 mg (0.152 mmol) of azido–deoxyribose sugar **2.84β** and 23.69 mg (0.182mmol) of 4-ethynyl benzaldehyde (**2.85J**), 77.75 mg (0.148 mmol) of the title compound **2.101β** was isolated as a white solid.Yield 97.4%; mp 188-190 ^oC; IR (KBr) 2852, 1727, 1714, 1695, 1610, 1280, 1112cm^- ^{1}; ^{1}H NMR ($CDCl_3$, 400 MHz) δ 2.36 (3H, s), 2.45 (3H, s), 2.94-2.96 (1H, m), 3.16-3.19 (1H, m), 4.54-4.57 (1H, m), 4.70 (1H, s), 4.76-4.79 (1H, m), 5.80-5.82 (1H, d, *J* = 2.4 Hz), 6.58 (1H, t, *J* = 6 Hz), 7.18 (1H, d, *J* = 7.2 Hz), 7.29 (2H, d, *J* = 8 Hz), 7.79 (2H, d, *J* = 7.6 Hz), 7.84-7.88 (4H, m), 7.96 (2H, d, *J* = 8 Hz), 8.05 (1H, s), 10.02 (1H, s); ^{13}C NMR (DMSO-d_6, 400 MHz) δ 21.9, 38.0, 64.8, 75.5, 83.7, 89.4, 122.9, 126.7, 127.6, 127.7, 130.2, 130.2, 130.4, 130.6, 131.1, 136.8, 137.2, 144.8, 145.2, 146.9, 166.4, 166.5, 193.1; HRMS calcd for $C_{30}H_{28}N_3O_6$ $[M+H]^+$ 526.1973, found 526.1982.

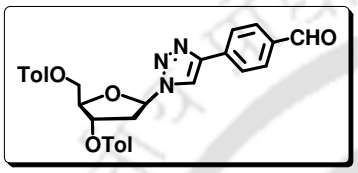

Synthesis of 3′, 5′-bis{O-(p-toluoyl)}-2′-deoxy-1′-α-triazolyl formylbenzene nucleoside (2.101α, bis-toluoyl-α-$^{TBenzal}B_{Ac}$): Using the general procedure, starting from 50 mg (0.126 mmol) of azido–deoxy ribose sugar **2.84α** and 19.65 mg (0.151 mmol) of 4-ethynylbenzaldehyde (**2.85J**), 52 mg (0.099mmol) of the title compound **2.101α** was isolated as a white solid. Yield 78.5%; mp142-145 ^oC; IR (KBr) 1717, 1694, 1610, 1286, 1107 cm^{-1} ; ^{1}H NMR ($CDCl_3$, 400 MHz) δ 2.23 (3H, s), 2.33 (3H, s), 2.94-3.11 (2H, m), 4.49-4.58 (2H, m), 4.78 (1H, s), 5.59 (1H, d, *J* = 5.6 Hz), 6.51 (1H, d, *J* = 6.8 Hz), 6.96 (2H, d, *J* = 7.6 Hz), 7.17 (2H, d, *J* = 8 Hz), 7.54 (2H, d, *J* = 7.6 Hz), 7.8-7.88 (6H, m), 8.16 (1H, s), 9.92 (1H, s); ^{13}C NMR ($CDCl_3$, 100 MHz) δ 21.7, 21.8, 38.9, 64.0, 74.8, 85.3, 90.4, 119.7, 126.1, 126.2, 126.8, 129.4, 129.5, 129.7, 129.8, 130.4, 135.9, 136.4, 144.4, 144.7, 146.6, 165.9, 166.2, 191.8. HRMS calcd for $C_{30}H_{28}N_3O_6$ $[M+H]^+$ 526.1973, found 526.1973.

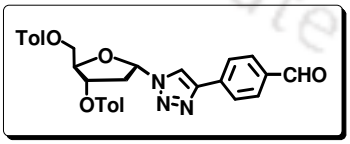

Synthesis of 3′, 5′-bis{O-(p-toluoyl)}-2′-deoxy-1′-β-triazolyl difluorophenyl nucleoside (2.91β, bis-toluoyl-β-$^{TDFB}B_{Ac}$): Using the general procedure, starting from 60 mg (0.152 mmol) of azido–deoxy ribose sugar **2.84β** and 25 mg (0.182 mmol) of 1-ethynyl 2,4 difluoro benzene (**2.85K**), 69.6 mg (0.130 mmol) of the title compound **2.102β** was isolated as a white solid. Yield 86%; mp 165-170 ^{o}C; IR (KBr) 1729, 1709, 1610, 1281, 1112 cm^{-1}; ^{1}H NMR ($CDCl_3$, 400 MHz) δ 2.36 (3H, s), 2.44 (3H, s), 2.88-2.92 (1H, m), 3.26-3.29 (1H, m), 4.56 (1H, dd, *J* = 4, 12 Hz), 4.65-4.69 (2H, m), 5.8-5.81 (1H, m), 6.54 (1H, t, *J* = 6 Hz), 6.82-6.88 (1H, m), 6.98 (1H, t, *J* = 8 Hz), 7.16 (2H, d, *J* = 8 Hz), 7.28 (2H, d, *J* = 8 Hz), 7.84 (2H, d, *J* = 8 Hz), 7.96 (2H, d, *J* = 8 Hz), 8.08-8.09 (1H, m), 8.18-8.25 (1H, m); ^{13}C NMR ($CDCl_3$, 400 MHz) δ 21.8, 21.9, 38.4, 63.9, 74.9, 83.8, 89.1, 104.2, 111.9, 112.1, 121.3, 126.6, 126.8, 129.3, 129.4, 129.8, 129.95, 141.1, 144.1, 144.6, 166.01, 166.29; HRMS calcd for $C_{29}H_{26}F_2N_3O_5$ $[M+H]^+$ 534.1835, found 534.1886.

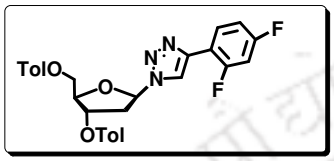

Synthesis of 3′, 5′-bis{O-(p-toluoyl)}-2′-deoxy-1′-α-triazolyl difluorophenyl nucleoside (2.91α, bis-toluoyl-α-$^{TDFB}B_{Ac}$): Using the general procedure, starting from 50 mg (0.126 mmol) of azido–deoxy ribose sugar **2.84α** and 20.88 mg (0.151 mmol) of 1-ethynyl 2,4-difluorobenzene (**2.85K**), 66.65 mg (0.125mmol) of the compound **2.102α** was isolated as a white solid. Yield 99.2%; mp117-120 ^{o}C; IR (KBr) 1716, 1610, 1281, 1270, 1101 cm^{-1} ; ^{1}H NMR ($CDCl_3$, 400 MHz) δ 2.24 (3H, s), 2.32 (3H, s), 2.96-3.02 (1H, m), 3.06 (1H, d, *J* = 14.8 Hz), 4.49-4.58 (2H, m), 4.74-4.77 (1H, m), 5.59 (1H, d, *J* = 6.4 Hz), 6.51 (1H, d, *J* = 5.2 Hz), 6.75-6.81 (1H, m), 6.88-6.93 (1H, m), 6.99 (2H, d, *J* = 8 Hz), 7.17 (2H, d, *J* = 8 Hz), 7.58(2H, d, *J* = 8 Hz), 7.86 (2H, d, *J* = 8 Hz), 8.14 (1H, d, *J* = 3.6 Hz), 8.15-8.21(1H, m); ^{13}C NMR ($CDCl_3$, 100 MHz) δ 21.8, 38.9, 64.1, 74.7, 85.1, 90.3, 103.9, 104.2, 104.4, 111.9, 112.2, 120.6, 120.7, 126.2, 126.8, 129.0, 129.1, 129.3, 129.5, 129.8, 140.8, 144.4, 144.5, 166.1, 166.3. HRMS calcd for $C_{29}H_{26}F_2N_3O_5$ $[M+H]^+$ 534.1835, found 534.1837.

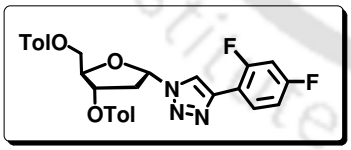

2.7.6. General Procedure for toluoyl deprotection of triazolyl donor/acceptor aromatic nucleosides

The bistoluoylated nucleoside (1 equiv) was dissolved in dry methanol. Sodium methoxide (3.5 equiv) was subsequently added. The solution was left for overnight stirring at room temperature. The solution was evaporated and the deprotected products were separated by column chromatography. All the β-epimers except **2.90β** ($^{TBenzal}\mathbf{B}_{Ac}$) and **2.91β** ($^{TDFB}\mathbf{B}_{Ac}$) were deprotected.

Synthesis of 2′-deoxy-1′-β–triazolyl-N,N-dimethylanilino nucleoside (2.103β, β-$^{TNDMB}B_{Do}$): Using the general procedure for deprotection starting from 98.2 mg (0.182mmol) of compound **2.92β**, 50.4 mg (0.165mmol) of compound **2.103β** was isolated as yellow solid. Yield 91.11%; mp 168 ^{o}C; IR (KBr) 3330, 1617, 1507, 1201, 1105, 1051, 1013 cm^{-1}; ^{1}H NMR (CD_3OD, 400 MHz) δ 2.36-2.42 (1H, m), 2.64-2.71 (1H, m), 2.84 (6H, s), 3.49-3.54 (1H, m), 3.59-3.64 (1H, m), 3.90 (1H, q, *J* = 4.2, 4.8 Hz), 4.43 (1H, q, *J* = 4.6, 6 Hz), 6.29 (1H, t, *J* = 6 Hz), 6.68 (2H, d, *J* = 8.4 Hz), 7.51 (2H, d, *J* = 8.8 Hz), 8.21 (1H, s); ^{13}C NMR (CD_3OD, 400 MHz) δ 40.9, 41.9, 63.5, 72.5, 89.9, 90.4, 113.9, 119.3, 119.8, 127.8, 149.8, 152.4; HRMS calcd. for $C_{15}H_{21}N_4O_3$ $[M+H]^+$ 305.16, found 305.1643.

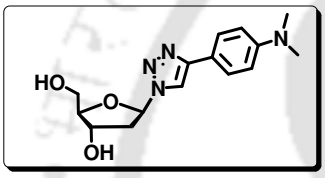

Synthesis of 2′-deoxy-1′-β–triazolyl-dimethoxyphenyl nucleoside (2.104β, β-$^{TDMB}B_{Do}$): Using the general procedure for deprotection starting from 290.9 mg (0.522 mmol) of compound **2.93β**, 160.3 mg (0.499 mmol) of compound **2.104β** was isolated as white solid. Yield 95.5%; mp 135-140 ^{o}C; IR (KBr) 3243, 1603, 1203, 1156, 1013 cm^{-1}; ^{1}H NMR (CD_3OD, 400 MHz) *δ* 2.51–2.57 (1H, m), 2.79-2.84 (1H, m), 3.66 (1H, dd, *J* = 4.8, 11.6 Hz), 3.73-3.75 (1H, m), 3.83 (6H, s), 4.03 (1H, q, *J* = 3.6 Hz), 4.58 (q, *J* = 4.8, 4.4 Hz), 6.38-6.48 (m, 1H), 7.01 (1H, s), 8.54 (1H, s); ^{13}C NMR (CD_3OD, 100 MHz) *δ* 41.7, 55.9, 63.2, 72.2, 90.3, 101.5, 104.7, 121.1, 130.7, 133.3, 148.9, 162.8; HRMS calcd. for $C_{15}H_{20}$ N_3O_5 ($[M+H]^+$) 322.1393, found 322.1397.

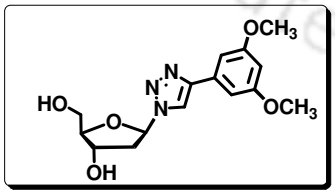

Synthesis of 2'-deoxy-1'-α–triazolyl-dimethoxyphenyl nucleoside (2.104α, α-$^{TDMB}B_{Do}$): Using the general procedure for deprotection starting from 260 mg (0.47

mmol) of compound **2.93α**, 144.0 mg (0.448 mmol) of compound **2.104α** was isolated as white solid. Yield 95.4%; IR (KBr) 3340, 1208, 1082, 1053 cm^{-1}; ^1H NMR

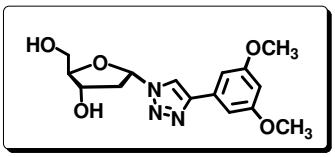

(CD_3OD, 400 MHz) δ 2.40 (1H, td, *J* = 2.4, 14.4 Hz), 2.73-2.80 (1H, m), 3.49-3.53 (1H, m), 3.56-3.60 (1H, m), 3.70 (6H, s), 4.16 (1H, q, *J* = 3.6 Hz), 4.32-4.35 (1H, m), 6.33 (1H, d, *J* = 2.4 Hz), 6.35(1H, d, *J* = 2.0 Hz), 6.87 (2H, d, *J* = 2.4 Hz), 8.47 (1H, s); ^{13}C NMR (CD_3OD, 100 MHz) δ 42.0, 56.0, 63.3, 72.7, 90.7, 91.5, 101.6, 104.8, 121.22, 130.3, 130.9, 133.5, 148.9, 162.9. HRMS calcd. for $C_{15}H_{20}O_5N_3$ $[M+H]^+$ 322.1402, found 322.1416.

Synthesis of 2′-deoxy-1′- β–triazolyl-phenoxyphenyl nucleoside (2.105β, β-$^{TPhOB}B_{Do}$): Using the general procedure for deprotection starting from 100.00 mg (0.169mmol) of compound **2.94β**, 54.1 mg (0.153mmol) of compound **2.105β** was isolated as white solid. Yield 90.67%; mp 143 °C; IR (KBr) 3399, 1488, 1241, 1090, 1067, 1039 cm^{-1}; ^1H NMR (CD_3OD, 400 MHz) δ 2.52-2.55 (1H, m), 2.79-2.83 (1H,

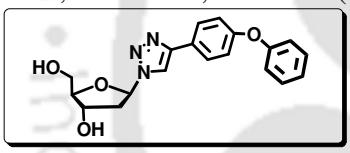

m), 3.64-3.77 (2H, m), 4.04-4.07 (1H, m), 4.56-4.59 (1H, m), 6.43-6.45 (1H, m), 7.01 (4H, d, *J* = 6.8 Hz), 7.13 (1H, t, *J* = 6.0 Hz.), 7.36 (2H, t, *J* = 6.4 Hz)7.78 (2H, d, *J* = 7.2), 8.45 (1H, s); ^{13}C NMR (CD_3OD, 100 MHz) δ41.9, 63.4, 72.4, 89.9, 90.5, 120.1, 120.4, 120.6, 124.9, 126.8, 128.5, 131.2, 148.7, 158.4, 159.2; HRMS calcd for $C_{19}H_{20}O_4N_3$ $[M+H]^+$ 354.1453, found 354.1480.

Synthesis of 2′-deoxy-1′-β-triazolylmethoxynapthalene nucleoside (2.106β, β-$^{MNap}B_{Do}$): Using the general procedure for deprotection starting from 85 mg (0.147 mmol) of compound **2.95β**, 52.92 mg (0.153 mmol) of compound **2.106β** was isolated as white solid. Yield 88 %; R_f = 0.5 in100% ethylacetate; mp 141-145 °C; IR (KBr) 3390, 1674, 1419, 1284, 1095 cm^{-1}; ^1H NMR (CD_3OD, 400 MHz) δ 2.41-2.47 (1H,

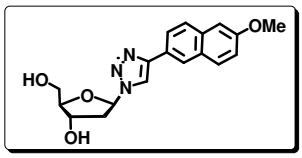

m), 2.69-2.76 (1H, m), 3.55 (1H, dd, *J* = 5.2, 12.0 Hz), 3.65 (1H, dd, *J* = 3.4, 12.0 Hz), 3.79 (3H, s) 3.92-3.95 (1H, m), 4.45-4.48 (1H, m), 6.36 (1H, t, *J* = 5.8 Hz), 7.04 (1H, dd, *J* = 4.0, 9.2 Hz), 7.13 (1H, s), 7.67-7.77 (3H, m), 8.11 (1H, s), 8.47 (1H, s); ^{13}C NMR (CD_3OD, 400 MHz) δ 41.9, 56.1, 63.5, 72.4, 90.0, 90. 5, 107.2, 120.8, 121.0, 125.5,

127.1, 128.9, 130.9, 136.2, 149.3, 159.8; HRMS calcd for $C_{18}H_{20}N_3O_4$ $[M+H]^+$ 342.1453, found 342.1479.

Synthesis of 2′-deoxy-1′-α-triazolyl methoxynapthalene nucleoside (2.106α, α-$^{MNap}B_{Do}$): Using the general procedure for deprotection starting from 280 mg (0.48 mmol) of compound **2.95α**, 141.1 mg (0.413mmol) of compound **2.106α** was isolated as white solid. Yield 86%; mp183-185 ^oC; IR (KBr) 3353, 1611, 1502, 1261, 1218, 1142, 1106, 861, 815 cm^{-1}; ^1H NMR (CD_3OD, 400 MHz) δ 2.42 (1H, td, *J* = 2.4, 14.4 Hz.), 2.75-2.82 (1H, m), 3.51-3.61 (2H, m), 3.79 (3H, s), 4.18 (1H, q, *J* = 3.6, 4.0 Hz.), 4.34-4.37 (1H, m), 6.37 (1H, dd, *J* = 2.4, 7.6 Hz.), 7.03 (1H, dd, *J* = 2.4, 9.2 Hz.), 7.13 (1H, d, *J* = 2.4 Hz.), 7.67-7.77 (3H, m), 8.10 (1H, s), 8.56 (1H, s);^{13}C NMR (DMSO, 100 MHz) δ 55.3, 61.4, 70.4, 88.5, 88.9, 106.0, 119.2, 119.5, 123.5, 124.1, 125.9, 127.4, 128.6, 129.6, 133.9, 146.7, 157.5; HRMS calcd for $C_{18}H_{20}O_4N_3$ $[M+H]^+$ 342.1453, found 342.1466.

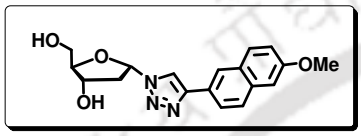

Crystallographic description for 2′-deoxy-1′-α-triazolyl methoxynapthalene nucleoside (2.106α, α-$^{MNap}B_{Do}$): Crystal dimension (mm): 0.29 x 0.22 x 0.15. $C_{18}H_{19}N_3O_4$, Mr = 341.36; Monoclinic, space group P 21; a = 5.808(7) Å, b = 29.856(4) Å, c = 9.539(11) Å; α = 90.00°, ß = 90.185°, γ = 90.00°, V = 1654.2(4) $Å^3$; Z = 4; ρcal = 1.371 g/cm^3; μ (mm^{-1}) = 0.099; *F(000)* = 720.00; Refinement method = Full-matrix least-squares on F^2; Final R indices [$I>2\sigma_I$] R(reflections) = 0.0478(2923), wR2(reflections) = 0.1066(4410); goodness of fit = 0.989.

Synthesis of 2′-deoxy-1′- β-triazolyl phenanthrene nucleoside (2.107β, β-$^{TPhen}B_{Do}$): Using the general procedure for deprotection starting from 278.7 mg (0.467 mmol) of compound **2.96β**, 155.2 mg (0.429 mmol) of compound **2.107β** was isolated as yellow solid. Yield 92.0%; mp 166-168 ^oC; IR (KBr) 3364, 1435, 1205, 1121, 1056, 1032 cm^{-1}; ^1H NMR (CD_3OD, 400 MHz) *δ* 2.59-2.64 (1H, m), 2.91-2.96 (1H, m), 3.71 (1H, dd, *J* = 4.4, 11.6 Hz), 3.79-3.82 (1H, m), 4.08-4.1 (1H, m), 4.62-4.65 (1H, m), 6.57 (1H, t, *J* = 5.6, 6.0 Hz), 7.62-7.7 (4H, m), 8.25 (1H, d, *J* = 8.4 Hz), 8.57 (1H, s), 8.78-8.86 (2H, m); ^{13}C NMR (CD_3OD, 100 MHz) *δ* 42.1, 63.5, 72.5, 90.1, 90.8, 123.9, 124.3, 124.4, 127.4, 128.0, 128.3, 128.4, 128.8, 129.9,

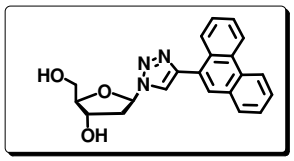

130.2, 131.6, 132.1, 132.3, 132.9, 148.1; HRMS calcd. for $C_{21}H_{20}N_3O_3$ ($[M+H]^+$) 362.1499, found 362.1510.

Crystallographic description for 2´-deoxy-1´-β-triazolyl phenanthrene nucleoside (2.107β, β-$^{TPhen}B_{Do}$): Crystal dimension (mm): 0.32 x 0.24 x 0.16. $C_{21}H_{19}N_3O_3$, Mr = 361.39; Orthorhombic, space group P 21 21 21; a = 10.054(3) Å, b = 12.268(3) Å, c = 14.054(3) Å; α = 90.00°, β = 90.00°, γ = 90.00°, V = 1732.4(8) Å3; Z = 4; ρcal = 1.386 Mg/m3; μ (mm^{-1}) = 0.095; *F (000)* = 760.00; Refinement method = Full-matrix least-squares on F^2; Final R indices [$I>2\sigma_I$] R(reflections)= 0.0522(1789), wR2(reflections)= 0.1184(3116); goodness of fit = 0.961.

Synthesis of 2´-deoxy-1´-α-triazolyl phenanthrene nucleoside (2.107α, α-$^{TPhen}B_{Do}$): Using the general procedure for deprotection starting from 280 mg (0.486mmol) of compound **2.96α**, 145.9 mg (0.404 mmol) of compound **2.107α** was isolated as pale yellow solid. Yield 83%; IR (KBr) 3364, 1121 1056, 857, 841, 746, 728 cm^{-1}; ^{1}H NMR (CD_3OD, 400 MHz) δ 2.50 (1H, td, *J* = 2.4,14.4 Hz.), 2.79-2.87 (1H, m), 3.52-3.63 (2H, m), 4.23 (1H, q, *J* = 3.8, 3.2Hz.), 4.36-4.39 (1H, m), 6.47 (1H,dd, *J* = 2, 7.4 Hz.), 7.48-7.53 (2H, m), 7.56-7.61 (2H, m), 7.83(1H, d, *J* = 8.0 Hz.), 7.85 (1H, s), 8.11 (1H, d, *J* = 8.4 Hz.), 8.52 (1H, s), 8.66 (1H, d, *J* = 8.4 Hz.), 8.73 (1H, d, *J* = 8.0 Hz.); ^{13}C NMR (CD_3OD, 100 MHz) δ 42.4, 63.6, 73.0, 91.2, 92.0, 124.1, 124.4, 124.6, 127.4, 128.4, 128.5, 128.9, 129.9, 130.3, 131.7, 132.1, 132.4, 132.9, 148.0. HRMS calcd for $C_{21}H_{20}N_3O_3$ $[M+H]^+$ 362.1499, found 362.1498.

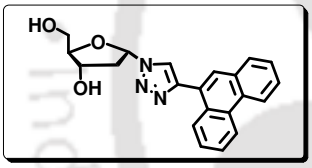

Synthesis of 2´-deoxy-1´-β-triazolyl pyrene nucleoside (2.108β, β-$^{TPy}B_{Do}$): Using the general procedure for deprotection starting from 60 mg (0.097 mmol) of compound **2.97β**, 30.61 mg (0.080mmol) of the title compound **2.108β** was isolated as white solid. Yield 81.4%; IR (KBr) 3376.8, 2942.5, 1068 cm^{-1};^{1}H NMR (CD_3OD+$CDCl_3$, 400 MHz) δ 2.64-2.68 (1H, m), 2.95-2.99 (1H, m), 3.73-3.86 (2H, m), 4.13 (1H, s), 4.55 (1H, s), 6.60 (1H, t, *J* = 5.6), 8.03-8.29 (8H, m), 8.56 (1H, d, *J* = 8), 8.67 (1H, s); ^{13}C NMR (CD_3OD, 100 MHz) δ 38.88, 41.39, 62.65, 71.59, 89.41, 89.79, 123.69, 125.56, 125.79, 126.04, 126.38, 127.23, 128.13, 128.68, 128.92,

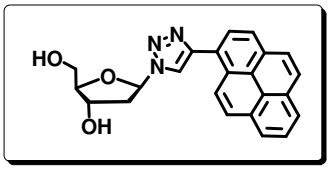

129.06, 131.65, 132.19, 147.69. HRMS calcd for $C_{23}H_{21}N_3O_3$ $[M]^+$ 387.1583, found 387.1532.

Synthesis of 2′-deoxy-1′-β-triazolyl butylpyrene nucleoside (2.109β, β-$^{TBPy}B_{Do}$): Using the general procedure for deprotection starting from 50 mg (0.069 mmol) of compound **2.98β**, 27.88 mg (0.058 mmol) of the title compound **2.109β** was isolated as white solid. Yield 83%; IR (KBr) 3432, 3356.8, 2926.8, 1715 cm^{-1}; ^1H NMR (CD_3OD, 400 MHz) δ 1.99-2.07 (2H, m), 2.25 (2H, t, *J* = 7.2), 2.29-2.35 (1H, m), 2.55-2.61 (1H, m), 3.19-3.24(2H, m)(merged with solvent peak), 3.24-3.58 (2H, m), 3.89 (1H, q, *J* = 4.4), 4.27-4.39 (3H, m), 6.24 (1H, t, *J* = 6), 7.74 (1H, d, *J* = 7.6), 7.84-8.06 (8H, m), 8.16 (1H, d, *J* = 9.2); ^{13}C NMR (CD_3OD, 100 MHz) δ 30.9, 33.8, 35.8 36.7, 41.9, 63.4, 72.4, 89.8, 90.3, 123.1, 124.5, 125.9, 126.0, 126.2, 126.3, 127.1, 127.8, 128.4, 128.5, 128.6, 129.9, 131.4, 132.4, 132.9, 137.4, 146.6, 175.93. HRMS calcd for $C_{28}H_{30}N_4O_4$ $[M]^+$ 486.2267, found 486.2230.

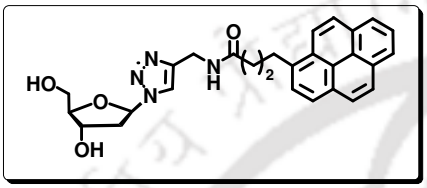

Synthesis of 2′-deoxy-1′-β-triazolyl nitrophenyl nucleoside (2.110β, β-$^{TNB}B_{Ac}$): Using the general procedure for deprotection starting from 255.6 mg (0.472 mmol) of compound **2.99β**, 132.05 mg (0.431 mmol) of the title compound **2.110β** was isolated as yellow solid. Yield 91.43%; IR (KBr) 3526, 3265, 1606,1516, 1346, 1072 cm^{-1}; ^1H NMR (CD_3OD, 400 MHz) *δ* 2.54-2.58 (1H, m), 2.81-2.86 (1H, m), 3.67 (1H, dd, *J* = 4.8, 12.0 Hz), 3.77 (1H, dd, *J* = 4, 12.0 Hz), 4.06 (1H, q, *J* = 4.8 Hz), 4.58 (1H, q, *J* = 4.8 Hz), 6.48 (1H, t, *J* = 5.2, 6.4 Hz), 8.09 (2H, d, *J* = 8.8 Hz), 8.33 (2H, d, *J* = 9.2 Hz), 8.76 (1H, s); ^{13}C NMR (CD_3OD, 100 MHz) *δ* 61.3, 70.0, 88.1, 121.7, 124.1, 125.7, 136.7, 144.4, 145.4; HRMS calcd. for $C_{13}H_{14}N_4O_5Na$ ($[M+Na]^+$) 329.0856, found 329.0867.

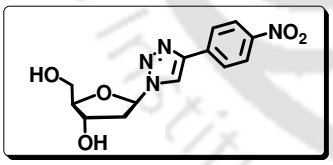

Crystallographic description for 2'-deoxy-1'-β-triazolyl nitrobenezene nucleoside (2.110β, β-$^{TNB}B_{Ac}$): Crystal dimension (mm): 0.30 x 0.26 x 0.17. $C_{13}H_{14}N_4O_5$, Mr = 306.28; Orthorhombic, space group P 21 21 21; a = 6.4456(7) Å, b = 9.8102(8) Å, c = 21.8210(19) Å; α = 90.00°, ß = 90.00°, γ = 90.00°, V = 1379.8(2) $Å^3$; Z = 4; ρcal = 1.474 g/cm^3; μ (mm^{-1}) = 0.116; *F(000)* = 640.00; Refinement

method = Full-matrix least-squares on F^2; Final R indices [I>2σ_l] R(reflections) = 0.0509(1701), wR2(reflections) = 0.1143(3180); goodness of fit = 0.933.

Synthesis of 2′-deoxy-1′-α-triazolyl nitrophenyl nucleoside (2.110α, α-$^{TNB}B_{Ac}$): Using the general procedure for deprotection starting from 290 mg (0.54 mmol) of compound **2.99α**, 135.5 mg (0.442 mmol) of the title compound **2.110α** was isolated as yellow solid. Yield 82%; mp147-150 ^{o}C; IR (KBr) 3523, 3473, 1513, 1341, 857 cm^{-1}; ^{1}H NMR (CD_3OD, 400 MHz) δ 2.52-2.57 (1H, m), 2.87-2.94 (1H, m), 3.63-3.74 (2H, m), 4.30-4.33 (1H, m), 4.46-4.49 (1H, m), 6.5-6.5 (1H, dd, *J* = 2, 7.6 Hz.), 8.07 (2H, d, *J* = 8.8 Hz.), 8.3 (2H, d, *J* = 8.8 Hz.), 8.8 (1H, s); ^{13}C NMR (CD_3OD, 100 MHz) δ 42.2, 63.4, 72.7, 91.0, 91.8, 122.7, 125.5, 127.5, 138.4, 146.9, 148.9.ESI calcd for $C_{13}H_{15}N_4O_5$ $[M+H]^+$ 307.1042, found 307.1376.

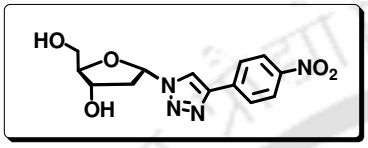

Synthesis of 2′-deoxy-1′- β-triazolyl cyanophenyl nucleoside (2.110β, β-$^{TCNB}B_{Ac}$): Using the general procedure for deprotection starting from 225 mg (0.431 mmol) of compound **2.100β**, 111.92 mg (0.391 mmol) of the title compound **2.111β** was isolated as white solid. Yield 90.8%; mp 142-145 ^{o}C; IR (KBr) 3243, 2230, 1359, 1167, 1100, 1063, 1037 cm^{-1}; ^{1}H NMR (CD_3OD, 400 MHz) *δ* 2.53-2.58 (1H, m), 2.79-2.85 (1H, m), 3.66 (1H, dd, *J* = 4.8, 12.0 Hz), 3.76 (1H, dd, *J* = 4.0, 12.4 Hz), 4.031-4.063 (1H, m), 4.56-4.62 (1H, m), 6.47 (1H, d, *J* = 5.6 Hz), 7.798 (2H, d, *J* = 8.4 Hz), 8.01 (2H, d, *J* = 8.4 Hz), 8.70 (1H, s); ^{13}C NMR (CD_3OD, 100 MHz) *δ* 41.9, 63.4, 72.3, 89.9, 90.6, 112.8, 119.8, 122.5, 127.4, 134.1, 136.5, 147.3; HRMS calcd. for $C_{14}H_{14}N_4O_3Na$ ($[M+Na]^+$) 309.0964, found 309.0969.

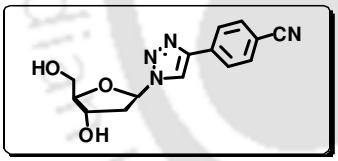

Synthesis of 2′-deoxy-1′-α-triazolyl cyanophenyl nucleoside (2.111α, α-$^{TCNB}B_{Ac}$): Using the general procedure for deprotection starting from 240 mg (0.46 mmol) of compound **2.100α**, 123.5 mg (0.431 mmol) of the title compound **2.111α** was isolated as white solid. Yield 93.8 %; mp124-129 ^{o}C; IR (KBr) 3450,3403, 2232, 1085 cm^{-1}; ^{1}H NMR (CD_3OD, 100 MHz) δ 2.40 (1H, td, *J* = 2, 14.8 Hz.), 2.73-2.80 (1H, m), 3.49-3.54 (1H, m), 3.56-3.59 (1H, m), 4.17 (1H, q, *J* = 3.8,

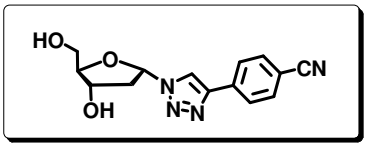

7.0 Hz.), 4.32-4.35 (1H, m), 6.37 (1H, dd, *J* = 2, 7.6 Hz.), 7.67 (2H, d, *J* = 8.4 Hz.), 7.89 (2H, d, *J* = 8.4 Hz.), 8.64 (1H, s); ^{13}C NMR (CD_3OD, 100 MHz) δ 42.1, 63.3, 72.9, 90.9, 91.8, 112.6, 122.4, 127.2, 127.4, 136.5, 147.1. HRMS calcd. for $C_{14}H_{15}N_4O_3$ $[M+H]^+$ 287.1144, found 287.1147.

2.7.7. Photophysical Studies of the Nucleosides

UV-visible measurements: All the *UV* –visible spectra of the compounds (10 μM) were measured in different solvents using a UV-Visible spectrophotometer with a cell of 1 cm path length. The measurements were carried out in absorbance mode. The absorbance values of the sample solutions were measured in the wavelength regime of 200–550 nm. All the sample solutions were prepared just before doing the experiment.

Fluorescence experiments: All the sample solutions were prepared as described in UV measurement experiments. Fluorescence spectra were obtained using a fluorescence spectrophotometer at 25 °C using 1 cm path length cell. The excitation wavelengths for all the cases were set at the excitation maxima of each sample in each solvents and emission spectra were measured in the wavelength regime of 300–700 nm with an integration time of 0.2 sec. All the sample solutions were prepared just before doing the experiment. Total volume of 1.0 ml from a stock solution of 2 ml of 10 μM concentration for each case was used for fluorescence experiment in 1 ml cell. Fluorescence emissions were collected exciting the samples at the wave length corresponding to their absorption maxima. Steady-state fluorescence emission spectra were recorded at room temperature as an average of five scans using an excitation slit of 3.0 nm, emission slit 3.0 nm, and scan speed of 120 nm/min. The fluorescence quantum yields (Φ_f) were determined using either quinine sulphate as a reference with the known Φ_f (0.55) in 0.1 molar solution in sulphuric acid or amino pyridine as a reference with the known Φ_f (0.6) in 0.1 molar solution in sulphuric acid. The following equation was used to calculate the quantum yield,

$$\Phi_S = \Phi_R \frac{Fl_S^{Area}}{Fl_R^{Area}} \frac{Abs_R}{Abs_S} \frac{n_S^2}{n_R^2}$$

where, Φ_R is the quantum yield of standard reference, Fl_S^{Area} (sample) and Fl_R^{Area} (reference) are the integrated emission peak areas, Abs_S (sample) and Abs_R (reference) are the absorbances at the excitation wavelength, and n_S (sample) and n_R (reference) are the refractive indices of the solutions.

The fluorescence lifetime experiment was carried out using a time resolved fluorescence spectrophotometer at 25 °C using 1 cm path length cell. 375 nm laser was used as excitation light source. The lifetime data were calculated by software with fixed fitting range. The time correlated single photon counting (TCSPC) method was used to calculate the lifetime data. The life time data (Global Analysis) were calculated by the software package with fitting range 205 – 4000 channels.

2.8. ^{1}H and ^{13}C NMR Spectra

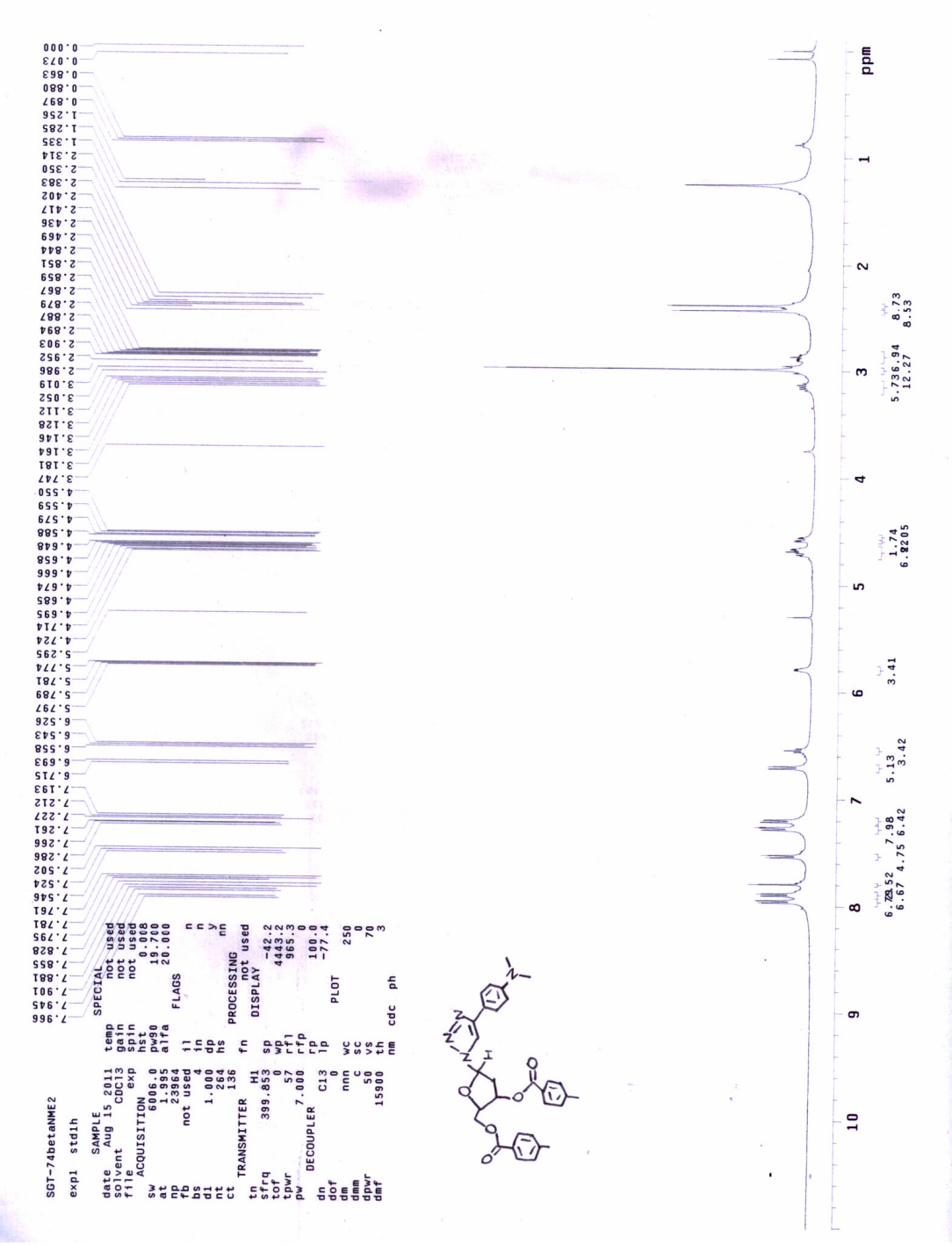

^{1}H NMR spectra of compound **2.92β**

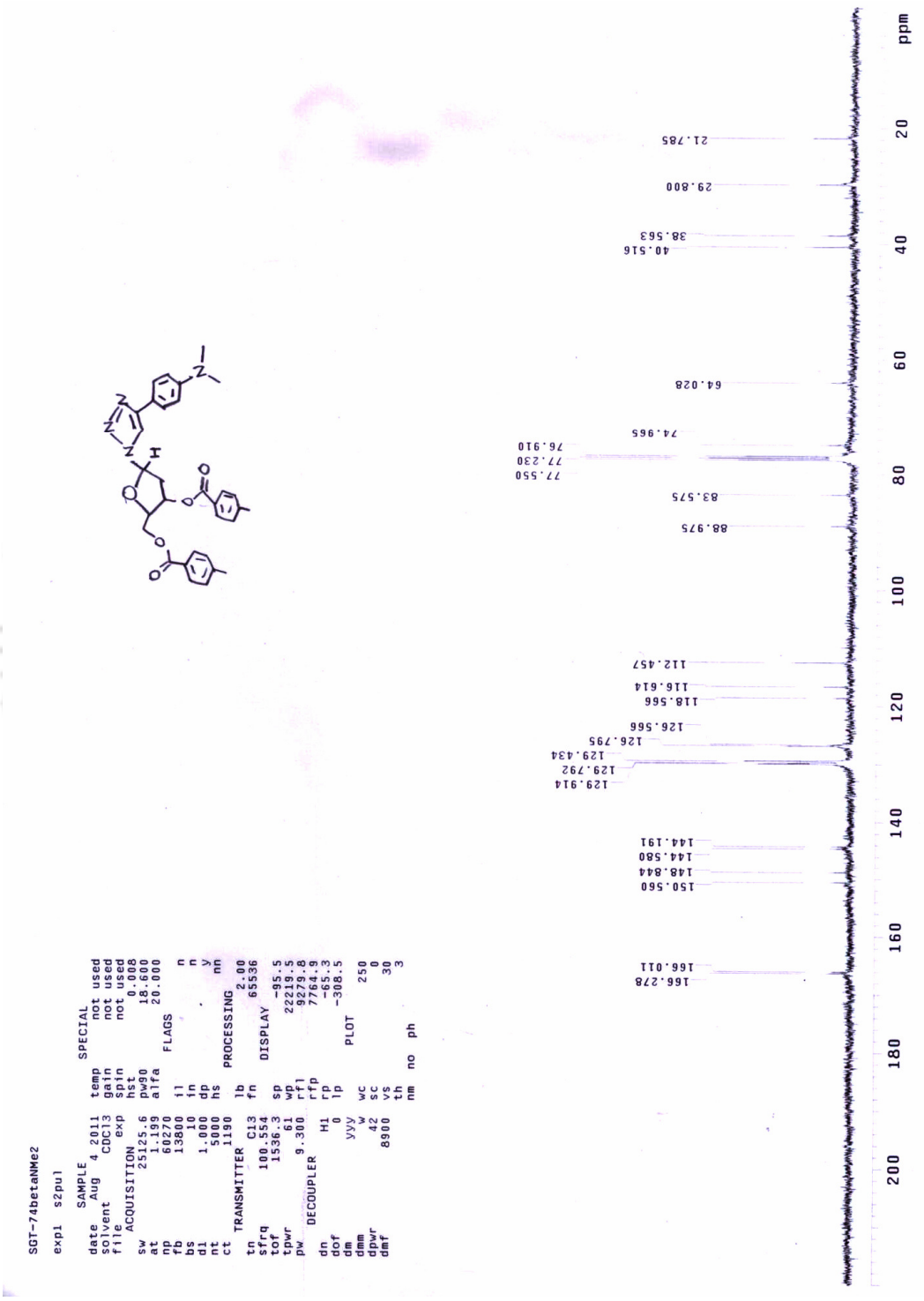

^{13}C NMR spectra of compound **2.92β**

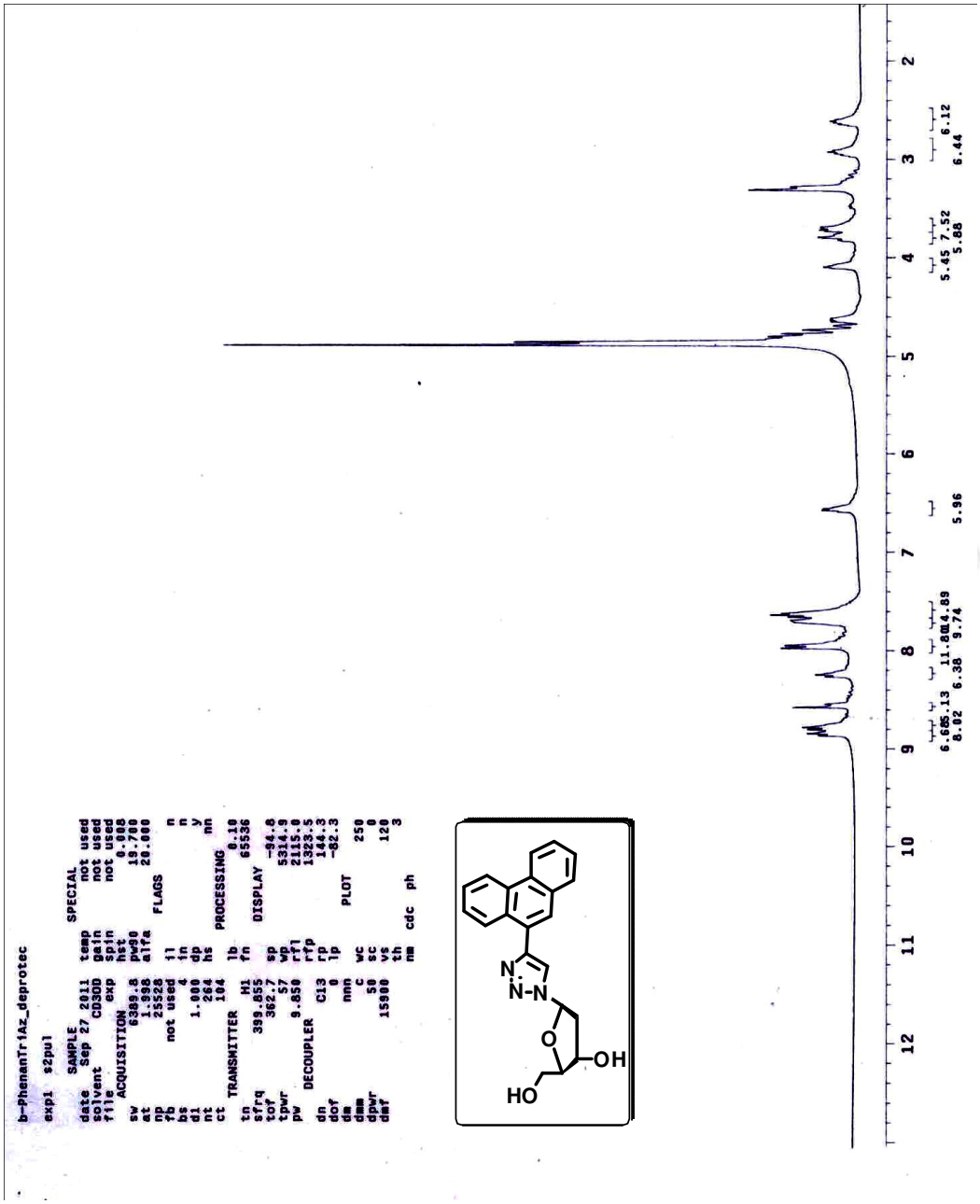

^{1}H NMR spectra of compound **2.107β**

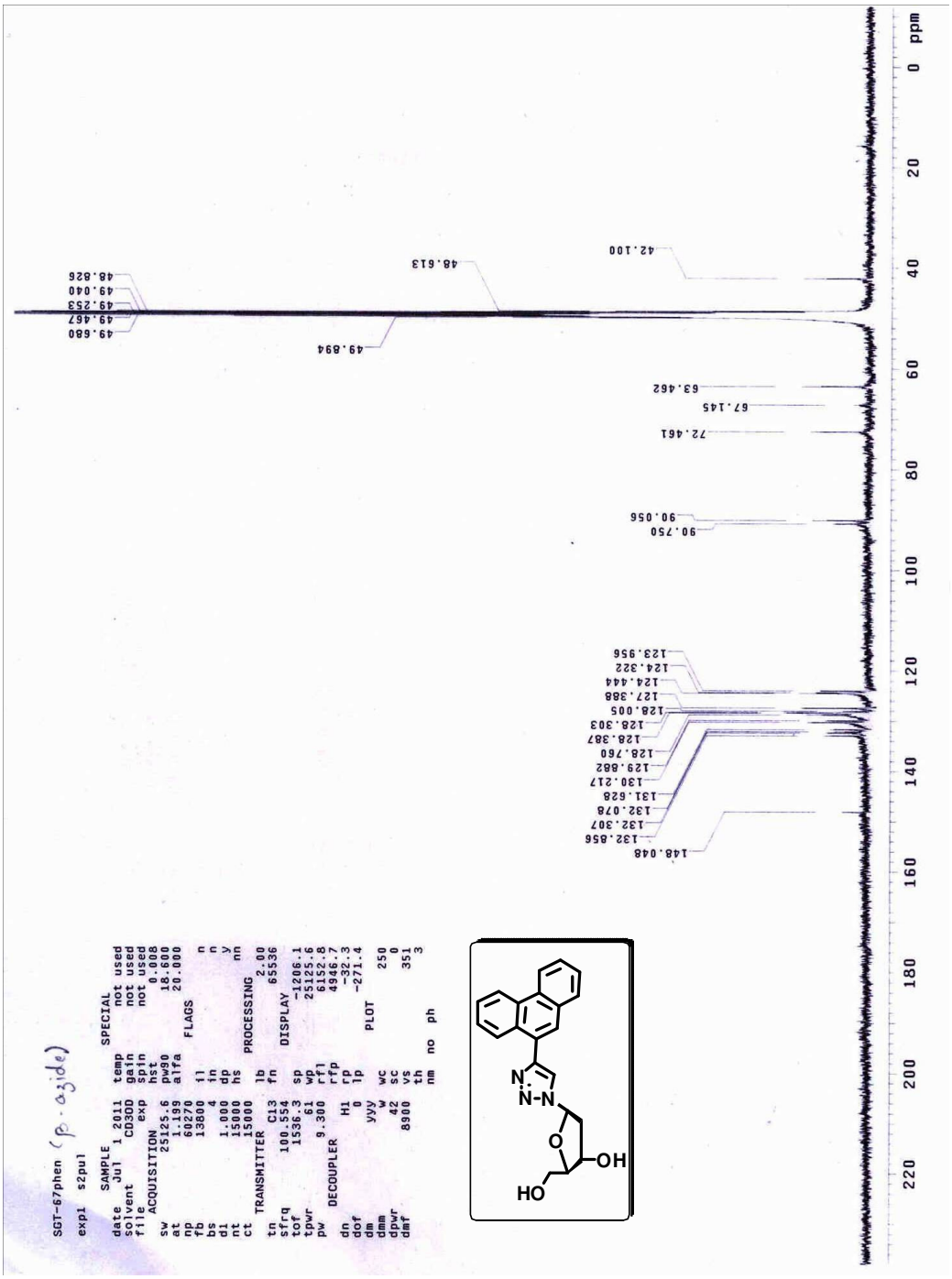

^{13}C NMR spectra of compound **2.107β**

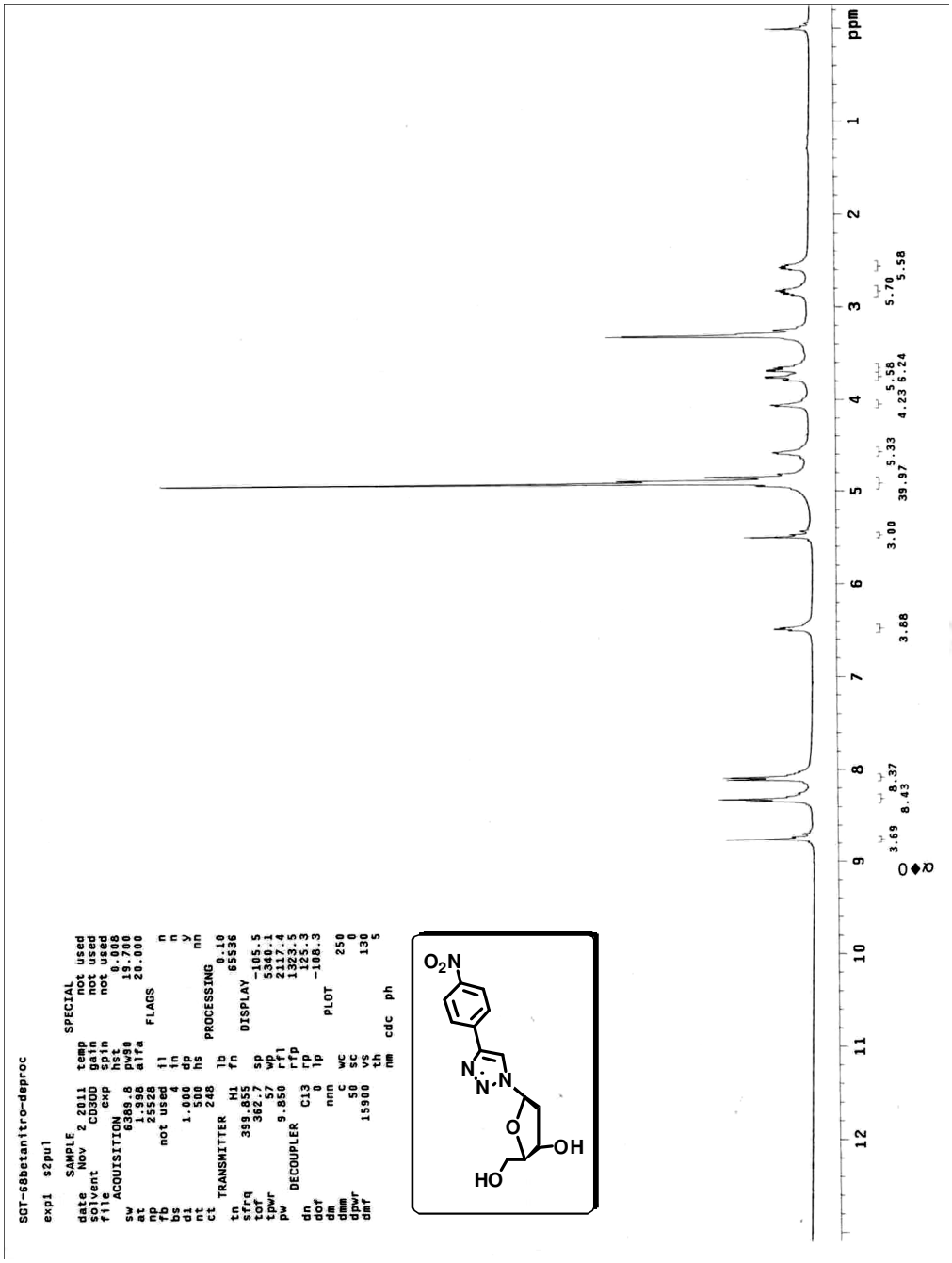

^{1}H NMR spectra of compound **2.110β**

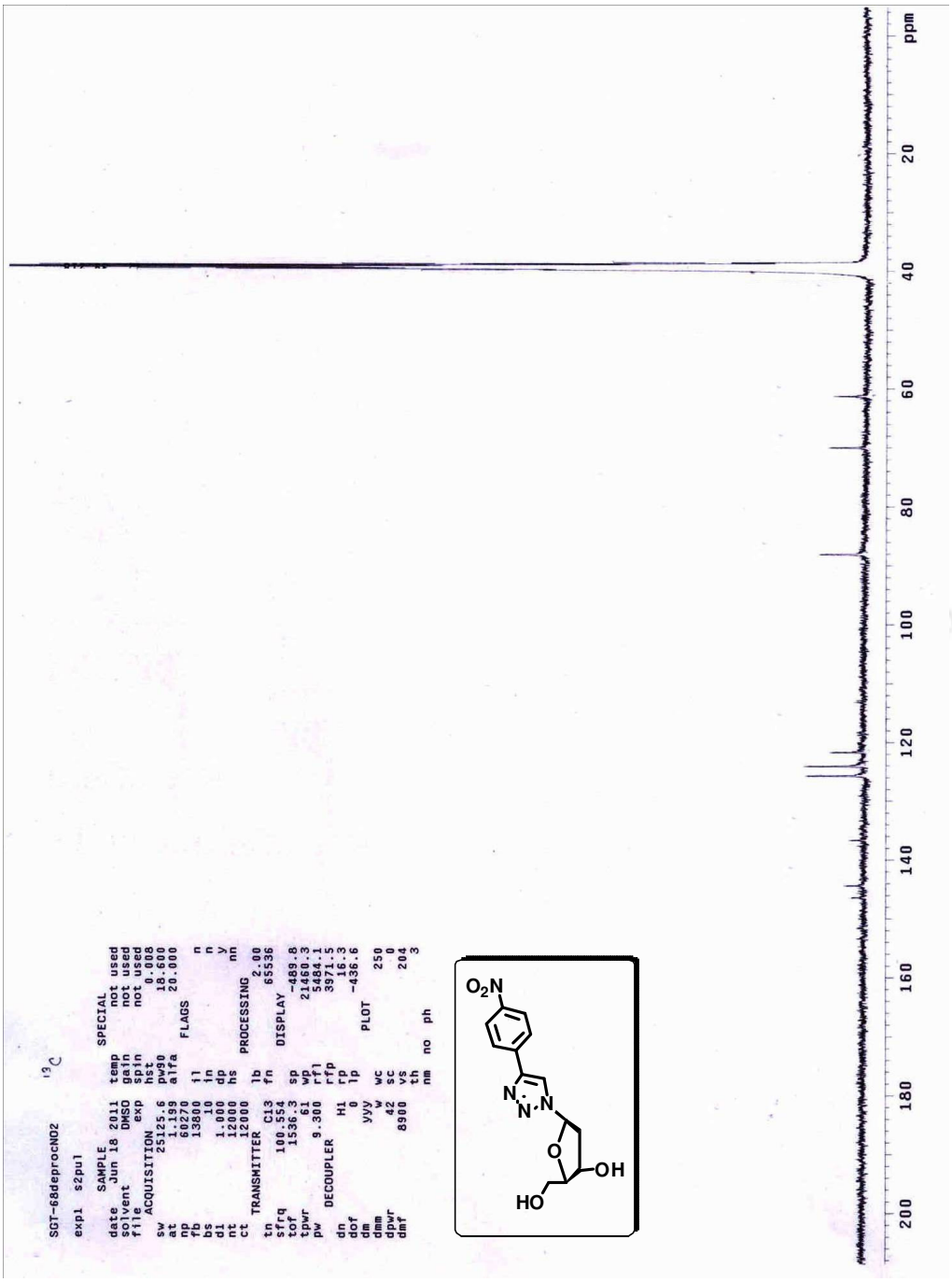

^{13}C NMR spectra of compound **2.110β**

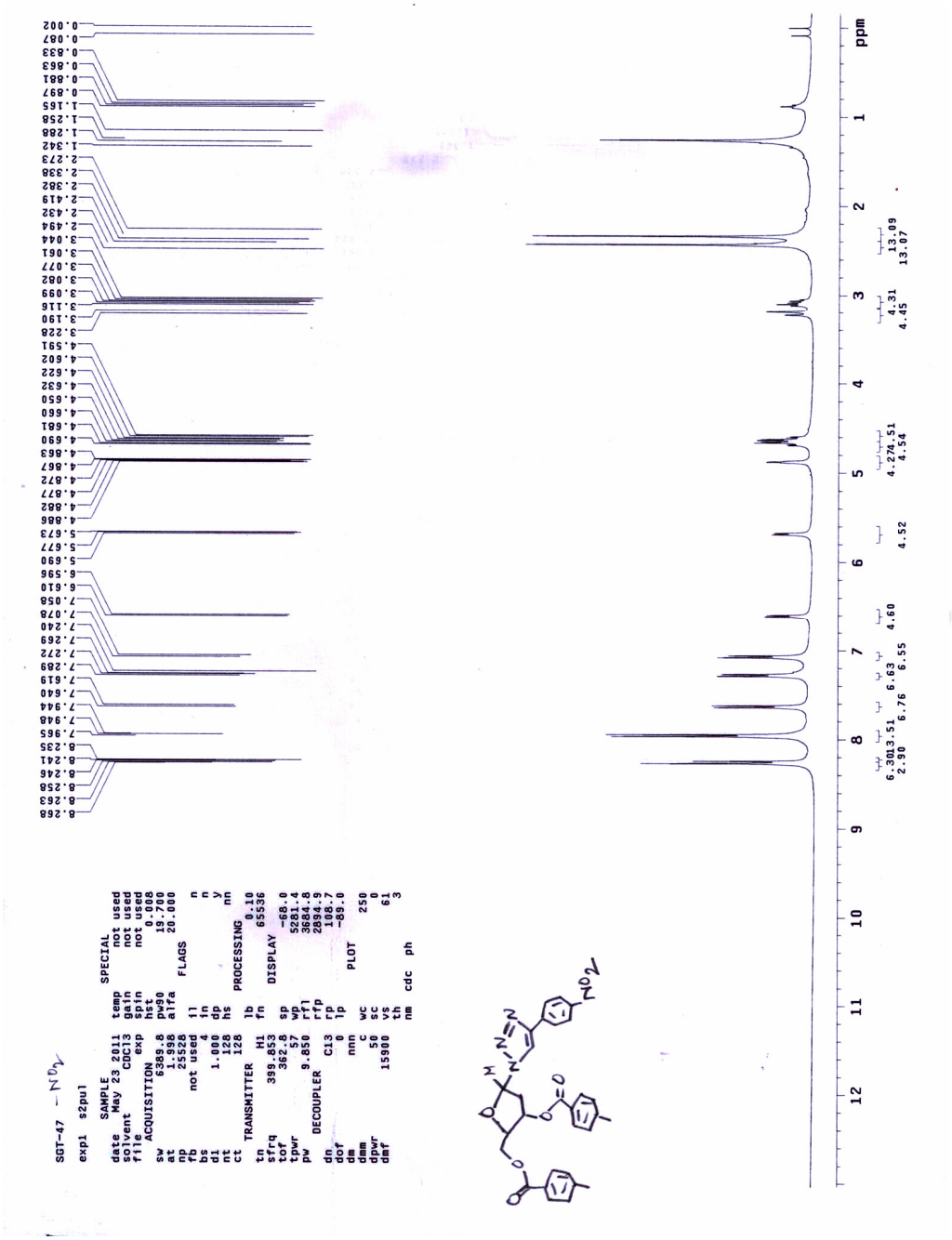

^{1}H NMR spectra of compound **2.99α**

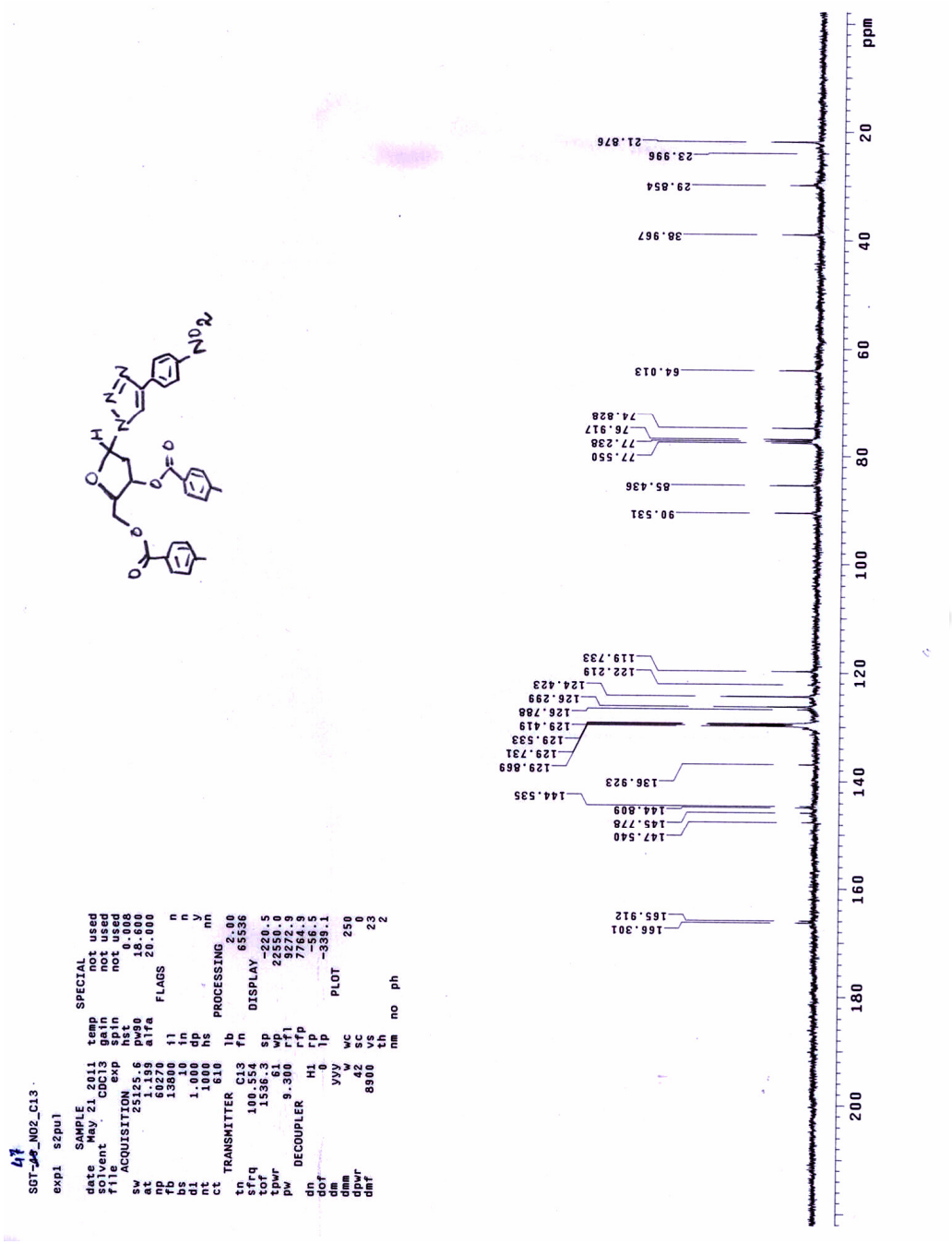

^{13}C NMR spectra of compound **2.99α**

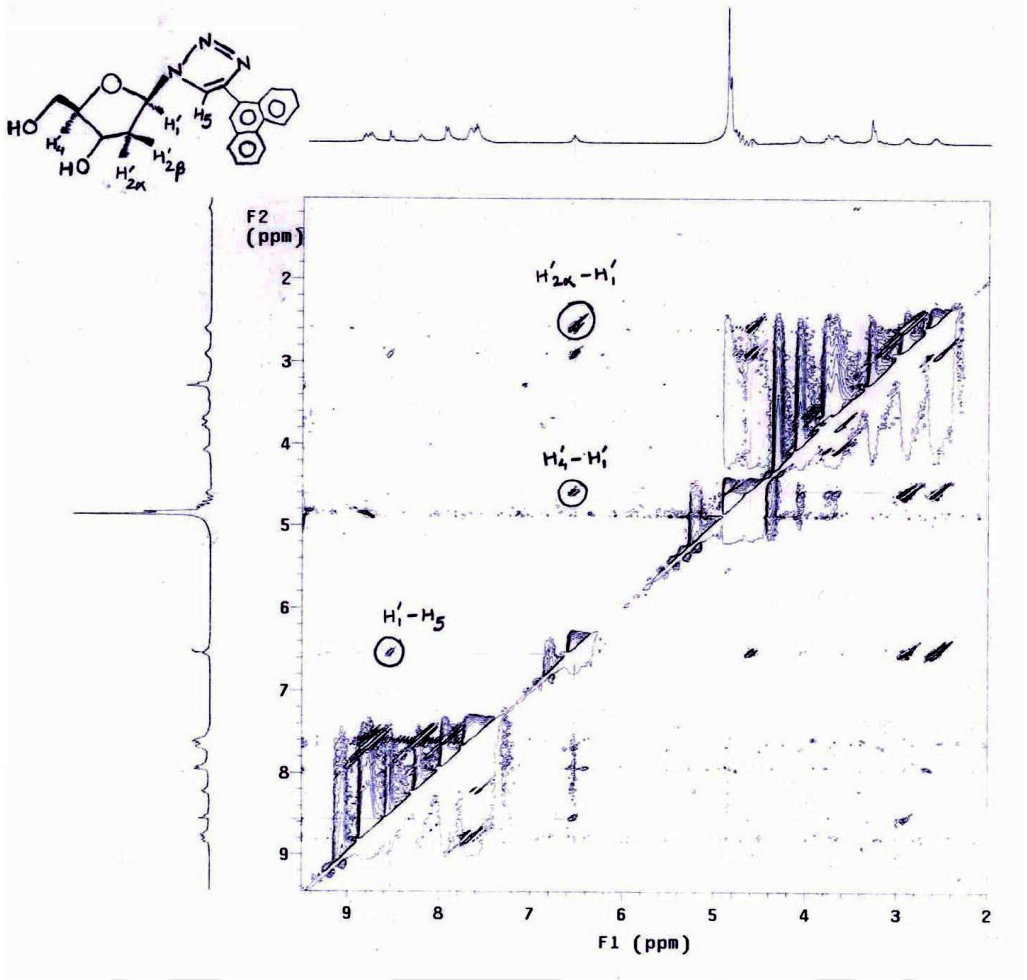

NOESY spectra of compound **2.107β**

2.9. References

1. (a) Morales, J. C.; Kool, E. T. *Biochemistry* **2000**, *39*, 2626. (b) Rubira, M.-J.; Jimeno, M.-L.; Balzarini, J.; Camarasa, M.-J.; Perez-Perez, M.-J. *Tetrahedron* **1998**, *54*, 8223. (c) Ali Md., M.; Imoto, S.; Li, Y.; Sasaki, S.; Nagatsugi, F. *Bioorg. Med. Chem.* **2009**, *17*, 2859. (d) McKenna, C. E.; Kashemirov, B. A.; Peterson, L. W.; Goodman, M. F. *Biochim. Biophys. Acta*, *Proteins and Proteomics* **2010**, *1804*, 1223. (e) Hatton, W.; Arosio, D.; Re, M.; Giudici, D.; Bernardi, A.; Seneci, P. *Comptes Rendus Chim.* **2010**, *13*, 1284.

2. (a) Taniguchi, Y.; Sasaki, S. *Org. Biomol. Chem.* **2012**, *10*, 8336. (b) Lavergne, T.; Malyshev, D. A.; Romesberg, F. E. *Chem.- A Eur. J.* **2012**, *18*, 1231. (c) Niu, C.; Murakami, E.; Furman, P. A. *Antiviral Therapy* **2008**, *13*, 263. (d) Srivatsan, S. G.; Weizman, H.; Tor, Y. *Org. Biomol. Chem.* **2008**, *6*, 1334. (e) Mitsui, T.; Kimoto, M.; Kawai, R.; Yokoyama, S.; Hirao, I. *Tetrahedron* **2007**, *63*, 3528. (f) Kim, Y.; Leconte, A. M.; Hari, Y.; Romesberg, F. E. *Angew. Chem., Int. Ed.* **2006**, *45*, 7809.

3. (a) Nakano, S.-i.; Fujii, M.; Sugimoto, N. *J. Nucleic Acids* **2011**, 967098, 11. (b) Ono, T.; Edwards, S. K.; Wang, S.; Jiang, W.; Kool, E. T. *Nucleic Acids Res.* **2013**, *41*, e127. (c) Furse, K. E.; Corcelli, S. A. *J. Phys. Chem. B* **2010**, *114*, 9934. (d) Moser, M. J; Marshall D. J; Grenier, J. K; Kieffer, C. D; Killeen, A. A; Ptacin, J. L.; Richmond, C. S.; Roesch, E. B.; Scherrer, C. W; Sherrill, C. B; *Clinical Chem.* **2003**, *49*, 407.(e) Kimoto, M.; Yamashige, R.; Matsunaga, K.-i.; Yokoyama, S.; Hirao, I. *Nature Biotech.* **2013**, *31*, 453. (f) Singh, V.; Wang, S.; Kool, E. T. *J. Am. Chem. Soc.* **2013**, *135*, 6184. (g) Wang, S.; Guo, J.; Ono, T.; Kool, E. T. *Angew. Chem., Int. Ed.* **2012**, *51*, 7176.

4. (a) Bag, S. S.; Heemstra, J. M.; Saito, Y.; Chenoweth, D. M. *J. Nucleic Acids* **2012**, *718582*, 2. (b) Li, L.; Degardin, M.; Lavergne, T.; Malyshev, D. A.; Dhami, K.; Ordoukhanian, P.; Romesberg, F. E. *J. Am. Chem. Soc.* **2014**, *136*, 826. (c) Kimoto, M.; Hikida, Y.; Hirao, I. *Israel J. Chem.* **2013**, *53*, 450. (d) Hirao, I.; Kimoto, M. *Pro. Jap. Acad., Series B: Phys. Biolo. Sc.* **2012**, *88*, 345. (e) Malyshev, D. A.; Dhami, K.; Quach, H. T.; Lavergne, T.;

Ordoukhanian, P.; Torkamani, A.; Romesberg, F. E. *PNAS, USA* **2012**, *109*, 12005. (f) Yamashige, R.; Kimoto, M.; Takezawa, Y.; Sato, A.; Mitsui, T.; Yokoyama, S.; Hirao, I. *Nucleic Acids Res.* **2012**, *40*, 2793. (g) Lavergne, T.; Malyshev, D. A.; Romesberg, F. E. *Chem. - A Eur. J.* **2012**, *18*, 1231. (h) Kimoto, M.; Cox, R. S., III; Hirao, I. *Expert Rev. Mol. Diagnos.* **2011**, *11*, 321. (i) Krueger, A. T.; Peterson, L. W.; Chelliserry, J.; Kleinbaum, D. J.; Kool, E. T. *J. Am. Chem. Soc.* **2011**, *133*, 18447. (j) Kimoto, M.; Hirao, I. *Methods Mol. Biolo.* **2010**, *634*, 355. (k) Romesberg, F. E; Yu, C.; Matsuda, S.; Henry, A. A. In Current protocols in nucleic acid chemistry, Ed., Serge, L. B. **2002**, Chapter 1, Unit 1.5.

5. (a) Mencin, N.; Smuc, T.; Vranicar, M.; Mavri, J.; Hren, M.; Galesa, K.; Krkoc, P.; Ulrich, H.; Solar, B. *J. Pharmaceutic. Biomed. Anal.* **2014**, *91*, 151. (b) Sefah, K.; Yang, Z.; Bradley, K. M.; Hoshika, S.; Jimenez, E.; Zhang, L.; Zhu, G.; Shanker, S.; Yu, F.; Turek, D. *PNAS, USA* **2014**, *111*, 1449. (c) Ulrich, H.; Wrenger, C. *Methods in Mol. Biol.* **2013**, *986*, 17. (d) Zhang, J.; Liu, B.; Liu, H.; Zhang, X.; Tan, W. *Nanomedicine* **2013**, *8*, 983. (e) Ho, C.; Yu, H.-Z. *Neuromethods* **2013**, *80*, 319. (f) Tonelli, R. R.; Colli, W.; Alves, M. J. M. *Frontiers in Microb. Immunol.* **2013**, *4*, 419. (g) Hong, P.; Li, W.; Li, J. *Sensors* **2012**, *12*, 1181. (h) Ayel, E.; Escude, C. *Nucleic Acids Res.* **2010**, *38*, e31/1. (i) Keefe, A. D.; Cload, S. T. *Curr. Opin. Chem. Biol.* **2008**, *12*, 448. (j) Lindemose, S.; Nielsen, P. E.; Mollegaard, N. E. *Nucleic Acids Res.* **2008**, *36*, 4797. (k) Gourdeau, H.; Leblond, L.; Hamelin, B.; Dong, K.; Ouellet, F.; Boudreau, C.; Custeau, D.; Richard, A.; Gilbert, M.-J.; Jolivet, J. *Clinical Cancer Res.* **2004**, *10*, 7692.

6. (a) Ding, P.; Wunnicke, D.; Steinhoff, H.-J.; Seela, F. *Chem. - A Eur. J.* **2010**, *16*, 14385. (b) Kimoto, M.; Hikida, Y.; Hirao, I. *Israel J. Chemistry* **2013**, *53*, 450. (c) Seo, Y. J.; Malyshev, D. A.; Lavergne, T.; Ordoukhanian, P.; Romesberg, F. E. *J. Am. Chem. Soc.* **2011**, *133*, 19878. (d) Hirao, I.; Kimoto, M.; Mitsui, T.; Fujiwara, T.; Kawai, R.; Sato, A.; Harada, Y.; Yokoyama, S. *Nat. Methods* **2006**, *3*, 729.

7. (a) Li, L.; Degardin, M.; Lavergne, T.; Malyshev, D. A.; Dhami, K.;

Ordoukhanian, P.; Romesberg, F. E. *J. Am. Chem. Soc.* **2014**, *136*, 826. (b) Lavergne, T.; Degardin, M.; Malyshev, D. A.; Quach, H. T.; Dhami, K.; Ordoukhanian, P.; Romesberg, F. E. *J. Am. Chem. Soc.* **2013**, *135*, 5408. (c) Yamashige, R.; Kimoto, M.; Takezawa, Y.; Sato, A.; Mitsui, T.; Yokoyama, S.; Hirao, I. *Nucleic Acids Res.* **2012**, *40*, 2793. (d) Malyshev, D. A.; Pfaff, D. A.; Ippoliti, S. I.; Hwang, G. T.; Dwyer, T. J.; Romesberg, F. E. *Chem. - A Eur. J.* **2010**, *16*, 12650. (e) Hirao, I.; Mitsui, T.; Kimoto, M.; Yokoyama, S. *J. Am. Chem. Soc.* **2007**, *129*, 15549. (f) Winnacker, M.; Kool, E. T. *Angew. Chem., Int. Ed.* **2013**, *52*, 12498. (g) Attwater, J.; Tagami, S.; Kimoto, M.; Butler, K.; Kool, E. T.; Wengel, J.; Herdewijn, P.; Hirao, I.; Holliger, P. *Chem. Sci.* **2013**, *4*, 2804. (h) Kellinger, M. W.; Ulrich, S.; Chong, J.; Kool, E. T.; Wang, D. *J. Am. Chem. Soc.* **2012**, *134*, 8231. (i) Ulrich, S.; Kool, E. T. *Biochemistry* **2011**, *50*, 10343. (k) Morales, J. C.; Kool, E. T. *Nature Str. Biol.* **1998**, *5*, 950. (j) Delaney, J. C.; Henderson, P.l T.; Helquist, S. A.; Morales, J. C.; Essigmann, J. M.; Kool, E. T. *PNAS, USA* **2003**, *100*, 4469.

8. (a) Kim, H.-J.; Leal, N. A.; Hoshika, S.; Benner, S. A. *J. Org. Chem.* **2014**, *79*, 3194. (b) Khakshoor, O.; Wheeler, S. E.; Houk, K. N.; Kool, E. T. *J. Am. Chem. Soc.* **2012**, *134*, 3154. (c) Benner, S. A. *Acc. Chem. Res.* **2004**, *37*, 784. (d) Geyer, C. R.; Battersby, T. R.; Benner, S. A. *Structure* **2003**, *11*, 1485. (e) Yang, Z.; Hutter, D.; Sheng, P.; Sismour, A. M.; Benner, S. A. *Nucleic Acids Res.* **2006**, *34*, 6095. (f) Schneider, K. C.; Benner, S. A. *J. Am. Chem. Soc.* **1990**, *112*, 453. (g) Lu, H.; Krueger, A. T.; Gao, J.; Liu, H.; Kool, E. T. *Org. Biomol. Chem.* **2010**, *8*, 2704. (h) Sintim, H. O.; Kool, E. T. *J. Am. Chem. Soc.* **2009**, *131*, 11270. (i) Delaney, J. C.; Gao, J.; Liu, H.; Shrivastav, N.; Essigmann, J. M.; Kool, E. T. *Angew. Chem., Int. Ed.* **2009**, *48*, 4524. (j) Minakawa, N.; Ogata, S.; Takahashi, M.; Matsuda, A. *J. Am. Chem. Soc.* **2009**, *131*, 1644. (k) Hirao, I.; Kimoto, M.; Yamakage, S.-i.; Ishikawa, M.; Kikuchi, J.; Yokoyama, S. *Bioorg. Med. Chem. Lett.* **2002**, *12*, 1391. (l) Gao, K. *Recent Res. Develop., Nucleosides Nucleotides* **2003**, *1*, 97. (m) Kim, Y.; Leconte, A. M.; Hari, Y.; Romesberg, F. E. *Angew. Chem., Int. Ed.* **2006**, *45*, 7809. (n) Hirao, I. *CSJ Curr. Rev.* **2011**, *6*, 101. (o) Tawarada, R.; Seio, K.;

Sekine, M. *J. Org. Chem.* **2008**, *73*, 383. (p) Polonius, F.-A.; Mueller, J. *Angew. Chem., Int. Ed.* **2007**, *46*, 5602. (q) Liu, H.; Gao, J.; Lynch, S. R.; Saito, Y. D.; Maynard, L.; Kool, E. T. *Science* **2003**, *302*, 868.

9. (a) Schweitzer, B. A.; Kool, E. T. *J. Org. Chem.* **1994**, *59*, 7238. (b) Schweitzer, B. A.; Kool, E. T. *J. Am. Chem. Soc.* **1995**, *117*, 1863. (c) Ren, R. X.-F.; Chaudhuri, N. C.; Paris, P. L.; Rumney, S., IV; Kool, E. T. *J. Am. Chem. Soc.* **1996**, *118*, 7671. (d) Moran, S.; Ren, R. X.-F.; Rumney, S., IV; Kool, E. T. *J. Am. Chem. Soc.* **1997**, *119*, 2056. (e) Moran, S.; Ren, R. X.-F.; Kool, E. T. *PNAS, USA* **1997**, *94*, 10506. (f) Matray, T. J.; Kool, E.T. *J. Am. Chem. Soc.* **1998**, *120*, 6191. (g) Morales, J. C.; Kool, E. T. *J. Am. Chem. Soc.* **1999**, *121*, 2323. (h) Barsky, D.; Kool, E. T.; Colvin, M. E. *J. Biomol. Str. Dyn.* **1999**, *16*, 1119. (i) Guckian, K. M.; Krugh, T. R.; Kool, E. T. *J. Am. Chem. Soc.* **2000**, *122*, 6841. (j) Kool, E. T. *Acc. Chem. Res.* **2002**, *35*, 936. (k) Takezawa, Y.; Shionoya, M. *Acc. Chem. Res.* **2012**, *45*, 2066. (l) Otsuka, T.; Miyazaki, T, *Int. J. Quan. Chem.* **2013**, *113*, 504. (m) Hwang, G. T.; Hari, Y.; Romesberg, F. E. *Nucleic Acids Res.* **2009**, *37*, 4757. (n) Hirao, I. *Curr. Opin. Chem. Biol.* **2006**, *10*, 622. (o) Hirao, I.; Kimoto, M.; Mitsui, T.; Fujiwara, T.; Kawai, R.; Sato, A.; Harada, Y.; Yokoyama, S. *Nat. Methods* **2006**, *3*, 729. (p) Henry, A. A.; Romesberg, F. E. *Curr. Opin. Chem. Biol.* **2003**, *7*, 727. (q) Betz, K.; Malyshev, D. A.; Lavergne, T.; Welte, W.; Diederichs, K.; Romesberg, F. E.; Marx, A. *J. Am. Chem. Soc.* **2013**, *135*, 18637. (r) Li, L.; Degardin, M.; Lavergne, T.; Malyshev, D. A.; Dhami, K.; Ordoukhanian, P.; Romesberg, F. E. *J. Am. Chem. Soc.* **2014**, *136*, 826. (s) Lavergne, T.; Degardin, M.; Malyshev, D. A.; Quach, H. T.; Dhami, K.; Ordoukhanian, P.; Romesberg, F. E. *J. Am. Chem. Soc.* **2013**, *135*, 5408. (t) Kimoto, M.; Hirao, I. *Methods Mol. Biol.* **2010**, *634*, 355. (u) Leconte, A. M.; Hwang, G. T.; Matsuda, S.; Capek, P.; Hari, Y.; Romesberg, F. E. *J. Am. Chem. Soc.* **2008**, *130*, 2336.

10. (a) Han, Li; Bu, Y. *Phys. Chem. Chem. Phys.* **2011**, *13*, 5906. (b) Teo, Y. N.; Kool, E. T. *Chem. Rev.* **2012**, *112*, 4221. (c) Kimoto, M.; Mitsui, T.; Yamashige, R.; Sato, A.; Yokoyama, S.; Hirao, I. *J. Am. Chem. Soc.* **2010**,

132, 15418. (d) Kimoto, M.; Mitsui, T.; Yokoyama, S.; Hirao, I. *J. Am. Chem. Soc.* **2010**, *132*, 4988. (e) Guo, J.; Wang, S.; Dai, N.; Teo, Y. N.; Kool, E. T. *PNAS, USA* **2011**, *108*, 3493. (f) Dai, N.; Kool, E. T. *Chem. Soc. Rev.* **2011**, *40*, 5756. (g) Koo, C.-K.; Wang, S.; Gaur, R. L.; Samain, F.; Banaei, N.; Kool, E. T. *Chem. Commun.* **2011**, *47*, 11435. (h) Koo, C.-K.; Samain, F.; Dai, N.; Kool, E. T. *Chem. Sci.* **2011**, *2*, 1910.

11. (a) Wojciechowski, F.; Leumann, C. J. *Chem. Soc. Rev.* **2011**, *40*, 5669. (b) Grigorenko, N. A.; Leumann, C. J. *Chem.-Eur. J.* **2009**, *15*, 639. (c) Wilson, J. N.; Teo, Y. N.; Kool, E. T. *J. Am. Chem. Soc.* **2007**, *129*, 15426. (d) Robertson, N.; McGowan, C. A. *Chem. Soc. Rev.* **2003**, *32*, 96. (e) Keren, K.; Krueger, M.; Gilad, R.; Ben-Yoseph, G.; Sivan, U.; Braun, E. *Science* **2002**, *297*, 72. (f) Hall, D. B.; Holmlin, R. E.; Barton, J. K. *Nature* **1996**, *382*, 731.

12. (a) Liu, J.; Cao, Z.; Lu, Y. *Chem. Rev.* **2009**, *109*, 1948. (b) Drummond, T.G.; Hill, M.G.; Barton, J. K. *Nature Biotech.* **2003**, *21,* 1192. (c) Kolpashchikov, D. M.; Gerasimova, Y. V.; Khan M. S. *ChemBioChem* **2011**, *12,* 2564. (d) Liu, L.; Li,Y.; Liotta, D.; Lutz, S. *Nucleic Acids Res.* **2009**, *37,* 4472.

13. (a) Stambasky, J.; Hocek, M.; Kouovsky, P. *Chem. Rev.*, **2009**, *109*, 6729 and references therein. (b) Kool, E. T. *Acc. Chem. Res.* **2002**, *35*, 936. (c) Tor, Y.; Dervan, P. B. *J. Am. Chem. Soc.* **1993**, *115*, 4461. (d) Clever, G. H.; Kaul, C.; Carell, T. *Angew. Chem., Int. Ed.***2007**, *46*, 6226.

14. (a) Schweitzer, B. A.; Kool, E. T. *J. Am. Chem. Soc.* **1995**, *117*, 1863. (b) Kool, E. T. *Annu. Rev. Biochem.* **2002**, *71*, 191. (c) Seo, Y. J.; Matsuda, S.; Romesberg, F. E. *J. Am. Chem. Soc.* **2009**, 131, 5046. (d) Jarchow-Choy, S. K.; Sjuvarsson, E.; Sintim, H. O.; Eriksson, S.; Kool, E. T. *J. Am. Chem. Soc.* **2009**, *131*, 5488.

15. (a) Rostovtsev, V. V.; Green, L. G.; Fokin, V. V.; Sharpless, K. B. *Angew. Chem., Int. Ed.* **2002**, *41*, 2596. (b) El-Sagheer, A. H.; Brown, T. *Chem. Soc. Rev.* **2010**, *39*, 1388. (c) Marks, I. S.; Kang, J. S.; Jones, B. T.; Landmark, K. J.; Cleland, A. J. Taton, T. A. *Biocon.Chem.* **2011**, *22*, 1259. (d) Xiong, H.; Seela, F. *J. Org. Chem.* **2011**, *76*, 5584. (e) Xiong, H.; Leonard, P.; Seela, F.

Biocon.Chem. **2012**, *23*, 856. (f) Sau, S. P.; Hrdlicka, P. J. *J. Org. Chem.* **2012**, *77*, 5.

16. (a) Tornøe, C. W.; Meldal, M. *Proceedings of the Second International and the Seventeenth American Peptide Symposium* **2001**, 263. (b) Tornøe, C. W.; Christensen, C.; Meldal, M. *J. Org. Chem.* **2002**, *67*, 3057.

17. (a) Kolb, H. C.; Finn, M. G.; Sharpless, K. B. *Angew. Chem.* **2001**, *40*, 2004. (b) Rostovtsev, V. V.; Green, L. G.; Fokin, V. V.; Sharpless, B. K. *Angew. Chem., Int. Ed.* **2002**, *41*, 2596. (c) Kolb, H. C.; Sharpless, K. B. *Drug Discovery Today* **2003**, *8*, 1128.

18. Droumaguet, C. L.; Wang, C.; Wang, Q. *Chem. Soc. Rev.,* **2010**, *39*, 1233.

19. Seela, F. ;Xiong, H.; Leonard, P.; Budow, S. *Org. Biomol. Chem*., **2009**, *7*, 1374.

20. Sirivolu, V. R.; Chittepu, P.; Seela, F.*ChemBioChem.* **2008**, *9*, 2305.

21. Bouillon, C.; Meyer, A.; Vidal, S.; Jochum, A.; Chevolot, Y.; Cloarec, J.-P.; Praly, J.-P.; Vasseur, J.-J.; Morvan, F. *J. Org. Chem.* **2006**, *71*, 4700

22. Kocalka, P.; El-Sagheer, A. H.; Brown, T. *ChemBioChem* **2008**, *9*, 1280.

23. Kumar, R.; El-Sagheer, A.; Tumpane, J.; Lincoln, P.; Wilhelmsson, L. M.; Brown, T. *J. Am. Chem. Soc.* **2007**, *129*, 6859.

24. El-Sagheer, A. H.; Kumar, R.; Findlow, S.; Werner, J. M.; Lane, A. N.; Brown, T. *ChemBioChem* **2008**, *9*, 50.

25. El-Sagheer, A. H.; Brown, T. *J. Am. Chem. Soc*. **2009**, *131*, 3958.

26. (a) Uhlmann, E.; Peyman, A. *Chem. Rev*. **1990**, *90*, 543. (b) *Via*ri, V.; Ballini, J. P.; Vigny, P.; Blonski, C.; Dousset, P.; Shire, D. *Tetrahedron Lett.* **1987**, *28*, 3349.

27. von Matt, P.; Lochmann, T.; Altmann, K.-H. *Bioorg. Med. Chem. Lett*. **1997**, *7*, 1549.

28. Freier, S. M.; Altmann, K.-H. *Nucleic Acids Res.* **1997**, *25*, 4429.

29. Nuzzi, A.; Massi, A.; Dondoni, A. *QSAR Comb. Sci.* **2007**, *26*, 1191.

30. (a) Lucas, R.; Neto, V.; Bouazza, A. H.; Zerrouki, R.; Granet, R. ; Krausz, P.; Champavier, Y. *Tetrahedron Lett.* **2008**, *49*, 1004. (b) Lucas, R.; Zerrouki, R.; Granet, R ; Krausz, P.; Champavier, Y. *Tetrahedron* **2008**, *64*, 5467.

31. Isobe, H.; Fujino, T.; Yamazaki, N.; Guillot-Nieckowski, M.; Nakamura, E. *Org. Lett.* **2008**, *10*, 3729**.**

32. Chittepu, P.; Sirivolu,V. R.; Seela, F. *Bioorg. Med. Chem.* **2008**, *16*, 8427.

33. Cosyn, L.; Palaniappan, K. K.; Kim, S.; Duong, H. T.; Gao, Z.; Jacobson, K. A.; and Calenbergh, S. V. *J. Med. Chem.* **2006**, *49*, 7373.

34. Lakshman, M. K.; Singh, M. K.; Parrish, D.; Balachandran, R.; Billy W.; Day, B. W. *J. Org. Chem.*, **2010**, *75*, 2461.

35. Lakshman, M. K.; Kumar, A.; Balachandran, R.; Day, B. W.; Andrei, G.; Snoeck, R.; Balzarini, J. *J. Org. Chem.*, **2012**, *77*, 5870.

36. Ingale, S. A.; Pujari, S. S.; Sirivolu, V. R.; Ding, P.; Xiong, H.; Mei, H.; Seela, F. *J. Org. Chem.*, **2012**, *77*, 188.

37. (a) Kovalovs, A.; Novosjolova, I.; Bizdena, E.; Bizane, I.; Skardziute, L.; Kazlauskas, K.; Jursenas, S.; Turks, M. *Tetrahedron Lett.* **2013**, *54*, 850. (b) Novosjolova, I.; Bizdēna, E.; Turks, M. *Tetrahedron Lett.* **2013**, *54*, 6557.

38. Ingale, S. A.; Seela, F. *Tetrahedron* **2014**, *70*, 380.

39. Nakahara, M.; Kuboyama, T.; Izawa, A.; Hari, Y.; Imanishi, T.; Obika, S. *Bioorg. Med. Chem. Lett*. **2009**, *19*, 3316.

40. Guezguez, R.; Bougrin, K.; Akria, K. E.; Benhida, R.; *Tetrahedron Lett.* **2006**, *47*, 4807.

41. Ermolat'ev, D. S.; Metha, V. P.; Van der Eycken, E. V. *QSAR Comb. Sci.* **2007**, *26*, 1266.

42. (a) Broggi, J.; Joubert, N.; Aucagne, V.; Berteina-Raboin, S.; Diez- Gonzalez, S.; Nolan, S. P.; Topalis, D.; Deville-Bonne, D.; Balzarini, J.; Neyts, J.; Andrei, G.; Snoeck, R.; Agrofoglio, L. *Nucleosides Nucleotides* **2007**, *26*, 1391. (b) Broggi, J.; Joubert, N.; Diez-Gonzalez, S.; Berteina-Raboin, S.; Zevaco, T.; Nolan, S. P.; Agrofoglio, L. *Tetrahedron* **2009**, *65*, 1162.

43. Driowya, M.; Puissant, A.; Robert, G.; Auberger, P.; Benhida, R.; Bougrin, K. *Ultrasonics Sonochemistry* **2012**, *19*, 1132.

44. Pradere, U.; Roy, V.; McBrayer, T. R.; Schinazi, R. F.; Agrofoglio, L. A.; *Tetrahedron* **2008**, *64*, 9044.

45. Akri, K. E.; Bougrin, K.; Balzarini, J.; Farajd, A.; Benhida, R. *Bioorg. Med. Chem. Lett*. **2007**, *17*, 6656.

46. (a)Ren, R. X.-F.;Chaudhuri, N. C.; Paris, P. L.;Rumney IV, S.; Eric T. Kool, E. T.*J. Am. Chem. Soc.* **1996,** *118,* 7671.(b) Cahová, H.; Havran, L.; Brázdilová, P.; Pivoňková, H.; Pohl, R.; Fojta, M.; Hocek,M.*Angew. Chem. Int. Ed.***2008**, *47*, 2059.

47. Mulliken, R. S. *J. Am. Chem. Soc*. **1952**, *74*, 811.

48. (a) Seidel, C. A. M.; Schulz, A.; Sauer, M. H. M. *J. Phys. Chem.* **1996,** *100,* 5541. (b) Poulin, K. W.; Smirnov, A. V.; Hawkins, M. E., Balis, F. M.; Knutson, J. R. *Biochemistry* **2009**, *48*, 8861. (c) Wierzbinski, E.; de Leon, A.; Davis, K. L.; Bezer, S.; Wolak, M. A.; Kofke, M. J.; Schlaf, R.; Achim, C.; Waldeck, D. H. *Langmuir* **2012**, *28*, 1971. (d) Hervas, M.; Navarro, J. A.; De la Rosa, M. A. *Acc. Chem. Res.* **2003**, *36*, 798. (e) Berlin, Y. A.; Grozema, F. C.; Siebbeles, L. D. A.; Ratner, M. A. *J. Phys. Chem. C* **2008**, *112*, 10988.

49. (a) Morrison, L.E.; Stols, L.M. *Biochemistry* 1993, 32, 3095. (b) Marras, S. A. E.; Kramer, F. R.; Tyagi, S. *Nucleic. Acids Res.* 2002, *30*, e122. (c) Li, Q.; Luan, G.; Guo, Q.; Liang, J. *Nucl. Acids Res.* 2002, 30, e5. (d) Nazarenko, I.; Pires, R.; Lowe, B.; Obaldy, M.; Rashtchian, A. *Nucl. Acids Res.* 2002, *30*, 2089. (e) Johansson, M. K.; Fidder, H.; Dick, D.; Cook, R. M. *J. Am. Chem. Soc.* 2002, *124*, 6950.

50. (a) You, Y.; Tataurov, A. V.; Owczarzy, R. *Biopolymers* 2011, *95*, 472. (b) Moreira, B. G.; You, Y.; Behlke, M. A.; Owczarzy, R. *Biochem. Biophys. Res. Commun.* 2005, *327*, 473. (c) Kimoto, M.; Mitsui, T.; Yamashige, R.; Sato, A.; Yokoyama, S.; Hirao, I. *J. Am. Chem. Soc.* 2010, *132*, 15418. (d) Sinkeldam, R. W.; Greco, N. J.; Tor, Y. *Chem. Rev.* 2010, *110*, 2579. (e) Bag, S. S.; Kundu, R.; Matsumoto, K, Saito, Y.; Saito, I. *Bioorg. Med.Chem. Lett.* 2010, *20*, 3227.

51. Bag, S. S.; Kundu, R. *J. Org. Chem.* **2011**, *76*, 3348.

52. (a) Štimac, A.; Leban, I.; Kobe, J. *Synlett.* **1999**, 1069. (b) Štimac, A.; Kobe, J. *Carbohydrate Res.* **2000***, 329*, 317. (c) Kolganova, N. A.; Florentiev, V. L.; Chudinov, A. V.; Zasedatelev, A. S.; Timofeev, E. N. *Chem. Biodivers.* **2011**,

8, 568. (d) Bag, S. S.; Talukdar, S.; Matsumoto, K.; Kundu, R. *J. Org. Chem.* **2013**, *78*, 278.

53. (a) Chen, D.-W.; Beuscher, IV, A. E.; Stevens, R. C.; Wirsching, P.; Lerner, R. A.; Janda, K. D. *J. Org. Chem.* **2001**, *66*, 1725. (b) Yamada, K.; Hayakawa, H.; Sakata, S.; Ashida, N.; Yoshimura, Y. *Bioorg. Med.Chem. Lett.* **2010**, *20*, 6013. (c) Deglane, G.; Morvan, F.; Debart, F.; Vasseur, J.-J. *Bioorg. Med.Chem. Lett.* **2007**, *17*, 951. (d) Morvan, F.; Debart, F.; Vasseur, J.-J. *ChemBioChem* **2005**, *6*, 1254. (e) Morvan, F.; Debart, F.; Vasseur, J.-J. *Chem. Biodiv.* **2010**, *7*, 494. (f) Abdel Aleem H.; Larsen, E.; Pedersen, E. B. *Tetrahedron* **1995**, *51*, 7867.

54. (a) Turro, N. J. *Modern Molecular Photochemistry*, University Science Books, Sausalito, **1991**. (b) Lakowicz, J. R. *Principles of Fluorescence Spectroscopy*, Springer,New York, 3rd edn, **2006**. (c) Yang, S.-W.; Elangovan, A.; Hwang, K.-C.; Ho, T.-I. *J. Phys. Chem. B* **2005**, *109*, 16628. (d) Benniston, A. C.; Harriman, A.; Lawrie, D. J.; Mayeux, A. *Phys. Chem. Chem. Phys.* **2004**, *6*, 51. (e) Benniston, A. C.; Harriman, A.; Lawrie, D. J.; Mayeux, A.; Rafferty, K.; Russell, O. D. *Dalton Trans.* **2003**, 4762. (f) Calvert, J. G.; Pitts Jr., J. N. *Photochemistry*, John Wiley and Sons, Inc., New York, **1966**. (g) Kovalenko, S. A.; Ernsting, N. P.; Ruthmann, J. *J. Chem. Phys.* **1997**, *106*, 3504. (h) Strehmel, B.; Seifert, H.; Rettig, W. *J. Phys. Chem. B* **1997**, *101*, 2232. (i) Kim, J.; Lee, M. *J. Phys. Chem. A* **1999**, *103*, 3378. (j) Fromherz, P. *J. Phys. Chem.* **1995**, *99*, 7188.

55. (a) Albinsson, B. *J. Am. Chem. Soc.* **1997**, *119*, 6369. (b) Chen, X.; Zhao, Y.; Cao, Z. *J. Chem. Phys.* **2009**, *130*, 144307. (c) Verhoeven, J. W.; Scherer, T.; Willemse, R. J. *Pure. Appl. Chem.* **1993**, *65*, 1717. (d) Thiagarajan, V.; Selvaraju, C.; Malar, E. J. P.; Ramamurthy, P. *Chem. Phys. Chem.* **2004**, *5*, 1200. (e) Pham, T. H. N.; Clarke, R. J. *J. Phys. Chem. B* **2008**, *112*, 6513. (f) Huang, Y.; Cheng, T.; Li, F.; Huang, C.; Hou, T.; Yu, A.; Zhao, X.; Xu, X. *J. Phys. Chem. B* **2002**, *106*, 10020. (g) Koti, A. S. R.; Bhattacharjee, B.; Haram, N. S.; Das, R.; Periasamy, N.; Sonawane, N. D.; Ragnekar, D. W. *J. Photochem. Photobiol. A: Chem.* **2000**, *137*, 115. (h) Shim, T.; Lee, M. H.;

Kim, D.; Ouchi, Y. *J. Phys. Chem. B.* **2008**, *112*, 1906. (i) Bingemann, D.; Ernsting, N. P. *J. Chem. Phys.* **1995**, *102*, 2691. (j) Sertova, N.; Nunzi, J.-M.; Petkov, I.; Deligeorgiev, T. *J. Photochem. Photobiol. A. Chem* **1998**, *112*, 187. (k) Panigrahi, M.; Dash, S.; Patel, S.; Behera, P. K.; Mishra, B. K. *Spectrochim. Acta, Part A* **2007**, *68*, 757.

56. (a) Grabowksi, Z. R.; Rotkiewicz, K.; Rettig, W. *Chem. Rev.* **2003**, *103*, 3899. (b) Badger, G. M.; Walker, I. S. *J. Chem. Soc.* **1956**, 122.

Chapter 3

STUDIES ON THE SYNTHESIS AND PHOTOPHYSICAL PROPERTIES OF TETRAZOLYL NUCLEOSIDES

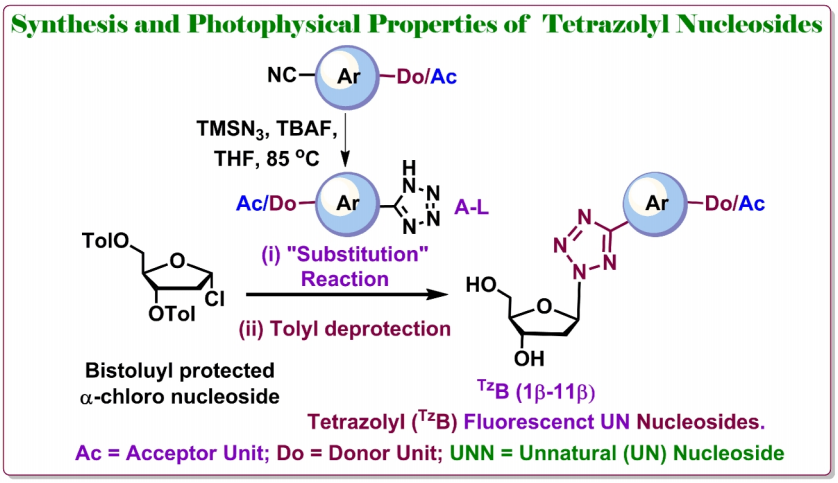

3.1. Introduction

The importance of non-covalent interactions in the stabilization of nucleic acids has been a topic of research since long time.[1] It has already been discussed in the previous chapters that hydrogen bonding interaction plays a significant role in the stability of DNA duplexes. However, recent studies have indicated that other than the H-bonding interaction, forces like π-π stacking/ hydrophobic interactions also play an important role in the stabilization of DNA duplexes.[2] In addition to these forces, electrostatic interactions /charge transfer interactions (discussed in **Chapter 2** and **4**) also play an important role in imparting stability to the DNA duplexes.[3] Therefore, large number of artificial base-pairs have been synthesized and incorporated into DNA in order to study the importance of π-π stacking interactions as well as other hydrophobic interactions in the stabilization of DNA duplexes.[1-3] However, there is no report of charge transfer complexation mediated DNA duplex stabilization wherein a designed donor-acceptor nucleobase pair inside a DNA duplex is held together *via* this force of interaction.[4] In this context, after the synthesis of unnatural triazolyl nucleosides as described in **Chapter 2** and the study of charge-transfer complexation between a donor/acceptor pair nucleoside, we extended our research towards the design of new tetrazolyl nucleosidic base-pairs which might find applications for the investigation of hydrophobic or charge transfer interactions operating in DNA duplexes.

Tetrazoles are known to exist in different tautomeric forms and also as cations and anions as shown in the **Figure 3.1**. The mono substituted NH-tetrazole can be represented as **3.1** and the two disubstituted tetrazoles can exist as two regioisomers i.e, 1,5- (**3.2**) and 2,5- (**3.3**) disubstituted tetrazoles. The mono substituted tetrazole can exist in the form of its anion also (**3.4**). Trisubstituted tetrazolium cations 1,4,5- (**3.5**), 1,3,5- (**3.6**) are also known which remain in the form of salts. The tetrazoles can also exist as bicyclic form (**3.7, 3.8**) or as partially dehydrogenated form as is represented by structure number **3.9** in **Figure 3.1**.

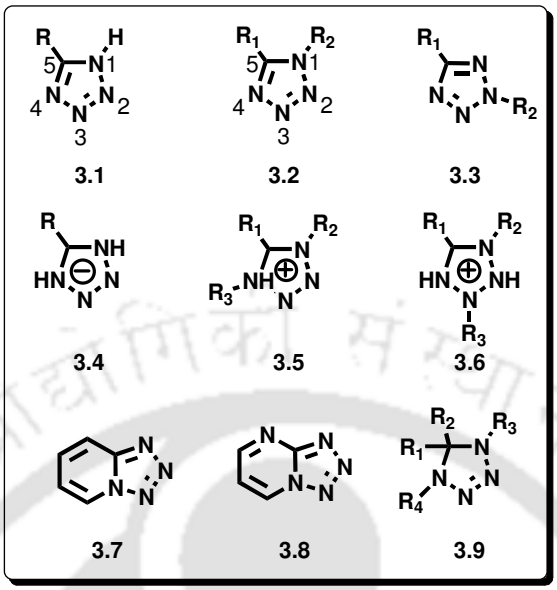

Figure 3.1: Structures of the different forms of tetrazole compounds.

3.2. Importance of Tetrazole Molecules

Tetrazole molecules exhibit a wide range of biological activity. More than 20 biological activities of tetrazoles are known such as (a) hypotensive action,[5] (b) antimicrobial and anti-inflammatory activity,[6] (c) antifungal activity,[7] (d) antiviral activity,[8] *etc.* Tetrazoles have the ability to form hydrogen bonds like purine and pyrimidine moiety. Since, two nitrogen atoms of the heterocyclic ring can simultaneously involve in hydrogen bonding interaction, they are known for their pronounced ability to form intermolecular hydrogen bonding. Thus, tetrazole unit possess several functional and structural properties which are given below:

(a) Tetrazole rings serve as non-classical isostere for the carboxylic acid moiety in biologically active molecules.

(b) In peptidomimetic drug design, 1,5-disubstituted tetrazoles are known as effective bioisosteres for *cis*-amide bonds.

(c) Tetrazoles are resistant to many biological metabolic degradation pathways.

(d) They can readily associate with other biological molecules *via* strong hydrogen bonding interactions.

Because of such attractive and important structural features and biological activity, tetrazoles have been successfully utilized for the design of various kinds of commercial drug candidates. Therefore, tetrazole derivatives have an adequate position in the modern pharmaceutical market.[9]

3.3. Synthetic Procedures for the Preparation of Tetrazole Compounds

Although a number of procedures for the preparation of the tetrazoles have been reported in literature, but the most direct method is the [2+3] cycloaddition of organic azides (R-N_3) and organic nitriles (R-CN). However, this methodology suffers from certain disadvantages, like the slow reaction rate except when potent electron-withdrawing groups activate the nitrile component, the use of both toxic metals and expensive reagents, drastic reaction conditions, water sensitivity and the presence of hazardous hydrazoic acid. Hallberg *et al.*[10] have reported a fast microwave assisted preparation of tetrazoles from the corresponding nitriles. This conversion has been carried out in one pot within a very short time and the methodology has been utilized to prepare a very potent HIV-1 protease inhibitor, comprising of two tetrazole heterocycles. Sharpless *et al.*[11] have reported the use of Zn(II) salts which act as an excellent catalyst for the union of azide ion with organic nitrile to form the respective tetrazoles. The coordination of the zinc ion with the organic nitrile is believed to substantially lower the activation energy for the nucleophilic attack by the azide in this case. However, this reaction needs high temperature (140-170 ^{o}C) in case of sterically hindered aromatic and inactivated alkyl nitriles. Amantani and Pizzo *et al.*[12] have reported the synthesis of 5-substituted 1-*H* tetrazoles using tetrabutylammonium fluoride (TBAF) as a catalyst under solvent free condition (**Scheme 3.1**). Tetrabutylammonium fluoride is an efficient catalyst in the [3 + 2] cycloaddition reaction of organic nitriles from which the corresponding 5-substituted 1-*H* tetrazoles have been obtained under mild reaction conditions with high yields (**Scheme 3.1**).

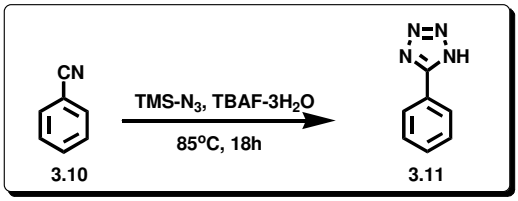

Scheme 3.1: Schematic representation of conversion of cyano moiety to the tetrazole ring.

A click chemistry based approach to the synthesis of tetrazoles has been adopted by Sharpless *et al.*[13] wherein the tetrazoles have been synthesized from azides and sulfonyl cyanides (**Scheme 3.2**). The procedure involved simple heating of toluenesulfonyl cyanide with one equivalent of unhindered azide in which quantitative conversion to the 1-alkyl-5-sulphonyl tetrazole was observed. The type of intermolecular cycloaddition of sulphonyl cyanide with unhindered aliphatic azides is a perfect mimic of click-chemistry reaction which can be carried out in neat condition applying heat and with 100% yield of the products, tetrazoles (**Scheme 3.2**).

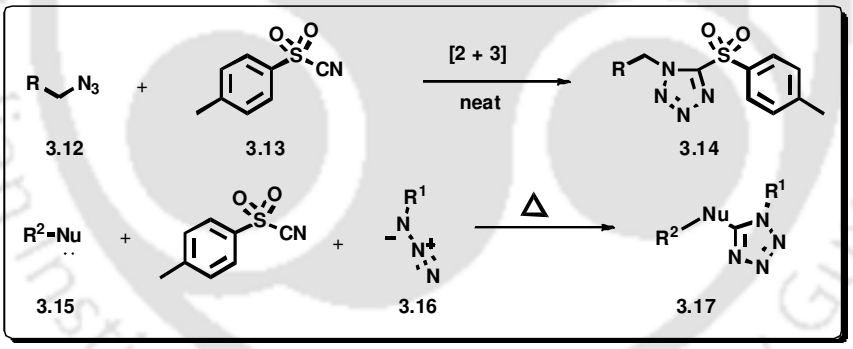

Scheme 3.2: Synthesis of 1,5 disubstituted tetrazole *via* [2+3] dipolar cycloaddition of unhindered azide and toluenesulphonyl cyanide.

Vilarrasa *et al.*[14] have reported the microwave assisted preparation of tetrazoles from organic nitriles and organic azides catalysed by $Cu_2(OTf)_2$ under mild reaction condition (**Scheme 3.3**). This reaction affords excellent yields of 1,5-disubstituted tetrazoles at ambient temperature with 1-10 mol% of the catalyst but under hetreogenous conditions with 50-100 mol% of the catalyst, which affords mainly 1, 4-disubstituted tetrazoles.

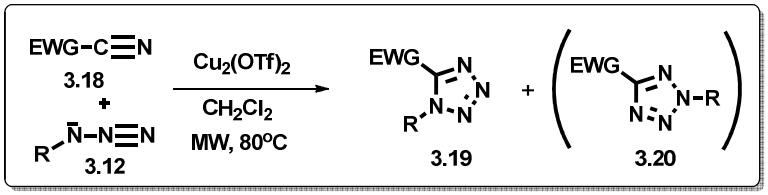

Scheme 3.3: Synthesis of 1,5 disubstituted tetrazole *via* Cu-catalysed [2+3] dipolar cycloaddition reaction.

3.4. Application of Tetrazoles as Amino Acid Analogues in Peptidomimetics

The replacement of the peptide bond with peptide bond surrogates in the biologically active peptides has been extensively studied in order to constrain the amide bond into a particular geometry.[15] Towards this end, *trans*-olefinic moiety has successfully been employed as a mimic of the *trans*-amide bond in a number of different peptides.[16] Although the *cis*-olefinic moiety is a perfect mimic of *cis*-amide bond, the isomerization of the *cis*-ß,γ- unsaturated carbonyl group to the more stable *trans*-α,ß- unsaturated carbonyl system has restricted the use of this peptide bond surrogate in the design of peptide analogues.[16a] The solution of this problem have come with the proposal of Marshell *et al.*[17,18] that the 1,5 disubstituted tetrazole ring can act as an ideal peptide bond surrogate for the *cis*-amide bond in order to lock the dipeptide bond into a geometry similar to that of *cis*-isomer. This concept has been utilized for the synthesis of the bradykinin analogues in which the proline residues of the nonapeptide have been replaced by the tetrazole surrogate.[19] This work is extended with the synthesis of α-keto tetrazole based di-peptide mimic which combines the conformational restriction of 1,5-disubstituted tetrazole ring with the potency of a non-hydrolysable α-keto-amide isostere (**Figure 3.2**).[20] The α-keto-tetrazole isostere is an important analogue of the amide bond for incorporation into enzyme inhibitors and conformational probes for peptidomimetic studies.

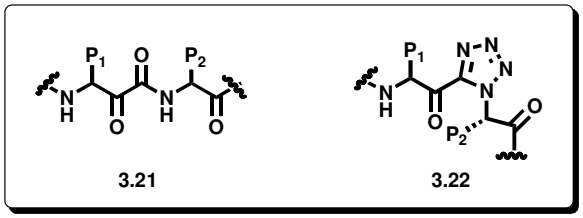

Figure 3.2: Structural representation of tetrazole analogue of the amide bond.

3.5. Application of Tetrazole as Nucleosidic Base Analouges and Linkers

After the discovery of ribavirin,[21a] shodomycin,[21b-f] pyrazomycin[21g-h] containing a heterocyclic ring as nucleobase which have shown significant biological activity, a great deal of research activity have been put forth for the synthesis of nucleosides containing 5-membered nitrogen containing heterocycles as a nucleobase surrogate or as a replacement of phosphate backbone. As for example, a number a triazole compounds have been synthesized with this aim as has been described in **Chapter 2**. Since the tetrazole ring is biologically important, so advances in the field of synthesis of tetrazole nucleosides is going on in a rapid manner.

The first example in the field of synthesis of tetrazole nucleosides and the study of antiviral property was reported by Pooniam *et al.*[22] in 1974. The synthesis of 1-ß-D-ribofuranosyltetrazole **3.23** and its 5-carboxamide **3.24** and 5-acetamide **3.25** derivatives has been described by them. These tetrazole N-nucleosides have been tested against influenza A2/Asian/J-305 virus infection in mice and have been found to be inactive at high doses.

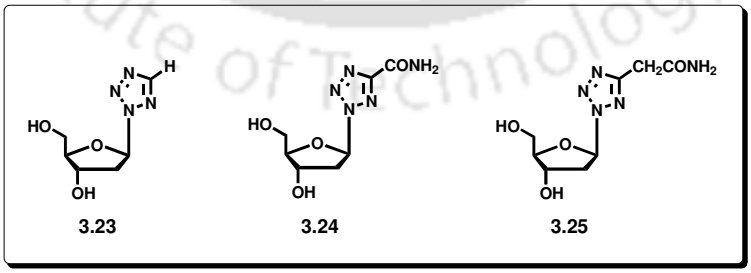

Figure 3.3: Structures of 1-ß-D-ribofuranosyltetrazole and its 5-carboxamide and 5-acetamide derivatives.

Tetrazole-related *C*-nucleosides also have been reported by Popsavin *et al.*[23] and their biological activity has been evaluated. The two tetrazole C-nucleosides synthesized are 2-benzamido-2-deoxy-ß-D-ribofuranose (**Figure 3.4, 3.26**) and 3-azido-3-deoxy-ß-D-xylofuranose (**Figure 3.4, 3.27**) from D-glucose out of which compound **3.27** shows moderate inhibitory activity against *in-vitro* growth of both N2a and BHK 21 tumor cell lines.

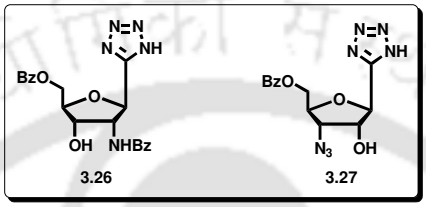

Figure 3.4: Structures of 2-benzamido-2-deoxy-ß-D-ribofuranose and 3-azido-3-deoxy-ß-D-xylofuranose.

As a part of their investigation on the reactivity of ditetrazole compounds with electrophilic sugar moiety, Filichev *et al.*[24] have synthesised mono- and bis-3′-substituted thymidine derivatives containing 1,5-bis(tetrazol-5-yl)- 3-oxapentane (**Figure 3.5**, **3.28**) as a linker. These compounds possess interesting properties of inhibition of DNA chain elongation and as antisense agents. Pedersen *et al.*[25] have reported the synthesis of the thymidine dimers in which 2,5-disubstituted tetrazole ring substituted the natural phosphodiester linkage (**Figure 3.5**, **3.29**). These thymidine dimers have been incorporated into oligodeoxynucleotides (ODNs) and the thermal stability of the duplexes formed by the modified oligonucleotides have been investigated by thermal denaturation study. It has been observed that the replacement of the phosphodiester linkage with tetrazole results in lowering of the thermal melting stability of the DNA duplexes by about 5.8 ^{o}C in thermal melting temperature (T_m).

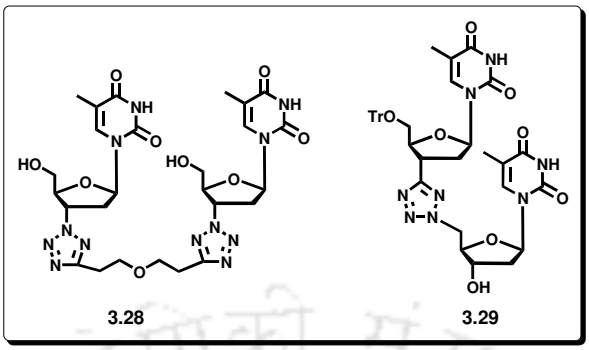

Figure 3.5: Stuctures of tetrazole used as linkers in thymidine dimers.

Thymidine- and AZT-linked 5-(1,3-dioxoalkyl)tetrazoles have also been designed and synthesized by Bosch *et al.*[26] by the condensation of nucleoside-derived 2-oxonitriles with the lithium salt of 5-acetyl-1-(4-fluorobenzyl)tetrazole (**Figure 3.6**). The evaluation of the biological activity of **3.31** revealed that it could serve as a lead compound for the treatment of AIDS.

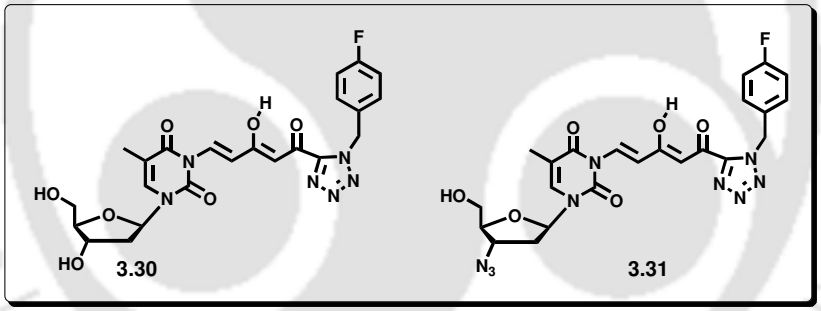

Figure 3.6: Structures of thymidine- and AZT-linked 5-(1,3-dioxoalkyl)tetrazoles.

Muller *et al.*[27] have reported the synthesis of the tetrazole nucleosides from Hoffer's chloro sugar (**Scheme 3.4**) and tested the metal ion coordination property of the compounds. It has been observed that tetrazole nucleosides do not form any complexes with the metal ion under any experimental conditions as the basicity of tetrazole nucleoside is far too low to allow any complexation.

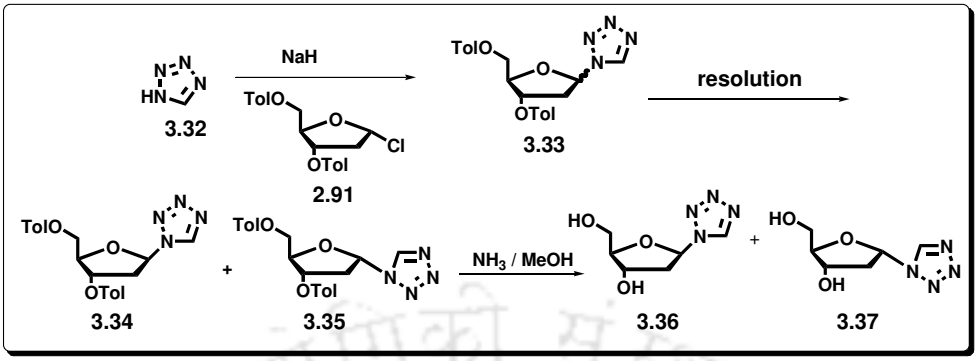

Scheme 3.4: Synthesis of tetrazole nucleosides; Tol = p-toluoyl). Additional isomeric products with N2-glycosidic bonds were also obtained.

Pedrosa *et al.*[28] have synthesized mono- and disubstituted tetrazoles from methyl D-glucopyranoside anomers (**Scheme 3.5**) wherein the tetrazole is exploited as a linker.

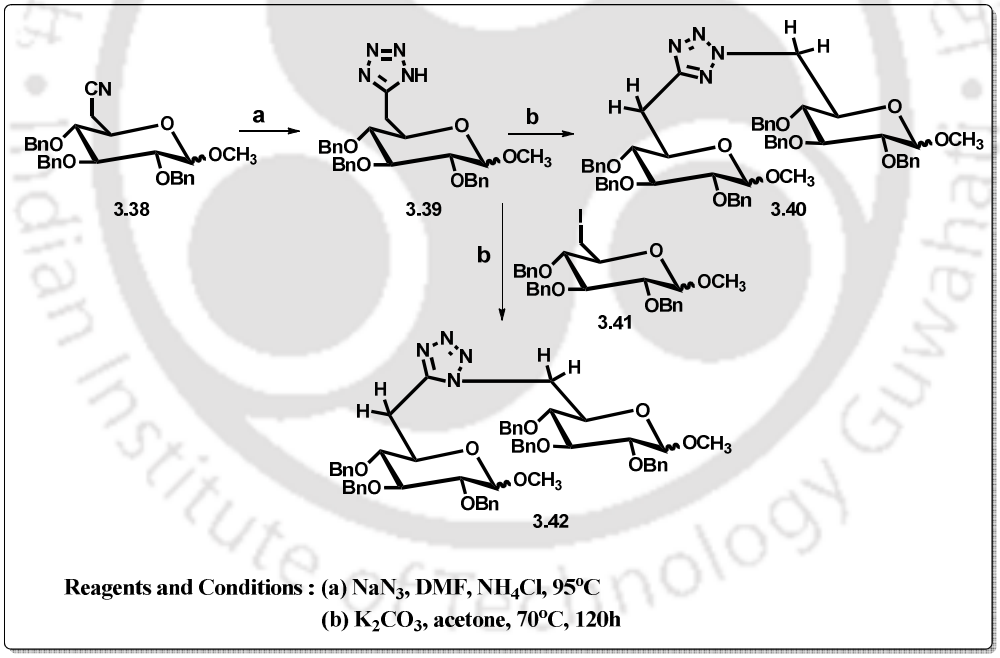

Scheme 3.5: Structures of mono- and di-substituted tetrazoles of methyl D-glucopyranoside.

Aldhoun *et al.*[29] have designed and synthesized *C*-glycosyl R-amino acids which contain the tetrazole ring holding the carbohydrate and glycinyl moiety. Since numerous mechanisms of carbohydrate action in glycoproteins are, at present, poorly

understood so natural and unnatural glycopeptides with a well-defined structure and composition can serve as synthetic probes in the studies for investigating the role of carbohydrate domain on the biological activity of glycoprotein. Hence, efforts are being made towards the development of synthetic methodologies of natural *O*- and *N*-linked glycosyl amino acids and glycopeptides[30] as well as of unnatural *C*-linked analogues[31] to be incorporated into peptides. The synthesis of *S*-linked glycosyl amino acids and thioglycopeptides has also received attention in the past.[32] Thus, two series of compounds have been prepared, one containing *C*-galactosyl and *C*-ribosyl *O*-tetrazolyl serine while the other containing *S*-tetrazolyl cysteine derivatives (**Figure 3.7**). In both the cases, the first step involved the thermal cycloaddition of a sugar azide with *p*-toluensulfonyl cyanide (TsCN) to give a 1-substituted 5-sulfonyl tetrazole which was developed by Demko *et al.* and the second step constituted the replacement of the tosyl group with a serine or cysteine residue.

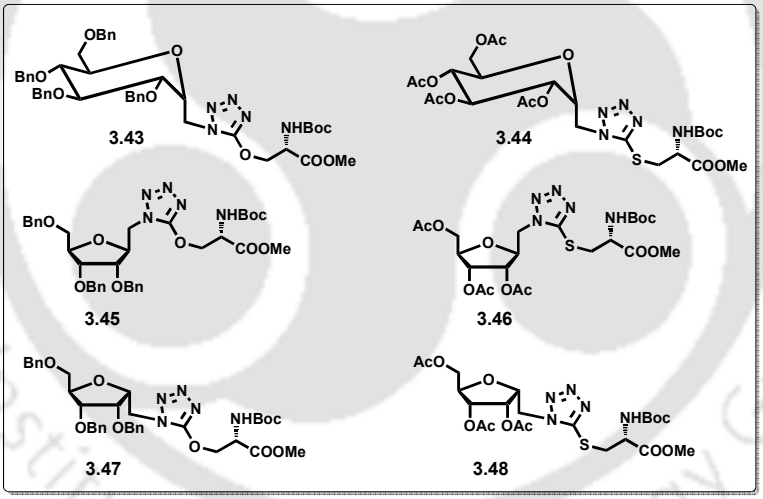

Figure 3.7: Structures of *C*-galactosyl and *C*-ribosyl *O*-tetrazolyl serines and *C*-galactosyl and *C*-ribosyl *S*-tetrazolyl serines.

Davis *et al.*[33] have reported the synthesis of bicyclic tetrazole derivatives of D-mannofuranose and D-rhamnofuranose and L-rhamnofuranose (**Figure 3.8**). Since the tetrazoles of pyranoses (**3.49)** possessed great inhibitory potential towards the glycosidase enzymes and other sugar possessing enzymes so their furanose tetrazole counterparts were synthesized. The key step to their synthesis involved an intramolecular [1,3]- dipolar cycloaddition of azide and nitrile moieties.

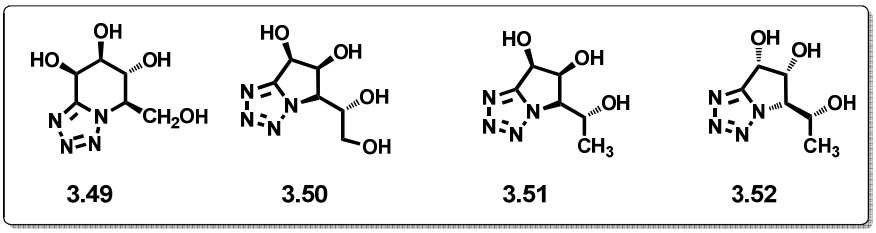

Figure 3.8: Structures of pyranose tetrazole (**3.49**), D-manno tetrazole (**3.50**), D-rhamno tetrazole (**3.51**) and L-rhamnofuranose tetrazole (**3.52**).

3.6. Background

From a literature study it is revealed that a vast majority of research efforts have been put forth for the synthesis of tetrazole derivatives of various classes including tetrazole containing carbohydrates and nucleosides. The efforts towards the synthesis of tetrazole nucleosides focused mainly on the synthesis and the design of medicinally important drug candidates. However, there exists only a very few reports on the use of tetrazole as a linker with aromatics to be the nucleobase surrogates.

3.7. Objective

The tetrazole unit as a nucleosidic base analogues have not been explored like their triazole counterparts. There exist only a few examples in literature where the synthesis of tetrazole-based *C*-nucleosides and tetrazole-based *N*-nucleosides has been shown. In this field, the 1,5-disubstituted tetrazoles have been synthesized but the 2,5-disubstituted tetrazoles have not been explored much. However, these tetrazole nucleosides have been generated mainly due to synthetic interest or to evaluate their medicinal properties. The synthetic pathway in any of these cases required harsh reaction conditions like the use of high temperature and solvents like DMF and DMSO. Morever, the interesting photophysical/biophysical property of our previously synthesized triazolyl donor-acceptor nucleosides, in particular, the triazolyl phenanthrene ($^{TPhen}\mathbf{B}_{\mathbf{D_0}}$) and triazolylnitrobenzene ($^{TNB}\mathbf{B}_{\mathbf{Ac}}$) nucleoside pair motivated us to generate tetrazolyl class of new unnatural nucleosides.[4] Therefore, in the context of design of nucleoside base surrogate, we wanted to use tetrazole as nucleoside base and framed our objective as below:

(a) To synthesize tetrazolyl donor/acceptor aromatic nucleosides.

(b) To study their photophysical properties in various organic solvents of varying polarity.

3.8. Results and Discussion

3.8.1. Synthesis of the Tetrazolyl Donor/Acceptor Nucleosides

The synthesis of the new class of donor/acceptor nucleosides in which the donor and the acceptor groups are linked to the deoxy-ribose sugar through tetrazole unit is shown in **Scheme 3.6**. First of all, we synthesized the aromatic tetrazoles following a modified literature protocol.[12] Thus, the aromatic tetrazoles of general structure **3.55** were prepared from the corresponding aromatic cyano compounds (**3.53A-3.53L**) with TMS-N_3 and TBAF under solvent free condition at 85 ^oC. The structures of the aromatic cyano used and the tetrazolyl aromatics synthesized are shown in **Figure 3.9**. After the synthesis, all the tetrazoles were purified by filtration and characterized. The tetrazoles **3.54A**,[12] **3.54B**,[12] **3.54H**[12] are known while others are new. The reported tetrazoles were characterized by ^1H, ^{13}C NMR while the new ones were characterized by ^1H, ^{13}C and mass spectrometry. Two of the tetrazoles such as **3.54D**, **3.54G** were found to sparingly soluble in the solvents like ethyl acetate, THF *etc.*, thus, were purified by recrystallization. The compound **3.54L** could not purified by recrystallisation or other methods so was used for the synthesis of nucleosides without further characterization.

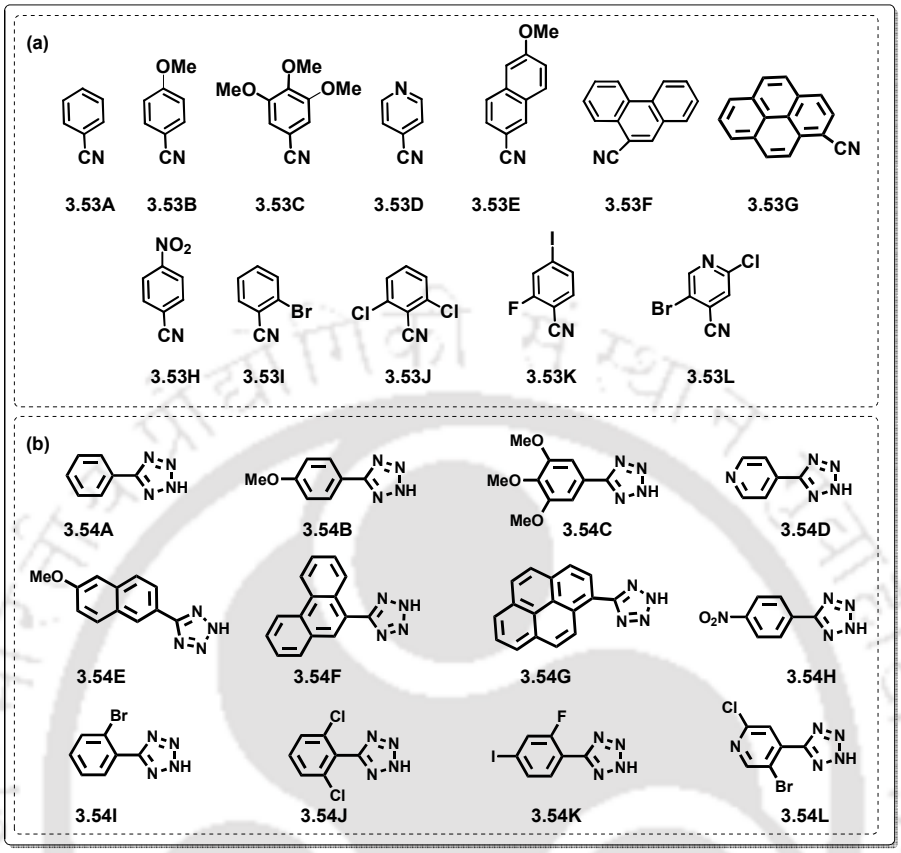

Figure 3.9: (a) Structures of the cyano compounds and (b) the tetrazole compounds synthesized from the corresponding cyano compounds.

The synthesis of the tetrazolyl aromatic nucleosides starts with 2-deoxy ribose sugar **2.88** which was converted to its 1-*O*-methyl derivative **2.89**. Subsequent treatment of 1-*O*-methyl-2-deoxy ribose (**2.89)** with *p*-toluoyl-chloride in pyridine afforded the bis-toluoyl protected sugar **2.90** with very good yield (70%). The treatment of dry HCl gas in a moderately dilute etherial solution of 1-*O*-methyl-3, 5-di-O-p-toluoyl-2-deoxy ribose sugar **2.90** yielded corresponding Hoffer's chlorosugar **2.91** with good yield (59%). The Hoffer's chlorosugar was then made to undergo substitution reaction with the aromatic tetrazoles (**3.54A-3.54L**) with K_2CO_3 as the base at room temperature. The substitution of the chloro by the tetrazolyl moiety yielded exclusively the β-nucleosides with very good yield (**Table 3.1**). The bis-toluoyl protected nucleosides of general structure **3.55** were then deprotected using NaOMe in methanol. The bis-toluoyl protected halogenated pyridyl (**3.66a**) tetrazole

was not deprotected. All the toluoyl protected and deprotected compounds were characterized by NMR, mass, IR, melting temperatures and in two cases by single crystal X-ray analysis. The experimental observation suggests the formation of β-isomer while no trace of α-tetrazolyl nucleosides were observed.

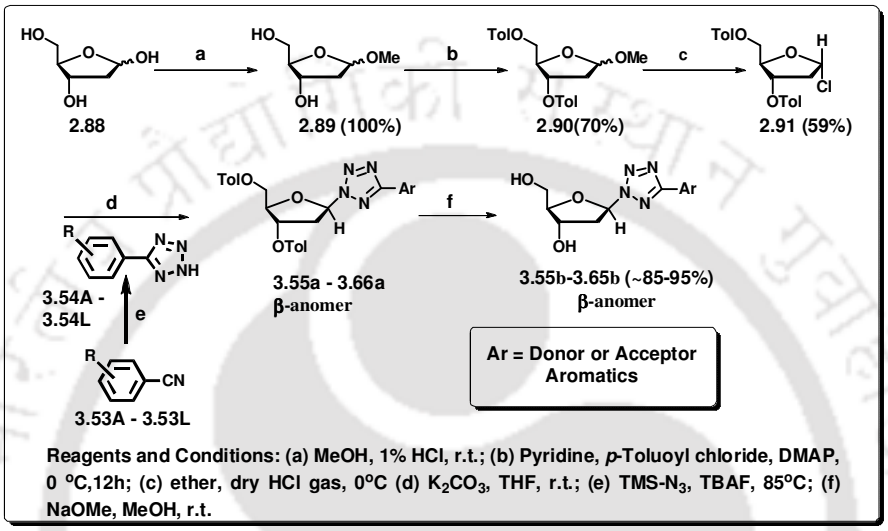

Scheme 3.6: Synthesis of the tetrazolyl unnatural nucleosides from deoxy-ribose sugar.

Table 3.1: Summary of yield of toluoyl protected and deprotected β-tetrazolyl donor-acceptor nucleosides.

Entry	Nucleosides [R = toluoyl or H]	Yield %	
		β-isomer[R = toluoyl](compound number)	β-isomer[R = H] (compound number)
1	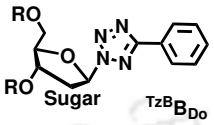	75 (3.55a)	95 (3.55b)
2	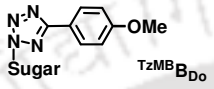	75 (3.56a)	98 (3.56b)
3	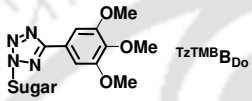	83 (3.57a)	86 (3.57b)
4	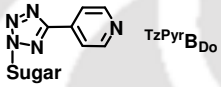	78 (3.58a)	81 (3.58b)
5	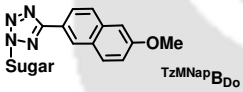	70 (3.59a)	95 (3.59b)
6	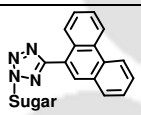	84 (3.60a)	92 (3.60b)
7	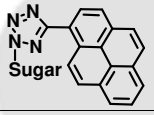	76 (3.61a)	92 (3.61b)
8	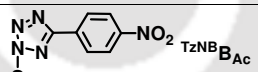	70 (3.62a)	96 (3.62b)
9	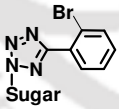	79 (3.63a)	90 (3.63b)
10	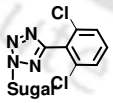	65 (3.64a)	91 (3.64b)
11	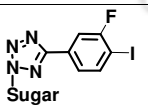	74 (3.65a)	85 (3.65b)
12	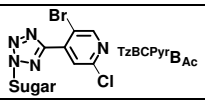	60 (3.66a)	---

3.8.2. Spectral Characterization of Tetrazolyl Nucleosides

NOESY Experiment: The nucleosides β-conformation was established *via* NOESY spectra of a representative tetrazolyl nucleoside, $^{TzPy}B_{Do}$ **(3.58a)**. The NOESY spectra of the representative nucleoside (**Figure 3.10**) showed the presence of a cross peak between H1' - H2'α and H1' – H4′.

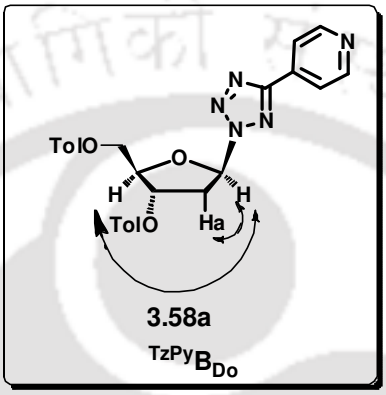

Figure 3.10: Presentation of NOESY cross peak in the representative β- toluoyl protected pyridine tetrazolyl nucleoside and the NOESY spectra.

The Single Crystal X-Ray Structure: The single crystal structure of $^{TzBB}B_{Ac}$ (**3.63a**) and $^{TzFIB}B_{Ac}$ **(3.65a)** further confirmed the β-anomeric conformation and the structure of bis-toluoyl protected tetrazolyl nucleosides (**Figure 3.11** and **3.12**).

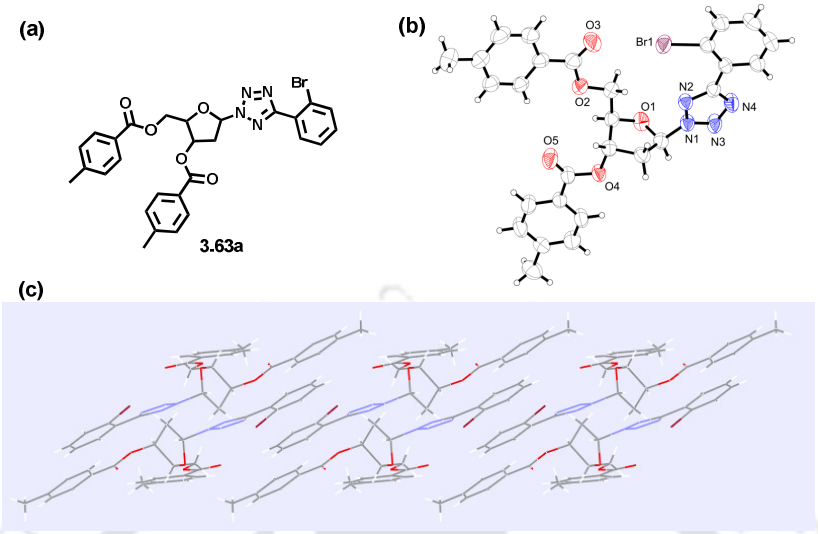

Figure 3.11: (a) Structure of toluoyl protected tetrazolyl bromobenzene nucleoside (b) ORTEP molecular diagram with thermal ellipsoid at 50% probability and the (c) crystal packing arrangement.

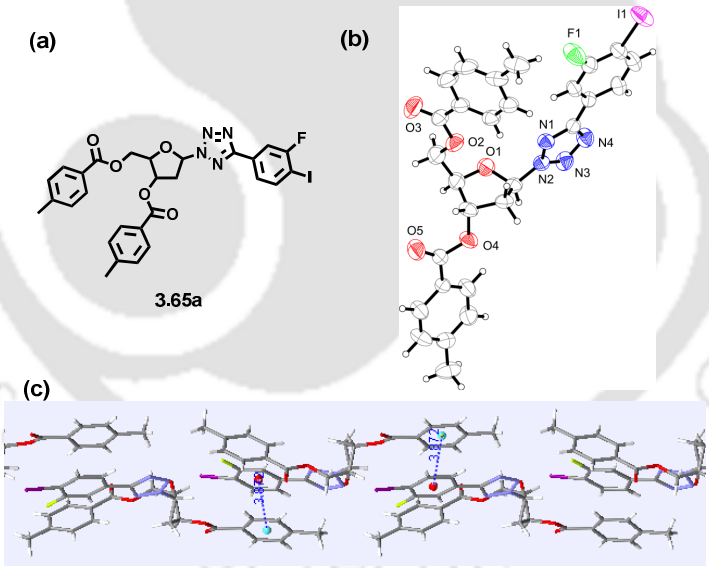

Figure 3.12: (a) Stucture of toluoyl protected tetrazolyl fluoro, iodo-benzene nucleoside (b) ORTEP molecular diagram with thermal ellipsoid at 50% probability. (c) π-π stacking interactions between the planes and the distance between the planes in the packing diagram.

Crystal data were collected with a CCD diffractometer using graphite monochromated MoKα radiation (λ = 0.71073 Å) at 296 K. Cell parameters were retrieved and refined with softwares on all observed reflections. Data reduction was

performed with the software and corrected for Lorentz and polarization effects. Absorption corrections were applied with the program. The structure was solved by direct methods implemented in a program and refined by full-matrix least-squares methods on F2. All non-hydrogen atomic positions were located in difference Fourier maps and refined anisotropically. The hydrogen atoms were placed in their geometrically generated positions. Colourless crystals were isolated in rectangular shape from ethylacetate at room temperature.

Table 3.2: Crystal parameters of the tetrazolyl nucleosides.

Data	**3.63a**	**3.65a**
Z	4	4
Molecular Formula	$C_{28}H_{25}BrN_4O_5$	$C_{28}H_{24}FIN_4O_5$
Temperature (K)	296	296
Space Group	P 21 Monoclinic	P 21 21 21 Orthorhomblc
a (Å)	10.1458(2)	11.6709(2)
b (Å)	12.4658(2)	11.8642(2)
c (Å)	10.7755(2)	19.6750(4)
α (degree)	90	90
β degree)	107.228(1)	90
γ (degree)	90	90
M_r	577.42	642.41
V ($Å^3$)	1301.97(4)	2724.32(9)
μ (mm^{-1})	1.625	1.227
F(000)	592.0	1288.0
R(reflections)	0.0380(1540)	0.0273(4514)
wR2(reflections)	0.0272(3780)	0.0643(4795)
Correction method	Multi Scan	Multi Scan

The crystal packing diagram of nucleoside **3.63a** showed that the molecules are packed in a layered structure. The layers are held together *via* weak van der walls and

hydrophobic interaction between tetrazole unit and sugar moiety of two layer. The crystal packing diagram of nucleoside **3.65a** showed that the molecules are held together *via* strong π-π stacking interactions between the phenyl rings of toluoyl protecting groups and the iodo fluoro aromatic ring. The distance between the two consecutive layers is 3.872 Å.

3.8.2 Study of Photophysical Properties

After getting all the pure tetrazolyl nucleosides in hand, we next studied their UV-visible and fluorescence photophysical properties. Previously, we[34] and subsequently others have shown that linking of fluorescent/non-fluorescent unit with a triazole moiety led to the installation of fluorescence emission properties to the non-fluorescent molecules and/or modulation of the same to a fluorescent molecule. The synthesized tetrazolyl building blocks also behaved in a similar way with respect to their photophysical properties. We studied the photophysical properties of few of our synthesized β-nucleosides in various organic solvents to test their microenvironment sensitive property.

The UV-visible spectra of the nucleoside $^{TzMB}B_{Do}$ (**3.56b, Table 3.1**) containing a 4-methoxybenzene exhibited very strong absorption maxima at around 255-257 nm in various organic solvents. Excitation at absorption maxima of each solvent showed emission at around 288 nm in lowest polar solvent dioxane which exhibited a bathochromic shift to 340 nm as the solvent polarity increases upto acetonitrile. In methanol and ethanol, the emission spectra showed two bands at 319 and 419 nm and at 316 and 436 nm, respectively (**Figure 3.13a-b**, **Table 3.3**).

The nucleoside $^{TzTMB}B_{Do}$ (**3.57b**, **Table 3.1**) containing a trimethoxybenzene aromatic unit exhibited very strong absorption at 266 nm in lowest polar solvent dioxane which showed a little blue shift to 263 nm as the solvent polarity increases. When excited at the absorption maxima of different solvents, it showed an intramolecular charge transfer (ICT) band appearing at 434 nm in dioxane with a red shift of 38 nm as the solvent polarity increases upto acetonitrile (434 nm in Dioxane→472 in ACN). The trimethoxy benzene acted as donor and the the tetrazole ring as an acceptor leading to an ICT band. This kind of installation and modulation

of photophysical properties has been observed between the donor and acceptor groups with triazolyl ring acting as the linker.[34] However, the ICT band disappeared in extremely polar solvents like ethanol and methanol most probably due the involvement of the lone pair of methoxy groups in hydrogen bonding with polar protic solvents like ethanol and methanol[35] (**Figure 3.13 c-d, Table 3.3**).

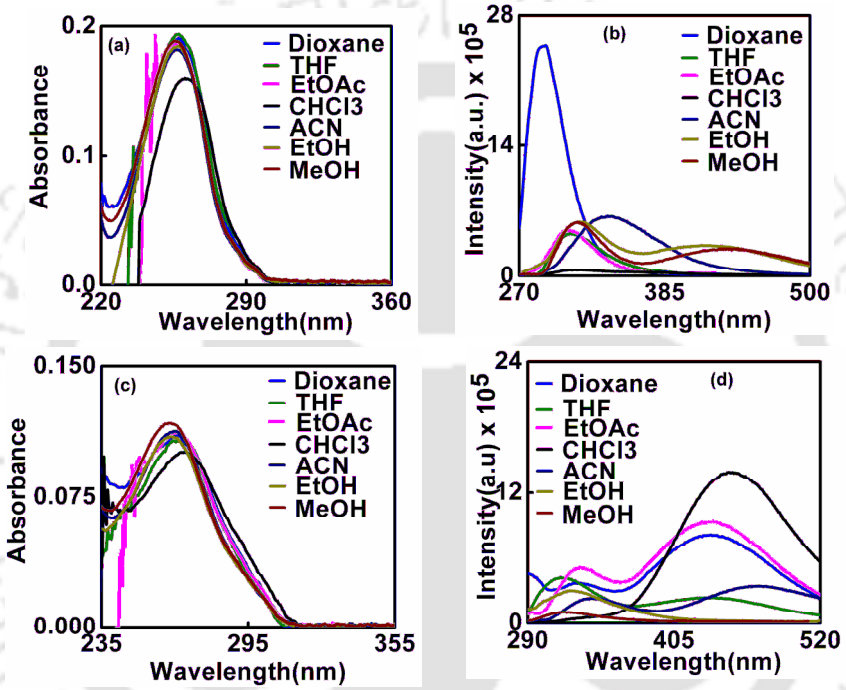

Figure 3.13: UV-visible and fluorescence spectra of (a-b) nucleoside $^{TzMB}B_{Do}$ (**3.58b**) and (c-d) nucleoside $^{TzTMB}B_{Do}$ (**3.57b**) in various organic solvents (Concentration of each nucleoside was 10 μM).

The nucleoside $^{TzMNap}B_{Do}$ (**3.59b**, **Table 3.1**) containing a methoxynapthalene aromatic unit exhibited very strong absorption at around 247 and 297 nm. The band at 247 nm showed a blue shift of 2 nm as the solvent polarity increases while the band at 297 nm showed a bathochromic shift followed by hypsochromic effect as the solvent polarity increases (**Figure 3.14a-b**, **Table 3.3**). Excitation at absorption maxima (290-300 nm) of each solvent showed structureless emission at around 362 nm with decrease in intensity as the solvent polarity increases. The quantum yield of

fluorescence also follows the same trend as for the case of intensity in various solvents (**Table 3.3**).

The $^{TzPhen}B_{Do}$ **(3.60b, Table 3.1)** nucleoside showed very little blue shifted absorbance as the polarity of the solvent increases from dioxane (λ_{max} = 258 nm) to methanol (λ_{max} = 255 nm). Upon excitation at 300 nm, the nucleoside $^{TzPhen}B_{Do}$ showed structured emission band at 363 and 379 nm in dioxane which were very little red shifted to 368 and 382 nm, respectively, as the solvent polarity increases upto chloroform. With further increase in solvent polarity upto methanol, the two structural bands shifted to the blue region and appeared at 360 and 376 nm, respectively (**Figure 3.14c-d**, **Table 3.4**).

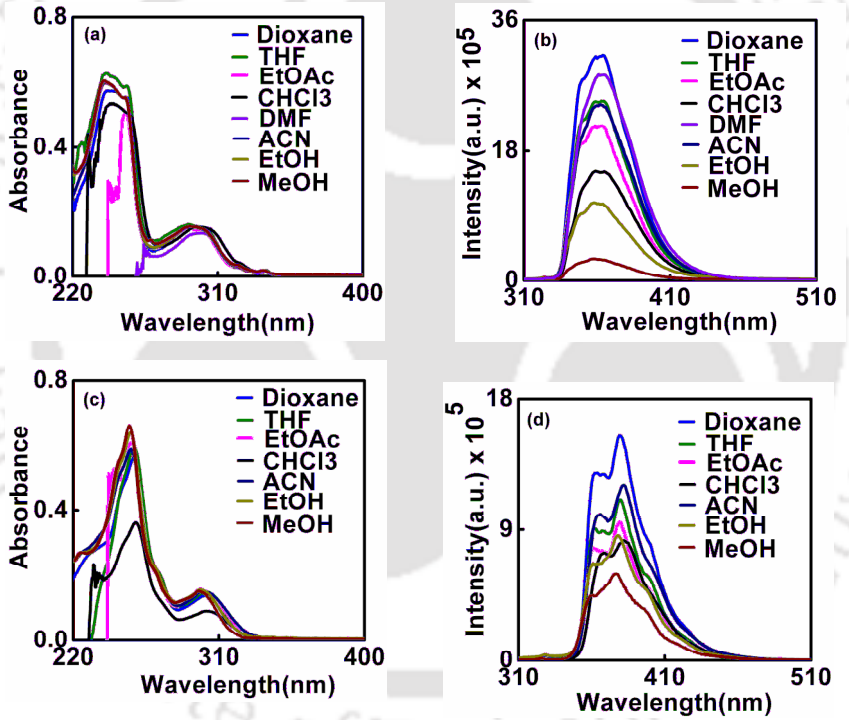

Figure 3.14: UV-visible and fluorescence spectra of (a-b) nucleoside $^{TzMNap}B_{Do}$ (**3.59b**, λ_{ex} ~ 290-300 nm) and (c-d) nucleoside $^{TzPhen}B_{Do}$ (**3.60b**, λ_{ex} = 300 nm) in various organic solvents (Concentration of each nucleoside was 10 μM).

Tetrazolylpyrene nucleoside $^{TzPy}B_{Do}$ **(3.61b, Table 3.1)** showed structureless absorption at 354 nm in dioxane which shifted to 346 nm as the solvent polarity increases from dioxane to methanol. This observation suggested an electronic coupling of pyrenyl π-electron with tetrazole unit. However, it showed a structured

emission when excited at 350 nm with appearance of prominent maxima at 385 and 406 nm of almost similar intensities in dioxane which showed a red shift to 387 and 408 nm as the solvent polarity increases upto $CHCl_3$ followed by blue shift to 384 and 405 nm as the solvent polarity further increases (**Figure 3.15a-b**, **Table 3.4**). The quantum yield also follows the same trend as for the case of intensity in various organic solvents (**Table 3.4**).

The nucleoside $^{TzNB}B_{Ac}$ (**3.62b**, **Table 3.1**) containing a nitro functionality exhibited very strong absorption at around 285 nm in all the solvents tested. Excitation at the absorption maxima of $^{TzNB}B_{Do}$ (280 nm) showed that it was non-fluorescent except in THF and ethanol in which it exhibited emission at 310 and 326 nm (**Figure 3.15c-d**, **Table 3.4**).

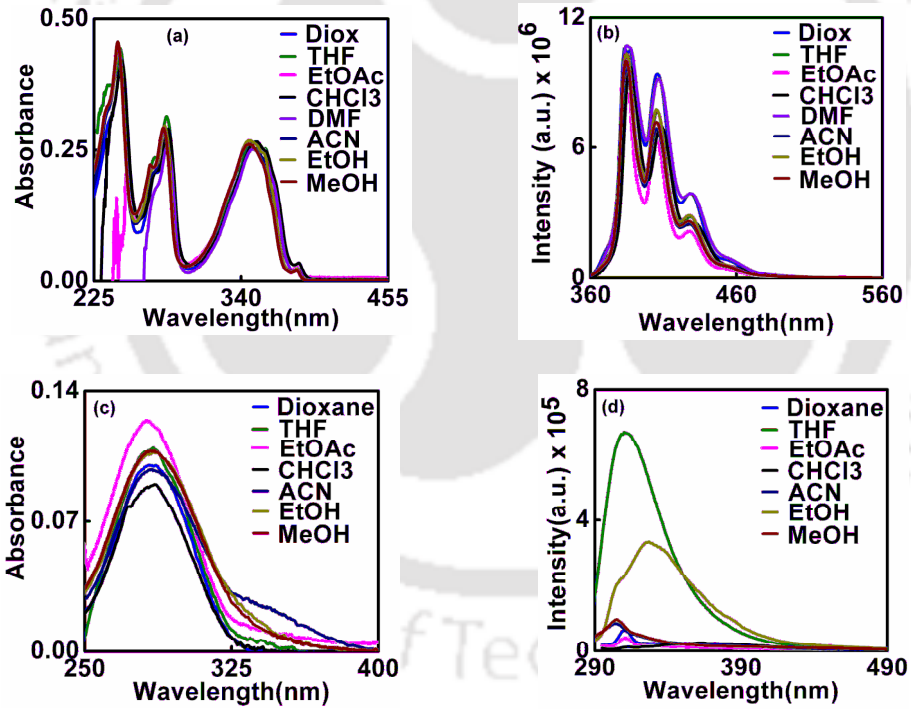

Figure 3.15: UV-visible and fluorescence spectra of (a-b) nucleoside $^{TzPy}B_{Do}$ (**3.61b**) λ_{ex} = 350 nm and (c-d) nucleoside $^{TzNB}B_{Ac}$ (**3.62b**) in various organic solvents (Concentration of each nucleoside was 10 μM).

Table 3.3: Summary of the photophysical properties of nucleosides **3.56b**, **3.57b**, **3.59b**.

	Solvents	UV-visible and fluorescence properties			
		λ_{abs} *(nm)*	ε_{max}	λ_{fl} *(nm)*	Φ_f [a]
$^{TzMB}B_{Do}$ (**3.56b**)	**Dioxane**	257	19072	288	0.03
	THF	257	19373	310	0.01
	EtOAc	256	18629	310	0.01
	CHCl3	261	15960	313	0.002
	ACN	256	18225	340	0.02
	EtOH	256	18480	319, 419	0.02
	MeOH	255	18874	316, 436	0.02
$^{TzTMB}B_{Do}$ (**3.57b**)	**Dioxane**	266	11083	330, 434	0.09
	THF	266	10733	317, 434	0.04
	EtOAc	266	11228	332, 435	0.07
	CHCl3	269	10099	450	0.10
	ACN	265	11282	339, 472	0.42
	EtOH	264	10968	325	0.22
	MeOH	263	11731	316	0.04
$^{TzMNap}B_{Do}$ (**3.59b**)	**Dioxane**	247, 297	14772	362	0.17
	THF	247, 297	15570	362	0.13
	EtOAc	297	14455	362	0.12
	$CHCl_3$	247, 300	15391	362	0.08
	DMF	298	13547	363	0.18
	ACN	245, 297	15268	362	0.14
	EtOH	245, 297	15312	360	0.06
	MeOH	245, 296	15312	358	0.02

[a] For all the cases aminopyridine was used as quantum yield standard.

Table 3.4: Summary of the photophysical properties of nucleosides **3.60b**, **3.61b**, **3.62b**.

	Solvents	**UV-v**isible **and f**luorescence **properties**			
		λ_{abs} *(nm)*	ε_{max}	λ_{fl} *(nm)*	Φ_f [a]
$^{TzPhen}B_{Do}$ (**3.60b**)	**Dioxane**	258, 303	56583	363, 379	0.09
	THF	258, 303	59662	361, 379	0.06
	EtOAc	256, 301	60870	362, 379	0.05
	CHCl3	259, 303	36495	368, 382	0.07
	ACN	256, 301	58933	365, 381	0.06
	EtOH	256, 299	64156	362, 378	0.04
	MeOH	255, 298	66431	360,376	0.03
$^{TzPy}B_{Do}$ (**3.61b**)	**Dioxane**	354	28888	385, 406	0.28
	THF	353	31433	385, 406	0.21
	EtOAc	352	29206	384, 405	0.17
	CHCl3	352	29107	387, 408	0.20
	DMF	350	25530	386, 406	0.29
	ACN	347	28422	386, 405	0.20
	EtOH	347	29645	385, 405	0.22
	MeOH	346	29278	384, 405	0.21
$^{TzNB}B_{Ac}$ (**3.62b**)	**Dioxane**	284	10024	---	**---**
	THF	285	10927	310	**---**
	EtOAc	282	12438	---	**---**
	$CHCl_3$	286	8990	---	**---**
	ACN	285	9794	---	**---**
	EtOH	285	10709	326	**---**
	MeOH	284	10818	---	**---**

[a] For **3.60b** and **3.61b** quinine sulphate and aminopyridine, respectively, were used for determination of quantum yield.

3.9. CONCLUSION

We have successfully synthesized few new tetrazolyl β-nucleosides *via* stereospecific substitution reaction as a key step of the synthesis with good yield. The reaction conditions employed are mild and the starting materials used are cheap. The ß-anomers of the tetrazole nucleosides are obtained from the α-chloro sugar *via* substitution reaction with aromatic tetrazoles in presence of K_2CO_3 as base. These tetrazole nucleosides constitute a new class of nucleoside base surrogates. Two of the

tetrazolyl aromatic nucleosides showed interesting solvatochromic photophysical property. As for example, the trimethoxyphenyl tetrazolyl nucleoside showed an intramolecular charge transfer (ICT) emission with large (38 nm) solvatochromicity. A combination of donor-acceptor pair tetrazolyl nucleosides might form suitable base pair of unnatural DNA and are expected to stabilize a duplex DNA *via* π-π stacking/charge transfer interaction. Therefore, the tetrazolyl unnatural nucleosides might find application in decorating unnatural DNA usable for various biotechnological and DNA based material science applications.

3.10. Experimental Section

3.10.1. General Experimental Section

All reactions were carried out under a nitrogen atmosphere. Organic extracts were dried over anhydrous sodium sulphate. Solvents were removed in a rotary evaporator under reduced pressure. Silica gel (60-120 mesh size) was used for the column chromatography. Reactions were monitored by TLC on silica gel 60 F254 (0.25mm). All ^{1}H NMR spectra were measured with Varian 400 (400 MHz) and ^{13}C NMR spectra were measured with Varian 400 (100 MHz) spectrometer except otherwise mentioned. Coupling constant (*J* value) was reported in hertz. The chemical shifts were shown in ppm downfield from tetramethylsilane, using residual chloroform (δ = 7.24 in ^{1}H NMR, δ = 77.23 in ^{13}C NMR), methanol (δ = 3.34 in ^{1}H NMR, δ = 49.2 in ^{13}C NMR), dimethyl sulfoxide (δ = 2.48 in ^{1}H NMR, δ = 39.5 in ^{13}C NMR), as an internal standard. Mass spectra were recorded using WATERS MS system, Q-tof premier and data analyzed using Mass Lynx 4.1. IR spectra were recorded in KBr or neat on a Perkin Elmer Spectrum one FT-IR spectrometer.

3.10.2. Crystallographic Description

Crystal data were collected with Bruker Smart Apex-II CCD diffractometer using graphite monochromated MoKα radiation (λ = 0.71073 Å) at 298 K. Cell parameters were retrieved using SMART [a] software and refined with SAINT[a] on all observed reflections. Data reduction was performed with the SAINT software and corrected for Lorentz and polarization effects. Absorption corrections were applied with the program SADABS[b]. The structure was solved by direct methods implemented in

SHELX-97[c] program and refined by full-matrix least-squares methods on F2. All non-hydrogen atomic positions were located in difference Fourier maps and refined anisotropically. The hydrogen atoms were placed in their geometrically generated positions. Colourless crystals were isolated in rectangular shape and needle shape from ethylacetate by slow evaporation at room temperature.

a. SMART V 4.043 Software for the CCD Detector System; Siemens Analytical Instruments Division: Madison, WI, 1995.

b. SAINT V 4.035 Software for the CCD Detector System; Siemens Analytical Instruments Division: Madison, WI, 1995.

c. Sheldrick, G. M. SHELXL-97, Program for the Refinement of Crystal Structures; University of Göttingen: Göttingen (Germany), **1997**.

3.10.3. Synthesis and Characterization of Tetrazolyl Unnatural Nucleosides

***Synthesis of 2-deoxy-3, 5-di-O-p-toluoyl-α-D-ribofuranosyl chloride (2.91)*:** The synthesis of the starting material *2-deoxy-3, 5-di-O-p-toluoyl-α-D-ribofuranosyl chloride* and its precursors were carried out following the procedure described in **Chapter 2** and the detailed procedure as well as characterization were described therein.

3.10.3.1. General procedure for the synthesis of aromatic tetrazoles from the aromatic nitriles (3.54A-3.54L)

The tetrazole compounds were prepared by a literature reported protocol.[12] Thus, the aromatic nitrile (1.0 equiv), TBAF.$3H_2O$ (0.5 equiv) and TMS-N_3 (1.5 equiv) were taken in a screw capped *via*l equipped with a magnetic stirrer and the resulting mixture was stirred vigorously at 85 ^oC. The reaction mixture was then transferred to a seperatory funnel and TBAF was removed by washing the organic phase with 1M aqueous HCl solution (20 ml). The organic phase was separated, washed with brine (20 ml) and dried over Na_2SO_4 and then concentrated in a rotary evaporator. The products were then purified by silica-gel (60-120 mesh) column chromatography or for some cases by recystallisation. Compound **3.54L** was used as a crude mixture for further reaction. The compounds were then characterized by IR, NMR spectroscopy

and mass spectrometry. Compounds **3.54A-B** and **3.54H** are reported compounds[12] whereas **3.54C**- **3.54G** and **3.54I**- **3.54L** are new.

Synthesis of 5-phenyl tetrazole (3.54A): Using the general procedure, starting

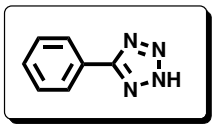

from 100 mg (0.969 mmol) of benzonitrile (**3.53A**), 120 mg (0.824 mmol) of the title compound (**3.54A**) was isolated as white solid. Yield 85%; mp 215-216 ^{o}C; ^{1}H NMR (600 MHz, d_6-DMSO) δ 7.60-7.61 (3H, m), 8.03 (2H, d, J = 6.0 Hz).

Synthesis of 5-(4-methoxyphenyl) tetrazole (3.54B): Using the general procedure,

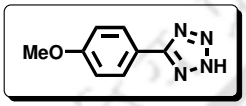

starting from 133 mg (0.999 mmol) of compound (**3.53B**), 165 mg (0.94 mmol) of the title compound (**3.54B**) was isolated as white solid. Yield 94%; mp 173-175 ^{o}C; ^{1}H NMR (600 MHz, d_6-DMSO) δ 3.84 (3H, s), 7.16 (2H, d, J = 9.0 Hz), 7.97 (2H, d, J = 9.0 Hz); HRMS calcd. for $C_8H_9N_4O$ $[M+H]^+$ 177.0771, found 177.0769.

Synthesis of 5-(3', 4', 5'-trimethoxyphenyl) tetrazole (3.54C): Using the general

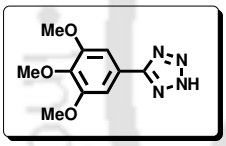

procedure, starting from 100 mg (0.517 mmol) of compound (**3.53C**), 121 mg (0.512 mmol) of the title compound (**3.54C**) was isolated as white solid. Yield 99%; mp 211-212 ^{o}C; ^{1}H NMR (400 MHz, CD_3OD) δ 3.83 (3H, s), 3.93 (6H, s), 7.33 (2H, s); ^{13}C NMR (100 MHz) δ 57.0, 61.4, 105.9, 120.7, 142.1, 155.5, 157.6; HRMS calcd. for $C_{10}H_{13}N_4O_3$ $[M+H]^+$ 237.0982, found 237.0980.

Synthesis of 4-(tetrazol-5'-yl)pyridine (3.54D): Using the general procedure,

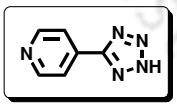

starting from 200 mg (1.92 mmol) of compound (**3.53D**), 237 mg (1.61 mmol) of the title compound (**3.54D**) was isolated as white solid. Yield 84%; mp 252-253 ^{o}C; ^{1}H NMR (400 MHz, CD_3SOCD_3) δ 8.00-8.02 (2H, m), 8.79 (2H, d, J = 5.5 Hz); ^{13}C NMR (100 MHz) δ 121.3, 134.5, 150.6, 156.3.

Synthesis of 5-(6'-acetylnapthalene) tetrazole (3.54E): Using the general

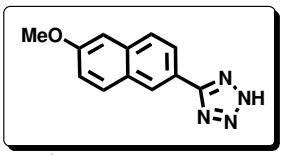

procedure, starting from 200 mg (1.092 mmol) of compound (**3.53E**), 222 mg (0.983 mmol) of the title compound (**3.54E**) was isolated as white solid. Yield 90%; mp 229-230 ^{o}C; ^{1}H NMR (400 MHz, d_6-DMSO) δ 3.91 (3H, s), 7.27 (1H, d, J = 8.4 Hz), 7.43 (1H, s), 7.98-8.04 (3H, m), 8.55 (1H, s); ^{13}C NMR (100 MHz) δ 65.2, 115.9, 129.7,

133.9, 136.6, 137.8, 137.8, 140.0, 145.4, 168.5; HRMS calcd. for $C_{12}H_{10}N_4O[M+H]^+$ 227.0927, found 227.0918.

Synthesis of 5-Phenanthrenyl tetrazole (3.54F): Using the general procedure, starting from 275 mg (1.353 mmol) of compound (**3.53F**), 290 mg (1.177 mmol) of the title compound (**3.54F**) was isolated as white solid. Yield 87%; mp 247-248 ^oC; ^1H NMR (600 MHz, d_6-DMSO) δ 7.76 (2H, t, J = 7.2 Hz), 7.81-7.84 (2H, m), 8.13 (1H, d, J = 7.8 Hz), 8.35 (1H, s), 8.48 (1H, d, J = 8.4 Hz), 8.94 (1H, d, J = 8.4 Hz), 8.99 (1H, d, J = 8.4 Hz); ^{13}C NMR (175 MHz) δ 120.7, 123.2, 123.6, 125.9, 127.7, 127.8, 127.8, 128.3, 128.9, 129.5, 130.1, 130.2, 130.7, 156.1.

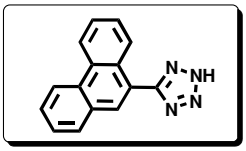

Synthesis of 5-Pyrenyl tetrazole (3.54G): Using the general procedure, starting from 140 mg (0.616 mmol) of compound (**3.53G**), 150 mg (0.555 mmol) of compound (**3.54G**) was isolated as light brown solid. Yield 90%; mp 259-260 ^oC; ^1H NMR (600 MHz, d_6-DMSO) δ 8.16 (1H, t, J = 7.2 Hz), 8.28 (1H, d, J = 9 Hz), 8.33-8.42 (4H, m), 8.47 (2H, s), 8.92 (1H, J = 6.4 Hz); ^{13}C NMR (175 MHz) δ 118.5, 123.8, 124.4, 124.6, 125.4, 126.4, 126.8, 127.3, 127.6, 128.9, 129.5, 129.6, 130.5, 131.1, 132.9, 156.4.

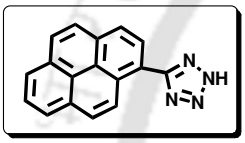

Synthesis of 5-(4'-nitrophenyl) tetrazole (3.54H): Using the general procedure, starting from 188mg (1.26 mmol) of compound (**3.53H**), 224 mg (1.17 mmol) of title compound (**3.54H**) was isolated as yellow solid. Yield 93%; mp 219-221 ^oC; ^1H NMR (400 MHz, d_6-DMSO) δ 8.29 (2H, d, J = 8 Hz), 8.44 (2H, d, J = 8.4 Hz); ^{13}C NMR (100 MHz) δ 119.4, 134.4, 138.0, 140.5, 158.6; HRMS calcd. for $C_7H_6N_5O_2[M+H]^+$ 192.0516, found 192.0510.

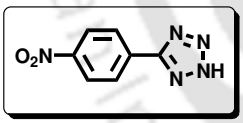

Synthesis of 5-(2'-bromophenyl) tetrazole (3.54I): Using the general procedure, starting from 100 mg (0.549 mmol) of compound (**3.53I**), 115 mg (0.510 mmol) of title compound (**3.54I**) was isolated as light white solid. Yield 93%; mp 190-191 ^oC; ^1H NMR (400 MHz, CD_3OCD) δ 7.22-7.31 (2H, m), 7.42 (1H, d, J = 7.2 Hz), 7.55 (1H, d, J = 7.6 Hz); ^{13}C NMR (100 MHz) δ 123.3, 127.7, 129.3, 133.1, 133.9, 135.1, 156.4; HRMS calcd. for

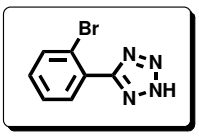

$C_7H_6N_4Br[M+H]^+$ 224.9770, found 224.9766, $C_7H_6N_4Br[M+H+2]^+$ 226.9770, found 224.9768.

Synthesis of 5-(2', 6'- dichlorophenyl) tetrazole (3.54J): Using the general procedure, starting from 320mg (1.86 mmol) of compound (**3.53J**), 348 mg (1.62 mmol) of title compound (**3.54J**) was isolated as white solid. Yield 87%; mp 213-214 ^oC; ^1H NMR (400 MHz, d_6-DMSO) δ 7.66-7.74 (3H, m); ^{13}C NMR (100 MHz) δ 124.9, 129.2, 133.9, 134.1, 135.2, 151.9; HRMS calcd. for $C_7H_5N_4Cl_2[M+H]^+$ 214.9886, found 214.9870.

Synthesis of 5-(3',4'-iodofluorophenyl) tetrazole (3.54K): Using the general procedure, starting from 300mg (1.215 mmol) of compound (**3.53K**), 315 mg (1.086 mmol) of title compound (**3.54K**) was isolated as light white solid. Yield 89%; mp 230-232 ^oC; ^1H NMR (400 MHz, CD_3OCD) δ 7.63-7.65 (1H, d, J = 8 Hz), 7.77-7.79 (1H, d, J = 8.8 Hz), 8.01-8.05 (1H, t, J = 8.0 Hz); ^{13}C NMR (100 MHz) δ 113.3, 113.6, 123.9, 127.0, 140.6, 160.9, 163.4; HRMS calcd. for $C_7H_4N_4FI$ $[M+H]^+$ 290.9537, found 290.9530.

3.10.3.2. General procedure for the synthesis of bis-toluoyl protected tetrazolyl donor/acceptor aromatic nucleosides *via* substitution reaction

In a 2-neck round bottom flask fitted with a septum and a stopper take-off, the aryl tetrazole **3.54A-L**, (1.5 equiv.) was dissolved in dry THF in an inert atmosphere. K_2CO_3 (3 equiv) was then added to the reaction mixture and the reaction mixture was stirred for half an hour. After that the bis-toulyl protected α-chloro-deoxy ribose sugar (**2.91**, 3.0 equiv) was added to the reaction mixture portionwise and the reaction mixture was stirred overnight. After completion of the reaction as monitored by TLC, the reaction mixture was evaporated and partitioned between water and ethyl acetate. The organic layer was then washed with water followed by brine solution, dried over Na_2SO_4, and then concentrated. The products were then separated by silica-gel (60-120 mesh) column chromatography and characterized. The average isolated yields of the tetrazolyl nucleosides were between 65-84%.

Synthesis of 3', 5'-bis{O-(p-toluoyl)}-2'-deoxy-1'-β-tetrazolyl benzene nucleoside (3.55a, bis-toluoyl-β-^{TzB}B): Using the general procedure, starting from 56.3 mg (0.386

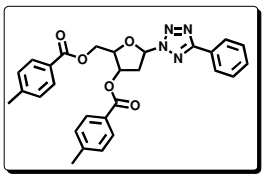

mmol) of the 5-phenyl tetrazole (**3.54A**) and 100 mg of α-chloro-deoxy ribose sugar (**2.91**, 0.257 mmol), 96 mg (0.193 mmol) of the title compound **3.55a** was isolated as a colourless oil. Yield 75%; IR (KBr) 1712, 1612, 1470, 1453, 1312, 1280, 1264, 1179, 1106, 1074, 752, 735 cm^{-1}; ^1H NMR (400 MHz, $CDCl_3$) δ 2.34 (3H, s), 2.40 (3H, s), 2.85-2.91 (1H, m), 3.39-3.46 (1H, m), 4.57-4.63 (1H, m), 4.69-4.73 (2H, m), 5.96-5.99 (1H, m), 6.84 (1H, t, J = 6.2 Hz), 7.12 (2H, d, J = 8.0 Hz), 7.25 (2H, d, J = 8.0 Hz), 7.43 (1H, s), 7.45 (2H, s), 7.91-7.97 (4H, m), 8.07-8.09 (2H, m); ^{13}C NMR (100 MHz) δ 21.8, 21.7, 37.5, 63.8, 74.7, 83.8, 90.5, 127.0, 127.1, 128.9, 129.2, 129.4, 129.9, 130.6, 143.9, 144.6, 165.7, 165.9, 166.2; HRMS calcd. for $C_{28}H_{26}N_4O_5Na$ ($[M+Na]^+$) 521.1795, found 521.1790.

Synthesis of 3', 5'-bis{O-(p-toluoyl)}-2'-deoxy-1'-β-tetrazolyl- methoxybenzene nucleoside (3.56a, bis-toluoyl-β-$^{TzMB}B_{Do}$): Using the general procedure, starting from

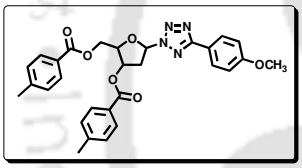

67.9 mg (0.386 mmol) of 5-(4-methoxyphenyl) tetrazole (**3.54B**) and 100 mg of α-chloro-deoxy ribose sugar (**2.91**, 0.257 mmol), 102 mg (0.193 mmol) of the title compound **3.56a** was isolated as a white solid. Yield 75%; IR (KBr) 1729, 1719, 1612, 1481, 1465, 1481, 1312, 1278, 1175, 1106, 1078, 834, 756 cm^{-1}; ^1H NMR (400 MHz, $CDCl_3$) δ 2.37 (3H, s), 2.44 (3H, s), 2.83-2.89 (1H, m), 3.39-3.45 (1H, m), 3.07 (3H, s), 4.56-4.62 (1H, m), 4.69-4.73 (2H, m), 5.96 (1H, bs), 6.82 (1H, t, J = 5.8 Hz), 6.97 (2H, d, J = 9.2 Hz), 7.15 (2H, d, J = 7.6 Hz), 7.27 (2H, d, J = 8.4 Hz), 7.92-7.97 (4H, m), 8.02 (2H, d, J = 9.2 Hz); ^{13}C NMR (100 MHz) δ 21.8, 21.9, 37.7, 55.6, 63.9, 74.8, 83.9, 90.5, 114.4, 119.8, 127.0, 128.8, 129.3, 129.5, 130.0, 144.0, 144.7, 161.6, 165.8, 166.1, 166.4; HRMS calcd. for $C_{29}H_{29}N_4O_6$ $[M+H]^+$ 529.2082, found 529.2078.

Synthesis of 3', 5'-bis{O-(p-toluoyl)}-2'-deoxy-1'-β-tetrazolyl-trimethoxybenzene nucleoside (3.57a, bis-toluoyl-β-$^{TzTMB}B_{Do}$): Using the general

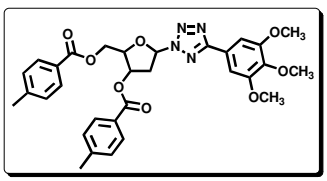

procedure, starting from 91.2 mg (0.386 mmol) of 5-(3′, 4′, 5′-trimethoxyphenyl) tetrazole (**3.54c**) and 100 mg of α-chloro-deoxy ribose sugar (**2.91**, 0.257 mmol), 125.5 mg (0.213 mmol) of the title compound **3.57a** was isolated as a white solid. Yield

83%; IR (KBr) 2923, 2852, 1733, 1719, 1612, 1593, 1485, 1464, 1426, 1279, 1268, 1129, 1105, 958, 851, 755 cm^{-1}; ^1H NMR (600 MHz, $CDCl_3$) δ 2.36 (3H, s), 2.44 (3H, s), 2.88-2.92 (1H, m), 3.42-3.46 (1H, m), 3.91 (3H, s), 3.92 (6H, s), 4.62 (1H, dd, J = 5.4, 12.0 Hz), 4.68 (1H, dd, J = 4.8, 12.0 Hz), 4.75-4.76 (1H, m), 5.92-5.94 (1H, m), 6.83 (1H, t, J = 6.3 Hz), 7.14 (2H, d, J = 8.4 Hz), 7.28 (2H, d, J = 8.4 Hz), 7.39 (2H, s), 7.89 (2H, d, J = 8.4 Hz), 7.96 (2H, d, J = 8.4 Hz); ^{13}C NMR (150 MHz) δ 21.8, 21.9, 37.7, 56.5, 61.2, 64.0, 74.8, 83.9, 90.8, 104.5, 122.5, 126.6, 126.9, 129.3, 129.5, 129.9, 130.0, 14.1, 144.8, 153.9, 165.8, 166.1, 166.4; HRMS calcd. for $C_{31}H_{33}N_4O_5$ $[M+H]^+$ 541.2445, found 541.2438.

Synthesis of 3', 5'-bis{O-(p-toluoyl)}-2'-deoxy-1'-β-tetrazolyl- pyridine nucleoside (3.58a, bis-toluoyl-β-$^{TzPy}B_{Do}$): Using the general procedure, starting from

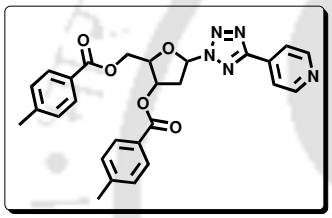

56.8 mg (0.386 mmol) of 4-(tetrazol-5′-yl)pyridine (**3.54D**) and 100 mg (**2.91**, 0.257 mmol) of α-chloro-deoxy ribose sugar, 100.1 mg (0.2 mmol) of the title compound **3.58a** was isolated as a white solid. Yield 78%; IR (KBr) 1722, 1612, 1457, 1273, 1176, 1094, 749 cm^{-1}; ^1H NMR (400 MHz, $CDCl_3$) δ 2.38 (3H, s), 2.45 (3H, s), 2.88-2.94 (1H, m), 3.40-3.47 (1H, m), 4.55-4.60 (1H, m), 4.73-4.77 (2H, m), 5.95-5.99 (1H, m), 6.86 (1H, t, J = 5.8 Hz), 7.16 (2H, d, J = 8.4 Hz), 7.29 (2H, d, J = 8.4 Hz), 7.88-7.91 (4H, m), 7.97 (2H, d, J = 8 Hz), 8.92 (2H, d, J = 6 Hz); ^{13}C NMR (100 MHz) δ 21.8, 21.9, 37.7, 63.7, 74.6, 84.1, 90.9, 121.0, 126.4, 126.8, 129.3, 129.4, 129.8, 129.9, 134.4, 144.1, 144.7, 150.7, 163.8, 165.9, 166.2; HRMS calcd. for $C_{27}H_{26}N_5O_5$ $[M+H]^+$ 500.1928, found 500.1919.

Synthesis of 3', 5'-bis{O-(p-toluoyl)}-2'-deoxy-1'-β-tetrazolyl-methoxynapthalene nucleoside (3.59a, bis-toluoyl-β-$^{TzMNapB}B_{Do}$): Using the general

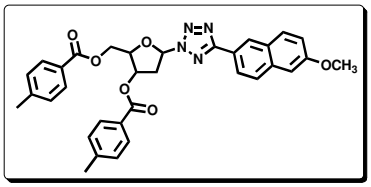

procedure, starting from 87.2 mg (0.386 mmol) of 5-(6′-acetylnapthalene) tetrazole (**3.54E**) and 100 mg (**2.91**, 0.257 mmol) of α-chloro-deoxy ribose sugar, 104.1 mg (0.180 mmol) of the title compound **3.59a** was isolated as a white solid. Yield 70%; IR (KBr) 1723, 1612, 1523, 1505, 1279, 1210, 1180, 1111, 1076, 754 cm^{-1}; ^1H NMR (400 MHz, $CDCl_3$) δ 2.29 (3H, s), 2.44

(3H, s), 2.87-2.93 (1H, m), 3.42-3.51 (1H, m), 3.95 (3H, s), 4.63-4.66 (1H, m), 4.70-4.74 (2H, m), 5.98-6.01 (1H, m), 6.86 (1H, t, *J* = 6.2 Hz), 7.12 (2H, d, *J* = 8 Hz), 7.17-7.21 (2H, m), 7.28 (2H, d, *J* = 8 Hz), 7.80 (2H, d, *J* = 6.8 Hz), 7.92-7.98 (4H, m), 8.11 (1H, d, *J* = 8.4 Hz), 8.57 (1H, s); ^{13}C NMR (100 MHz) δ 21.8, 21.9, 37.7, 55.6, 63.9, 74.8, 83.9, 90.6, 106.0, 119.8, 122.4, 124.8, 126.6, 127.1, 127.6, 128.8, 129.3, 129.5, 130.0, 130.5, 135.9, 144.1, 144.7, 158.9, 166.1, 166.2, 166.5; HRMS calcd. for $C_{33}H_{31}N_4O_6$ $[M+H]^+$ 579.2238, found 579.2230.

Synthesis of 3', 5'-bis{O-(p-toluoyl)}-2'-deoxy-1'-β-tetrazolyl- phenantherene nucleoside (3.60a, bis-toluoyl-β-$^{TzPhenB}B_{Do}$): Using the general procedure, starting

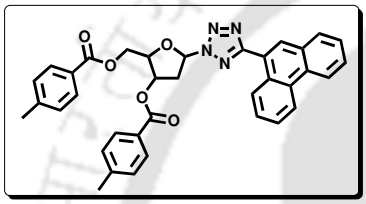

from 81 mg of (0.328 mmol) of 5-phenanthrenyl tetrazole (**3.54F**) 85 mg of α-chloro-deoxy ribose sugar (**2.91**, 0.219 mmol), 110 mg (0.184 mmol) of the title compound **3.60a** was isolated as a white solid. Yield 84%; IR (KBr) 1719, 1611, 1491, 1278, 1179, 1109, 751 cm^{-1}; ^{1}H NMR (600 MHz, $CDCl_3$) δ 2.17 (3H, s), 2.44 (3H, s), 2.95-2.99 (1H, m), 3.54-3.58 (1H, m), 4.69 (1H, dd, *J* = 5.4, 12.0 Hz), 4.75-4.80 (2H, m), 6.02-6.05 (1H, m), 6.95 (2H, d, *J* = 8.4 Hz), 6.97 (1H, d, *J* = 6.6 Hz), 7.27 (2H, d, *J* = 7.8 Hz), 7.64 (1H, t, *J* = 7.2 Hz), 7.68-7.75 (3H, m), 7.89 (2H, d, *J* = 8.4 Hz), 7.96 (1H, d, *J* = 7.8 Hz), 7.99 (2H, d, *J* = 7.8 Hz), 8.49 (1H, s), 8.73 (1H, d, *J* = 7.8 Hz), 8.79 (1H, d, *J* = 7.8 Hz), 8.89 (1H, d, *J* = 7.8 Hz); ^{13}C NMR (150 MHz) δ 21.6, 21.9, 37.8, 63.8, 74.7, 84.0, 90.8, 122.7, 122.9, 123.1, 126.5, 126.6, 126.8, 127.1, 127.6, 128.2, 129.0, 129.1, 129.4, 129.7, 129.8, 129.9, 130.7, 130.8, 130.9, 131.4, 143.9, 144.6, 165.9, 166.0, 166.4; HRMS calcd. for $C_{36}H_{31}N_4O_5$[M+H]$^+$ 599.2289, found 599.2281.

Synthesis of 3', 5'-bis{O-(p-toluoyl)}-2'-deoxy-1'-β-tetrazolyl- pyrene nucleoside (3.61a bis-toluoyl-β-$^{TzPyB}B_{Do}$): Using the general procedure, starting from 83.4 mg of

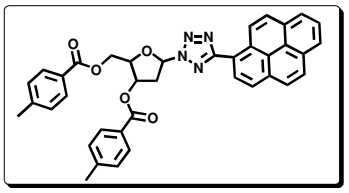

(0.308 mmol) of 5-pyrenyl tetrazole (**3.54G**)and 100 mg (**2.91**, 0.257 mmol) of α-chloro-deoxy ribose sugar, 122 mg (0.195 mmol) of the title compound **3.61a** was isolated as a white solid. Yield 76%; IR (KBr) 2922, 2852, 1726, 1612, 1470, 1276, 1264, 1107, 1074, 841, 753 cm^{-1}; ^{1}H NMR (400 MHz, $CDCl_3$) δ 2.07 (3H, s), 2.44 (3H, s), 2.94-3.01 (1H, m), 3.53-3.59

(1H, m), 4.65-4.69 (1H, m), 4.75-4.81 (2H, m), 6.05-6.06 (1H, m), 6.88 (2H, d , *J* = 8.0 Hz), 6.98 (1H, t, *J* = 6.0 Hz), 7.29 (2H, d, *J* = 8.0 Hz), 7.86 (2H, d, *J* = 7.6 Hz), 7.98 (2H, d, *J* = 8.4 Hz), 8.03-8.13 (2H, m), 8.16-8.19 (2H, m), 8.24 (3H, d, *J* = 7.6 Hz), 8.69 (1H, d, *J* = 8.4 Hz), 9.18 (1H, d, *J* = 9.2 Hz); ^{13}C NMR (100 MHz) δ 21.5, 21.9, 37.9, 63.8, 74.6, 83.9, 90.8, 120.9, 124.9, 125.0, 125.2, 125.9, 126.1, 126.4, 126.6, 126.8, 127.5, 127.8, 128.9, 129.1, 129.3, 129.5, 129.9, 130.0, 130.9, 131.4, 133.0, 143.9, 144.7, 166.1, 166.4, 166.6; HRMS calcd. for $C_{38}H_{30}N_4O_5Na$ $[M+Na]^+$ 645.2265, found 645.2258.

Synthesis of 3', 5'-bis{O-(p-toluoyl)}-2'-deoxy-1'-β-tetrazolyl- nitro benzene nucleoside (3.62a, bis-toluoyl-β-$^{TzNB}B_{Ac}$): Using the general procedure, starting from

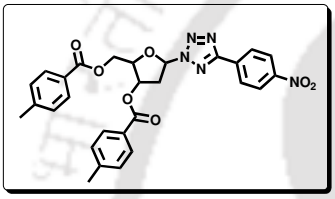

73.8 mg of (0.386 mmol) of 5-(4′-nitrophenyl) tetrazole (**3.54H**) and 100 mg of α-chloro-deoxy ribose sugar (**2.91**, 0.257 mmol), 140 mg (0.258 mmol) of the title compound **3.62a** was isolated as a yellow solid. Yield 70%; IR (KBr) 1717, 1611, 1521, 1343, 1275, 1180, 1089, 960, 855, 754 cm^{-1}; ^{1}H NMR (600 MHz, $CDCl_3$) δ 2.38 (3H, s), 2.45 (3H, s), 2.89-2.94 (1H, m), 3.42-3.46 (1H, m), 4.57-4.60 (1H, m), 4.73-4.76 (2H, m), 5.97-5.99 (1H, m), 6.86 (1H, t, *J* = 6.0 Hz), 7.17 (2H, d, *J* = 7.8 Hz), 7.29 (2H, d, *J* = 7.8 Hz), 7.9 (2H, d, J = 8.4 Hz), 7.97 (2H, d, *J* = 8.4 Hz), 8.22 (2H, d, *J* = 6.0 Hz), 8.29 (2H, d, *J* = 6.0 Hz); ^{13}C NMR (150 MHz) δ 21.8, 21.9, 63.8, 74.6, 84.2, 91.1, 124.3, 126.5, 126.9, 128.1, 129.4, 129.6, 130.0, 130.1, 133.0, 144.2, 144.9, 149.2, 164.0, 166.1, 166.3; HRMS calcd. for $C_{28}H_{26}N_5O_7$ $[M+H]^+$ 544.1827, found 544.1822.

Synthesis of 3', 5'-bis{O-(p-toluoyl)}-2'-deoxy-1'-β-tetrazolyl- bromo benzene nucleoside (3.63a, bis-toluoyl-β-$^{TzBrB}B_{Ac}$): Using the general procedure, starting from

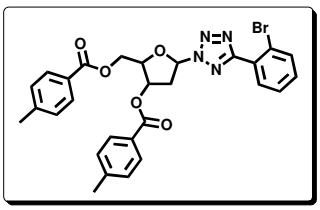

86.5 mg of (0.386 mmol) of 5-(2′-bromophenyl) tetrazole (**3.54I**) and 100 mg (**2.91**, 0.257) of α-chloro-deoxy ribose sugar, 117 mg (0.203 mmol) of the title compound **3.63a** was isolated as a white solid. Yield 79 %; IR (KBr) 1711, 1613, 1466, 1308, 1270, 1178, 1101, 1080, 961, 754 cm^{-1}; ^{1}H NMR (400 MHz, $CDCl_3$) δ 2.35 (3H, s), 2.44 (3H, s), 2.87-2.94 (1H, m), 3.38-3.44 (1H, m), 4.59-4.63 (1H, m), 4.72-4.78 (2H, m), 5.97-6.01 (1H, m), 6.89 (1H, t, *J* = 5.2 Hz), 7.12 (2H, d, *J*

= 8 Hz), 7.27 (1H, d, *J* = 8.8 Hz), 7.35 (1H, t, *J* = 8.0 Hz), 7.42 (1H, t, *J* = 7.6 Hz), 7.74 (1H, d, *J* = 8.0 Hz), 7.88 (2H, dd, *J* = 1.8, 7.8 Hz), 7.91 (2H, d, *J* = 8.0 Hz), 7.96 (2H, d, *J* = 8.0 Hz);^{13}C NMR (100 MHz) δ 22.1, 22.2, 38.1, 64.4, 75.0, 84.2, 91.1, 122.6, 126.9, 127.2, 127.9, 128.6, 129.5, 129.7, 130.3, 131.8, 132.2, 134.6, 144.2, 144.9, 165.0, 166.3, 166.6; HRMS calcd. for $C_{28}H_{25}N_4O_5BrNa[M+Na]^+$ 599.0901, found 599.0899, $C_{28}H_{27}N_4O_5BrNa[M+Na+2]^+$ 601.0901, found 601.0896.

Crystallographic description for 3', 5'-bis{O-(p-toluoyl)}-2'-deoxy-1'-β-tetrazolyl-bromo benzene nucleoside (3.63a, bis-toluoyl-β-$^{TzBrB}B_{Ac}$): Crystal dimension (mm): 0.28 x 0.30 x 0.35. $C_{28}H_{25}BrN_4O_5$, Mr = 577.42; Monoclinic, space group P 21; a = 10.1458(2) Å, b = 12.4658(2) Å, c = 10.7755(2) Å; α = 90.00°, ß = 107.228°, γ = 90.00°, V = 1379.8(2) Å^3; Z = 4; ρcal = 1.473 g/cm^3; μ (mm^{-1}) = 1.625; *F(000)* = 592.00; Refinement method = Full-matrix least-squares on F^2; Final R indices [I>2σ_I] R(reflections) = 0.0272(3780), wR2(reflections) = 0.0625(4592); goodness of fit = 1.017.

Synthesis of 3', 5'-bis{O-(p-toluoyl)}-2'-deoxy-1´-β-tetrazolyl- dichloro benzene nucleoside (3.64a, bis-toluoyl-β-$^{TzDClB}B_{Ac}$): Using the general procedure, starting from 157.6 mg (0.733 mmol) of 5-(2′, 6′-dichlorophenyl) tetrazole (**3.54J**) and 170 mg (**2.91**, 0.488 mmol) of α-chloro-deoxy ribose sugar, 180 mg (0.318 mmol) of the title compound **3.64a** was isolated as a colourless semisolid compound. Yield 65%; ^{1}H NMR (400 MHz, $CDCl_3$) δ 2.23 (3H, s), 2.31 (3H, s), 2.81-2.87 (1H, m), 3.31-3.37 (1H, m), 4.42-4.46 (1H, m), 4.57-4.61 (1H, m), 4.65-4.68 (1H, m), 5.84-5.87 (1H, m), 6.82 (1H, t, *J* = 5.8 Hz), 6.99 (2H, d, *J* = 7.6 Hz), 7.15 (2H, d, *J* = 8 Hz), 7.26-7.32 (3H, m), 7.83 (4H, q, *J* = 3.2, 8.4 Hz); ^{13}C NMR (100 MHz) δ 21.7, 21.8, 37.8, 63.9, 74.8, 84.1, 90.9, 126.4, 126.9, 128.2, 129.0, 129.3, 129.9, 131.9, 136.3, 143.7, 144.5, 161.2, 165.9, 166.2; HRMS calcd. for $C_{28}H_{25}N_4O_5Cl_2$ [M+H]$^+$ 567.1197, found 567.1188.

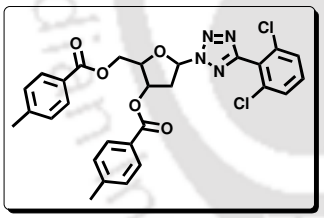

Synthesis of 3', 5'-bis{O-(p-toluoyl)}-2'-deoxy-1'-β-tetrazolyl- fluoroiodo benzene nucleoside (3.65a, bis-toluoyl-β-$^{TzFIB}B_{Ac}$): Using the general procedure, starting from 111.8 mg of (0.386 mmol) of 5-(3′,4′-iodofluorophenyl) tetrazole

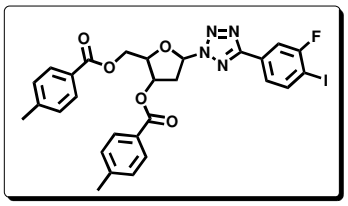

(**3.54K**)and 100 mg (**2.91**, 0.257 mmol) of α-chloro-deoxy ribose sugar, 122 mg (0.190 mmol) of the title compound **3.65a** was isolated as a white solid. Yield 74%; IR (KBr) 2936, 1717, 1609, 1448, 1258, 1176, 1099, 1090, 750 cm^{-1}; ^1H NMR (400 MHz, $CDCl_3$) δ 2.38 (3H, s), 2.44 (3H, s), 2.86-2.92 (1H, m), 3.39-3.46 (1H, m), 4.56-4.60 (1H, m), 4.69-4.74 (2H, m), 5.94-5.98 (1H, m), 6.83 (1H, t, *J* = 5.8 Hz), 7.15 (2H, d, *J* = 8 Hz), 7.28 (2H, d, *J* = 8 Hz), 7.61 (1H, dd, *J* = 2.0, 8.4 Hz), 7.71 (1H, dd, *J* = 1.6, 8.4 Hz), 7.83 (1H, t, *J* = 8.4 Hz), 7.89 (2H, d, *J* = 8.0 Hz), 7.96 (2H, d, *J* = 8.0 Hz); ^{13}C NMR (100 MHz) δ 21.8, 21.9, 37.7, 63.7, 74.6, 84.1, 84.3, 90.8, 114.0, 114.3, 124.3, 126.5, 126.9, 129.3, 129.5, 129.9, 129.97, 140.2, 144.2, 144.7, 160.9, 164.2, 166.0, 166.3; HRMS calcd. for $C_{28}H_{25}N_4O_5FI[M+H]^+$ 643.0848, found 648.0844.

Crystallographic description for 3', 5'-bis{O-(p-toluoyl)}-2'-deoxy-1'-β-tetrazolyl- fluoroiodo benzene nucleoside (3.65a, bis-toluoyl-β-$^{TzFIB}B_{Ac}$): Crystal dimension (mm): 0.29 x 0.26 x 0.10. $C_{28}H_{24}FIN_4O_5$, Mr = 642.41; Orthorhombic, space group P 212121; a = 11.6709(2) Å, b = 11.8642(2) Å, c = 19.6750(4) Å; α = 90.00°, ß = 90.00 °, γ = 90.00°, V = 2724.32(9) $Å^3$; Z = 4; ρcal = 1.566 g/cm^3; μ (mm^{-1}) = 1.227; *F(000)* = 1288.00; Refinement method = Full-matrix least-squares on F^2; Final R indices [$I>2\sigma_I$] R(reflections) = 0.0273(4515), wR2(reflections) = 0.0643(4795); goodness of fit = 1.057.

Synthesis of 3', 5'-bis{O-(p-toluoyl)}-2'-deoxy-1'-β-tetrazolyl- chloro bromo pyridine nucleoside (3.66a, bis-toluoyl-β-$^{TzBCPyr}B_{Ac}$): Using the general procedure,

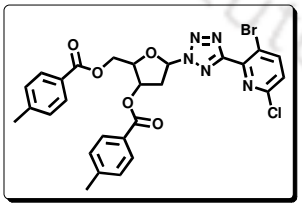

starting from 60.3 mg (0.231 mmol) of bromo, chloro pyridine tetrazole (**3.54L**) and 60 mg (0.154 mmol) of α-chloro-deoxy ribose sugar (**2.91**), 94.4 mg (0.154 mmol) of the title compound **3.66a** was isolated as a white solid. Yield 60%; IR (KBr) 3038, 2923, 1713, 1612, 1434, 1402, 1271, 1178, 1108, 1011, 753 cm^{-1}; ^1H NMR (600 MHz, $CDCl_3$) δ 2.36 (3H, s), 2.43 (3H, s), 2.90-2.94 (1H, m), 3.39-3.44 (1H, m), 4.58-4.61 (1H, m), 4.69-4.72 (1H, m), 4.72-4.78 (1H, m), 5.96-5.98 (1H, m), 6.91 (1H, t, *J* = 6 Hz), 7.15 (2H, d, *J* = 7.8 Hz), 7.27 (2H, d, *J* = 7.8 Hz), 7.34 (1H, d, *J* = 8.4 Hz), 7.91 (2H, d, *J* = 7.8 Hz), 7.95

(2H, d, J = 7.8 Hz),7.99 (1H, d, J = 8.4 Hz); ^{13}C NMR (150 MHz) δ 21.8, 21.9, 37.9, 64.1, 74.7, 84.1, 91.2, 119.2, 126.5, 126.8, 126.9, 129.2, 129.5, 129.9, 143.9, 144.5, 144.7, 146.0, 150.3, 162.9, 165.9, 166.4; HRMS calcd. for $C_{27}H_{23}N_5O_5BrClNa$ $[M+Na]^+$ 634.0463, found 634.0468.

3.10.3.3 General procedure for toluoyl deprotection of triazolyl donor/acceptor aromatic nucleosides (3.55b-3.66b)

The bis-toluoylated nucleoside (**3.55a-3.55a**, 1.0 equiv.) was dissolved in dry methanol. Sodium methoxide (3.0 equiv.) was subsequently added. The solution was stirred at room temperature for 2.5 hours. Then, NH_4Cl was added to the reaction mixture until the reaction mixture was weakly acidic. The solvent methanol was evaporated and around 15 ml of ethylacetate was added to the reaction mixture. The organic layer was washed with water followed by brine solution, dried over Na_2SO_4, and then concentrated. The deprotected products were separated by silica gel (60-120 mesh) column chromatography.

Synthesis of 2'-deoxy-1'-β-tetrazolyl benzene nucleoside (3.55b, β-^{TzB}B): Using

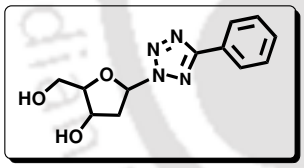

the general procedure for deprotection starting from 100 mg (0.201 mmol) of **3.55a**, 50 mg (0.191 mmol) of title compound (**3.55b**) was isolated as colourles semi-solid. Yield 95%; IR (KBr) 3442, 2922, 2852, 1564, 726 cm^{-1}; ^{1}H NMR (400 MHz, CD_3OD) δ 2.46-2.53 (1H, m), 2.83-2.89 (1H, m), 3.52-3.57(1H, m), 3.63-3.67(1H, m), 3.98-3.99 (1H, m), 4.63 (1H, q, J = 4.8, 6.0 Hz), 6.58 (1H, q, J = 3.2, 4.0 Hz), 7.36-7.37 (3H, m), 7.96-7.98 (2H, m); ^{13}C NMR (100 MHz) δ 40.8, 63.7, 72.3, 90.2, 92.4, 127.9, 128.5, 130.3, 131.9, 166.5; HRMS calcd. for $C_{12}H_{15}N_4O_3[M+H]^+$ 263.1139, found 263.1128.

Synthesis of 2'-deoxy-1'-β-tetrazolyl methoxy benzene nucleoside (3.56b, β-$^{TzMB}B_{Do}$): Using the general procedure for deprotection starting from 100 mg (0.189

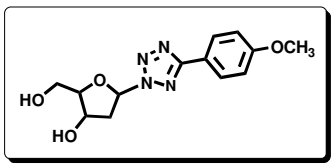

mmol) of compound **3.56a**, 54 mg (0.185 mmol) of the title compound (**3.56b**) was isolated as white crystalline solid. Yield 98%; mp 71-75 ^{o}C; IR (KBr) 3339, 2924, 2852, 1616, 1467, 1429, 1253, 1175, 834, 763, 681 cm$^-$

[1]; ^{1}H NMR (400 MHz, CD_3OD) δ 2.57-2.64 (1H, m), 2.94-2.99 (1H, m), 3.63-3.68 (1H, m), 3.74-3.78 (1H, m), 3.85 (3H, s), 4.08 (1H, q, *J* = 4.8, 5.2 Hz), 4.73 (1H, q, *J* = 5.2, 5.6 Hz), 6.67-6.69 (1H, m), 7.05 (2H, d, *J* = 8.4 Hz), 8.03 (2H, d, *J* = 8.8 Hz); ^{13}C NMR (150 MHz) δ 40.9, 56.1, 63.8, 72.4, 90.3, 92.3, 115.7, 120.9, 129.6, 163.3, 166.5; HRMS calcd. for $C_{13}H_{17}N_4O4[M+H]^+$ 293.1244, found 293.1238.

Synthesis of 2'-deoxy-1'-β-tetrazolyl trimethoxy benzene nucleoside (3.57b, β-$^{TzMB}B_{Do}$): Using the general procedure for deprotection starting from 74 mg (0.126 mmol) of compound **3.56a**, 38 mg (0.108 mmol) of compound (**3.57b**) was isolated as white solid. Yield 86%; mp 135-140^{o}C; IR (KBr) 3545, 3460, 3297, 2922, 2853, 1595, 1485, 1469, 1425, 1245, 1127, 1065, 999, 962, 755 cm^{-1}; ^{1}H NMR (400 MHz, CD_3OD) δ 2.48-2.55 (1H, m), 2.88-2.94 (1H, m), 3.53-3.57 (1H, m), 3.63-3.67 (1H, m), 3.72 (3H, s), 3.82(6H, s), 3.98 (1H, q, *J* = 4.6, 5.2 Hz), 4.64 (1H, q, *J* = 4.8, 6 Hz), 6.57-6.59 (1H, m), 7.31 (2H, s); ^{13}C NMR (100 MHz) δ 40.9, 57.0, 61.4, 63.7, 72.4, 90.4, 92.6, 105.6, 124.1, 155.4, 166.5; HRMS calcd. for $C_{15}H_{21}N_4O_6[M+H]^+$ 353.1456, found 353.1450.

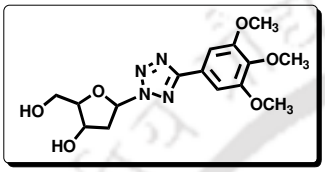

Synthesis of 2'-deoxy-1'-β-tetrazolyl pyridine nucleoside (3.58b β-$^{TzPyr}B_{Do}$): Using the general procedure for deprotection starting from 60 mg (0.120 mmol) of compound **3.58a**, 27 mg (0.103 mmol) of the title compound (**3.58b**) was isolated as white solid. Yield 85%; IR (KBr) 3440, 2924, 1634, 1530, 751 cm^{-1}; ^{1}H NMR (400 MHz, CD_3OD) δ 2.51-2.54 (1H, m), 2.87-2.92 (1H, m), 3.52-3.55 (1H, m), 3.62-3.65 (1H, m), 3.97 (1H, bs), 4.64 (1H, bs), 6.64 (1H, bs), 8.02 (2H, bs), 8.62 (2H, bs); ^{13}C NMR (100 MHz, CD_3OD) δ 40.9, 63.5, 72.2, 90.4, 92.9, 122.6, 137.2, 151.4, 164.3; HRMS calcd. for $C_{11}H_{14}N_5O_3[M+H]^+$ 264.1091, found 264.1011.

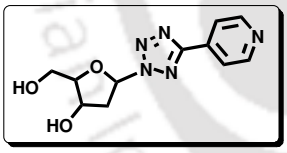

Synthesis of 2'-deoxy-1'-β-tetrazolyl methoxynapthalene nucleoside (3.59b, β-$^{TzMNap}B_{Do}$): Using the general procedure for deprotection starting from 100 mg (0.173 mmol) of compound **3.59a**, 56 mg (0.164 mmol) of the title compound (**3.59b)** was isolated as white solid. Yield 95%; mp 125-127 ^{o}C; IR (KBr) 3392, 3308, 1629, 1528, 1506, 1260, 1219, 1089, 1030, 868, 818

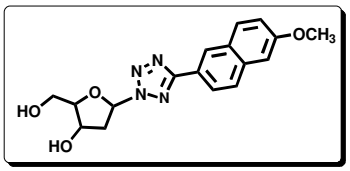

cm^{-1}; ^1H NMR (400 MHz, CD_3OD) δ 2.6-2.67 (1H, m), 2.99-3.05 (1H, m), 3.66-3.71 (1H, m), 3.77-3.81 (1H, m), 3.95 (3H, s), 4.09 (1H, q, *J* = 5.2 Hz), 4.78 (1H, q, *J* = 5.2, 5.8 Hz), 6.72-6.75 (1H, m), 7.21 (1H, dd, *J* = 2, 8.8 Hz), 7.31 (1H, bs), 7.90 (2H, t, *J* = 9.8 Hz), 8.12 (1H, d, *J* = 8.4 Hz), 8.57 (1H, s); ^{13}C NMR (150 MHz) δ 39.4, 54.5, 62.2, 70.9, 88.8, 90.9, 105.6, 119.5, 123.8, 126.1, 127.5, 128.7, 129.8, 159.07, 165.3; HRMS calcd. for $C_{17}H_{19}N_4O_5[M+H]^+$ 359.1350, found 359.1330.

Synthesis of 2'-deoxy-1'-β-tetrazolyl phenantherene nucleoside (3.60b, β-$^{TzPhen}B_{Do}$): Using the general procedure for deprotection starting from 140 mg (0.234 mmol) of compound **3.60a**, 78 mg (0.215 mmol) of the title compound (**3.60b**) was

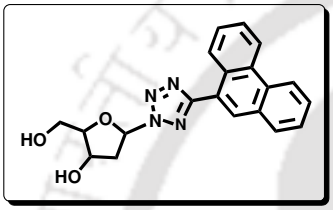

isolated as white solid. Yield 92%; mp 220-225 °C; IR (KBr) 3391, 2878, 2721, 1567, 1451, 1112, 1056, 772, 740, 723cm^{-1}; ^1H NMR (400 MHz, CD_3OD) δ 2.51-2.58 (1H, m), 2.89-2.96 (1H, m), 3.56-3.61 (1H, m), 3.66-3.71 (1H, m), 3.99 (1H, q, *J* = 4.8, 6 Hz), 4.68 (1H, q, *J* = 4.8, 6.2), 6.66-6.69 (1H, m), 7.45-7.57 (4H, m), 7.81 (1H, m), 8.26 (1H, s), 8.57-8.66 (3H, m); ^{13}C NMR (100 MHz) δ 40.9, 63.6, 72.3, 90.3, 92.5, 123.9, 124.3, 124.4, 127.5, 128.3, 128.4, 128.4, 129.5, 130.2, 130.6, 131.4, 132.2, 132.6, 166.5; HRMS calcd. for $C_{20}H_{19}N_4O_3[M+H]^+$ 363.1452, found 363.1443.

Synthesis of 2'-deoxy-1'-β-tetrazolyl pyrene nucleoside (3.61b, β-$^{TzPy}B_{Do}$): Using

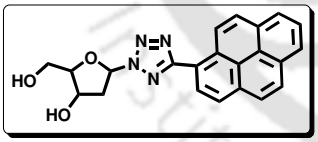

the general procedure for deprotection starting from 70 mg (0.112 mmol) of compound **3.61a**, 40 mg (0.103 mmol) of the title compound (**3.61b**) was isolated as light green solid. Yield 92%; mp 113-115 °C; IR (KBr) 3379, 3291, 2922, 1531, 1431, 1319, 1090, 1062, 838, 745, 712 cm^{-1}; ^1H NMR (400 MHz, CD_3OD) δ 2.56-2.62 (1H, m), 2.95-3.01 (1H, m), 3.62-3.66 (1H, m), 3.71-3.75 (1H, m), 4.03 (1H, q, *J* = 4.6, 5.6 Hz), 4.74 (1H, q , *J* = 5.6, 5.6 Hz), 6.71-6.73 (1H, m), 7.83-7.88 (2H, m), 7.93-7.98 (2H, m), 8.04-8.05 (3H, m), 8.44 (1H, d, *J* = 8Hz), 8.88 (1H, d, *J* = 9.6 Hz); ^{13}C NMR (100 MHz) δ 41.1, 63.8, 72.4, 90.4, 92.6, 122.1, 125.6, 125.8, 125.9, 126.1, 126.9, 127.2, 127.6, 128.4, 128.5, 130.0, 130.1, 130.3, 132.1, 132.7, 134.3, 167.1; HRMS calcd. for $C_{22}H_{18}N_4O_3Na[M+Na]^+$ 409.1428, found 409.1426.

Synthesis of 2'-deoxy-1'-β-tetrazolyl nitrobenzene nucleoside (3.62b, β-$^{TzNB}B_{Ac}$):

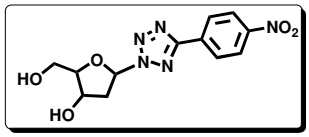

Using the general procedure for deprotection starting from 120 mg (0.221 mmol) of compound **3.62a**, 65 mg (0.212 mmol) of the title compound (**3.62b**) was isolated as cream white solid. Yield 96%; mp 105-108 ^{o}C; IR (KBr) 3367, 3106, 2940, 1604, 1521, 1459, 1426, 1345, 1313, 1066, 947, 855, 732 cm^{-1}; ^{1}H NMR (400 MHz) δ 2.49-2.56 (1H, m), 2.86-2.92 (1H, m), 3.52-3.56 (1H, m), 3.62-3.66 (1H, m), 3.97 (1H, q, *J* = 4.8, 5.2 Hz), 4.64 (1H, q, *J* = 4.8, 6.2 Hz), 6.61-6.64 (1H, m), 8.23-8.29 (4H, m); ^{13}C NMR (100 MHz) δ 40.9, 63.6, 72.3, 90.4, 92.8, 125.5, 129.1, 134.6, 150.7, 164.9; HRMS calcd. for $C_{12}H_{14}N_5O_5[M+H]^+$ 308.0989, found 308.0978.

Synthesis of 2'-deoxy-1'-β -tetrazolyl bromo benzene nucleoside (3.63b, β-$^{TzNB}B_{Ac}$): Using the general procedure for deprotection starting from 117 mg (0.203 mmol) of compound **3.63a**, 62mg (0.182 mmol) of the title compound (**3.63b**)was isolated as white solid. Yield 90%; ^{1}H NMR (400 MHz, CD_3OD) δ 2.48-2.55 (1H, m), 2.81-2.87 (1H, m), 3.53-3.57 (1H, m), 3.62-3.67 (1H, m), 3.97 (1H, q, *J* = 4.4, 6.4 Hz), 4.63 (1H, q, *J* = 5.2, 6.0 Hz), 6.63-6.66 (1H, m), 7.3 (1H, t, *J* = 8.0 Hz), 7.39 (1H, t, *J* = 7.6 Hz), 7.67 (1H, d, *J* = 8.0 Hz), 7.72 (1H, d, *J* = 8.0 Hz); ^{13}C NMR (100 MHz) δ 41.1, 63.9, 72.4, 90.4, 92.7, 123.2, 129.0, 129.9, 132.9, 133.1, 135.4, 165.6; HRMS calcd. for $C_{12}H_{13}N_4O_5BrNa[M+Na]^+$ 363.0063, found 363.0057, $C_{12}H_{13}N_4O_5BrNa[M+Na+2]^+$ 365.0063, found 363.0055.

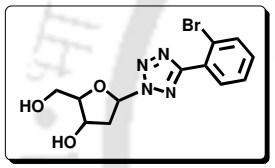

Synthesis of 2'-deoxy-1'-β-tetrazolyl dichloro benzene nucleoside (3.64b, β-$^{TzDCB}B_{Ac}$): Using the general procedure for deprotection starting from 170 mg (0.299 mmol) of compound **3.64a**, 90 mg (0.272 mmol) of the title compound (**3.64b**) was isolated as white solid. Yield 91%; mp 145-148 ^{o}C; IR (KBr) 3400, 2936, 1605, 1561, 1435, 1394, 1193, 1106, 1072, 994, 787 cm^{-1}; ^{1}H NMR (400 MHz, CD_3OD) δ 2.49-2.56 (1H, m), 2.79-2.85 (1H, m), 3.44-3.49 (1H, m), 3.57-3.61 (1H, m), 3.96 (1H, q, *J* = 5.2, 5.6 Hz), 4.56 (1H, q, *J* = 5.6, 5.8 Hz), 6. 65-6.67 (1H, m), 7.42-7.47 (3H, m); ^{13}C NMR (100 MHz) δ 41.1, 64.0, 72.5, 90.4, 92.9, 129.7,

133.9, 137.4, 162.1; HRMS calcd. for $C_{12}H_{13}N_4O_3Cl_2[M+H]^+$ 331.0359, found 331.0345.

Synthesis of 2'-deoxy-1'-β-tetrazolyl fluoro, iodo benzene nucleoside (3.65b, β-$^{TzFIB}B_{Ac}$): Using the general procedure for deprotection starting from 130mg (0.202 mmol) of compound **3.65a**, 70 mg (0.172 mmol) of the title compound (**3.65b**) was isolated as white solid. Yield 85%; mp 99-100 °C; IR (KBr) 3412, 2926, 1523, 1452, 1439, 1399, 1233, 1098, 1052, 963, 882, 757 cm^{-1}; ^1H NMR (400 MHz, CD_3OD) δ 2.46-2.53 (1H, m), 2.83-2.88 (1H, m), 3.49-3.54 (1H, m), 3.60-3.65 (1H, m), 3.95 (1H, q, *J* = 4.4, 5.4 Hz), 4.61 (1H, q, *J* = 5.2, 6 Hz), 6.57-6.59 (1H, m), 7.59 (1H, d, *J* = 7.6 Hz), 7.71 (1H, d, *J* = 8.0 Hz), 7.86 (1H, d, *J* = 7.4 Hz); ^{13}C NMR (100 MHz, CD_3OD) δ 39.3, 62.0, 70.7, 88.7, 91.0, 112.9, 113.2, 123.6, 129.9, 141.9, 162.5, 164.9; HRMS calcd. for $C_{12}H_{13}N_4O_3FI[M+H]^+$ 407.0011, found 407.0008.

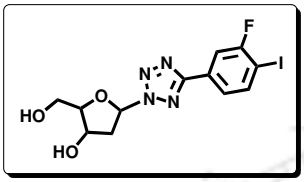

3.10.4. Study of Photophysical Property of the Nucleosides

UV-visible measurements: All the *UV* –visible spectra of the compounds (10 µM) were measured in different solvents using Shimadzu 2550 UV-Visible spectrophotometer with quartz optical cell of 1.0 cm path length. The measurements were carried out in absorbance mode. The absorbance values of the sample solutions were measured at a scanning rate of 0.5 nm with wavelength range of 200-500 nm and slit width of 2 nm. All the sample solutions were prepared just before doing the experiment.

Fluorescence experiments: All the sample solutions were prepared as described in UV measurement experiments. Fluorescence spectra were recorded using a Fluoromax-4 fluorescence spectrophotometer at 25 °C using quartz cell of 1.0 cm path length. The excitation wavelengths for all the cases were set at the excitation maxima of each sample in each solvents and emission spectra were measured in the wavelength regime of 300–600 nm with an integration time of 0.2 sec. All the sample solutions were prepared just before doing the experiment. Total volume of 1.0 ml from a stock solution of 2 ml of 10 µM concentration for each case was used for

fluorescence experiment in 1 ml cell. Fluorescence emissions were collected exciting the samples at the wave length corresponding to their absorption maxima. Steady-state fluorescence emission spectra were recorded at room temperature as an average of five scans using an excitation slit of 3.0 nm, emission slit 3.0 nm, and scan speed of 120 nm/min. The fluorescence quantum yields (Φ_f) were determined using quinine sulphate as a reference with the known Φ_f (0.55) in 0.1 molar solution in sulphuric acid or amino pyridine as a reference with the known Φ_f (0.6) in 0.1 molar solution in sulphuric acid. The following equation was used to calculate the quantum yield,

$$\Phi_S = \Phi_R \frac{Fl_S^{Area}}{Fl_R^{Area}} \frac{Abs_R}{Abs_S} \frac{n_S^2}{n_R^2}$$

where, Φ_R is the quantum yield of standard reference, Fl_S^{Area} (sample) and Fl_R^{Area} (reference) are the integrated emission peak areas, Abs_S (sample) and Abs_R (reference) are the absorbances at the excitation wavelength, and n_S (sample) and n_R (reference) are the refractive indices of the solutions.

3.11. ^{1}H and ^{13}C NMR spectra

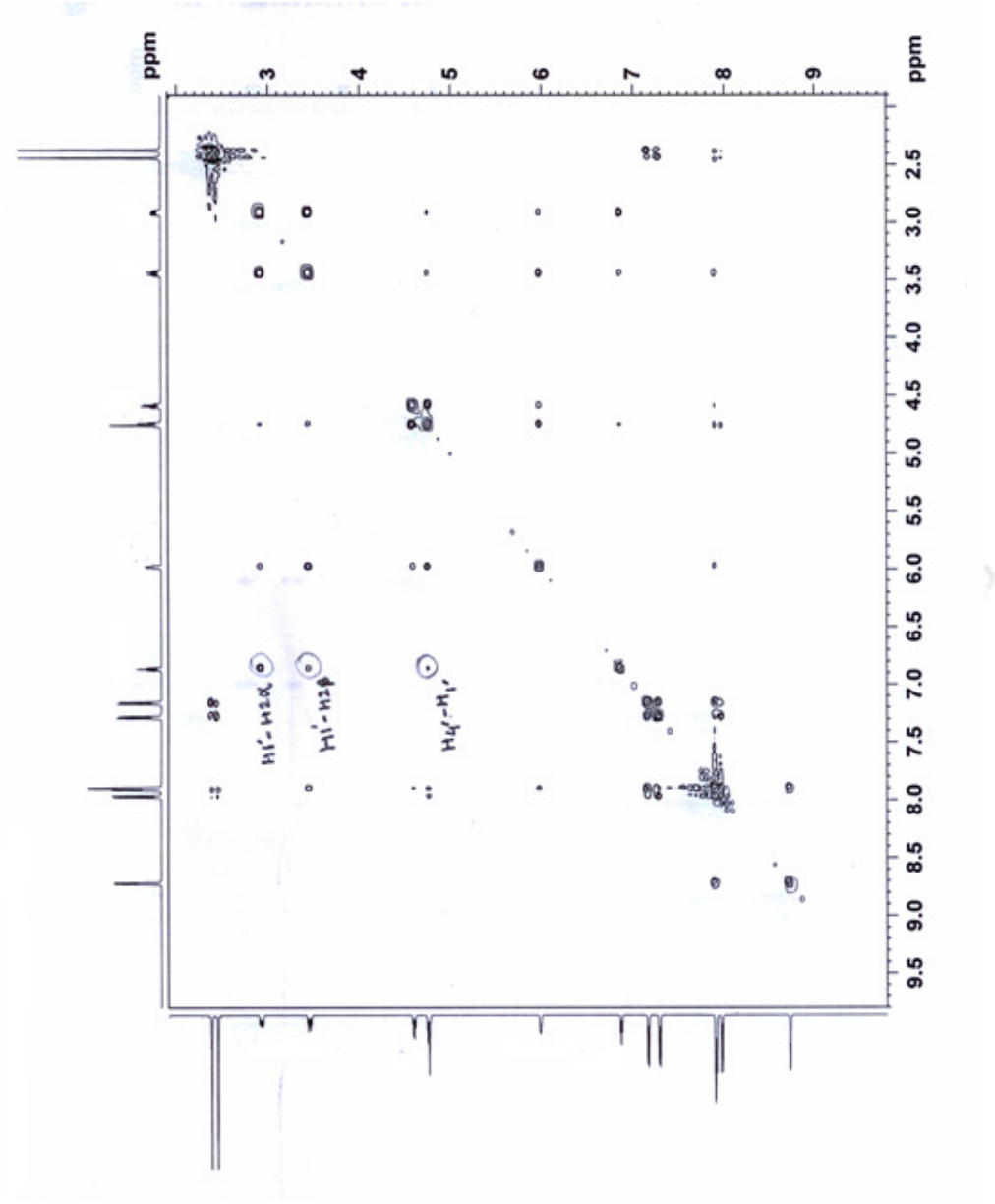

NOESY spectra of compound **3.58a**

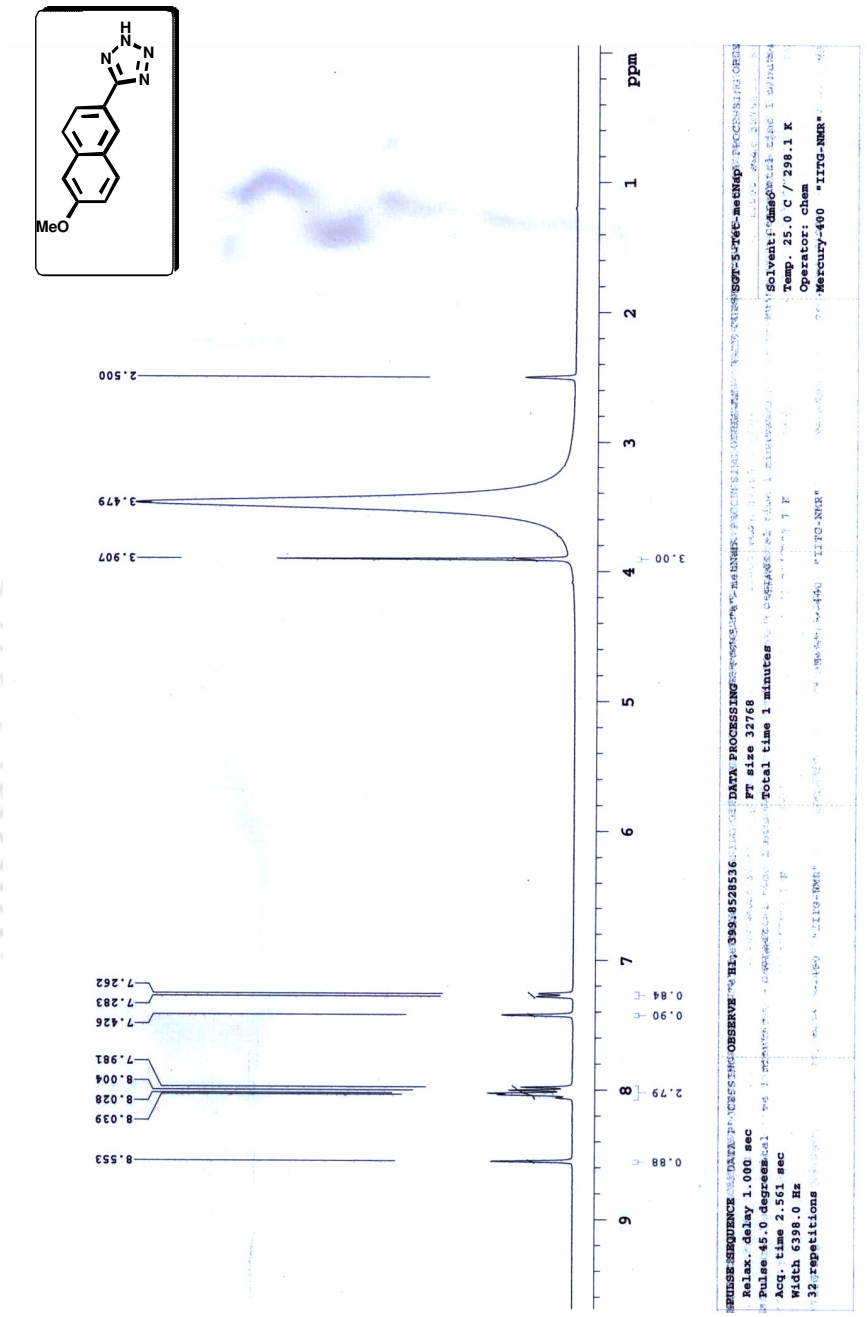

^{1}H spectra of compound **3.54E**

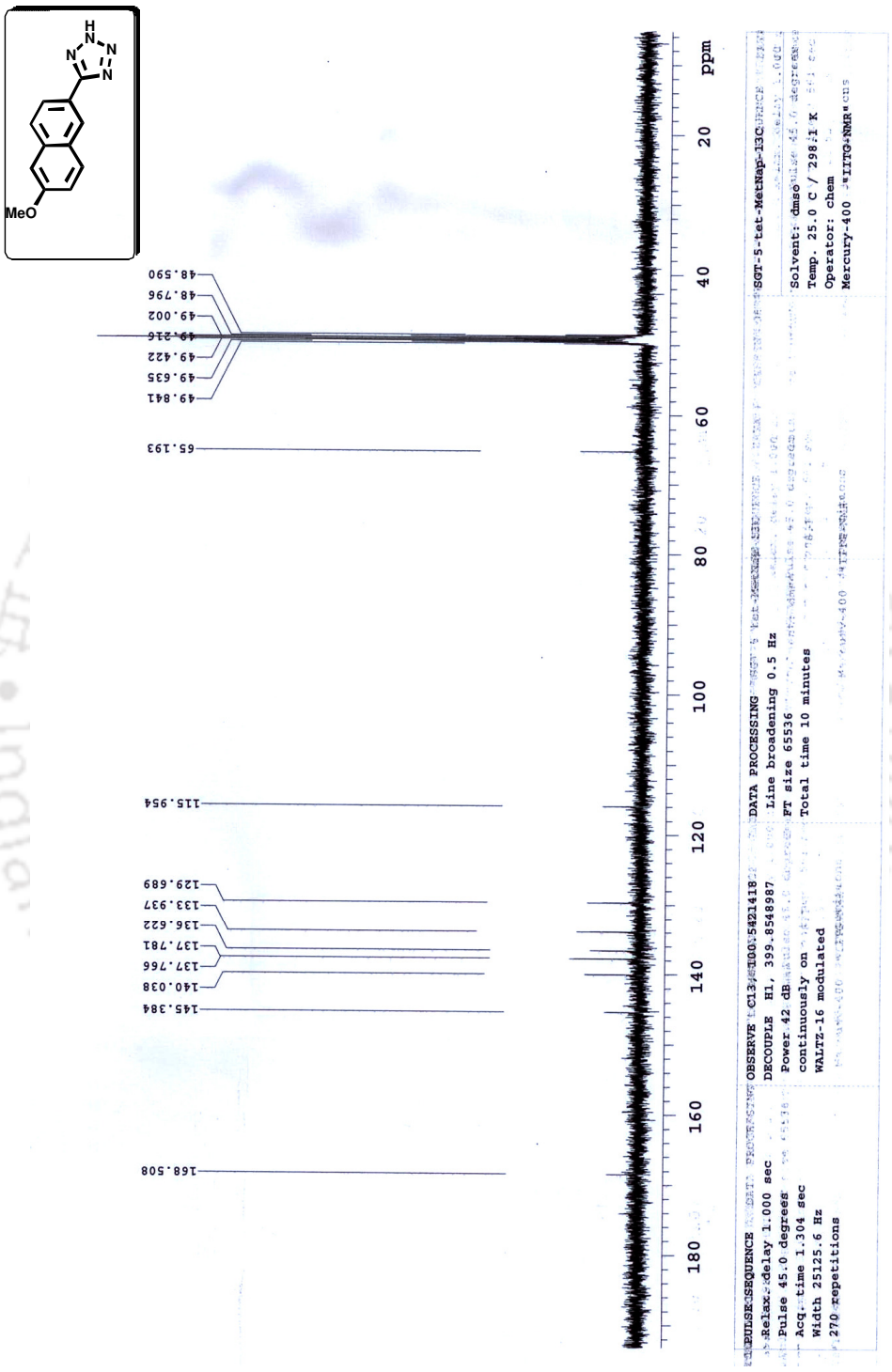

^{13}C spectra of compound **3.54E**

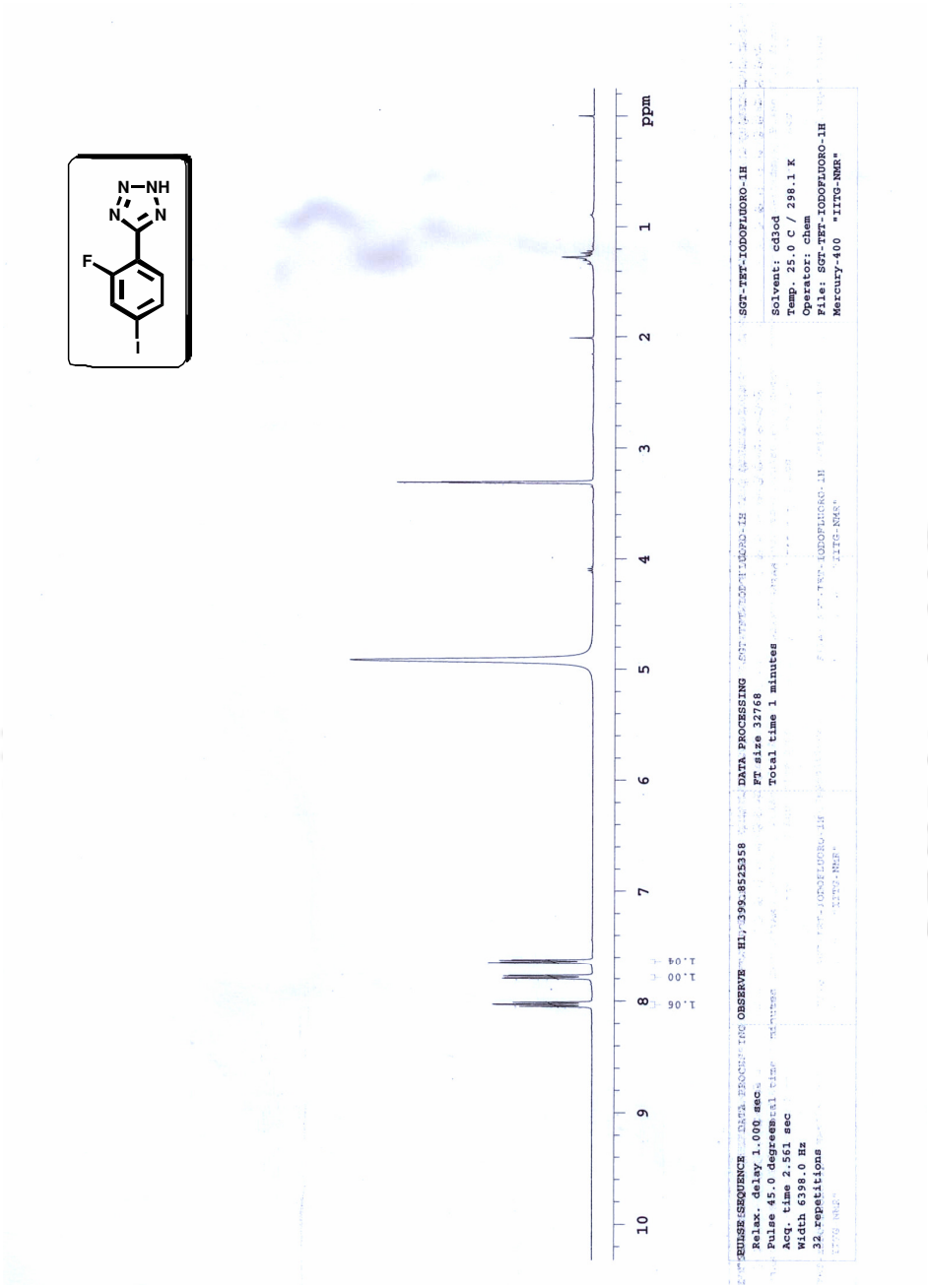

^{1}H spectra of compound **3.54K**

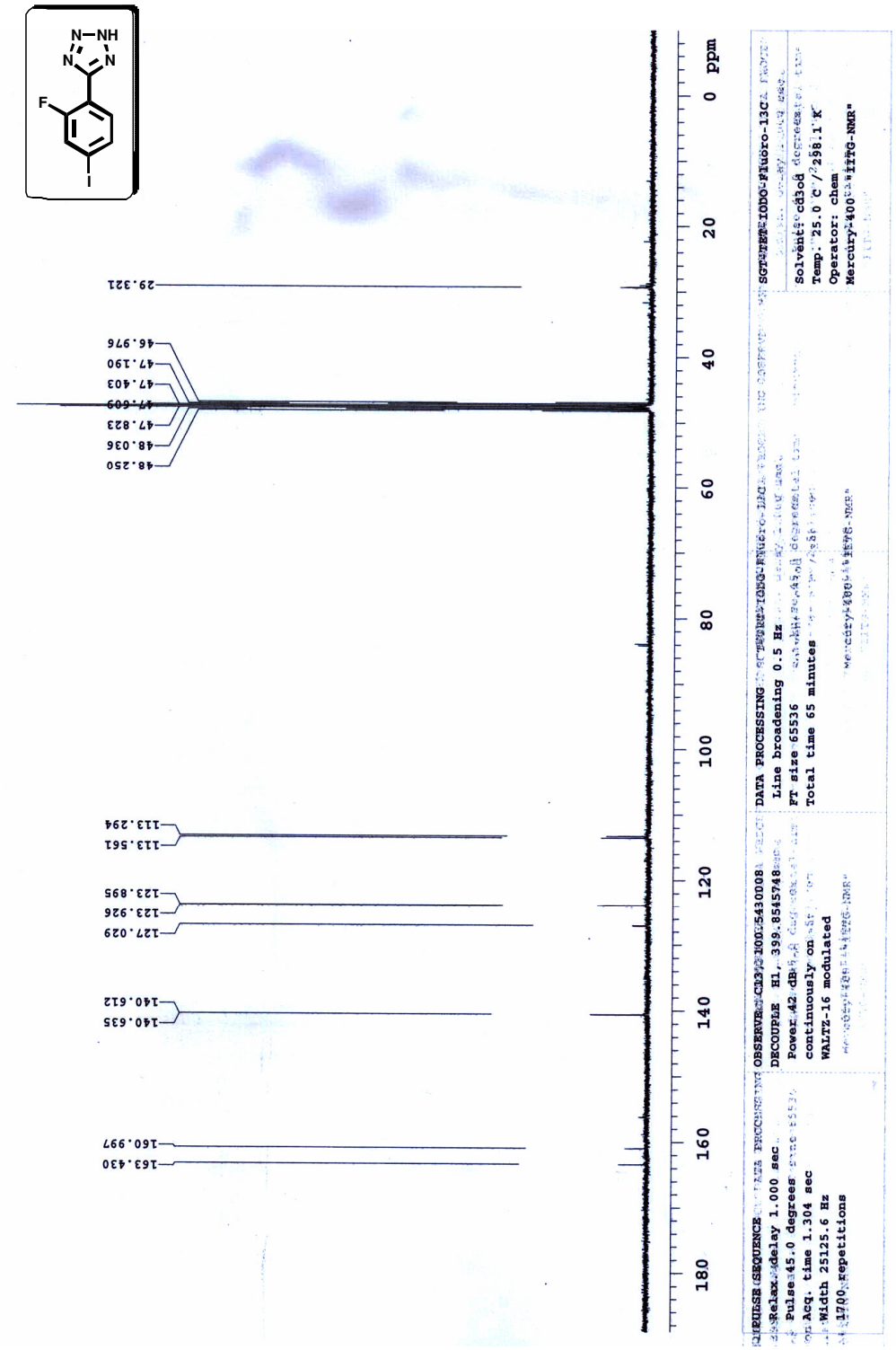

^{13}C Spectra of compound **3.54K**

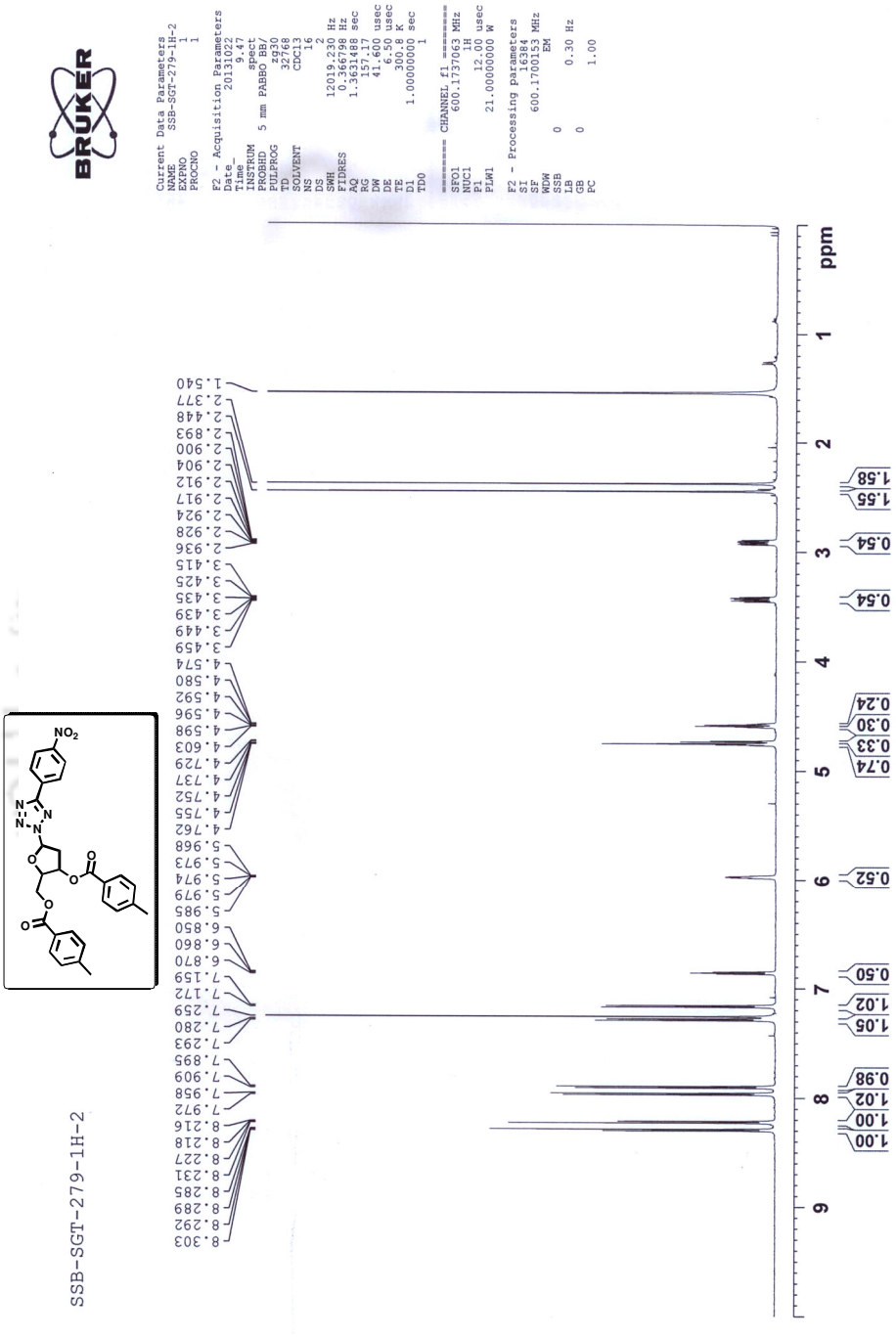

^{1}H spectra of compound **3.62a**

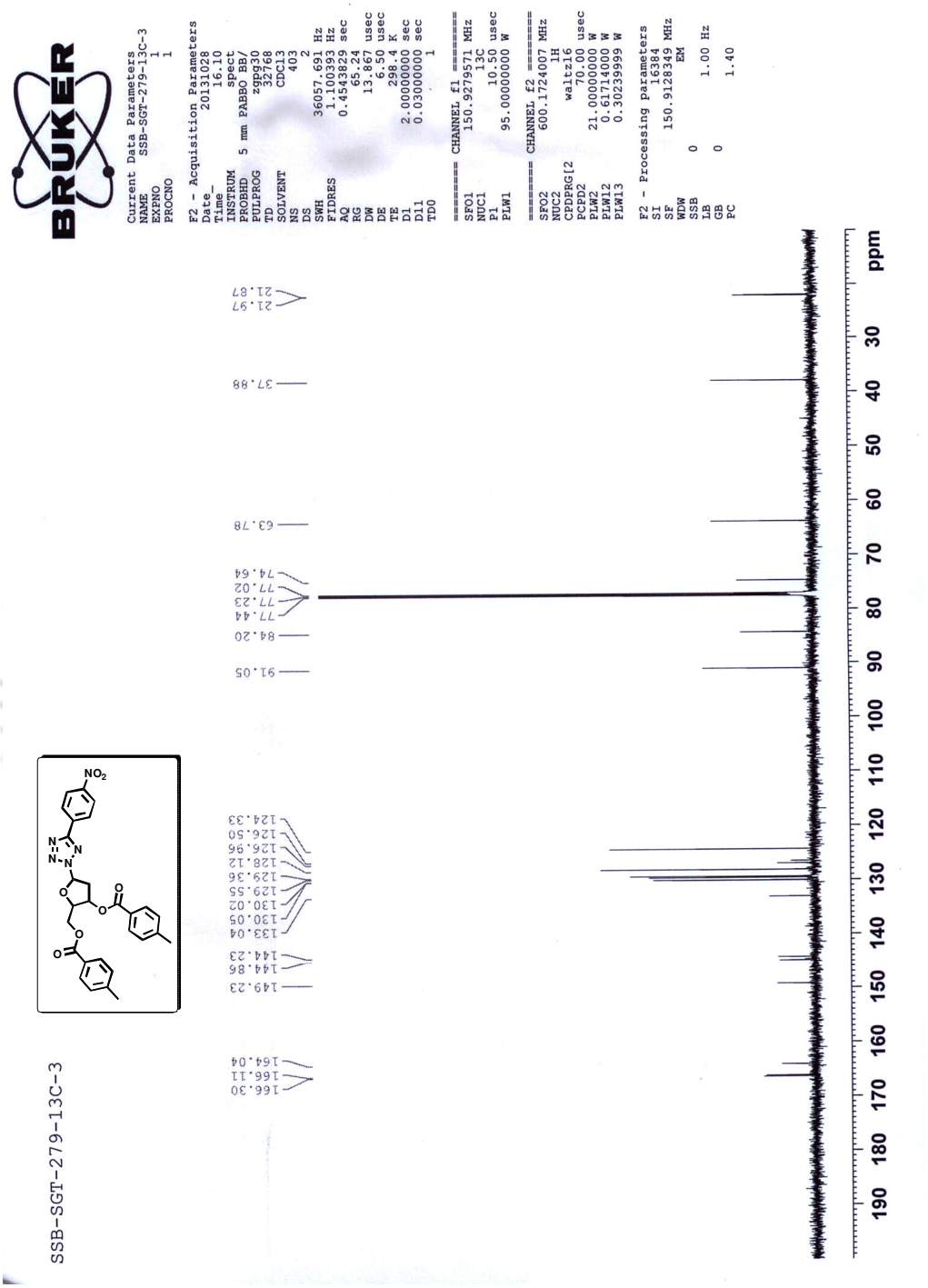

^{13}C spectra of compound **3.62a**

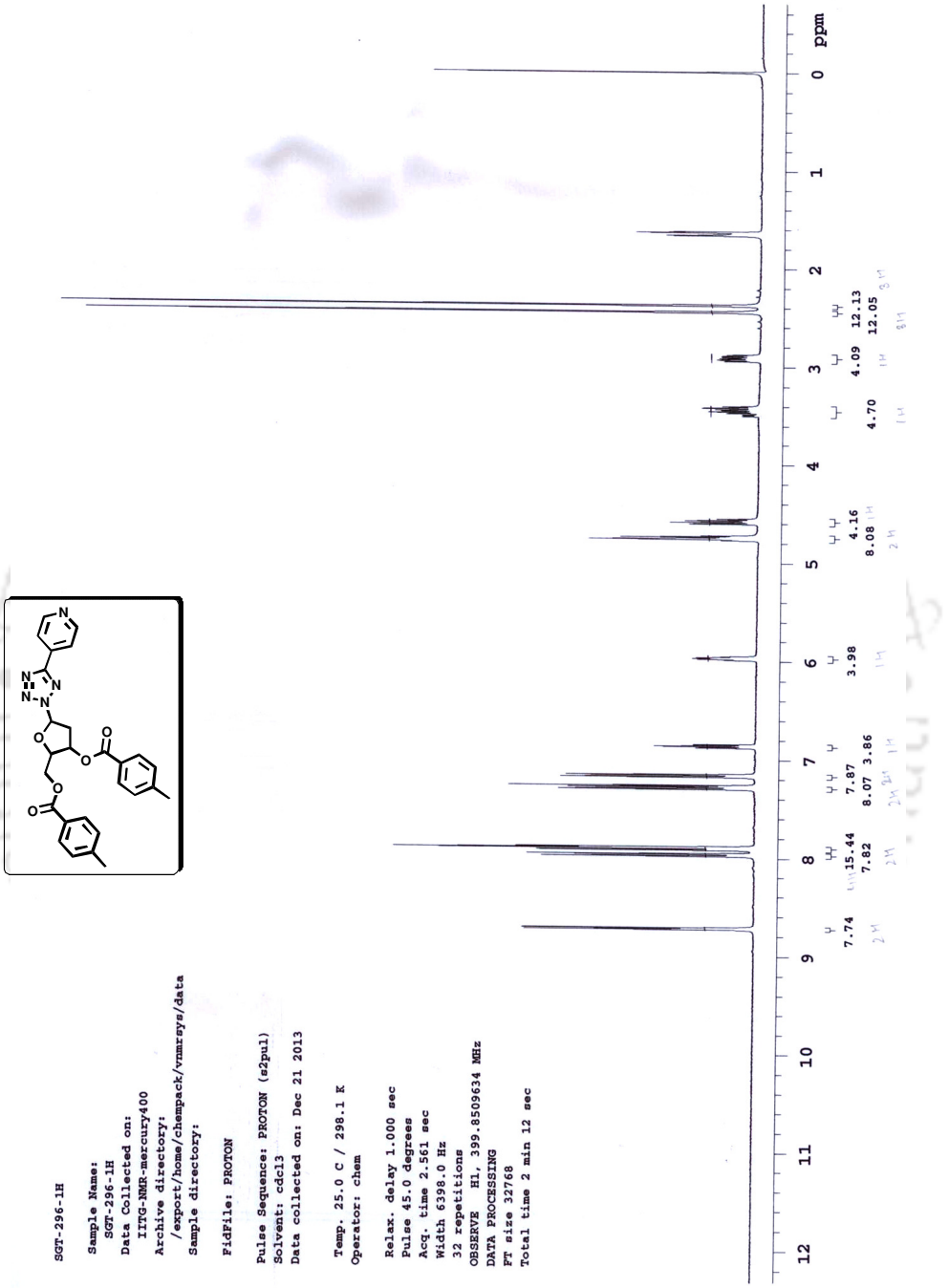

^{1}H spectra of compound **3.58a**

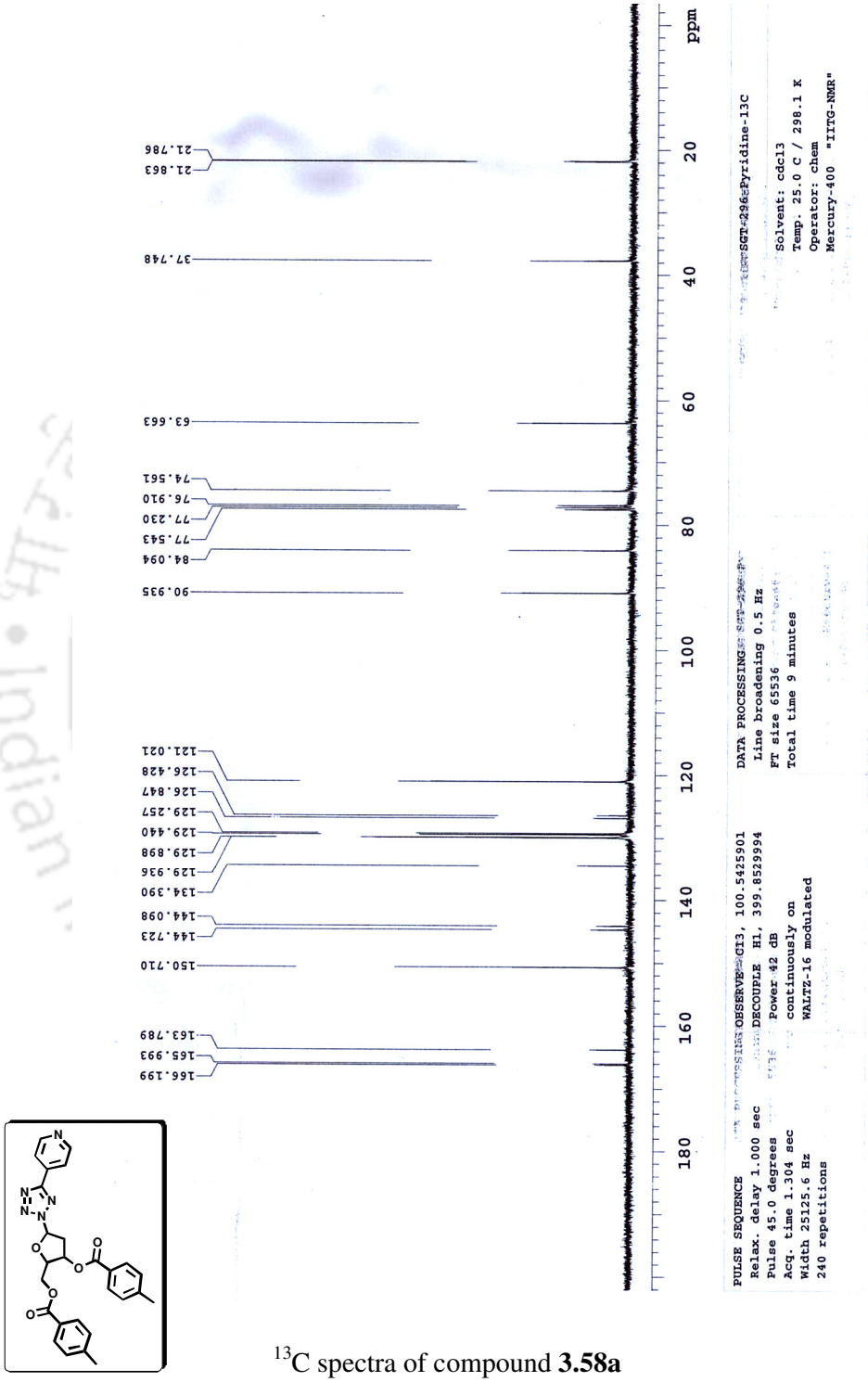

^{13}C spectra of compound **3.58a**

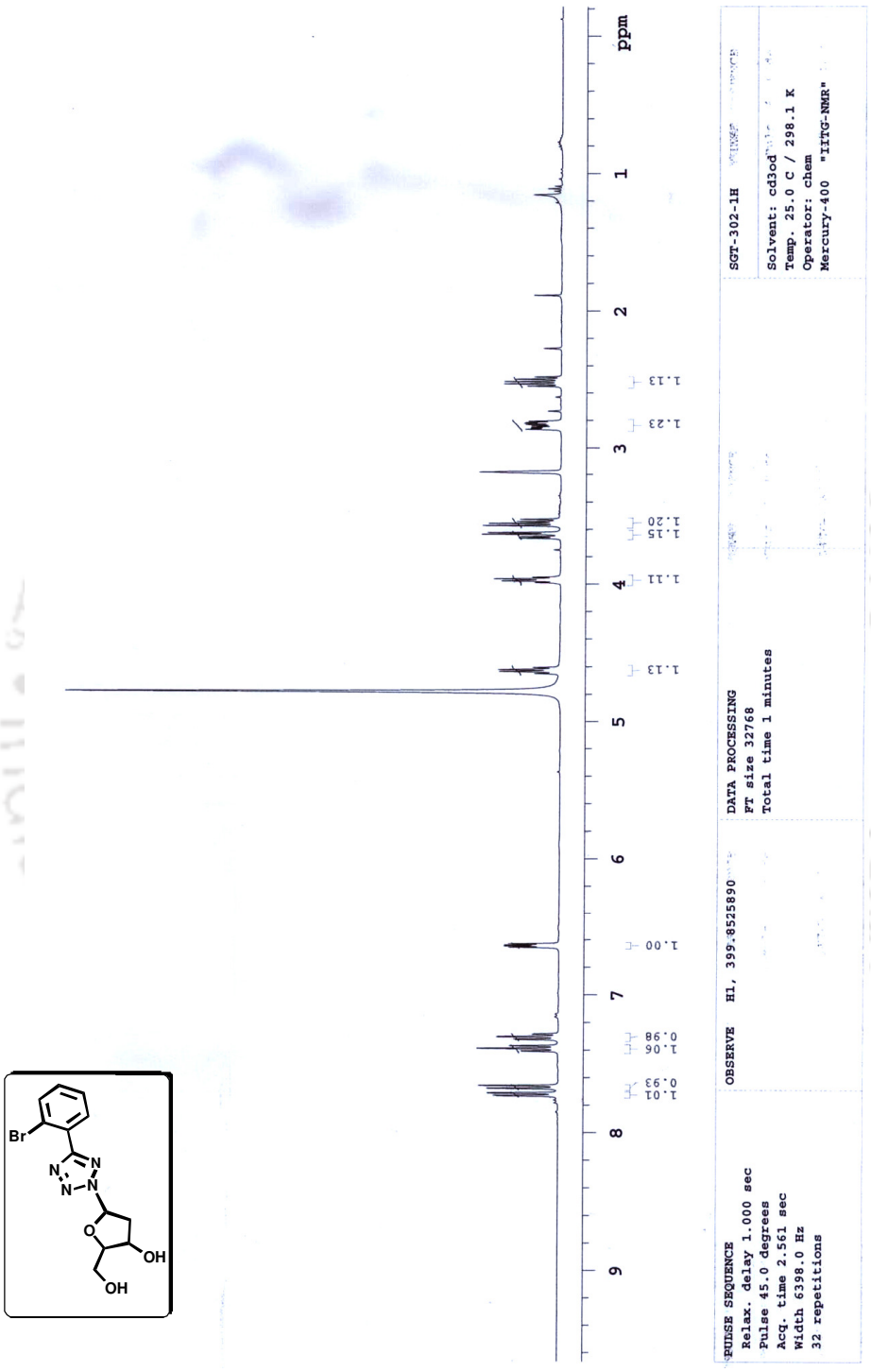

^{1}H spectra of compound **3.63b**

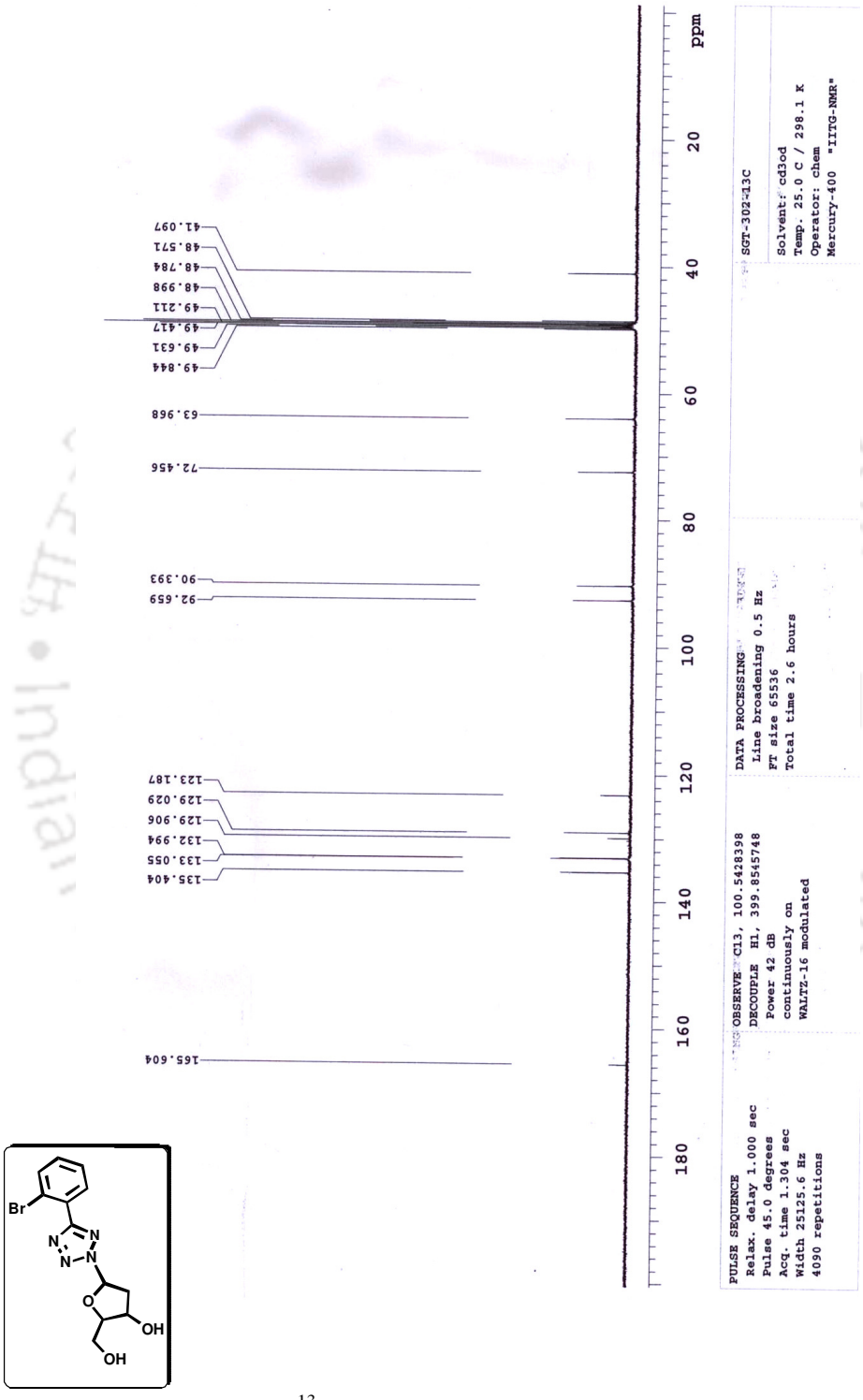

^{13}C spectra of compound **3.63b**

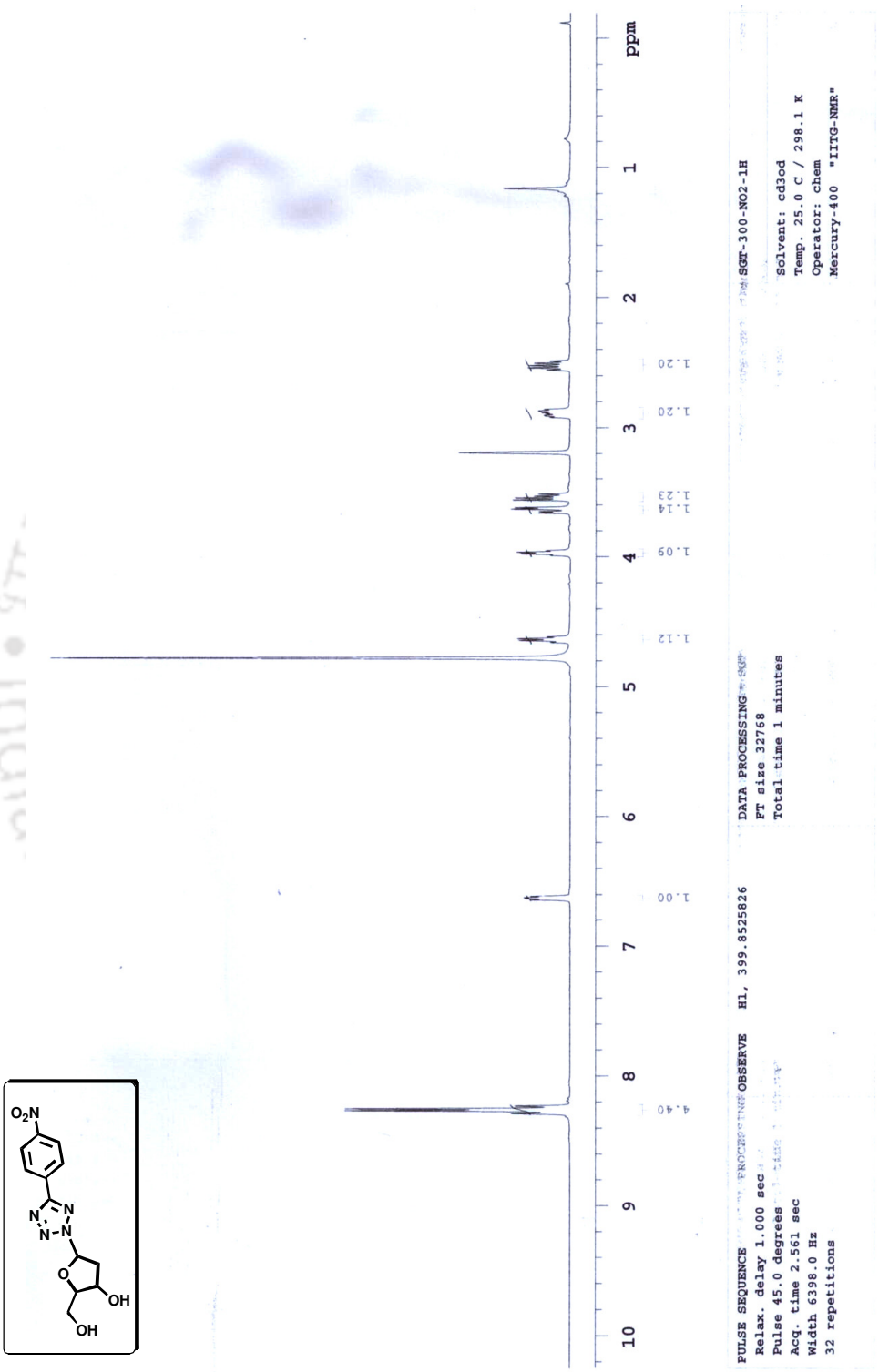

^{1}H spectra of compound **3.62b**

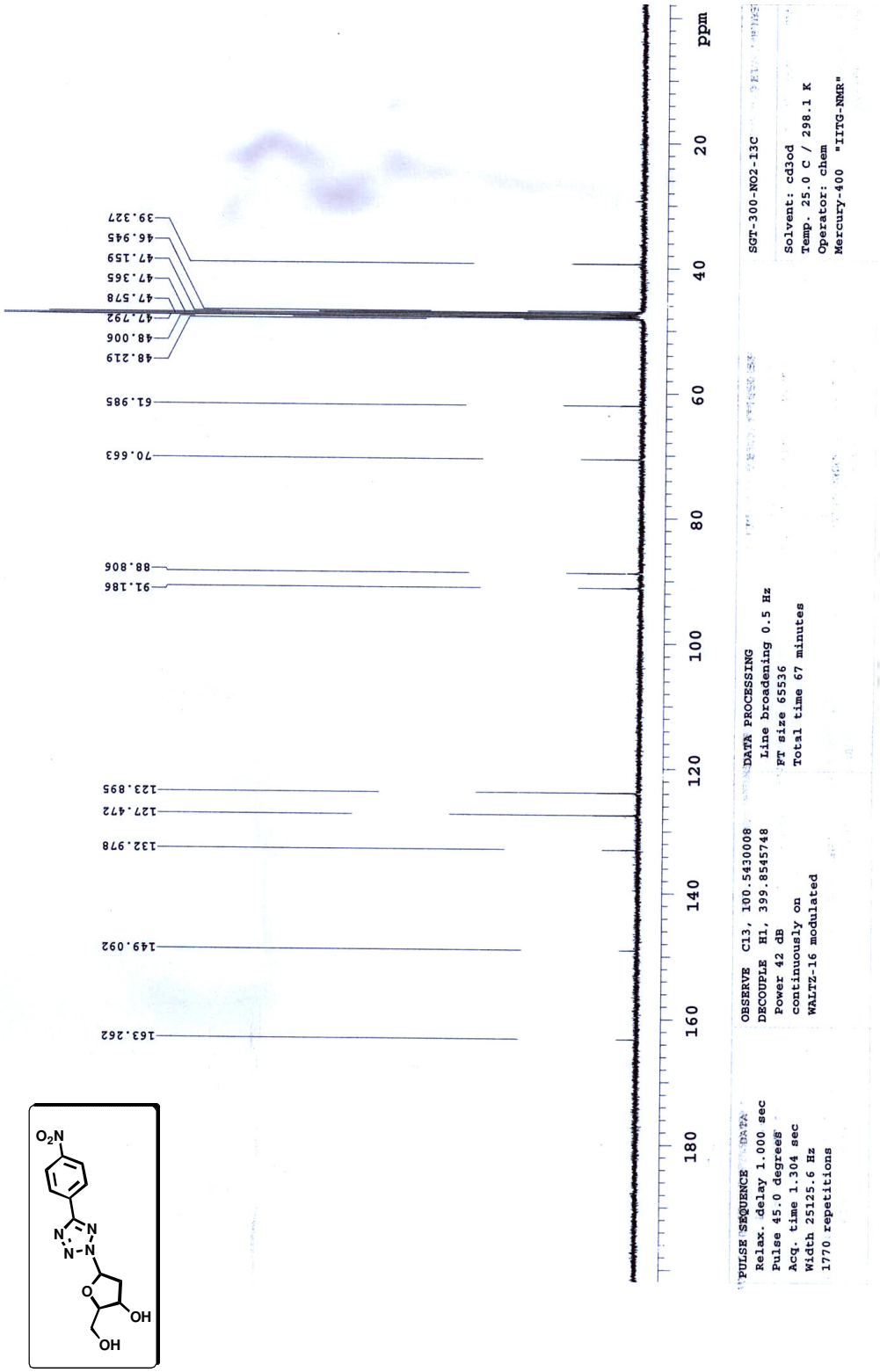

^{13}C spectra of compound **3.62b**

3.12. References

1. (a) Kool, E. T. *Annu. Rev. Biophys. Biomol. Struct.* **2001**, *30*, 1. (b) Kool, E. T. *Annu. Rev. Biochem.* **2002**, *71*, 191. (b) Schweitzer, B. A.; Kool, E. T. *J. Org. Chem.* **1994**, *59*, 7238. (c) Schweitzer, B. A.; Kool, E. T. *J. Am. Chem. Soc.* **1995**, *117*, 737. (d) Moran, S.; Ren, R. X. F.; Rumney, S. I. V.; Kool, E. T. *J. Am. Chem. Soc.* **1997**, *119*, 2056. (e) Moran, S.; Ren, R. X. F.; Kool, E. T. *Proc. Natl. Acad. Sci. U.S.A.* **1997**, *94*, 10506. (f) Morales, J. C.; Kool, E. T. *Nat. Struct. Biol.* **1998**, *5*, 950. (g) Morales, J. C.; Kool, E. T. *J. Am. Chem. Soc.* **1999**, *121*, 2323. (h) Ogawa, A. K.; Wu, Y.; Berger, M.; Schultz, P. G.; Romesberg, F. E. *J. Am. Chem. Soc.* **2000**, *122*, 8803. (i) Matsuda, S.; Romesberg, F. E. *J. Am. Chem. Soc.* **2004**, *126*, 14419. (j) Matsuda, S.; Henry, A. A.; Romesberg, F. E. *J. Am. Chem. Soc.* **2006**, *128*, 6369. (k) Henry, A. A.; Olsen, A. G.; Matsuda, S.; Yu, C.; Geierstanger, B. H.; Romseberg, F. E. *J. Am. Chem. Soc.* **2004**, *126*, 6923.

2. (a) Ren, R. X.-F.; Chaudhuri, N. C.; Paris, P. L.; Rumney IV, S.; Kool, E. T. *J. Am. Chem. Soc.* **1996**, *118*, 7671. (b) Guckian, K. M.; Schweitzer, B. A.; Rex X.-F. R.; Sheils, R. C. J.; Paris, P. L. ; Tahmassebi, D. C.; Kool E.T. *J. Am. Chem. Soc.* **1996,** *118,* 8182. (c) Brotschi, C.; Häberli, A.; Leumann, C. J. *Angew. Chem., Int., Ed.* **2001**, *40*, 3012; (d) Brotschi, C.; Leumann, C. J. *Angew. Chem., Int., Ed.* **2003**, 42, 1655. (e) Kaufmann, M.; Gisler, M.; Leumann, C. J. *Angew. Chem., Int. Ed.* **2009**, *48*, 3810. (f) Matsuda, S.; Henry, A. A.; Schultz, P. G.; Romesberg, F. E. *J. Am.Chem. Soc.* **2003**, *125*, 6134.(g) Hwang, G. T.; Romesberg, F. E. *Nucleic Acids Res.* **2006**, *34*, 2037.(h) Berger, M.; Luzzi, S. D.; Henry, A. A.; Romesberg, F. E. *J. Am.Chem. Soc.* **2002**, *124*, 1222. (i) Matsuda, S.; Leconte, A. M.; Romesberg, F. E. *J. Am. Chem. Soc.* **2007**, *129*, 5551.

3. (a) You, Y.; Tataurov, A. V.; Owczarzy, R. *Biopolymers* **2011**, *95*, 472. (b) Moreira, B. G.; You, Y.; Behlke, M. A.; Owczarzy, R. *Biochem. Biophys. Res. Commun.* **2005**, *327*, 473. (c) Zahn, A.; Leumann, C. J. *Chem. Eur. J.* **2008**, *14*, 1087. (d) Grigorenko, N. A.; Leumann, C. J. *Chem. Eur. J.* **2009**, *15*, 639. (e) Grigorenko, N. A.; Leumann, C. J. *Chem. Commun.* **2008**, 5417.

(f) Roethlisberger, P.; Wojciechowski, F.; Leumann, C. J. *Chem. Eur. J.* **2013**, *19*, 11518. (g) Ikkanda, B. A.; Samuel, S.A.; Iverson, B. L. *J. Org. Chem.* **2014**, *79*, 2029.

4. Bag, S. S.; Talukdar, S.; Matsumoto, K.; Kundu, R. *J. Org. Chem.* **2013**, *78*, 278.

5. (a) Yoo, S.-E.; Lee, Se.-H.; Kim, S.-K.; Lee, Su.-H. *Bioorg. Med. Chem.* **1997**, *5*, 445. (b) Shih, T. L.; Candelore, M. R.; Cascieri, M. A.; Chiu, S.-H. L.; Colwell, Jr. L. F.; Deng, L.; Feeney, W. P.; Forrest, M. J.; Hom, G. J.; MacIntyre, D. E.; Miller, R. R.; Stearns, R. A.; Strader, C. D.; Tota, L.; Wyvratt, M. J.; Fisher, M. H.; Weber, A. E. *Bioorg. Med. Chem. Lett*. **1999**, *9*, 1251. (c) Chung, J. Y. L.; Ho, G.-J.; Chartrain, M.; Roberge, C.; Zhao, D.; Leazer, J.; Farr, R.; Robbins, M.; Emerson, K.; Mathre, D. J.; McNamara, J. M.; Hughes, D. L.; Grabowski, E. J. J.; Reider, P. J. *Tetrahedron Lett*. **1999**, *40*, 6739.

6. (a) Wagner, R.; Mollison, K. W.; Liu, L.; Henry, C. L.; Rosenberg, T. A.; Bamaung, N.; Tu, N.; Wiedeman, P. E.; Or, Y.; Luly, J. R.; Lane, B. C.; Trevillyan, J.; Chen, Y.-W.; Fey, T.; Hsieh, G.; Marsh, K.; Nuss, M.; Jacobson, P. B.; Wilcox, D.; Carlson, R. P.; Carter, G. W.; Djuric, S. W. *Bioorg. Med. Chem. Lett*. **2005**, *15*, 5340.(b) Naidu, B. N.; Sorenson, M. E.; Bronson, J. J.; Pucci, M. J.; Clark, J. M.; Ueda, Y. *Bioorg. Med. Chem. Lett*. **2005**, *15*, 2069. (c) Diwakar, S. D.; Bhagwat, S. S.; Shingare, M. S.; Gill, C. H. *Bioorg. Med. Chem. Lett.* **2008**, *18*, 4678.

7. (a) Upadhayaya, R. S.; Jain, S.; Sinha, N.; Kishore, N.; Chandra, R.; Arora, S. K. *Eur. J. Med. Chem*. **2004**, *39*, 579. (b) Upadhayaya, R. S.; Jain, S.; Sinha, N.; Kishore, N.; Chandra, R.; Arora, S. K. *Bioorg. Med. Chem*. **2004**, *12*, 2225.(c) Kumar, Ch. N. S. S. P.; Parida, D. K.; Santhoshi, A.; Kota, A. K.; Sridhar, B.; Rao, V. J. *Med. Chem. Commun*. **2011**, *2*, 486.

8. (a) Chang, C.-S.; Lin, Y.-T.; Shih, S.-R.; Lee, C.-C.; Lee, Y.-C.; Tai, C.-L.; Tseng, S.-N.; Chern, J.-H. *J. Med. Chem*. **2005**, *48*, 3522. (b) Zarubaev, V. V.; Golod, E. L.; Anfimov, P. M.; Shtro, A. A.; Saraev, V. V.; Gavrilov, A. S.; Logvinov, A. V.; Kiselev, O. I. *Bioorg. Med. Chem. Lett.* **2010**, *18*, 839.

(c) Abell, A. D.; Foulds, G. J. *J. Chem. Soc., Perkin Trans. 1* **1997**, 2475. (d). May, B. C. H.; Abell, A. D. *J. Chem. Soc., Perkin Trans. 1* **2002**, 172.

9. (a) Myznikov, L. V.; Hrabalek, A.; Koldobskii, G. I. *Chem. Het.Compounds.***2007**, *43*, 1. (b) Schocken, M. J.; Creekmore, R.W.; Theodoridis, G.; Nystrom, G. J.; Robinson, R. A. *Appl. Environ. Micobiol*. **1989**, *55*, 1220. (c) Mavromoustakos, T.; Kolocouris, A.; Zervou, M.; Roumelioti, P.; Matsoukas, J.;Weisemann, R. *J. Med. Chem.* **1999**, *42*, 1714. (d) Mekni, N.; Bakloiti, A.. Synthesis of new 1-substituted 4-perfluoroalkyl tetrazol-5-ones. *J. Fluorine Chem.* **2008**, **129**, 1073. (e) Toney, J. H.; Fitzgerald, P. M.D.; Grover-Sharma, N.; Olson, S. H.; May, W. J.;Sundelof, J. G.; Venderwall, D. E.; Cleary, K. A.; Grant, S. K.; Wu, J. K.; Kozarich, J. W.; Pompliano, D. L.; Hammond, G. G. *Chem. Biol*. **1998**, *5*, 185. (f) Tamura, Y.; Watanabe, F.; Nakatani, T.; Yasui, K.; Fuji, M.; Komurasaki, T.; Tsuzuki, H.; Maekawa, R.; Yoshioka, T.; Kawada, K.; Sugita, K.; Ohtani, M. *J. Med. Chem*. **1998**, *41*, 640. (g) Katritzky, A. R.; Jain, R.; Petrukhin, R.; Denisenko, S.; Schelenz, T. *SAR QSAR Environ. Res.* **2001**, *12*, 259. (h) Howard, N.; Abell, C.; Blakemore, W.; Chessari, G.; Congreve, M.; Howard, S.; Jhoti, H.; Murray, C. W.; Seavees, L. C. A.; van Montfort, R. L. M. *J. Med. Chem*. **2006**, *49*, 1346.

10. Alterman, M.; Hallberg, A. *J. Org. Chem.* **2000**, *65,* 7984.

11. Himo, F.; Demko, Z. P.; Noodleman, L.; Sharpless, K. B. *J. Am. Chem. Soc.* **2003**, *125*, 9983.

12. Amantini, D.; Beleggia, R; Fringuelli, F; Pizzo, F; Vaccaro, L. *J. Org. Chem.* **2004**, *69*, 2896.

13. Demko, Z. P.; Sharpless, K. B. *Angew. Chem., Int., Ed.* **2002**, *41*, 2110.

14. Bosch, L.; Vilarassa, J. *Angew. Chem. Int. Ed.* **2007**, *46*, 3926.

15. (a) For a review of amide bond surrogates, see: Spatola, **A.** F. In *Chemistry and Biochemistry of Amino Acids, Peptides and Proteins;* Weinstein,B., Ed.; Dekker: New York, **1983**, *7*, 267. (b) Andersen, B. B.; Lenz, S. M.; Skjarbak, N.; Søby, K. K.; Hansen, H. O.; Ebert, B.; Bøgsø, K. P.; Krogsgaard-Larsen, P. *J. Med. Chem.* **1997**, *40*, 2831. (c) Brauner-Osborne, H.; Egenbjerg, J.;

Nielsen, E. Ø.; Mads-en, U.; Krogsgaard-Larsen, P. *J. Med. Chem*. **2000**, *43*, 2609. (d) Costantino, G.; Maltoni, K.; Marinozzi, M.; Camaioni, E.; Prezeau, L.; Pin, J.-P.; Pellicciari, R. *Bioorg. Med. Chem*. **2001**, *9*, 221. (e) Hallinan, E. A.; Tsymbalov, S.; Dorn, C. R.; Pitzele, B. S.; Hansen, Jr., D. W. *J. Med. Chem.* **2002**, *45*, 1686. (f) Liljebris, C.; Larsen, S. D.; Ogg, D.; Palazuk, B. J.; Bleas-dale, J. E. *J. Med. Chem*. 2002, *45*, 1785. (g) Demko, Z. P.; Sharpless, K. B. *Org. Lett*. **2002**, *4*, 2525. (h) Zhang, J. Y.; Wang, Y.; Milton, M. N.; Kraus, L.; Breau, A. P.; Paulson, S. K. *J. Pharm. Sci*. **2004**, *93*, 1229. (i) Vogensen, S. B.; Clausen, R. P.; Greenwood, J. R.; Johansen, T. N.; Pickering, D. S.; Nielsen, B.; Ebert, B.; Krogs-gaard-Larsen, P. *J. Med. Chem*. **2005**, *48*, 3438.

16. (a) Hann, M. M.; Sammes, P. *G.;* Kennewell, P. D.; Taylor, J. B. *J. Chem. Soc., Chem. Commun.* **1980**, 234. (b) Hann, M. M.; Sammes, P. *G.;* Kennewell, P. D.; Taylor, J. B. *J. Chem. Soc., Perkin Trans. 1* **1982**, 307. (c) Cox, M. T.; Gormley, J. J.; Hayward, C. F.; Petter, N. N. *J. Chem. Soc., Chem. Commun.* **1980**, 800. (d) Johnson, R. L. J. *Med. Chem.* **1984**, 27, 1351.

17. Zabrocki, J.; Smith, G. D.; Dunbar, J. B., Jr.; Iijima, H.; Marshall, G. R. ***J.*** *Am. Chem. Soc.* **1988,** *110***,** 5875.

18. Yu, K-L.; Johnson, R. L. *J. Org. Chem.* **1987**, *52*, 2051.

19. Zabrocki, J.; Dunbar, J. B., Jr.; Marshall, K. W.; Toth, M. V.; Marshall, G. R. *J. Org. Chem.* **1992**, *57*, 202.

20. May, B. C. H.; Abell, A. D. *Tetrahedron Lett.* **2001**, *42*, 5641.

21. (a) Witkowski, J. T.; Robins, R. K.; Sidwell, R. W.; Simon, L. N.; *J. Med. Chem.* **1972**, *15*, 1150. (b) Damall, R. K.; Townsend, L. B.; Robins, R. K. *Proc. Natl. Acad. Sci. U.S.A.* **1967**, *57*, 548. (c) Nishimura, H.; Mayama, M.; Komatsu, Y.; Kato, H.; Shimaoka, N.; Tanaka, Y. *J. Antibiot., Ser. A* **1964**, *17*, 148. (d) Rabinovitz, M.; Uehara, Y.; Vistica, D. T. *Science* **1979**, *206*, 1085. (e) Barett, A. G. M.; Broughton, H. B. *J. Org. Chem.* **1986**, *51*, 495. (f) Shaban, M. A. E.; Nasr, A. Z. *Advances in Heterocyclic Chemistry*, **1998**, *70*, 230. (g) DeLong, D. C.; Baker, L. A. ; Gerzon, K.; Gutowski, G. E.; Williams, R. H.; Hamill, R. L. *Adu. Antimicrob. Antineoplast. Chemother.,*

Proc. Int. Congr. Chemother. 7th, **1970**, *1*, A-5/35(1971). (h) Sweeney, M. J.; Davis, F. A.; Gutowski, G. E.; Marnili, R. L.; Hoffman, D. H.; Poore, G. A. *Cancer Research* **1973**, *33*, 2619.

22. Poonian, M. S.; Nowoswiat, E. F.; Blount, J. F.; Williams, T. H.; Pitcher, R. G.; Kramer, M. J. *J. Med. Chem,* **1976***, 19,* 286.

23. Popsavin, M.; Torovic, L.; Spaic´, S.; Stankov, S.; Kapor, A; Tomic´, Z.; Popsavin, V. *Tetrahedron* **2002**, *58*, 569.

24. Filichev, V. V.; Jasko, M. V.; Malin, A. A.; Zubareva V. Y. ; Ostrovskii, V. A. *Tetrahedron Lett.* **2002**, *43*, 1901.

25. Filichev, V. V.; Malin, A. A.; Ostrovskii, V. A.; Pedersen, E. B. *Helv. Chim. Acta*, **2002**, *85*, 2847.

26. Bosch, L.; Delelis, O.; Subra, Deprez, F. E.; Witvrow, M.; Vilarrasa, J. *Tetrahedron Lett.* **2012**, *53*, 514.

27. Müller, J.; Böhme, D.; Lax, P.; Cerdá, M. M.; Roitzsch, M. *Chem. Eur. J.* **2005**, *11*, 6246.

28. Pedrosa, M. T. C.; Alves, R. B.; Prado, M. A. F.; Filho, J. D. S.; Alves, R. J.; Accorso, N. B. *J. Carbohydr. Chem*. **2003**, *22*, 433.

29. Aldhoun, M.; Massi,A.; Dondoni, A. *J. Org. Chem.* **2008**, *73*, 9565.

30. (a) Seitz, O. *ChemBioChem* **2000**, *1*, 214. (b) Arsequell, G.; Valencia, G. *Tetrahedron: Asymmetry* **1997**, *8*, 2839. (c) Taylor, C. M. *Tetrahedron* **1998**, *54*, 11317. (d) Herzner, H.; Reipen, T.; Schultz, M.; Kunz, H. *Chem. Re*V. **2000**, *100*, 4495. (e) Davis, B. G. *Chem. Re*V. **2002**, *102*, 579.

31. (a) McNabb, S. B.; Ueda, M.; Naito, T.*Org. Lett.* **2004**, *6*, 1911. (b) Kuijpers, B. H. M.; Groothuys, S.; Keereweer, A. R.; Quaedflierg, P. J. L. M.; Blaaauw, R. H.; van Delft, F. L.; Rutjes, F. P. J. T. *Org. Lett.* **2004**, *6*, 3123. (c) Czifra´k, K.; Szila´gyi, P.; Somsa´k, L. *Tetrahedron: Asymmetry* **2005**, *16*, 127. (d) Chambers, D. J.; Evans, J. R.; Fairbanks, A. J. *Tetrahedron: Asymmetry* **2005**, *16*, 45. (e) Nishikawa, T.; Koide, Y.; Kanakubo, A.; Yoshimura, H.; Isobe, M. *Org. Biomol. Chem.* **2006**, *4*, 1268. (f) Gustafsson, T.; Hedenstro¨m, M.; Kihlberg, J. *J.Org. Chem.* **2006**, *71*, 1911.

32. (a) Marcaurelle, L. A.; Bertozzi, C. R. *Chem.sEur. J.* **1999**, *5*, 1384. (b) Pachamuthu, K.; Schmidt, R. R. *Chem. Re*V. **2006**, *106*, 160.

33. B. G. Davis, R. J. Nash, A. A. Watson, C. Smith, G. W. J. Fleet, *Tetrahedron* **1999**, *55*, 4501.

34. Bag, S. S.; Kundu, R. *J. Org. Chem.* **2011**, *76*, 3348.

35. Shigeru Amemiya, Philippe B¨uhlmann and Yoshio Umezawa *Chem. Commun*. **1997**, 1027.

Chapter 4

STUDIES ON THE STABILIZATION OF A DNA DUPLEX DECORATED WITH UNNATURAL TRIAZOLYL DONOR/ACCEPTOR NUCLEOSIDES: ROLE OF π-STACKING AND CHARGE TRANSFER INTERACTIONS

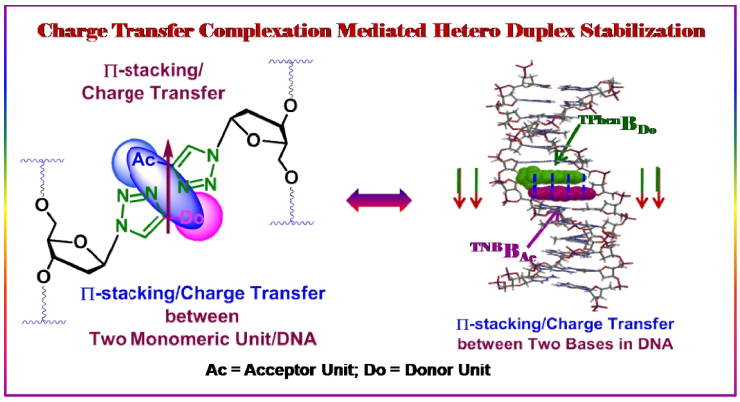

4.1. Introduction

The DNA double helix is stabilized by two major forces: the hydrogen bonding interactions and the aromatic π-π stacking interactions between the DNA bases.[1] In addition to these solvation forces also play their role in stabilizing a DNA duplex. Hydrogen bonds contribute 2-3 kcal/mol. Stacking interactions contribute about 4-15 kcal/mol per base pair. Although weak in nature, H-bonding plays a major role in stabilizing the DNA double helix due to large number of hydrogen bonds present in DNA.

Besides these, other forces of stabilization includes van der Waals interaction force, electrostatic interaction among the nucleobase pairs. The van der Waals interaction is important in DNA because the DNA bases are polarizable and the flat aromatic surfaces of the DNA bases allow close contact between them ultimately leading to a stabilization of the duplex DNA. The significant charge localization of all the four nucleobases or the attractive force between aromatic π-electrons and nuclei in σ-framework in suitably geometrical orientation makes electrostatic interaction force also to stabilize duplex DNA. Moreover, hydrophobic interaction plays an important role in stabilizing a DNA double helix by burying the bases in the interior of the helix.

4.2. Exploration of H-Bonding and Hydrophobic Interactions in DNA

In order to examine the importance of hydrogen bonding interactions, aromatic π-stacking interactions, and to generate DNA and RNA with enhanced functional abilities, the pioneering concept of orthogonal base pairing between the designed *iso-G* and *iso-C* has been proposed by led Alex Rich in 1962.[2] Later on, the Benner idea of the expansion of the genetic alphabet[3] attracted a great research interest, resulting in increasing amounts of research aimed at the development of new base pairs having hydrogen bonding patterns orthogonal to those in canonical Watson-Crick base pairs. Therefore, a number of base analogues with orthogonal H-bonding complementarities[4] in relation to the natural Watson-Crick H-bonding have been exploited to examine the importance of hydrogen bonding interactions in the stabilization of nucleic acids structure, in the study of interbiomolecular

interactions,[5a-b] and in the base recognition ability of enzymes.[5c-g] Several modified nucleosides with reporter functionalities have also been synthesized for monitoring the local microenvironmental change around the nucleic acids associated with interbiomolecular interactions.[6] Few important examples of H-bonded base pairs have already been discussed in **Chapter 1** and **Chapter 2**.

On the other hand, introduction of non-H-bonding unnatural DNA base analogues by Kool *et al.* has opened a new dimension in the design of more potent non-H-bonding unnatural nucleobases to explore the importance of aromatic stacking, hydrophobic or CH-π interactions between the bases in stabilizing the duplex DNA.[7] Thus, they have explored the possible aromatic stacking, hydrophobic or CH-π interactions between the bases and shown that these attractive forces are good enough to stabilize a DNA duplex and are well recognized by DNA polymerases. As for example, Kool *et al.* have synthesized difluorotoluene isostere (**F**) as a nucleoside (d**F**) which is a perfect mimic of thymidine in both crystalline and solution state.[8] Although it lacks strong hydrogen bond donors or acceptors, it was selectively incorporated as a free nucleotide opposite adenine and the DNA produced was found to be replicated very efficiently by Klenow DNA polymerase enzyme. When incorporated into DNA and paired against adenosine of a target DNA, it maintained similar structure to that of **T:A** base pair. Similarly, deoxyribonucleoside derivative of 4-methylbenzimidazole which is a non-polar isostere of deoxyadenosine have been synthesized by Kool and co-workers.[9] When incorporated into DNA and its pairing selectivity was assessed it was found to have low affinity for all the four natural bases. However it had strong preference for pairing with non polar difluorotoluene nucleoside (**F**), an analogue of thymidine. Deoxyribonucleoside of 4-fluoro-6-methylbenzimidazole has also been synthesized as a non polar isostere of deoxyguanosine and its base pairing properties studied.[10] It was found to be a non-selective as well as destabilizing base when paired against any of the natural bases in a DNA duplex as compared to the natural **A:T** pair. However, when paired against difluorotoluene (d**F**) in a DNA duplex the stabilization of the base pair [d(4 fluoro-6-methyl benzimidazole) **:** d**F**], was found to be similar to that of a G-T wooble base-pair.

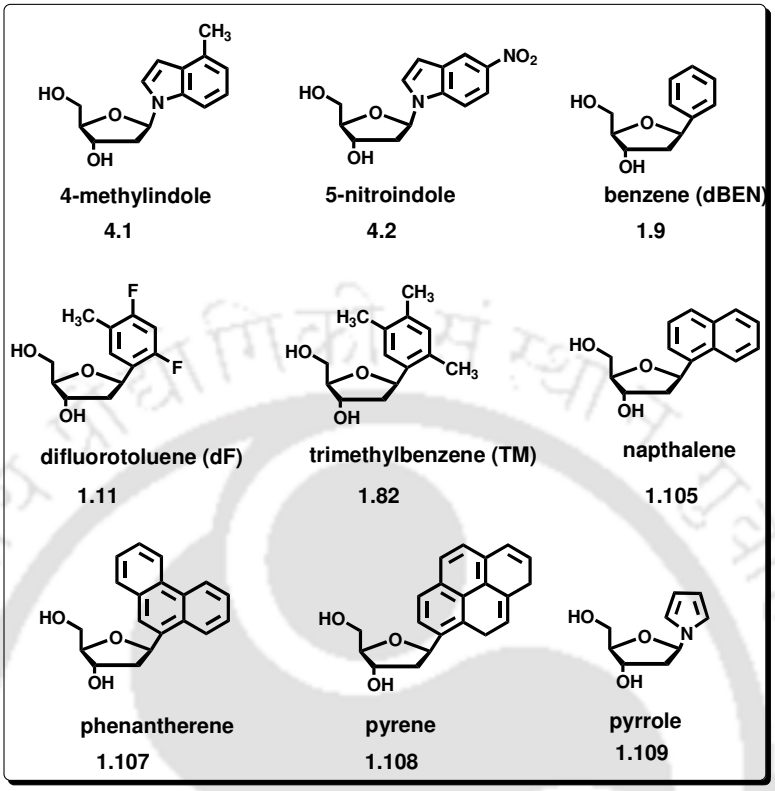

Figure 4.1: Structures at the dangling ends and the nucleosides studied with the dangling end experiments.

In order to study the aromatic stacking interactions separately from hydrogen bonding interactions, Kool *et al.*, have designed oligonucleotide by placing the natural and non-natural nucleotides at the ends of duplex (*i.e.* without a pairing partner)[11] and studied the aromatic stacking affinities in the context of duplex DNA. In this connection, simple polycyclic compounds such as benzene,[12] trimethylbenzene,[12] difluorotoluene,[13] 4-methylindole,[13] pyrrole,[14,15] naphthalene,[12] phenanthrene,[15] and pyrene[15] deoxynucleoside phosphoramidites were synthesized and introduced as bases in the nucleosides (**Figure 4.1**). The thermal denaturation experiments of the duplexes with dangling end thymine and adenine shows that the purine stacks more strongly on the duplex than the smaller pyrimidine base. The nonpolar DNA base isosteres stack considerably more strongly than their natural counterparts indicating that the surface area alone is not the determining factor of stacking ability.[12-15] The effect of size and hydrophobicity on stacking interactions were also investigated by placing a series of four nucleotides at the dangling ends. The results showed that the stacking

interactions became stronger with the increasing size of the base. However, a comparison between the molecules of same size revealed that the less polar molecules stack more strongly than the more polar ones. Moreover, it was observed that the stacking interactions increased with the increase in surface area of nonpolar bases of different sizes.

The base replacements by polyaromatic hydrocarbons not only introduced the fluorescence property into DNA but also increased the thermal stability of modified duplexes when incorporated at the dangling ends and also in the middle of the DNA duplexes. As for example, 1-pyrenyl[16] and 2-pyrenyl[17] nucleoside could replace the entire adenine-thymine base pair without a large decrease in thermal stability. Duplexes containing interstrand pyrene residues were found to be more stable than the unmodified duplex sequences. Similarly, when bipyridine,[18] biphenyl[19] and phenantherene[20] were incorporated into the middle of the DNA duplexes, they recognized each other through interstrand stacking interactions resulting in gradual increase in duplex stability.

Thus, in a series of experiments with hydrophobic aromatic nucleobases Kool *et al.* and latter on by others have shown that attractive forces other than hydrogen bonding interaction such as aromatic π-π stacking, hydrophobic interactions are good enough to stabilize a DNA duplex. It was also established that not only the H-bonded base pairs but also the hydrophobic base pair and hence hydrophobic force could be recognized by DNA polymerase enzyme. This establishment inspired the next generation chemists for taking the challenge of developing more of such hydrophobic base pairs towards an effort of expanding the genetic alphabets as well as generating the DNA/RNA with more functional and application potential. Few examples of such types of bases have already been discussed in **Chapter 1** and **Chapter 2**.

4.3. Other Possible Forces of DNA Duplex Stabilization

Oligonucleotides labeled with fluorescent probes are of immense research interest and have been used in genomic assays such as SNP typing, gene quantitation, allelic discrimination, etc.[21] Fluorescence based assay system generally relies on the study of differential signal generated during the course of hybridization. In a dual labeled probe containing a fluorophore and a quencher often generates quenched fluorescence

signal either in single stranded form or upon hybridization due to static quenching (contact mediated quenching) or dynamic quenching often *via* Forster resonance energy transfer (FRET) processes. In order to study the quenching processes in such oligonucleotide probe the fluorophore and the quencher are generally attached to the two ends of the same oligonucleotide probe or to the ends of two different oligonucleotide probes of same or different length.[22] Such a fluorophore quencher pair can also be attached to the ends of molecular beacons. [23] Molecular beacons are the probes with a stem-loop structure in which the complementary bases are present in the 5′- and 3′- ends of the probe that brings the reporter and the quencher dyes closer.[23]

While utilizing such fluorescent DNA probes or designing the same for DNA analysis or investigating the structure, dynamics and inter-biomolecular interactions through the study of biophysical/photophysical properties (like FRET process, quenching of fluorescence etc.) of such DNA probe systems, it is in some reports found that other than H-bonding/hydrophobic/π-π stacking interaction forces, some new forces of interaction are considered in order to explain the origin of extra stabilization in such DNA duplexes. As for an example, the static quenching phenomena have been explored by various research groups in the context of DNA probe design.[22-23, 24-25]. Thus, it has been shown *via* studying the molecular beacons[23] and complementary linear probes[24c] that when the fluorescent dyes and quenchers come in close contact, a significant enhancement of duplex stabilization occurs. Thus, Tyagi and Marras *et al.* have investigated that the tested configurations of various duplex DNA with fluorophores and quenchers conjugated as 5′- and 3′-terminal on complementary ODNs showed increase in duplex stability by 2–10 °C when fluorophores and quenchers interacted strongly (**Figure 4.2**).[24c]

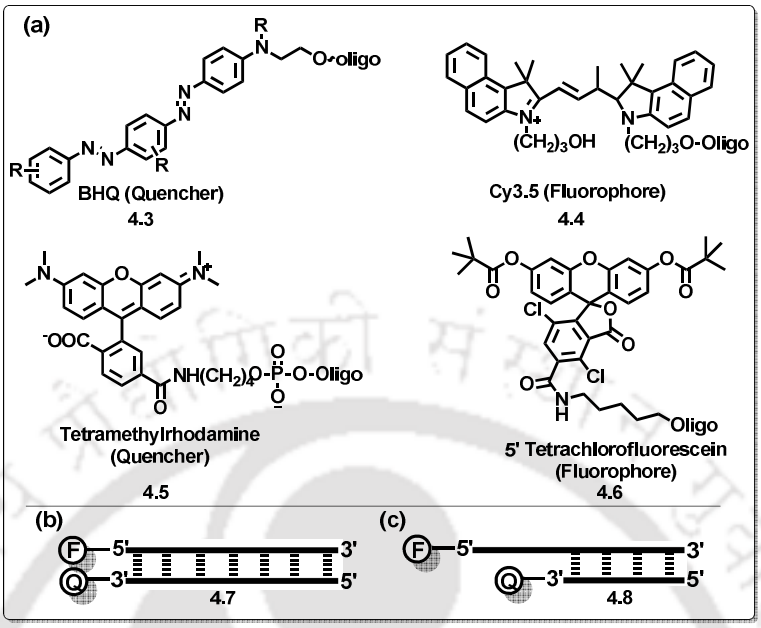

Figure 4.2: (a) Structures of some of fluorophores and quenchers, (c) schematic of blunt-ended hybrids that place the fluorophore (F) and quencher (Q) so close that contact quenching occurs, and the (d) schematic of staggered hybrids that place the fluorophore and quencher at a distance at which FRET is the predominant mode of quenching. These were used in their study by Tyagi and Marras *et al.*[24c]

The study of Morrison and Stols showed an enhancement of duplex stabilization when dye and quencher are directly adjacent on opposite strands and comes in potential physical contact.[25a] These results suggested that the adjacent dye/quencher pairs when have the potential to form complexes can offer significant additional duplex stability. In all of such examples signature of ground state complexation was evident from the UV-visible spectra. The designed DNA containing a donor in one strand and acceptor in the other strand has led to static quenching *via* ground state charge transfer complexation and stabilizing the duplex. The "strand-displacement probe" assays utilized the same ground state complexation phenomenon.[25b]

Johansson *et al.* have reported that properly chosen dye-quencher pairs in dual-labeled oligonucleotides can have a strong enough affinity for each other to form a ground state complex (Figure 4.3).[25d] Their experiment was well documented by UV-visible spectral changes and fluorescence lifetime measurements of a series of singly labeled and dual-labeled oligonucleotides. This report suggested that the efficient

static quenching can be obtained without the use of molecular beacon structures that might lead to new design for DNA analysis.

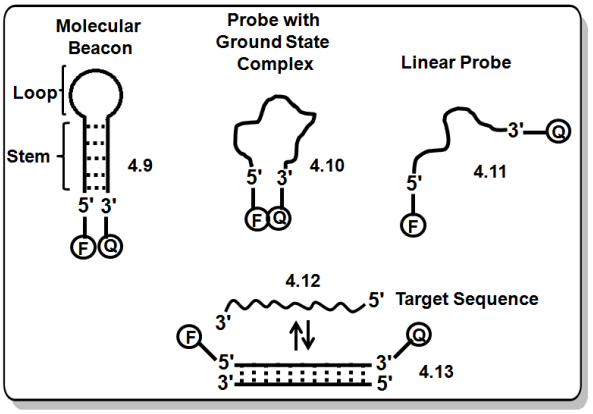

Figure 4.3: In molecular beacons and probes with a ground-state complex, the reporter dye and quencher are close together, preventing fluorescence. Linear probes have an uncontrolled dye-quencher distance. All three structures extend and fluoresce when complementary sequence is present. The strategy was used by Johansson *et al.*

Owczarzy *et al.,* have investigated that fluorophore-quencher labeled probe duplexes gathered increased duplex stabilization *via* the formation of ground state charge transfer complex between donor-acceptor pairs.[26a] Recently, they have shown that a DNA duplex can be stabilized by interaction and ground state complexation between a dye and a quencher attached at the terminus of the two single stranded DNA. [26b]

In order to study the pairing and fluorescence properties of 2-phenanthrenyl-DNA, Leumann *et al.* have synthesized three 2′-phenanthrenyl-*C*-deoxyribonucleosides with donor (**phenNH_2**), acceptor (**phenNO_2**), or no substitution (**phenH**) on the phenanthrenyl unit and incorporated them into oligonucleotides (**Figure 4.4**). [27] The thermal stability of the duplexes containing the donor and acceptor groups varied between -2.7 to +11.1 ^{o}C, depending on the nature of the substituents. When **phenNO_2** was placed opposite to the fluorophores **phenNH_2** and **phenH** inside a DNA duplex, efficient quenching of the fluorescence was observed. Similarly, when **phenH** and **phenNH_2** were placed opposite to each other, efficient quenching of fluorescence of **phenH** with simultaneous enhancement of fluorescence

of **phenNH$_2$** was observed which indicated the occurrence of electron- or energy-transfer processes between the aromatic units.

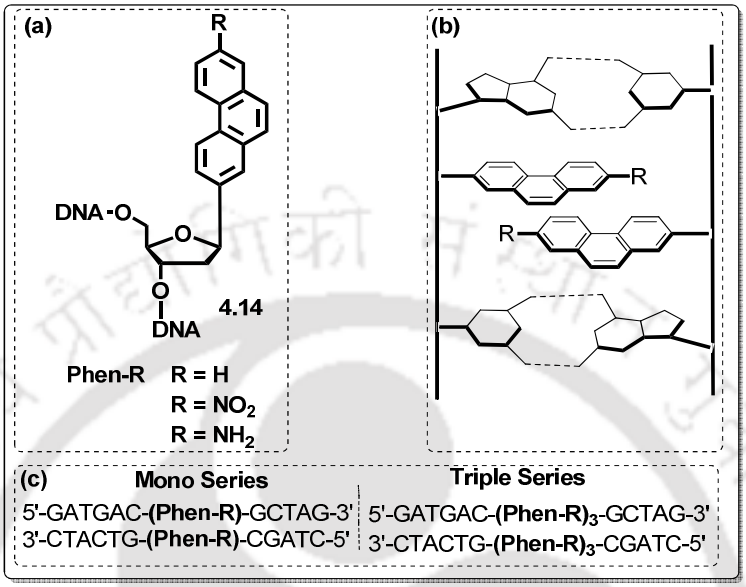

Figure 4.4: (a) Structure of the phenanthrenyl-*C*-nucleoside units; (b) Schematic representation of the expected zipper-like duplex structure; (c) DNA sequences of the mono- and triple-modified duplexes used.

A similar kind of study of the recognition properties of duplexes containing donor and acceptor biphenyl residues was carried out by Leumann *et al.*[27] The donor-byphenyl residues were modified with -OMe and -NH_2 substituents whereas the acceptor biphenyl residues were modified with -NO_2 (**Figure 4.5**). The thermal denaturation experiments revealed that the stabilities of duplexes with one biphenyl pair increase in the order: donor/donor < acceptor/donor < acceptor/acceptor substitution. In duplexes with three consecutive biphenyl pairs, the DNA duplex stability was found to increase in the inverse order (acceptor/acceptor < donor/acceptor < donor/donor) relative to an unmodified duplex. The fluorescence of the amino biphenyl residues in oligonucleotide is largely quenched when they are paired with themselves or with nitrobiphenyl containing duplex partners.

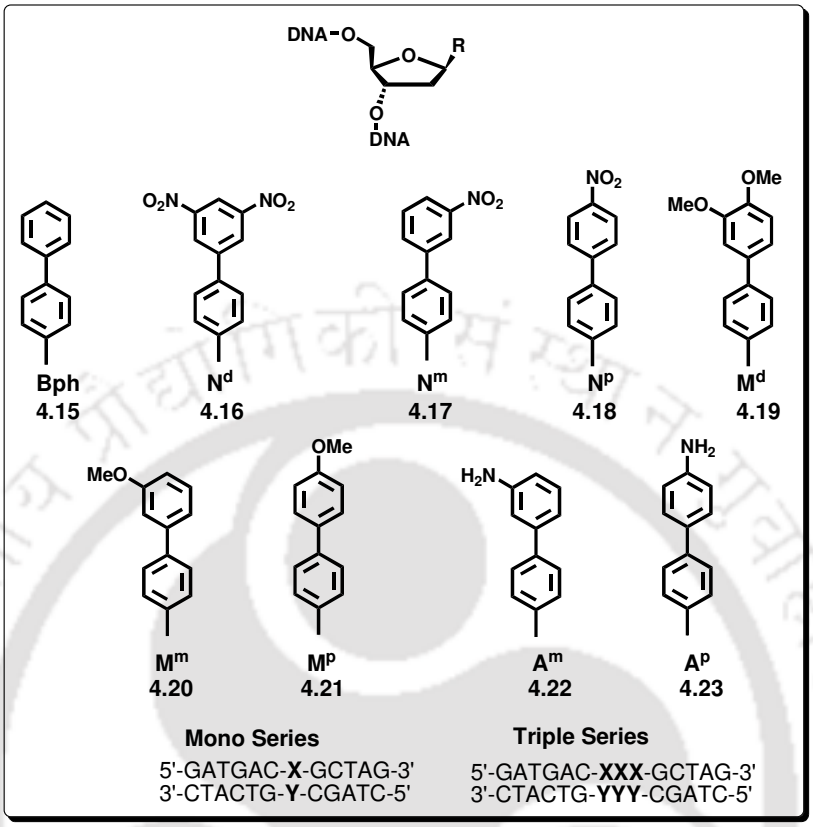

Figure 4.5: Chemical structures of the biphenyl-*C*-nucleosides together with the sequences of corresponding oligodeoxynucleotide duplexes.

Electron transport through the π-stacked DNA base pairs has recently attracted considerable interest.[28] A better understanding of excess electron transfer (EET), could allow development of DNA nanoscale devices for sensing of single-nucleotide polymorphism. Towards this end, Leumann *et al.* have designed DNA assemblies based on unnatural aromatic nucleobases with favorable electronic conducting properties. [29a] In this context they have designed oligonucleotides containing 5-(pyren-1-yl) uridine, 5-bromouridine phenantherene units in which two phenantherene units are sandwiched between the 5-(pyren-1-yl) uridine and 5-bromouridine units (**Figure 4.6**). It was observed that electron transfer occurred from an excited 5-(pyren-1-yl) uridine (an electron donor) to 5-bromouridine (an electron acceptor) through the internal stacked phenanthrenyl pair. Another example of electron transfer was provided by the Leumann group in which phenothiazine-β-*C*-nucleoside (**PTZ**) was placed against an abasic site (**Φ**) along with an interstrand stacked phenanthrenyl

(**Phen**) base pair and 5-bromouracil (**BrU**) (**Figure 4.7**).[29b] They observed that an excess electron transfer (EET) from a photoexcited π-stacked **PTZ**-b-*C*-nucleoside (**PTZ**) occurred *via* an interstrand stacked phenanthrenyl (Phen) base pair as electron carriers to 5-bromouracil as an electron trap. They also have observed that an increasing the number of phenanthrenyl base pairs increased the EET efficiency.

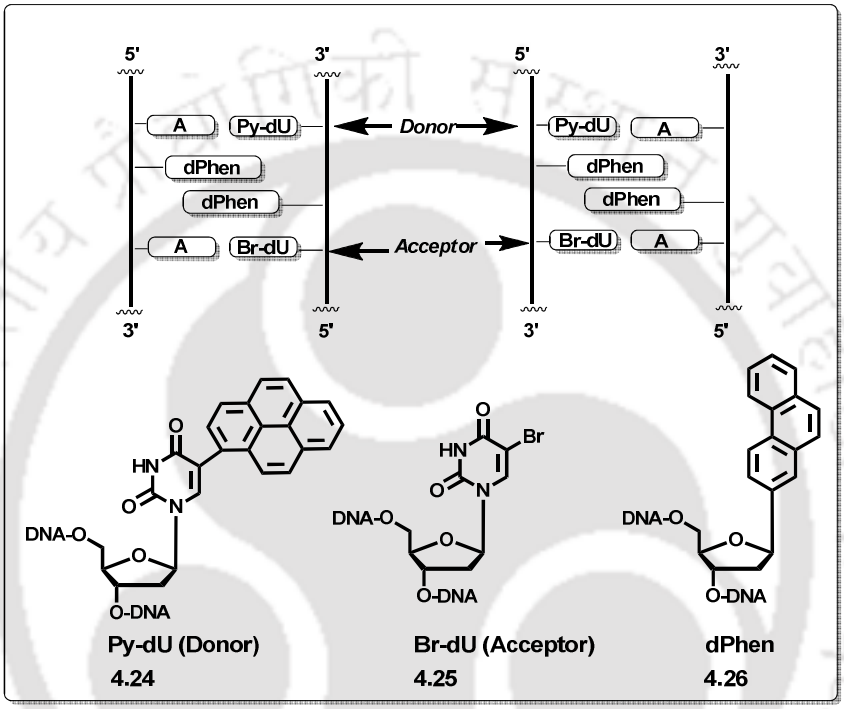

Figure 4.6: Schematic representation of the phenanthrenyl duplexes and the chemical structures of electron donating (**Py-**d**U**), electron accepting (**Br-**d**U**) as well as phenanthrenyl (d**Phen**) nucleosides.

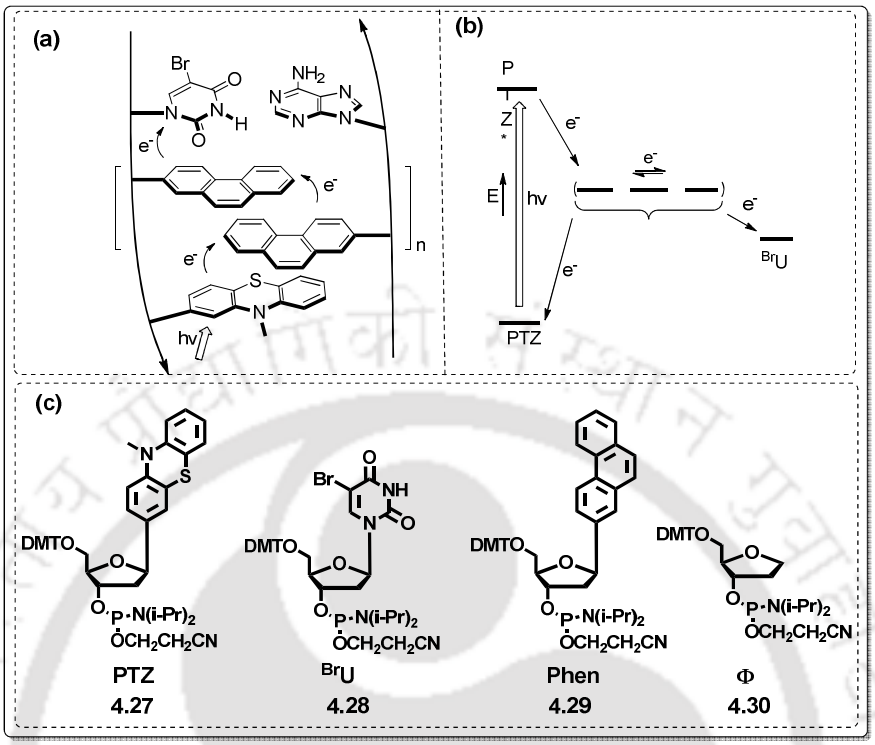

Figure 4.7: (a) Schematic representation highlighting EET from a photoexcited **PTZ**-β-*C*-nucleoside (**PTZ**) placed against an abasic site (**Φ**) to a interstrand stacked phenanthrenyl (**Phen**) base pair and 5-bromouracil (**BrU**); (b) an EET pathway from photoexcited (**PTZ***) to three **Phen** base pairs and (c) the chemical structures of electron donating **PTZ**-β-*C*-nucleoside (**PTZ**), electron accepting (**Br-dU**) as well as phenanthrenyl (**dPhen**) nucleosides.

Recently, Iversion *et al.*[30] have demonstrated that the DNA duplex stability and specificity can be driven by the electrostatic complementarity between an electron-rich and an electron deficient non-nucleosidic base pair. Thus, they have incorporated two novel non-nucleosidic DNA base surrogates, one of which is a relatively electron-deficient 1,4,5,8-naphthalenetetracarboxylic diimide (**NDI**) (**4.31**) and another is relatively electron-rich 1,5-dialkoxynaphthalene (**DAN**) (**4.32**), into short oligonucleotide strands (**Figure 4.8**). Three base pair replacement by two **NDI** and one DAN of a 12-mer oligonucleotide duplex in various sequential arrangements revealed an associative interction between the non-nucleoside donor-acceptor bases and interstrand π-π-stacking interaction with the natural bases inside the duplex DNA leading to a high duplex stabilization maintaining the B-form DNA duplex conformation. They have also shown that an **NDI–DAN–NDI** arrangement in the

middle of the DNA duplex was found to be approximately as stabilizing as three **A:T** base pairs.

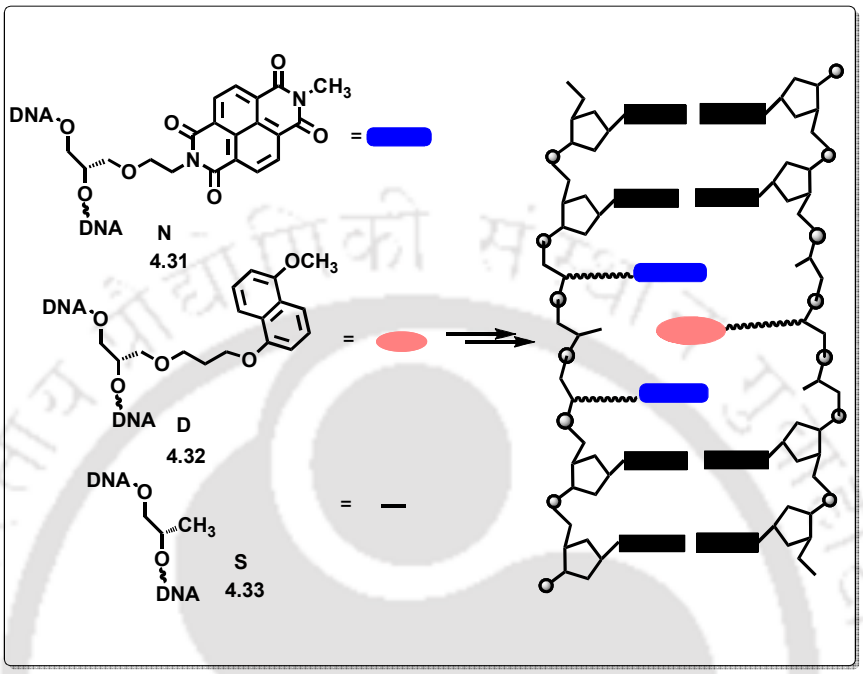

Figure 4.8: Chemical structures of 1,4,5,8-naphthalenetetracarboxylic diimide (**NDI**) and 1,5-dialkoxynaphthalene (**DAN**) and their arrangement in a double stranded oligonucleotide.

4.4. Background

After the introduction of non-H-bonding unnatural nucleobase surrogates by Kool *et al.* several research efforts for the design of hydrophobic unnatural DNA base analogues have been undertaken by various research groups.[1, 7, 9-11] Thus, the possible aromatic stacking, hydrophobic or CH-π interactions between the bases have been well explored in order to study the importance of such forces that stabilize the DNA duplex without Watson–Crick hydrogen bonding interaction. In the design of non-hydrogen bonding base pairs, researchers have concentrated mainly on the factors like π-stacking, hydrophobicity, steric shape mimicry and in few cases the dipole moment *etc.*, in the stabilization of the DNA duplex. However, the idea of charge transfer complexation mediated DNA duplex stabilization in a designed donor/acceptor pair of nucleobases has not solely been explored till the date.

4.5. Objective

About sixty years ago, Mulliken have suggested that the charge-transfer (CT) complexes "may afford new possibilities for understanding intermolecular interactions in biological systems".[31] Since then several biochemical phenomena were explained based on CT interactions.[32] As stated earlier in **Section 4.1.2**, various research groups have considered the ground state complexation as a possible source of extra stabilization observed in the DNA duplexes in course of their study of static quenching phenomena in a doubly labeled DNA probe. All of such examples considered the ground state complexation between a dye and a quencher attached at the terminus of the two single stranded DNA. However, a dye-quencher pair at the middle of the probe led to a destabilization of the duplex DNA as was revealed from their discussion.[23-26] Moreover, there is no report of charge transfer complexation mediated duplex stabilization wherein the DNA duplex is decorated with unnatural nucleobases at the central position of each single strand. Therefore, we wanted to explore the possibility of exploring the CT force to stabilize a DNA duplex by utilizing our newly designed triazolyl donor/acceptor nucleosides pair described in **Chapter 2**. Accordingly, we framed our objective as follows:

(a) Incorporation of triazolylphenanthrene ($^{TPhen}\mathbf{B}_{\mathbf{Do}}$) as a donor nucleoside and triazolylnitrobenzene ($^{TNB}\mathbf{B}_{\mathbf{Ac}}$) as an acceptor nucleoside into two short oligonucleotide sequences in two sequence contexts.

(b) Study of their photophysical and DNA duplex stabilizing properties during the course of hybridization to form self-pair and hetero-pair duplex.

(c) Study of the thermal melting as well as thermodynamic stability of the various duplexes.

(d) Examination of pairing selectivity and the sequence dependency in stabilization.

(e) Exploring the role of π-stacking/hydrophobic or electrostatic repulsion interaction in a self-pair duplex stabilization or destabilization.

(f) Establishment of the role of ground state charge transfer (CT) complexation force in the stabilization of a donor/acceptor hetero-pair duplex *via* the analysis of the photophysical spectra.

We envisaged that the pseudoaromatic 1,2,3-triazole can modulate the electronic characteristics of the bases and endow new properties to the unnatural nucleosides and/or oligonucleotides. In addition, triazole as well as aromatic units may play an important role in stabilizing a duplex *via* π-stacking interaction. Furthermore, triazolyl nucleosides capable of self- and/or hetero-pairing as well as stable and predictable pairing with other nucleobases, may shed light into the duplex stabilizing forces and may facilitate biophysical approach to DNA detection and can improve charge transfer interaction properties in DNA.[33] Thus, we observed that our unnatural bases have good selectivity to form hetero-pair and/or self-pair *via* charge transfer and/or π-stacking interactions. We are the first, to the best of our knowledge to explore the possibility of unnatural hetero-duplex stabilization *via* charge transfer interaction along with π-stacking interaction.

4.6. Results and Discussion

4.6.1. Synthesis and Characterization of the Two Nucleosides

With this background, aim and objective, we have designed and synthesized triazolyl unnatural nucleoside base $^{TPhen}\mathbf{B}_{\mathbf{Do}}$ and $^{TNB}\mathbf{B}_{\mathbf{Ac}}$ for incorporation into short oligonucleotide sequences and studying their DNA duplex stabilizing property. The synthesis of these two nucleosides was already discussed in **Chapter 2**. In short, the bis-toluoyl protected triazolylphenanthrene and triazolylnitrobenzene nucleosides were prepared *via* click reaction at 60 ^{o}C in THF between the β-azidosugar, 2-deoxy-3,5-bis[*O*-(*p*-toluoyl)]-β-D-ribofuranosyl azide (**2.84b**, **Scheme 2.23**, **Chapter 2**), and aromatic alkynes, 9-ethynylphenanthrene (**F**, **Scheme 2.22b**, **Chapter 2**) and 4-ethynyl nitrobenzene (**I**, **Scheme 2.22b**, **Chapter 2**), respectively, in very good yield. The final deprotected nucleosides, $^{TPhen}\mathbf{B}_{\mathbf{Do}}$ and $^{TNB}\mathbf{B}_{\mathbf{Ac}}$ were generated, then, after deprotection of the bis-toluoyl protecting groups using NaOMe in dry MeOH in 90% and 98% yields, respectively (**Scheme 2.23**, **Table 2.1**, **Chapter 2**). The nucleosides were characterized by NMR, mass, IR, melting temperatures and by single crystal X-ray analysis.

4.6.2. Logic behind Choosing $^{TPhen}B_{Do}$ and $^{TNB}B_{Ac}$ Pair for Incorporation in Short DNA: Study of Stacking and/or Charge Transfer Interaction Property

After getting the nucleosides in hand, the π-stacking and/or charge transfer interactions abilities of $^{TPhen}B_{Do}$ and $^{TNB}B_{Ac}$ nucleosides were examined prior to incorporation into oligonucleotides by studying photophysical properties as well as preliminary theoretical study in combination with natural bases.

Out of few synthesized triazolyl acceptor nucleosides, we have choosen triazolyl nitrobenzene nucleoside as a potent acceptor because it is more charge-deficient compared to other acceptor nucleosides synthesized such as cyanobenzene. Thus, it would involve in efficient charge transfer interaction with donor triazolyl phenanthrene nucleoside when placed closed to each other. Therefore, owing to the interest in emission and charge transfer interaction, we have chosen phenanthrene/nitrobenzene pair for incorporation in DNA and expected that they could form charge transfer complexation in close proximity in the duplex DNA. Exploration of other possible fluorescent donor/acceptor pair is the future scope of the thesis.

4.6.2.1. Spectroscopic Study

To evaluate the ^{T}B nucleosides' potential to form charge transfer and/or π-stacked pair as well as the ability to sense microenvironment, the photophysical properties of individual as well as of Do/Ac pair nucleosides ($^{TPhen}B_{Do}$ and $^{TNB}B_{Ac}$) have been evaluated in different solvents which were discussed in **Chapter 2** under **Section 2.5.3**. Analyses of the UV-visible spectra of a 1:1 mixture in low polar dioxane solvent and in polar phosphate buffer of donor triazolylphenanthrene nucleoside ($^{TPhen}B_{Do}$) and acceptor triazolylnitrobenzene nucleoside ($^{TNB}B_{Ac}$) showed the possibility of ground state association property which is reflected in the appearance of a new absorption band at longer wavelength region, longer than any of the parent nucleosides. The results were discussed in **Chapter 2** under **Section 2.5.3**, **Figure 2.18**. A quenching of the fluorescence of $^{TPhen}B_{Do}$ in presence of $^{TNB}B_{Ac}$ was also clear from the fluorescence emission of a solution of 1:1 mixture that indicated either the possibility of static (ground state charge transfer complexation) or collisional

quenching between the donor and the acceptor nucleosides. However, analysis of the UV-visible spectra of the mixture and the combined spectra of the individual nucleosides both in dioxane and in buffer revealed a possible formation of ground state charge transfer complexation. The results were discussed in **Chapter 2** under **Section 2.5.3**, **Figure 2.18**. Therefore, the spectroscopic study suggested that the triazolyl phenanthrene/nitrobenzene nucleoside pair ($^{TPhen}\mathbf{B}_{Do}$:$^{TNB}\mathbf{B}_{Ac}$) can indeed engage in ground state charge transfer complexation interaction if incorporated in DNA.

4.6.2.2. Solid State Structure Analysis

The crystal packing of the donor $^{TPhen}\mathbf{B}_{Do}$ nucleosides, presented in **Chapter 2**, under **Section 2.5.2**, showed an intermolecular π-stacked and H-bonded helical layer network wherein the phenanthrene units held by π-π stacking interaction among themselves and aromatic CH…..N hydrogen bonding with triazole moiety. This suggested that the triazolyl phenanthrene nucleoside can indeed engage in H-bonding as well π-stacking interaction. However, the $^{TPhen}\mathbf{B}_{Do}$ nucleoside showed a twist between the triazole and the phenanthrene suggesting that all rings of the phenanthrene unit might be unable to engage fully in stacking interaction upon incorporation into a DNA. However, it is possible that the third ring of phenanthrene might involve in groove binding stabilization event leaving other rings for stacking interaction with the bases in a duplex DNA.

On the other hand, both the packing diagram and crystal arrangement of $^{TNB}\mathbf{B}_{Ac}$ showed H-bonded helical layer chain like structure. The two adjacent layers are also involved in stabilized π-stacking interaction between phenyl ring of β-nitrobenzene of one layer and closely spaced triazole ring of another layer (**Figure 2.11**, **Chapter 2**). It was revealed that the nitrobenzene and the triazole moiety of $^{TNB}\mathbf{B}_{Ac}$ remained in the same plane that would allow the triazolylnitrobenzene unit to take part in intercalation/or in full stacking interaction within the nucleobases inside a DNA duplex after incorporation into DNA. Therefore, crystal packing suggested that the triazolyl phenanthrene/nitrobenzene nucleoside pair ($^{TPhen}\mathbf{B}_{Do}$:$^{TNB}\mathbf{B}_{Ac}$) can indeed engage in H-bonding as well π-stacking interaction if incorporated in DNA.

4.6.2.3. Theoritical Study

Next we have carried out theoretical calculation to get a preliminary idea about the charge transfer and the stacking propensity between the triazolyl donor/acceptor heteropairs and/or self pairs or between natural nucleoside bases using Guassian 09[34] and ADF2[35] programme package.

Thus, we have carried out a theoretical investigation on the charge transfer property between triazolyl phenanthrene as donor and triazolyl nitrobenzene as an acceptor with ADF program package which showed a considerable amount of charge transfer characteristics.[35] A considerable amount of stacking interactions were also observed between triazolyl phennanthrene/Nitrobenzene pair and pairs with natural nucleosides from DFT calculation using M05-2X/6-31+G(d,p)[36] level of theory using G09 program package.[34, 36-37]

All the geometries of natural and unnatural bases were optimized by B3LYP/6-31+g(d,p) and stacked bases were optimized using the M05-2X density functional developed by Truhlar and Zhao.[36] The M05-2X functional is a hybrid meta GGA (generalized gradient approximations) functional having 54% Hartree–Fock exchange contribution. Because of the large Hartree–Fock exchange contribution, this functional is a better choice than other functional. This newly developed M05-2X functional has been found very suitable for studying a number of chemical problems, especially shows its wide applicability to the study of noncovalent interactions. In the present preliminary calculation, the initial starting geometries of stacked dimers natural/unnatural hybrids in B-DNA conformation were generated using the Schrodinger Macromodel program. From the generated structures in B-DNA conformation, we removed the sugar, phosphate backbone attached to the bases and satisfied all valences of all atoms with hydrogen atoms. In case of trimeric B-DNA duplex, the initial structure thus generated retains the B-DNA base conformation. We used the 6-31+G(d,p) basis set for geometry optimization to make these calculations feasible in the B-DNA conformation using the M05-2X density functional developed by Truhlar and Zhao.[36]

Calculation of Stacking Energy: For calculating the stacking energy of the stacked bases, natural and non-natural, the monomers (single base) as well as the two intra-strand stacked bases were optimized at the M05-2X/6-31+G(d, p) level of

theory. For the stacked bases, natural and non-natural, the stacking energy, ΔE was determined by the following equation:

$$\mathbf{A} + \mathbf{B} \longrightarrow \begin{matrix}\mathbf{A}\\ \vdots \\ \mathbf{B}\end{matrix}$$

$$\Delta E = E_{A\ldots B} - (E_A + E_B)$$

where, $E_{A\ldots B}$ is the energy of the stacked bases; E_A and E_B are the energies of the optimized single bases. Basis set superposition error (BSSE) corrections were carried out to obtain the corrected interaction energy by using the counterpoise correction procedure (CP).[37]

Table 4.1: BSSE corrected energy, stacking energy of the pair and individual pairing partner.

BSSE corrected energy and stacking energy of the nucleobase pairs		
Entry	**BSSE corrected energy (a. u.)**	**Stacking Energy* (kcal/mol) BSSE corrected**
$^{TNB}B_{Ac}$-A	-1145.060645	-6.59
$^{TNB}B_{Ac}$-G	-1220.29469	-9.76
$^{TNB}B_{Ac}$-C	-1072.675012	-11.45
$^{TNB}B_{Ac}$-T	-1131.865809	-7.21
$^{TPhen}B_{Do}$:A	-1247.861163	-8.47
$^{TPhen}B_{Do}$:G	-1323.086243	-6.02
$^{TPhen}B_{Do}$:C	-1175.472795	-11.61
$^{TPhen}B_{Do}$:T	-1234.661982	-6.36
$^{TPhen}B_{Do}$:$^{TNB}B_{Ac}$	-1458.308791	-13.27
BSSE corrected energy of individual pairing partners		
Adenine (A)	-467.3050871	---
Thymine (T)	-454.1092599	---
Guanine (G)	-542.534076	---
Cytosine (C)	-394.9117116	---
$^{TNB}B_{Ac}$	-677.7450605	---
$^{TPhen}B_{Do}$	-780.5425813	---

Therefore, our preliminary observation stated that a considerable amount of stacking interaction is operating between various pairing partners which are comparable to the stacking energies between natural bases. Our calculation showed that the stacking energy between **$^{TPhen}B_{Do}$:$^{TNB}B_{Ac}$** is highest (-13.27 kcal/mole) among any other pairs studied.

AIM Calculation: The obtained wave-functions at the M05-2X/6-31+G(d,p) computational level have been used to analyze the electron density within the AIM methodology by AIM2000 package.[38] It shows a potential nonbonding interaction between the pairing partners.

Charge Transfer Possibility: Calculation Using ADF: The charge transfer integral for the electrons and holes in between the two donor-acceptor nucleobases was calculated preliminary by Density Functional Theory using the fragment orbital approach implemented in ADF 2010.02.[34-36] The wave function of a hole can be written as a linear superposition of the highest occupied molecular orbitals (HOMOs) on the individual bases – natural and non-natural. The site energies and charge-transfer integrals were obtained from the ADF output. The charge transfer integrals for the natural/non-natural stacks were calculated with the generalized gradient approximation (GGA) at dispersion-corrected BLYP-D level with a TZ2P basis set.[39]

The preliminary parameters suggested that a considerable amount of charge transfer is possible between heteropair ($^{TPhen}\mathbf{B}_{Do}$:$^{TNB}\mathbf{B}_{Ac}$) as well as between several possible mispairs.

QM/MM Stacking Energy in Trimeric Duplex[40]: We have also performed QM/MM calculation using the Gaussian 09 program package. The triazolyl base and the natural bases of the system (Tp$^{Phen}\mathbf{B}_{Do}$pT:Ap**C**pA) were chosen as the QM region and the rest sugar-phosphate parts were chosen as MM region. Multilayer ONIOM calculation was performed. Quantum Mechanics calculation with M05-2X/6-31+G(d, p) for QM region and Molecular mechanics calculation using UFF force field for MM region were performed. Then we have calculated the stabilization energy of the system (Tp$^{Phen}\mathbf{B}_{Do}$pT**:**Ap**C**pA) from the optimized geometries using the equation below.

$$E_{SE} = E_{Total} - (E_{T:A} + E_{PhenB4\text{-}C} + E_{T:A})$$

We observed that the system Tp$^{Phen}\mathbf{B}_{Do}$pT**:**Ap**C**pA is stabilized by -27.34 kcal/mol energy which imply that the stabilisation is possibly due of a combination of inter-/intra-strand stacking, H-bonding and charge transfer interaction.

Table 4.2 : QM/MM stacking energy of a trimeric duplex.

ONIOM Total Energy	**ONIOM** Total Energy
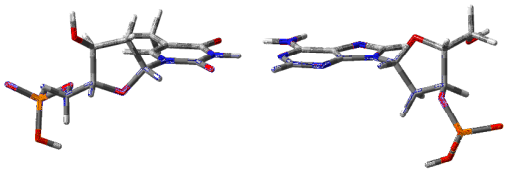 $E_{T:A}$= -921.37753096 a.u. 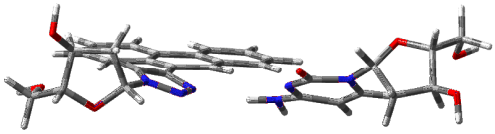 $E_{PhenB4-C}$ = -1175.404326 a.u. 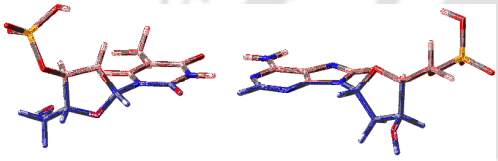 $E_{T:A}$ = -921.37869667 a.u.	**T--------A** **^{TPhen}B$_{Do}$-----C** **T--------A** 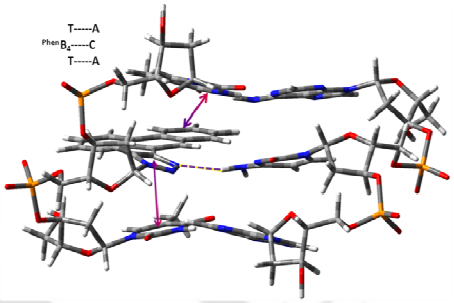 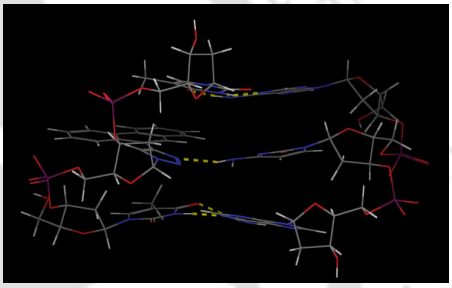 E_{Total} = -3018.20412865 a.u. $E_{SE} = E_{Total} - (E_{T:A} + E^{Phen}_{B_{Do}-C} + E_{T:A})$ E_{SE} = -0.0435745 a.u. E_{SE} = -27.3434345 kcal/mol

This stabilization is originated mainly from the stacking of inner ring of phenanthrene and triazole unit within the strand as well as H-bonding interaction between opposite cytosine and the N-3 of triazole moiety. The H-bonding is also observed from the Macromodel minimized structure (see next section **4.4.3**). Thus, from the AMBER* energy minimized geometry we observed that there is a strong Hydrogen bonding interaction between triazole N-3 and cytosine-NH_2 hydrogen. The distance of hydrogen bond is 2.16 Å which is closer to natural hydrogen bonds (**T:A**, 1.94, 1.82 and 1.73, 2.04 Å) of that system.

Though the gas phase calculations do not take into account solvent interactions, our preliminary observations suggested and gave us the idea that the pairing partners ^{TPhen}**B**$_{Do}$ and ^{TNB}**B**$_{Ac}$ in a close proximity might involve in charge transfer as well as stacking interactions among themselves in a duplex DNA.

In summary, all the experimental as well as gas phase theoretical calculation showed that in close proximity the donor/acceptor nucleobase pair, $^{TPhen}\mathbf{B}_{Do}$ and $^{TNB}\mathbf{B}_{Ac}$ would involve in charge transfer as well as stacking interactions among themselves with high possibility when they would form a base pair of a rigid DNA duplex. Inspiring results of π-stacking and charge transfer complexation interaction among the donor/acceptor pair ($^{TPhen}\mathbf{B}_{Do}$ and $^{TNB}\mathbf{B}_{Ac}$) led us to choose these particular two nucleosides for incorporation into oligonucleotide sequences to investigate the possibility of occurrence of charge transfer between two pairing partner in a hetero-duplex and to study the role of charge transfer complexation interaction in duplex stabilization.

4.6.3. Synthesis and Properties of Oligonucleotides Containing Triazolyl Donor/Acceptor Nucleosides

Driven by the photophysical study, single crystal X-ray structure analysis and theoretical calculations of possible stacking as well as ground state interactions between donor ($^{TPhen}\mathbf{B}_{Do}$) and acceptor ($^{TNB}\mathbf{B}_{Ac}$) triazolyl nucleosides, we next turned our attention to incorporate these two nucleosides into short 13-mer oligonucleotide sequences to evaluate the stable duplex formation abilities.

For the synthesis of oligonucleotide containing $^{TPhen}\mathbf{B}_{Do}$ and $^{TNB}\mathbf{B}_{Ac}$, we first protected 5′-OH group of the nucleosides, $^{TPhen}\mathbf{B}_{Do}$ and $^{TNB}\mathbf{B}_{Ac}$, with 4,4′-dimethoxytrityl group by reaction with 4,4′-dimethoxytrityl chloride in presence of catalytic amount of *N,N*-dimethylamino pyridine (DMAP) in anhydrous pyridine solvent. The DMTr protected nucleosidic base surrogates were isolated in pure form by a silica gel column chromatography and characterized by NMR and mass spectrometry. Next, the DMTr protected nucleosides ($^{TPhen}\mathbf{B}_{Do}$**-DMTr** and $^{TNB}\mathbf{B}_{Ac}$**-DMTr**) were converted to their phosphoramidite derivatives (**4.36, 4.37, Scheme 4.1**) by the reaction with 2-cyanoethyl-*N,N,N′,N′*-tetraisopropyldiphosphoramidite in presence of (1*H*)-tetrazole in anhydrous acetonitrile under nitrogen atmosphere. The phosphoramidite derivatives so produced was filtered through a short and basic silica gel column and dried and then used for the DNA synthesis without further purification (**Scheme 4.1**). We synthesized two complementary 13-mer oligonucleotides with $^{TPhen}\mathbf{B}_{Do}$ (ODN **1**, **7**) and two with $^{TNB}\mathbf{B}_{Ac}$ (ODN **2**, **8**) in two

sequence contexts placing the triazolyl nucleosides (^{T}**B**s) at a central position of the strands *via* automated DNA/RNA synthesizer using phosphoramidite chemistry (**Table 4.3**).

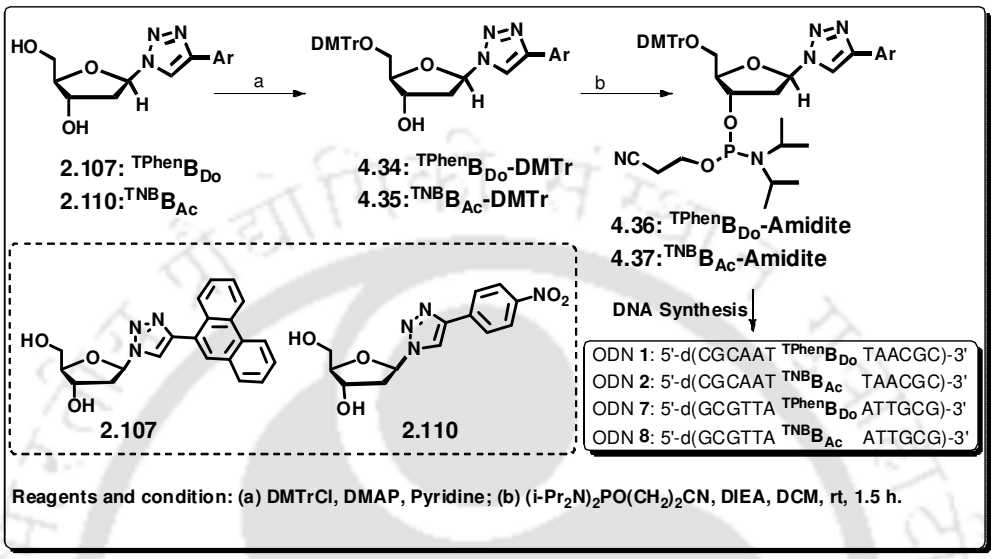

Scheme 4.1: Schematic representation of oligonucleotide synthesis.

Table 4.3: Oligonucleotide sequences containing ^{TPhen}**B**$_{Do}$ **:**^{TNB}**B**$_{Ac}$ nucleosides and their natural complements.

ODNs Sequences	
1. 5′-CGCAAT ^{TPhen}**B**$_{Do}$ TAACGC -3′	**7.** 3′- GCGTTA ^{TPhen}**B**$_{Do}$ ATTGCG - 5′
2. 5′-CGCAAT ^{TNB}**B**$_{Ac}$ TAACGC -3′	**8.** 3′- GCGTTA ^{TNB}**B**$_{Ac}$ ATTGCG - 5′
3. 3′- GCGTTA **A** ATTGCG - 5′	**9.** 5′-CGCAAT **A** TAACGC -3′
4. 3′- GCGTTA **G** ATTGCG - 5′	**10.** 5′-CGCAAT **G** TAACGC -3′
5. 3′- GCGTTA **C** ATTGCG - 5′	**11.** 5′-CGCAAT **C** TAACGC -3′
6. 3′- GCGTTA **T** ATTGCG - 5′	**12.** 5′-CGCAAT **T** TAACGC -3′

Each single stranded ODN containing ^{T}**B**s was hybridized to all possible natural nucleobases (ODN **3**-**6**; **9**-**12**) and the thermal melting stability and photophysical property of which were measured. The duplex forming capabilities and photophysical properties of the homo-duplexes formed between two identical ^{T}**B**s (self pair; ODN **1•7** and ODN **2•8**) and hetero-duplexes formed between two different ^{T}**B**s (heteropairs; ODN **1•8** and ODN **2•7**) were also evaluated. For comparison, the perfectly matched native oligonucleotide duplexes having an **A:T** base pair in the

same central position (ODN **3•12**) and the natural mismatched duplexes (A:A, T:T, G:G, and C:C) were also examined.

4.6.4. Evaluation of Global Property of the Duplexes

Study of Circular Dichroism Spectroscopy: Before going to measure the thermal stability, we examined the global property of all possible duplexes using circular dichroism spectroscopy. Thus, all spectra showed a positive band at around λ = 278 ~ 286 nm and a negative band at around λ = 248 ~ 252 nm of nearly equal magnitude with intersection at around λ = 260-262 nm similar to the natural A:T pair duplex (**Figure 4.9**). The CD-spectra analyses supported that all unnatural duplexes adopted stable B-form DNA conformation.

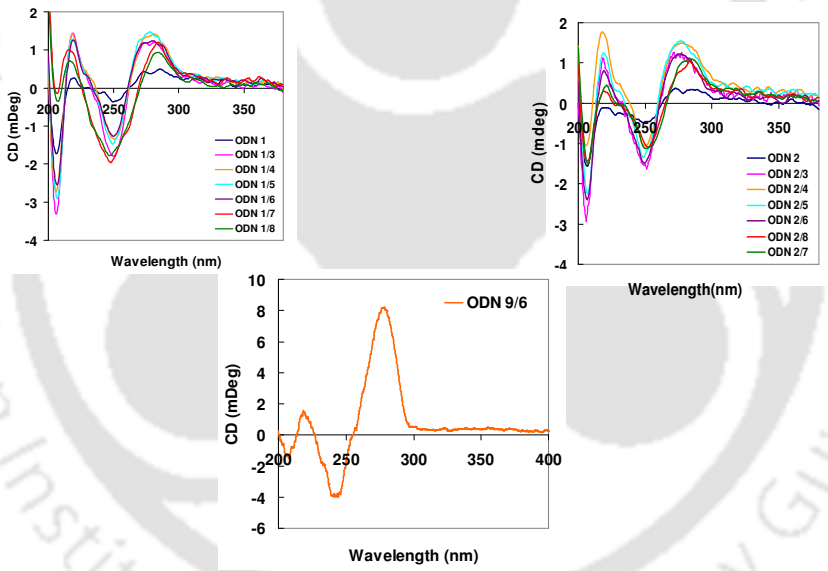

Figure 4.9: Circular dichroism spectra of (a) ODN **1** and its several duplexes (at 25 °C, all samples contained 2.5 μM each strand of DNA), (b) ODN **2** and its several duplexes (at 25 °C, all samples contained 2.5 μM each strand of DNA) and (c) natural **A:T** duplex (concentration was 20 μM) [50 mM sodium phosphate, 0.1 M sodium chloride, pH 7.0, room temperature.

Macromodel Study: To support the global B-form conformation of the duplexes of our novel unnatural ^{T}Bs self-pair/hetero-pair, we have carried out molecular modeling study of the duplexes using Schrodinger Macro Model (Maestro vs. 9.0) software with Amber* force field in water. The optimized geometries of the duplexes

suggests (**Figure 4.10**) that the introduction of our novel unnatural ^{T}Bs self pair/heteropair or mispair with natural bases within a duplex does not perturb the conformation of B-form DNA rather they stabilize the duplexes *via* aromatic stacking interaction which supported our observation from the CD measurement.

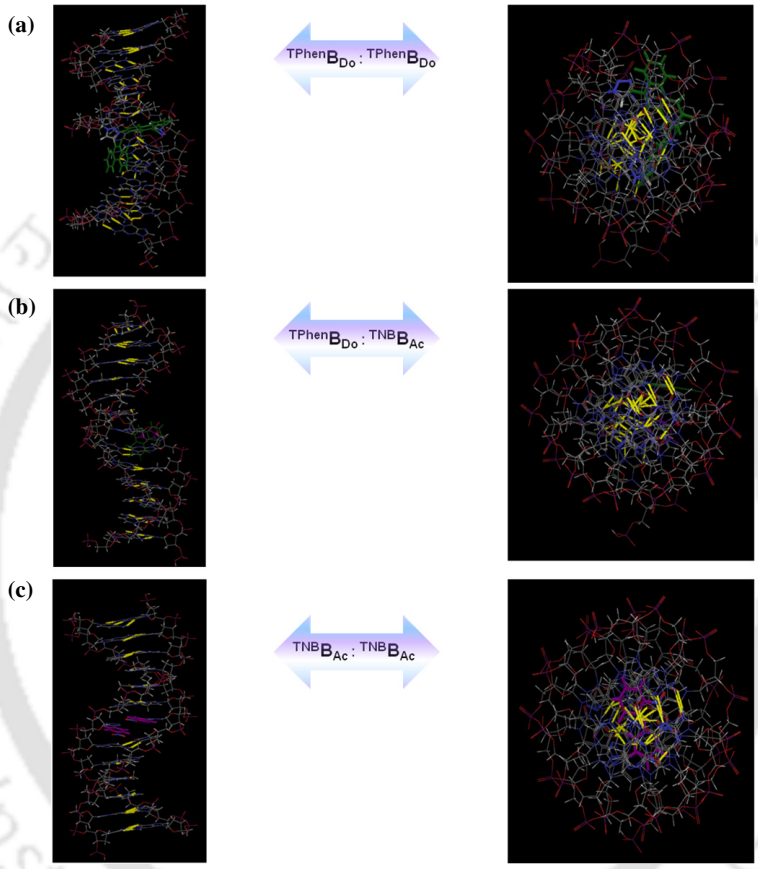

Figure 4.10 AMBER* energy minimized conformations in water of self pair (^{TPhen}**B**$_{Do}$:^{TPhen}**B**$_{Do}$), (^{TNB}**B**$_{Ac}$:^{TNB}**B**$_{Ac}$) and heteropair (^{TPhen}**B**$_{Do}$:^{TNB}**B**$_{Ac}$).

4.6.5. Study of Thermal Melting Stability and Pairing Selectivity of Various Unnatural Duplexes

Encouraged by all the above results, we, next, evaluated the thermal stabilities of the unnatural self pairs, hetero pairs, and mispairs [(5'-CGCAAT **X** TAACGC-3': (5'-GCGTTA **Y** ATTGCG-3') by thermal denaturation experiment. The two sequence context was so chosen as to examine the effects of flanking pyrimidines (T base for

X) and purines (A base for **Y**) (**Table 4.4**) on the duplex stability. For a comparison, the T_m for **A:T** natural matched and mismatched pairs were also evaluated.

Table 4.4: T_m values for several duplexes.

5'-CGC AAT **X** TAA CGC-3'

3'-GCG TTA **Y** ATT GCG-5'

ODNs	X:Y	T_m	ODNs	X:Y	T_m
1•7	$^{TPhen}B_{Do}$:$^{TPhen}B_{Do}$	53.6	**2•8**	$^{TNB}B_{Ac}$:$^{TNB}B_{Ac}$	50.2
1•8	$^{TPhen}B_{Do}$:$^{TNB}B_{Ac}$	52.3	**2•7**	$^{TNB}B_{Ac}$:$^{TPhen}{}_{Do}$	54.4
1•3	$^{TPhen}B_{Do}$:A	48.5	**2•3**	$^{TNB}B_{Ac}$:A	44.8
1•4	$^{TPhen}B_{Do}$:G	49.4	**2•4**	$^{TNB}B_{Ac}$:G	47.0
1•5	$^{TPhen}B_{Do}$:C	51.3	**2•5**	$^{TNB}B_{Ac}$:C	44.7
1•6	$^{TPhen}B_{Do}$:T	50.0	**2•6**	$^{TNB}B_{Ac}$:T	43.4
9•7	A:$^{TPhen}B_{Do}$	47.1	**9•8**	A:$^{TNB}B_{Ac}$	43.9
10•7	G:$^{TPhen}B_{Do}$	48.0	**10•8**	G:$^{TNB}B_{Ac}$	44.3
11•7	C:$^{TPhen}B_{Do}$	48.3	**11•8**	C:$^{TNB}B_{Ac}$	43.5
12•7	T:$^{TPhen}B_{Do}$	46.9	**12•8**	T:$^{TNB}B_{Ac}$	43.4
9•6	A:T	51.2	**12•3**	T:A	53.2
10•5	G:C	56.0	**11•4**	C:G	55.5

All samples contained 2.5 μM each strand of DNA, 50 mM sodium phosphate, 0.1 M sodium chloride, pH 7.0, with 0.1 mM EDTA room temperature. Error in T_m is estimated as ± 0.3°C. T_m of natural mismatched duplexes = 40.8 °C (T:T); 42.9 °C (A:A); 44.5 °C (G:G); 35.5 °C (C:C).

Table 4.4 shows the thermal melting temperature (T_m) values of all possible duplexes. Thus, from the T_m values, we observed the following decreasing order of stability for ODN **1** with its various target partners: $^{TPhen}B_{Do}$:$^{TPhen}B_{Do}$ > $^{TPhen}B_{Do}$:$^{TNB}B_{Ac}$ > **A:T** > $^{TPhen}B_{Do}$:C ≥ $^{TPhen}B_{Do}$:T > $^{TPhen}B_{Do}$:G ≥ $^{TPhen}B_{Do}$:A. Similarly, for ODN **2**, the stability follow the trend: $^{TNB}B_{Ac}$:$^{TPhen}B_{Do}$ > **A:T** ≥ $^{TNB}B_{Ac}$:$^{TNB}B_{Ac}$ > $^{TNB}B_{Ac}$:G ≥ $^{TNB}B_{Ac}$:C > $^{TNB}B_{Ac}$:A ≥ $^{TNB}B_{Ac}$:T. Our results interestingly demonstrated that the stabilities of the self pair (ODN **1•7**), and heteropair (ODN **2•7**) of $^{TPhen}B_{Do}$ are slightly higher than any of the natural **A:T** or **T:A** pairs. The highest stability of the $^{Tphen}B_{Do}$:$^{Tphen}B_{Do}$ self pair is most probably the result of strong hydrophobic and π-π stacking interaction between two triazolyl phenanthrene units of two strands of the self pair. Also, the hetero pair ODN **1•8** is slightly more stable than natural **A:T** pair. The stability of the highest stable

unnatural heteropair $^{TNB}\mathbf{B}_{Ac}$:$^{Tphen}\mathbf{B}_{Do}$ is found to be 3.2 ^{o}C higher than that of a natural **A:T** or **T:A** pair and comparable to that of (only slightly less stable by 1.1-1.6 ^{o}C) a natural C:G or G:C pair. The $^{Tphen}\mathbf{B}_{Do}$:$^{Tphen}\mathbf{B}_{Do}$ self pair is also slightly less stable (less by only 1.9-2.4 ^{o}C) than a natural **C:G** or **G:C** pair but more stable (by 2.4 ^{o}C) than a natural **A:T** or **T:A** pair (**Table 4.4**). Therefore, we can conclude that the triazolyl donor/acceptor nucleoside containing unnatural DNA are promising to offer at least a comparable stabilities as that of a natural **A:T** or **T:A** pair.

Other than duplex stabilizing property, an unnatural base pair should be highly selective against mispairing with the natural nucleobases so that the DNA with that unnatural pair would be efficient to perform job like natural DNA.[41] Thus, we next studied the selectivity if at all shown by the unnatural bases in mispairing with the natural nucleobases. To examine the sequence dependency in mispairing, ODNs **7**-**8** were hybridized to the corresponding complementary natural sequences, ODN **3-6** and ODN **9**-**12**. The thermal denaturation experiments showed the following trend of stability for ODN **7**: C≥ G> A> T and ODN **8**: G> A≥ C ≥T, reflecting the possible role of hydrophobic/dipole-dipole interaction (**Table 4.4**). In general, however, higher T_m values were observed when the flanking bases are pyrimidine (dT). Better interstrand base stacking (T-$^{T}\mathbf{Bs}$-T) interaction resulted in more stable duplexes compared to the corresponding A-$^{T}\mathbf{Bs}$-A duplexes in case of mispairing with natural bases (**Table 4.4**). However, for heteropair formation the opposite is true *i.e.,* in case of $^{TPhen}\mathbf{B}_{Do}$, strong aromatic intrastrand stacking with purine (dA) as well as hydrophobic and charge transfer interaction between $^{TPhen}\mathbf{B}_{Do}$ and $^{TNB}\mathbf{B}_{Ac}$ endow with the highest duplex stabilization of the $^{TNB}\mathbf{B}_{Ac}$:$^{TPhen}\mathbf{B}_{Do}$ heteropair (T_m= 54.4 ^{o}C). These observations are significant considering the intrastrand stacking interaction within the nearby natural bases in the duplex suggesting that the nucleobases possibly slip in order to stack on each other within the self-pair and/or hetero-pair.[42] It is noteworthy to mention that a significant portion of base stacking most probably resulted from a partial overlap of the polar moiety of nitrobenzene unit of $^{TNB}\mathbf{B}_{Ac}$ nucleoside with the polarizable triazolyl phenanthrene ring system and adjacent natural bases.[42d]

4.6.6. Study of Thermodynamic Stability of Various Duplexes

To better understand the thermodynamic origin of higher stability of the heteropair and self pair, we have calculated thermodynamic parameters from van't Hoff analyses of the thermal denaturation curves for fluorescent duplexes containing $^{TPhen}\mathbf{B}_{Do}$. Thermodynamic parameters were determined by van't Hoff analysis using the relation: $T_m^{-1} = R[\ln([C_T]/4)]/\Delta H + \Delta S°/\Delta H°$, where $\Delta H°$ and $\Delta S°$ are the standard enthalpy and entropy changes determined from UV experiments, respectively, R is the universal gas constant and $[C_T]$ is the total strand concentration. The slope of the plot of $1/Tm$ vs. $\ln([C_T]$ gives the value ΔH and then sustitution of this in the value of intercept yielded $\Delta S°$ and then we have calculated ΔG. Thermodynamic parameters (at 25 °C) were determined from van't Hoff plots using at least four to five different concentrations for each duplex (**Figure 4.11**).

Thus, it was evident that the self pair stabilization ($^{TPhen}\mathbf{B}_{Do}$:$^{TPhen}\mathbf{B}_{Do}$, ΔS = -305.04 cal/K/mol and $^{TNB}\mathbf{B}_{Ac}$:$^{TNB}\mathbf{B}_{Ac}$, ΔS = -266.46 cal/K/mol) is driven by more favorable (less negative) entropic change compared to natural A:T pair (ΔS = -337.08 cal/K/mol). While the process of coil to helix formation is accompanied with a comparable change in free energy for $^{TPhen}\mathbf{B}_{Do}$:$^{TPhen}\mathbf{B}_{Do}$ self pair (ΔG^o = -12.85 Kcal/mol), due to unfavorable enthalpy change the free energy change of the process is very low in case of $^{TNB}\mathbf{B}_{Ac}$: $^{TNB}\mathbf{B}_{Ac}$ self pair (ΔG^o = -10.89 Kcal/mol) (**Table 4.5**) . This is probably because of smaller surface area and extremely unfavorable electrostatic repulsive forces between two highly polar triazolyl nitrobenzene (μ = 8.3 D).

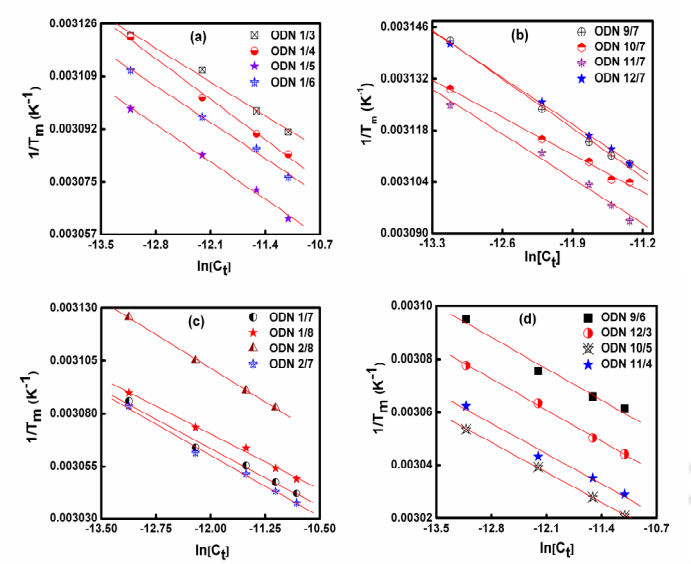

Figure 4.11: Van't Hoff fits for data for the concentration range from 1 to 7.5 μM for 13 bp duplexes containing self-pairs, heteropairs (a-b), mispairs with natural bases (c) and natural pairs in a central position (d).

Table 4.5. T_m values and thermodynamic parameters for several duplexes.

Duplexes	X:Y	T_m	$-\Delta G^0_{37}$	$-\Delta H^0$	$-\Delta S^0$
1•7	$^{TPhen}B_{Do}$:$^{TPhen}B_{Do}$	53.6	12.85	107.41	305.04
1•8	$^{TPhen}B_{Do}$:$^{TNB}B_{Ac}$	52.5	12.86	113.43	324.41
2•8	$^{TNB}B_{Ac}$: $^{TNB}B_{Ac}$	50.2	10.89	93.49	266.46
2•7	$^{TNB}B_{Ac}$:$^{TPhen}B_{Do}$	54.4	12.71	101.07	285.03
1•3	$^{TPhen}B_{Do}$:A	48.5	12.09	127.57	372.49
1•4	$^{TPhen}B_{Do}$:G	49.4	11.39	106.25	306.00
1•5	$^{TPhen}B_{Do}$:C	51.3	12.72	115.33	330.99
1•6	$^{TPhen}B_{Do}$:T	50.0	12.38	118.90	343.61
9•7	A: $^{TPhen}B_{Do}$	47.1	10.87	104.46	301.88
10•7	G: $^{TPhen}B_{Do}$	48.0	12.16	137.23	403.45
11•7	C: $^{TPhen}B_{Do}$	48.3	11.57	114.59	332.30
12•7	T: $^{TPhen}B_{Do}$	46.9	10.78	110.14	320.51
9•6	A : T	51.2	12.95	117.45	337.08
12•3	T : A	53.2	13.36	117.77	336.82
10•5	G : C	56.0	14.75	123.32	350.23
11•4	C : G	55.5	14.15	121.48	346.23

All samples contained 2.5 μM each strand of DNA, 50 mM Na-phosphate, 0.1M NaCl, 0.1mM Na_2EDTA, pH 7.0. Units of ΔG *and* ΔH are in kcal/mole, while for $-\Delta S$ is in cal/K/mol. Error in T_m is estimated at ± 0.3°C, and in free energy, ± 5%.

4.6.7. Summary of the Observations from the Study of Thermal and Thermodynamic Stability

The higher stability of the $^{TNB}\mathbf{B}_{Ac}$:$^{TPhen}\mathbf{B}_{Do}$ heteropair compared to $^{TPhen}\mathbf{B}_{Do}$:$^{TNB}\mathbf{B}_{Ac}$ pair is due to large surface area of triazolyl phenanthrene (**TPhen**) compared to triazolyl nitrobenzene (**TNB**) wherein more intrastrand stacking with flanking purin (A) in the sequence -A-$^{TPhen}\mathbf{B}_{Do}$-A- is operating. Furthermore, all the unnatural self-pairs or hetero-pairs are entropically more favourable compared to any natural pairs. In the heteropairs, $^{TNB}\mathbf{B}_{Ac}$ is involved in ground state charge transfer interaction as well as in intercalative interstrand stacking interactions.[42] Interestingly, all the mispairs of either of $^{TPhen}\mathbf{B}_{Do}$ or $^{TNB}\mathbf{B}_{Ac}$ in any sequence context were found to be thermodynamically more stable compared to any combinations of natural mismatched pairs (A:A, T:T, G:G, and C:C). Overall, the unnatural bases are more selective for hetero-pairing as well as self-pairing possibly *via* π-stacking and/or charge transfer interaction between two donor and/or acceptor pairing partners and natural bases within a duplex.

The stability order of the self-pairs or hetero-pairs observed from thermal melting and thermodynamic study can be explained by considering the stacking as well as electrostatic repulsion and charge transfer interaction which was also supported by the Amber* optimized geometry of the corresponding duplexes. Thus, in the highest stable hetero-pair, $^{TNB}\mathbf{B}_{Ac}$:$^{TPhen}\mathbf{B}_{Do}$ both the triazoles are involved in intrastrand stacking, the third ring of the phenanthrene unit is engaged in major groove binding and nitrobenzene is involved in intercalative stacking between phenanthrene and its other natural flanking base pairs. Nitrobenzene unit also involved in charge transfer interaction with phenanthrene unit *via* a stacking between polar $-NO_2$ and polarizable phenanthrene unit. Other two ring of the phenanthrene stacked with natural A base in the same strand (A-$^{TPhen}\mathbf{B}_{Do}$-A) very strongly as the stacking propensity of A is highest among all four natural bases (A > G > C =T). It was calculated that the vertical distance between triazole and natural base of the same strand is comparable to the distance between natural bases (3.4 Å) and thus, is sufficient enough for strong intrastrand stacking. The two dipolar units, phenanthrene and nitrobenzene with dipole moment of 3.5 D and 8.3 D, (derived from Gaussian 03 optimized geometries) respectively, are face to face with each other which probably allow them in strong π-π

stacking and charge transfer interaction (**Figure 4.10**). Thus, a charge transfer interaction between $^{TPhen}\mathbf{B}_{Do}$ and $^{TNB}\mathbf{B}_{Ac}$ as well as stacking interaction is most probably operative leading to highest duplex stability among all the unnatural and natural A:T or T:A duplex. The evidence for both the forces are discussed below.

4.6.8. Evidence of Charge Transfer and π-π Stacking Interaction and Duplex Stabilization

The proof of our concept of charge transfer complexation came from the analysis of UV-visible spectra and fluorescence quenching experiment. Thus, from a careful analysis of the UV-visible spectra of single stranded ODNs, their addition spectra and the spectra of the duplex ODN **2•7** [ODN **2** contains acceptor triazolyl nitrobenzene nucleoside ($^{TNB}\mathbf{B}_{Ac}$) and ODN **7** contains donor triazolylphenanthrene nucleoside ($^{TPhen}\mathbf{B}_{Do}$)], we observed about 8 nm shift in wave length when compared between the combined absorption spectra of the individual ODNs (ODN **2** and **7**) and the hybrid duplex ODN (ODN **2•7**). This observation in change in UV-visible spectra indicated a possible formation of ground state charge transfer complex between the two nucleosides $^{TPhen}\mathbf{B}_{Do}$ and $^{TNB}\mathbf{B}_{Ac}$, in the duplex ODN **2•7** (**Figure 4.12a**).[22,24a,25]. The ground state complexation phenomenon is further supported by a static quenching of fluorescence of donor nucleoside by the acceptor nucleoside in a hybrid duplex ODN **2•7** and ODN **1•8** (**Figure 4.12b-c**). The static quenching of fluorescence is supported by the quenching of emission of both the donor and acceptor nucleosides upon hybridisation that is clear from the resolved emission spectra from the duplex ODN **2•7** (**Figure 4.12d**).[24a, 22] Similar phenomenon was also reported by Tyagi *et al.*[22]

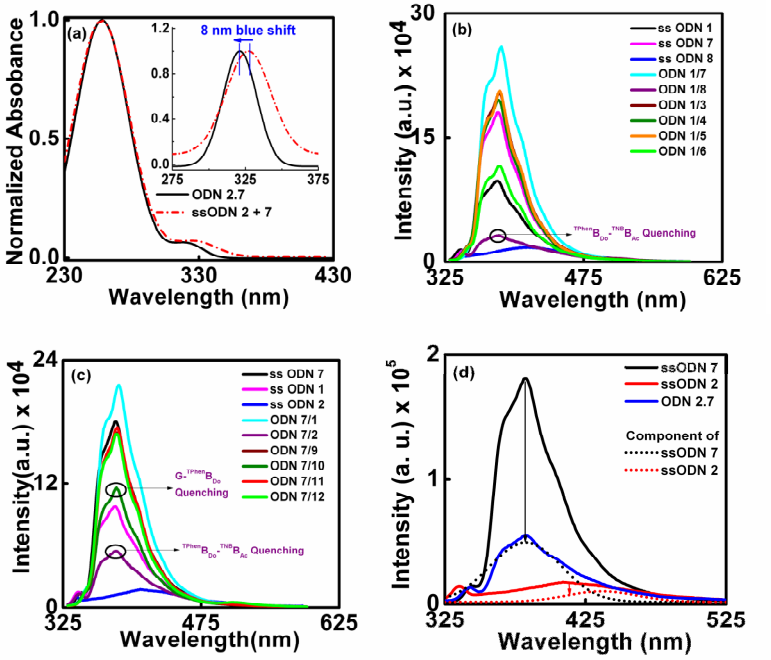

Figure 4.12: (a) UV-visible absorption spectra of the hybrid ODN **2•7** (solid line) and the absorption spectra obtained by combining the absorption spectra of the individual oligonucleotides, ODN **2** and ODN **7** (dotted line). Inset: Guassian fit spectra of the chromophoric region to show the differences. Fluorescence emission spectra (λ_{ex} = 315 nm) of (b) ODN **1** and (c) ODN **7** in their single stranded as well as duplex state with various complementary ODNs (2.5 μM conc. of different ODNs in 50 mM sodium phosphate, 0.1 M sodium chloride, pH 7.0, room temperature). (d) Emission spectra of the single stranded ODNs (ODN **7** and ODN **2**) containing donor and/or acceptor nucleoside ($^{TPhen}\mathbf{B_{Do}}$ and/or $^{TNB}\mathbf{B_{Ac}}$) and of the hybrid they form ODN **2•7**. The duplex ODN **2•7** was excited at 310 nm that is the optimal excitation wavelength for donor nucleoside, $^{TPhen}\mathbf{B_{Do}}$. The emission from the OND **7** and ODN **2** originates when stimulated by 310 nm and 330 nm light that are the optimal excitation for donor nucleoside ($^{TPhen}\mathbf{B_{Do}}$) and acceptor nucleoside ($^{TNB}\mathbf{B_{Ac}}$) respectively. Resolving the emission spectra from the duplex ODN **2•7** into its components showed decrease in intensity of both the donor and acceptor nucleosides upon hybridization. (ODN **7** or **2** = 15 μM; 50 mM sodium phosphate, 100 mM NaCl, pH 7.0; λ_{ex} = 310 nm, λ_{em} = 384 nm).

In addition to this, ground state complexation becomes obvious from a bathochromic shift of about 8 nm and 14 nm of the absorption and fluorescence excitation spectra, respectively, of the probe ODN **7** containing the donor fluorescent nucleoside in the presence of target ODN **2** containing the acceptor (quencher)

fluorescent nucleoside with a static quenching efficiency. The prominent bathochromic shift is observed in the duplex ODN **2•7** compared to single stranded ODN **7** (**Figure 4.13**).[24a, 25d]

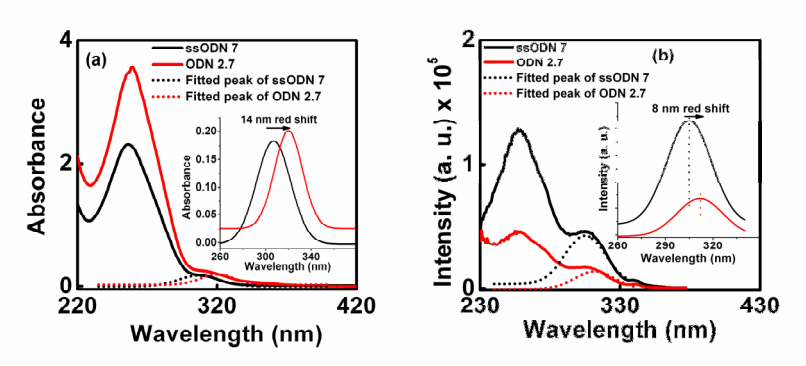

Figure 4.13: (a) UV-visible and (b) fluorescence excitation spectra of ssODN **7** and hybrid ODN **2•7** at room temperature. Dotted lines are the Gaussian fit spectra of the chromophoric region to show the differences. Inset: Magnifying Gaussian fit spectra of the chromophoric region which clearly showed the blue shifting of λ_{abs}^{max} (14 nm) and λ_{ex}^{max} (8 nm) of ODN **7** upon hybridization with ODN **2**. ([ODN **7**] = [ODN **2**] = 15 µM; 50 mM Na-phosphate, 100 mM NaCl, pH 7.0; λ_{em} = 384 nm).

We have also tested the static quenching event in detail, considering donor nucleoside containing ODN **7** as a probe (fluorophore) and the acceptor nucleoside containing ODN **2** as a target quencher. Thus, from the fluorescence experiment and life time data we observed a decreased F_0/F value at high temperature compared to that at room temperature for the duplex ODN **2•7** (**Figure 4.14a-b**). Moreover, the time-resolved fluorescence experiment revealed the constant value of τ_0/τ (τ_0/τ = 1) for both the single stranded (ODN **7**) and duplex state (ODN **2•7**) (**Figure 4.14 c-d**). This result clearly indicated that the quenching incidence is purely a static quenching in nature. Recently, Owczarzy *et al.* have shown that a DNA duplex can be stabilized by interaction and complexation between a dye and a quencher attached at the terminus of the two single stranded DNA. They also have investigated that fluorophore-quencher labeled probe duplexes gathered increased duplex stabilization *via* the formation of ground state charge transfer complex between donor-acceptor pairs.[25d] Our experimental results follow the similar trend. A correlation between the

reported literature data and our experimental observations supported the ground state charge transfer complex formation between the donor ($^{TPhen}\mathbf{B}_{Do}$) and the acceptor ($^{TNB}\mathbf{B}_{Ac}$) triazolyl unnatural nucleosides in the duplex ODN **2•7** ($^{TNB}\mathbf{B}_{Ac}$ **:** $^{TPhen}\mathbf{B}_{Do}$) and the static quenching of fluorescence event.[24a, 25]

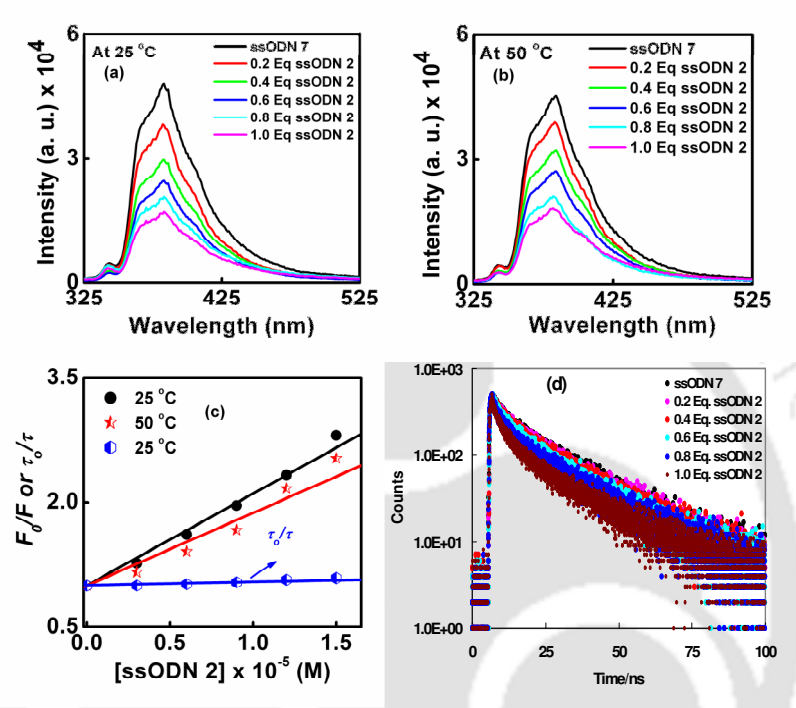

Figure 4.14: Fluorescence titration of ODN **7** (as donor/fluorophore) with ODN **2** (as acceptor/quencher) at (a) room temperature and at (b) 50 °C. (c) Plot of F_0/F and/or τ_0/τ *vs.* concentration of ODN **2**. (ODN **7** = 15 µM; 50 mM Na-phosphate, 100 mM NaCl, pH 7.0; λ_{ex} = 310 nm, λ_{em} = 384 nm). (d) Time resolved fluorescence titration curves of ODN **7** (as donor/fluorophore) with ODN **2** (as acceptor/quencher) at room temperature. (ODN **7** = 15 µM; 50 mM Na-phosphate, 100 mM NaCl, pH 7.0; λ_{ex} = 308 nm LED, λ_{em} = 384 nm).

Moreover, ground state complexation becomes obvious by a bathochromic shift of the absorption and fluorescence excitation spectra of the probe ODN **7** containing the donor fluorescent nucleoside in the presence of increasing concentration of target ODN **2** containing the acceptor (quencher) fluorescent nucleoside with a static quenching efficiency (**Figure 4.15 a-b**). The prominent bathochromic shift of 14 nm is observed in the duplex ODN **2•7** compared to single stranded ODN **7** (**Figure 4.15c**).

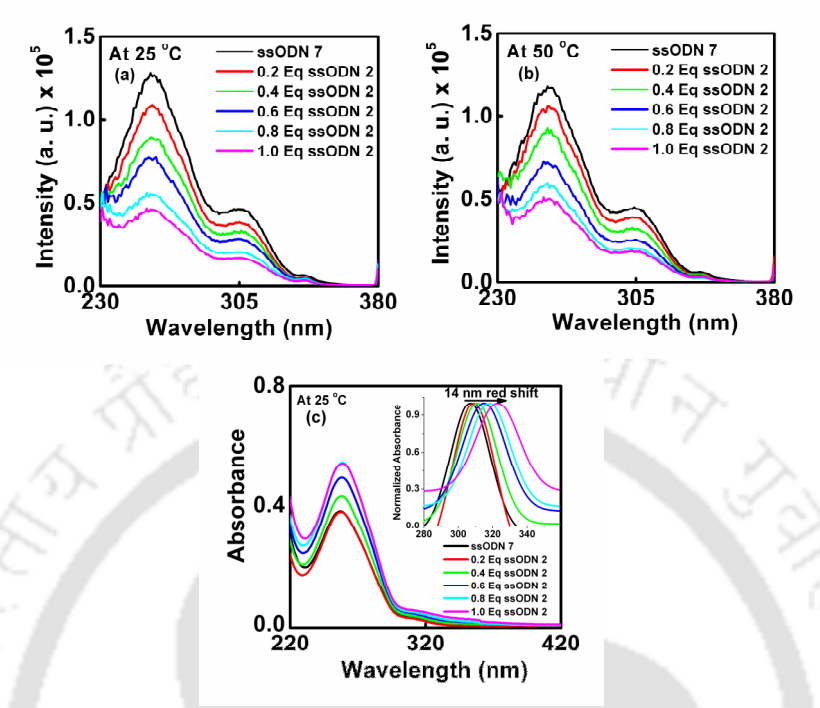

Figure 4.15: Fluorescence excitation spectra of **ODN 7** (as donor/fluorophore) titrated with ODN **2** (as acceptor/quencher) at (a) room temperature and at (b) 50 °C. (c) UV-visible spectra of ODN **7** (as donor/fluorophore) titrated with ODN **2** (as acceptor/quencher) at room temperature showing a bathochromic shift of 14 nm for duplex ODN **2•7**.

Therefore, all the photophysical phenomenon supported that the hybridization of ODN **7** and ODN **2** brought the donor/acceptor pair in close contact leading to a charge transfer complexation which played an important role in giving highest duplex stabilization in the heteroduplex ODN **2•7** among all other unnatural/natural duplex tested.

While both the self-pairs are accommodated within duplex DNA without significant loss of duplex stability, one of the two large aromatic triazolylphenanthrene of homo-duplex, $^{TPhen}\mathbf{B}_{Do}$:$^{TPhen}\mathbf{B}_{Do}$ invlove in an intercalative stacking and the other involves in stacking interaction inside the groove position. The stacking interaction within the $^{TPhen}\mathbf{B}_{Do}$:$^{TPhen}\mathbf{B}_{Do}$ self-pair is consistent with its high stability and is supported from Amber* optimized geometry of the duplex (**Figure 4.10a**). Thus, it is clear from the MacroModel study that one phenanthrene is engaged in major groove binding while other one involves in interacalative inter/intra-strand

stacking between its flanking base pair leading to second most stable complex compared to all the unnatural and natural **A:T** or **T:A** duplex. These nucleotides are not pair in an edge-on manner as observed with natural Watson-Crick base pairs.

In contrast to the $^{TPhen}\mathbf{B}_{Do}$ self-pair, the nucleobase analogues of the $^{TNB}\mathbf{B}_{Ac}$ self-pair are not sufficiently large to bridge the duplex and cannot intercalate. They are not optimally edge-to-edge packed rather their packing is probably arose from the triazole moieties which might engaged in intrastrand stacking/electrostatic interactions between their flanking natural base pair. As was clear from the Amber* optimized geometry (**Figure 4.10c**), both the highly polar nitrobenzene units are tilted out of the helix and their negative dipoles are faced each other. The distance between two repelling $-NO_2$ groups was found to be 3.6 Å; therefore the two dipoles (dipole moment = 8.3 Debye) are extended enough to repel each other. Thus, a dipole-dipole/electrostatic repulsion is operative to some extent leading to duplex destabilisation compared to all unnatural self-pair/hetero-pair as well as natural **A:T** or **T:A** duplex.

In summary, the concept of duplex stabilization through possible involvement of π-stacking and/or charge transfer interactions was supported by the highest stabilization of the heteropair (ODN **2•7**) as well as a static quenching of fluorescence of $^{TPhen}\mathbf{B}_{Do}$ in this heteropair (**Figure 4.12b-c**). The charge transfer interaction is evident from the UV-visible and fluorescence excitation spectra (**Figure 4.12a**, **4.13**, **4.15**). That the quenching of fluorescence in the heteropair (ODN **2•7**) is purely a static quenching was also evident from the UV-visible as well as fluorescence spectral data (**Figure 4.12a**, **4.12d**, **4.13**). The possible charge transfer mediated quenching was also evident in case of heteropair ODN **1•8** (**Figure 4.12 b-c**). That the electrostatic/dipole-dipole interaction possibly plays a role in duplex stability and/or instability was evident from the lower T_m of self-pair of $^{TBN}\mathbf{B}_{Ac}$ than that of hetero-pair which is mostly due to electrostatic repulsion between two $-NO_2$ groups. A bathochromic shift of the absorbance maxima and hypochromicity of $^{TPhen}\mathbf{B}_{Do}$ in a single strand ODN **7** of the reverse sequence (-A- $^{TPhen}\mathbf{B}_{Do}$-A-) compared to its' normal sequence ODn **2**(-T- $^{TPhen}\mathbf{B}_{Do}$-T-) indicated the possibility of stacking interaction between $^{TPhen}\mathbf{B}_{Do}$ and natural base **A** which also was reflected in the more

intense fluorescence of single strand ODN **7**. The possible stacking interaction was also evident from the chromophore's absorbances in a single strand and duplex DNA.

4.7. Conclusion

In summary, we have shown that our new and novel triazolyl unnatural donor/acceptor nucleobases offer a good stabilization of the heteropair/self pair duplexes that are comparable to that of a natural **A:T** pair. The stabilization of the duplexes and the pairing selectivity was explained on the basis of possible involvement of π-stacking and/or charge transfer interactions. Both the theoretical and spectroscopic evidences supported the role of the π-π-stacking and charge transfer interaction force in stabilizing self-pair and hetero-pair duplexes. This is the first direct evidence of charge transfer complexation mediated DNA hetero-duplex stabilization. Therefore, our results might shed light to design such type of donor-acceptor base pair and to further elaborate this new force of duplex stabilization in the context of recognition by polymerase enzymes. The static quenching of fluorescence of $^{TPhen}\mathbf{B}_{Do}$ by $^{TNB}\mathbf{B}_{Ac}$ in any sequence context clearly shows that our unnatural DNA might find applications in studying charge transfer process in DNA.

4.8. Experimental Section

4.8.1. General Experimental

All reactions were carried out under a nitrogen atmosphere. Organic extracts were dried over anhydrous sodium sulphate. Solvents were removed in a rotary evaporator under reduced pressure. Silica gel (60-120 mesh size) was used for the column chromatography. Reactions were monitored by TLC on silica gel 60 F254 (0.25mm). ^{1}H NMR spectra were measured with Varian 400 (400 MHz) and ^{13}C NMR spectra were measured with Varian 400 (100 MHz) spectrometer. Coupling constant (*J* value) was reported in hertz. The chemical shifts were shown in ppm downfield from tetramethylsilane, using residual chloroform (δ = 7.24 in ^{1}H NMR, δ = 77.23 in ^{13}C NMR), dimethyl sulfoxide (δ = 2.48 in ^{1}H NMR, δ = 39.5 in ^{13}C NMR), as an internal standard. Mass spectra were recorded using WATERS MS system, Q-tof premier and data analyzed using Mass Lynx 4.1. IR spectra were recorded in KBr or neat on a

Perkin Elmer Spectrum one FT-IR spectrometer. The *UV*–visible spectra were recorded by Shimadzu UV-2550 UV-Visible spectrophotometer with a cell of 1 cm path length. Fluorescence spectra were obtained using Fluoromax-4 fluorescence spectrophotometer at 25 °C using 1 cm path length cell. Circular Dichroism spectra were recorded on a JASCO CD J-810 spectropolarimeter. The reagents for DNA synthesis were purchased from Glen Research. Reversed-phase HPLC was performed on CHEMCOBOND 5-ODS-H columns (10x150 mm, 4.6x150 mm) using UV detector (260 nm). Mass spectra of the oligonucleotides were recorded using a MALDI-TOF mass spectrometer. The natural complementary DNAs were purchased from Integrated DNA Technologies.

4.8.2. General Procedure for the Tritylation of 5'-OH (4.34-DMTr, 4.35-DMTr)

A solution of **2.107** (99.34 mg, 0.150 mmol) or **2.110** (91.08 mg, 0.150 mmol), with 4-dimethylaminopyridine (catalytic amount), and 4,4′-dimethoxytrityl chloride (56.0 mg, 0.165 mmol) in anhydrous pyridine (3.0 mL) was stirred at room temperature for 16 h. After concentration of the solution to dryness, the residue was purified by silica gel column chromatography ($CHCl_3$/MeOH = 20:1) to yield the tritylated product (70%, 91.1 mg) as a pale yellow solid.

1-(5'-O-(4,4'-dimethoxytrityl)-2-deoxy-β-D-ribofuranosyl)-4 (phenanthren-9-yl)-1H-1,2,3-triazole (4.34, $^{TPhen}B_{Do}$-DMTr): ^{1}H NMR (CD_3OD, 300 MHz) δ 2.68 (1H,

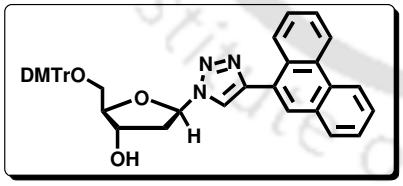

quintet, J = 6.9 Hz), 3.04-3.1 (1H, m), 3.49 (3H, s), 3.51 (3H, s), 4.06-4.19 (3H, m), 4.79-4.82 (1H, m), 6.61-6.67 (5H, m), 7.13-7.21 (7H, m), 7.32-7.40 (2H, m), 7.61-7.80 (5H, m), 8.04 (1H, d, J = 7.5 Hz), 8.44 (1H, s), 8.80 (2H, q, J = 9.0 Hz); ^{13}C NMR (CD_3OD, 75 MHz) δ 13.1, 40.3, 54.1, 63.2, 70.7, 86.4, 87.2, 89.2, 112.6, 122.3, 122.8, 125.9, 126.3, 126.6, 126.7, 127.1, 127.4, 128.1, 128.4, 128.7, 129.8, 129.9, 130.6, 131.2, 135.6, 140.8, 146.5,158.6; HRMS calcd. for $C_{42}H_{36}O_5N_3Na$ ([M+Na]$^+$) 686.2622, found 686.2626.

1-(5'-O-(4,4'-dimethoxytrityl)-2-deoxy-β-D-ribofuranosyl)-4-(4-nitrophenyl)-1H-1,2,3-triazole (4.35, $^{TNB}B_{Ac}$-DMTr): ^{1}H NMR (CD_3OD, 300 MHz) δ 2.59-2.64 (3H, m), 2.94-3.01 (1H, m), 3.69 (6H, s), 4.13-4.16 (1H, m), 4.72 (1H, q, J = 6.0 Hz), 6.49

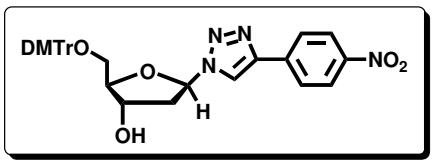

(1H, q, *J* = 6.0 Hz), 6.76 (4H, dd, *J* = 9.0 Hz), 7.24 (7H, dd, *J* = 2.4, 4.5 Hz), 7.36 (2H, d, *J* = 6.9 Hz), 7.75 (2H, d, *J* = 6.0 Hz), 8.2 (2H, d, *J* = 6.9 Hz), 8.63 (1H, s); ^{13}C NMR (CD_3OD, 300 MHz) δ 54.3, 63.3, 70.6, 86.4, 87.1, 89.2, 112.8, 121.3, 123.9, 125.9, 126.6, 127.5, 128.2, 129.9, 135.6, 135.7, 136.6, 144.5, 145.5, 147.3, 158.8. HRMS calcd for $C_{34}H_{31}O_7N_4Na$ ($[M+Na]^+$) 631.2161 found 631.2157.

4.8.3. General Procedure for Phosphoramidite Reaction (4.36, $^{TPhen}B_{Do}$-Amidite; 4.37, $^{TPhen}B_{Ac}$-Amidite)

To a solution of **4.34** (54.54 mg, 0.060 mmol) or **4.35** (47.87 mg, 0.060 mmol) and 1H-tetrazole in anhydrous acetonitrile (0.078 mmol) was added 2-cyanoethyl tetraisopropylphosphorodiamidite (24.8 µL, 0.078 mmol) under nitrogen atmosphere. The mixture was stirred at room temperature for 1 h. The mixture was filtered off and passed through a short basic silica gel column. The organic eluent was dried and used for oligodeoxynucleotide synthesis without further purification and characterization.

4.8.4. General Procedure for Oligonucleotide Synthesis

The synthesis of the oligonucleotide probes containing the unnatural nucleotide, triazolylphenanthrene, $^{TPhen}B_{Do}$ (ODN **1** and **7**), and triazolyl nitrobenzene, $^{TNB}B_{Ac}$ (ODN **2** and **8**) at the centre of each sequence was performed by a conventional phosphoramidite method using an automated DNA/RNA synthesizer. Synthesis was performed on a controlled pore glass (CPG) supported cartridge containing the 3'-nucleoside (dC for ODN **1** and ODN **2** and dG for ODN **7** and **8**) attached to CPG support. Synthesis was carried out automatically by sequential addition of natural and modified β-cyanoethyl phosphoramidite monomers from 3'- to 5'- direction. The monomers and most of the other reagents were prepared with 10 ppm acetonitril (p.a) and left for overnight on pre dried molecular sieves (4Å) in dark. Extended coupling (10 min, 4,5-dicyanoimidazole as activator) and oxidation (60 sec) times were used during incorporation of modified phosphoramidite monomers for achieving very good coupling yields (>90%). The unmodified phosphoramidites- DMTr-dA^{Bz}, DMTr-

dC^{Bz}, DMTr-dG^{iBu}, and DMTr-T, controlled pore glass (CPG) supported cartridges, TCA deblock, activator (4,5-dicyanoimidazole (DCI) , Cap A and Cap B solutions were purchased and used. A 1 µmol scale-solid phase synthesis of the desired ODNs was carried out in trityl-on mode using modified-phosphoramidite as the extra (fifth) phosphoramidite and programmed to cleave the trityl group from the last unmodified nucleoside. The advancement of the synthesis was monitored with a 'trityl viewer' on the basis of the outgoing trityl group produced during detritylation. The coupling yield was 90%.

After the DNA synthesis was over, the cartridges from the synthesizer was taken out and transferred into an eppendorf (2 mL). Then the oligonucleotide was cleaved from the solid support under standard conditions (conc. aq. NH_3, 55 ^oC, 12 h) by incubating the solution for at least 12 hr at 55 ^oC in a temperature-controlled incubator. After deprotection, the ammonia was evaporated in a *speed vac*, the ODN was diluted with double distilled water (0.5 mL) and the glass beads were filtered 'off' through a Whatman 0.2 µm syringe filter. Next, the solution was concentrated in a *speed vac* and made it a final solution of 1 mL. The deprotected DNA was purified from the unsuccessfully coupled sequences by reversed-phase HPLC on a 5-ODS-H column (10×150 mm, elution with 50 mM ammonium formate buffer (AF), pH 7.0, with a linear gradient over 45 min from 3% to 40% acetonitrile at a flow rate of 2.0 ml/min). The desired purified fractions were collected in 10 mL eppendorf tubes, evaporated and finally transferred into 2 mL eppendorf (**Figure 4.16**). The purified ODN was dissolved in 1 mL double-distilled water in an eppendorf tube and characterized by *m/z* value obtained from *MALDI-TOF* mass spectrometry using 2,4,6-trihydroxyacetophenon (0.5 M in EtOH)/Diammoniumcitrate (0.1 M in water) in 1:1 v/v as matrix. The *MALDI-TOF* was measured in normal positive mode with 19 KV acceleration voltage. The characterized and pure DNA stock solution (1-1.5 ml) was then kept in refrigerator at -80 °C for further studies.

(a) ODN 1: HPLC Trace of 5'-CGCAAT **X** TAACGC-3' [**X** = $^{TPhen}\mathbf{B}_{Do}$]

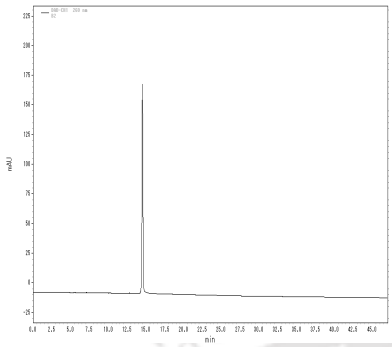

(b) ODN 7: HPLC Trace of 5'-GCGTTA **X** ATTGCG-3' [**X** = $^{TPhen}\mathbf{B}_{Do}$]

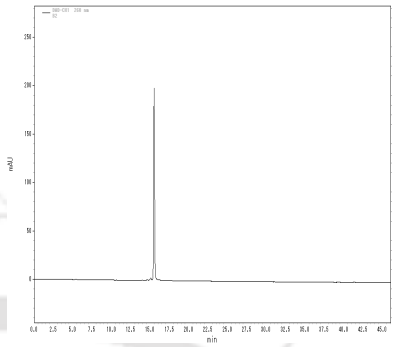

(c) ODN 2: HPLC Trace of 5'-CGCAAT **Y** TAACGC-3' [**Y** = $^{TNB}\mathbf{B}_{Ac}$]

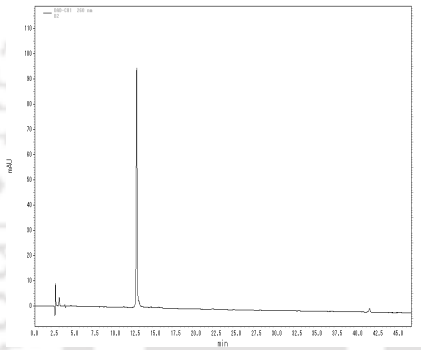

(d) ODN 8: HPLC Trace of 5'-GCGTTA **Y** ATTGCG-3' [**Y** = $^{TNB}\mathbf{B}_{Ac}$]

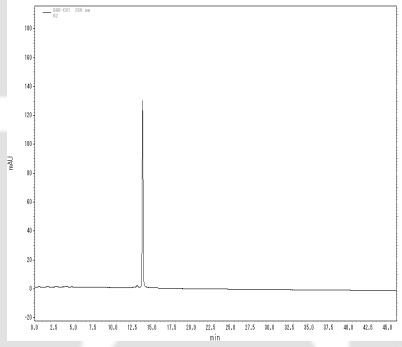

Figure 4.16: HPLC trace of purified unnatural oligonucleotides.

The concentration of the DNA stock solution was then determined applying *Lamberts-Beer's* equation: $A_{260} = \log I/I_0 = c \times \varepsilon_{260} \times l$ where $\varepsilon_{260} = \Sigma i\ \varepsilon_I$; *A260* is the absorbance of the probe at 260 nm which is determined from the intensity of the transmitted light (*I*) compared to the intensity of the emerging light (I_0), *c* is the concentration of the probe DNA, ε_{260} is the algebraic sum of extinction-coefficients of the individual nucleosides at 260 nm, (for natural nucleosides, this is calculated with Oligo Analyser) and *l* is the pathlength of the light through the sample.

The concentration of stock ODN **1**, ODN **7**, ODN **2** and ODN **8** were 609, 554, 354 and 291 μM (2 ml). All the natural complementary ODNS (ODN **3-6** and **9-12**) were purchased and used as supplied.

4.8.4 Studies of Photophysical Properties of the Oligonucleotide Probes

Preparation of ODNs solutions for thermal denaturation and spectroscopic studies: The two complementary DNA strands were mixed togather in a solution of buffer, NaCl solution, the final volume of 1 ml was made up by adding Millipore water to get a DNA solution wherein the concentration of each single strand DNA is 2.5 μM. All the DNA solutions were prepared in separate 2 ml micro centrifuge tubes which were undergone through sonication for 2 minutes, vortex mixing for 4 minutes and finally microcentrifugation for 2 minutes. In summary, first we prepared 2.5 μM DNA solutions (probe or target DNA, 1 ml) in 50 mM sodium phosphate buffer, 100 mM NaCl, pH 7.0 for melting point (T_m) determination and all other spectroscopic studies. Next, the two complementary DNA strands were hybridize just by mixing and sonicating for 5 min to get various double stranded ODNs. In all the cases the concentration of each single stranded ODN is 2. 5 μM in the above mentioned buffer and salt at pH 7.0. Thus, prepared single strand DNA and double strand DNAs solutions were used for all the spectroscopic investigations.

UV-visible and thermal melting temperature (T_m) measurements of the oligonucleotides: All UV-visible and T_ms of the ODNs (2.5 μM, final duplex concentration) were measured in 50 mM sodium phosphate buffers (pH 7.0) containing 100 mM sodium chloride. The measurements were taken in absorbance mode. The absorbance values of the sample solutions were measured in the wavelength regime of 200–500 nm with a scanning rate of 0.5 nm slit width of 2 nm. All the sample solutions were prepared just before doing the experiment. Total volume of 120 μL from a stock solution of 700 μL of 2.5 μM concentration for each set was used for UV and *Tm* experiments in 8-micro cell. Absorbance vs. temperature profiles were measured at 260 nm using Shimadzu UV-2550 UV-Visible spectrophotometer with quartz optical 8-micro cell (120 μl DNA) of 1.0 cm path length. The absorbance of the samples was monitored at 260 nm from 20 to 90 °C with a heating rate of 1 °C/min. From these profiles, average method was used to determine T_m values using in built software.

For the experiment related to the ground state complexation phenomenon the concentration of ODN **7** in 50 mM sodium phosphate buffers (pH 7.0) containing 100 mM sodium chloride was taken 15 μM.

Calculation of thermodynamic parameters: Thermodynamic parameters were determined by van't Hoff analysis using the relation: T_m^{-1} = R[ln([C_T]/4)]/ΔH+ $\Delta S°/\Delta H°$, where $\Delta H°$ and $\Delta S°$ are the standard enthalpy and entropy changes determined from UV experiments, respectively, R is the universal gas constant and [C_T] is the total strand concentration. From the slope of the plot of $1/T_m$ vs. ln([C_T], ΔH was calculated and then sustitution of this in the value of intercept yielded $\Delta S°$ and then we have calculated ΔG. Thermodynamic parameters (25 °C) were determined from van't Hoff plots using at least four to five different concentrations for each duplex. For thermal denaturation studies samples were prepared in 50 mM sodium phosphate buffers (pH 7.0) containing 100 mM sodium chloride and 0.1 mM sodium-EDTA.

Fluorescence experiments: ODNs solutions were prepared as described in UV-visible and T_m measurement experiments. Fluorescence spectra were obtained using a Fluoromax-4 fluorescence spectrophotometer at 25 °C using quartz cell of 1.0 cm path length with a slit width of 3 nm. The excitation wavelengths for single strand duplex ODN were set at λ_{abs}^{max} (~307 – 340 nm), and emission spectra were measured in the wavelength regime of 300–600 nm with an integration time of 0.2 sec. All the sample solutions were prepared just before doing the experiment. Total volume of 500 μL from a stock solution of 700 μL of 2.5 μM concentration for each set was used for fluorescence experiment in 1 ml cell. The fluorescence quantum yields (Φ_f) were determined using quinine sulphate as a reference with the known Φ_f (0.54) in 0.1 molar solution in sulphuric acid. For fluorescence experiment at two temperatures and life time measurement experiment of ODN **7** and its hybrids with ODN **2**, the concentration of ODN **7** was 15 μM in 50 mM sodium phosphate buffers (pH 7.0) containing 100 mM sodium chloride.

The fluorescence lifetime experiment was carried out using Edinburgh instrument, Life Space II time resolved fluorescence spectrophotometer time resolved fluorescence spectrophotometer at 25 °C using 1 cm path length cell. The concentration of ODN **7** was taken as 15 μM and ODN **2** were 0, 3, 6, 9, 12, 15 μM.

308 nm LED was used as excitation light source. The lifetime data were calculated by FAST software with fitting range 205 – 4000 channels.

Circular dichroism measurement: CD experiments were performed with a JASCO CD J-810 Spectropolarimeter equipped with a peltier thermoelectric type temperature control system (2.5 μM strand concentration, 50 mM sodium phosphate, 0.1 M sodium chloride, pH 7.0, room temperature). The data were collected using a 1 cm path length quartz cuvette with scanning from 380 to 200 nm, a time constant of 3 s and a wavelength step size of 0.5 nm at 25°C.

4.8.5 Theoretical Study

For the calculation of charge transfer propensity between a donor-acceptor unnatural pair or unnatural-natural nucleoside pair, ADF programme package was utilized. On the other hand, we have carried out density functional theory (DFT) for calculating the stacking interaction between a pair of nucleosides with M05-2X density functional and 6-31+G(d,p) basis set using Gaussian 09 (G 09) program package.[34, 36-37] For that purpose all the geometries of natural and unnatural bases were optimized by B3LYP/6-31+g(d,p) and stacked bases were optimized using the M05-2X density functional developed by Truhlar and Zhao.[36] The M05-2X functional is a hybrid meta GGA (generalized gradient approximations) functional having 54% Hartree–Fock exchange contribution. Because of the large Hartree–Fock exchange contribution, this functional is a better choice than other functional. This newly developed M05-2X functional has been found very suitable for studying a number of chemical problems, especially shows its wide applicability to the study of noncovalent interactions. In the present preliminary calculation, the initial starting geometries of stacked dimmers natural/unnatural hybrids in B-DNA conformation were generated using the macromodel program. From the generated structures in B-DNA conformation, we removed the sugar and phosphate backbone attached to the bases and satisfied all valences of all atoms with a hydrogen atom. In case of trimeric B-DNA duplex, the initial structure thus generated retains the B-DNA base conformation. We used the 6-31+G(d,p) basis set for geometry optimization to make these calculations feasible in the B-DNA conformation using the M05-2X density functional developed by Truhlar and Zhao.[36]

Calculation of Stacking Energy: For calculating the stacking energy of the stacked bases, natural and non-natural the monomers (single base) as well as the two intra-strand stacked bases were optimized at the M05-2X/6-31+G(d,p) level. For the stacked bases, natural and non-natural the stacking energy, ΔE was determined by:

$$\mathbf{A} + \mathbf{B} \longrightarrow \begin{matrix}\mathbf{A}\\ \vdots\\ \mathbf{B}\end{matrix}$$

$$\Delta E = E_{A...B} - (E_A + E_B)$$

where, $E_{A...B}$ is the energy of the stacked bases; E_A and E_B are the energies of the optimized single bases. Basis set superposition error (BSSE) corrections were calculated to obtain the corrected interaction energy by using the counterpoise correction procedure (CP).[37]

Calculation for Non Bonding Interaction: The obtained wave-functions at the M05-2X/6-31+G(d,p) computational level have been used to analyze the electron density within the AIM methodology by AIM2000 package.[38] It shows a potential nonbonding interaction between the pairing partners.

Calculation of Charge Transfer Possibility: The charge transfer integral for the electrons and holes in between the two molecules was calculated preliminary by Density Functional Theory using the fragment orbital approach implemented in ADF 2010.02.[35-37] The wave function of a hole can be written as a linear superposition of the highest occupied molecular orbitals (HOMOs) on the individual bases – natural and non-natural. The site energies and charge-transfer integrals were obtained from the ADF output. The charge transfer *integrals* for the natural/non-natural stacks were calculated with the generalized gradient approximation (GGA) at dispersion-corrected BLYP-D level with a TZ2P basis set.[39]

The preliminary parameters suggest that a considerable amount of charge transfer is possible between heteropair ($^{TPhen}\mathbf{B}_{Do}$: $^{TNB}\mathbf{B}_{Ac}$) as well as between several possible mispairs.

Charge transfer integrals relevant for hole or electron mobility calculations	
$^{TPhen}\mathbf{B}_{Do}$: $^{TNB}\mathbf{B}_{Ac}$ Site energy (hole) HOMO fragment 1 (eV): -5.49838 Site energy (hole) HOMO fragment 2 (eV): -5.63035 Charge transfer integral (hole) HOMO fragment 1 - HOMO fragment 2 (eV): -0.19312 Site energy (electron) LUMO fragment 1 (eV): -2.20120 Site energy (electron) LUMO fragment 2 (eV): -3.06183 Charge transfer integral (electron) LUMO fragment 1 - LUMO fragment 2 (eV): 0.06063	AIM-geometry 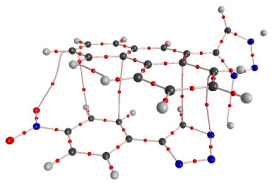

Calculation of Stacking Energy in Trimeric Duplex[40]- A Sample QM/MM Study: The QM/MM calculations were performed using the Gaussian 09 program package. The triazolyl base and the natural bases of the system (Tp$^{Phen}\mathbf{B}_{Do}$pT:Ap**C**pA) were chosen as the QM region and the sugar-phosphate parts were chosen as MM region. Multilayer ONIOM model calculation were performed, Quantum Mechanics calculation with M05-2X/6-31+G(d,p) for QM region and Molecular mechanics calculation using UFF force field for MM region. Then we have calculated the stabilization energy of the system (Tp$^{Phen}\mathbf{B}_{Do}$pT:Ap**C**pA) from the optimized geometries as follows.

$$E_{SE} = E_{Total} - (E_{T:A} + E_{PhenB4\text{-}C} + E_{T:A})$$

We observed that the system Tp$^{Phen}\mathbf{B}_{Do}$pT:Ap**C**pA is stabilized by -27.34 kcal/mol energy which imply that the stabilisation is possibly due of a combination of inter/intra strand stacking, H-bonding, and charge transfer interaction. A QM/MM calculation using multilayer ONIOM model in Gaussian 09 program package showed a is stabilization energy of -27.34 kcal/mol for the system Tp ($^{TPhen}\mathbf{B}_{Do}$) pT**:**ApCpA which imply that the stabilization is possibly due of a combination of inter/intra strand stacking, H-bonding, and charge transfer interaction.

4.8.5.1. Optimized Geometry and Coordinates

4.8.5.1.1. B3LYP/6-31+g(d,p) Optimized structure and energy of $^{TPhen}B_{Do}$

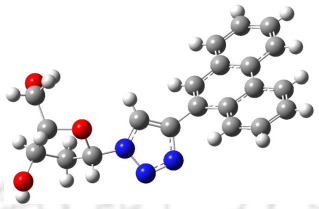

E(RB+HF-LYP) = -1201.27633645 a.u.

0 1

C	1.89480526	3.32604737	0.55665263
C	0.75380526	2.48704737	0.64265263
C	3.31480526	1.32804737	0.23365263
C	-0.25719474	0.16204737	0.71265263
C	-0.51519474	3.09204737	0.77465263
H	-1.27119474	2.55304737	0.81165263
C	2.13780526	0.52904737	0.35865263
H	2.21780526	-0.39495263	0.28965263
C	0.90280526	1.06004737	0.57565263
C	4.39180526	3.47804737	0.26665263
H	4.35780526	4.40404737	0.34865263
C	-0.75819474	-0.80495263	-0.10134737
H	-0.42519474	-1.06695263	-0.93034737
C	3.20180526	2.72604737	0.35565263
C	4.55680526	0.74104737	0.03265263
H	4.61980526	-0.18295263	-0.04434737
C	1.70780526	4.72104737	0.64365263
H	2.44480526	5.28504737	0.59165263
C	5.58780526	2.86504737	0.06165263
H	6.35780526	3.38204737	-0.00334737
C	0.45780526	5.25604737	0.80365263
H	0.36380526	6.17804737	0.88265263
C	5.68780526	1.50204737	-0.05434737
H	6.51480526	1.10104737	-0.18834737
C	-0.66219474	4.45704737	0.85365263
H	-1.50719474	4.83504737	0.93865263
N	-1.82819474	-1.30395263	0.53165263
N	-2.01319474	-0.68795263	1.71265263
N	-1.05719474	0.20404737	1.82565263
O	-2.86819474	-2.26395263	-1.27534737
O	-4.57219474	-4.77795263	-0.08734737
H	-4.52719474	-5.09395263	0.66965263
O	-1.41819474	-4.44495263	-2.77734737
H	-0.87519474	-3.84495263	-2.65234737
C	-2.78519474	-2.31695263	0.13665263
H	-3.66019474	-2.12295263	0.53165263
C	-2.39719474	-3.74995263	0.42065263
H	-2.61219474	-3.99995263	1.33265263
H	-1.45219474	-3.89695263	0.26365263
C	-3.37419474	-3.51595263	-1.75334737
H	-4.32619474	-3.40295263	-1.95534737
C	-3.24519474	-4.51195263	-0.57334737

H	-2.80219474	-5.33795263	-0.85734737
C	-2.67719474	-3.88995263	-3.00534737
H	-3.22219474	-4.52895263	-3.48934737
H	-2.58019474	-3.10095263	-3.55934737

4.8.5.1.2. B3LYP/6-31+g(d,p) Optimized structure and energy of $^{TNB}B_{Ac}$

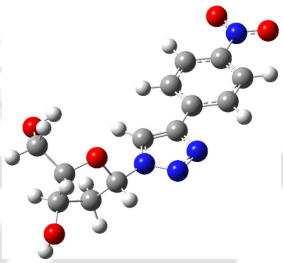

E(RB+HF-LYP) = -1098.85672180 a.u.

0 1

C	-4.41226000	-0.98955300	-0.32237600
C	-3.07875400	-1.37918700	-0.38727400
C	-3.72095600	1.22841500	0.41506600
C	-0.65020900	-0.90937300	-0.12779400
C	-2.39194900	0.82644800	0.34645600
H	-1.61622100	1.53852400	0.60989000
C	-2.04961000	-0.47851500	-0.05442100
C	0.51999000	-0.21182700	0.11898500
H	0.71835100	0.80647800	0.41052400
C	-4.71831100	0.31172000	0.07901800
N	1.50949400	-1.11188700	-0.10501900
N	0.98880600	-2.30917500	-0.47812900
N	-0.30214800	-2.18922700	-0.48584800
O	3.35673200	0.02389900	-0.97404800
O	5.94686600	-0.62185800	1.10766600
H	6.18494600	-0.63879900	2.04374900
O	3.90605800	2.77874900	-0.46392800
H	3.03203900	2.54861300	-0.80680400
C	2.94753700	-0.95344900	-0.02401400
H	3.35644300	-1.93943400	-0.27162300
C	3.47962000	-0.42889700	1.31656100
H	3.60615000	-1.22235400	2.05740100
H	2.79202400	0.32111000	1.71961700
C	4.68031800	0.45967500	-0.60741000
H	5.42793000	-0.17451500	-1.10441400
C	4.81480900	0.23009600	0.92091800
H	4.95918100	1.17915300	1.44803700
C	4.84558700	1.89963400	-1.07287200
H	5.84022600	2.25577800	-0.78822300
H	4.76997300	1.94028100	-2.16768500
H	-3.99394100	2.23019700	0.72251900
H	-5.21214700	-1.67407000	-0.57633700
H	-2.81828500	-2.38492000	-0.69639500
N	-6.12503400	0.72961000	0.15074100
O	-6.98777800	-0.09872000	-0.14835500
O	-6.36430000	1.88637900	0.50647300

4.8.5.1.3. ONIOM(M05-2x/6-31+g(d,p):uff) Optimized structure of "$Tp^{Phen}B_{Do}$pT:ApCpA" system

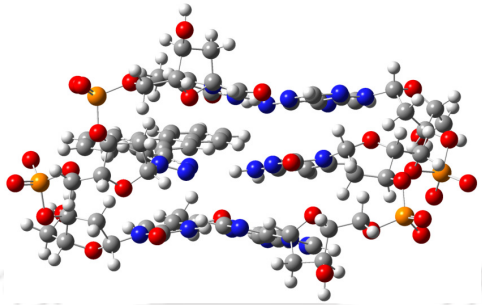

Oniom Total Energy = -3018.20412865 a.u. and E_{SE} = -27.3434345 kcal/mol

6	-9.042736	2.558467	-3.844561
6	-8.148142	1.324497	-4.009138
8	-6.879125	1.709335	-4.476937
6	-7.962519	0.561921	-2.703072
8	-8.960182	-0.43368	-2.579502
6	-6.590141	-0.041756	-2.868945
6	-5.963851	0.729566	-4.033006
7	-4.688371	1.320901	-3.653577
6	-3.603355	0.454547	-3.460135
8	-3.718457	-0.762432	-3.407372
7	-2.384142	1.063816	-3.334933
6	-2.124083	2.409011	-3.265145
8	-0.972862	2.820876	-3.095103
6	-3.286823	3.276545	-3.406393
6	-3.083666	4.761082	-3.367405
6	-4.489521	2.697177	-3.587889
1	-1.572259	0.407346	-3.182041
15	8.060549	-4.020358	-1.866673
8	8.987439	-5.214538	-1.803919
8	8.743408	-2.867822	-2.900735
8	6.534764	-4.479122	-2.475011
6	6.140595	-5.683389	-1.857168
6	4.671733	-5.978053	-2.179913
8	3.855988	-4.924281	-1.723282
6	4.427566	-6.166264	-3.671602
6	3.000423	-5.720273	-3.825011
6	2.781089	-4.794354	-2.63005
7	2.674969	-3.423772	-3.059597
6	3.701392	-2.612669	-3.490558
7	3.333127	-1.375356	-3.689007
6	1.990753	-1.373634	-3.370632
6	1.022783	-0.352868	-3.381952
7	1.304649	0.911174	-3.748598
7	-0.229515	-0.67778	-3.033493
6	-0.516402	-1.949286	-2.694521
7	0.305036	-2.981575	-2.639916
6	1.554236	-2.634929	-2.973865
1	0.610152	1.634006	-3.595528
1	2.266218	1.153934	-3.909993
1	-10.013097	2.256871	-3.389405
1	-9.244072	2.99447	-4.848305
1	-8.613391	0.656375	-4.770608

1	-7.950453	1.28685	-1.857733
1	-6.008175	0.069892	-1.931769
1	-6.654476	-1.122122	-3.125743
1	-5.795334	0.031048	-4.88498
1	-4.041786	5.282057	-3.387485
1	-2.543512	5.053528	-2.467757
1	-2.486639	5.083002	-4.223375
1	-5.359055	3.338118	-3.660615
1	6.762393	-6.52781	-2.230266
1	6.236739	-5.624641	-0.748361
1	4.374356	-6.903706	-1.635476
1	5.093007	-5.507946	-4.278019
1	2.838968	-5.212468	-4.801846
1	2.31036	-6.591064	-3.753934
1	1.846202	-5.09758	-2.107822
1	4.700916	-2.984221	-3.647771
1	-1.555935	-2.127843	-2.456352
15	-9.169825	-0.829686	-0.931095
8	-10.236028	-1.897158	-0.813722
8	-9.692347	0.536153	-0.081293
8	-7.694531	-1.370128	-0.260804
6	-7.524273	-2.734515	-0.572974
6	-6.103332	-3.184843	-0.215449
8	-5.159544	-2.412341	-0.917938
6	-5.802839	-3.073189	1.275116
8	-6.198436	-4.258415	1.93803
6	-4.30701	-2.896627	1.272144
6	-4.006359	-2.326024	-0.109201
15	9.354306	1.774242	-0.693713
8	10.631323	1.056431	-1.070605
8	8.91907	2.792182	-1.973602
8	8.101094	0.644858	-0.434858
6	8.546418	-0.319022	0.493005
6	7.40894	-1.295205	0.81728
8	6.238825	-0.595245	1.165321
6	7.082651	-2.202954	-0.358636
8	7.890279	-3.363441	-0.300748
6	5.62743	-2.520452	-0.126262
6	5.148793	-1.437481	0.844379
1	-8.246588	-3.353715	0.004824
1	-7.671938	-2.922742	-1.661836
1	-5.987003	-4.24569	-0.537465
1	-6.289439	-2.157307	1.684369
1	-3.983497	-2.220222	2.09048
1	-3.797359	-3.878748	1.384049
1	-3.200226	-2.93237	-0.581428
1	9.402503	-0.899514	0.080169
1	8.869108	0.158188	1.443445
1	7.719211	-1.913311	1.691971
1	7.187423	-1.62243	-1.306949
1	5.073693	-2.498871	-1.087475
1	5.505344	-3.522393	0.340864
1	4.815819	-1.91557	1.794066
15	-6.271728	-3.975531	3.622093
8	-6.864472	-5.191641	4.299171
8	-7.269284	-2.647346	3.94661
8	-4.710556	-3.660229	4.235942

6	-3.979861	-4.866123	4.264022
6	-2.500103	-4.577871	4.546829
8	-1.976394	-3.712146	3.567704
6	-2.276825	-3.940014	5.911124
6	-1.017252	-3.141834	5.699076
6	-0.940206	-2.970305	4.179243
7	-1.048037	-1.5719	3.807489
6	0.102776	-0.867077	3.425283
8	1.231264	-1.31766	3.468628
7	-0.139955	0.422682	3.010899
6	-1.31319	1.128281	3.088418
8	-1.358523	2.321523	2.783292
6	-2.462303	0.376785	3.576376
6	-3.770142	1.091121	3.739247
6	-2.264526	-0.912727	3.909818
1	0.715064	0.960307	2.772997
6	9.136873	5.890975	0.953909
6	8.838069	4.678677	1.8429
8	7.782214	4.972329	2.730359
6	8.469018	3.439906	1.035838
8	9.633714	2.705013	0.711717
6	7.602178	2.696976	2.009546
6	6.994586	3.805047	2.863296
7	5.63111	4.070792	2.471676
6	5.084493	5.284502	2.098539
7	3.787935	5.243668	1.961849
6	3.455182	3.941394	2.271793
6	2.212937	3.27782	2.341057
7	1.049481	3.893845	2.087266
7	2.221672	1.97644	2.668548
6	3.384317	1.36465	2.942464
7	4.601422	1.89311	2.944054
6	4.576854	3.188449	2.599416
1	0.177887	3.406814	2.289135
1	1.053259	4.896592	2.012232
1	-4.371507	-5.53304	5.06441
1	-4.036861	-5.402167	3.28862
1	-1.942038	-5.541165	4.491298
1	-3.115722	-3.254971	6.177546
1	-1.065906	-2.171288	6.241007
1	-0.127641	-3.706187	6.058789
1	0.023844	-3.399995	3.824404
1	-4.561627	0.389919	4.009778
1	-3.696499	1.855555	4.515347
1	-4.042564	1.60167	2.814721
1	-3.095268	-1.486517	4.301673
1	9.935536	5.628632	0.223999
1	9.503467	6.724872	1.593257
1	9.746709	4.465209	2.451511
1	7.858223	3.741745	0.151187
1	6.845201	2.082135	1.47979
1	8.22203	2.040738	2.659549
1	7.001369	3.494361	3.931426
1	5.681681	6.167369	1.932583
1	3.296696	0.312172	3.191111
7	-3.584649	-0.954074	-0.016228
6	-4.356858	0.122768	0.283649
6	-3.533235	1.205819	0.042193

7	-2.325894	0.691741	-0.362954
7	-2.372468	-0.59119	-0.403644
1	-5.356998	0.018645	0.660358
6	-2.521305	3.393511	0.146256
6	-3.67815	2.674348	0.123981
1	-1.573775	2.873318	0.149042
6	-4.961231	4.800116	0.207456
6	-4.94833	3.378795	0.136244
6	-6.188501	2.706365	0.06546
6	-7.388773	3.384817	0.10346
6	-7.3988	4.782395	0.201114
6	-6.203985	5.467202	0.243055
1	-6.206425	1.635207	-0.041938
1	-8.322528	2.840682	0.054546
1	-8.336608	5.322241	0.235575
1	-6.230457	6.545484	0.306749
6	-3.711121	5.544258	0.216156
6	-2.501594	4.820255	0.17067
6	-1.266744	5.503015	0.111479
6	-1.223642	6.879126	0.115542
6	-2.425594	7.607197	0.183162
6	-3.640681	6.954515	0.229565
1	-0.359021	4.915564	0.039488
1	-0.275232	7.398906	0.058828
1	-2.400317	8.68989	0.188895
1	-4.541652	7.55032	0.266851
6	1.805092	0.722713	-0.371881
7	1.660665	-0.53908	-0.030887
7	4.035136	-0.683685	0.28644
6	4.166446	0.607121	-0.145963
6	3.094776	1.342432	-0.517978
1	5.154529	1.044836	-0.199486
1	3.207686	2.362889	-0.853407
1	0.755991	2.329432	-1.071044
7	0.693123	1.459012	-0.57146
1	-0.197792	0.980126	-0.615165
6	2.74587	-1.326593	0.216477
8	2.67125	-2.535407	0.379028
8	-2.105507	-4.922856	6.898351
1	-2.113381	-4.448621	7.770458
8	7.981165	6.29742	0.273189
1	8.247856	7.076102	-0.281028
8	-8.410891	3.516473	-3.039479
1	-9.053244	4.267161	-2.948057
8	4.590475	-7.511199	-4.038378
1	4.562578	-7.536777	-5.03041

4.8.5.1.4. Optimized Structure and Energy of Stacked form: M05-2X/6-31+G(d,p)

Optimized Structure and Energy of A : $^{TPhen}B_{Do}$ (without sugar unit)

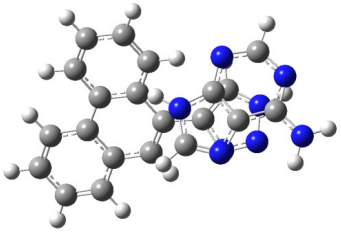

BSSE Corrected Total Energy = -1247.86116255 a.u.

0 1

N	1.44658300	0.86729100	1.70021100
C	1.56515900	-0.28303700	2.44398600
N	2.64836900	-0.96245400	2.18146400
C	3.26730900	-0.22865100	1.19393800
C	4.42849200	-0.45415300	0.43236200
N	5.19978200	-1.54199200	0.62246100
N	4.76901400	0.43967400	-0.50777600
C	3.98756100	1.51891500	-0.67366900
N	2.86190100	1.83519000	-0.04473000
C	2.53979800	0.91490000	0.87667900
H	5.93763700	-1.72087600	-0.03569700
H	4.83241400	-2.29894300	1.17348400
H	0.81363100	-0.56642400	3.16395100
H	4.32147400	2.21736500	-1.43339000
N	2.30723000	-1.12331000	-1.95320300
N	2.09745200	-2.16799900	-1.15644000
N	0.92438100	-2.02870700	-0.63983800
C	0.35489100	-0.86881800	-1.09335000
C	1.25694800	-0.27651200	-1.95326400
H	1.23473000	0.62054500	-2.54564400
C	-1.89407000	-1.52917700	-0.47760700
C	-1.01739400	-0.51017700	-0.69146300
H	-1.55434200	-2.54966400	-0.60631900
C	-2.80103800	1.12426100	-0.13991600
C	-1.45214500	0.86168800	-0.50029200
C	-0.55729300	1.95007100	-0.62386300
C	-0.97158800	3.25015200	-0.42153000
C	-2.31046500	3.51196500	-0.09242500
C	-3.19802500	2.46650800	0.04712000
H	0.48454400	1.77225800	-0.84846900
H	-0.25777400	4.05952100	-0.51369100
H	-2.64615900	4.52975300	0.06199400
H	-4.21993600	2.69175400	0.31683600
C	-3.73200500	0.02116500	0.05072400
C	-3.25533900	-1.30026200	-0.10239300
C	-4.12780200	-2.39299800	0.09437500
C	-5.44660500	-2.18973900	0.43267000
C	-5.92848500	-0.87690100	0.58020800
C	-5.08955300	0.20239800	0.39332400
H	-3.73719000	-3.39658300	-0.02805100
H	-6.10985800	-3.03230800	0.58249600

H	-6.96570300	-0.70904000	0.84237800
H	-5.49656800	1.19637000	0.51347200
H	0.66430000	1.50295100	1.68380500
H	3.20570700	-1.01013000	-2.39585800

4.8.5.1.5. Optimized Structure and Energy of Stacked form: M052x/6-31+g(d,p)

Optimized Structure and Energy of A:$^{TNB}B_{Ac}$ (without sugar unit)

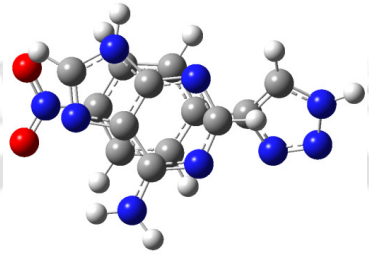

Corrected Total Energy = -1145.06064467 a.u.

0 1

N	-1.61110800	1.88307900	-1.72356900
C	-2.73096300	1.55091400	-0.99543400
N	-2.49433700	1.42359800	0.28195200
C	-1.14521000	1.68740600	0.40065700
C	-0.27490800	1.70790200	1.50654700
N	-0.70021200	1.42379700	2.75204100
N	1.01438700	2.00757100	1.30619200
C	1.42303400	2.26077800	0.05623400
N	0.71549300	2.25918100	-1.07031500
C	-0.57101900	1.97265400	-0.83355600
H	-0.05748400	1.52915800	3.51685000
H	-1.67934800	1.27593000	2.92295400
H	-3.68999900	1.40026000	-1.46567300
H	2.47651900	2.49721100	-0.04286900
N	4.60087200	-0.35728000	-0.67683500
N	4.65157600	-1.05427900	0.45828300
N	3.45112700	-1.43549900	0.72937700
C	2.60178400	-0.98840400	-0.24098300
C	3.34447900	-0.28077400	-1.16202100
H	3.08097000	0.27293600	-2.04668800
C	-1.57059000	-1.62981900	-0.08849900
C	-0.98654000	-1.33670800	-1.31409100
C	0.38636700	-1.14406700	-1.36163900
C	1.15991800	-1.24322800	-0.19937000
C	0.54592000	-1.56915800	1.01524800
C	-0.82682000	-1.76464100	1.07708300
H	-1.60280500	-1.26232100	-2.19830400
H	0.86088500	-0.91521800	-2.30754300
H	1.15268000	-1.63944900	1.90805800
H	-1.32514700	-1.99253800	2.00803100
N	-3.02679600	-1.77366300	-0.02070000
O	-3.66431300	-1.55901700	-1.03809300
O	-3.51669200	-2.09270700	1.04498300
H	5.44950600	0.03430600	-1.05049900
H	-1.55747900	2.04084400	-2.71549000

4.8.5.1.6. Optimized Structure and Energy of Stacked form: M052x/6-31+g(d,p)

Optimized Structure and Energy of $^{TPhen}B_{Do}$: $^{TNB}B_{Ac}$ (without sugar unit)

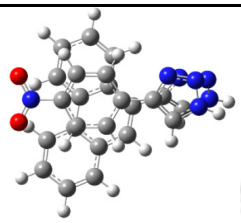

Top view

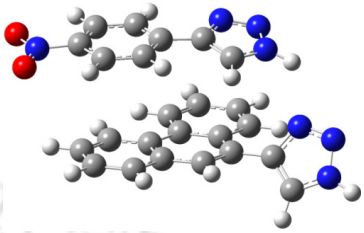

Side view

E(RM052X) = -1458.31152230 a.u.

0 1

C	2.49910800	1.25857500	0.83085400
N	4.64593800	0.65446100	0.94638300
N	4.63545400	1.96400000	0.76216800
C	1.04558200	1.40138500	0.65354200
C	0.59810300	2.18265200	-0.36984100
C	0.09648000	0.73000600	1.51909800
C	-0.79579000	2.37269900	-0.63150100
H	1.30866500	2.65499100	-1.04137000
C	-1.29345600	0.89203000	1.28299200
C	0.52562100	-0.07008000	2.59983000
C	-1.21235800	3.16774400	-1.72100800
C	-1.75394700	1.73416400	0.18784900
C	-2.19869300	0.21433300	2.12644300
H	1.58328800	-0.16061800	2.80500200
C	-0.38326600	-0.72377600	3.40396700
C	-2.55124800	3.33179000	-2.00037000
H	-0.45895000	3.64695100	-2.33654000
C	-3.11901700	1.92622500	-0.11490800
C	-1.75788700	-0.58658900	3.15825500
H	-3.26378900	0.31029900	1.96853300
H	-0.03499900	-1.33614600	4.22610100
C	-3.50941800	2.70337000	-1.18606700
H	-2.86496700	3.93986500	-2.83943900
H	-3.88627100	1.45013600	0.47813200
H	-2.47826900	-1.10329500	3.77953400
H	-4.56366200	2.82206500	-1.40150000
N	3.94809900	-1.31290400	-1.82892200
C	2.69271800	-0.86473900	-2.02785500
C	1.91147200	-1.77623900	-1.34802700
N	2.74589800	-2.70096200	-0.78885800
N	3.96834300	-2.41230400	-1.08115300
H	2.47063100	0.03183400	-2.57930900
C	-2.24110700	-1.82268200	-0.58430200
C	-1.41030300	-2.66846100	0.14118100
C	-0.05240700	-2.66044200	-0.13575300
C	0.46382700	-1.81136800	-1.12366100
C	-0.40168600	-0.98638100	-1.85018000
C	-1.76356300	-0.98258800	-1.58328600
H	-1.82714300	-3.29676000	0.91490400

H	0.62512000	-3.29560000	0.41832000
H	-0.01392000	-0.33200800	-2.62088400
H	-2.44366600	-0.33062800	-2.11354100
N	-3.66353200	-1.77853300	-0.24655600
O	-4.37778300	-1.03027800	-0.89065300
O	-4.05352000	-2.47582200	0.67291600
H	3.08602300	3.29269000	0.60226100
H	4.82177300	-0.89407700	-2.10476700
N	3.36411800	0.21009400	1.00038700
C	3.34140200	2.33824000	0.68693300
H	5.49933500	2.48292600	0.75721800

4.9. ^{1}H and ^{13}C NMR Spectra

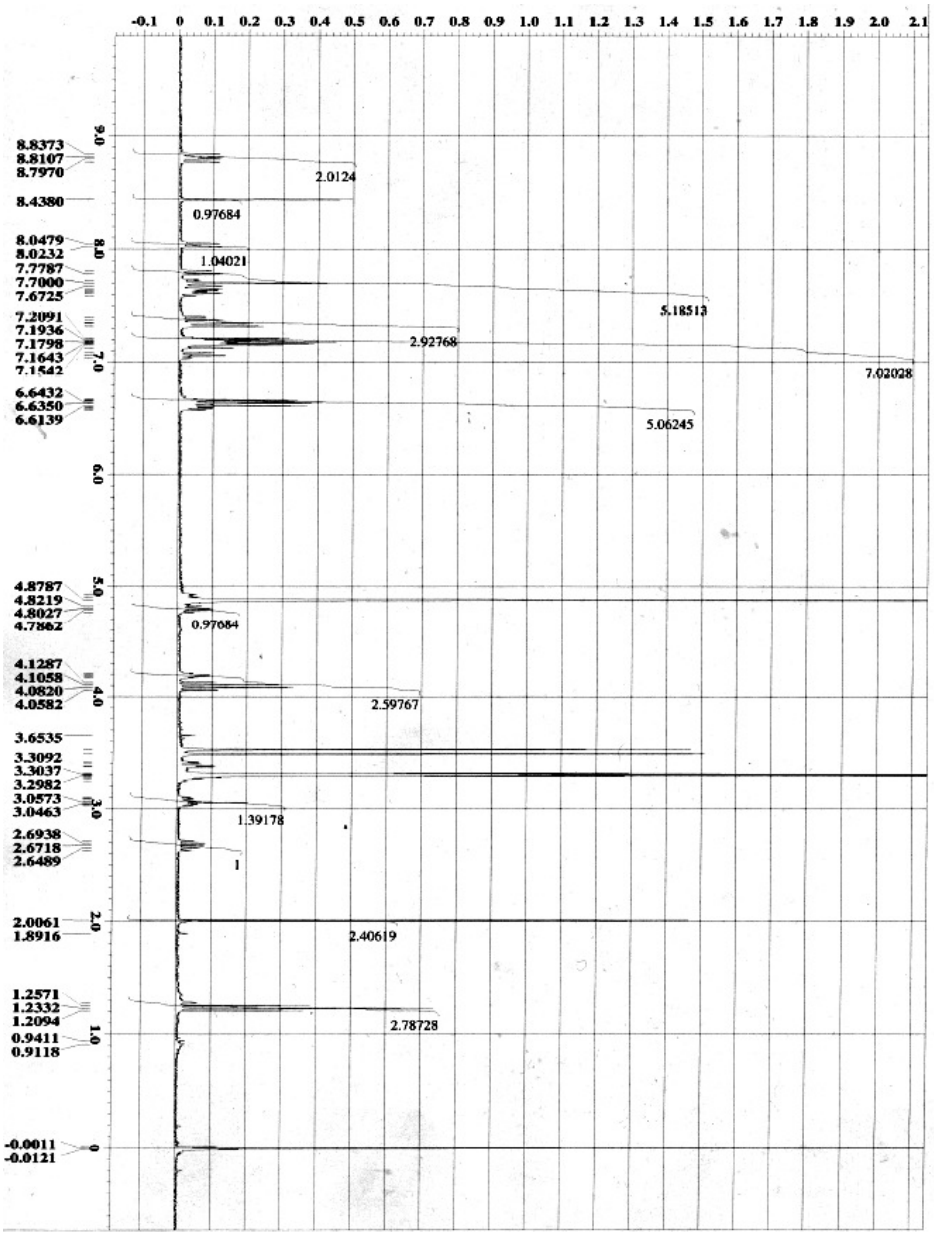

^{1}H NMR spectra of $^{TPhen}\mathbf{B_{Do}}$-**DMTr** nucleoside **4.34.**

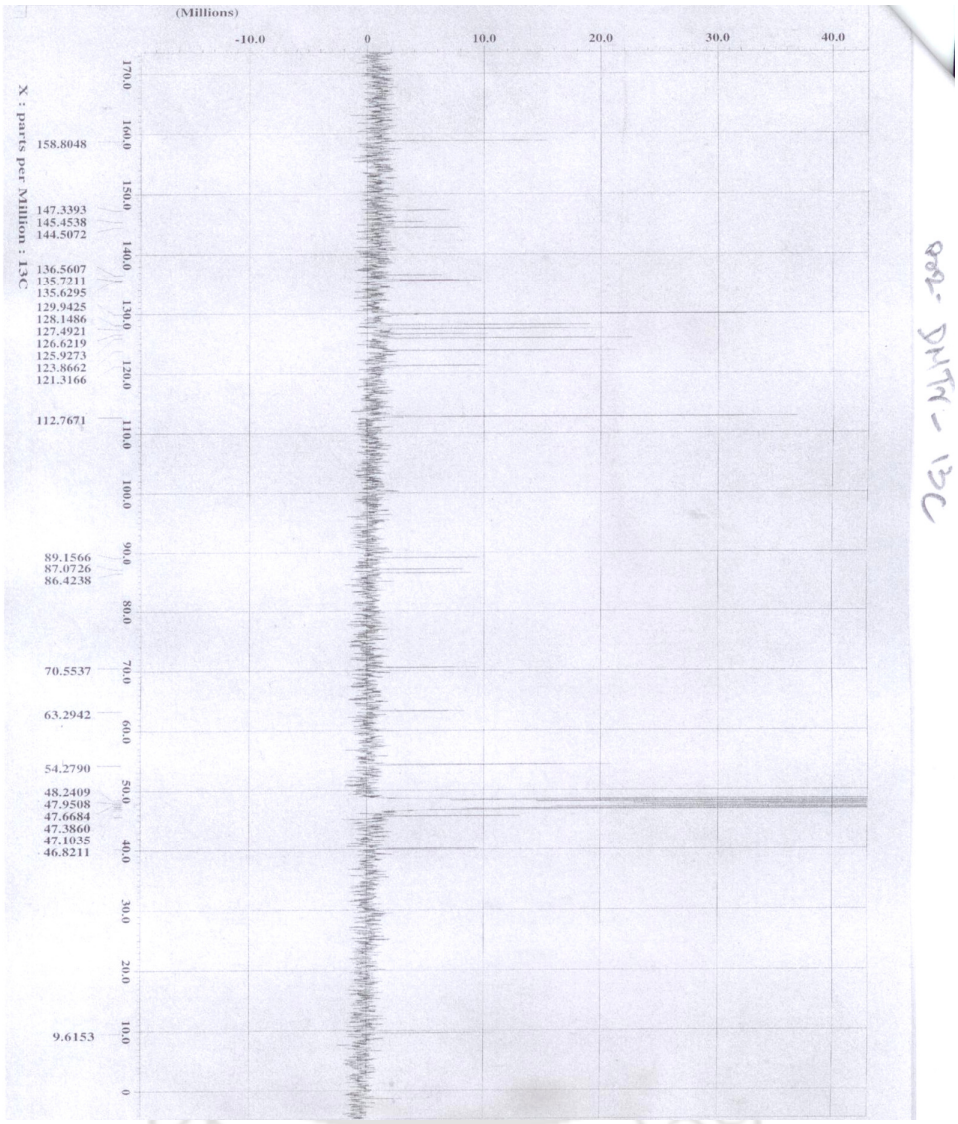

^{13}C NMR spectra of $^{TPhen}B_{Do}$-**DMTr** nucleoside **4.34.**

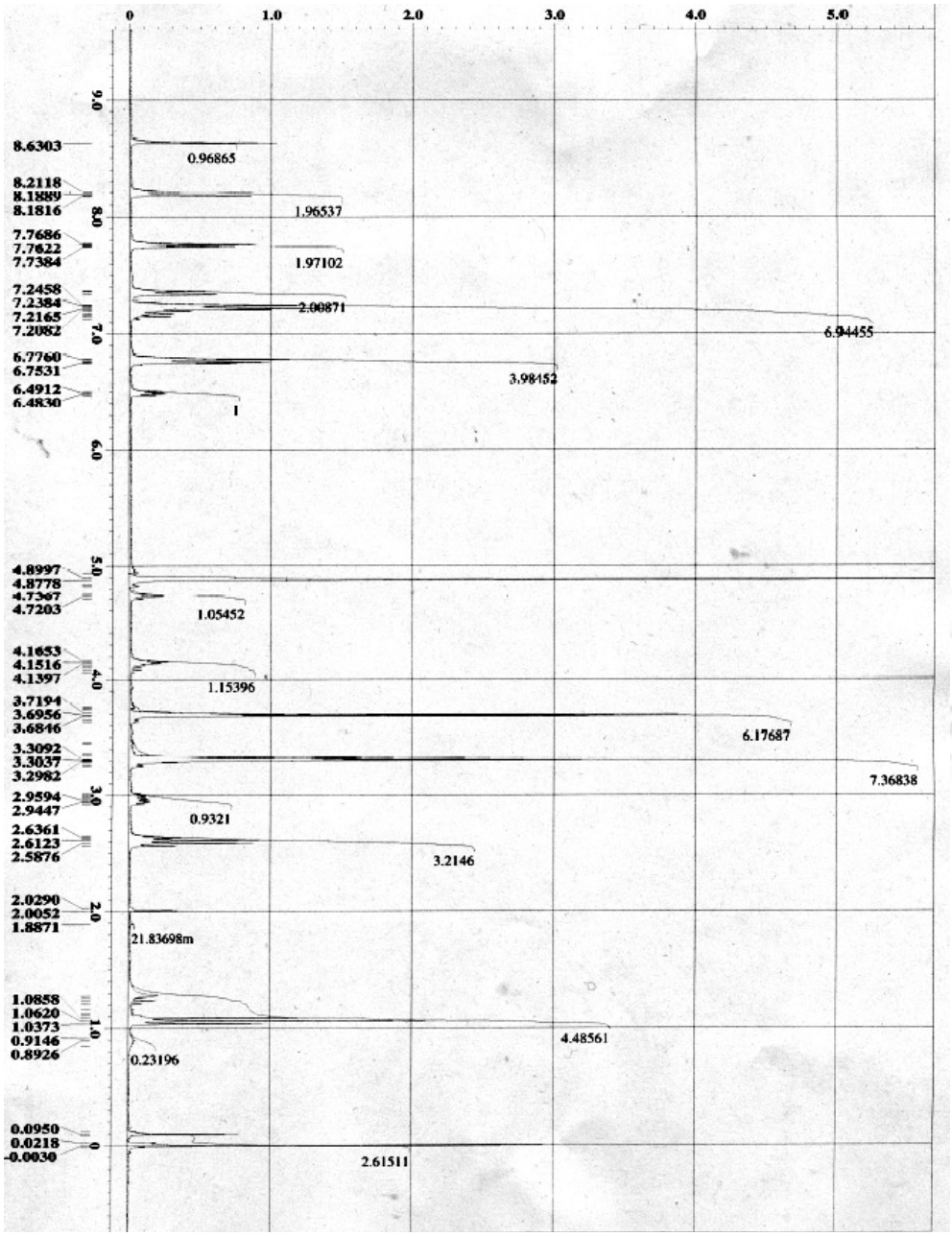

^{1}H NMR spectra of $^{TNB}\mathbf{B}_{\mathbf{Ac}}$**-DMTr** nucleoside **4.35**.

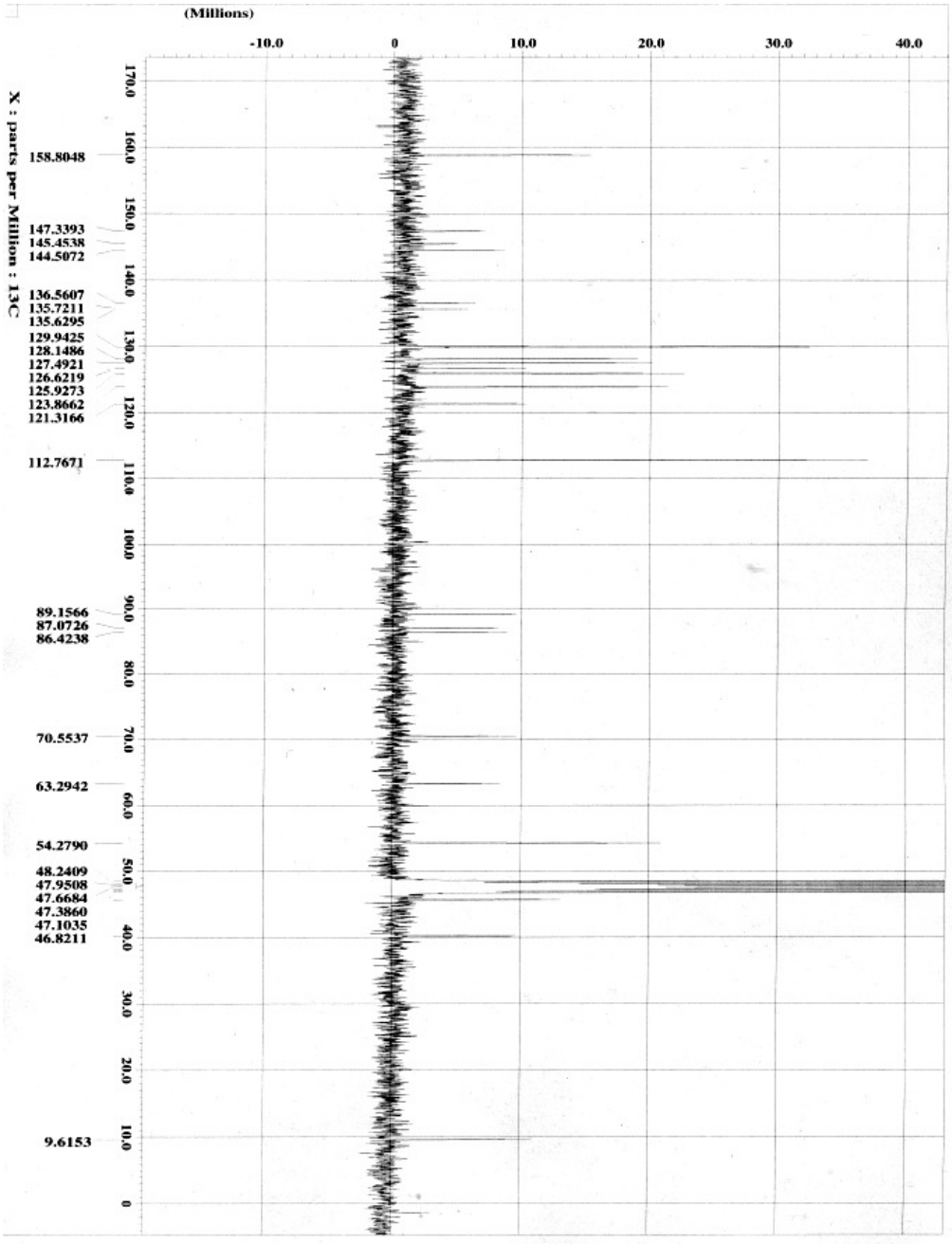

^{13}C NMR spectra of $^{TNB}\mathbf{B_{Ac}}$ **-DMTr** nucleoside **4.35**.

4.10. References

1. (a) Santa Lucia, J.; Kierzek, R.; Turner, D. H. *Science* **1992**, *256*, 217. (b) Cantor, C. R.; Schimmel, P. R. *Biophysical Chemistiy Part III: The Behavior of Biological Macromolecu1es;'W.* H. Freeman: -Sari Francisco, **1980**; 1117. (c) Petersheim, M.; Turner, D. H. *Biochemistry* **1983**, *22*, 256.

2. Rich, A.; Kasha, M.; Pullmann, B. *Horizons in Biochemistry.***1962**, 103.

3. (a) Switzer, C.; Moroney, S. E.; Benner, S. A. *J. Am. Chem. Soc.* **1989**, *111*, 8322. (b) Switzer, C.Y.; Moroney, S. E.; Benner, S. A. *Biochemistry* **1993**, *32*, 10489.

4. (a) Piccirilli J. A.; Krauch, T.; Moroney, S. E.; Benner, S. A. *Nature* **1990**, *343*, 33. (b) Yang, Z.; Hutter, D.; Sheng, P.; Sismour, A. M.; Benner, S. A. *Nucleic Acids Res.* **2006**, *34*, 6095. (c) Hirao, I.; Kimoto, M.; Mitsui, T.; Fujiwara, T.; Kawai, R.; Sato, A.; Harada, Y.; Yokoyama, S. *Nat. Methods* **2006**, *3*, 729. (d) Doi, Y.; Chiba, J.; Morikawa, T.; Inouye, M. *J. Am. Chem. Soc.* **2008**, *130*, 8762. (e) Delaney, J. C.; Gao, J.; Liu, H.; Shrivastav, N.; Essigmann, J. M.; Kool, E. T. *Angew. Chem., Int. Ed.* **2009**, *48*, 4524.

5. (a) Smith, S. A.; Rajur, S. B.; McLaughlin, L. W. *Nat. Struct. Biol.* **1994**, *1*, 198. (b) Lesser, D. R.; Kurpiewski, M. R.; Jen-Jacobson, L. *Science* **1990**, *250*, 776. (c) Kornberg, A.; Baker, T. A. *DNA Replication*, 2nd ed.; W. H.Freeman: New York, **1992**. (d) Echols, H.; Goodman, M. F. *Ann. Rev. Biochem.* **1991**, *60*, 477. (e) Strazewski, P.; Tamm, C. *Angew. Chem. Int. Ed. Engl.* **1990**, *29*, 36.(f) Seo, Y. J.; Matsuda, S.; Romesberg, F. E. *J. Am. Chem. Soc.* **2009**, 131, 5046. (g) Teo, Y. N.; Wilson, J. N.; Kool, E. T. *J. Am. Chem. Soc.* **2009**, 131, 3923.

6. (a) Kempe, T.; Sundquist, W. I.; Chow, F.; Hu, S. L. *Nucleic Acids Res.* **1985**, *13*, 45. (b) Zischler, H.; Nanda, I.; Schafer, R.; Schmid, M.; Epplen, J. T. *Hum. Genet.* **1989**, *82*, 227 (c) Hustedt, E. J.; Spaltenstein, A.; Kirchner, J. J.; Hopkins, P.B.; Robinson, B. H. *Biochemistry* **1993**, *32*, 1774. (d) Haugland, R. P. *The Handbook: A Guide to Fluorescent Probes and Labeling Technologies*; Molecular Probes. **2005**. (e) Okamoto, A.; Saito, Y.; Saito, I. *J. Photochem. Photobiol. C* **2005**, *6*, 108. (f) Bag, S. S.; Kundu, R.;

Matsumoto, K; Saito, Y.; Saito, I. *Bioorg. Med. Chem. Lett.* **2010**, *20*, 3227. (g) Teo, Y. N.; Kool, E. T. *Chem. Rev.* **2012**, *112*, 4221.

7. (a) Schweitzer, B. A.; Kool, E. T. *J. Am. Chem. Soc.* **1995**, *117*, 1863. (b) Kool, E. T. *Annu. Rev. Biochem.* **2002**, *71*, 191. (c) Seo, Y. J.; Matsuda, S.; Romesberg, F. E. *J. Am. Chem. Soc.* **2009**, 131, 5046. (d) Jarchow-Choy, S. K.; Sjuvarsson, E.; Sintim, H. O.; Eriksson, S.; Kool, E. T. *J. Am. Chem. Soc.* **2009**, *131*, 5488.

8. Moran, S.; Ren, R. X.-F.; Rumney IV, S.; Kool, E. T. *J. Am. Chem. Soc*. **1997**, *119*, 2056.

9. Guckian, K. M.; Morales, J. C.; Kool, E. T. *J. Org. Chem.* **1998**, *63*, 9652.

10. O'Neill, B. M.; Ratto, J. E.; Good, K. L.; Tahmassebi, D. C.; Helquist, S. A.; Morales, J. C.; Kool, E. T. *J. Org. Chem.* **2002**, *67*, 5869.

11. (a). Guckian, K. M.; Schweitzer, B. A.; Ren, R. X.-F.; Sheils, C. J.; Paris, P. L.; Tahmassebi, D. C.; Kool, E. T. *J. Am. Chem. Soc.* **1996**, *118*, 8182. (b) Guckian, K. M.; Schweitzer, B. A.; Ren, R. X.-F.; Tahmassebi, D. C.; Kool, E. T. *J. Am. Chem. Soc*. **2000**, *122*, 2213.

12. Chaudhuri, N. C.; Kool, E. T. *Tetrahedron Lett.* **1995**, *36*, 1795.

13. Moran, S.; Ren, R. X.; Sheils, C. J.; Rumney, S. t.; Kool, E. T. *Nucleic Acids Res.* **1996**, *24*, 2044.

14. Durland, R. H.; Rao, T. S.; Bodepudi, V.; Seth, D. M.; Jayaraman, K.; Revankar, G. R. *Nucleic Acids Res.* **1995**, *23*, 647.

15. Ren, R. X. F.; Chaudhuri, N. C.; Paris, P. L.; Rumney, S.; Kool, E. T. *J. Am. Chem. Soc.* **1996**, *118*, 7671.

16. Matray, T. J.; Kool, E. T. *J. Am. Chem. Soc.* **1998**, *120*, 6191.

17. Wojciechowski, F.; Lietard, J.; Leumann, C. J.; *Org. Lett.* **2012**, *14*, 5176.

18. Brotschi, C.; Haberli, A.; Leumann, C. J. *Angew. Chem. Int. Ed*. **2001**, *40*, 3012.

19. Brotschi, C.; Leumann, C. J. *Angew. Chem. Int. Ed.* **2003**, *42*, 1655.

20. Langenegger, S. M.; Häner, R. *Helv. Chim. Acta* **2002**, *85*, 3414.

21. (a) Bustin, S.A. *J. Mol. Endrocrinol.* **2000**, *25*, 169. (b) Ferrė, F., Ed. *Gene Quantification*, Birkhauser: Basel, **1998**.

22. Marras, S. A. E.; Kramer, F. R.; Tyagi, S. *Nucleic Acids Res.* **2002**, *30*, e122.

23. Tyagi, S.; Kramer, F. R. *Nat.Biotechnol.* **1996**, *14*, 303.

24. (a) Lakowicz, J. R. Principles of Fluorescence Spectroscopy, 3rd. ed.; Springer: New York, **2006**; (b) Bernacchi, S.; Mely, Y. *Nucleic Acids Res.* **2001**, *29*, e62.

25. (a) Morrison, L.E.; Stols, L.M. *Biochemistry* **1993**, *32*, 3095. (b) Li, Q.; Luan, G.; Guo, Q.; Liang, J. *Nucleic Acids Res.* **2002**, *30*, e5. (c) Nazarenko, I.; Pires, R.; Lowe, B.; Obaldy, M.; Rashtchian, A. *Nucleic Acids Res.* **2002**, *30*, 2089. (d) Johansson, M. K.; Fidder, H.; Dick, D.; Cook, R. M. *J. Am. Chem. Soc.* **2002**, *124*, 6950.

26. (a) You, Y.; Tataurov, A. V.; Owczarzy, R. *Biopolymers* **2011**, *95*, 472. (b) Moreira, B. G.; You, Y.; Behlke, M. A.; Owczarzy, R. *Biochem. Biophys. Res. Commun.* **2005**, *327*, 473.

27. (a) Zahn, A.; Leumann, C. J. *Chem. Eur. J.* **2008**, *14*, 1087. (b) Grigorenko, N. A.; Leumann, C. J. *Chem. Eur. J.* **2009**, *15*, 639.

28. (a) Wagenknecht, H. A. *Nat. Prod. Rep.* **2006**, *23*, 973. b) Genereux, J. C.; Barton, J. K. *Chem. Rev.* **2010**, *110*, 1642.

29. (a) Grigorenko, N. A.; Leumann, C. J. *Chem. Commun.* **2008**, 5417. (b) Roethlisberger, P.; Wojciechowski, F.; Leumann, C. J. *Chem. Eur. J.* **2013**, *19*, 11518.

30. Ikkanda, B. A.; Samuel, S.A.; Iverson, B. L. *J. Org. Chem.* **2014**, *79*, 2029.

31. Mulliken, R. S. *J. Am. Chem. Soc.* **1952**, *74*, 811.

32. (a) Seidel, C. A. M.; Schulz, A.; Sauer, M. H. M. *J. Phys. Chem.* **1996,** *100,* 5541. (b) Poulin, K. W.; Smirnov, A. V.; Hawkins, M. E., Balis, F. M.; Knutson, J. R. *Biochemistry* **2009**, *48*, 8861. (c) Wierzbinski, E.; de Leon, A.; Davis, K. L.; Bezer, S.; Wolak, M. A.; Kofke, M. J.; Schlaf, R.; Achim, C.; Waldeck, D. H. *Langmuir* **2012**, *28*, 1971. (d) Hervas, M.; Navarro, J. A.; De la Rosa, M. A. *Acc. Chem. Res.* **2003**, *36*, 798. (e) Berlin, Y. A.; Grozema, F. C.; Siebbeles, L. D. A.; Ratner, M. A. *J. Phys. Chem. C* **2008**, *112*, 10988.

33. (a) Liu, J.; Cao, Z.; Lu, Y. *Chem. Rev.* **2009**, *109*, 1948. (b) Drummond, T.G.; Hill, M.G.; Barton, J. K. *Nat. Biotechnol.* **2003,** *21,* 1192. (c)

Kolpashchikov, D. M.; Gerasimova, Y. V.; Khan M. S. *ChemBioChem* **2011,** *12,* 2564. (d) Liu, L.; Li,Y.; Liotta, D.; Lutz, S. *Nucleic Acids Res.* **2009**, *37,* 4472. (e) Bag, S. S.; Kundu, R.; Matsumoto, K, Saito, Y.; Saito, I. *Bioorg. Med.Chem. Lett.* **2010**, *20*, 3227. (f) Sinkeldam, R. W.; Greco, N. J.; Tor, Y. *Chem. Rev.* **2010**, *110*, 2579.

34. Frisch, M. J.; Trucks, G. W.; Schlegel, H. B.; Scuseria, G. E.; Robb, M. A.; Cheeseman, J. R.; Montgomery, J. A., Jr.; Vreven, T.; Kudin, K. N.; Burant, J. C.; Millam, J. M.; Iyengar, S. S.; Tomasi, J.; Barone, V.; Mennucci, B.; Cossi, M.; Scalmani, G.; Rega, N.; Petersson, G. A.; Nakatsuji, H.; Hada, M.; Ehara, M.; Toyota, K.; Fukuda, R.; Hasegawa, J.; Ishida, M.; Nakajima, T.; Honda, Y.; Kitao, O.; Nakai, H.; Klene, M.; Li, X.; Knox, J. E.; Hratchian, H. P.; Cross, J. B.; Bakken, V.; Adamo, C.; Jaramillo, J.; Gomperts, R.; Stratmann, R. E.; Yazyev, O.; Austin, A. J.; Cammi, R.; Pomelli, C.; Ochterski, J. W.; Ayala, P. Y.; Morokuma, K.; Voth, G. A.; Salvador, P.; Dannenberg, J. J.; Zakrzewski, V. G.; Dapprich, S.; Daniels, A. D.; Strain, M. C.; Farkas, O.; Malick, D. K.; Rabuck, A. D.; Raghavachari, K.; Foresman, J. B.; Ortiz, J. V.; Cui, Q.; Baboul, A. G.; Clifford, S.; Cioslowski, J.; Stefanov, B. B.; Liu, G.; Liashenko, A.; Piskorz, P.; Komaromi, I.; Martin, R. L.; Fox, D. J.; Keith, T.; Al-Laham, M. A.; Peng, C. Y.; Nanayakkara, A.; Challacombe, M.; Gill, P. M. W.; Johnson, B.; Chen, W.; Wong, M. W.; Gonzalez, C.; Pople, J. A. Gaussian 09, revision A.1, Gaussian, Inc., Wallingford, CT, **2009**.

35. (a) te Velde, G.; Bickelhaupt, F.M.; van Gisbergen, S. J. A.; Guerra, C. F.; Baerends, E. J.; Snijders, J.G.; Ziegler, T. *J. Comput. Chem.* **2001**, *22,* 931. (b) Guerra, C. F.; Snijders, J.G.; te Velde, G.; Baerends, E. J. *Theo. Chem. Acc.* **1998**, *99,* 391. (c) ADF2010, SCM, Theoretical Chemistry, Vrije Universiteit, Amsterdam, The Netherlands, http://www.scm.com (a) Grimme, S. *J. Comput. Chem.* **2004**, *25*, 1463. (b) Grimme, S. *J. Comput. Chem.* **2006**, *27*, 1787. (c) van der Wijst, T.; Lippert, B.; Swart, M.; Guerra, C. F.; Bickelhaupt, F. M. *J. Biol. Inorg. Chem.* **2010**, *15*, 387.

36. (a) Zhao, Y.; Schultz, N. E.; Truhlar, D. G. *J. Chem. Theory Comput.* **2006**, *2,* 364. (b) Zhao, Y.; Truhlar, D. G. *Acc. Chem. Res.* **2008**, *41,* 157. (c) Zhao, Y.; Truhlar, D. G. *J. Chem. Phys.* **2006**, *125,* 194101. (d) Zhao, Y.; Truhlar, D. G. *J. Chem. Theory Comput.* **2007**, *3,* 289.

37. Boys, S. F.; Bernardi, F. *Mol. Phys.* **1970**, *19*, 553.

38. (a) Biegler König F. W.; Schöbohm, J.; Bayles, D. *J. Comput. Chem.* **2001**, *22*, 545. (b) Robertazzi, A.; Platts, J. A. *J. Phys. Chem. A* **2006**, *110*, 3992.

39. (a) Grimme, S. *J. Comput. Chem.* **2004**, *25*, 1463. (b) Grimme, S. *J. Comput. Chem.* **2006**, *27*, 1787. (c) van der Wijst, T.; Lippert, B.; Swart, M.; Guerra, C. F.; Bickelhaupt, F. M. *J. Biol. Inorg. Chem.* **2010**, *15*, 387.

40. (a) Swart, M.; van der Wijst, T.; Guerra, C. F.; Bickelhaupt, F. M. *J. Mol. Model.* **2007**, *13*, 1245. (b) Gao, J. *Acc. Chem. Res.* **1996**, *29,* 298. (c) Monard, G.; Merz Jr., K. M. *Acc. Chem. Res.* **1999**, *32*, 904. (d) Svensson, M.; Humbel, S.; Froese, R. D. J.; Matsubara, T.; Sieber, S.; Morokuma, K. *J. Phys. Chem.* **1996**, *100*, 19357. (e) Kosugi, T.; Hayashi, S. *J. Chem. Theory Comput.* **2012**, *8*, 322.

41. Zimmermann, N.; Meggers, E.; Schultz, P. G. *J. Am. Chem. Soc.* **2002**, *124*, 13684. (b) Atwell, S.; Meggers, E.; Spraggon, G.; Schultz, P. G. *J. Am. Chem. Soc.* **2001**, *123*, 12364. (b) Takezawa, Y.; Shionoya, M. *Acc. Chem. Res.* **2012**, *45*, 2066.

42. (a) Matsuda, S.; Fillo, J. D.; Henry, A. A.; Rai, P.; Wilkens, S. J.; Dwyer, T. J.; Geierstanger, B. H.; Wemmer, D. E.; Schultz, P. G.; Spraggon, G.; Romesberg, F. E. *J. Am. Chem. Soc.* **2007**, *129*, 10466. (b) Malyshev, D. A.; Pfaff, D. A.; Ippoliti, S. I.; Hwang, G. T.; Dwyer, T. J.; Romesberg, F. E. *Chemistry* **2010**, *16*, 12650. (c) Hirao, I.; Kimoto, M.; Yamashige, R. *Acc. Chem. Res.* **2012**, *45*, 2055.

Chapter 5

STUDIES ON THE STABILIZATION OF AN ABASIC SITE PAIRED AGAINST AN UNNATURAL TRIAZOLYL NUCLEOSIDE

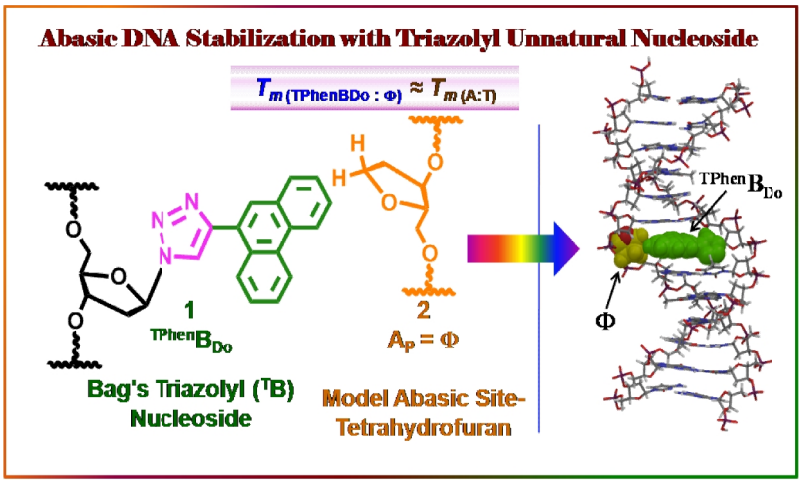

5.1 Introduction

An abasic site in genomic DNA is frequent among the most common forms of DNA lesions.[1] It is produced due to the cleavage of the glycosidic bond between the deoxy-ribose sugar and the nucleobase which results in the loss of purine or a pyrimidine base leaving behind the deoxyribose sugar in the DNA strand (**Figure 5.1**). Generation of an abasic site can occur spontaneously as a result of exogenous agents or as an intermediate in the repair of modified or abnormal bases by base-excision repair mechanism.[2,3,1b] As many as 10,000 abasic sites per cell cycle can be formed by spontaneous depurination alone.[4] Due to lack of coding information, if left unrepaired by the base excision repair (BER) machinery, an abasic site (Ap) can lead to deleterious mutations that are dangerous to cellular survival and replication.[1] An abasic site being chemically unstable can lead to strand breakage which may ultimately lead to cell death. Structurally the formation of an abasic site leads to a discontinuity in the DNA strand and thus leads to a deviation from the regular DNA duplex structure.[5]

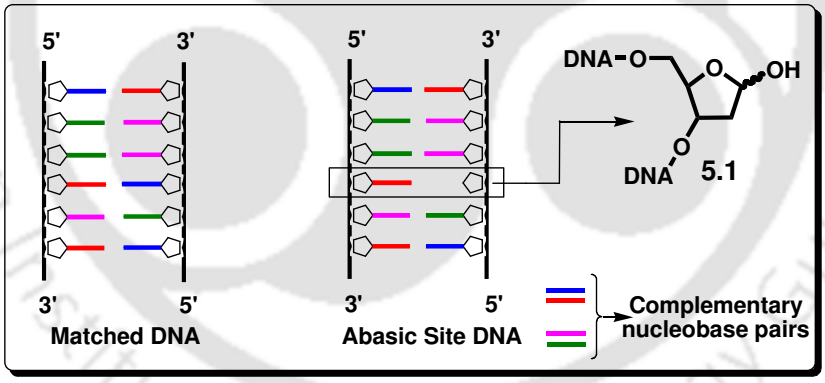

Figure 5.1: Schematic illustration of an abasic site in DNA.

5.2. Generation, Reactivity of Abasic Sites and the Structure of Abasic DNA

The diversity of the biological implications of AP-sites stimulated a great research interest during the past four decades to understand the chemistry and enzymology of abasic DNA that largely relies upon the study of synthetic abasic duplexes. It is well known that the abasic sites result from hydrolytic cleavage of the *N*-glycosidic bond.

This cleavage process is augmented by any factor or by chemical modification that develops a positive charge on the nucleobase and labilizes the glycosidic bond.[6] Generation of abasic sites in DNA or in synthetic oligonucleotides is based on this strategy. Towards this end, various efficient synthetic methods have been developed to synthesize oligonucleotides containing abasic sites at predetermined positions out of which most strategies involve synthesis of unnatural or modified deoxynucleoside precursors and their incorporation into oligomers by automated DNA/RNA synthesizer *via* phosphoramidite chemistry.[7] Moreover, several chemically stable analogues of abasic sites that mimick both the cyclic[8] and the open-chain[8a] forms of the deoxyribose moiety, have been designed. The structures of natural and synthetic models of abasic sites are given in **Figure 5.2**. A pyrrolidine analogue has also been prepared by Verdine and colleagues as inhibitor of the DNA repair enzyme AlkA, the enzyme that creates abasic sites by cleavage of the N3-methyl-deoxyadenosine glycosidic bond.[9]

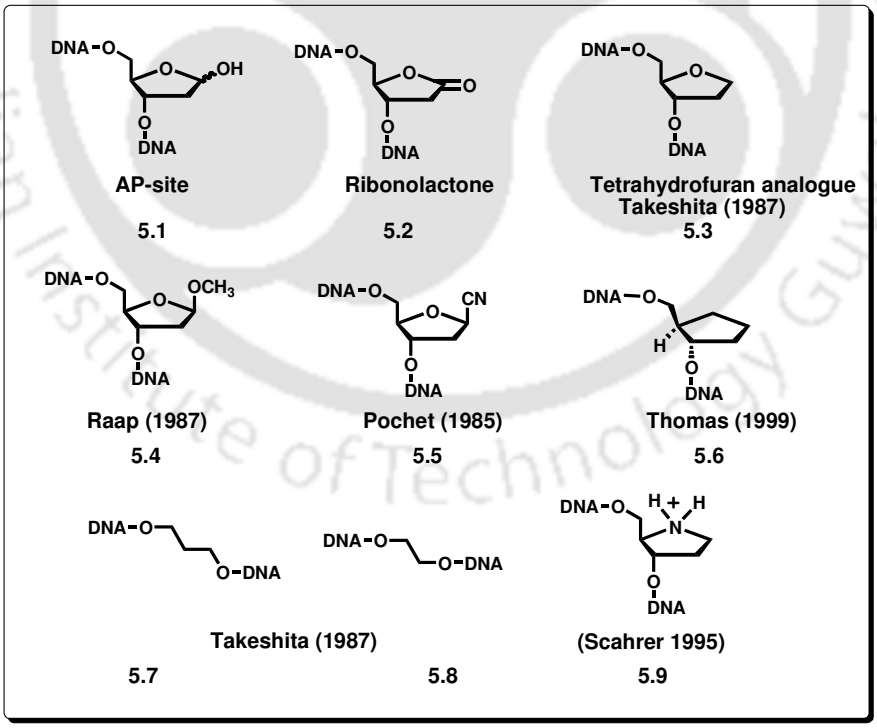

Figure 5.2: Abasic sites structures and their analogues.

The detailed structure of abasic sites has been characterized by NMR spectroscopy analysis of ^{17}O- and ^{13}C-labeled abasic site containing oligodeoxynucleotides.[10] The abasic sites in a cell exist as a 40:60 mixture of α- and β-hemiacetal anomers in equilibrium with a minor ring-opened aldehylic form that represents less than 1% of total sites (**Scheme 5.1**).[11] Due to the existence of the aldehydic form the abasic site is highly sensitive to alkaline conditions undergoing a β-elimination reaction with formation of an α,β-unsaturated aldehyde.[12] The δ-elimination has also been proposed to follow β-elimination cleavage of AP sites during enzymatic repair of damaged DNA (**Scheme 5.1**).[12, 13]

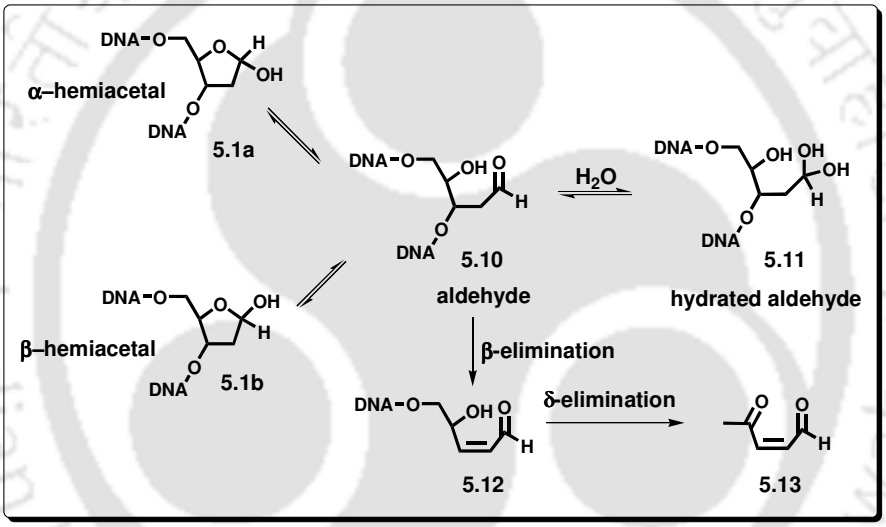

Scheme 5.1: The structure and chemistry of abasic sites. Illustration of the equilibrium of abasic sites between the two major hemiacetal anomers and the minor aldehylic and hydrated aldehylic forms and the mechanisms of hydrogen abstraction.

Several research groups have studied the influence of an abasic site on the conformation of DNA and the stability of the duplexes. The general approach has been to examine the properties using synthetic oligonucleotides containing an abasic site,[14] or most frequently, the stable tetrahydrofuran analogue of the abasic site[15,16] or the open analogue[17] (**Figure 1**), by physicochemical and spectroscopic means such as, calorimetry, thermal denaturation experiment, high-field NMR spectroscopy and molecular modeling study. Different types of abasic duplexes have been examined, according to the nature of the base opposite the abasic site, a purine or a pyrimidine

and according to the nature of the flanking bases.[14,16,17] All of these research efforts have revealed that the abasic lesion strongly destabilizes the duplex, although canonical B-form conformation of DNA is retained with structural modifications strictly located at the site of the abasic lesion. The conformation of the unpaired base complementary to the abasic site can be extra- or intrahelical depending upon its identity and that of the surrounding bases.[18] Unpaired purines are almost always intrahelical, whereas unpaired pyrimidines exist in equilibrium between extrahelical and intrahelical forms, with the extrahelical form favored when the base is flanked by other pyrimidines. Therefore, the duplexes containing abasic site are thermodynamically destabilized by 3-11 kcal/mol as compared to native DNA duplex.[19] The magnitude of destabilization is dependent on both the sequence context and the identity of the unpaired base. In general, abasic sites when flanked by purines are more stable than those flanked by pyrimidines and to a lesser degree sites with unpaired purines are more stable than those with unpaired pyrimidines. [20]

When an Ap (Φ) site is formed, it destabilizes the DNA locally and provides special affinity for repair enzymes to repair it.[1, 21] Under normal condition, the cell quickly and efficiently repairs the abasic site defect through base excision repair (BER) machinery thus preventing any lasting damage to the cell or its genome. However, the suppression or disabling of these repair mechanism is often met with dreadful consequences like abasic sites can lead to single nucleotide polymorphisms (SNPs), block transcription, inhibit DNA replication and can act as potent topoisomerase poisons.[22] Because of the tremendous biological implication estimating the abasic site is of great research interest which might provide a measure of the exposure of DNA to various mutagens or genotoxic compounds such as environmental or chemotherapeutic agents. Moreover, recognition of the AP site is very important in evaluating DNA damage and screening antitumor/antioxidation drugs that would target a cancer cell.[23] Therefore, several probes have been developed to titrate the damage in DNA *in vitro*. Series of molecules have been designed to recognize the abasic site specifically that exhibit a cleavage activity and mimicking the action of AP nucleases. The third approach to target the abasic site is

to design molecules that bind strongly to the abasic site. Therefore, detection and stabilization of an abasic site is important for the design of new diagnostics and chemotherapeutics. In the context of abasic DNA duplex detection and stabilization several small molecule intercalators, unnatural nucleosidic/non-nucleosidic base surrogates have been reported in literature few of which are discussed below.

5.3. Targeting Abasic Site by Small Molecule Intercalators

It has already been mentioned that the abasic site exist as an equilibrium mixture of cyclic hemiacetals and the open chain aldehyde in which the aldehydic form exist in less than 1% of the total (**Scheme 5.2**). The AP endonucleases recognise the abasic sites by cleaving the DNA at the AP-sites *via* β-elimination of the 3'-phosphate that is shown in **Scheme 5.3**.

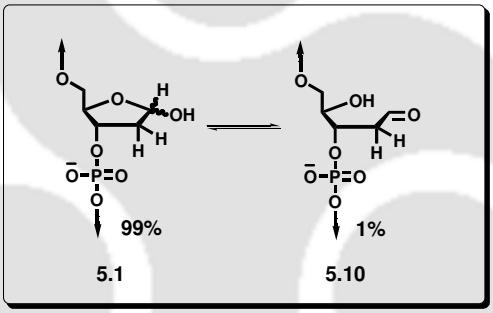

Scheme 5.2: Equilibrium mixture of abasic sites between the hemiacetal anomers (99%) and the minor aldehylic form (1%).

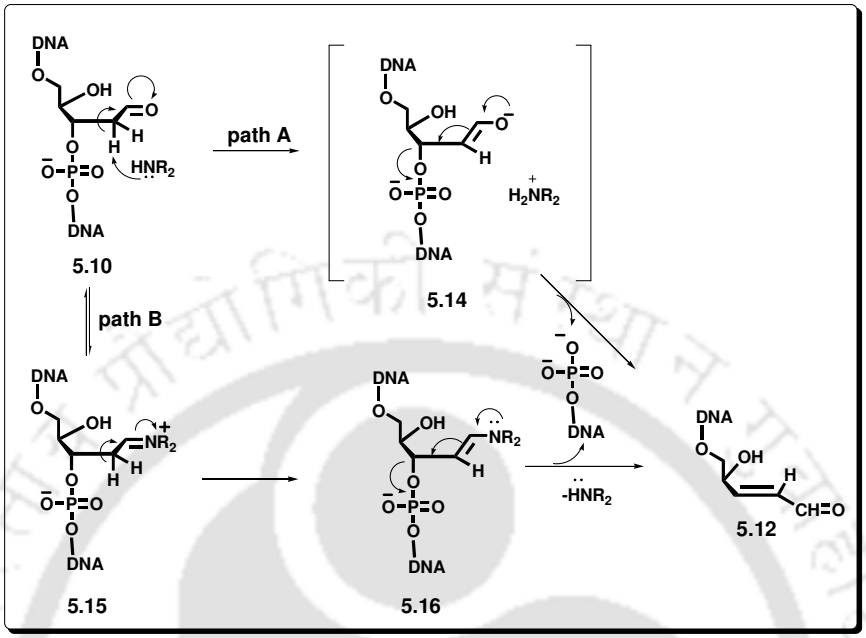

Scheme 5.3: Proposed mechanism for cleavage of DNA at the abasic site by AP endonucleases (AP-lyases) and the AP-endonucleases mimics.

Previously, the covalent reaction of the deoxyribose hemiacetal isomer of the AP site was employed to investigate the binding specificity of amino-containing substrates at the AP site.[24] Inspired by the large numbers of research studies on specific recognition of the AP site in DNA by AP-related enzymes,[25] several works have been carried out in respect of targeting the AP site by designer artificial nucleases. As for an example, based on the activity of the AP-endonucleases, artificial nucleases containing amino functionality has been designed by Lhomne *et al.*[26] which is found to recognise and cleave the abasic sites in DNA with great selectivity and efficiency. The structure of the artificial nuclease constitutes three different units designed for specific functions: (1) an intercalator for DNA binding, (2) a nucleobase for abasic site recognition and (3) a linker for binding and cleavage of DNA at abasic site (**5.17**, **Figure 5.3**). Their study revealed that the nucleophilic amine of the linker reacted with the minor aldehydic form of the natural abasic site which ultimately resulted in strand cleavage at abasic sites.

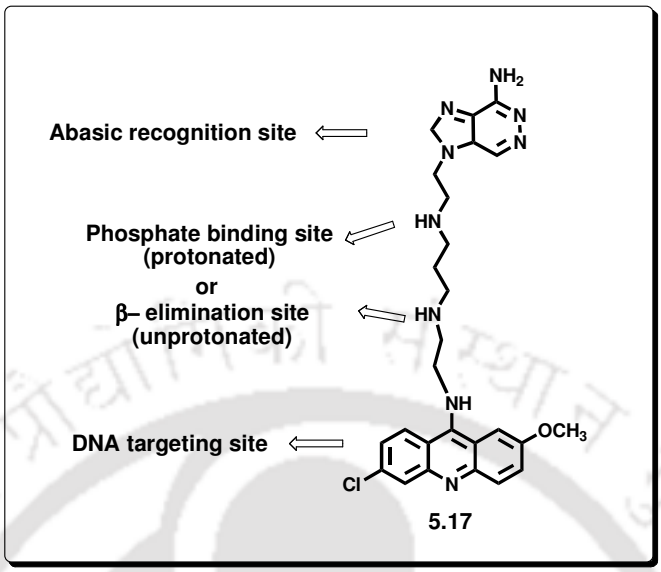

Figure 5.3: Structures of the synthetic molecules which acted as artificial nucleases at the abasic site.

Rather than targeting the AP-sites with covalent interaction, selective targeting based on noncovalent interaction[27] is much more favorable for achieving flexibility in activity and molecular design. In this respect, a pioneer work was carried out by Constant and Demeunynck using heterodimer, a conjugate of a DNA base and an intercalator, to target an AP site. However, this heterodimer structure is too intricate to identify which moiety is mainly responsible for its binding at the AP site.[28] Later on, Lhomne and co-workers have synthesized fluorescent probes which are highly specific and sensitive for the detection of abasic site (**5.18** and **5.19**, **Figure 5.4**).[29] Their mode of action is based on the reactivity of the amino-oxy function present in the molecule which formed oxime ethers by reacting with the aldehydic functionality of the ring opened deoxyribose residue.

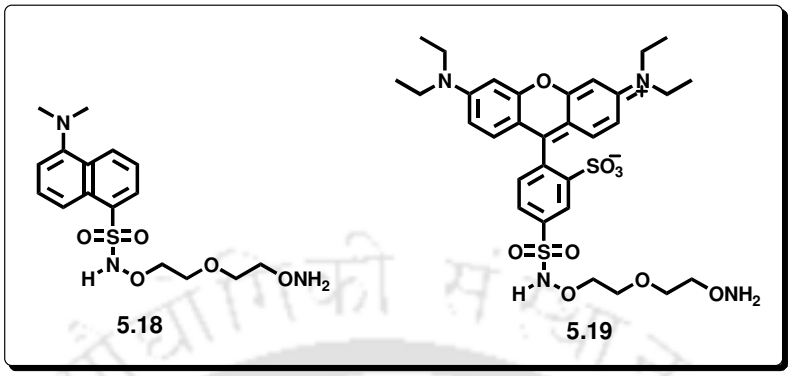

Figure 5.4: Abasic site recognition agents (fluorophore conjugated nucleophilic amine).

Some much simpler molecules in structure like nitroxide spin labels,[30] metalloinsertors[31] are also effective in targeting the AP site. Barton *et al.* have synthesized the metal complexes, $Rh(bpy)_2(chrysi)^{3+}$ (chrysi = chrysene-5,6-quinone diimine) (**5.20**) and $Rh(bpy)_2(phzi)^{3+}$ (phzi = benzo[a]phenazine-5,6-quinone diimine) (**5.21**) (**Figure 5.5**) bearing sterically bulky ligands and applied in targeting mismatched sites. They have found that the complex not only recognized the mismatched site but also promoted cleavage of the DNA backbone upon irradiation with UV light at the binding site with high affinity and selectivity. The complex employed a unique way of binding to the DNA termed as metalloinsertion in which the complex after binding to the minor groove ejected the mismatched bases into the major groove and replaced them with its aromatic ligand. This insertion mode indicates that there is a correlation between site recognition and thermodynamic destabilization-the less stable the mismatch, the easier the ejection of the mismatched bases. This relationship between thermodynamic instability of the mismatched pair and metalloinsertor binding events led Barton *et al.* to exploit those complexes in recognising abasic sites.[31] Thus, they have observed that both the metal complexes, $Rh(bpy)_2(chrysi)^{3+}$ (chrysi = chrysene-5,6-quinone diimine) (**5.20**) and $Rh(bpy)_2(phzi)^{3+}$ (phzi = benzo[a]phenazine-5,6-quinone diimine) (**5.21**) selectively bind with the abasic site *via* insertion mode of interaction leading to cleavage of the abasic site at the binding site upon irradiation with UV light. The specificity, affinity

and reactivity of both the metal complexes proved as reliable probes for abasic site detection and hence serve as useful candidates for diagnostic and chemotherapeutic agents.

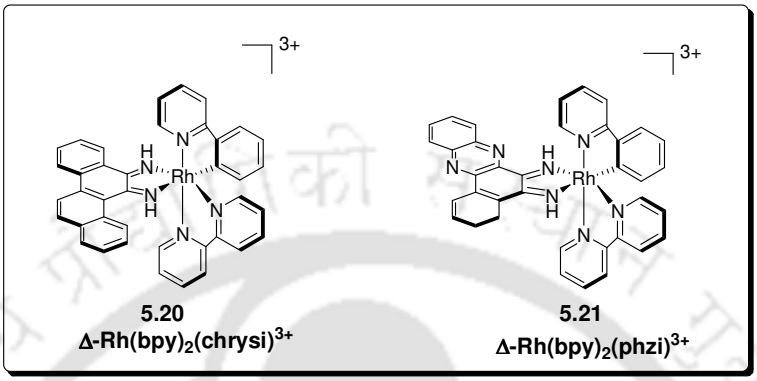

Figure 5.5: Structures of two metalloinsertors. The Δ-enantiomers of $Rh(bpy)_2(chrysi)^{3+}$ (left) and $Rh(bpy)_2(phzi)^{3+}$ (right); each complex bears two 2,2'-dipyridine ligands and a sterically demanding inserting ligand.

Rokita *et al.* have synthesized a solvatochromic naphthalene derivative which is found to detect the nonpolar microenvironment of abasic site *via* binding at that particular lesion site.[32] Very recently, Ihmels *et al.* have exploited annelated quinolizinium derivatives for AP-DNA stabilization.[32] They have investigated the interactions of abasic site containing DNA with several quinolizinium derivatives (**5.22-5.26, Figure 5.6**) with the help of fluorimetric titrations and thermal DNA denaturation experiments. They have observed that the parent quinolizinium ion (**5.22**) and the benzo-annelated derivatives **5.23**, **5.24** and **5.25** exhibit no significant affinity to AP-DNA. However, additional benzo-annelated quinolizinium ion **5.26** leads to an increased selective stabilization of AP-DNA. From their studies with several quinolizinium derivatives it can be concluded that the compound **5.26** represents the first example of a ligand that does not require ancillary substituents for efficient AP-DNA stabilization. Their study also reveals that a chloro substituent affects the propensity of a ligand to bind to AP-DNA in a similar way as the methyl substituent and may be employed complementary to the known methyl effect to increase the binding affinity of a ligand.

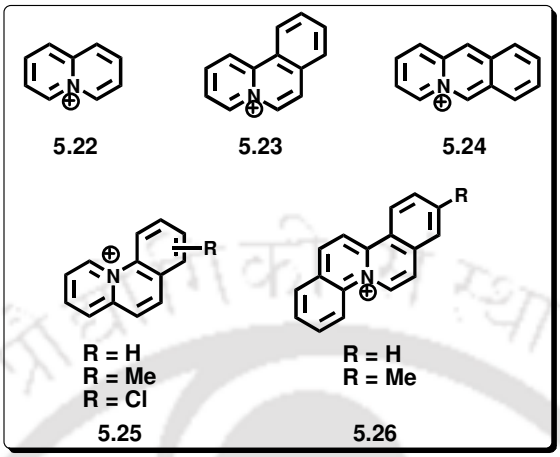

Figure 5.6: Structure of quinolizinium ion and the benzo-annelated derivatives.

5.4. Stabilization of Abasic Site by Non-Nucleosidic Base Surrogate

As is revealed from the previous section, several small molecule intercallators have been found to recognise and stabilize an abasic lesion. The stabilization of abasic lesion relies mainly on the adjustment of the molecule within the gap created by the Ap site. The molecules with good intercalating property and volume comparable to a natural **A:T** pair, in general, are expected to cover the full space along the Ap site which in turn involve in inter-/intrastrand π-π stacking interaction with the bases of the abasic DNA duplex leading to stabilization of the abasic DNA. Research efforts towards the expanding of the genetic alphabet and searching for DNA based materials have evolved several new nucleosidic as well as non-nucleosidic base surrogates out of which many of them have been found having intercalation property with similar size as that of a natural **A:T** pair. Therefore, with this concept of abasic duplex stabilization, many of the designed fluorescent nucleosidic and non nucleosidic base surrogates have been exploited in fluorimetric sensing as well as stabilization of an abasic DNA. In this section the abasic duplex stabilization by few of the designer non-nucleosidic base surrogates have been discussed. Next section will be devoted to the stabilization by few reported nucleosidic base surrogates. Placement of extended aromatic residues as a nucleobase surrogate opposite to the abasic site can substitute for the missing nucleobase maintaining the aromatic stacking throughout the duplex, ultimately, leading to the stabilization of the

abasic DNA. Such aromatic building blocks might present a considerable practical advantage for stabilizing abasic site with high specificity over free intercallators.

Towards this end, Häner *et al.* have designed and synthesized few non-nucleosidic base-surrogates and studied their abasic site stabilization properties. They have first reported the influence of a phenanthrene-3,6-dicarboxamide derivative with flexible, aliphatic linkers on the duplex stability opposite an abasic site. The flexible aliphatic linker constitutes the methylene groups and the buiding blocks have been incorporated into the DNA by standard phosphoramidite chemistry. The length of the aliphatic linkers was varied and the influence of the linker length on the abasic DNA duplex stability containing phenantherene as non-nucleosidic base surrogate has been investigated. It has been observed from the thermal denaturation experiment that phenanthrene with a tetramethylene linker (**P_4**) led to a significant stabilization of the abasic site relative to the duplex containing a natural base opposite to the abasic site (**Table 5.1**).[33a] Later on, Häner and co-workers have analyzed the effect of phenanthroline and pyrene building blocks on the stability of an abasic site containing DNA duplex[33b-c]. Thermal denaturation experiments suggested a remarkable stabilization of the duplex DNA containing an abasic site by non-nucleosidic base surrogate, 2,9-disubstituted 1,10-phenanthroline as well as by 1,8-disubstituted pyrene. The influence of the aliphatic linker length has also been investigated in both the cases. It has been observed that both the building blocks have led to a significant stabilization of the abasic DNA duplexes as compared to the natural **A:Φ** pair which is evident from the thermal melting experiments. In the pyrene series, the T_m varies within a narrow range of approximately 1 °C on going from two to five methylene linker length in both linker arms (**Table 5.1**). Thus, the stabilization of abasic DNA by pyrene derivatives remains relatively insensitive to changes of the linker length. However, in the phenanthroline series, a strong influence of the linker length on the thermal melting stability has been observed which is reflected in the T_m increased by about 4.2 °C as the linker length is increased from 2 to 5 (**Table 5.1**). The highest stabilization of the abasic site in the duplexes is seen in case of 1,10-phenanthroline-2,9-dicarboxamide bearing two pentamethylene linkers. The stabilization is explained

to arise from the stacking interactions between polyaromatic systems and the adjacent base pairs.

Table 5.1: Influence of phenantherene-, phenanthroline- and pyrene-derived non-nucleosidic building blocks on the stability of the duplex DNA containing an abasic site [**Δ T_m = d**ifference in T_m relative to the duplex containing an adenosine opposite to the abasic site (T_m = 56.3 °C)].

Duplexes	T_m (°C)	**Δ T_m (°C)**			
5′ AGC TCG GTC A **T** C GAG AGT GCA 3′ 3′ TCG AGC CAG T **A** G CTC TCA CGT 5′	67.7	n=2	n=3	n=4	n=5
5′ AGC TCG GTC A **ϕ** C GAG AGT GCA 3′ 3′ TCG AGC CAG T **A** G CTC TCA CGT 5′	56.3				
5′ AGC TCG GTC A **ϕ** C GAG AGT GCA 3′ 3′ TCG AGC CAG T**^{n}Pn**G CTC TCA CGT 5′		0.4	2.3	5.7	4.9
5′ AGC TCG GTC A **ϕ** C GAG AGT GCA 3′ 3′ TCG AGC CAG T**^{n}An**G CTC TCA CGT 5′		4.2	6.2	5.9	8.4
5′ AGC TCG GTC A **ϕ** C GAG AGT GCA 3′ 3′ TCG AGC CAG T**^{n}Bn**G CTC TCA CGT 5′		5.9	6.2	6.9	5.5

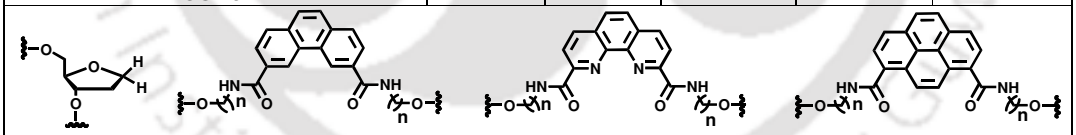

Stabilization of abasic site with oligonucleotide (ODN) modified with 2-methoxy-6-chloro-9-aminoacridine (**Acr**) (**Figure 5.7**) has been demonstrated by Shimidzu *et al.*[34] The thermodynamic studies indicated that the duplexes containing the acridine derivative opposite to an abasic site are more stable by about 11.2 °C as compared to that of duplexes containing abasic site opposite natural bases. The UV- visible and

fluorescence spectroscopic investigation revealed that acridine is selectively intercalated along the abasic site in the duplex.

Tanaka *et al.* have studied the interactions of the intercalating agent, 9-amino-6-chloro-2-methoxyacridine (ACMA) with tri- and pentamethylene linker at three types of abasic sites of the DNA helix *i.e.* abasic frameshift, apurinic (purine base missing) and apyrimidinic (pyrimidine base missing).[35] It has been elucidated through the thermal denaturation experiment that the ACMA with the pentamethylene linker and apyrimidinic site is the most stable system. The UV-visible and the fluorescence experiments have revealed that ACMA selectively intercalated to the apyrimidinic site rather than the frameshift abasic site[36] (**Figure 5.8**).

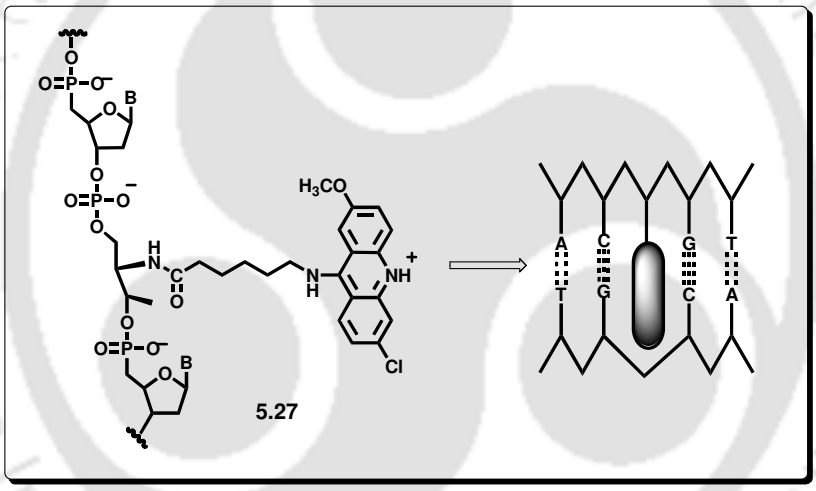

Figure 5.7: Structure of oligonucleotide (ODN) modified with 2-methoxy-6-chloro-9-aminoacridine (**Acr**) and its intercalation in a DNA duplex.

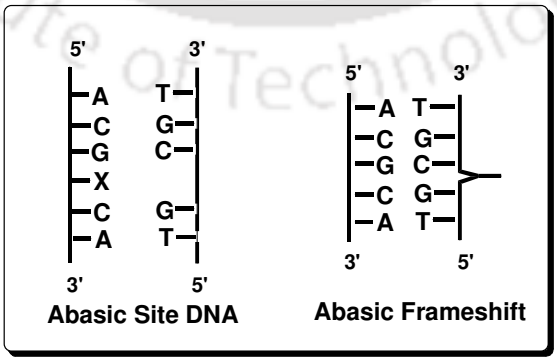

Figure 5.8: Structure of abasic site and abasic frameshift site in DNA.

5.5. Targeting Abasic Site with Nucleosidic Base Surrogate

The abasic sites are known to destabilize DNA when paired opposite natural bases.[37] It has already been discussed in the previous section that many non nucleosidic aromatic base surrogates are able to stabilize abasic DNA out of intercalation and aromating stacking along the abasic site. Stabilisation of abasic sites has also been reported using complementary oligonucleotides carrying modified nucleosides. The idea behind using the deoxyribose-derived nucleosidic base surrogates is to cause as little change as possible to the sugar-phosphate backbone. In this context, deoxyribose-derived extended aromatic residues have been placed opposite to the abasic site which can substitute for the missing nucleobase and maintain the aromatic stacking throughout the duplex. Deoxyribofuranosides carrying 1-pyrene and 2-pyrene have been used for this purpose because pyrene nucleoside analogue is sterically large enough to fit well against an abasic site.

The first example of stabilization of an abasic site by nucleosidic base surrogate has been reported by Kool *et al.*[38a-d] *via* the synthesis of 1-pyrenyl C-nucleoside. It has been observed that 1-pyrenyl C-nucleoside stabilizes well an abasic duplex. However, the pyrene/abasic duplex are found to slightly less stable than the control natural **A:T** pair. The thermal denaturation experiments also revealed that the pyrene selectively paired against an abasic site as compared to the natural bases since the replacement of the central pyrene-abasic pair with P-X pair (P = pyrene and X = A. T, C, G) destabilized the DNA duplex relative to P-ϕ pair (**Table 5.2**).

Table 5.2: Influence of 1-pyrene-, 2-pyrene nucleosidic base surrogates on the stability of duplex DNAs containing an abasic site [**Δ T_m** = difference in T_m relative to the duplex containing an adenosine opposite to the thymine (T_m = 43.2 °C and 49.6 °C in case of 1-pyrene and 2-pyrene, respectively)].

Duplexes	T_m (°C)	Δ T_m (°C)
5′ CTT TTC **T**TT CTT 3′ 3′ GAAAAG**A**AAGAA 5′	43.2	
5′ CTT TTC **P**TT CTT 3′ 3′ GAAAAG**ϕ**AAGAA 5′	41.0	2.2
5′ CTT TTC **ϕ**TT CTT 3′ 3′ GAAAAG**P**AAGAA 5′	41.6	1.6
5′ CTT TTC **P**TT CTT 3′ 3′ GAAAAG**A**AAGAA 5′	38.7	4.5
5′ CTT TTC **P**TT CTT 3′ 3′ GAAAAG**C**AAGAA 5′	37.6	5.6
5′ CTT TTC **P**TT CTT 3′ 3′ GAAAAG**T**AAGAA 5′	36.4	6.8
5′ CTT TTC **P**TT CTT 3′ 3′ GAAAAG**G**AAGAA 5′	38.2	5
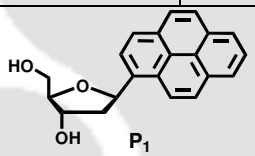 **P_1** **1.108** 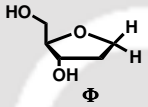 **Φ** **5.3**		

A similar experiment relating the stabilization of abasic site has been carried out by Leumann *et al.* with 2-pyrenyl-C-nucleoside.[39] The synthesis of 2-pyrenyl C-nucleoside has been carried out in order to maximize π-π stacking interactions and to minimize conformational isomerism around the *C*-glycosidic bond. Thus, it is observed that a duplex containing 2-pyrene residue opposite to an abasic site has led to minor decrease in its thermal stability as compared to the duplex containing a natural **A:T** base pair (**Table 5.3**). Duplexes containing two or three intrastacked pyrene residues paired against two or three abasic sites (duplexes **3**, **4**, **6**, and **7**) results in a gradual decrease in thermal stability.

Table 5.3: Influence of 1-pyrene-, 2-pyrene nucleosidic base surrogates on the stability of duplex DNA containing an abasic site [ΔT_m = difference in T_m relative to the duplex containing an adenosine opposite to the thymine (T_m = 43.2 °C and 49.6 °C in case of 1-pyrene and 2-pyrene respectively)].

	Duplexes	T_m (°C)	ΔT_m (°C)
1.	5′ GATGAC**T**GCTAG 3′ 3′ CTACTG**A**CGATC 5′	49.6	
2.	5′ GATGAC**P_2**GCTAG 3′ 3′ CTACTG**ϕ** CGATC 5′	47.6	2.0
3.	5′ GATGAC(**P_2**)$_2$GCTAG 3′ 3′ CTACTG (**ϕ**)$_2$ CGATC 5′	41.5	8.1
4.	5′ GATGAC(**P_2**)$_3$GCTAG 3′ 3′ CTACTG (**ϕ**)$_3$ CGATC 5′	38.2	11.4
5.	5′ GATGAC**ϕ**GCTAG 3′ 3′ CTACTG**P_2**CGATC 5′	46.9	2.7
6.	5′ GATGAC (**ϕ**)$_2$ GCTAG 3′ 3′ CTACTG(**P_2**)$_2$CGATC 5′	45.6	4
7.	5′ GATGAC (**ϕ**) GCTAG 3′ 3′ CTACTG(**P_2**)$_3$CGATC 5′	37.7	11.9

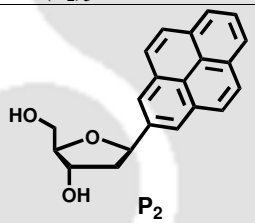

P_2

1.134

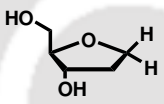

Φ

5.3

The results obtained by pairing 1-pyrene deoxynucleoside and 2-pyrene deoxynucleoside opposite an abasic site are thus comparable demonstrating that both the pyrene nucleosides stabilize well an abasic site. Pyrene was chosen to be paired against the abasic site as it occupies (220 Å^2) the same area as that covered by a natural **A:T** pair (269 Å^2). The pairing selectivity between pyrene and the abasic nucleoside (compared to the natural bases) can be rationalized on the basis of its large surface area and strong stacking ability which is nearly twice that of natural adenine. Model study also suggests that the aromatic building block replaces for the missing base by intercalation into the cavity resulting from loss of a nucleobase.

Hence, stabilisation of abasic sites in duplex DNA can be achieved with complementary oligonucleotides carrying extended aromatic residues opposite to the

abasic site.

5.6. Background

It is now clear that several research efforts have been put forth to recognise/stabilize abasic DNA *via* the design of small molecule intercallators, oligonucleotide (ODNs) probes containing non-nucleosidic building blocks[33-35] and/or modified nucleosides [38,39] as nucleobase surrogates. All of these research efforts have been aimed at unfolding the mechanism by which DNA repair enzymes recognize and distinguish abasic DNA from normal one. While all the reported non-nucleoside base surrogates[33-35] have led to a remarkable thermal stabilization of abasic site (by 0-8 ^{o}C in T_m), probes containing modified nucleosides[38,39] have been found to stabilize abasic site to a much greater extent than those of the corresponding natural duplexes with adenine-abasic (**A:Φ**) pair. However, those nucleoside/non-nucleoside base surrogates stabilize abasic duplexes that are less stable than a natural **A:T** pair. As for an example, ODN containing pyrenyl deoxyriboside offers highest reported thermal stability of an abasic DNA, though the stability is slightly lower (by 1.6–2.2 °C) than a natural **A:T** pair.[38]

All of the above results of abasic DNA stabilisation are highly inspiring for the design of nonpolar hydrophobic nucleoside isosteres for stabilizing an abasic site without H-bonded base-pairing. However, it is still reasonable to think that dipole moment and polarizability imparted by heteroatoms and large surface area might play a significant role in bringing high stacking ability[33b] as well as polymerase fidelity.[40] Therefore, it seems that considering geometric fit hypothesis combined with efficient stacking propensity and polarizability might allow one to design nucleoside bases which would expectedly result in high stabilization of abasic DNA and be a promising candidate for studying polymerase replication fidelity. Therefore, the design of such nucleoside isosteres is highly demanding. Despite the few successes, the rational design of more efficient hydrophobic nucleoside analogues to target abasic site remains a challenge.

5.7. Objective

As a part of our ongoing research effort towards the design of unnatural nucleosides with tuned photophysical properties, we have observed that the click chemistry generated triazolyl donor/acceptor aromatic chromophores containing unnatural nucleoside base $^{TPhen}\mathbf{B}_{\mathbf{Do}}$ produce self pair and hetero-pair, the stability of which is comparable to the stability of a control **A:T** pair.[41] The highest stability in self-pairing is most likely a result of the large size of triazolylphenanthrene which helped in slipping past one another leading to strong stacking interaction. The synthesis of the nucleosides and the DNA dulex stabilizing property has already been discussed in **Chapter 2** and **Chapter 4** respectively.

Model study suggests that the aromatic nucleoside isosteres can reinstate the DNA base stack by intercalation into the cavity leading to stabilization of the abasic duplex.[38,39] Therefore, inspired by the large surface area, high polarizability, high stacking propensity (stacking propensity of phenanthrene is higher than Adenine)[38a, e] and our recent observation on strong self-pair/hetero-pair stabilization, we thought that it would be worthwhile to study abasic DNA stabilization using our triazolyl phenanthrene unnatural nucleoside $^{TPhen}\mathbf{B}_{\mathbf{Do}}$ (**2.107**, **Figure 5.9**). Amber* optimized geometry of B-form DNA suggests that the triazolylphenanthrene moiety is geometrically large enough (surface area 248 $Å^2$ against natural **A:T** pair surface area 273 $Å^2$)[42] to fit well against model abasic site **5.3** (**Φ**) by covering almost full space and maintaining contiguous stacked π-systems in both strands of the duplex as that normally be done by a natural base pair. Therefore, we have envisaged that a combination of all the factors might enable our designed nucleoside to impart better stabilization of abasic DNA than any of the reported studies.

With this aim and the preliminary inspiration from macromodel study, we plan our objective as below:

(A) Synthesis of two complementary 13-mer oligonucleotides containing $^{TPhen}\mathbf{B}_{\mathbf{Do}}$ (ODN **1**, **7**) in two sequence context placing the $^{T}\mathbf{B}$s at a central position of the strands *via* automated DNA synthesizer. This sequence context was so chosen

as to study the effects of flanking bases (T base for **X** and A base for **Y**) on the abasic duplex stability.

(B) Evaluation of the stabilities in aqueous buffer of all the duplexes containing ^{T}**Bs-Φ** pairs with thermal denaturation studies and the investigation of pairing selectivity.

(C) Evaluation of Thermodynamic origin of the abasic site stabilization by ^{TPhen}**B$_{Do}$** nucleoside.

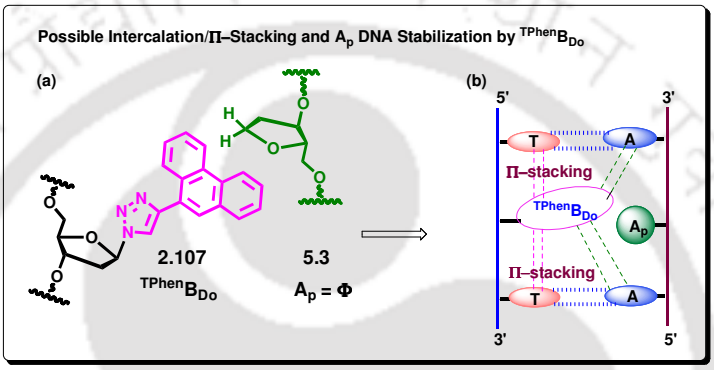

Figure 5.9: (a) Structure of the unnatural triazolyl nucleoside (^{T}**B** = ^{TPhen}**B$_{Do}$**) and model abasic site (Φ). (b) Schematic presentation of possible intercalative π-stacking interaction along the abasic site.

5.8. Result and Discussion

5.8.1. Synthesis of Triazolylphenanthrene Nucleoside (^{TPhen}B$_{Do}$) Containing Oligonucleotide Probes

We have synthesized ^{TPhen}**B$_{Do}$** nucleoside following the procedure described in **Chapter 2** under section **2.5.1**. The nucleoside **2.107** was then incorporated into two short oligonucleotide sequences (ODN **1**, **7**) following phosphoroamidite chemistry *via* automated DNA/RNA synthesizer (**Scheme 5.4**). The synthesis and characterization by MALDI-TOF mass spectrometry of the two oligonucleotides (ODNs) containing ^{TPhen}**B$_{Do}$** (ODN **1** and ODN **7**) at the central position of each strand have already been discussed in **Chapter 4** under section **4.6.3**.

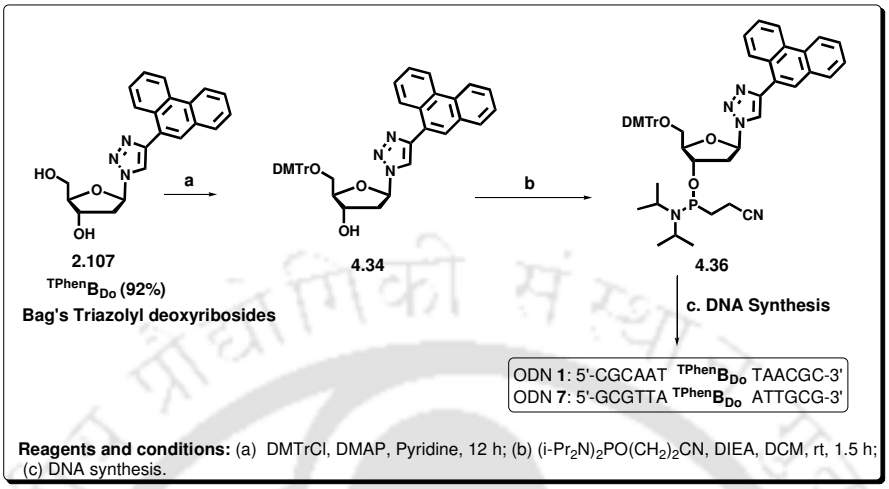

Scheme 5.4: Synthesis of $^{TPhen}B_{Do}$ nucleoside and the oligonucleotides.

The abasic site containing ODNs (**ODN 2** and **ODN 8**) and all possible natural ODNs (**ODN 3-6** and **ODN 9-12**) were purchased. The two sequence context was chosen to study the effects of flanking bases (T base for **X** and A base for **Y**) on the abasic duplex stability. **Table 5.4** lists the sequences of all the ODNs used for the study.

Table 5.4: Oligonucleotide sequences containing $^{TPhen}B_{Do}$ nucleoside/ abasic site (**Φ**) and their natural complements.

5'-CGCAAT **X** TAACGC-3' 5'-GCGTTA **Y** ATTGCG-3'			
ODNs	**Sequences**	**ODNs**	**Sequences**
1	5'-CGCAAT $^{TPhen}B_{Do}$ TAACGC-3'	**7**	5'-GCGTTA $^{TPhen}B_{Do}$ ATTGCG-3'
2	5'-GCGTTA **Φ** ATTGCG-3'	**8**	5'-CGCAAT **Φ** TAACGC-3'
3	5'-GCGTTA **A** ATTGCG-3'	**9**	5'-CGCAAT **A** TAACGC-3'
4	5'-GCGTTA **G** A TTGCG-3'	**10**	5'-CGCAAT **G** TAACGC-3'
5	5'-GCGTTA **C** A TTGCG-3'	**11**	5'-CGCAAT **C** TAACGC-3'
6	5'-GCGTTA **T** A TTGCG-3'	**12**	5'-CGCAAT **T** TAACGC-3'

5.8.2. Study of Thermal Melting and Thermodynamic Stability of the Duplexes: Investigatiing the Pairing Selectivity and the Effect of Flanking Base Pair

The stabilities in aqueous buffer of all duplexes containing **^{T}Bs-Φ** pairs were then evaluated with thermal denaturation studies (**Table 5.5 and Figure 5.10**). To compare duplex stability and pairing selectivity, ODN **1-2**, **7-8** were also paired against the four natural bases and the thermal stability of natural **A:T** pair in the same central position (ODN **9•6**) was also examined.

From the thermal melting temperature it was evident that all the duplexes containing unnatural nucleosides (**^{T}Bs:Φ** or **Φ:^{T}Bs**) paired against an abasic site were more stable than the duplexes between any of the natural bases and the abasic site [**X** (= A, G, C, T)**:**Φ or **Φ:Y** (= A, G, C, T)] in both the sequence contexts. The natural **A : T** pair duplex (**ODN 9•6**), has a T_m of 51.2 ^{o}C. A strong destabilization of 14.0 ^{o}C in T_m was the result when A was paired against an abasic site (**9•2, A:Φ**) which is possibly due to the disruption of continuous stacking in the helix along the abasic site.[38a] However, triazolylphenanthrene nucleobase well stabilized abasic site leading to thermal stabilization of duplexes (**^{T}Bs-Φ** or **Φ-^{T}Bs**) by 13.4-15 ^{o}C higher than that of the duplexes **A:Φ** and/or **Φ:A** (**Table 5.5**). Furthermore, when triazolylphenanthrene nucleoside **^{TPhen}B$_{Do}$** (**2.107**, **Scheme 5.4**) was paired opposite to the abasic site, the duplex formed (ODN **1•2**, **^{TPhen}B$_{Do}$:Φ**) was found to be equally stable as the control **A:T** pair (ΔT_m = + 1.0 ^{o}C and ΔG = + 0.5 kcal/mol) (**Table 5.5**).

Table 5.5: T_m values and thermodynamic parameters for several duplexes.

5'-CGC AAT **X** TAA CGC-3'

3'-GCG TTA **Y** ATT GCG-5'

ODNs	X:Y	T_m	ΔT_m	$-\Delta G^0_{37}$	$-\Delta H^0$	$-\Delta S^0$
1•2	$^{TPhen}B_{Do}$:Φ	52.2	+1.0	13.4	129.1	373.1
9•2	A:Φ	37.2	–14.0	7.5	111.7	336.3
10•2	G:Φ	37.5	–13.7	7.7	97.5	289.7
11•2	C:Φ	35.1	–16.1	6.9	90.5	269.6
12•2	T:Φ	35.8	–15.4	7.4	101.6	303.9
8•7	Φ:$^{TPhen}B_{Do}$	49.0	–2.2	12.0	125.8	367.3
8•3	Φ:A	35.6	–15.6	7.3	81.9	240.9
8•4	Φ:G	35.7	–15.5	7.2	87.3	258.5
8•5	Φ:C	33.4	–17.8	6.8	63.4	182.6
8•6	Φ:T	33.5	–17.7	6.7	75.9	223.3
9•6	A:T	51.2	--	12.9	117.4	337.1
1•7	$^{TPhen}B_{Do}$:$^{TPhen}B_{Do}$	53.6	+2.4	12.8	107.4	305.0
1•3	$^{TPhen}B_{Do}$:A	48.5	-2.7	12.09	127.6	372.5
1•4	$^{TPhen}B_{Do}$:G	49.4	-1.8	11.39	106.2	306
1•5	$^{TPhen}B_{Do}$:C	51.3	+0.1	12.72	115.3	331
1•6	$^{TPhen}B_{Do}$:T	50.0	-1.2	12.38	118.9	343.6
9•8	A:$^{TPhen}B_{Do}$	47.1	-4.1	10.87	104.5	301.9
10•8	G:$^{TPhen}B_{Do}$	48	-3.2	12.16	137.2	403.4
11•8	C:$^{TPhen}B_{Do}$	48.3	-2.9	11.57	114.6	332.3
12•8	T:$^{TPhen}B_{Do}$	46.9	-4.3	10.78	110.1	320.5

All samples contained 2.5 μM each strand of DNA in 50 mM sodium phosphate, 100 mM sodium chloride, 0.1 mM EDTA, pH 7.0, room temperature. Units of ΔG and ΔH are in kcal/mole, while for ΔS is in cal/K/mol. Error in T_m is estimated at ± 0.3 °C and in free energy ± 3%. ΔT_m = Difference in T_m compared to corresponding natural **A:T** pair.

It was also evident that the $^{TPhen}B_{Do}$ showed significant selectivity (by 0.7-1.3 kcal mol^{-1} and 0.8- 3.7 ^{o}C in T_m higher stability) for pairing with the abasic site over all four natural bases (**Table 5.5**). The model abasic nucleoside **5.3** (**Φ**) also showed a strong preference for pairing with $^{TPhen}B_{Do}$ over any of the natural bases by 14.7-17.1 ^{o}C increase in T_m and a gain of 5.7-6.5 kcal mol^{-1} in stability. The self-pair duplex formed by $^{TPhen}B_{Do}$ (ODN **1 • 7,** $^{TPhen}B_{Do}$:$^{TPhen}B_{Do}$) was found to be 2.4 ^{o}C more

stable than a control **A:T** pair which was discussed in detail in **Chapter 4**. Moreover, $^{TPhen}\mathbf{B_{Do}}$ offers better thermal stabilization (by ~ 2.6-3.2 ^{o}C) of the abasic duplex than the highest reported stabilization provided by unnatural nucleoside base surrogates.[38a, 39] To the best of our knowledge this is the strongest stabilization of an abasic duplex achieved by our designed nucleoside, $^{TPhen}\mathbf{B_{Do}}$.

We have next examined the role of flanking bases of the abasic site on the stabilization of the duplex upon pairing with natural or unnatural nucleosides. An examination of the role of flanking bases on stabilization of abasic site reveals that the flanking -A- bases lead to higher duplex stability compared to flanking -T- bases irrespective of natural or unnatural bases opposite to the abasic site (**Table 5.5**). This is probably because of the fact that the larger surface area possessed by purine neighbor -A- tends to close the gap in the abasic site by stacking more than that of the pyrimidine neighbor. This observation is also supported by the observation of Sagi *et al*.[20] On the other hand, nucleoside $^{TPhen}\mathbf{B_{Do}}$ in general, (which can be seen from our study in **Chapter 4**) when flanked between -T- bases shows higher duplex stability compared to the stability of the duplexes when flanked between -A- bases in case of mis-pairing with any natural bases (**Table 5.5**). Therefore a cooperative effect of flanking bases was reflected in higher stabilization of the duplex $^{TPhen}\mathbf{B_{Do}}$**:Φ** (by 3.2 ^{o}C) than the **Φ:**$^{TPhen}\mathbf{B_{Do}}$ duplex which was only slightly less stable (by 2.2^{o}C) compared to a control **A:T** pair (**Table 5.5**). However, in the reverse sequence (**Φ:**$^{TPhen}\mathbf{B_{Do}}$) the stabilization of abasic DNA was also high but comparable to that offered by reported pyrene nucleosides.[38a, 39] These observations are remarkable considering especially the fact that large surface area of triazolylphenanthrene rendered it to offer both the inter- and intra-strand stacking interactions within the nearby natural bases in the duplex along the abasic site; thus covering the full space leading to higher abasic duplex stabilization than any other reported bases. [33-39]

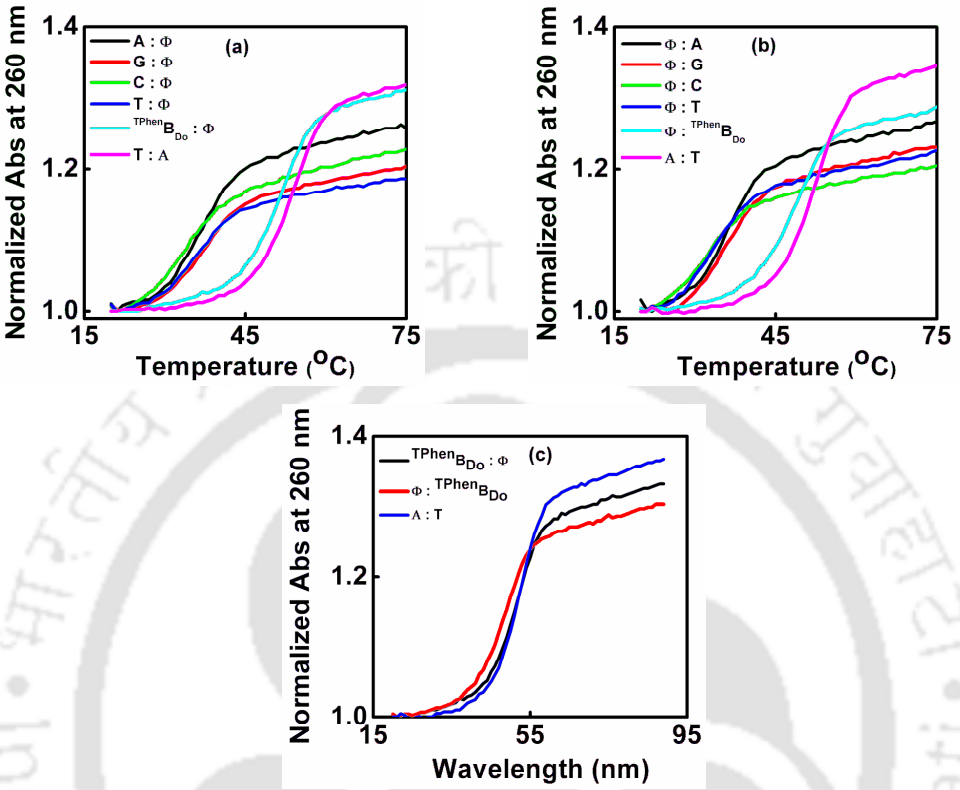

Figure 5.10: Normalized thermal melting curves (2.5 μM of duplex concentration) of four to five different concentrations of ODNs-(a) ODN **X** :**Φ** (**X** = A, G, C, T, $^{TPhen}\mathbf{B_{Do}}$) and (b) ODN **Φ** : **Y** (**Y** = A, G, C, T, $^{TPhen}\mathbf{B_{Do}}$). All the solutions were prepared in 50 mM sodium phosphate, 100 mM sodium chloride, 0.1 mM sodium-EDTA, pH 7.0.

To better understand the thermodynamic origin of higher stability of the abasic DNA, we have calculated thermodynamic parameters from van't Hoff analyses of the thermal denaturation curves for all the duplexes. Thus, the van't Hoff analyses of thermal denaturation curves (**Figure 5.11**) for all the duplexes reveal that the abasic site stabilization by unnatural $^{TPhen}\mathbf{B_{Do}}$ nucleoside ($^{TPhen}\mathbf{B_{Do}}$**:Φ** and **Φ:**$^{TPhen}\mathbf{B_{Do}}$) was driven by more favourable enthalpy (higher $\Delta\Delta H$ by 8.4-11.7 kcal mole^{-1}) change compared to a natural **A:T** pair (**Table 5.5**). Also the process of coil to helix formation is accompanied with a slightly higher and a comparable change in free energy for $^{TPhen}\mathbf{B_{Do}}$**:Φ** and **Φ:**$^{TPhen}\mathbf{B_{Do}}$ pairs, respectively. This is probably because of

comparable surface area that leads to proper geometric fit and stacking with the neighboring bases along the abasic site.

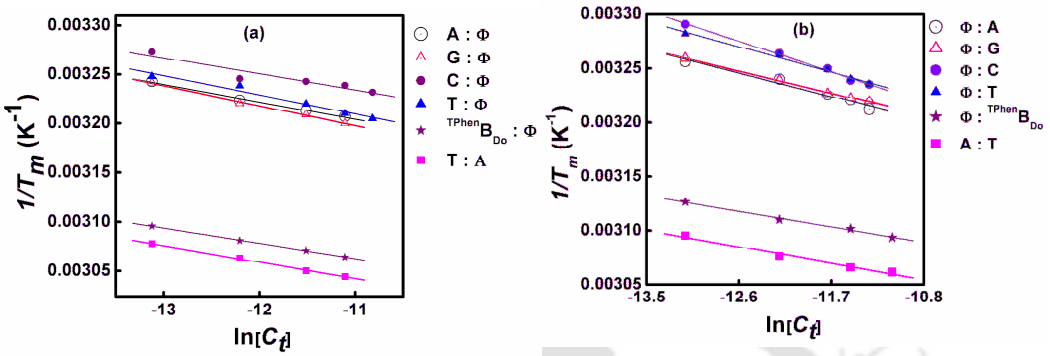

Figure 5.11: Van't Hoff Isotherms of four to five different concentrations of ODNs- (a) ODN **X** :**Φ** (**X** = A, G, C, T, $^{TPhen}\mathbf{B_{Do}}$) and (b) ODN **Φ** : **Y** (**Y** = A, G, C, T, $^{TPhen}\mathbf{B_{Do}}$). All the solutions were prepared in 50 mM sodium phosphate, 100 mM sodium chloride, 0.1 mM sodium-EDTA, pH 7.0.

These results showed that intercalative stacking interaction of $^{TPhen}\mathbf{B_{Do}}$ with DNA bases played a dominant role in stabilizing a duplex containing an abasic site paired with hydrophobic $^{TPhen}\mathbf{B_{Do}}$ unnatural base. The strong pairing selectivity between $^{TPhen}\mathbf{B_{Do}}$ and the abasic nucleoside (compare to the natural bases) and equal stabilization of $^{TPhen}\mathbf{B_{Do}}$**:Φ** duplex to that of a control **A:T** pair can be rationalized through a best geometric fit, high polarizability, large size and strong stacking ability of triazolylphenanthrene moiety of $^{TPhen}\mathbf{B_{Do}}$ nucleoside.[38a, 39]

To gain further insight into the structural preference, we, next, analyzed UV-visible, CD spectra, fluorescence anisotropy and life time data of both the $^{TPhen}\mathbf{B_{Do}}$**:Φ** and **Φ:**$^{TPhen}\mathbf{B_{Do}}$ duplexes and the single strand ODNs.

5.8.3. Study of UV-visible Spectroscopy of ODNs : Support of Intercalative Stacking

To understand the stacking interaction inside the duplex we performed the spectroscopic investigation. Thus, the UV-visible spectra of both the duplexes clearly show bathochromic shift (of ~9-10 nm) along with 27-28% increase in hypochromicities in comparison to the corresponding single stranded ODNs

containing $^{TPhen}B_{Do}$ in both the sequence contexts (**Figure 5.12, Table 5.6**) indicating strong intercalative stacking interaction between the trizolylphenanthrene and DNA base pairs along the abasic site.[43]

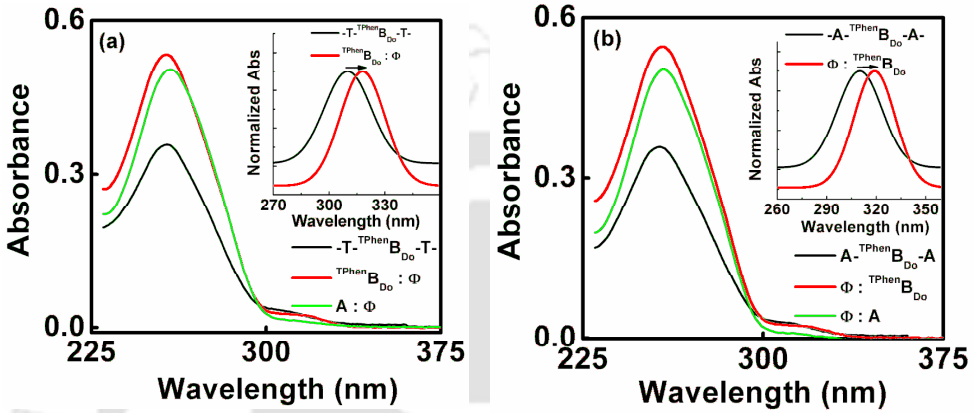

Figure 5.12: UV-visible spectra of (a) single strand ODN **1** containing $^{TPhen}B_{Do}$ (T-flanking base), its duplex ($^{TPhen}B_{Do}$:**Φ**; ODN **1•2**) with abasic site (**Φ**) containing complementary strand ODN **2** and duplex ODN **9•2** (**A** :Φ); (b) single strand ODN **7** containing $^{TPhen}B_{Do}$ (A-flanking base), its duplex (**Φ**:$^{TPhen}B_{Do}$; ODN **8•7**) with abasic site (**Φ**) containing complementary strand ODN **8** and duplex ODN **8•3** (**Φ**:**A**). Insets: Gaussian fit at the chromophoric region.

Table 5.6: Summary of UV-visible and fluorescence photophysical property

5'-CGC AAT **X** TAA CGC-3'
3'-GCG TTA **Y** ATT GCG-5'

ODNs	X : Y	λ_{max} (nm)	Abs.	% Hypochr-omicity	ε (M^{-1} cm^{-1})	λ_{max} (nm)	Φ_f
ODN **7**	**-A-** $^{TPhen}B_{Do}$ **-A-**	310	0.0285	--	11400	384	0.039
ODN **8•7**	**Φ :** $^{TPhen}B_{Do}$	320	0.0207	27.39	8280	384	0.062
ODN **1**	**-T-** $^{TPhen}B_{Do}$ **-T-**	309	0.0313	--	12520	384	0.021
ODN **1•2**	$^{TPhen}B_{Do}$ **: Φ**	318	0.0224	28.43	8960	384	0.048

5.8.4. Study of Steady State and Time Resolved Fluorescence of ODNs

The support of stacking interactions also comes from fluorescence spectroscopic studies. Thus, the steady state fluorescence studies showed increase of fluorescence intensity and quantum yield of both ODNs **1**, **7** when they form duplexes with abasic

site containing complementary strand (ODN **1•2,** ODN **8•7; Figure 5.13, Table 5.6**). The increase of fluorescence intensity of the duplexes compared to their single strand ODNs is due to the strong intercalative stacking interaction.

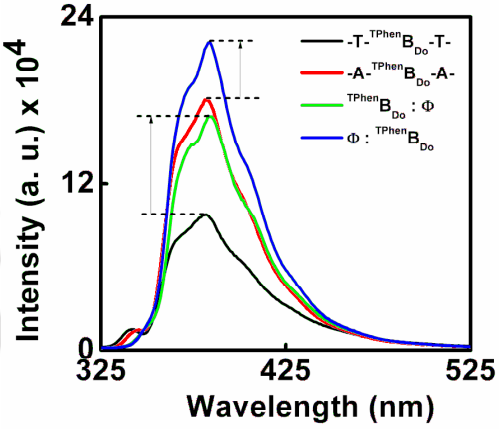

Figure 5.13: Fluorescence emission spectra of single strand ODNs **1**, **7** and their duplexes with abasic site containing complementary strand (ODN **1•2,** ODN**8•7**). Concentration of each single strand ODNs was 2.5 µM in 50 mM sodium phosphate, 100 mM sodium chloride, 0.1 mM sodium-EDTA, pH 7.0, room temperature.

Fluorescence life time experiment showed single exponential decay of $^{TPhen}\mathbf{B_{Do}}$ nucleoside in both the abasic duplexes (**Figure 5.14, Table 5.7**). The higher decay time was observed in the duplexes compared to their single stranded form. This result suggested only one mode of interaction, possibly intercalation, of $^{TPhen}\mathbf{B_{Do}}$ with the neighbouring base pairs along the abasic site. Steady state fluorescence anisotropy of triazolylphenanthrene in the duplexes ODN **1•2** ($^{TPhen}\mathbf{B_{Do}}$**:Φ**) and ODN **8•7** (**Φ:**$^{TPhen}\mathbf{B_{Do}}$) showed three times and two times, respectively, higher anisotropy values (**Table 5.7**) compared to their corresponding single strands ODN **1** or ODN **7** indicating that the triazolylphenanthrene is more strongly stacked possibly *via* intercalation between the base pairs in the duplexes. This result is also consistent with the observations from the UV-visible spectral analyses. [44]

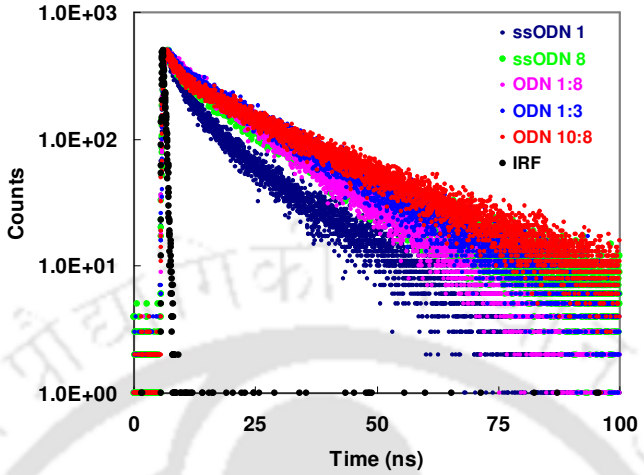

Figure 5.14: Time resolved fluorescence spectra (λ_{ex} = 308 nm LED) of the ODNs. Concentration of each single strand ODNs was 10.0 μM in 50 mM sodium phosphate, 100 mM sodium chloride, 0.1 mM sodium-EDTA, pH 7.0, room temperature.

Table 5.7: Summary of time resolved fluorescence and steady state fluorescence anisotropy

Time Resolved Fluorescence Summary			
ODNs	**X : Y**	**τ (ns)**	**χ^2**
ODN **1**	**-T-$^{TPhen}B_{Do}$-T-**	13	1.05
ODN **1•2**	**$^{TPhen}B_{Do}$: Φ**	18	1.13
ODN **7**	**-A-$^{TPhen}B_{Do}$-A-**	17	1.24
ODN **8•7**	**Φ : $^{TPhen}B_{Do}$**	21	1.20
ODN **1•7**	**$^{TPhen}B_{Do}$: $^{TPhen}B_{Do}$**	15	1.05
Steady State Fluorescence Anisotropy and Polarization Summary			
ODNs	**X : Y**	**Anisotropy (x 10^{-2})**	**Polarization (x 10^{-2})**
ODN **1**	**-T-$^{TPhen}B_{Do}$-T-**	1.5	2.2
ODN **1•2**	**$^{TPhen}B_{Do}$: Φ**(1:1)	3.5	5.1
ODN **1•2**	**$^{TPhen}B_{Do}$: Φ**(1:2)	5.8	8.5
ODN **7**	**-A-$^{TPhen}B_{Do}$-A-**	1.5	2.2
ODN **8•7**	**Φ : $^{TPhen}B_{Do}$**(1:1)	2.7	4.0
ODN **8•7**	**Φ : $^{TPhen}B_{Do}$**(1:2)	3.7	5.4

5.8.5. Study of Circular Dichroism (CD) Spectroscopy

The global conformation as well as the spatial disposition of the $^{TPhen}B_{Do}$ unit inside the abasic duplex was determined by circular dichroism (CD) spectroscopy. CD

spectral analysis of the duplexes ($^{TPhen}B_{Do}$:Φ or $^{TPhen}B_{Do}$:Φ) revealed typical B-form DNA conformation with appearance of slightly red shifted (by 3-6 nm) positive and negative ellipticities compared to those of natural A/T pair duplex. The presence of negative induced CD signals for both the duplexes $^{TPhen}B_{Do}$:Φ or $^{TPhen}B_{Do}$:Φ at ~307 nm corresponding to the chromophores' absorption band supporting possible intercalative stacking interaction operative in the duplex containing abasic site paired with unnatural nucleoside, $^{TPhen}B_{Do}$ (**Figure 5.15**).[39, 44d] The slight difference in relative intensity of these bands in two sequence context is indicative of a subtle change in intercalation site or a shift of the chromophore along the abasic site that is also supported from a macromodel study which is described below.[44d]

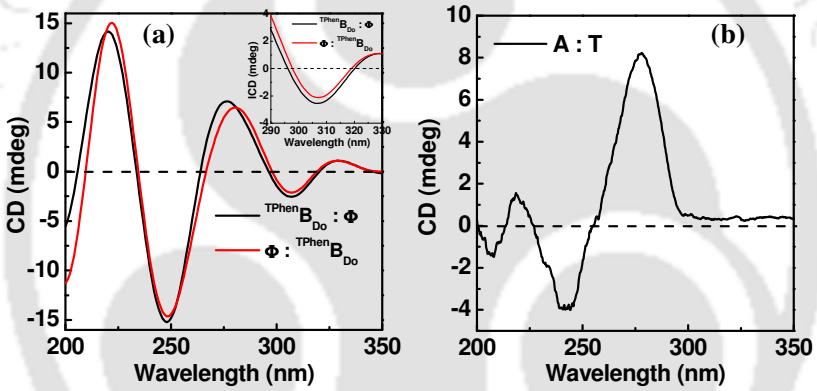

Figure 5.15: CD spectra of the duplexes shown (2.5 μM duplex concentration and 50 mM sodium phosphate, 0.1 M sodium chloride, pH 7.0).

5.8.6. Macromodel Calculations : Insight into the Conformation of Abasic Duplexes

Next, we have carried out macromodel calculation using Schrodinger MacroModel, Maestro version 9.3[45]/Macromodel version 9.9[46] by using water as solvent with Amber* force field to gain further insight into the conformation of B-form abasic duplexes and the spatial disposition of the triazolylphenanthrene unit inside the duplex. Thus, the conformations of DNA duplexes with triazolylphenanthrene ($^{TPhen}B_{Do}$) nucleoside opposite to abasic sites were minimized with the Amber* force field using Maestro, version 9.0, Schrödinger Macromodel software. The Amber* minimized structures of the abasic duplexes paired against

$^{TPhen}\mathbf{B_{Do}}$ showed intrahelical conformation of both the $^{TPhen}\mathbf{B_{Do}}$ and abasic site wherein the $^{TPhen}\mathbf{B_{Do}}$ reaches deeper into the interior of the helix along the abasic site enabling an optimal positioning for stacking interactions. Both the inter-/intra strand stacking is more in duplex $^{TPhen}\mathbf{B_{Do}}$**:Φ** compared to its reverse sequence resulted in comparatively less gap that is reflected in space filling model indicating the more mobile nature of the reverse sequence (**Φ:**$^{TPhen}\mathbf{B_{Do}}$) which is probably the cause of less stability compared to the normal sequence.

Table 5.8: Rise between base pairs

Duplex ODNs	**Sequences**		
ODN 1•2	**5'-C_1-G_2-C_3-A_4-A_5-T_6-($^{TPhen}B_{Do}$)$_7$-T_8-A_9-A_{10}-C_{11}-G_{12}-C_{13}-3'** **3'-G_{26}-C_{25}-G_{24}-T_{23}-T_{22}-A_{21}-(Φ)$_{20}$-A_{19}-T_{18}-T_{17}-G_{16}-C_{15}-G_{14}-5'**		
ODN 8•7	**5'-C_1-G_2-C_3-A_4-A_5-T_6-------(Φ)$_7$------T_8-A_9-A_{10}-C_{11}-G_{12}-C_{13}-3'** **3'-G_{26}-C_{25}-G_{24}-T_{23}-T_{22}-A_{21}-($^{TPhen}B_{Do}$)$_{20}$-A_{19}-T_{18}-T_{17}-G_{16}-C_{15}-G_{14}-5'**		
	X : Y	**Rise**	**Å**
ODN 1•2	$^{TPhen}\mathbf{B_{Do}}$ **: Φ**	T_6—($^{TPhen}B_{Do}$)$_7$	3.4–3.5
	$^{TPhen}\mathbf{B_{Do}}$ **: Φ**	($^{TPhen}B_{Do}$)$_7$—T_8	3.3–3.5
ODN 8•7	**Φ :** $^{TPhen}\mathbf{B_{Do}}$	A_{21}—($^{TPhen}B_{Do}$)$_{20}$	3.3 – 3.6
	Φ : $^{TPhen}\mathbf{B_{Do}}$	($^{TPhen}B_{Do}$)$_{20}$—A_{19}	3.3 – 3.5

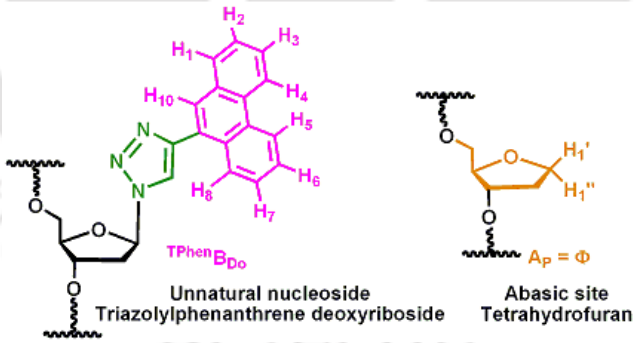

Figure 5.16: Chemical structure of $^{TPhen}\mathbf{B_{Do}}$ and **Φ** with atom number.

The Amber* optimized geometries of the duplexes ODN **1•2** ($^{TPhen}\mathbf{B_{Do}}$ **:Φ**) and ODN **8•7** (**Φ:**$^{TPhen}\mathbf{B_{Do}}$) showed that all both of them are right–handed helix with all residues having *anti* glycosidic bond and C2'-*endo*/C3'-*exo* sugar conformations. Helical rise values [Rise T_6/($^{TPhen}\mathbf{B_{Do}}$)$_7$: 3.4–3.5 Å; and Rise ($^{TPhen}\mathbf{B_{Do}}$)$_7$/ T_8: 3.3–3.5 Å] are close to those observed in B–form DNA (3.4 Å), with slight deviations at and

near the abasic site. In both of the structures the triazolylphenanthrene residue resided inside the helix (**Table 5.8**). The abasic site residue was also found to be intrahelical with C2′-*endo* sugar conformation in both the duplexes. The C1′ and C2′ of abasic residues in $^{TPhen}\mathbf{B_{Do}}$**:Φ** duplex are close to the H_3-H_4-H5 edges of its aromatic partner, triazolylphenanthrene (**Figure 5.17**) while H2-H3 edges of triazolyl phenanthrene are in close proximity with C1′ and C2′ of abasic residues of **Φ:**$^{TPhen}\mathbf{B_{Do}}$ duplex.

In $^{TPhen}\mathbf{B_{Do}}$**:Φ** duplex the H3-edge pointed toward the C1'-*β-H* and C2'-*β-H* of abasic site with distance 3.57 Å, and = 3.10 Å respectively. Also, H4-edge pointed toward the C1'-*β-H* and C2'-*β-H* of abasic site with distance 2.40 Å, and 2.96 respectively. Moreover, H5-edge pointed toward the C1'-*β-H* of abasic site with distance only 3.04 Å. In the same duplex H6-H7 pointed toward minor groove side and H1-H2 pointed towards major groove side (**Figure 5.17**).

In **Φ:**$^{TPhen}\mathbf{B_{Do}}$ duplex the H2-edge pointed toward the C2'-*β-H* of abasic site with distance 2.70 Å. Also, H3-edge pointed toward the C1'-*β-H* of abasic site with distance 2.42 Å. In the same duplex H10 pointed toward minor groove side while H5-H6 pointed towards major groove side (**Figure 5.17**).

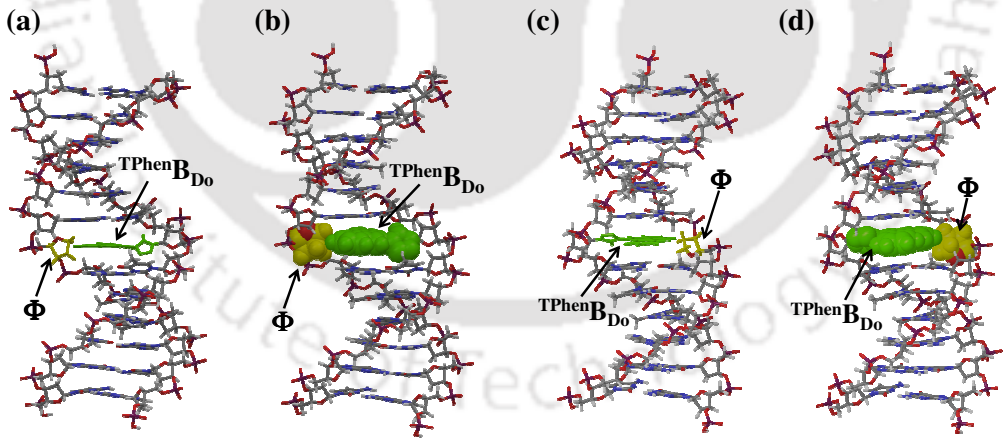

Figure 5.17: Amber* optimized geometry of the duplexes $^{TPhen}\mathbf{B_{Do}}$ **:Φ** (a-b) and **Φ:** $^{TPhen}\mathbf{B_{Do}}$ (c-d). The pictures show the $^{TPhen}\mathbf{B_{Do}}$ residues in green and the abasic sites in yellow colour.

When viewed from the helical axis of the duplex $^{TPhen}\mathbf{B_{Do}}$**:Φ**, it was observed that the triazole ring involved in stacking with flanking T_6 residue of same strand in T-shaped fashion. The full part of triazolyl phenanthrene stack extensively with the

flanking T_8 residue of the same strand (intrastrand stacking). Moreover, phenanthrene moiety fully stacked with both A_{19} and A_{21} bases in the tetrahydrofuran-containing strand (interstrand stacking) (**Figure 5.18**).

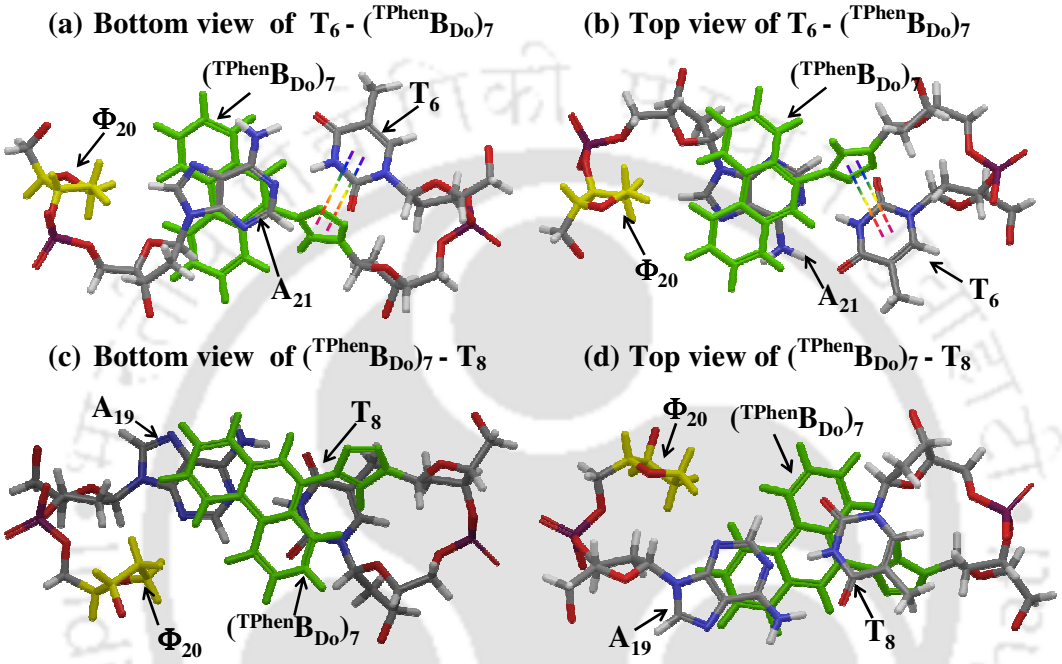

Figure 5.18: Amber* optimized and helical axis view of the ($^{TPhen}B_{Do}$ **:Φ**) duplexes showing both the interstrand and intrastrand stacking interactions of $^{TPhen}B_{Do}$ and the bases inside the duplexes. The pictures show the $^{TPhen}B_{Do}$ residues in green and the abasic sites in yellow color.

When viewed from the helical axis of the duplex **Φ-** $^{TPhen}B_{Do}$, it was observed that the phenanthrene moiety fully stacked with flanking A_{21} and partially stacked with flanking A_{19} bases in the same strand (intrastrand stacking). However, only one benzene ring of phenanthrene partially stacked with T_8 residue (interstrand stacking) and no interstrand stacking was observed with T_6 residue of tetrahydrofuran–containing strand (interstrand stacking) (**Figure 5.19**).

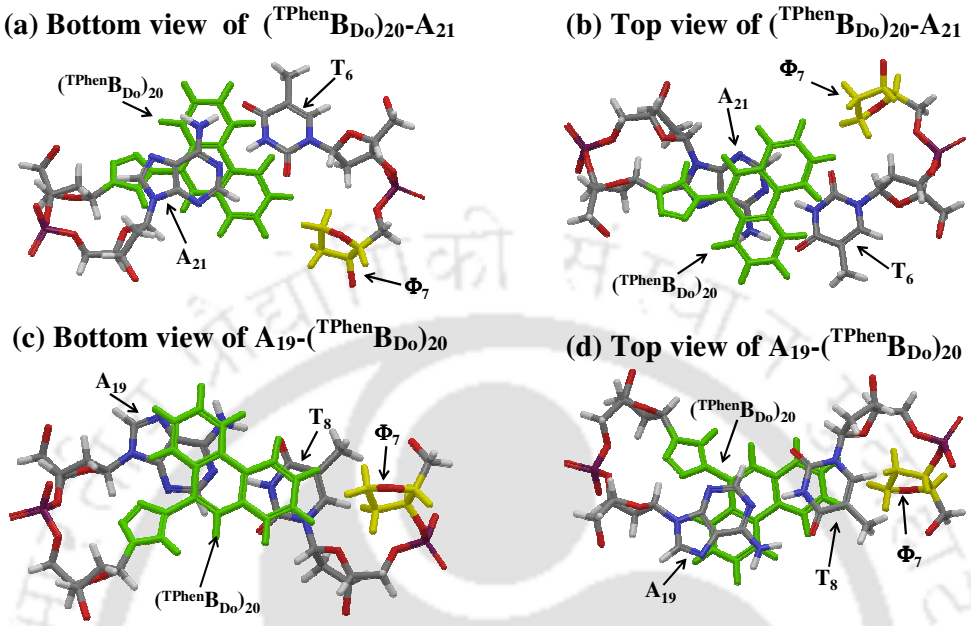

Figure 5.19: Amber* optimized and helical axis view of the (**Φ:**^{TPhen}**B$_{Do}$**)-duplexes showing both the interstrand and intrastrand stacking interactions of ^{TPhen}**B$_{Do}$** and the bases inside the duplexes. The pictures show the ^{TPhen}**B$_{Do}$** residues in green and the abasic sites in yellow coloure.

The space-filling models revealed that the size of the triazolylphenanthrene (248 Å^2) is comparable to that of natural **A:T** pair (273 Å^2) and is sufficient enough to establish tight Van der Waals contacts with the abasic site residue in the opposing strand.[38] In the case of the ^{TPhen}**B$_{Do}$:Φ** duplex (ODN **1•2**), there is negligible gap within the ^{TPhen}**B$_{Do}$:Φ** pair when viewed from major groove of the duplex but a small space was seen when viewed from minor groove side (**Figure 5.20a-b**).

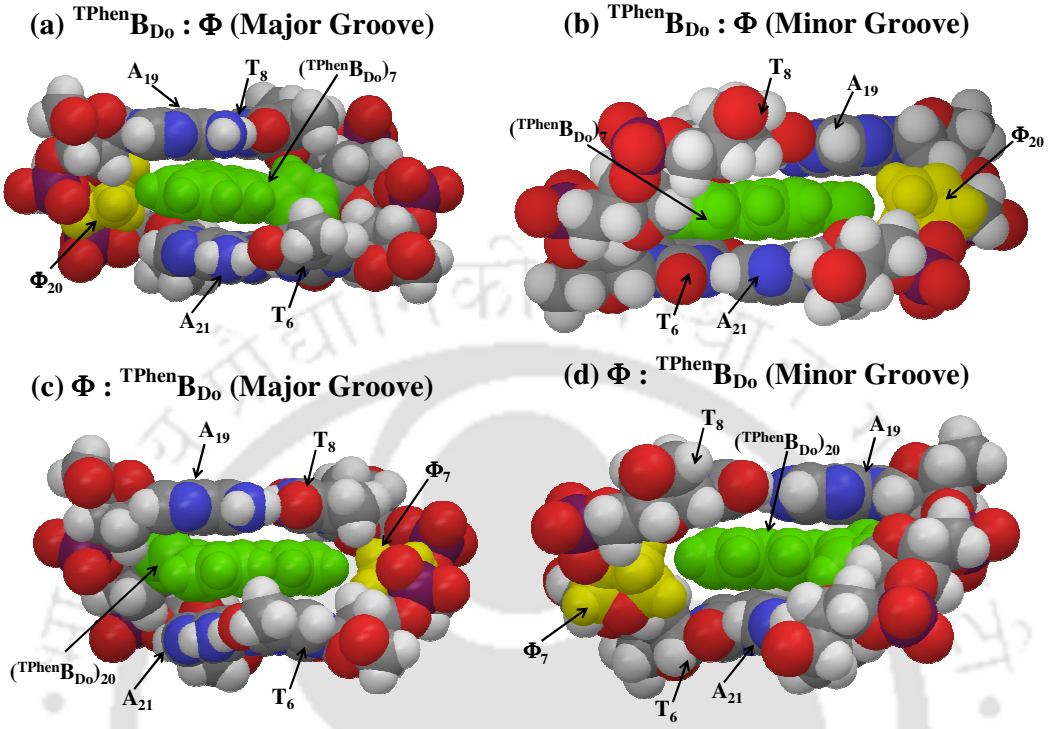

Figure 5.20: Spacefilling model of the $^{TPhen}B_{Do}$:Φ (a-b) and Φ: $^{TPhen}B_{Do}$ (c-d) duplexes and flanking base pairs with the prominent major groove (left) and minor groove (right). The pictures show the $^{TPhen}B_{Do}$ residues in green and the abasic sites in yellow coloure.

However, a small empty space is present in the Φ:$^{TPhen}B_{Do}$ duplex structure when viewed from both the grooves. As a result, percent of the triazolylphenanthrene surface accessible to solvent in the Φ:$^{TPhen}B_{Do}$ (ODN **8•7**)-duplex is more than the $^{TPhen}B_{Do}$:Φ duplex. Therefore, Φ: $^{TPhen}B_{Do}$ duplex is conformationally more mobile than $^{TPhen}B_{Do}$:Φ duplex to accommodate a water molecule after a minor adjustment of the structure. Comparatively more flexible nature of the Φ: $^{TPhen}B_{Do}$ duplex is probably the cause of less stability of the duplex compared to the duplex $^{TPhen}B_{Do}$:Φ (**Figure 5.20 c-d**).

5.9. Conclusion

In summary, high stabilization of $^{TPhen}B_{Do}$:Φ duplex that is comparable to that of a natural **A:T** pair represents a remarkable improvement in stability and selectivity

over previously reported stabilization of abasic site with non-hydrogen-bonded base. The large surface area, polarizability and strong stacking propensity play a major role to offer high duplex stabilization *via* strong intercalative stacking interaction which is evident from high duplex stability, UV-visible spectroscopy, increased fluorescence anisotropy and negative induced CD signal. The nucleoside $^{TPhen}\mathbf{B_{Do}}$ has very good pairing selectivity to pairing against an abasic site. A cooperative effect of stacking interaction of the flanking bases was reflected in higher stabilization of the duplex $^{TPhen}\mathbf{B_{Do}}$**:Φ** (by 3.2 ^{o}C) than the **Φ:**$^{TPhen}\mathbf{B_{Do}}$ duplex which was only slightly less stable (by 2.2 ^{o}C) compared to a control **A:T** pair. Though the stability offered by $^{TPhen}\mathbf{B_{Do}}$ in the reverse sequence context is slightly less than the natural **A:T** pair but comparable to that yielded by reported highest stabilizing pyrene nucleoside base. The strong pairing selectivity between $^{TPhen}\mathbf{B_{Do}}$ and the abasic nucleoside (compare to the natural bases) and equal stabilization of $^{TPhen}\mathbf{B_{Do}}$**:Φ** duplex to that of a control **A:T** pair can be rationalized through a best geometric fit, high polarizability, large size and strong stacking ability of triazolylphenanthrene moiety of $^{TPhen}\mathbf{B_{Do}}$ nucleoside.

5.10. Experimental Section

5.10.1. General Experimental

The reagents for DNA synthesis were purchased from Glen Research. Reversed-phase HPLC was performed on CHEMCOBOND 5-ODS-H columns (10x150 mm, 4.6x150 mm) using UV detector (260 nm). Mass spectra of the oligonucleotides were recorded using a MALDI-TOF mass spectrometer. The natural complementary DNAs were purchased from Integrated DNA Technologies. The *UV*–visible spectra were recorded by Shimadzu UV-2550 UV-Visible spectrophotometer with a cell of 1 cm path length. Fluorescence spectra were obtained using Fluoromax-4 fluorescence spectrophotometer at 25 °C using 1 cm path length cell. Circular Dichroism spectra were recorded on a JASCO CD J-810 spectropolarimeter.

5.10.2. Synthesis and Characterization of Modified Oligonucleotides

The synthesis of the oligonucleotide probes containing the labeled nucleodide, unnatural triazolylphenanthrene nucleoside, $^{TPhen}\mathbf{B_{Do}}$ (ODN **1** and **7**), at the centre of

each sequence was performed by a conventional phosphoramidite method using an automated DNA/RNA synthesizer. Synthesis was performed on a controlled pore glass (CPG) supported cartridge containing the 3'-nucleoside (dC for ODN **1** and dG for ODN **7)** attached to CPG support. Synthesis was carried out automatically by sequential addition of natural and modified β-cyanoethyl phosphoramidite monomers from 3'- to 5'- direction. The monomers and most of the other reagents were prepared with 10 ppm acetonitril (p.a) and left for overnight on pre dried molecular sieves (4Å) in dark. Extended coupling (10 min, 4,5-dicyanoimidazole as activator) and oxidation (60 sec) times were used during incorporation of modified phosphoramidite monomers for achieving in very good coupling yields (>90%). The unmodified phosphoramidites- DMTr-dA^{Bz}, DMTr-dC^{Bz}, DMTr-dG^{iBu}, and DMTr-T, controlled pore glass (CPG) supported cartridges, TCA deblock, activator (4,5-dicyanoimidazole (DCI) , Cap A and Cap B solutions were purchased and used. A 1 μmol scale-solid phase synthesis of the desired ODNs was carried out in trityl-on mode using modified-phosphoramidite as the extra (fifth) phosphoramidite and programmed to cleave the trityl group from the last unmodified nucleoside. The advancement of the synthesis was monitored with a 'trityl viewer' on the basis of the outgoing trityl group produced during detritylation. The coupling yield is 90%.

After the DNA synthesis was over, the cartridges from the synthesizer was taken out and transferred into an eppendorf (2 mL). Then the oligonucleotide was cleaved from the solid support under standard conditions (conc. aq. NH_3, 55 ^oC, 12 h) by incubating the solution for at least 12 hr at 55^oC in a temperature-controlled incubator. After deprotection, the ammonia was evaporated in a *speed vac*, the ODN was diluted with double distilled water (0.5 mL) and the glass beads were filtered 'off' through a Whatman 0.2 μm syringe filter. Next the solution was concentrated in a *speed vac* and made it a final solution of 1 mL. The deprotected DNA was purified from the unsuccessfully coupled sequences by reversed-phase HPLC on a 5-ODS-H column (10×150 mm, elution with 50 mM ammonium formate buffer (AF), pH 7.0, with a linear gradient over 45 min from 3% to 40% acetonitrile at a flow rate 2.0 ml/min). The desired fractions were collected in 10 mL eppendorf tubes, evaporated and finally

transferred into 2 mL eppendorf. The purified ODN was dissolved in 1 mL double-distilled water in an eppendorf tube and characterized by its *m/z* value obtained from *MALDI-TOF* using 2,4,6-trihydroxyacetophenon (0.5 M in EtOH)/Diammoniumcitrate (0.1 M in water) in 1:1 v/v as matrix. The *MALDI-TOF* was measured in normal positive mode with 19 KV acceleration voltage (**Table 5.9**). The characterized and pure DNA stock solution (1-1.5 ml) was then kept in refrigerator at -80 °C for further studies.

The concentration of the DNA stock solution was then determined applying *Lamberts-Beer's* equation: $A_{260} = \log I/I_0 = c \times \varepsilon_{260} \times l$ where $\varepsilon_{260} = \Sigma i\ \varepsilon_I$; *A260* is the absorbance of the probe at 260 nm which is determined from the intensity of the transmitted light (*I*) compared to the intensity of the emerging light (I_0), *c* is the concentration of the probe DNA, ε_{260} is the algebraic sum of extinction-coefficients of the individual nucleosides at 260 nm (for natural nucleosides, this is calculated with Oligo Analyser and *l* is the pathlength of the light through the sample.

The concentration of stock ODN **1** and ODN **7** was 609 µM and 554 µM, respectively (2.0 ml). All the natural complementary ODNs and abasic ODNs (ODN **2-6** and **8-12**) were purchased and used as supplied.

Table 5.9: MALDI-TOF-MS of synthesized ODNs.

ODNs	Sequences	*m/z* calcd. $[M + H]^+$	*m/z* found $[M + H]^+$
ODN **1**	5'- CGCAAT**Y**TTACGC -3' [**Y** = $^{TPhen}B_{Do}$]	4036.01	4036.24
ODN **7**	5'- GCGTTA**Y**ATT GCG -3'[**Y**= $^{TPhen}B_{Do}$]	4098.00	4097.56

5.10.3. General Spectroscopic Measurements

UV-visible measurements: UV-visible spectra of all the ODNs (2.5 µM concentration of each single strand) were measured in 50 mM sodium phosphate buffers (pH 7.0) containing 100 mM sodium chloride and 0.1 mM sodium-EDTA using Shimadzu 2550 UV-Visible spectrophotometer. with quartz optical cell of 1.0 cm path length and scanning rate of 0.5 nm with wavelength range of 200-500 nm and slit width of 2 nm.

Thermal melting temperature (T_m) experiments of the oligonucleotides: The thermal denaturation studies (T_m), absorbance *vs.* temperature profiles of the duplexes (2.5 µM concentration of each single strand) were measured at 260 nm using Shimadzu 2550 UV-Visible spectrophotometer equipped with a Peltier temperature controller using 1 cm path length cell in 50 mM sodium phosphate buffers (pH 7.0) containing 100 mM sodium chloride and 0.1 mM sodium-EDTA. The absorbance of the samples was monitored at 260 nm from 20 to 90 °C with a heating rate of 0.5 °C/min. From these profiles, average method was used to determine T_m values using in built software.

Calculation of thermodynamic parameters: Thermodynamic parameters were determined by van't Hoff analysis using the relation: $T_m^{-1} = R[ln(C_T)]/\Delta H + \Delta S°/\Delta H°$, where $\Delta H°$ and $\Delta S°$ are the standard enthalpy and entropy changes determined from UV experiments, respectively, R is the universal gas constant and $[C_T]$ is the total strand concentration. From the slope of the plot of $1/T_m$ vs. $\ln(C_T)$, ΔH was calculated and then substitution of this in the value of intercept yielded ΔS° and then we have calculated ΔG. Thermodynamic parameters (25 °C) were determined from van't Hoff plots using at least four to five different concentrations for each duplex.

Steady state fluorescence experiments: ODNs solutions were prepared as described in UV-visible and T_m measurement experiments. Fluorescence spectra were recorded using Fluoromax-4 fluorescence spectrophotometer at 25 °C using quartz cell of 1.0 cm path length with a slit width of 3 nm, integration time 0.2 sec and wavelength range 300-600 nm. Excitation spectra were monitored at 307 (for single standed ODNs) and 319 nm (for duplexes) emission wavelength. Fluorescence emissions were collected exciting the ODNs at the wave length corresponding to their absorption maxima. Steady-state fluorescence emission spectra were recorded at room temperature as an average of five scans using an excitation slit of 3.0 nm, emission slit 3.0 nm, and scan speed of 120 nm/min. The fluorescence quantum yields (Φ_f) were determined using quinine sulphate as a reference with the known Φ_f (0.55) in 0.1 molar solution in sulphuric acid. The following equation was used to calculate the quantum yield,

$$\Phi_S = \Phi_R \frac{Fl_S^{Area}}{Fl_R^{Area}} \frac{Abs_R}{Abs_S} \frac{n_S^2}{n_R^2}$$

where, Φ_R is the quantum yield of standard reference, Fl_S^{Area} (sample) and Fl_R^{Area} (reference) are the integrated emission peak areas, Abs_S (sample) and Abs_R (reference) are the absorbances at the excitation wavelength, and n_S (sample) and n_R (reference) are the refractive indices of the solutions.

The steady state anisotropy experiment was performed with the Fluoromax-4 fluorescence spectrophotometer at 25 °C using 1 cm path length cell. The fluorescence anisotropy (r) was calculated using the following equation-

$$r = \frac{(I_{VV} - I_{VH}G)}{(I_{VV} + 2I_{VH}G)}; \quad G = \frac{I_{HV}}{I_{HH}}$$

where, I_{VV} and I_{VH} are the emission intensities when the excitation polarizer is vertically oriented and the emission polarizer is oriented vertically and horizontally respectively. G is the correction factor. The terms I_{HV} and I_{HH} are the emission intensity when the excitation polarization is horizontally oriented and the emission polarization is oriented vertically and horizontally, respectively.

Time resolved fluorescence experiments: The time resolved fluorescence spectra were obtained by using Edinburgh instrument, Life Space II time resolved fluorescence spectrophotometer at 25 °C using 1 cm path length cell in 50 mM sodium phosphate buffers (pH 7.0) containing 100 mM sodium chloride and 0.1 mM sodium-EDTA. 308 nm LED was used as the excitation light source and the monitoring emission wavelength was fixed at 384 nm. The time correlated single photon counting (TCSPC) method was used to calculate the lifetime data. The life time data (Global Analysis) were calculated by the FAST software package with fitting range 205 – 4000 channels.

Circular dichroism (CD) measurement: CD spectra were recorded with a JASCO CD, J-810 spectropolarimeter equipped with a Peltier thermoelectric temperature control system (2.5 μM concentration of each strand in 50 mM sodium phosphate, 100 mM sodium chloride, and 0.1 mM sodium-EDTA, pH 7.0, at room temperature). The data were collected using quartz optical cells with a 1.0 cm path length.

Measurements were conducted using 2.5 μM of strands in T_m buffer. Corrections were made for buffer background CD spectra (200-400 nm) were recorded at 25 °C as an average of five scans and with a scan speed of 100 nm/min. The spectral data were analyzed with the spectra manager software.

5.10.4. Macromodel Calculations

The conformations of DNA duplexes with triazolylphenanthrene ($^{TPhen}\mathbf{B_{Do}}$) nucleosides opposite to abasic sites were minimized with the Amber* force field in water using Schrodinger Macro Model (Maestro vs. 9.0) software.

5.11. References

1. (a) Vesnaver, G; Chang, C-N; Eisenberg, M.; Grollmann, A. P.;Breslaur, K.G.; *Proc. Natl. Acad. Sci. USA* **1989**, *86*, 3614. (b) Scharer, O. D. *Angew. Chem. Int. Ed.* **2003**, *42*, 2946.
2. Lindahl, T.; Nyberg, B. *Biochemistry* **1972**, *11*, 3610.
3. (a) Demple, B.; Harrison, L. *Annu. Rev. Biochem.* **1994**, *63*, 915. (b) Lhomme, J.; Constant, J. F.; Demeunynck, M. *Biopolymers* **1999**, *52*, 65.
4. Lindahl, T.; Nyberg, B. *Biochemistry* **1972**, *11*, 3610.
5. (a) Berthet, N.; Constant, J. F.; Demeunynck, M.; Michon, P.; Lhomme, J. *J. Med. Chem* **1997**, *40*, 3346. (b) Boiteux, S.; Guillet, M. *DNA Repair* **2004**, *3*, 1.
6. Singer, B.; Grunberger, D. *Molecular Biology of Mutagens and Carcinogens: Plenum Press: New York* **1983**, 16.
7. (a) Stuart, G. R.; Chambers, R. W. *Nucleic Acids Res.* **1987**, *15*, 7451. (b) Vasseur, J. J.; Rayner, B.; Imbach, J.-L. *Biochem. Biophys. Res. Commun.* **1986**, *134*, 1204. (c) Vasseur, J.-J.; Peoch, D.; Rayner, B.; Imbach, J.-L. *Nucleosides Nucleotides* **1991**, *10*, 107. (d) Iocono, J. A.; Gildea, B.; McLaughlin, L. W. *Tetrahedron Lett.* **1990**, *31*, 175. (e) Laayoun, A.; Décout, J.-L.; Lhomme, J. *Tetrahedron Lett.* **1994**, *35*, 4989. (f) Laayoun,

A.; Décout, J.-L.; Defrancq, E.; Lhomme, J. *Tetrahedron Lett.* **1994**, *35*, 4991 (g) Groebke, K.; Leumann, C. *Helv. Chim. Acta* **1990**, *73*, 608 (h) Peoch, D.; Meyer, A.; Imbach, J.-L.; Rayner, B. *Tetrahedron Lett.* **1991**, *32*, 207.

8. (a) Takeshita, M.; Chang, C. N.; Johnson, F.; Will, S.; Grollman, A. P. *J. Biol. Chem.* **1987**, *262*, 10171. (b) Raap, J.; Dreef, C. E.; Van der Marel, G. A.; Van Boom, J. H.; Hilbers, C. W. *J. Biomol. Struct. Dynam* **1987**, *5*, 219. (c) Pochet, S.; Huynh-Dinh, T.; Neumann, J.-M.; Tran- Dinh, S.; Taboury, J. A.; Taillandier, E.; Igolen, J. *Tetrahedron Lett.* **1985**, *26*, 2085. (d) Thomas, M.; Castaing, B.; Fourrey, J.-L.; Zelwer, C. *Nucleosides Nucleotides* **1999**, *18*, 239.

9. Scharer, O. D.; Ortholand, J.-Y.; Ganesan, A.; Ezaz-Nikpay, K.; Verdine, G. L. *J. Am. Chem. Soc.* **1995**, *117*, 6623.

10. (a) Manoharan, M.; Gerlt, J. A. *J. Am. Chem. Soc.* **1987**, *109*, 7217.(b) Manoharan, M.; Ransom, S. C.; Mazumder, A.; Gerlt, J. A.; Wilde, J. A.; Withka, J. A.; Bolton, P. H. *J. Am. Chem. Soc.* **1988**, *110*, 1620. (c) Wilde, J. A.; Bolton, P. H.; Mazumder, A.; Manoharan, M.; Gerlt, J. A. *J. Am. Chem. Soc.* **1989**, *111*, 1894.

11. Wilde, J. A.; Bolton, P. H.; Mazumder, A.; Manoharan, M.; Gerlt, J. A. *J. Am. Chem. Soc.* **1989**, *111*, 1894.

12. (a) Bailly, V.; Derydt, M.; Verly, W. G. *Biochem. J.* **1989**, *261*, 707. (b) Bailly, V.; Verly, W. G. *Biochem. J.* **1988**, *253*, 553.

13. Latham, K. A.; Lloyd, R. S. *Biochemistry* **1995**, *34*, 8796.

14. (a) Goljer, I.; Withka, J. M.; Kao, J. Y.; Bolton, P. H. *Biochemistry* **1992**, *31*, 11614. (b) Goljer, I.; Kumar, S.; Bolton, P. H. *J. Biol. Chem.* **1995**, *270*, 22980. (c) Singh, M. P.; Hill, G. C.; Peoch, D.; Rayner, B.; Imbach, J. L.; Lown, J. W. *Biochemistry* **1994**, *33*, 10271. (d) Withka, J. M.; Wilde, J. A.; Bolton, P. H.; Mazumder, A.; Gerlt, J. A. *Biochemistry* **1991**, *30*, 9931.

15. Raap, J.; Dreef, C. E.; Van der Marel, G. A.; Van Boom, J. H.; Hilbers, C. W. *J. Biomol. Struct. Dynam* **1987**, *5*, 219.

16. (a) Coppel, Y.; Berthet, N.; Coulombeau, C.; Garcia, J.; Lhomme, J. *Biochemistry* **1997**, *36*, 4817. (b) Cuniasse, P.; Sowers, L. C.; Eritja, R.; Kaplan, B.; Goodman, M. F.; Cognet, J. A.; LeBret, M.; Guschlbauer, W.; Fazakerley, G. V. *Nucleic Acids Res.* **1987**, *15*, 8003. (c) Cuniasse, P.; Sowers, L. C.; Eritja, R.; Kaplan, B.; Goodman, M. F.; Cognet, J. A.; Le Bret, M.; Guschlbauer, W.; Fazakerley, G. V. *Biochemistry* **1989**, *28*, 2018. (d) Kalnik, M. W.; Chang, C. N.; Grollman, A. P.; Patel, D. J. *Biochemistry* **1988**, *27*, 924.

17. Kalnik, M. W.; Chang, C. N.; Johnson, F.; Grollman, A. P.; Patel, D. J. *Biochemistry* **1989**, *28*, 3373.

18. (a) Goljer, I.; Kumar, S.; Bolton, P. H. *J. Biol. Chem.* **1995**, *270*, 22980. (b). Coppel, Y.; Berthet, N.; Coulombeau, C.; Garcia, J.; Lhomme, J. *Biochemistry* **1997**, *36*, 4817.(c). Feig, M.; Zacharias, M.; Pettitt, B. M. *Biophys. J.* **2001**, *81*, 351. (d). Chen, J.; Dupradeau, F.−Y.; Case, D. A.; Turner, C. J.; Stubbe, J. *Nucleic Acids Res.* **2008**, *36,* 253. (e). Hoehn, S. T.; Turner, C. J.; Stubbe, J. *Nucleic Acids Res.* **2001**, *29*, 3413.

19. (a) Vesnaver, G.; Chang, C. N.; Eisenberg, M.; Grollman, A. P.; Breslauer, K. J. *Proc. Natl. Acad. Sci. USA*, **1989**, *86*, 3614. (b) Gelfand, C. A.; Plum, G. E.; Grollman, A. P.; Johnson, F.; Breslauer, K. J. *Biochemistry* **1998**, *37*, 7321.

20. Sagi, J.; Guliaev, A. B.; Singer, B. *Biochemistry* **2001**, *40*, 3859.

21. (a) Hoehn, S. T.; Turner, C. J.; Stubbe, J. *Nucleic Acids Res.* **2001**, *29*, 3413. (b) Chen, J.; Dupradeau, F.-Y.; Case, D. A.; Turner, C. J.; Stubbe, J. *Nucleic Acids Res.* **200**8, *36*, 253.

22. (a) Lhomme, J.; Constant, J. F.; Demeunynck, M. *Biopolymers* **1999**, *52*,65. (b) Boiteux, S.; Guillet, M. *DNA Repair* **2004**, *3*, 1. (c) Cline, S. D.; Jones, W.; Stone, M. P.; Osheroff, N. *Biochemistry* **1999**, *38*,15500.

23. Atamna, H.; Cheung, I.; Ames, B.N. *Proc. Natl. Acad. Sci. USA* **2000**, *97*, 686.

24. Behmoaras, T.; Helene, C.A. *Nature* **1981**, *292*, 858.

25. **25.** Lhomme, J.; Constant, J.F.; Demeunynck, M. *Biopolymers* **1999**, *52*, 65.

26. Fkyerat, A.; Demeunynck, M.; Constant, J. F.; Michon, P.; Lhomme, J. *J. Am. Chem. Soc.* **1993**, *115*, 9952.

27. Strekowski, L.; Wilson, B. *Mutat. Res.* **2007**, *623*, 3

28. (a) Constant, J.F.; Demeunynck, M. *In Small Molecule DNA and RNA Binders, Wiley-VCH, Weinheim,* **2003**. (b) Martelli, A.; Jourdan, M.; Constant, J. F.; Demeunynck, M.; Dumy, P. *Bioorg. Med. Chem. Lett.* **2006**, *16*, 154. (c) K. Benner, A. Granzhan, H. Ihmels, G. Viola Eur. *J. Org. Chem.* **2007,** *28*, 4721.

29. Boturyn, D.; Boudali, A.; Constant, J. F.; Defrancq, E.; Lhomme, J. *Tetrahedron* **1997**, *53*, 5485.

30. (a) Jakobsen, U.; Shelke, S.A.; Vogel, S.; Sigurdsson, S.T. *J. Am. Chem. Soc.* **2010**, *132*, 10424. (b) Zeglis, B. M.; Boland, J. A.; Barton, J. K. *J. Am. Chem. Soc.* **2008**, *130*, 7530. (c) Zeglis, B. M.; Boland, J.A.; Barton, J.K. *Biochemistry* **2009**, *48*, 839.

31. (a) Zeglis, B. M.; Boland, J. A.; Jacqueline K. Barton, J. K. *J. Am. Chem. Soc.* **2008**, *130*, 7530. (b) Zeglis, B. M.; Boland, J. A.; Jacqueline K. Barton, *Biochemistry* **2009**, *48,* 839.

32. (a) Fakhari, M. A.; Rokita, S. E. *Chem. Commun.* **2011**, *47*, 4222. (b) Benner, K.; Ihmels, H.; Kolsch, S.; Pithan, P. M. *Org. Biomol. Chem.* **2014**, *12*, 1725.

33. (a) Langenegger, S. M.; Haner, R. *Chem. Biodiversity* **2004**, *1*, 259. (b) Langenegger, S. M.; Haner, R. *ChemBioChem.* **2005**, *6*, 848. (c) Malinovskii, V. L. ; Wenger, D.; Haner, R. *Chem. Soc. Rev.* **2010**, *39*, 410.

34. Fukui, K.; Morimoto, M.; Segawa, H.; Tanaka, K.; Shimidzu, T. *Bioconjugate Chem.* **1996**, *7*, 349.

35. Fukui, K; Tanaka, K. *Nucleic Acids Res.* **1996***, 24,* 3962.

36. Cuniasse, P. ; Sowers, L. C.; Eritja, R.; Kaplan, B.; Goodman, M. F.; Cognet, J. A. H.; Bret, M. L.; Guschlbauer, W.; Fazakerley, G. **V.** *Biochemistry* **1989**, *28,* 2018 **.**

37. Millican, T. A.; Mock, G. A.; Chauncey, M. A.; Patel, T. P.; Eaton, M. A.; Gunning, J.; Cutbush, S. D.; Neidle, S.; Mann, J. *Nucleic Acid Res.* **1984**, *12*, 7435.

38. (a) Matray, T. J.; Kool, E. T. *J. Am. Chem. Soc.* **1998**, *120*, 6191. (b) Kool, E. T.; Morales, J. C.; Guckian, K. M. *Angew. Chem. Int. Ed.* **2000**, *39*, 990. (c) Smirnov, S.; Matray, T. J.; Kool, E. T.; los Santos, C. *Nucleic Acids Res.* **2002**, *30*, 5561.(d) Matray, T. J.; Kool, E. T. *Nature* **1999**, *399*, 704. (e) Guckian, K. M.; Schweitzer, B. A.; Ren, R. X.-F.; Sheils, C. J.; Paris, P. L.; Tahmassebi, D. C.; Kool, E. T. *J. Am. Chem. Soc.* **1996**, *118*, 8182.

39. Wojciechowski, F.; Lietard, J.; Leumann, C. J. *Org. Lett.* **2012**, *14,* 5176.

40. (a) Smirnov, S.; Matray, T. J.; Kool, E. T.; Santos, C. l. *Nucleic Acids Res.* **2002**, *30*, 5561. (b) Hwang, G. T.; Romesberg, F. E. *Nucleic Acids Res.* **2006**, *34*, 2037. (c) Seo, Y. J.; Romesberg, F. E. *Chembiochem.* **2009**, *10*, 2394.

41. Bag, S. S.; Talukdar, S.; Matsumoto, K.; Kundu, R. *J. Org. Chem.* **2013**, *78*, 278.

42. Maestro, version 9.0, Schrödinger, LLC, New York, NY, **2009**.

43. (a) Dougherty, G.; Pilbrow, J. R. *Int. J. Biochem.* **1984**, *16*, 1179. (b) Nakamura, M.; Fukunaga, Y.; Sasa, K.; Ohtoshi, Y.; Kanaori, K.; Hayashi, H.; Nakano, H.; Yamana, K. *Nucleic Acids Res.* **2005**, *33*, 5887.

44. (a) Murakami, A.; Nakaura, M.; Nakatsuji, Y.; Nagahara, S.; Tran-Cong, Q.; Makino, K. *Nucleic Acids Res.* **1991**, *19*, 4097. (b) Nakamura, M.; Fukunaga, Y.; Sasa, K. ; Ohtoshi, Y.; Kanaori, K.; Hayashi, H.; Nakano, H.; Yamana, K. *Nucleic Acids Res.* **2005**, *33*, 5887; (d) Lyng, R. ; Rodger, A.; Norden, B. *Biopolymers* **1991**, *31*, 1709.

45. Maestro, Version 9.3 Schroëdinger, LLC, New York, NY, **2012.**

46. MacroModel, Version 9.9 Schroëdinger, LLC, New York, NY, **2012.**

Chapter 6

STUDIES ON THE DUAL MECHANISM OF EXCIPLEX EMISSION IN A CHIMERIC DNA DUPLEX CONTAINING NON-NUCLEOSIDE-NUCLEOSIDE BASE PAIR

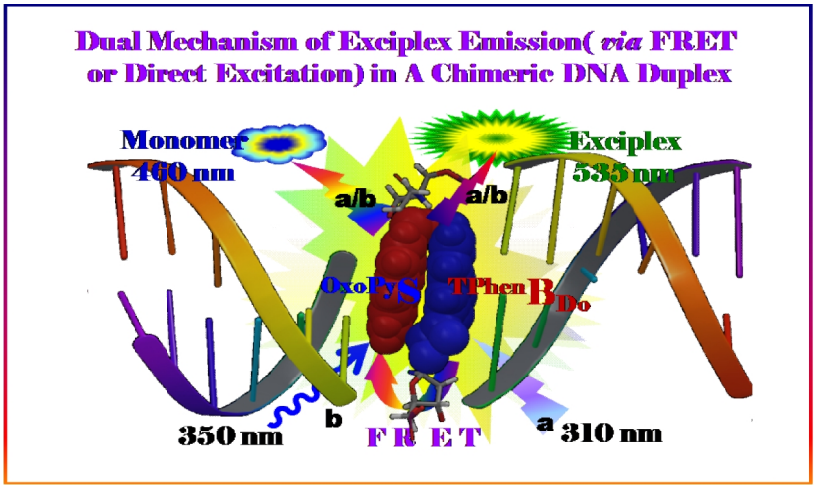

6.1. Introduction

The phenomena of exciplex emission and Förster resonance energy transfer (FRET) find widespread applications in chemistry, biology and material sciences.[1] FRET is a nonradiative photophysical phenomenon in which the energy of a donor (D) in an excited state is transferred to an acceptor (A) in the ground state. This nonradiative transfer of energy occurs through long range resonance coupling between the relaxation transition dipole of the donor and the excitation transition dipole of the acceptor.[2] The FRET process is diagrammatically represented in Jablonski diagram below in **Figure 6.1.**

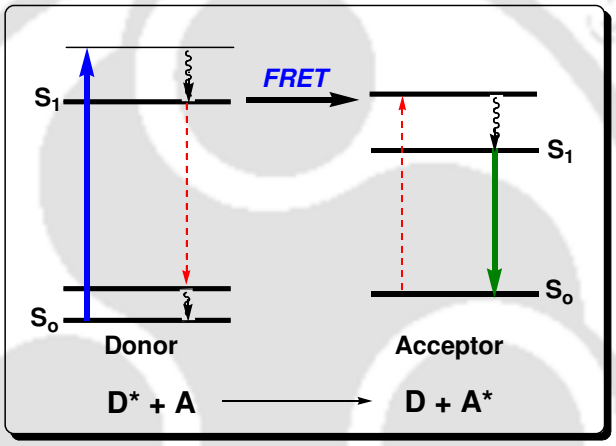

Figure 6.1: Jablonski diagram indicating energy transfer through FRET.

The process of resonance energy transfer *via* FRET occurs when the emission spectra of a donor overlap with the absorption spectra of an acceptor and the donor and acceptor remain within the characteristic Förster distance (R_o). Thus, FRET is a distance dependent phenomenon and hence is used to determine distances in biomolecular assemblies. The rate of energy transfer is dependent on the intermolecular distance between the D and A.[1,3] In general, the fluorescence intensity and the quantum efficiency of the acceptor increases and that of the donor decreases in a FRET event.[1,3] FRET as a spectroscopic ruler, thus, can probe the molecular proximity quantitatively in many biological events at angstrom distances with much more accuracy than other methods can provide.[4] As for example, FRET based

imaging techniques have been used in the study of cellular events.[5,4c] FRET is also being widely used as sensor to probe cell structure,[5b] protein folding/unfolding status, [4c] for detection of glucose in clinical diagnostic,[5d] and to study antigen-antibody[5e] interactions.

Recently, our group observed the FRET process in a tripeptide containing fluorescent triazolyl donor and acceptor unnatural amino acids separated by a natural amino acid which might find application in studying solution conformational distribution of an unstructured peptide and FRET based bioassay (**Figure 6.2 a**).[6a]

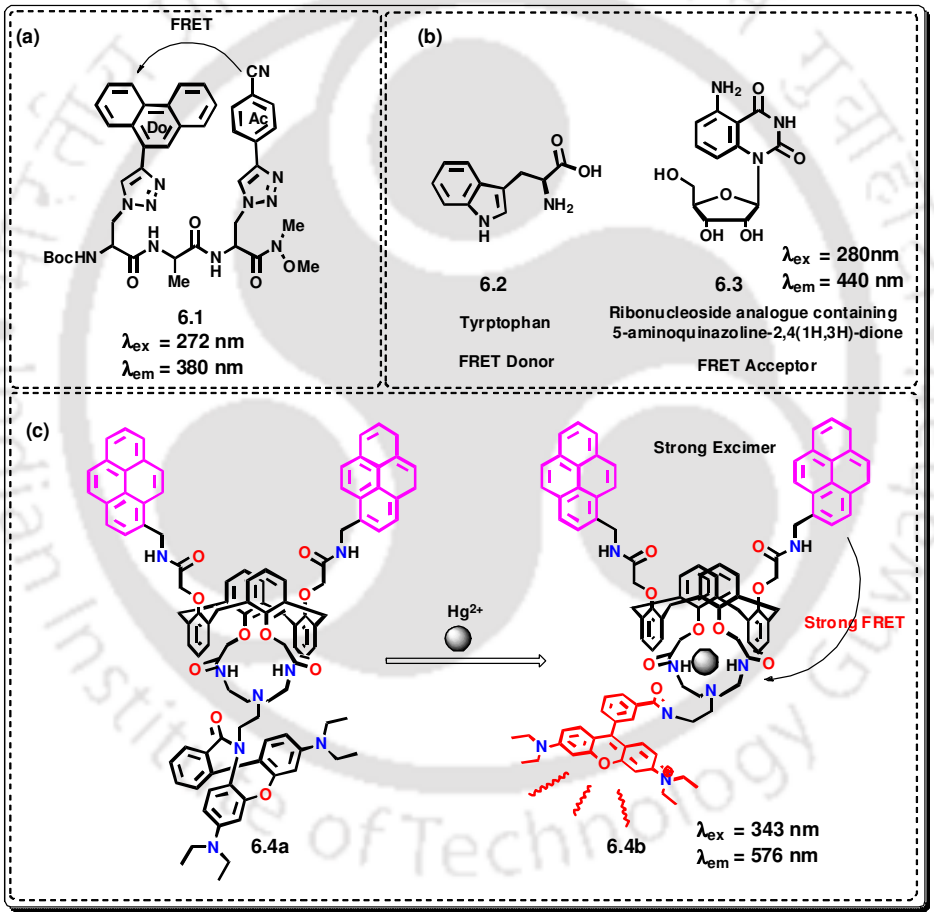

Figure 6.2: (a) FRET in unnatural peptide. (b) FRET between amino acid and ribonucleoside analogue. (c) FRET in sensory application.

A fluorescent ribonucleoside analogue containing 5-aminoquinazoline-2,4(*1H,3H*)- dione acts as a FRET acceptor of tryptophan (**Figure 6.2 b**) has been

reported by Tor *et al*. Thus, this FRET pair is suitable for monitoring protein-RNA interactions with native tryptophan residues in proteins and peptides.[6b] Besides these applications, the FRET phenomenon has been utilized in sensing metal ions. For example, Lee *et al.* have developed a novel calix[4]arene derivative appended to two pyrene moieties and a rhodamine fluorophore which acts as a selective sensor for Hg^{2+} ion (**Figure 6.2 c**).[6c] Rigid structure of double helical DNA is of no exception that also allows the opportunity for studying distance dependence of FRET process few examples of which will be presented under **Section 6.2**.[7]

On the other hand, exciplex formation involves the complexation between the excited state of a donor and/or acceptor and the ground state of an acceptor and/or donor and is always characterized by a long radiative decay time and red-shifted fluorescence emission. Exciplex formation is presented in **Figure 6.3**.[8]

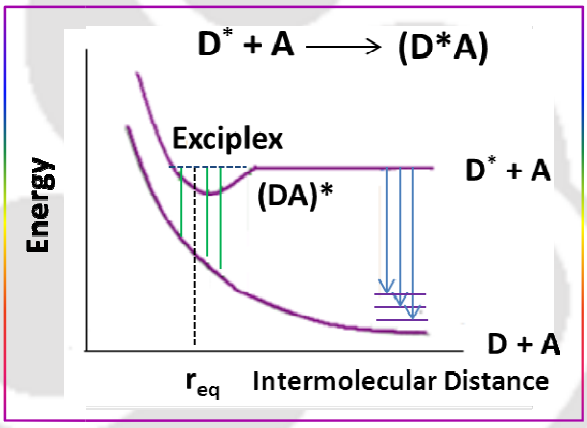

Figure 6.3: Jablonski diagram indicating exciplex emission.

Exciplex emission has also got considerable attention due to its diverse range of potential applications such as in nucleic acid detection, in biosensing and signaling devices in material science.[1,9] For example, fluorescent chemosensors exhibiting exciplex emission have been utilized in fluoride ion detection as well as a pH sensor.[10] Thus, the fluorescent chemosensor **6.5a** was found to selectively recognize the fluoride ion *via* the generation of exciplex emission (**Figure 6.4**). The fluorescence of the compound **6.5a** (λ_{em} = 360 nm) was quenched upon addition of fluoride ion and simultaneously a new band appeared at longer wavelength (λ_{em} = 455

nm). The appearance of the new band was attributed to the formation of an exciplex.[10a]

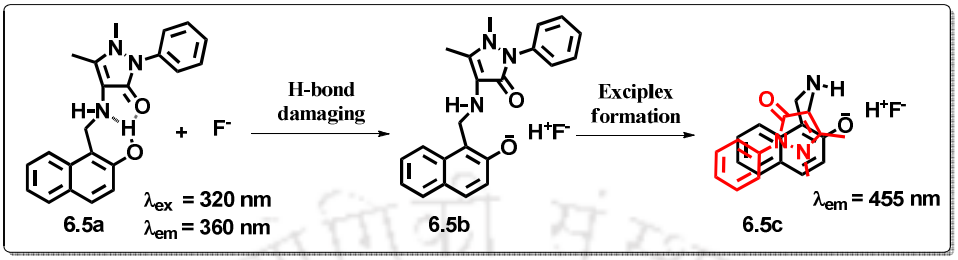

Figure 6.4: Schematic illustration of breaking of intramolecular hydrogen bonding upon addition of fluoride ion-the molecular structure changes from rigid to flexible leading to an exciplex emission.

Bencini and Biianchi *et al.* have reported an exciplex emission based fluorescent chemosensor which acted as a pH sensor.[10b] Thus, their synthesized Zn(II) complex of the macrocyclic ligand **6.6a** shown in **Figure 6.5** was known to exhibit pH modulated exciplex emission driven by the coordination of the pendent arm to the metal ion resulting in π-π stacking interaction between the anthracene and the phenanthroline moieties of the same molecule (**Figure 6.5**).

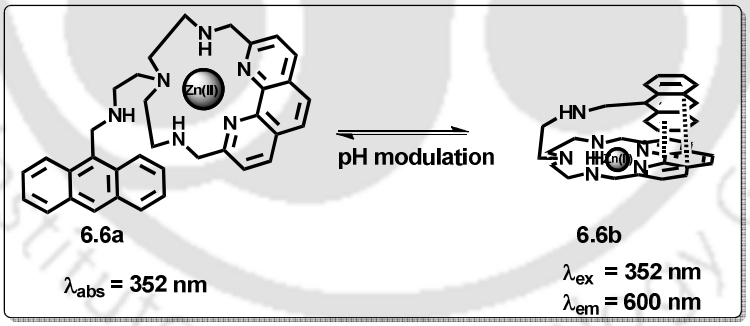

Figure 6.5: pH modulated formation of the π-stacking complex (exciplex) in presence of Zn(II).

6.2. Application of FRET in DNA

Monitoring the DNA hybridization by fluorescence spectroscopy using fluorescent dye labelled DNA is a well established and relatively inexpensive technique. Förster resonance energy transfer (FRET) has been widely used to study

the structure and dynamics of molecules in the gas phase, solution, and solid state.[8,11] During the past two decades, FRET has also been employed in studies of DNA duplex formation, determination of duplex structure and investigating protein binding events. Monitoring the nucleic acid hybridization events is possible *via* FRET technique if different fluorophores (donor/acceptor pairs) are attached within two complementary DNA whose spectral overlap satisfy the fluorescence energy transfer from donor to acceptor. In this connection, the pioneering work by Clegg *et al.*[12] is highly appreciative wherein they have reported, for the first time, the use of donor and acceptor probes in nucleic acid separated by a variable number of base pairs in a helical geometry of double-stranded DNA in solution leading to a Förster resonance energy transfer process. Their study provided an excellent opportunity for structural investigation of DNA by the FRET technique. Later on, Hurley and Tor *et al.*[13] extended this FRET technique in nucleic acid system and concluded that the DNA double helix is an intriguing platform for the study of FRET processes. As a result of tremendous research efforts, several FRET based systems have been designed to target DNA. As for example, in-situ optical DNA detection has been demonstrated by measuring the amplified fluorescence of dye-labelled DNA generated *via* FRET in an electrostatic complex of a cationic conjugated polymer and a dye-labelled anionic DNA strand.[14] A conjugate FRET system consisting of oligonucleotides, chromophores, and gold nanoparticles (GNPs) have been utilized for the detection of DNA complementary to probe G-quadruplex. It was observed that after hybridization with target DNA, the G-quadruplex stretched and resulted in an enhancement of fluorescence. This FRET system can be used for sensing of target DNA with detection limit as low as 40 pM (S/N=3). The result of this study reflected that bigger GNPs had higher fluorescence enhancement after hybridization with target DNA.[15] Highly water soluble quantum dots with cadmium selenide cores and coated with zinc sulfide shells attached to the ligand, 3-mercaptopropionic acid have been exploited as donor which transfer the energy *via* FRET to the acceptor dye Cy3 attached to DNA. This system was able to determine the hybridization event of DNA.[16] The fluorescence decay on a picoseconds time scale of a donor was employed by Luca *et al.* in a suitable donor-acceptor FRET system to reveal DNA sequences that are

specific of genetically correlated diseases.[17] Employing this strategy they were able to identify an individual, even heterozygote, carrying the sequences of the DQB1 gene that confers susceptibility to the development of insulin-dependent diabetes mellitus without performing DNA extraction, purification or PCR amplification.[17]

From the above discussion, it is clear that over the years many FRET-based DNA systems have, therefore, been developed and widely utilized in the genetic analysis such as the detection of genetic mutations and monitoring the DNA hybridization events.[18] A number of laboratories have also explored FRET interactions in multichromophoric DNA using traditional monomeric fluorescent dyes. However, we will restrict our discussion only to a few of those FRET–DNA systems wherein the DNA scaffolds such as non-nucleosidic base surrogates,[19a] labels of nucleobases,[19b] or unnatural nucleobase[19c] comprise the part of a FRET DNA system.

Therefore, there is no doubt that FRET is an emerging technique in DNA research and also it has been nicely established by various research groups. However, the donor/acceptor pairs used in FRET studies are structurally limited and of very specific combinations. Previously, the donor/acceptor pairs were composed of dyes belonging to fluorescein and rhodamine family, respectively (**Figure 6.6**).[20] These dyes are often attached to the nucleobases through a flexible linker and thereby enabling them to move freely in space and involve in FRET interaction process.

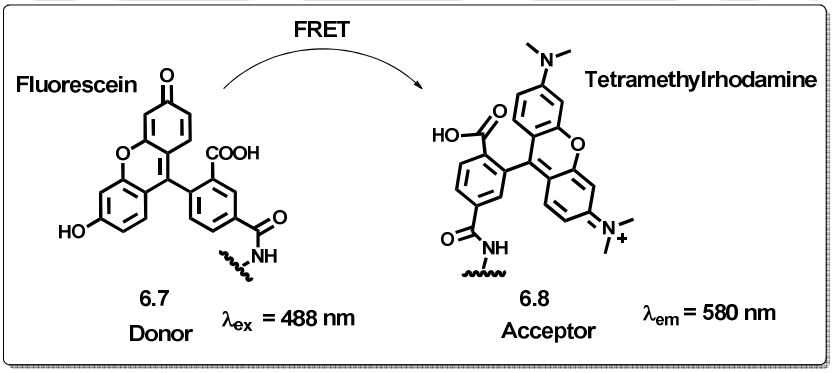

Figure 6.6: Structures of fluorescein-rhodamine FRET donor-acceptor pair labelled in DNA and involved in FRET process.

Polycyclic aromatic hydrocarbons based on pyrene as donor and perylene as acceptor are also of significant interest to design another donor/acceptor pairs and thereby expand the field of FRET-based applications.[21,22] Perylene has high quantum yield. The absorption spectrum of perylene overlaps with the emission spectrum of pyrene and thereby allowing these two aromatic hydrocarbons to constitute a FRET pair. Masuko and coworkers were the first to introduce pyrene and perylene as FRET pair to study the nucleic acid hybridization event.[22] They have reported a FRET efficiency approaching 100% when the two fluorophores were in close proximity upon DNA hybridization.

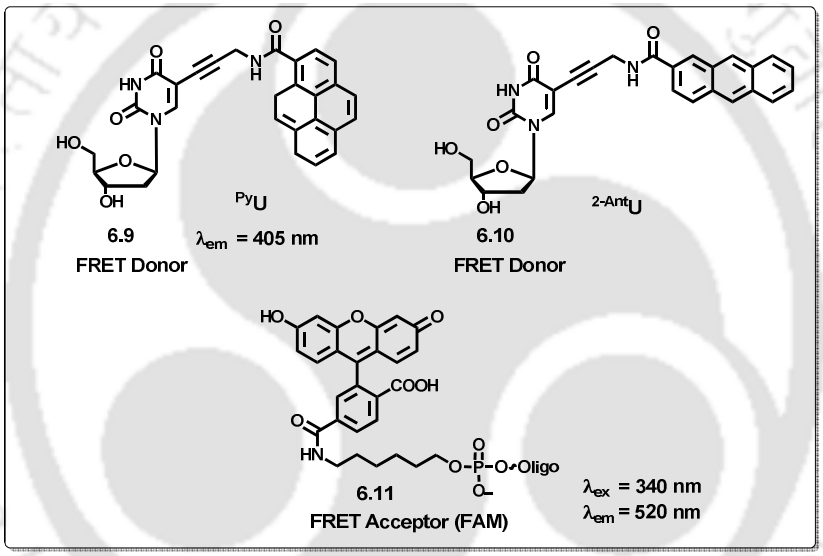

Figure 6.7: Chemical structures of the two BDF nucleosides, ^{Py}**U** and $^{2\text{-Ant}}$**U**, as donors and the **FAM** (**F**) as the acceptor fluorophore used in the probe design for DNA detection.

Dual-labeled oligonucleotide probe for sensing adenosine *via* FRET was reported by Saito *et al.*[23] They incorporated the fluorescent labelled nucleoside containing pyrene and/or anthracene derivative in the middle of a DNA which acted as FRET donor and fluorescein at the 5′-end of the oligonucleotide probe acted as a FRET acceptor (**Figure 6.7**). The phenomenon of FRET was observed between the donor and the acceptor. Thus, the dual labelled oligonucleotide probe showed selective emission from the acceptor upon excitation at the donor only when the opposite base

of the base-discriminating fluorescence (BDF) nucleoside ^{Py}**U** and/or $^{2\text{-}Ant}$**U**, was adenine on the complementary target sequence. Thus, they were able to detect the presence/absence of complementary DNA base of a target DNA opposite of labeled BDF base of probe DNA by a discriminating fluorescence signal generated *via* FRET.

Non-nucleosidic base surrogates tethered with fluorophores have also been utilized and reported by various research groups to study the photophysical properties during DNA hybridization event. Thus, two non-nucleosdic base surrogates based on D-threoninol labelled with perylene and pyrene fluorophores were developed by Asanuma and co-workers to elucidate the DNA structure, dynamics and hybridization events.[24] They incorporated the pyrene and perylene units covalently attached on D-threoninol acyclic scaffold into the middle of the DNA and established that pyrene-perylene couple formed an efficient FRET donor-acceptor pair (**Figure 6.8**).

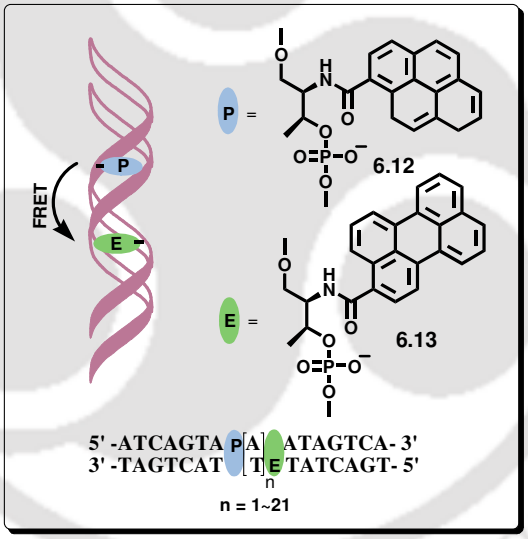

Figure 6.8: FRET between non-nucleosidic base surrogate pyrene and perylene incorporated in DNA.

An accurate and detailed investigation on the structure and dynamics of nucleic acids as well as their interactions with other biomacromolecules *via* FRET was presented by Wilhelmsson *et al.*[25] *via* the design of doubly labelled DNA duplex containing two nucleobase analogues in two strands acting as FRET-pair. In their designed DNA duplex, one strand contained the unnatural nucleoside, **tC^{O}** (1,3-diaza-

2-oxophenoxazine) acting as an energy donor while the complementary strand consisted of unnatural nucleoside, **tC_{nitro}** (7-nitro-1,3-diaza-2-oxophenothiazine) acting as an energy acceptor. In the duplexes both the base analogues were rigidly located within the base stack which enabled very high control of the orientation factor in the FRET event. They observed that the FRET-pair monitors distances covering up to more than one turn of the DNA duplex successfully. Moreover, the rigid stacking of the two nucleobase analogues enabled excellent control of their exact positions and orientations which resulted in a very distinct change in FRET signal as the number of bases, separating the two nucleobase analogs, **tC^{O}** and **tC_{nitro}**, was varied. The importance of their findings lies on the fact that the placement of FRET-pair chromophores inside the base stack might have a great advantage in studying the interaction between nucleic acid and other molecules/biomacromolecules. This is the first experimental support to the dependence of energy transfer efficiency on orientation of involved transition dipoles as predicted by the Förster theory (**Figure 6.9**).

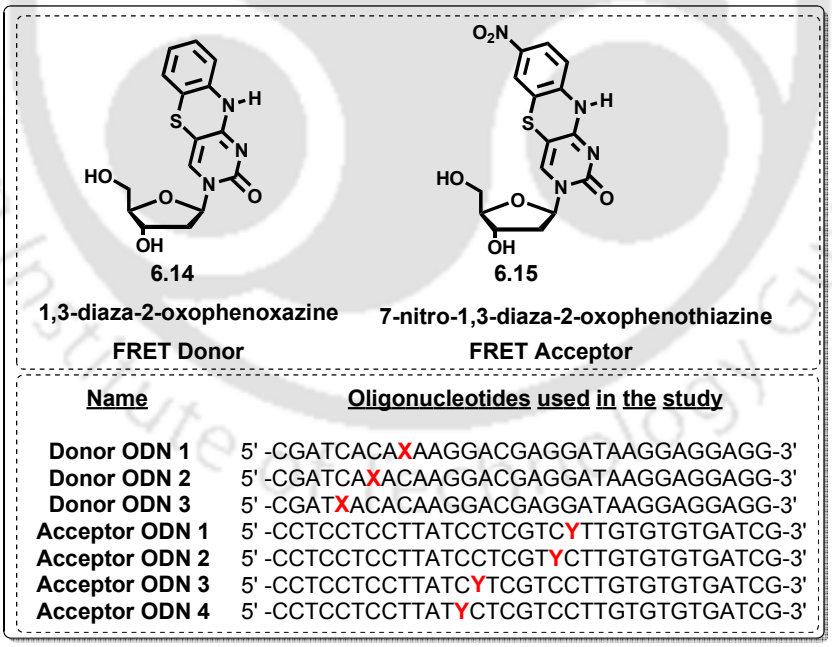

Figure 6.9: Nucleosidic base surrogate 1,3-diaza-2-oxophenoxazine and 7-nitro-1,3-diaza-2-oxophenoxazine demonstrating FRET and the oligonucleotides used in the study.

6.3. Application of Excimer/Exciplex in DNA

Similar to the FRET process in nucleic acid systems, fluorescent excimers/exciplexes also have a great potential in the application of biosensing and bioimaging due to the fact that they exhibit unique absorption and emission spectra often with unusually large Stokes shifts.[1] Excimer/exciplex based probes allow the analysis of target *via* the shift in emission wavelength and/or colour changes between the monomeric fluorophores and the excimer/exciplex leading to high detection sensitivity of biomolecules.[18c, 26] Natural nucleobases interact with each other in the excited state with very low efficiency as fluorophores and excimers of adenine have been observed.[27] Häner and co-workers have studied the DNA hybridization through the pyrene-pyrene excimer emission.[28] They have also extended their efforts and reported that pyrene-pyrene excimer emission can also be an efficient FRET donor to perylene[28d] or Cy5 dye.[28e]

Although FRET and excimer emission phenomena have been mainly studied in DNA analyses, but exciplex emission has not received much attention. One of the possible reasons is that FRET and excimer emission work efficiently in aqueous media but an exciplex emission is weak due to the dissociation of an exciplex in hydrophilic environment. Despite this problem, exciplex-based approaches offer more property diversity than excimers such as in exciplex there is a freedom in selection of exciplex-partners, variability in excitation and emission wavelength *etc.* and hence might find potential application in nucleic acids research.

Therefore, with the advent of DNA modification technologies and interest of designing functional DNA based materials, new stacks of modified base pairs have been engineered and incorporated into DNA to discover new capabilities of showing interesting photophysical properties like excimer/exciplex. The majority of excimer/exciplex systems on nucleic acids are based on labeling of multiple chromophores into DNA scaffolds.[28b, 29] As for example, polyaromatic hydrocarbons such as pyrene and perylene have been utilized to form excimer/exciplexe in DNA conjugates for sensing of nucleic acids, proteins and small molecules.[30] However, the excitation wavelength falls in the UV region which limits the applications of these

systems in cell detection process. Exciplex emission between pyrene and guanine in DNA scaffolds has also been reported. However, the low bathochromicity and UV incident wavelength of the exciplex emission are not ideal for application in biological sensing system.[31]

In the studies of oligodeoxyfluoroside (ODF) dyes developed by Kool *et al.* it has been shown that ODF dyes exhibit properties which can not be observed in common organic fluorophores. Large Stokes shifts of more than 200 nm have been observed and numerous excimers and exciplexes have been characterized in their study. [32]

Alkynyl C-nucleosides with pyrene, perylene and anthracene as nucleobase substitutes were synthesized by Inouye and co-workers who studied their photophysical interaction property.[33] In the designed DNA these aromatic residues remained fixed rigidly *via* an alkyne bond which allowed them to interact photophysically with each other leading to an excimer and exciplex formation.

Wagenknecht *et al.* have exploited the rigid double helical structure of DNA to organize chromophores in a array at predictable positions and distances which ultimately led to emergent spectroscopic behaviour such as band narrowing and band shifts, formation of excimer/exciplex that are not observed in single dyes.[34a] They have synthesised 5-arylsubstituted uridine wherein clusters of aromatic chromophores, such as pyrene (^{Py}**dU**), 1-ethynylpyrene, phenothiazine and Nile red have been covalently attached to the 5-position of uridine through a C–C bond. These labelled natural nucleobases displayed a strong electronic coupling between uracil and π-electron cloud of the chromophore.[34b] They observed an exciplex formation between uracil and pyrene with spectra exhibiting an intense structureless red-shifted fluorescence emission band at 475 nm. Pyrene has also been observed to form exciplex with guanosine upon stacking interactions. The resultant colour change from blue to green has been utilized in the detection of G-quadruplex formation.[34c] Besides pyrene, pairs of perylene diimides and thiazole orange[34d] have also been incorporated into molecular beacons wherein strong excitonic interactions between the chromophores result in a red-shifted excimer emission.

The excimer emission in the visible region is much more beneficial because in such a case the background autofluorescence from cell does not produce any

misinterpretation of the analysis. Thus, thiazole orange (**TO**) labeled DNA probes have been developed. These probes were found to form interstrand thiazole orange (**TO**) dimers upon DNA hybridization which exhibited excimer fluorescence with excitation in the visible region and hence such system would be more suitable for applications in biologically relevant devices and protocols.[34d, 35]

Bichenkova *et al.* [36] have designed a "split probe" DNA system and studied the exciplex emission utilizing which they have been able to detect single nucleotide polymorphism of a target DNA *via* the generation of exciplex emission. In their design, two labelled probe, one with pyrene at the 5′-end and the other with *N*-methyl napthylamine attached to the 3′- end, were utilized as a "split probe" system. Upon hybridization with the complementary target sequence and excitation at 340~350 nm of pyrene absorption wavelength, the probe emits at a longer wavelength (~480 nm) which was assigned as pyrene-naphthalene exciplex (**Figure 6.10**). However, trifluoroethanol was inevitably required for exciplex emission in this case.

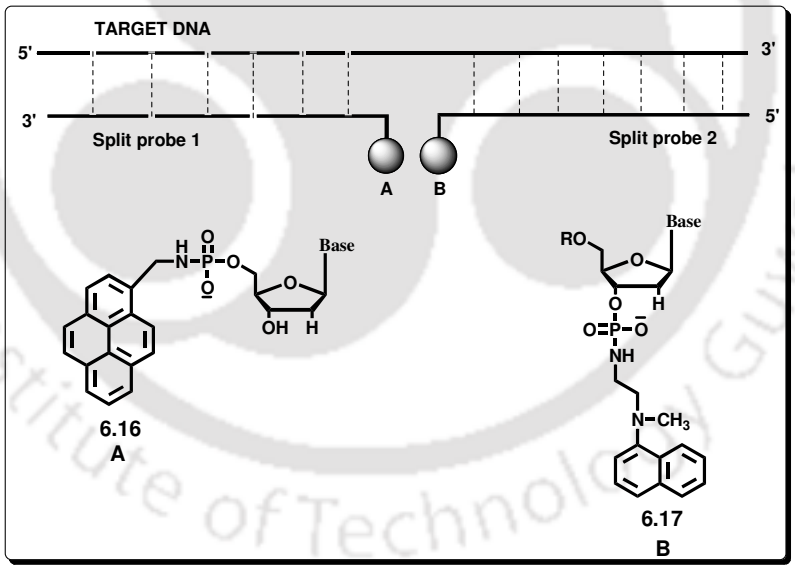

Figure 6.10: (a) Schematic presentation of split-probe approach showing self-assembly of exciplex components (**A** and **B**) induced by hybridization of oligonucleotide probes with complementary nucleic acid target. (b) Chemical structures of the modified bases involved in intramolecular exciplex formation.

Asanuma *et al.* have taken a strategy for the detection of SNPs and/or *indel* polymorphisms based on wedge-type insertions of chromophores tethered to a chiral D-threoninol as an acyclic non-nucleosidic base surrogate.[37] In their strategy two dye moieties separated by a single nucleotide were tethered to an oligonucleotide probe. In case of a fully matched duplex DNA, both dye moieties intercalate and thus the interaction between the two dyes is suppressed by the intervening base-pair leading to only monomer emission from the duplex (**Figure 6.11a**).

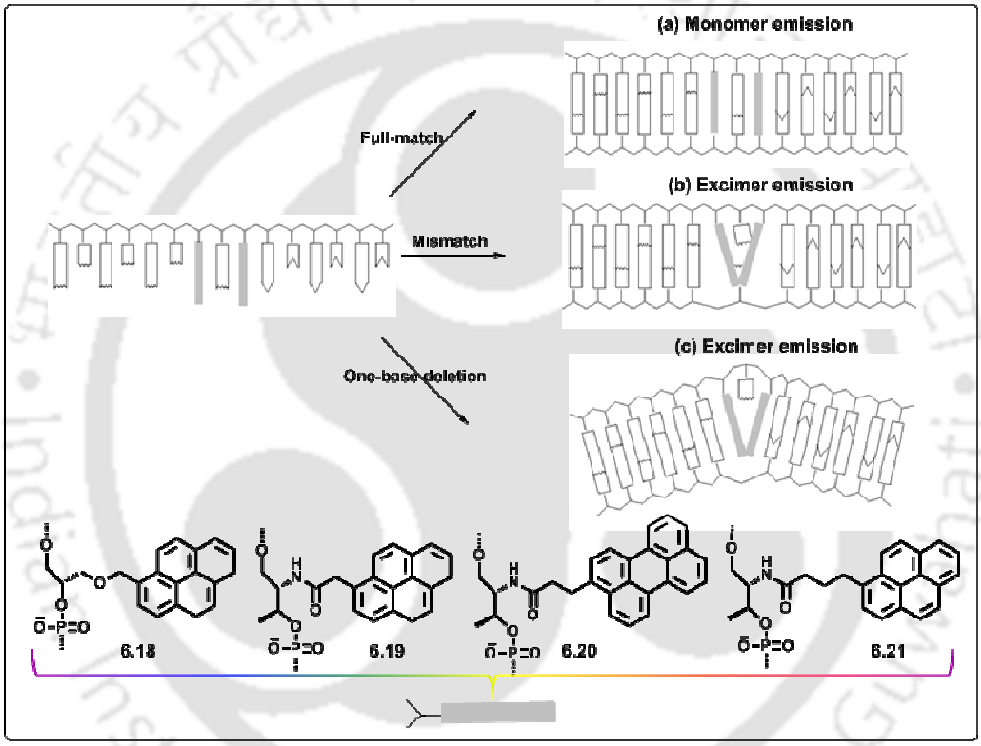

Figure 6.11: Schematic illustration of the strategy for the detection of SNPs and /or indel polymorphisms based on the wedge-type insertion with the help of acyclic non-nucleosidic base surrogate, D-threoninol.

On the other hand, hybridization of the probe DNA containing two dyes separated by a base with a mismatch target DNA causes disordering around the mismatched base pair allowing interaction of the two adjacent dyes that quench monomer emission and exhibit excimer emission in case of homo dye pair and/or exciplex in case of hetero dye pair (**Figure 6.11b**). This effect *i.e.* the strong excimer/exciplex emission

is more pronounced in case of hybridization with target DNA with one-base deletion (**Figure 6.11c**). The hybridization of the probe DNA with a target DNA containing a deletion mutant results in a three-base bulge including two dye moieties. This led to a close proximity and hence the strong interaction between two dyes which ultimately resulted in a strong excimer/exciplex emission. Thus, mismatch or deletion polymorphism can be distinguished from fully-matched DNA by monitoring excimer/exciplex emission.[37] Applying this concept they have reported two pyrene labeled probe DNA[38] as well as two perylene labeled probe DNA[39] for the detection of deletion polymorphism *via* the generation of excimer emission. They have shown that a one-base deletion can be detected even at a lower concentration as low as 5 nM due to its high quantum yield of the excimer emission. Moreover, such differences can be detected even with the naked eye as both the monomer and the excimer emissions appear in the visible region. [38d] They have also applied this strategy for the detection of deletion polymorphism *via* an exciplex emission between a pyrene and *N,N*-dimethylaniline attached *via* a D-threoninol unit in the probe DNA (**Figure 6.12**).[38c]

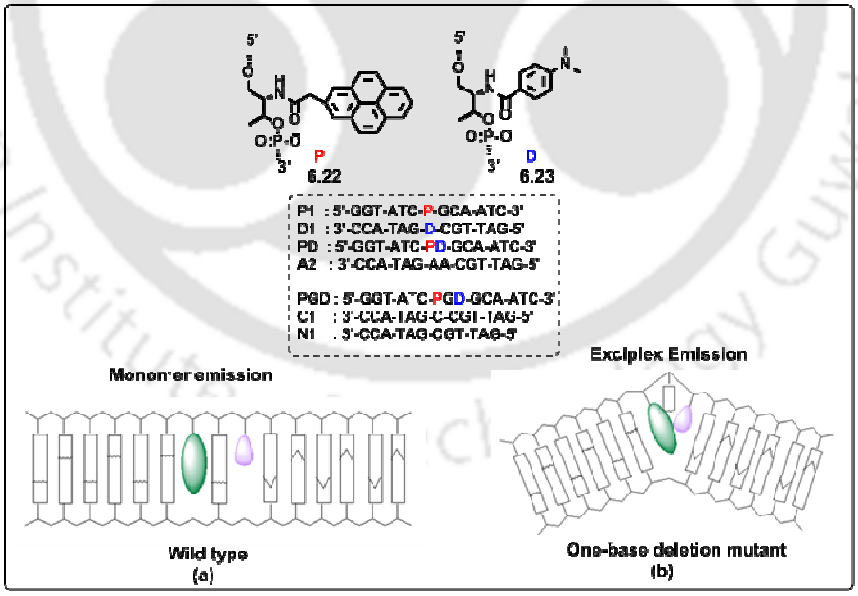

Figure 6.12: Exciplex emission between pyrene and *N,N*-dimethylaniline in DNA.

In 2007, Kool and co-workers showed exciplex emission from pyrene and perylene when these dyes were incorporated as nucleosidic base surrogates in DNA. Fluorescence lifetime data and emission spectra indicated the formation of an exciplex when excited at a single wavelength (**Figure 6.13**).[40]

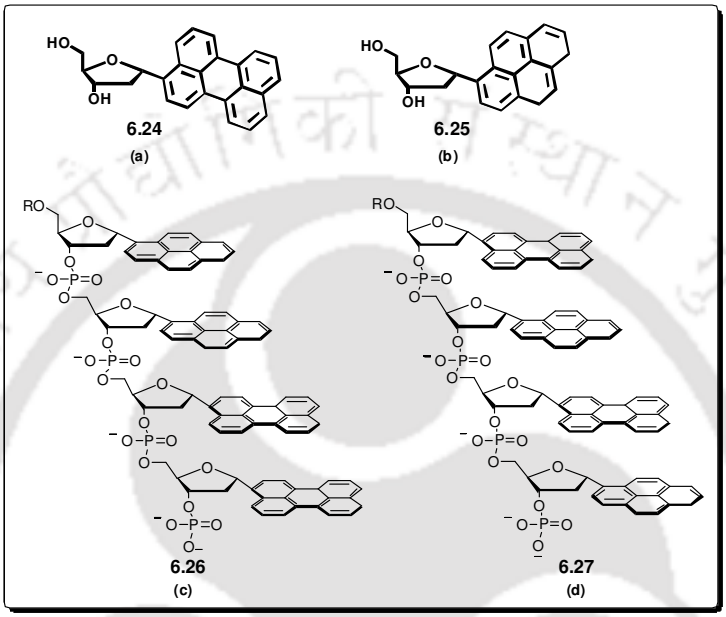

Figure 6.13: The structure of (a) α-perylenedeoxyribonucleoside, (b) α-pyrenedeoxyribonucleoside, and (c-d) oligodeoxy fluoroside showing the possible stacking of pyrene and perylene aromatic bases resulting in an exciplex emission.

Häner *et al.* have reported the synthesis and properties of triple-helical hybrids containing non-nucleosidic polyaromatic building blocks, pyrene or phenanthrene. It was observed that the clamp-type oligonucleotides containing a non-nucleosidic pyrene linker form stable triple helices with a polypurine target strand containing a terminal pyrene or phenanthrene moiety (**Figure 6.14**). Strong π-π-stacking interactions between the unnatural building blocks was found to enhance the stability of the triplex helix. The study of fluorescence photophysical property of the triple helices showed that two pyrene or the pyrene/phenanthrene pair involved in strong π-stacking complexation leading to an excimer (pyrene/pyrene) or exciplex (pyrene/phenanthrene) emission from the corresponding triple helices.[41]

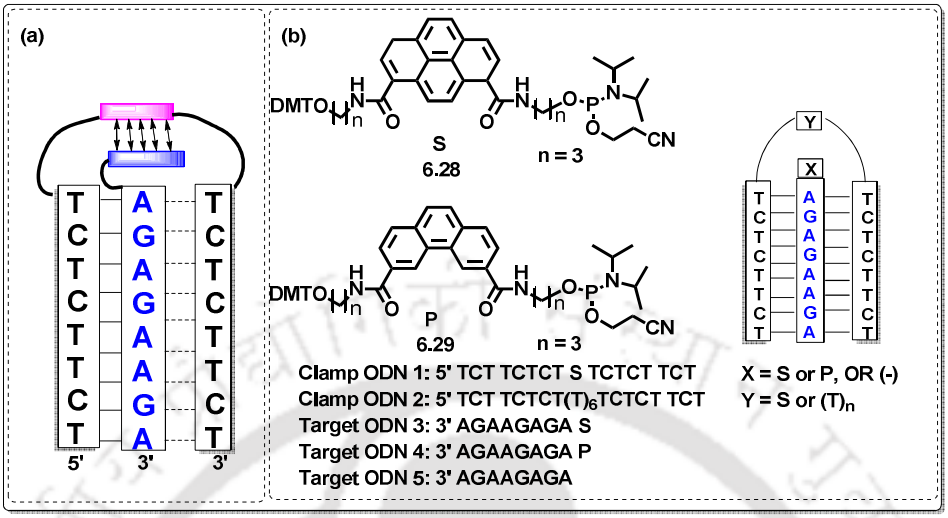

Figure 6.14: (a) Schematic representation of triplex formation between clamps ODN **1** or **2** and target ODN **3**-**5** and (b) the structures of pyrene and phenanthrene phosphoramidite building blocks and the sequences of oligonucleotides.

Construction of stable and well-defined π-stacks of chromophores can be achieved using DNA as a molecular scaffold wherein the arrangement of non-nucleosidic, polyaromatic chromophores might produce interesting photophysical properties.[28c, 42-43] Towards this end, Häner *et al.* have reported on the light harvesting properties of DNA decorated with multichromophoric arrays.[44] They have shown that the light is absorbed by multiple, π-stacked phenanthrenes (**P**) which is then efficiently transferred to pyrene (**S**) unit. Therefore, the assembly of light-absorbed multiple phenanthrene form phenanthrene-pyrene (**PS**) π-stacked complex resulting in an exciplex emission. This type of multichromophoric array in DNA might serve as a prototype for the design of synthetic light harvesting systems (**Figure 6.15**).

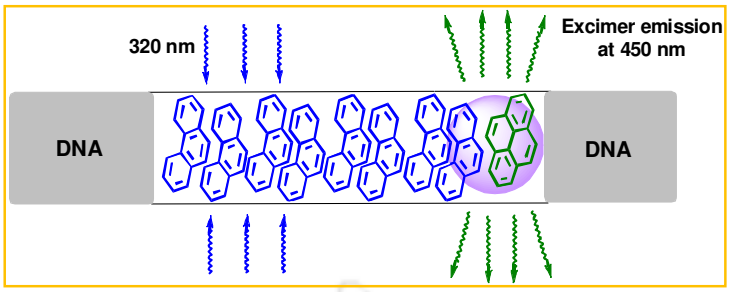

Figure 6.15: Schematic of a DNA-embedded, light-harvesting antenna composed of π-stacked phenanthrenes and a fluorescent phenanthrene–pyrene exciplex.

Häner's earlier study system contained only A:T base pairs and the **PS**-exciplex acted as the major energy collector where there is no chance of quenching of fluorescence coming out from the exciplex. The presence of a G:C base pair at the opposite end of the π-stack might lead to quenching of some of the excitation energy which can be directly measured by a reduction of the exciplex fluorescence signal. This concept led them to investigate the same light harvesting phenanthrene array system in more detail to uncover the effect of a G:C base pair on the excitation energy transfer in a multichromophoric DNA consisting of light harvesting assembly of π-stacked phenanthrene (**P**) and pyrene (**S**) chromophores.[45] They have shown that upon excitation of stacked **P** building blocks at 320 nm the excitation energy is transferred to **S** leading to the formation of a fluorescent **PS**-exciplex (**Figure 6.16**).

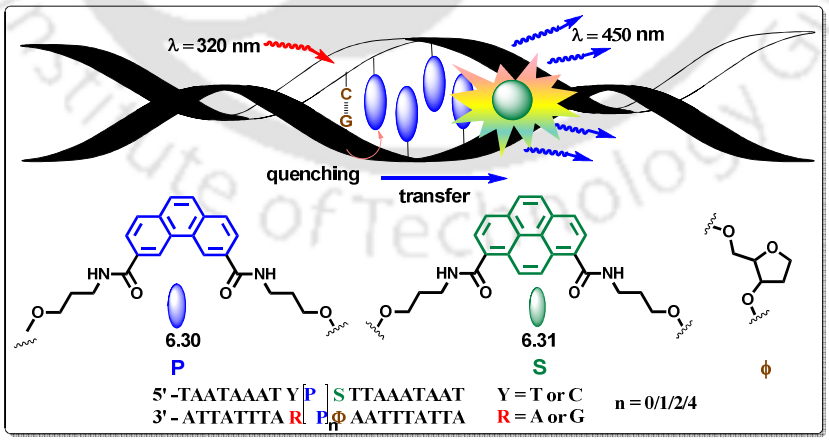

Figure 6.16: Structures of the chromophores and the oligonucleotides used in the study of light harvesting DNA system.

To test the dependency of fluorescence intensity on the number of light absorbing **P** units as well as on the nature of the DNA base pair next to the **P**-stack they have studied several double-stranded hybrids containing zero, two, four and eight units of **P**-stacks. They observed that, the excitation of the hybrids at 320 nm resulted in a steady increase of exciplex fluorescence with increasing numbers of the **P**-stack. Furthermore, a G:C base pair adjacent to the **P**-stack was found to quench the emission intensity which was not the case when a A:T base pair was there at this location. The inverse relation between quenching by a G:C pair and enhancement by the number of **P**-units led them to conclude that the stacked **P** units have a length-dependent, insulating effect[46] which prevented quenching of the exciplex by the G:C base pair. More interestingly, the **PS**-exciplex was found to be generated by excitation of the **S** unit which also followed the similar property with respect to an A:T or a G:C pair as in the case of excitation of **P**-units. Therefore, the π-stacked multichromophoric DNA represent a valuable model system of light harvesting DNA based material.[45]

Saito *et al.* have reported direct observation of exciplex emission in aqueous solution in their designed dual labelled DNA in the major groove by photoirradiation. In their design the probe DNA was labelled with 5-(1-naphthalenylethynyl)-2′-deoxyuridine (^{N}**U**) and 5-[(4-cyano-1-naphthalenyl)ethynyl]-2′-deoxyuridine (^{CN}**U**) sequentially (**Figure 6.17**).[47] They observed that the fluorescence emissions of modified duplexes containing double ^{N}**U** were efficiently quenched depending upon the sequence pattern of the naphthalenes in DNA major groove, as compared to the duplex possessing single ^{N}**U**. The fluorescence quenching was explained considering the photoinduced electron transfer (PET) between photoexcited ^{N}**U** and surrounding DNA bases including proximal second ^{N}**U**. However, on replacement of one of the ^{N}**U** by ^{CN}**U** the exciplex emission from the chromophores in DNA major groove was observed at longer wavelength (492 nm) (**Figure 6.17**). Therefore, their study reflects a unique property of DNA major groove as an interaction site and the exciplex emitting probe might find application for probing the structure of DNA or RNA.[47]

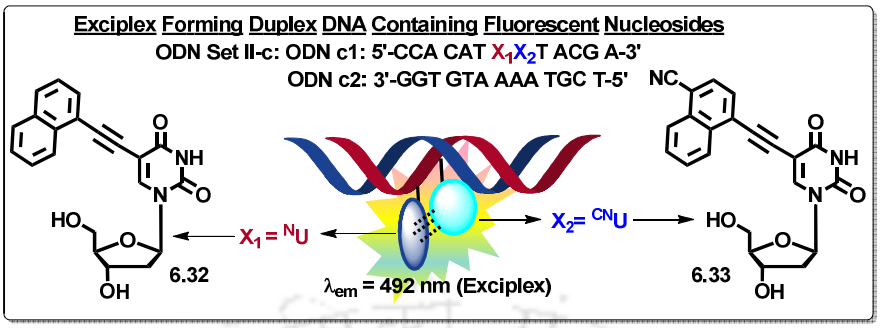

Figure 6.17: Exciplex forming duplex DNA containing consecutive two fluorescent nucleosides, ^{N}**U** and ^{NC}**U**.

The folded three dimensional structures of DNA quadruplexes extended the opportunity to the noncanonical base for their confined spatial orientations and for the formation of excimer/exciplex systems *via* dye–dye or dye–DNA π-stacking interaction.[48] The i-motif is a DNA quadruplex structure formed by cytosine-rich sequences under acidic pH conditions which is stabilized by hemiprotonated cytosine–cytosine (CH^+–C) pairs and three lateral loops.[49] This unique spatial orientation of the dual loop region in the i-motif provides a defined scaffold to form a fluorescent exciplex between dye molecules and nucleobases. This feature was exploited by Kim *et al.* for the study of structural transition of i-motif.[50] Thus, they have developed an oligonucleotide probe containing two 9-ethynylpyrene-modified deoxyadenosine (^{Py}**A**) [ODN I: 5′-T ^{Py}**A**A CCC CT ^{Py}**A** ACC CCT-3'] aiming for probing interstrand i-motif structures based on the stable stacking interactions of two nonpolar aromatic fluorophore (^{Py}**A**) units at the terminal and mid-loop positions of the i-motif structure.[50a] Thus, the probe was found to be capable of distinguishing structural transitions from random coil to interstrand i-motif structures *via* the generation of exciplex emission along with a distinct colour change from blue (monomer emission in coil form) to yellowish green (exciplex in i-motif). They also observed that the ^{Py}**A** units can induce interstrand i-motif structures that have a high transition midpoint (pH 7.2) as well as very stable i-motif structures (T_m = 80.4 °C) at pH 5.0. Therefore this simple probe system might find application in the development of stable DNA-based nanostructures.[50a] Recently, they have applied the same

fluorescent labelled nucleoside, 9-ethynylpyrene-modified deoxyadenosine (^{Py}**A**), to develop a fluorescent oligonucleotide probe system for monitoring the i-motif structures, focusing on the 4A-loop of the Rb gene [Sequence: 5′-GCCGCCCAAAACCCCCCG-3'] (**Figure 6.18**).[48b] Interestingly, it was observed that the i-motif structures modified with fluorescent nucleoside ^{Py}**A** at the 1,2 position of the probe O**DN i2** and 1,4 position of probe **ODN i4** of the 4A loop showed the most dramatic fluorescence changes at a single excitation wavelength upon conformational transitions from single-stranded to duplex to i-motif structures, respectively. Therefore, these probes are unique in their ability to discriminate among these three structural states through fluorescence emissions at three different colours upon excitation at a single wavelength. The result demonstrated in this report is expected to have potential applications in monitoring gene structure and studying gene regulation.

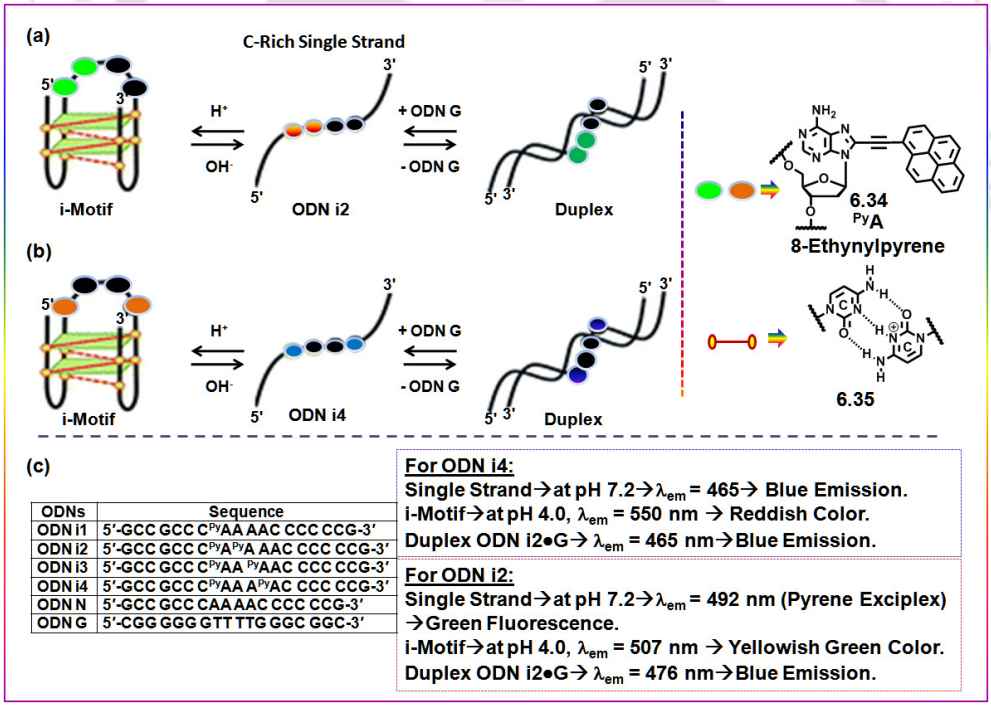

ODNs	Sequence
ODN i1	5′-GCC GCC C^{Py}AA AAC CCC CCG-3′
ODN i2	5′-GCC GCC C^{Py}A^{Py}A AAC CCC CCG-3′
ODN i3	5′-GCC GCC C^{Py}AA ^{Py}AAC CCC CCG-3′
ODN i4	5′-GCC GCC C^{Py}AA A^{Py}AC CCC CCG-3′
ODN N	5′-GCC GCC CAA AAC CCC CCG-3′
ODN G	5′-CGG GGG GTT TTG GGC GGC-3′

Figure 6.18: The schematic of structural transition between i-motif to single stranded form to duplex state revealed from a drastic change in fluorescent colour of the DNA containing fluorescent nucleoside, ^{Py}**A**.

The unique spatial orientation of the dual loop region in i-motif has also been exploited by Shao *et al. via* construction of G-quadruplex DNA containing a single thiazole orange (**TO**) molecule covalently conjugated to the DNA i-motif.[51a] In their recent design the non-nucleosidic scaffod, D-threoninol was used to covalently tether a single **TO** in the DNA backbone through phosphodiester bonds leading to the formation of a DNA with the telomeric sequence **TO-cHT22** (**Figure 6.19**).[51b] The **TO** labelled non-nucleosidic base surrogate replaced a thymine (T_{16}) of the telomeric sequence. Because of the good flexibility of the acyclic linker the **TO** chromophore find the opportunity to involve in strong stacking interaction with the natural nucleobases. They observed that upon excitation with visible light the single **TO** molecule emits orange exciplex fluorescence in the i-motif structure and green emission (**TO** monomer emission) in the duplex DNA when the probe **TO-cHT22** hybridized to its complementary target DNA. The exciplex emission was attributed to the involvement of four adenines in the dual loop region by either defining the spatial conformation and/or to π-electron stacking with the **TO** dye molecule.

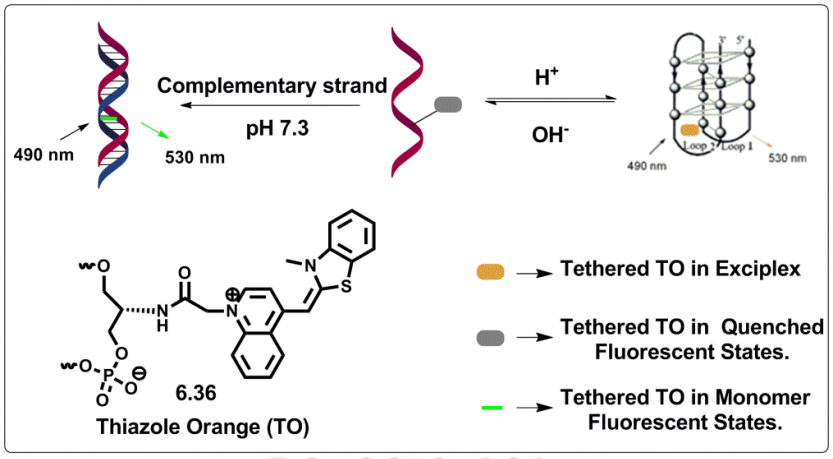

Figure 6.19: Schematics of exciplex formation by **TO** in i-motif of **TO-cHT22**.

6.4. Background

From the literature search it is thus clear that both the phenomena of exciplex and FRET process have been widely used in the field of nucleic acid chemistry to

elucidate the DNA structures, dynamics, interactions with other small or large biomolecules, in the study of DNA hybridization processes and in quest of light harvesting DNA based materials. To explore FRET interaction and exciplex formation in DNA multiple chromophore labeled oligonucleotide probes have also been developed for possible application in optical devices, light harvesting materials and in diagnostic applications. However, all the design relies either on the purely fluorescent nucleoside or on the fluorescent non-nucleosidic base surrogates. Moreover, a chimeric DNA duplex wherein a fluorescent nucleosidic base surrogate paired against a non-nucleosidic base surrogate involved in FRET or exciplex formation is not known.

6.5. Objective

With this above background it is clear that there exist a large number of DNA systems involving a limited number of FRET donor-acceptor pairs or exciplex forming pair. These systems have been designed mainly to elucidate the structure and dynamics of DNA, phtophysics in DNA, DNA detection, studying the hybridization events of DNA or to find DNA based light harvesting materials. All the reported design considers either the FRET process or the exciplex/excimer process in DNA separately. There exists only one example by Kool *et al.*[9d] wherein an excimer serves as an energy donor for the next stage FRET process. Moreover, it is also known that both the exciplex partner can be excited to achieve the exciplex emission. Till the date no donor acceptor decorated DNA systems have been reported to address any other alternative mechanism of formation of exciplex between a donor-acceptor pair. Moreover, as is pointed out earlier there is no report of non-nucleoside-nucleoside base chimera which might result in interesting photophysical property to the designed DNA.

Therefore, inspired by the π-π stacking/hydrophobic interaction mediated stabilization of self-pair DNA duplex, charge transfer complexation mediated hetero-duplex stabilization and abasic DNA stabilization by our designed fluorescent unnatural nucleoside, triazolylphenanthrene ($^{TPhen}\mathbf{B}_{\mathbf{Do}}$)[52], we thought that it would be worthwhile if we could design a fluorescently labelled flexible non-nucleosidic base

surrogate (^{Oxopy}**S**) and allow it to pair with our unnatural nucleoside, ^{TPhen}**B$_{Do}$** in a duplex, we could end up with chimeric DNA duplex which might offer interesting photophysical property like exciplex and/or FRET emission. The logic behind choosing serinol as non-ribose acyclic scaffold was its more flexible and achiral nature compared to other similar scaffolds used and its ability for insertion of a fluorophoric unit to DNA without affecting much duplex stability.[53] Moreover, the spectral overlap between the emission spectra of triazolylphenanthrene and absorption spectra of γ-oxopyreneserinol (^{Oxopy}**S**) led us to envision that during hybridization process the two chromophoric units would come closer and might involve in Förster resonance energy transfer and in π-stacking interaction to form an exciplex. With this aim and designing concept, we framed our objective as below:

(a) Synthesis and study of the photophysical properties of monomeric nucleosides ^{Oxopy}**S** and ^{TPhen}**B$_{Do}$**.

(b) Synthesis of the oligonucleotide probe containing ^{Oxopy}**S** as a non-nucleosidic base surrogate and the target oligonucleotide containing ^{TPhen}**B$_{Do}$** as an unnatural nucleoside.

(c) Study of thermal stability and pairing selectivity among the ^{Oxopy}**S** and ^{TPhen}**B$_{Do}$** base pair in the cimeric duplex DNA.

(d) Study of photophysical phenomena during hybridization of probe DNA containing ^{Oxopy}**S** with target oligonucleotide containing ^{TPhen}**B$_{Do}$**.

(e) Exploring the possibility of FRET and exciplex emission from the hybrid DNA duplex.

6.6. Result and Discussion

6.6.1. Synthesis of Fluorescent Nucleosidic and Non-nucleosidic Base Surrogate

The synthesis of the fluorescent nucleosidic base surrogate ^{TPhen}**B$_{Do}$** was accomplished following our previously published protocol[52a] and was discussed in **Chapter 2**. The synthesis of fluorescent non-nucleosidic base surrogate ^{OxoPy}**S** is shown in **Scheme 1**. Thus, γ-oxopyrenebutyric acid (**6.37, OxoPy**) was reacted with

serinol **6.38** in dry DMF in presence of pyBop and anhydrous diisopropylethylamine (DIPEA) at room temperature. After completion of the reaction monitored by TLC, DMF was removed by high vacuum and the reaction mixture was partitioned between ethyl acetate and water. Finally, the organic layer was evaporated and the residue was purified by silica gel column chromatography to afford oxopyreneserinol (^{OxoPy}**S, 6.39**) in 80% yield.

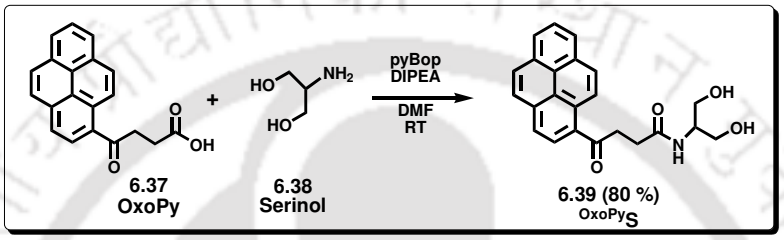

Scheme 6.1: Synthesis of acyclic non-nucleosidic base surrogate ^{OxoPy}**S**.

6.6.2. Spectral Characterization of Fluorescent Non-nucleosidic Base Surrogate (^{OxoPy}S)

After synthesis of the pure ^{OxoPy}**S**, it was characterized by ^{1}H, ^{13}C NMR and mass spectrometry. Thus, the ^{1}H NMR study of the fluorescent non-nucleoside base ^{OxoPy}**S, 6.39** showed that the serinol hydrogen (-CH_2- and –CH-) resonated at 4.65 ppm as multiplet. The hydrogen (-CH_2-) of butyric group appeared at 2.48 and 2.66 ppm in their respective field of resonance. The aromatic protons of pyrene unit appeared within the range of 7.69-8.72 ppm as multiplet (**Figure 6.20**).

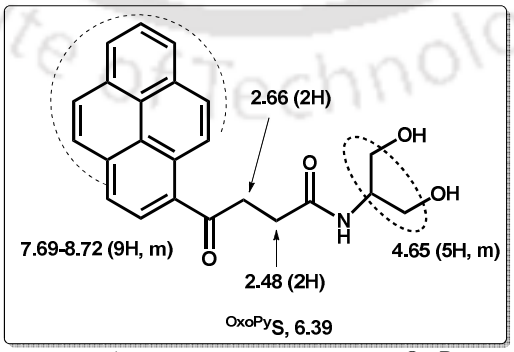

Figure 6.20: ^{1}H-NMR assignment of ^{OxoPy}**S** (**6.39**).

6.6.3. Study of Photophysical Properties of ^{OxoPy}S

After getting the pure ^{OxoPy}S monomer we first measured the photophysical property in various organic solvents and in acetonitrile-water mixture to test its microenvironment sensitivity. The UV-visible spectra did not show much shift in absorbance wavelength. However, the emission intensity increased as the polarity of the solvents and the % H_2O increases with a large stokes shift of about 61 nm indicating the potential solvofluorochromicity of ^{OxoPy}S monomer (**Figure 6.21**). The photophysical property of nucleosidic base surrogate $^{TPhen}B_{Do}$ was discussed in **Chapter 2**.

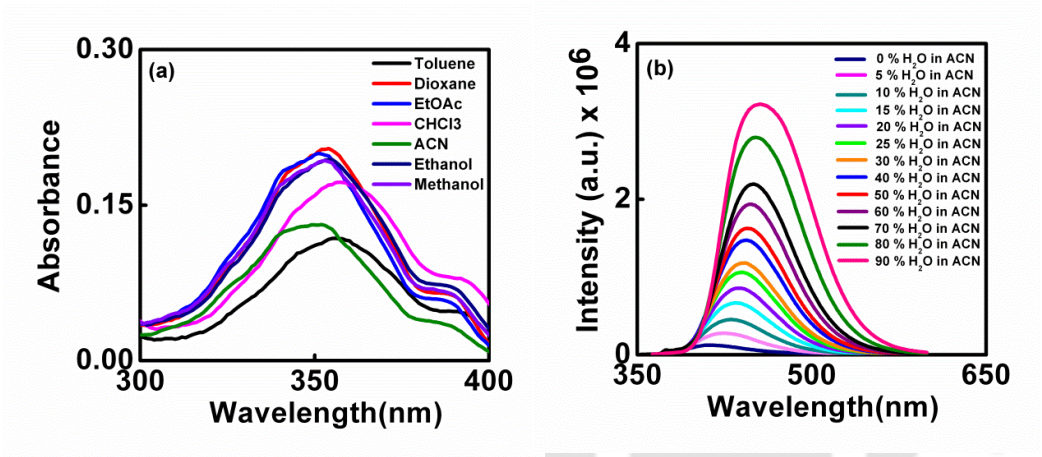

Figure 6.21: (a) UV-visible and (b) Fluorescence titration spectra of ^{OxoPy}S in ACN-H_2O mixture. Excitation wavelength was the λ_{max} of excitation spectra of each solvent. Sample concentration was 10 μM.

6.6.4. Synthesis of the Oligonucleotides

Being interested by the photophysical properties of the oxopyrene labeled non-nucleosidic base surrogate (^{OxoPy}S, **6.39**), especially the spectral overlap of the emission spectra of triazolylphenanthrene ($^{TPhen}B_{Do}$) and the absorbance spectra of oxopyreneserinol (^{OxoPy}S) (will be discussed under the **Section 6.6.7.5.**, **Figure 6.30**), we next incorporated the oxopyreneserinol into short oligonucleotide sequences *via* phosphoramidite chemistry using automated DNA/RNA synthesizer. The synthesis of $^{TPhen}B_{Do}$ was described in **Chapter 2**. For the synthesis of oligonucleotide containing ^{OxoPy}S, we first protected one -OH group of the serinol unit of oxopyreneserinol

(**^{OxoPy}S**, **6.39**) with 4,4′-dimethoxytrityl group by reaction with 4,4′-dimethoxytrityl chloride in presence of catalytic amount of *N,N*-dimethylamino pyridine (DMAP) in dry pyridine solvent. The DMTr protected non-nucleosidic base surrogate (**^{OxoPy}S-DMTr**, **6.40**) was isolated in pure form by a silica gel column chromatography and characterized by NMR and mass spectrometry. Next, the DMTr protected racemic nucleoside (**^{OxoPy}S-DMTr**, **6.40**) was converted to its phosphoramidite derivative (**6.41**) by reaction with 2-cyanoethyl-*N,N,N′,N′*-tetraisopropyldiphosphoramidite in presence of (1*H*)-tetrazole in anhydrous acetonitrile under nitrogen atmosphere. The phosphoramidite derivative **6.41** so produced was passed through a short column and dried and used for the DNA synthesis without further purification (**Scheme 6.2**).

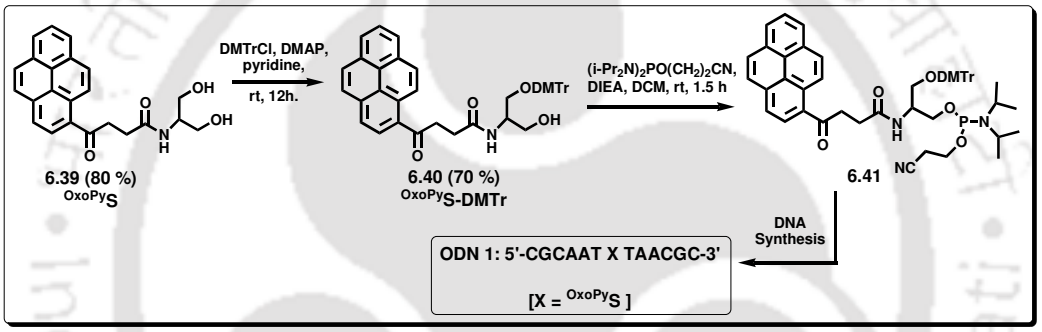

Scheme 6.2: Synthesis of fluorescent probe ODN **1** cotaining nonnucleosidic base surrogate, **^{OxoPy}S**.

The incorporation of the non-nucleosidic base surrogate **^{OxoPy}S** into DNA (ODN **1**) is shown in **Scheme 6.2**. The incorporation of nucleosidic base surrogate **$^{TPhen}B_{Do}$** into the DNA (ODN **2**) has already been discussed in **Chapter 4** which was named as ODN **7** there. The synthesis of probe ODN **1** was carried out *via* the phosphoramidite chemistry using an automated DNA/RNA synthesizer following same protocol as was described for the synthesis of DNA containing **$^{TPhen}B_{Do}$** nucleoside described in **Chapter 4**. The modified base surrogates were placed at the center of each palindromic 13-mer DNA sequence (**Table 6.1**). Incorporation of the racemic amidite **6.41** generated two isomeric ODNs, (ODN **1**and ODN **1'**), containing **^{OxoPy}S**. Both the isomers were purified and without characterizing the absolute configuration, they were utilized for sensing the presence of opposite natural base of a target natural DNA

by recording the fluorescence photophysical properties. The isomer with longer retention time (ODN **1**) was used in the study of hybridization with oligonucleotide containing unnatural base, $^{TPhen}\mathbf{B}_{\mathbf{Do}}$. The study with other isomer was not carried out and is left as a future scope of the thesis.

Table 6.1: Synthesized fluorescent oligonucleotide sequences.

ODNs	Sequence
ODN **1**	5'-CGCAAT $^{OxoPy}\mathbf{S}$ TAACGC-3'
ODN **2**	3'-GCGTTA $^{TPhen}\mathbf{B}_{\mathbf{Do}}$ ATTGCG-5'

6.6.5. Characterization of the Synthesized ODNs

The synthesized isomeric ODNs containing $^{OxoPy}\mathbf{S}$ were purified by reverse phase HPLC on a 5-ODS-H column (10×150 mm, elution with 50 mM ammonium formate buffer (AF), pH 7.0, linear gradient over 45 min from 3% to 40% acetonitrile at a flow rate 2.0 ml/min) (**Figure 6.22**). The concentration of each ODN was determined from molar extinction coefficient at 260 nm at 80 ^{o}C. Mass spectra of ODNs purified by HPLC were determined with a MALDI-TOF mass spectrometer (**Table 6.2**). The isolation in very pure form of B-isomer (ODN **1**) with longer retention time was little easier than the A-isomer (ODN **1'**) in HPLC. The calculated masses of the ODNs are in good agreement with the experimentally found masses. The concentrations of all the oligonucleotides [ODN **1'** = 160 µM (2.0 ml) and ODN **1** = 450 µM (2.0 ml)] were measured using the extinction coefficients at 260 nm (ε_{260}) which were calculated with OligoAnalyser (http://eu.idtdna.com). Complementary natural ODNs (ODN **3-6**) were purchased and used as supplied.

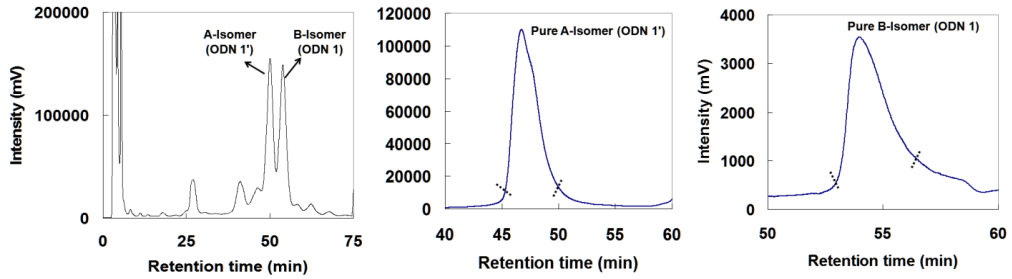

Figure 6.22: HPLC profiles of crude ODNs and isolated pure A-isomer (**ODN** 1') and B-isomer (**ODN** 1) containing fluorescent non-nucleosidic base surrogate, ^{OxoPy}**S**.

Table 6.2: MALDI-TOF mass spectral data for the synthesized ODNs.

ODNs	Sequences	MALDI-TOF mass calcd. [M+H]+	MALDI-TOF mass found [M+H]+
ODN **1** **(B-Isomer)**	5'-CGCAAT ^{OxoPy}**S** TAACGC-3'	4052.83	4054.03
ODN **1'** **(A-Isomer)**	5'-CGCAAT ^{OxoPy}**S** TAACGC-3'	4052.83	4052.61
ODN **2**	3'-GCGTTA ^{TPhen}**B**$_{Do}$ATTGCG-5'	4097.56	4098.00

6.6.6. Comparative Study of Photophysical Properties of Probe ODN 1 and ODN 1' Containing ^{OxoPy}S in Presence of Natural Complementary ODNs

After synthesizing the ODNs, the photophysical properties of the single strand ODNs as well as their various duplex ODNs formed *via* hybridization with various natural complementary ODNs were studied. **Table 6.3** shows the oligonucleotide sequences used for the photophysical studies.

Table 6.3: Oligonucleotide sequences used for the photophysical studies.

ODNs	Sequence
ODN **1**	5'-CGCAAT ^{OxoPy}**S** TAACGC-3' (**B-isomer**)
ODN **1'**	5'-CGCAAT ^{OxoPy}**S** TAACGC-3' (**A-isomer**)
ODN **3**	3'-GCGTTA A ATTGCG-5'
ODN **4**	3'-GCGTTA G ATTGCG-5'
ODN **5**	3'-GCGTTA C ATTGCG-5'
ODN **6**	3'-GCGTTA T ATTGCG-5'

From the UV-visible spectra, it was observed that the UV-absorptions of the single strand ODNs and the duplex ODNs were almost similar for both the isomeric modified ODNs. **Figure 6.23** shows the UV-visible spectra of the single strand oligonucleotides, ODN **1** (B-isomer with longer retention time in HPLC) and ODN **1'** (A-isomer with shorter retention time in HPLC) and their various duplexes formed by hybridization with various natural complementary ODNs.

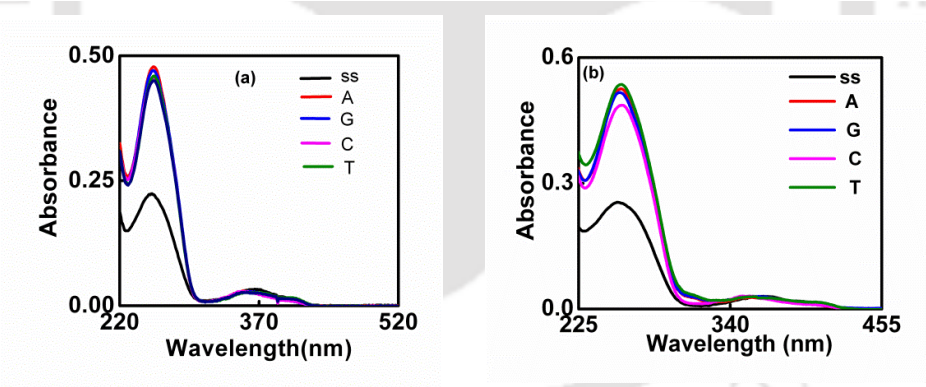

Figure 6.23: UV-visible spectra of (a) ODN **1'** (A-Isomer) and (b) ODN **1** (B-isomer) hybridized with various natural complementary ODN **3-6** at 298 K [Final duplex concentration was 2.5 μM, [buffer] (sodium phosphate) = 50 mM, pH = 7.0, [NaCl] = 0.1 M].

Being interested by the solvent polarity dependent fluorescence property of the fluorescent nucleoside (**6.39**, ^{OxoPy}**S**), we thought that ^{OxoPy}**S** would be usable for

monitoring the change in DNA microenvironment. Therefore, we studied the fluorescence properties of single stranded ODN **1'** and ODN **1** in the presence and absence of their various natural complementary strands (**Figure 6.24**).

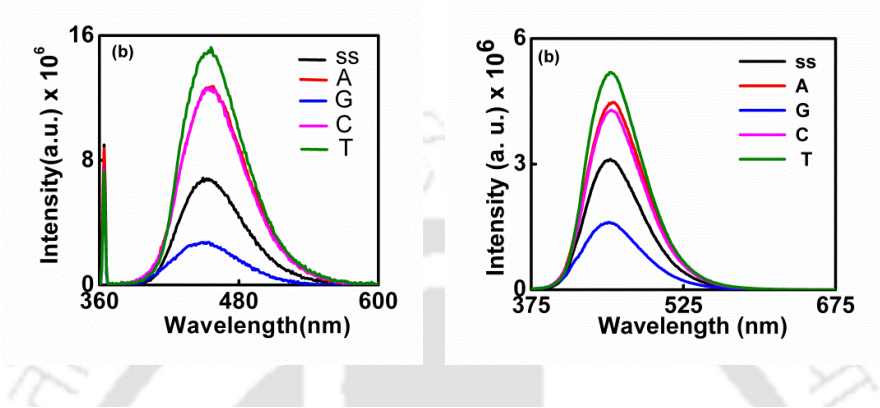

Figure 6.24: Fluorescence emission (a) ODN **1'** (**A-Isomer**) and (b) ODN **1** (B-isomer) hybridized with various natural complementary ODN **3-6** at 298 K [Final duplex concentration was 2.5 μM, [buffer] (sodium phosphate) = 50 mM, pH = 7.0, [NaCl] = 0.1 M]

As revealed from the fluorescence spectra it was observed that the fluorescence of both the probe ODNs was quenched when hybridized to the target ODN **4** containing G base opposite of ^{OxoPy}**S** of probe ODN **1** or ODN **1'**. On the other hand, upon hybridization with all other complementary ODNs **3**, **5**, **6** containing A, C, T base, respectively, opposite of ^{OxoPy}**S** of probe ODN **1** or ODN **1'**, enhanced emission at around 452-457 nm was observed in all cases. Therefore, both the probes (ODN **1** or ODN **1'**) are unable to discriminate well the presence of natural bases opposite of labeled non-nucleosidic base, ^{OxoPy}**S** of probe ODNs (**Figure 6.24**). This is because of the flexibility of the chromophore which led to almost similar interaction with the opposite bases of target ODNs. The fluorescence spectra revealed that the probe ODN **1** (B-Isomer) exhibited enhanced and almost equal emission intensity for A, C, T bases while probe ODN **1'** produced less enhanced emission for A and equal enhancement for C and T bases opposite of ^{OxoPy}**S** of probe ODNs. In both the cases the probes emitted quenched emission in presence G base of target ODN **4** opposite of ^{OxoPy}**S** of probe ODNs. Therefore, the probe ODN **1** (B-Isomer) at least provided

comparatively better discriminating fluorescence signal between G and the other bases (A, C, or T) of target ODNs opposite of ^{OxoPy}**S** of probe ODN **1** *via* quenching of fluorescence intensity (**Figure 6.24**).

Thus, quick and initial study of fluorescence photophysical property of various duplexes of both the isomers, A-isomer (ODN **1'**) and B-isomer (ODN **1**) showed almost no discriminating fluorescence signal. However, the probe ODN **1** (B-Isomer with longer retention time in HPLC) at least provided comparatively little better discriminating fluorescence signal between G and the other bases (A, C, or T) of target ODNs opposite of ^{OxoPy}**S** of probe ODN **1** *via* quenching of fluorescence intensity.

6.6.7. Study of Hybridisation of Non-Nucleosidic-Unnatural Nucleosidic Chimeric DNA Duplex (ODN 1•2; ^{OxoPy}S:^{TPhen}B$_{Do}$)

Next, the B-isomer with longer retention time (ODN **1**) was used in the study of hybridization with various natural oligonucleotide and unnatural target oligonucleotide containing unnatural base, ^{TPhen}**B**$_{Do}$ in detail because of comparatively little better discriminating fluorescence signal achieved in sensing the presence of opposite natural base **G** of a target DNA as stated above. The study of other isomer, A-isomer (ODN **1'**) with shorter retention time in HPLC was not carried out and is left as a possible future scope of the thesis.

It is revealed from our objective that we were curious to know whether in a designed chimeric DNA duplex containing a non-nucleosidic-unnatural nucleosidic base pair interact photophysically leading to either FRET or exciplex emission. Therefore, we have next studied the possibility of occurrence of FRET and exciplex formation using chimeric DNA duplex ODN **1•2** (^{OxoPy}**S**:^{TPhen}**B**$_{Do}$) *via* the study of photophysical and thermal melting properties. For that purpose the ODNs used in this study is given below in **Table 6.4**.

Table 6.4: Sequence of ODNs Used in this Study

5'-CGCAAT **X** TAACGC-3' 3'-GCGTTA **Y** ATTGCG-5'	
ODNs	**Sequence**
ODN **1**	5'-CGCAAT ^{OxoPy}**S** TAACGC-3'
ODN **2**	3'-GCGTTA ^{TPhen}**B**$_{Do}$ ATTGCG-5'
ODN **3**	3'-GCGTTA **A** ATTGCG-5'
ODN **4**	3'-GCGTTA **G** ATTGCG-5'
ODN **5**	3'-GCGTTA **C** ATTGCG-5'
ODN **6**	3'-GCGTTA **T** ATTGCG-5'

6.6.7.1. Study of Thermal Stability of the Duplexes

First, we studied the thermal stability and pairing selectivity via thermal denaturation experiment. Thus, the study of thermal stability of various duplexes showed that the stability of the chimeric duplex ODN **1•2** (52.3 °C) was comparable to that of a natural A:T pair (51.2 °C). It was also evident that the chimeric duplex ODN **1•2** was more stable than the duplexes with any of the natural bases (**Figure 6.25**). Moreover, the acyclic non-nucleosidic base surrogate ^{OxoPy}**S** showed significant selectivity (by 1.9- 3.9 ^{o}C in T_m higher stability) for the nucleosidic base surrogate ^{TPhen}**B**$_{Do}$ over all four natural bases (**Figure 6.25b**). These results showed that strong hydrophobic and π-π stacking interaction possibly played a dominant role in stabilizing a chimeric duplex containing ^{OxoPy}**S** paired against hydrophobic nucleoside ^{TPhen}**B**$_{Do}$. The strong pairing selectivity between ^{OxoPy}**S** and ^{TPhen}**B**$_{Do}$ (compared to the natural bases) and slightly higher stabilization (by 1.1 ^{o}C in T_m) of ^{OxoPy}**S** **:** ^{TPhen}**B**$_{Do}$ (ODN **1•2**) duplex compared to that of a control A:T pair could be rationalized through strong intercalative stacking interaction between oxopyrene unit of ^{OxoPy}**S** and phenanthrene moiety of ^{TPhen}**B**$_{Do}$ inside the duplex. However, the stability of the highest stable chimeric duplex ODN **1•2** was found to be less by 3.2 ^{o}C compared to that of a natural C-G pair (**Figure 6.25b**).

(a) Thermal denaturation curve of various duplexes

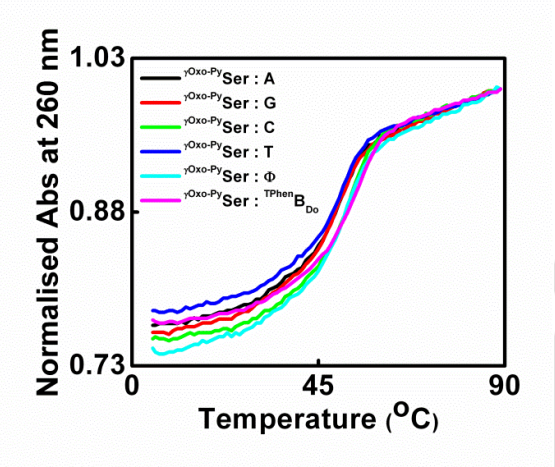

(b)Values of thermal melting temperatures (T_m) of various duplex ODNs

ODNs	X : Y	T_m (°C)
ODN **1•2**	^{OxoPy}**S:**^{TPhen}**B$_{Do}$**	52.3
ODN **1•3**	^{OxoPy}**S: A**	48.5
ODN **1•4**	^{OxoPy}**S:G**	48.5
ODN **1•5**	^{OxoPy}**S:C**	50.4
ODN **1•6**	^{OxoPy}**S:T**	49.2

T_m of natural A•T and C•G pair was 51.2 °C and 55.5 °C respectively. Error in T_m is estimated at ± 0.3°C.

Figure 6.25: (a) Thermal denaturation curve of various duplexes of ODN **1** (^{OxoPy}**S**) with various natural complementary ODNs [ODN **3-6** (A, G, C, T)] and unnatural complementary ODN **2** (^{TPhen}**B$_{Do}$**) and (b) The values of thermal melting temperatures (T_m) of various duplex ODNs [Concentration of each single stranded ODNs = 2.5 µM, 50 mM sodium phosphate, 0.1 M sodium chloride, pH 7.0, room temperature].

6.6.7.2. Study of UV-visible Absorption Property of Various ODNs

Next, we examined the UV-visible absorption property of single stranded ODN **1** and its various duplexes. While the duplexes of ^{OxoPy}**S** with natural bases [ODN **1•Y** (= A, G, C, T)] exhibited increased absorbance with blue shift of absorbance maxima (of about 3-6 nm), the chimeric duplex ODN **1•2** (^{OxoPy}**S** :^{TPhen}**B$_{Do}$**) showed a bathochromic shift (~10 nm) in absorption wavelength with 20% hypochromicity in oxopyrene absorbance in comparison to the corresponding single stranded ODN **1** (**Figure 6.26**). This observation indicated that the oxopyrene unit of non-nucleosidic base surrogate ^{OxoPy}**S** involved in strong intercalative stacking interaction inside the chimeric DNA duplex.[54] Thus, there is a chance of π-π stacking interaction between chromophoric moieties of two chimeric bases inside the duplex which was also supported by the high thermal melting stability of the chimeric duplex (**Figure 6.25b**, **Table 6.5**).

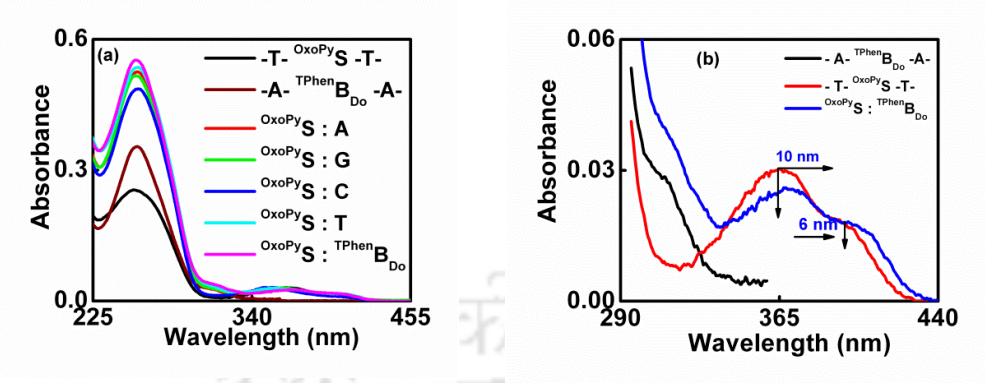

(c)	X : Y	λ_{abs} (nm)	$\Delta\lambda_{abs}$ (nm)	% Hypo-chromicity 362 → 372	% Hypo-chromicity 402 →408
ODN **1**	-T-^{OxoPy}S-T-	362, 402	---	---	---
ODN **1•2**	^{OxoPy}S:^{TPhen}B$_{Do}$	315, 372, 408	10, 6	20	6

Figure 6.26: (a) UV-visible of ODN **1** (^{OxoPy}S) and its various duplex ODNs with natural ODNs [ODN **3-6** (A, G, C, T)] and unnatural ODN **2** (^{TPhen}B$_{Do}$). (b) Magnifying area of chromophoric region. (c) % Hypochromicity of the chimeric duplex.

Table 6.5: Summary of photophysical properties of the ODNs at room temperature.

ODNs	X : Y	λ_{abs} (nm)	ε ($\times 10^3$) $M^{-1}cm^{-1}$	λ_{fl} (nm)	Φ_f	T_m (^oC)
ODN **1**	-T-^{OxoPy}S-T-	362, 402	12, 6	452	0.24	---
ODN **2**	-A-^{TPhen}B$_{Do}$-A-	310	11	384	0.04	---
ODN **1•2**	^{OxoPy}S:^{TPhen}B$_{Do}$ [a]	315, 372, 407	14, 10, 6	460, 535	0.46	52.3
ODN **1•3**	^{OxoPy}S: A	357, 405	11, 4	455	0.41	48.5
ODN **1•4**	^{OxoPy}S:G	358, 407	12, 4	452	0.13	48.5
ODN **1•5**	^{OxoPy}S:C	356, 403	12, 4	454	0.40	50.4
ODN **1•6**	^{OxoPy}S:T	359, 408	11, 6	453	0.44	49.2

T_m of natural A•**T** and C•G pair was 51.2 ^{o}C and 55.5 ^{o}C respectively. Error in T_m is estimated at ± 0.3 °C. [a]Monomer and exciplex quantum yield = 0.18 and 0.28 respectively.

6.6.7.3. Study of Fluorescence Photophysical Property of Various ODNs

Next, we studied the fluorescence emission property of various ODNs. Thus, the fluorescence spectra revealed that upon excitation at the absorbance maximum of ^{OxoPy}**S** (365 nm) all the duplexes with natural nucleoside, except guanosine, showed strong fluorescence emission compared to the single strand ODN **1**. The duplex ODN **1•4** wherein ^{OxoPy}**S** paired against strong electron donor guanosine exhibited strongly quenched emission. **Figure 6.27a-b** represents the excitation and the emission spectra respectively, of various duplexes. The emission maxima in all cases centered at ~ 452 nm with a tail expanded upto 575 nm. Surprisingly, the chimeric duplex ODN **1•2** (^{OxoPy}**S**) showed strong and broad emission band centered at 460-535 nm and span upto 675 nm (**Figure 6.27b**). The long tail and broad shape of the emission knocked our mind to re-examine and resolve the spectra. We could clearly resolve the broad spectra which indicated dual emission-one from the pure oxopyrene monomer emission at 460 nm and another intense emission centered at 535 nm and span upto 675 nm (**Figure 6.27b**). The intense and broad long wavelength emission was most likely from the exciplex of **OxoPy-TPhen** (**Figure 6.26**).

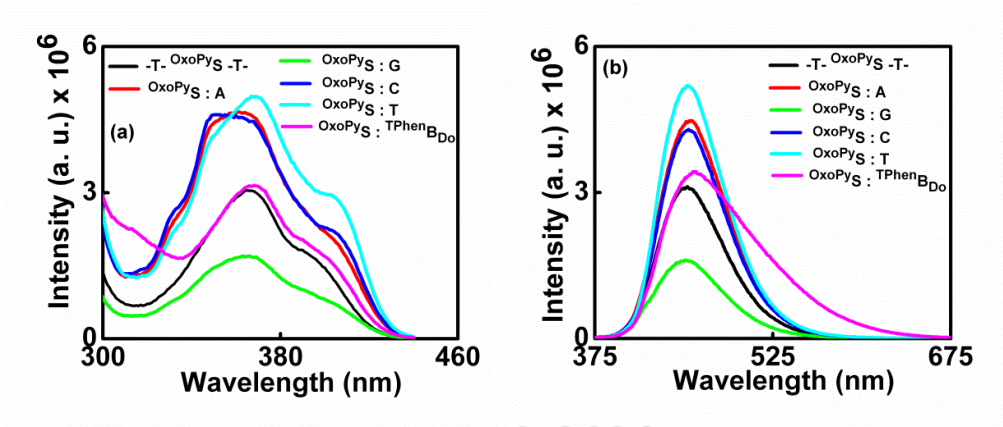

Figure 6.27: (a) Fluorescence excitation spectra and (b) fluorescence emission (λ_{ex} = 365 nm) spectra of ODN **1** (^{OxoPy}**S**) and its various duplex ODNs with natural ODNs [ODN **3-6** (A, G, C, T)] and unnatural ODN **2** (^{TPhen}**B$_{Do}$**). Concentration of each single stranded ODNs = 2.5 μM, 50 mM sodium phosphate, 0.1 M sodium chloride, pH 7.0, room temperature.

6.6.7.4. Evidence of Exciplex Formation Between $^{OxoPy}S$ and $^{TPhen}B_{Do}$ Residues in the Chimeric Duplex ODN $^{OxoPy}S$:$^{TPhen}B_{Do}$ (ODN 1•2) upon Excitation at $^{OxoPy}S$

As the oxopyrene moiety involved in intercalative stacking interaction inside the duplex DNA, there is a high possibility of formation of π-π stacked complex between excited oxopyrene and ground state of triazolylphenanthrene which might be the probable cause of appearance of intense and long wavelength emissive band at 535 nm in the resolved fluorescence spectra of duplex ODN **1•2** (**Figure 6.28**).

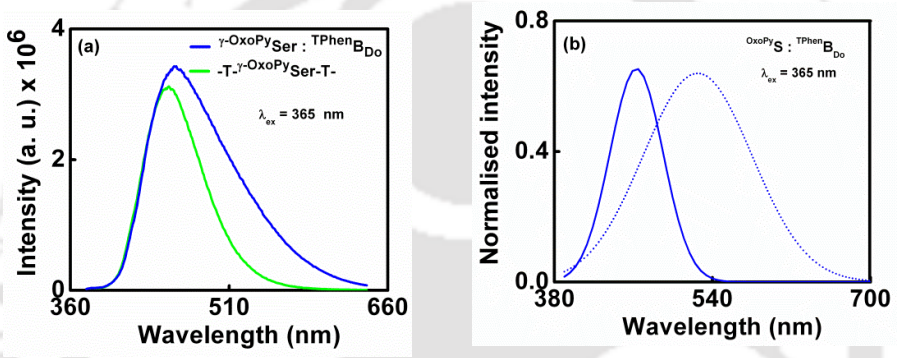

Figure 6.28: (a) Emission spectra of the chimeric duplex $^{OxoPy}S$:$^{TPhen}B_{Do}$ (ODN **1•2**) excited at 365 nm. (b) Resolved emission spectra shows bands at 460 and 535 nm.

To prove our thought into practical we recorded variable temperature emission spectra maintaining the same condition of excitation. Thus, we observed that as the temperature was increased, the emission intensity at 535 nm was going to decrease indicating the breakdown of π-stacked excited state complex (exciplex) between **OxoPy** and **TPhen** (**Figure 6.29**).[2b-c]

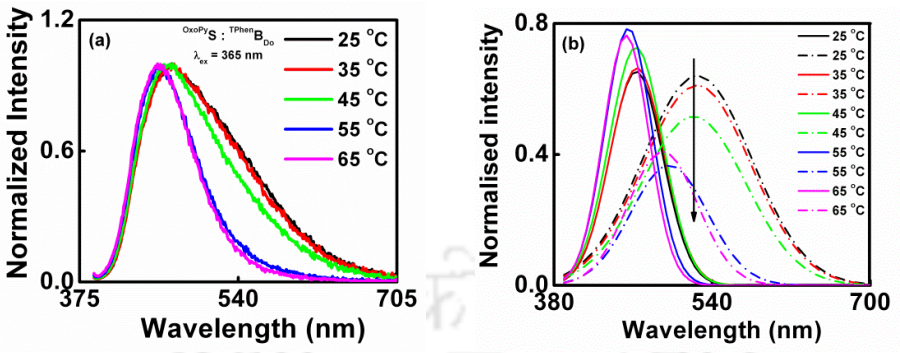

Figure 6.29: Normalized variable temperature fluorescence emission spectra of duplex ODN **1•2** (^{OxoPy}**S:**^{TPhen}**B$_{Do}$**)-(a) λ_{ex} = 365 nm and it's (b) multi gaussian peak fitting showing evidence of exciplex emission with decreased intensity.

Therefore, it was clear that excitation (365 nm) at oxopyrene of ^{OxoPy}**S** of chimeric duplex gave rise to the generation of **OxoPy**-**TPhen** exciplex emission at around 535 nm along with the **OxoPy** monomer emission at 460 nm (**Figure 6.28-6.29**). The exciplex was formed in a ground state complex in a π-π stacked fashion was also evident from excitonic interactions seen in the absorption spectra (**Figure 6.26**).

To further investigate the broad emission band at 535 nm as exciplex emission we next studied the time resolved fluorescence of ODN **1** (^{OxoPy}**S**) and its various duplex ODNs with natural ODNs [ODN **3-6** (A, G, C, T)] and unnatural ODN **2** (^{TPhen}**B$_{Do}$**) (**Figure 6.30** and **Table 6.6**). It was found that the life time of the duplex ODNs with natural and unnatural complementary target was longer than the corresponding single strand ODN **1**. However, the duplex ODN **1•4** (^{OxoPy}**S:G**) showed slightly smaller lifetime than the corresponding single strand ODN **1** and this is because of fluorescence quenching of ^{OxoPy}**S** by opposite guanine base. We observed higher lifetime (τ_{av} = 7.13 ns) in case of the duplex ODN **1•2** (^{OxoPy}**S:**^{TPhen}**B$_{Do}$**) compared to other duplexes when monitored at oxopyrene emission (λ_{em} = 460 nm). Surprisingly, the highest lifetime was observed (τ_{av} = 13.9 ns) for the duplex ODN **1•2** when monitored at 535 nm, the center of broad emission band. This longer lifetime most probably is due to the exciplex.

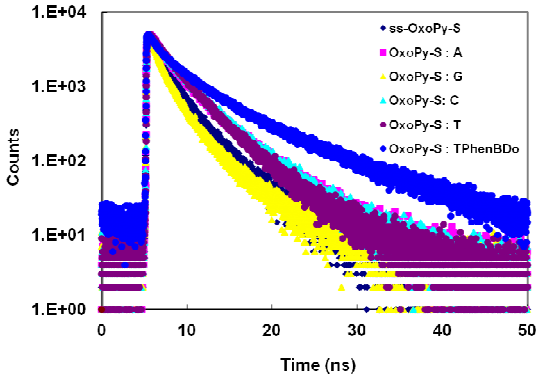

Figure 6.30: Time resolved fluorescence traces of various ODNs.

Table 6.6: Summary of time resolved fluorescence of various ODNs at room temperature.

ODNs	X : Y	τ_1 (ns)	τ_2 (ns)	a_1 %	a_2 %	$\langle\tau\rangle$ (ns)	B1	B2	χ^2
ODN **1**	-T-^{OxoPy}**S** -T-[a]	1.60	4.14	75.71	24.29	2.75	3982.9	1277.8	1.06
ODN **1•2**	^{OxoPy}**S:**^{TPhen}**B**$_{Do}$[a]	2.1	7.6	59.84	40.16	7.13	2650.1	1589.4	1.15
ODN **1•3**	^{OxoPy}**S: A**[a]	2.23	5.14	70.05	29.95	3.67	3684.8	1575.7	1.12
ODN **1•4**	^{OxoPy}**S:G**[a]	1.39	4.43	84.44	15.56	2.51	4309.2	794.2	1.12
ODN **1•5**	^{OxoPy}**S:C**[a]	2.43	5.30	71.94	28.06	3.75	3783.6	1475.8	1.11
ODN **1•6**	^{OxoPy}**S:T**[a]	2.62	5.41	81.24	18.76	3.52	4303.6	993.8	1.10
ODN **1•2**	^{OxoPy}**S:**^{TPhen}**B**$_{Do}$[b]	7.5	14.84	49.97	50.03	13.9	1048.0	1049.4	1.07
[a]**Monitoring λ_{em} = 460 nm;** [b] **Monitoring λ_{em} = 535 nm**									

To further investigate the exciplex formation, we studied the variable temperature time resolved fluorescence of the chimeric duplex ^{OxoPy}**S:** ^{TPhen}**B**$_{Do}$ (**Figure 6.31** and **Table 6.7**). Thus, we observed a clear decrease of lifetime (λ_{em} = 460 nm) from 7.13 ns to 2.23 ns when temperature was increased from 25 ^{o}C to 65 ^{o}C with decrease of % composition of the second component from 40.16% to 12.47%. Similar kind of decreasing trend of lifetime and % composition was observed when we monitored at the centre of the broad emission, λ_{em} = 535 nm (**Table 6.7**). This observation also

corroborated with the exciplex emission. Therefore, the broad emission centered at 535 nm originates as a result of exciplex emission between ^{OxoPy}**S** and ^{TPhen}**B**$_{Do}$ when the duplex ODN **1•2** is excited at the absorption maxima (at 365 nm) of ^{OxoPy}**S**.

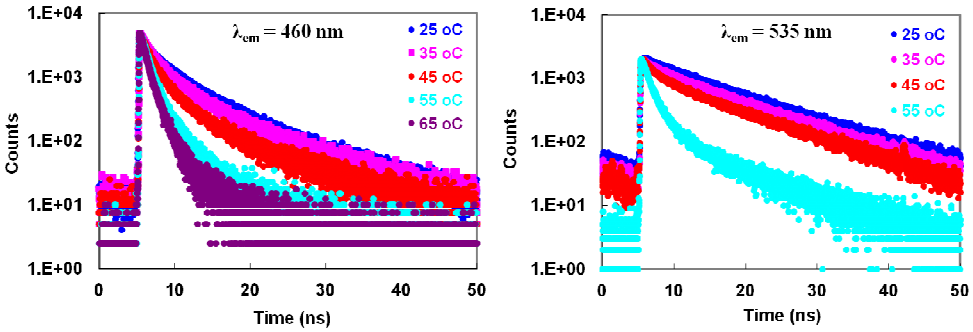

Figure 6.31: Variable temperature time resolved fluorescence spectra (λ_{ex} = 375 nm) of chimeric ODN^{OxoPy}**S :**^{TPhen}**B**$_{Do}$ ([ODN^{OxoPy}**S**] = [ODN ^{TPhen}**B**$_{Do}$] = 2.5 μM, 50 mM sodium phosphate, 0.1 M sodium chloride, pH 7.0, room temperature).

Table 6.7: Summary of variable temperature time resolved fluorescence of chimeric duplex ^{OxoPy}**S:** ^{TPhen}**B**$_{Do}$.

ODN	Temp (°C)	τ_1 (ns)	τ_2 (ns)	a_1 %	a_2 %	<τ> (ns)	B1	B2	χ^2
^{OxoPy}**S :**^{TPhen}**B**$_{Do}$ [a]	25	2.1	7.6	59.84	40.16	**7.13**	2650.1	1589.4	1.15
	35	1.88	7.65	74.05	25.95	**7.34**	1308.0	458.4	1.09
	45	1.51	7.21	84.75	15.25	**7.05**	1513.3	272.3	1.09
	55	1.00	3.04	85.99	14.01	**2.94**	1631.9	265.8	1.01
	65	0.83	2.30	87.53	12.47	**2.23**	1646.2	234.4	0.94
^{OxoPy}**S :**^{TPhen}**B**$_{Do}$ [b]	25	7.47	14.84	49.97	50.03	**13.91**	1048.0	1049.4	1.07
	35	3.30	11.77	27.75	72.25	**9.74**	533.4	1388.4	1.06
	45	1.85	10.85	47.17	52.83	**9.86**	960.9	1076.1	1.09
	55	1.29	8.03	89.99	10.01	**7.92**	1781.4	198.2	1.08

[a]Monitoring λ_{em} = 460 nm; [b] Monitoring λ_{em} = 535 nm

6.6.7.5. Evidence of Exciplex Emission Between ^{OxoPy}S and ^{TPhen}B$_{Do}$ upon Excitation at ^{TPhen}B$_{Do}$: Exciplex Emission *via* FRET from ^{TPhen}B$_{Do}$ to ^{OxoPy}S

After establishing the exciplex emission upon excitation of ^{OxoPy}**S** from the chimeric duplex ODN **1•2** (^{OxoPy}**S:**^{TPhen}**B$_{Do}$**), we were curious to know whether the same exciplex emission could be observed from the same duplex upon excitation at the absorption wavelength of other pairing partner, *i.e.* ^{TPhen}**B$_{Do}$** (λ_{abs} = 310 nm). If so, we also wanted to know whether the exciplex would generate *via* the π-π-stacking complexation between the excited ^{TPhen}**B$_{Do}$** and ground state of ^{OxoPy}**S** or the reverse upon excitation of the duplex at 310 nm. The reverse one, *i.e.* the exciplex generation *via* the π-π-stacking complexation between the excited ^{OxoPy}**S** and ground state of ^{TPhen}**B$_{Do}$** upon excitation of the duplex at 310 nm, is only possible if the energy from the excited ^{TPhen}**B$_{Do}$** is transferred to ^{OxoPy}**S** *via* FRET process.

To clear our understanding we first analyzed the fluorescence emission spectra of the duplex ODN **1•2** (^{OxoPy}**S:**^{TPhen}**B$_{Do}$**) which was excited at the absorbance maximum of ^{TPhen}**B$_{Do}$** (λ_{ex} = 310 nm). Thus, the fluorescence spectra exhibited a strong and broad emission centered at 460-535 nm and span upto 675 nm along with a very weak emission which is characteristic emission of ^{TPhen}**B$_{Do}$** (**Figure 6.32a**). Interestingly, the broad emission was found to be superimposable to the spectrum that was observed when the same duplex was excited at the absorbance maximum of ^{OxoPy}**S** (λ_{ex} = 365 nm) (**Figure 6.28**). The broad emission spectra could be resolved into two bands, at 460 nm characteristic emission of **OxoPy** monomer emission and at 535 nm which could be assigned as **OxoPy**-**TPhen** exciplex emission (**Figure 6.32b**).

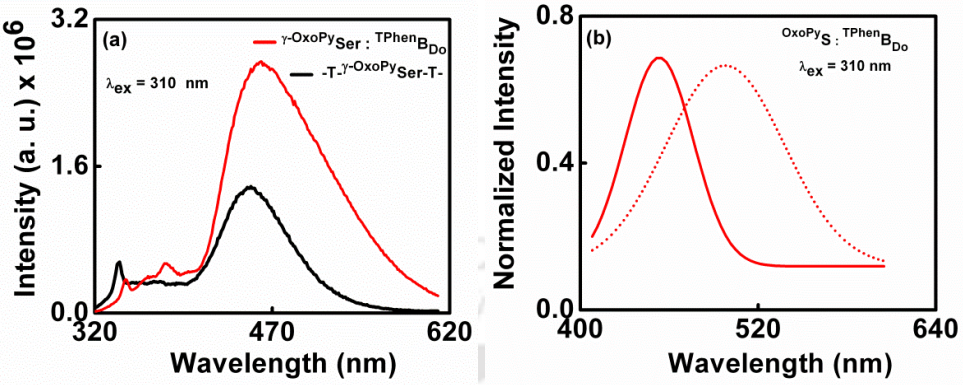

Figure 6.32: (a) Emission spectra of the chimeric duplex ^{OxoPy}**S :**^{TPhen}**B**$_{Do}$ (ODN **1•2**) excited at 310 nm. (b) Resolved emission spectra shows bands at 460 and 535 nm.

Therefore, excitation at ^{TPhen}**B**$_{Do}$ (λ_{ex} = 310 nm) resulted in 3 emission bands- at around 375 nm corresponding to ^{TPhen}**B**$_{Do}$ monomer emission, 460 nm characteristic emission of **OxoPy** monomer and at 535 nm which could be assigned as **OxoPy-TPhen** exciplex emission. The appearance of the band at 535 nm along with the **OxoPy** monomer emission band at 460 nm clearly suggested that the exciplex band at 535 coming *via* the π-π-stacking complexation between the excited ^{OxoPy}**S** and ground state of ^{TPhen}**B**$_{Do}$. Moreover, the presence of a weak band at around 375 nm corresponding to ^{TPhen}**B**$_{Do}$ monomer emission (which is a decreased emission compared to the emission intensity from the monomer in the single strand ODN **2**) along with 460 nm characteristic emission of **OxoPy** monomer further indicated a dipolar photophysical interaction between **TPhen** moiety of ^{TPhen}**B**$_{Do}$ and **OxoPy** moiety of ^{OxoPy}**S**.

To prove that the emission at 535 nm upon excitation at 310 nm is an exciplex emission we recorded the emission spectra at various temperatures and resolved the same into two bands. Thus, we observed that as the temperature was increased, the emission intensity at 535 nm was going to decrease indicating the breakdown of π-stacked excited state complex (exciplex) between **OxoPy** and **TPhen** (**Figure 6.33**).[2b-c] Therefore, it was clear that excitation at 310 nm *i.e.* at **TPhen** of ^{TPhen}**B**$_{Do}$ of chimeric duplex gave rise to the generation of **OxoPy-TPhen** exciplex emission at

around 535 nm along with the **OxoPy** monomer emission at 460 nm and a decreased (compared to the single strand ODN **2**) **TPhen** monomer emission at 375 nm (**Figure 6.33**).

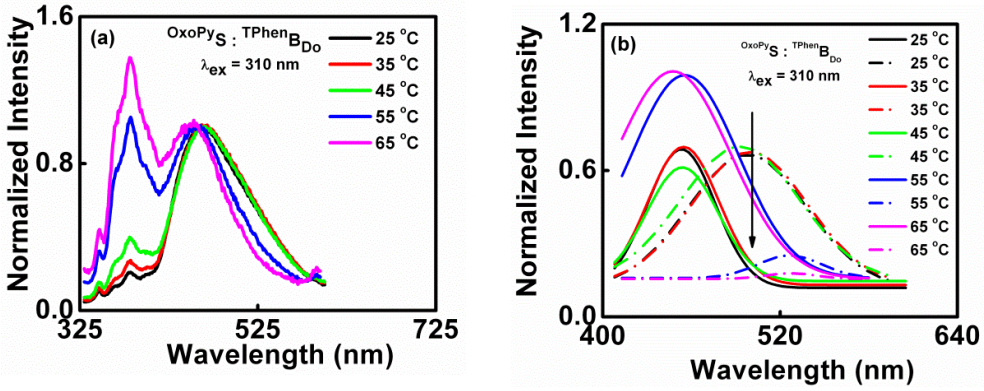

Figure 6.33: Normalized variable temperature fluorescence emission spectra of duplex ODN **1•2** (^{OxoPy}**S :** ^{TPhen}**B$_{Do}$**)-(a) λ_{ex} = 310 nm and it's (b) multi gaussian peak fitting showing evidence of exciplex emission with decreased intensity.

All the spectral features upon excitation at 310 nm can only be explained clearly if we consider the fact that the excited triazolylphenanthrene transfers its energy to the closely spaced oxopyrene chromophore of ^{OxoPy}**S** paired against ^{TPhen}**B$_{Do}$** in the chimeric duplex ODN **1•2**. Absorbing the transferred energy (FRET energy), **OxoPy** chromophore goes to the excited state and form a π-stacked complex (exciplex) with relaxed **TPhen** chromophore which then released its energy in the form of emission light at 535 nm.

Therefore, we next have examined whether there is a possibility of FRET process to occur between ^{TPhen}**B$_{Do}$** as donor and ^{OxoPy}**S** as an acceptor upon excitation of the chimeric duplex ODN **1•2** at the absorption maximum of the donor ^{TPhen}**B$_{Do}$** (λ_{ex} = 310 nm). The primary condition for the FRET to take place was satisfied by the overlap of emission spectra of ^{TPhen}**B$_{Do}$** containing target ODN **2** (donor) with the absorption spectra of ^{OxoPy}**S** containing probe ODN **1** (acceptor) (**Figure 6.34a**) [3a, 55]. Thus, it was observed that the fluorescence intensity of the acceptor ^{OxoPy}**S** in chimeric duplex ODN **1•2** increased from the emission in single stranded ODN **1** by

almost two times in presence of donor $^{TPhen}\mathbf{B_{Do}}$ in duplex ODN **1•2** when excited at absorption maximum of $^{TPhen}\mathbf{B_{Do}}$ (λ_{max} = 310 nm wherein negligible absorbance was there for $^{OxoPy}\mathbf{S}$). On the other hand, the fluorescence intensity of the donor $^{TPhen}\mathbf{B_{Do}}$ in the chimeric duplex ODN **1•2** decreased compared to the emission in the single stranded ODN **2** in presence of the acceptor $^{OxoPy}\mathbf{S}$. This change in fluorescence intensity revealed the visual evidence of FRET process from $^{TPhen}\mathbf{B_{Do}}$ to $^{OxoPy}\mathbf{S}$ in the chimeric dulex ODN **1•2** ($^{OxoPy}\mathbf{S}$ **:** $^{TPhen}\mathbf{B_{Do}}$) (**Figure 6.34b**).[55e]

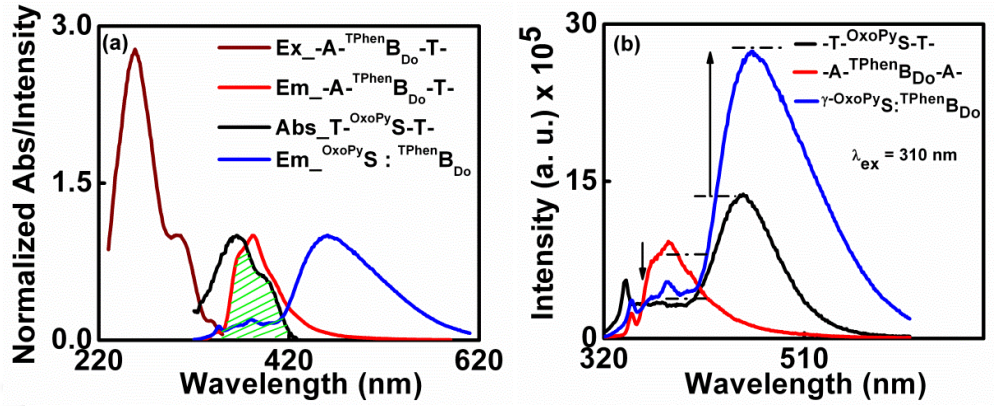

Figure 6.34: (a) Normalized absorption spectra of ODN **1** ($^{OxoPy}\mathbf{S}$), excitation and emission spectra of ODN **2** ($^{TPhen}\mathbf{B_{Do}}$), and emission spectra of chimeric duplex ODN **1•2** ($^{OxoPy}\mathbf{S}$ **:** $^{TPhen}\mathbf{B_{Do}}$). (b) Fluorescence emission spectra (λ_{ex} = 310 nm) of single strand ODN **1** ($^{OxoPy}\mathbf{S}$), ODN **2** ($^{TPhen}\mathbf{B_{Do}}$) and their hybrid ODN **1•2** ($^{OxoPy}\mathbf{S}$ **:** $^{TPhen}\mathbf{B_{Do}}$). ([ODN $^{OxoPy}\mathbf{S}$] = [ODN $^{TPhen}\mathbf{B_{Do}}$] = 1 μM, 50 mM sodium phosphate, 0.1 M sodium chloride, pH 7.0, room temperature).

In summary, upon excitation of the duplex ODN **1•2** at the absorbance maximum of the donor $^{TPhen}\mathbf{B_{Do}}$ (λ_{ex} = 310 nm) a broad and intense emission was observed. This emission was superimposable to the spectrum that was observed when excited at the absorbance maximum (λ_{ex} = 365 nm) of the acceptor, $^{OxoPy}\mathbf{S}$. If the emission was the only emission from oxopyrene chromophore due to FRET from $^{TPhen}\mathbf{B_{Do}}$ donor, we could observe only one emission band at around 460 nm. However, we observed a broad emission with two resolvable bands at 460 nm characteristic emission of **OxoPy** monomer and at 535 nm which was clearly be assigned as **OxoPy-TPhen**

exciplex emission (**Figure 6.33**). Therefore, it was clear from the emission spectra that upon excitation at 310 nm, the excited triazolylphenanthrene transfer its energy to the closely spaced oxopyrene chromophore of $^{\mathbf{OxoPy}}\mathbf{S}$ paired against $^{\mathbf{TPhen}}\mathbf{B_{Do}}$ in the chimeric duplex ODN **1•2**. Absorbing the FRET energy, **OxoPy** chromophore of $^{\mathbf{OxoPy}}\mathbf{S}$ goes to the excited state and formed a π-stacked complex (exciplex) with relaxed **TPhen** chromophore of $^{\mathbf{TPhen}}\mathbf{B_{Do}}$ which then released its energy in the form of emission light at 535 nm. Therefore, our result suggests that the exciplex emission originates *via* a FRET process between a donor and an acceptor chromophore.

Next, we calculated the efficiency of energy transfer, *E*, using the equation (1)

$$E=\frac{R_0^6}{R_0^6+r^6}=1-\frac{F}{F_0} \quad \ldots\ldots\ldots\ldots\ldots\ldots\ldots\ldots (1)$$

where, *F* and F_0 are the fluorescence intensity of donor ($^{\mathbf{TPhen}}\mathbf{B_{Do}}$) in the presence and absence of acceptor, *r* is the distance between donor and the acceptor and R_0 is the critical distance when the energy transfer efficiency is 50% . The efficiency of energy transfer (*E*) from donor to acceptor was calculated using the equation 1, and it was found that there was 43 % efficiency of energy transfer from donor residue ($^{\mathbf{TPhen}}\mathbf{B_{Do}}$) to acceptor residue ($^{\mathbf{OxoPy}}\mathbf{S}$) in the chimeric duplex ODN **1•2** ($^{\mathbf{OxoPy}}\mathbf{S}$ **:** $^{\mathbf{TPhen}}\mathbf{B_{Do}}$).

We also calculated the Förster distance R_0 (Å) using the following equation (2)

$$R_0=[8.79\times10^{-5}\kappa^2 n^{-4}\Phi_D J(\lambda)]^{1/6} \quad \ldots\ldots\ldots\ldots\ldots\ldots....(2)$$

where, κ^2 is the orientation, *n* is the refractive index of the medium, Φ_D is the quantum yield of the donor in the absence of acceptor $J(\lambda)$ is the overlap integral of the fluorescence emission spectrum of the donor and the absorption spectrum of the acceptor given by the following equation (3)

$$J=\frac{\int_0^\infty F_D(\lambda)\varepsilon_A(\lambda)\lambda^4 d\lambda}{\int_0^\infty F_D(\lambda)d\lambda} \quad \ldots\ldots\ldots\ldots\ldots\ldots\ldots\ldots (3)$$

where $F_D(\lambda)$is the fluorescence intensity of the donor in the wavelength range λ to $\lambda + \Delta\lambda$ with the total intensity normalized to unity. $\varepsilon_A(\lambda)$ is the molar extinction coefficient of the acceptor as a function of wavelength (λ). Using the values of κ^2= 2/3, *n* = 1.33,

Φ_D = 0.0395, and the obtained overlap integral, $J(\lambda)$ = 1.65873 x 10^{14} the R_0 and r values were calculated which were found as R_0 = 22.29Å and r = 23.39Å.

In conclusion the duplex ODN **1•2** (**^{OxoPy}S :^{TPhen}B$_{Do}$**) represents an highly interesting system wherein we established that the exciplex formation can take place *via* two mechanism-(a) FRET from the donor **^{TPhen}B$_{Do}$** to the acceptor **^{OxoPy}S** (**Section 6.6.7.5**) or (b) direct excitation of FRET acceptor **^{OxoPy}S** (**Section 6.6.7.4**). The full process of exciplex emission either *via* FRET from the donor **^{TPhen}B$_{Do}$** or direct excitation of FRET acceptor **^{OxoPy}S** is schematically represented below in **Figure 6.35**.

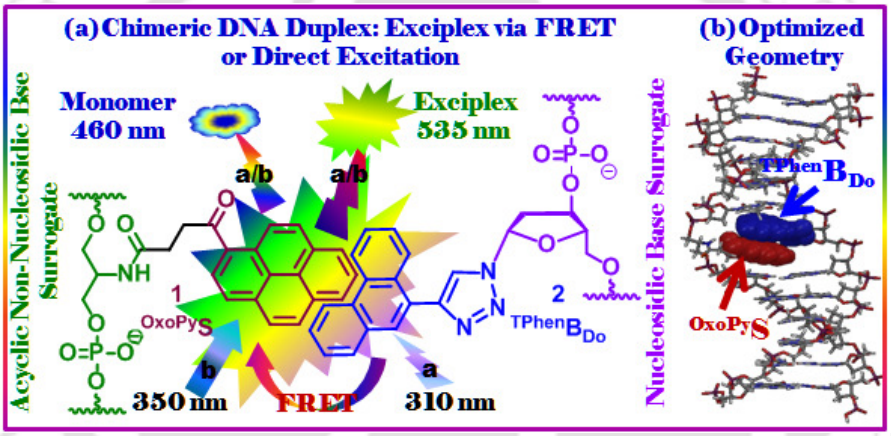

Figure 6.35: (a) Schematics of exciplex formation and structures of the acyclic non-nucleosidic base surrogate **^{OxoPy}S** and nucleosidic base surrogate **^{TPhen}B$_{Do}$**. (b) Amber* optimized geometry of the chimeric base pair (**^{OxoPy}S**:**^{TPhen}B$_{Do}$**) held by intercalative inter-strand π-stacking interaction showing the possibility of exciplex formation

6.6.7.6. Macromodel Study to Support Exciplex Formation

Next, we have carried out molecular modeling study using Schrödinger Macro Model software (Maestro, version 9.0) with Amber* force field in water to support the possibility of exciplex emission in the chimeric duplex ODN **1•2** (**^{OxoPy}S :^{TPhen}B$_{Do}$**).[56] Thus, the conformations of DNA duplex with triazolylphenanthrene (**^{TPhen}B$_{Do}$**) nucleoside opposite to oxo-pyreneserinol (**^{OxoPy}S**) was minimized with the Amber* force field. During the course of modelling study, both the isomers of the

probe ODN **1**, namely R- and S-configurations of the chiral centre of ^{OxoPy}**S**, were taken into consideration in constructing the duplex ODN **1•2** (^{OxoPy}**S :**^{TPhen}**B**$_{Do}$). Both the isomeric duplexes were then optimized with Amber* force field in water. A conjugate gradient minimization scheme [PRCG (Polak-Ribiere Conjugate Gradient)] that uses the Polak-Ribiere first derivative method with restarts every 3N iterations were employed for the minimization of the B-form duplexes. The optimized geometry of the B-form duplex ODN **1•2** (^{OxoPy}**S :**^{TPhen}**B**$_{Do}$) with R-configuration at the chiral centre of ^{OxoPy}**S** showed an intercalated stacked structure in triazolylphenanthrene (**TPhen**) while the oxopyrene (**OxoPy**) remained in the groove side indicating the impossibility of interaction between **OxoPy** and **TPhen** residues *via* π-π stacking interaction. On the other hand, the optimized geometry of the B-form duplex ODN **1•2** (^{OxoPy}**S :**^{TPhen}**B**$_{Do}$) with S-configuration at the chiral centre of ^{OxoPy}**S** showed an intercalated stacked structure in both triazolylphenanthrene (**TPhen**) and oxopyrene (**OxoPy**) inside the duplex suggesting a strong π-π stacking interaction between **OxoPy** and **TPhen** residues (**Figure 6.36a-b**). Therefore, the modeling study supported the high possibility of π-π stacking interaction and therefore, the exciplex formation between **OxoPy** and **TPhen** residues in the chimeric duplex ODN **1•2** (^{OxoPy}**S :**^{TPhen}**B**$_{Do}$) with S-configuration at the chiral centre of ^{OxoPy}**S**. This observation also indicates, though not evidencing, the possible isomeric status of the single strand probe ODN **1** containing ^{OxoPy}**S** which we dealt with here in this full chapter. We also observed the similar result while carried out a molecular dynamic simulation with the duplex ODN **1** using Schrodinger Macromodel (Maestro vs. 9.0) software package with OPLS 2005 force field in which the systems were subjected to 100 ps simulations time (with time step of 1.5 fs and equilibrium time 1.0 ps) at constant temperature (300 K) and pressure (1 atm) with shaking bonds to hydrogens. The triazolylphenanthrene (**TPhen**) and oxopyrene (**OxoPy**) units were choosen as freely moving moieties during the simulation. An optimal minimization method was chosen for minimizing the generating structure (with maximum iteration of 1000) with gradient convergence threshold of 0.05 (**Figure 6.36c-d**).

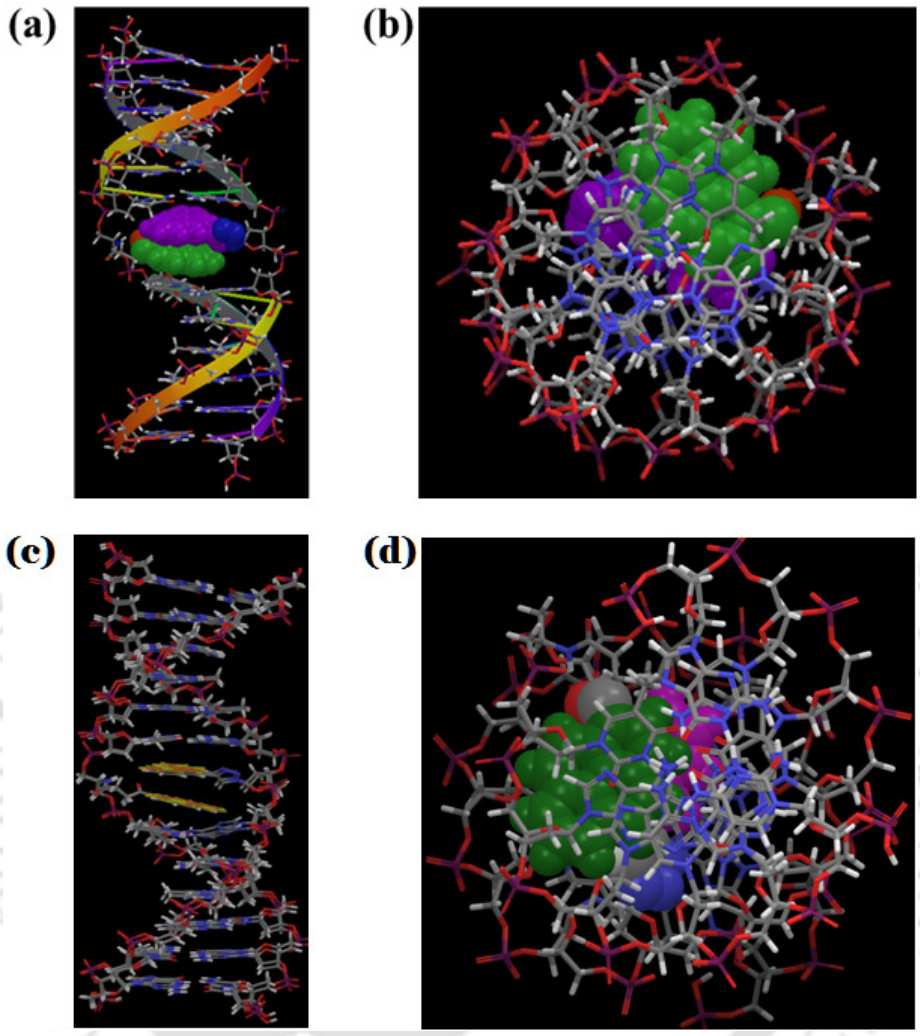

Figure 6.36: Amber* optimized geometry of the chimeric duplex ODN **1•2** (^{OxoPy}**S :**^{TPhen}**B**$_{Do}$)-(a) Side view and (b) top view. (c) Superimposed structures (6 out of 11 generated) of various conformations of the chimeric duplex ODN **1•2** (^{OxoPy}**S :**^{TPhen}**B**$_{Do}$) derived from a MD simulation using OPLS 2005 force field. (d) Top view of MD simulated lowest energy minimized conformation. Chiral centre of ^{OxoPy}**S** possess S-configuration in all cases. The pictures show the ^{OxoPy}**S** residue in green and ^{Tphen}**B**$_{Do}$ residue in cyan colour.

6.7. Conclusion

In summary, the designed novel chemeric DNA duplex wherein a non-nucleosidic base surrogate ^{OxoPy}**S** selectively paired against an unnatural triazolylphenanthrene nucleoside (^{TPhen}**B**$_{Do}$) represents a very interesting dual door entry system for exciplex emission. All the spectroscopic evidences suggested that both the process of excitation of oxopyrene chromophore of ^{OxoPy}**S**-either energy transfer from excited triazolylphenanthrene to oxopyrene *via* FRET or direct excitation of ^{OxoPy}**S** at its absorbance maximum-led to the exciplex emission. The mechanism of exciplex formation *via* FRET which we have shown would become possible further by judicious designing and proper positioning the donor/acceptor pair in a probe wherein the pair involves in strong intercalative π-π stacking interaction. To the best of our knowledge this is the start of a new generation of probes which could find wide applications in the field of chemical biology and in designing light harvesting DNA materials. We also hope that the design of such systems would have great impact in devising optoelectronics and might find application in chemistry, biology, material sciences and in diagnostic technology.

6.8. Experimental Section

6.8.1. General Experimental

All reactions were carried out under a nitrogen atmosphere. Organic extracts were dried over anhydrous sodium sulphate. Solvents were removed in a rotary evaporator under reduced pressure. Silica gel (60-120 mesh size) was used for the column chromatography. Reactions were monitored by TLC on silica gel 60 F254 (0.25mm). ^{1}H NMR spectra were measured with Bruker 300 (300 MHz) and ^{13}C NMR spectra were measured with Bruker 75 (75MHz) spectrometer. Coupling constant (*J* value) was reported in hertz. The chemical shifts were shown in ppm downfield from tetramethylsilane, using residual chloroform (δ = 7.24 in ^{1}H NMR, δ = 77.23 in ^{13}C NMR), dimethyl sulfoxide (δ = 2.48 in ^{1}H NMR, δ = 39.5 in ^{13}C NMR), as an internal standard. Mass spectra were recorded using WATERS MS system, Q-tof premier and data analyzed using Mass Lynx 4.1. The *UV*–visible spectra were recorded by

Shimadzu UV-2550 UV-Visible spectrophotometer with a cell of 1 cm path length. Fluorescence spectra were obtained using Fluoromax-4 fluorescence spectrophotometer at 25 °C using 1 cm path length cell. The reagents for DNA synthesis were purchased from Glen Research. Reversed-phase HPLC was performed on CHEMCOBOND 5-ODS-H columns (10x150 mm, 4.6x150 mm) using UV detector (260 nm). Mass spectra of the oligonucleotides were recorded using a MALDI-TOF mass spectrometer. The natural complementary DNAs were purchased from Integrated DNA Technologies.

6.8.2. Synthesis of Non-Nucleosidic/Nucleosidic Base Surrogates

N-(1,3-dihydroxypropan-2-yl)-4-oxo-4-(pyren-1-yl)butanamide ***($^{OxoPy}S$,*** **6.39*):*** To a solution of γ-oxopyrenebutyric acid in 5 ml dry DMF [(**6.37**, **OxoPy**); 200 mg, 0.66 mmol] synthesized *via* our previously published protocol, pyBop (413 mg, 0.80 mmol) and anhydrous diisopropylethyl amine (DIPEA) (253 µl, 1.5 mmol) were added. The reaction mixture was stirred for 30 minutes at room temperature. A solution of serinol (**6.38**, 90 mg, 0.99 mmol) in dry DMF (2 ml) and DIEPA (172 µl, 0.99 mmol) were added then to this reaction mixture and was stirred for 12 h at room temperature. After completion of the reaction monitored by TLC, DMF was removed by high vacuum, and ethyl acetate (30 ml) was added. The solution was washed with saturated aqueous $NaHCO_3$ solution (3 x 15 ml) and brine (3 x 15 ml). The organic layers were collected, dried over anhydrous sodium sulfate and then concentrated to dryness by rotary evaporator. The residue was purified by silica gel column chromatography to afford oxopyreneserinol (^{OxoPy}**S**, **6.39**) in 80% yield (198 mg). M.p.156-158 ^{o}C; IR (KBr) 3502, 3411, 3391, 3297, 1681, 1665, 841 cm^{-1} ;^{1}H NMR (DMSO-d_6, 300 MHz) δ 2.48 (2H, s), 2.66 (2H, d, J = 7.5 Hz), 4.65 (5H, m), 7.69 (2H, d, J = 9.0 Hz), 8.09-8.72 (7H, m); ^{13}C NMR (DMSO-d_6, 75 MHz) δ 30.1, 37.5, 53.1, 60.3, 124.5, 124.7, 126.5, 126.8, 127.3, 129.1, 129.3, 132.9, 133.1, 171.4, 203.9; ESI-TOF-MS m/z 376 $[M + H]^+$; HRMS calcd for $C_{23}H_{22}NO_4$ ($[M+H]^+$) 376.1549, found 376.1558.

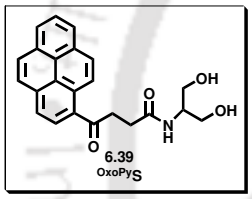

N-(3-(bis(4-methoxyphenyl)(phenyl)methoxy)-1-hydroxypropan-2-yl)-4-oxo-4-(pyren-1-yl)butanamide (^{OxoPy}***S-DMTr*, 6.40*):*** To a solution of oxopyreneserinol [(^{OxoPy}**S**, **6.39**)120 mg, 0.32 mmol] in 5 ml dry pyridine DMTr-Cl (129 mg, 0.38 mmol) was added under nitrogen atmosphere at room temperature. The reaction mixture was allowed to stir overnight. After completion the reaction monitored by TLC the reaction mixture was quenched by adding 1 ml of MeOH. The reaction mixture was then concentrated to dryness, the residue was dissolved in ethylacetate (40 ml), washed with water, 5% $NaHCO_3$, and brine. The organic phases were dried over anhydrous sodium sulfate and concentrated to dryness by rotary evaporator. The crude product was purified by silica gel column chromatography to afford compound **6.40** (^{OxoPy}**S-DMTr**) in 70 % yield (151 mg). IR (KBr) 3397, 1668, 1508, 1249, 1176, 848, 829 cm^{-1}; ^{1}H NMR (CD_3OD, 300 MHz) δ 2.67-2.69 (2H, m), 2.82-2.84 (2H, m), 3.18-3.22 (2H, m), 3.57-3.59 (2H, m), 3.67 (6H, s), 4.17-4.21 (1H, m), 6.78-6.81 (4H, d, J = 8.4 Hz), 7.17-7.19 (1H, m), 7.25-7.32 (6H, m), 7.46 (2H, d, J = 7.8 Hz), 8.11-8.18 (3H,m), 8.24-8.34(4H, m), 8.49 (1H, d, J = 9 Hz), 8.83 (1H, d, J = 9 Hz); ^{13}C NMR (CD_3OD, 75 MHz) δ 24.1, 39.5, 45.3, 47.8, 54.9, 56.0, 79.5, 106.2, 117.5, 118.1, 119.3, 119.6, 119.8, 119.9, 119.9, 120.5, 120.9, 121.5, 122.6, 122.8, 123.5, 124.1, 129.5, 129.6, 138.8, 152.2; ESI-TOF-MS m/z 678 $[M + H]^+$.

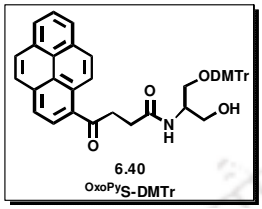

6.40
^{OxoPy}S-DMTr

3-(bis(4-methoxyphenyl)(phenyl)methoxy)-2-(4-oxo-4(pyrenyl)butanamido) propyl-2- cyanoethyldiisopropylphosphoramidite (6.41): Compound **6.41** was synthesised by dissolving compound **6.41** (100 mg, 0.14 mmol) in dry CH_2Cl_2 (5 ml) and stirred. To this stirring solution was added 1-methylimidazole (3 mg, 0.04 mmol) and *N,N*-diisopropylethylamine (0.15 ml) under argon atmosphere followed by 2-cyanoethyl *N,N*-diisopropylchlorophosphoramidite (50 µl, 0.21 mmol). The reaction mixture was allowed to stir at room temperature for 0.5 h and was monitored by TLC. After that CH_2Cl_2 (15 ml) was added and washed with 5% aqueous sodium carbonate and brine. The organic phases were dried over anhydrous sodium sulphate and concentrated to dryness by rotary evaporator. The crude product phosphoramidite

6.41 was purified by silica gel chromatography, dried in vacuum and used immediately for DNA synthesis without characterization.

Synthesis of 1-(2'-deoxy-β-D-ribofuranosyl)-4-(phenanthren-9-yl)-1H-1,2,3-triazole ($^{TPhen}B_{Do}$): The synthesis of triazolylphenanthrene decorated nucleoside, $^{TPhen}\mathbf{B_{Do}}$, was discussed in **Chapter 2**.

6.8.3. Procedure for Oligonucleotide Synthesis, Purification and Characterization

The synthesis, purification and characterization of the oligonucleotide target containing unnatural triazolylphenanthrene nucleoside, $^{TPhen}\mathbf{B_{Do}}$ (here it is named as ODN **2**) at the centre of 13-ODN sequence was performed by a conventional phosphoramidite method using an automated DNA/RNA synthesizer and was already discussed in the experimental section of **Chapter 4**. Following the same procedure, the oligonucleotide probe containing non-nucleosidic base surrogate, $^{OxoPy}\mathbf{S}$ (ODN **1**) at the centre of 13-ODN sequence was synthesized, purified and characterized.

The concentration of the DNA stock solution was then determined applying *Lamberts-Beer's* equation: $A_{260} = \log I/I_0 = c \times \varepsilon_{260} \times l$ where $\varepsilon_{260} = \Sigma i\ \varepsilon_I$; *A260* is the absorbance of the probe at 260 nm which is determined from the intensity of the transmitted light (*I*) compared to the intensity of the emerging light (I_0), *c* is the concentration of the probe DNA, ε_{260} is the algebraic sum of extinction-coefficients of the individual nucleosides at 260 nm (for natural nucleosides, this is calculated with Oligo Analyser and *l* is the pathlength of the light through the sample.

The concentration of stock ODN **1** and ODN **2** was 550 and 626 μM (2.0 ml), respectively. All the natural complementary ODNS (ODN **3-6**) were purchased and used as supplied.

6.8.4. Study of Photophysical Properties of the Oligonucleotides

Preparation of ODNs solutions for thermal denaturation and spectroscopic studies: The two complementary DNA strands were mixed together in a solution of buffer and NaCl. The final volume of 1 ml was made up by adding Millipore water to get a DNA solution wherein the concentration of each single strand DNA is 2.5 μM.

All the DNA solutions were prepared in separate 2 ml micro centrifuge tubes which were undergone through sonication for 2 minutes, vortex mixing for 4 minutes and finally microcentrifugation for 2 minutes. In summary, first we prepared 2.5 μM DNA solutions (probe or target DNA, 1 ml) in 50 mM sodium phosphate buffer, 100 mM NaCl, pH 7.0 for melting point (T_m) determination and all other spectroscopic studies. Next, the two complementary DNA strands were hybridize just by mixing and sonicating for 5 min to get various double stranded ODNs. In all the cases the concentration of each single stranded ODN was 2. 5 μM in the above mentioned buffer and salt at pH 7.0. Thus prepared single strand DNA and double strand DNAs solutions were used for all the spectroscopic investigations.

UV-visible and thermal melting temperature (T_m) measurements of the oligonucleotides: All UV-visible and T_m of the ODNs (2.5 μM, final duplex concentration) were measured in 50 mM sodium phosphate buffers (pH 7.0) containing 100 mM sodium chloride. The measurements were taken in absorbance mode. The absorbance values of the sample solutions were measured in the wavelength regime of 200–500 nm with a scanning rate of 0.5 nm slit width of 2 nm. All the sample solutions were prepared just before doing the experiment. Total volume of 120 μL from a stock solution of 700 μL of 2.5 μM concentration for each set was used for UV and *Tm* experiments in 8-micro cell. Absorbance vs. temperature profiles were measured at 260 nm using Shimadzu UV-2550 UV-Visible spectrophotometer with quartz optical 8-micro cell (120 μl DNA) of 1.0 cm path length. The absorbance of the samples was monitored at 260 nm from 20 to 90 °C with a heating rate of 1 °C/min. From these profiles, average method was used to determine T_m values using in built software.

Fluorescence experiments: ODNs solutions were prepared as described in UV-visible and T_m measurement experiments. Fluorescence spectra were recorded using Fluoromax-4 fluorescence spectrophotometer at 25 °C using quartz cell of 1.0 cm path length with a slit width of 3 nm, integration time 0.2 sec and wavelength range. The excitation wavelengths for single strand duplex ODN were set at λ_{abs}^{max} (~310 – 370 nm), and emission spectra were measured in the wavelength regime of 300–750

nm with an integration time of 0.2 sec. All the sample solutions were prepared just before doing the experiment. Total volume of 500 µL from a stock solution of 700 µL of 2.5 µM concentration for each set was used for fluorescence experiment in 1 ml cell. The fluorescence quantum yields (Φ_f) were determined using quinine sulphate as a reference with the known Φ_f (0.54) in 0.1 molar solution in sulphuric acid. The following equation was used to calculate the quantum yield,

$$\Phi_S = \Phi_R \frac{Fl_S^{Area}}{Fl_R^{Area}} \frac{Abs_R}{Abs_S} \frac{n_S^2}{n_R^2}$$

where, Φ_R is the quantum yield of standard reference, Fl_S^{Area} (sample) and Fl_R^{Area} (reference) are the integrated emission peak areas, Abs_S (sample) and Abs_R (reference) are the absorbances at the excitation wavelength, and n_S (sample) and n_R (reference) are the refractive indices of the solutions.

Time resolved fluorescence experiments: The time resolved fluorescence spectra were obtained by using Edinburgh instrument, Life Space II time resolved fluorescence spectrophotometer at 25 °C using 1 cm path length cell in 50 mM sodium phosphate buffers (pH 7.0) containing 100 mM sodium chloride. 375 nm LED was used as the excitation light source and the monitoring emission wavelength was fixed at 460 and 535nm. The time correlated single photon counting (TCSPC) method was used to calculate the lifetime data. The life time data (Global Analysis) were calculated by the software package with fitting range 205 – 4000 channels. The concentration of ODN **1** and ODN **2** were taken as 1 µM.

6.8.5. Macromodel Calculations

Molecular modelling study of the duplex ODN **1•2** (^{OxoPy}**S** : ^{TPhen}**B**$_{Do}$) was carried out using Schrodinger Macro Model (Maestro vs. 9.0)[55] software with Amber* force field in water. MD simulation was carried out using OPLS 2005 force field with optimal mode of minimization of the generated structures with a convergence threshold of 0.05.

6.9. ^{1}H and ^{13}C Spectra

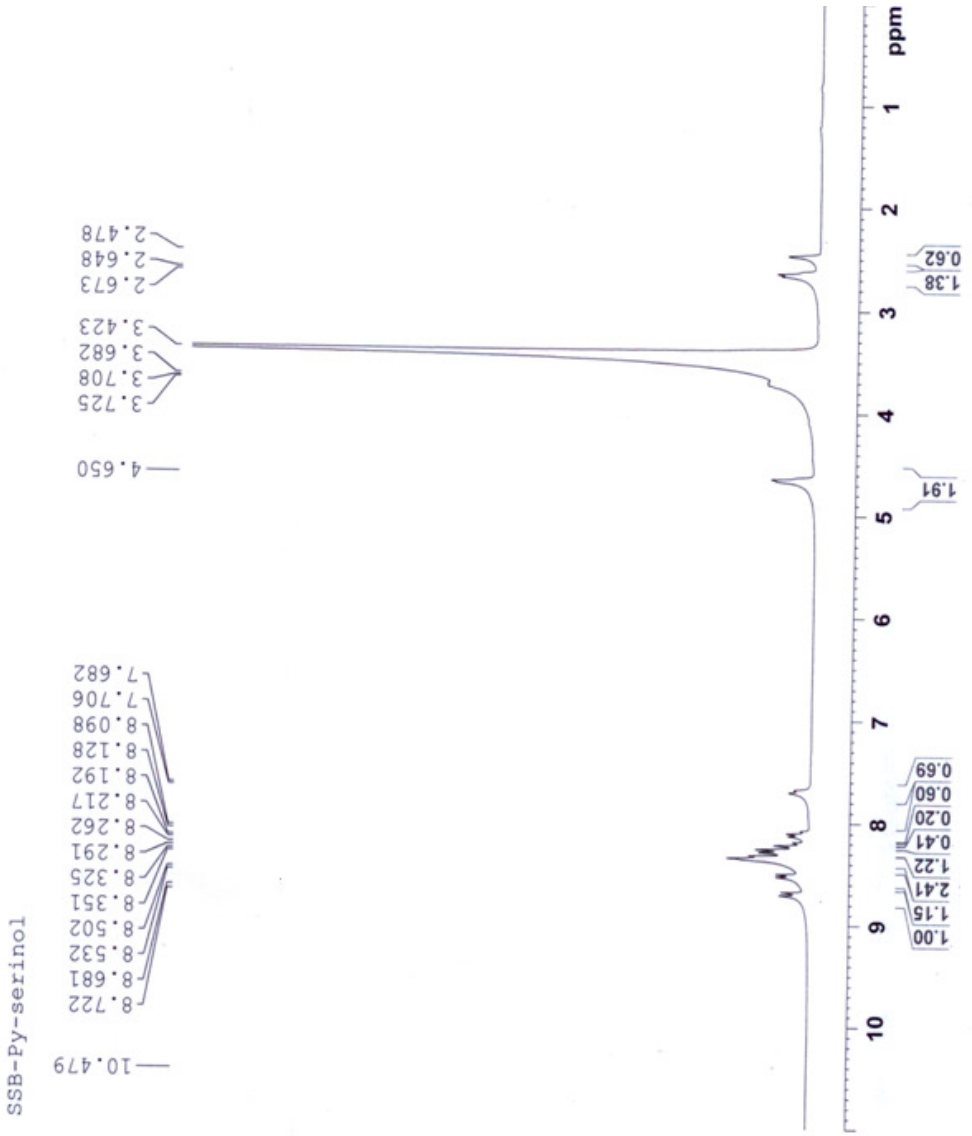

^{1}H NMR spectra of ^{OxoPy}**S** (**6.39**).

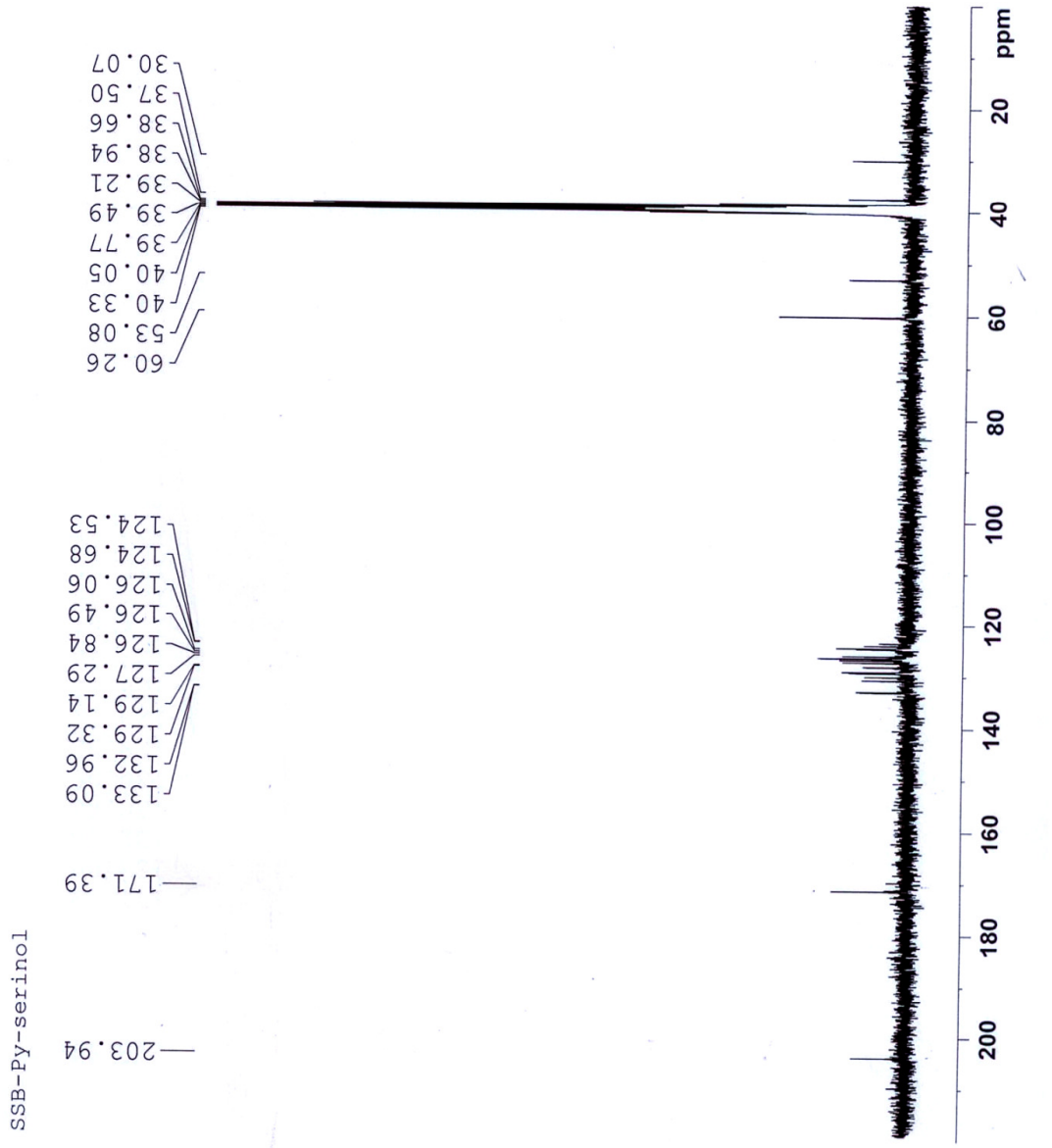

^{13}C NMR spectra of $^{\text{OxoPy}}$**S** (**6.39**).

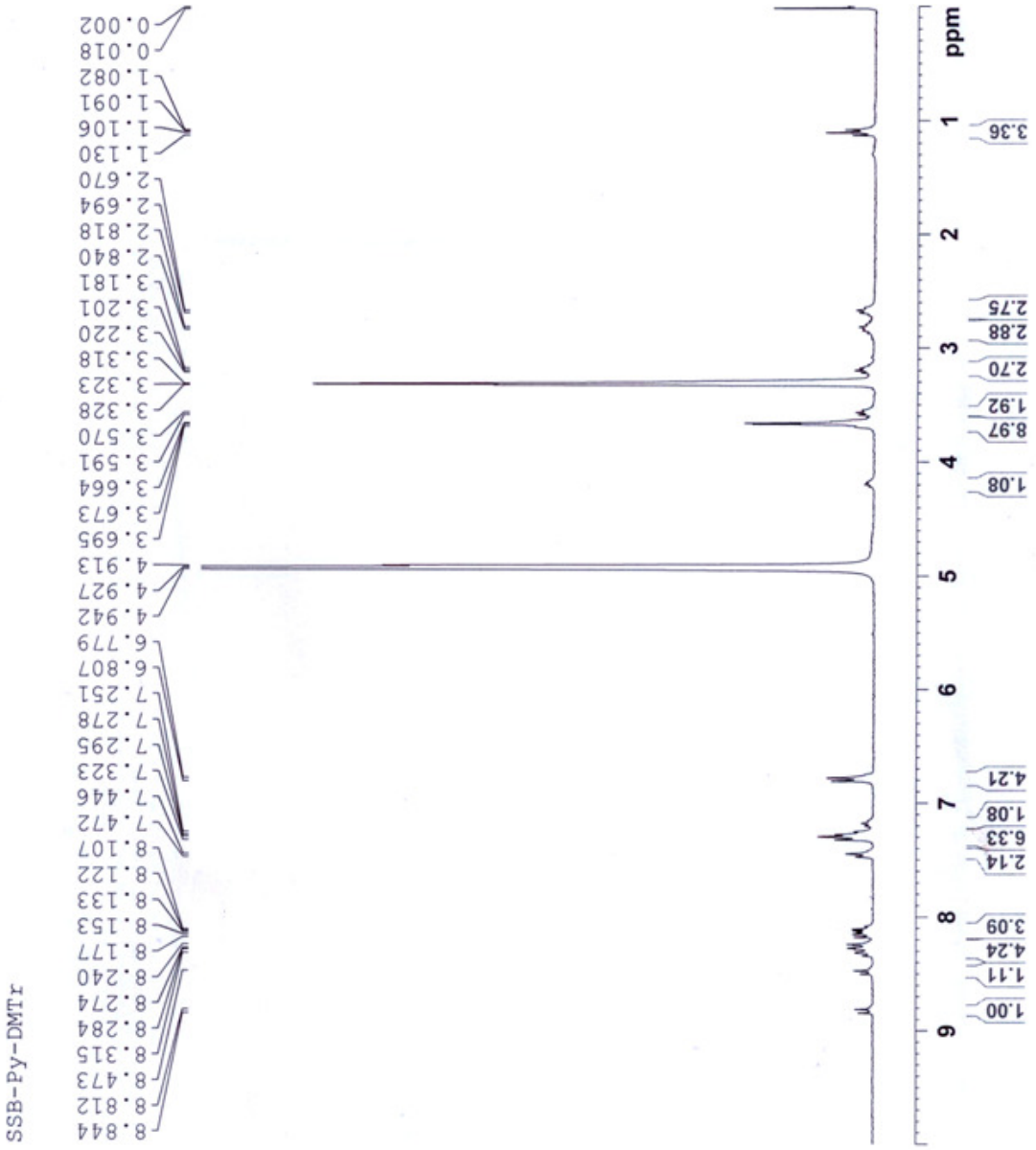

^{1}H NMR spectra of **DMTr-^{OxoPy}S** (**6.40**).

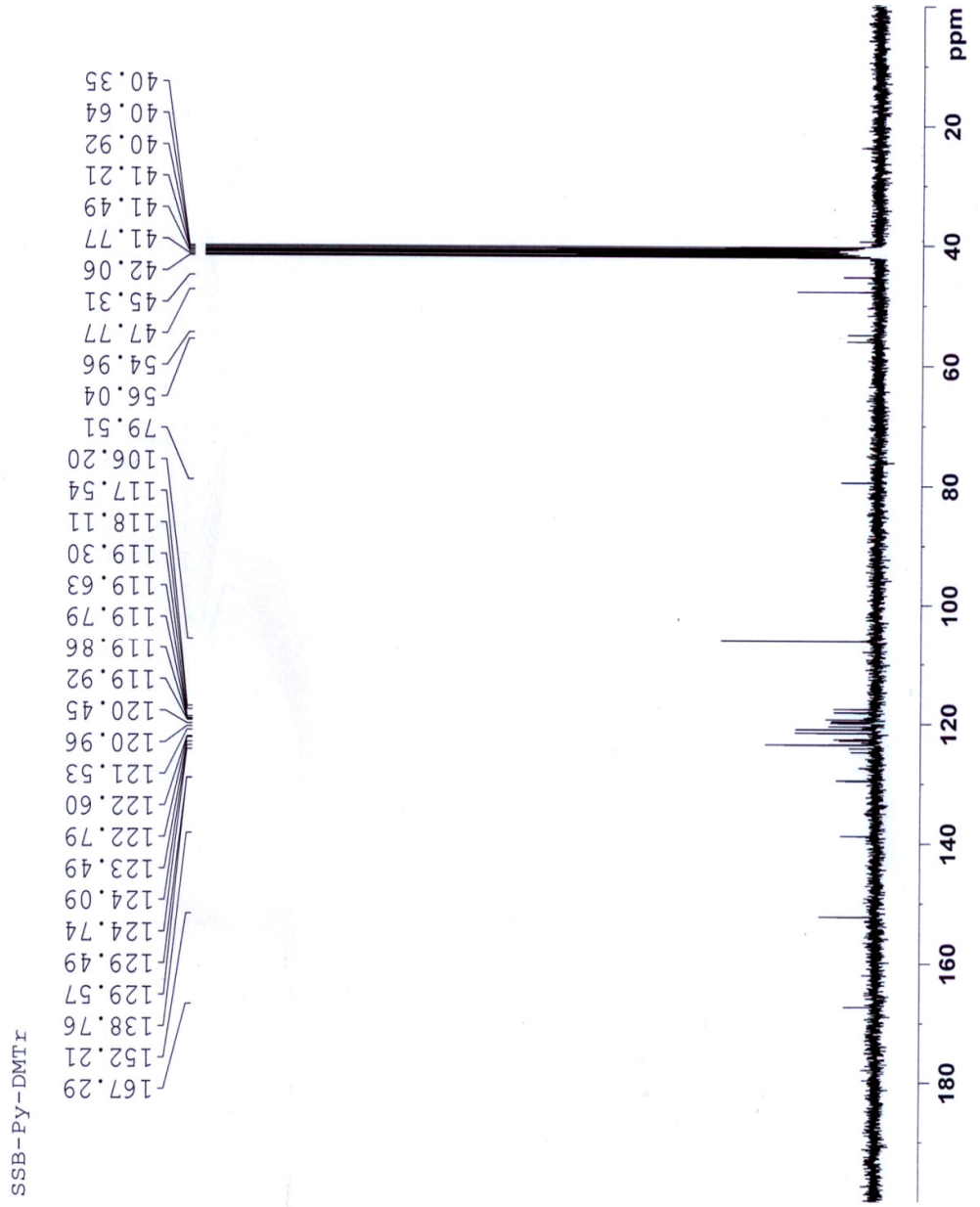

^{13}C NMR spectra of **DMTr-^{OxoPy}S** (**6.40**).

6.10. References

1. Lakowicz, J. R. Principles of Fluorescence Spectroscopy, 3rd. ed.; Springer: New York, **2006**.

2. *DNA Technology*; Lakowicz, J. R., Ed.; Kluwer Academic/Plenum Publishers: New York, **2003**; Vol. 7.

3. (a) Förster, T. *Naturwissenschaften* **1946**, *6*, 166. (b) Valeur, B.; Berberan-Santos, M. *Molecular Fluorescence: Principles and Applications*, 2nd ed. Weinheim: Wiley-VCH. **2012**.

4. (a) Stryer, L. *Annu. Rev. Biochem.* **1978**, *47*, 819. (b) Selvin, P. R. *Methods Enzymol.* **1995**, *246*, 300. (c) Sapsford, K. E.; Berti, L.; Medintz, I. L. *Angew. Chem. Int. Ed.* **2006**, *45*, 4562. (d) Kato, T.; Kashida, H.; Kishida, H.; Yada, H.; Okamoto, H.; Asanuma, H. *J. Am. Chem. Soc.* **2013**, *135*, 741.

5. (a) Peter, M.; Ameer-Beg, S. M.; Hughes, M. K. Y.; Keppler, M. D.; Prag, S.; Marsh, M.; Vojnovic, B.; Ng, T. *Biophys. J.* **2005**, *88*, 1224. (b) Petty, H. R.; Poo, H.; Fox, B. *J. Cell. Biol.* **1994**, *159*, 176. (c) Ge, X. D.; Tolosa, L.; Rao, G. *Anal. Chem.* **2004**, *76*, 1403. (d) Ohiro, Y.; Ueda, H.; Shibata, N.; Nagamune, T. *Anal. Biochem.* **2007**, *360*, 266.

6. (a) Bag, S. S.; Jana, S.; Yashmeen, A.; Kumar, S.; Bag, R. *Chem. Commun.* **2014**, *50*, 433. (b) Xie, Y.; Maxson, T.; Tor, Y. *J. Am. Chem. Soc*. **2010**, *132*, 11896. (c) Lee, Y. H.; Lee, M. H.; Zhang, J. F.; Kim, J. S. *J. Org. Chem.* **2010**, *75*, 7159.

7. (a) Flehr, R.; Kienzler, A.; Bannwarth W.; Kumke, M. U. *Bioconjugate Chem.* **2010**, *21*, 2347. (b) Kupstat, A.; Ritschel, T.; Kumke, M. U. *Bioconjugate Chem.* **2011**, *22*, 2546.

8. (a) Förster, T. *Naturwissenschaften* **1946**, *6*, 166. (b) Iqbal, A.; Arslan, S.; Okumus, B.; Wilson, T. J.; Giraud, G.; Norman, D. G.; Ha, T.; Lilley, D. M. J. *Proc. Natl. Acad. Soc. U.S.A.* **2008**, *105*, 11176. (c) Juskowiak, B. *Anal. Bioanal.Chem.* **2011**, *399*, 3157. (d) Preus, S.; Wilhelmsson, L. M. *ChemBioChem.* **2012**, *13*, 1990. (e) Kato, T.; Kashida, H.; Kishida, H.;

Yada, H.; Okamoto H.; Asanuma, H. *J. Am. Chem. Soc.* **2013**, *135*, 741. (f) Nedumparaa, R. J.; Manua, P. J.; Vallabhanb, C. P. G.; Nampooria, V. P. N.; Radhakrishnana, P. *Opt. Laser Tech.* **2008**, *40*, 953.

9. (a) Trkulja, I.; Haner, R. *J. Am. Chem. Soc*. **2007**, *129*, 7982. (b) Trkulja, I.; Haner, R. *Bioconjugate Chem.* **2007**, *18*, 289. (c) Mac, M.; Uchacz, T.; Danel, A.; Miranda, M. A.; Paris, C.; Pischel, U. *Photochem. Photobiol. Sci.* **2008**, *7*, 633. (d) Teo, Y. N.; Kool, E. T. *Bioconjugate Chem.* **2009**, *20*, 2371. (e) Teo, Y. N.; Wilson J. N.; Kool, E. T. *J. Am. Chem. Soc.*, **2009**, *131*, 3923. (f) Garo, F.; Haner, R. *Angew. Chem., Int. Ed.* **2012**, *51*, 916.

10. (a) Wu, J-S.; Zhou, J-H.; Wang, P-F.; Zhang X-H.; Wu, S-K.; *Org. Lett*. **2005**, *7*, 2133. (b) Bencini, A.; Bianchi, A.; Lodeiro, C.; Masotti, A.; Parola, A. J.; Pina, F.; Meloc, J. S.; Valtancolia, B. *Chem. Commun.*, **2000**, 1639.

11. (a) Stryer, L. *Annu. Rev. Biochem.* **1978**, *47*, 819. (b) Selvin, P. R. *Nat. Struct. Biol.* **2000**, *7*, 730.

12. (a) Clegg, R. M. *Methods Enzymol.* **1992**, *211*, 353. (b) Clegg, R. M.; Murchie, A. I. H.; Zechel, A.; Lilley, D. M. J. *Proc. Natl. Acad. Sci. U.S.A.* **1993**, *90*, 2994.

13. Hurley, D. J.; Tor, Y. *J. Am. Chem. Soc.* **2002**, *124*, 13231.

14. (a) Epstein, J. R.; Biran, I.; Walt, D. R. *Anal. Chim. Acta* **2002**, *469*, 3. (b) Pinto, M. R.; Schanze, S. *Proc. Nat. Acad. Sci. U.S.A* **2004**, *101*, 7505. (c) Gaylord, B. S.; Heeger, A. J.; Bazan, G. C. *Proc. Nat. Acad. Sci. U.S.A* **2002**, *99*, 10954 (d) Wang, S.; Liu, B.; Gaylord, B. S.; Bazan, G. C. *Adv. Funct. Mater.* **2003**, *13*, 463. (e) Xu, Q. -H.;Gaylord, B.; Wang, S.; Bazan, G. C.; Moses, D.; Heeger A. J. *Proc. Nat. Acad. Sci. U.S.A* **2004**, *101*, 11634. (f) Liu, B.; Bazan, G. C. *Chem. Mater*. **2004,** *16*, 4467. (g) Wang, S.; Gaylord, B. S.; Bazan, G. C. *J. Am. Chem. Soc.* **2004,** *126*, 5446 (h) Wang, S.; Bazan, G. C. *Chem. Commun.* **2004**, 2508. (i) Liu, B.; Bazan, G.

C. *J. Am. Chem. Soc.* **2006,** *128*, 1188. (j) Woo, H. Y.; Vak, D.; Korystov, D.; Mikhailovsky, A.; Bazan, G. C.; Kim, D-Y. *Adv. Funct. Mater.* **2007**, *17*, 290. (k) Kyhm, K.; Kim, I.; Kang, M.; Woo, H. Y. *J. Nanosci. Nanotechnol.* **2012**, *12*, 7733. (l) Kim, I.; Kyhm, K.; Kang, M.; Woo, H. Y. *JOL* **2014**, *149*, 185.

15. Qiaoli, Y.; Tongfei, S.; Changna, W.; Lei, W.; Haibo, L.; Shuling, X.; Huaisheng, W.; Jifeng, L. *Biosens. Bioelectron.* **2013**, *40*, 75.

16. Jade, H.; Dane, S.; Barrett, E.; Daniel, E. Abstracts of Papers, 245th ACS National Meeting & Exposition, New Orleans, LA, United States, 2013, BIOT-324.

17. Alessandra, A.; Maria, B.; Marco, L.; Luca, N. *IEEE J. Sel. Top. Quant. Electron.* **2014**, *20*, 7100207.

18. (a) Liu, C. -W.; Lin, Y. -W.; Huang, C. -C.; Chang, H. T. *Biosens. Bioelec.* **2009**, *24*, 2541. (b) Malinovskii, V. L.; Wenger, D.; Haner, R. *Chem. Soc. Rev*. **2010**, *39*, 410. (c) Teo, Y. N.; Kool, E. T. *Chem. Rev.* **2012**, *112*, 4221.

19. (a) Malinovskii, V. L.; Samain, F.; Haner, R. *Angew. Chem., Int. Ed. Engl.* **2007**, *46*, 4464. (b) Wagenknecht, H. A. *Ann. N.Y. Acad. Sci.* **2008**, *1130*, 122. (c) Chiba, J.; Takeshima, S.; Mishima, K.; Maeda, H.; Nanai, Y.; Mizuno, K.; Inouye, M. *Chem.-Eur. J.* **2007**, *13*, 8124.

20. (a) Rist, M. J.; Marino, J. P. *Curr. Org. Chem.* **2002**, *6*, 775. (b) Marras, S. A. E.; Kramer, F. R.; Tyagi, S. *Nucleic Acids Res.* **2002**, *30*, e122.

21. Malakhov, A. D.; Skorobogatyi, M. V.; Prokhorenko, I. A.; Gontarev, S. V.; Kozhich, D. T.; Stetsenko, D. A.; Stepanova, I. A.; Shenkarev, Z. O.; Berlin, Y. A.; Korshun, V. A. *Eur. J. Org. Chem.* **2004**, 1298.

22. Masuko, M.; Ohuchi, S.; Sode, K.; Ohtani, H.; Shimadzu, A. *Nucleic Acids Res.* **2000**, *28*, e34.

23. Saito, Y.; Bag, S. S.; Kusakabe, Y.; Nagai, C.; Matsumoto, K.; Mizuno, E.; Kodate, S.; Suzuka, I.; Saito, I. *Chem. Commun*., **2007**, *43*, 2133.

24. (a) Kashida, H.; Liang, X. G.; Asanuma, H. *Curr. Org. Chem.* **2009**, *13*, 1065. (b) Kashida, H.; Takatsu,T.; Sekiguchi, K.; Asanuma, H. *Chem. Eur. J.* **2010**, *16*, 2479. (c) Kato, T.; Kashida, H.; Kishida, H.; Yada, H.; Okamoto, H.; Asanuma, H. *J. Am. Chem. Soc.* **2013**, *135*, 741.

25. Borjesson, K.; Preus, S.; El-Sagheer, A. H.; Brown, T.; Albinsson, B.; Wilhelmsson, L. M. *J. Am. Chem. Soc.* **2009**, *131*, 4288.

26. (a) Marti, A. A.; Jockusch, S.; Stevens, N.; Ju, J. Y.; Turro, N. J. *Acc. Chem. Res.* **2007**, *40*, 402 ; (b) Wang, C. M.; Wu, C. C.; Chen, Y.; Song, Y. L.; Tan, W. H.; Yang, C. J. *Curr. Org. Chem.* **2011**, *15*, 465.

27. Olaso-González, G.; Merchán, M.; Serrano-Andrés, L. *J. Am. Chem. Soc.* **2009**, *131*, 4368.

28. (a) Langenegger. S. M.; Haner, R. *Chem. Commun*. **2004**, *40*, 2792. (b) Haner, R.; Biner, S. M.; Langenegger, S. M.; Meng, T.; Malinovskii, V. L. *Angew. Chem. Int. Ed*. **2010**, *49*, 1227. (c) Biner, S. M.; Haner, R. *ChemBioChem* **2011**, *12*, 2733. (d) Bouquin, N.; Malinovskii, V. L.; Haner, R. *Chem. Commun*. **2008**, *44*, 1974. (e) Adeyemi, O. O.; Malinovskii, V. L.; Biner, S. M.; Calzaferri, G.; Haner, R. *Chem. Commun*. **2012**, *48*, 9589.

29. (a) Lewis, F. D.; Zhang, Y. F.; Letsinger, R. L. *J. Am. Chem. Soc.* **1997**, *119*, 5451. (b) Mahara, A.; Iwase, R.; Sakamoto, T.; Yamana, K.; Yamaoka, T.; Murakami, A. *Angew. Chem., Int. Ed.* **2002**, *41*, 3648. (c) Fujimoto, K.; Shimizu, H.; Inouye, M. *J. Org. Chem.* **2004**, *69*, 3271. (d) Yang, C. J.; Jockusch, S.; Vicens, M.; Turro, N. J.; Tan, W. H. *Proc. Natl. Acad. Sci. U. S. A.* **2005**, *102*, 17278. (e) Kashida, H.; Kondo, N.; Sekiguchi, K.; Asanuma, H. *Chem. Commun.* **2011**, *47*, 6404.

30. (a) Okamoto, A.; Ichiba, T.; Saito, I. *J. Am. Chem. Soc.* **2004**, *126*, 8364. (b) Yamana, K.; Iwai, T.; Ohtani, Y.; Sato, S.; Nakamura, M.; Nakano, H. *Bioconjugate Chem.* **2002**, *13*, 1266.

31. (a) Kawai, T.; Ikegami, M.; Arai, T. *Chem. Commun.* **2004**, 824. (b) Seo, Y. J.; Lee, I. J.; Yi, J. W.; Kim, B. H. *Chem. Commun.* **2007**, 2817.

32. Cuppoletti, A.; Cho, Y.; Park, J. S.; Strassler, C.; Kool, E. T. *Bioconjugate Chem.* **2005**, *16*, 528.

33. Chiba, J.; Takeshima, S.; Mishima, K.; Maeda, H.; Nanai, Y.; Mizuno, K.; Inouye, M. *Chem. Eur. J.* **2007**, *13*, 8124.

34. (a) Varghese, R.; Wagenknecht, H.-A. *Chem. Commun.* **2009**, *19*, 2615. (b) Varghese, R.; Wagenknecht, H. A. *Chem. Eur. J.* **2010**, *16*, 9040. (c) Holzhauser, C.; Wagenknecht, H.-A. *Angew. Chem., Int. Ed.* **2011**, *50*, 7268. (d) Berndl, S.; Wagenknecht, H.-A. *Angew. Chem., Int. Ed.* **2009**, *48*, 2418.

35. (a) Hovelmann, F.; Gaspar, I.; Ephrussi, A.; Seitz, O. *J. Am. Chem. Soc.* **2013**, *135*, 19025. (b) Kummer, S.; Knoll, A.; Socher, E.; Bethge, L.; Herrmann, A.; Seitz, O. *Angew. Chem., Int. Ed.* **2011**, *123*, 1972. (c) Kummer, S.; Knoll, A.; Socher, E.; Bethge, L.; Herrmann, A.; Seitz, O. *Angew. Chem., Int. Ed.* **2011**, *50*, 1931.

36. Bichenkova, E. V.; Savage, H. E.; Sardarian, A. R.; Douglas, K. T. *Biochem. Biophys. Res. Commun*. **2005**, *332*, 956.

37. Kashida, H.; Liang, X.; Asanuma, H. *Curr. Org. Chem.* **2009**, *13,* 1065.

38. (a) Christensen U. B.; Pedersen, E. B. *Helv. Chim. Acta*. **2003**, *86*, 2090. (b) Kashida, H.; Asanuma, H.; Komiyama, M. *Chem. Commun*., **2006**, 2768. (c) Kashida, H.; Komiyama, M.; Asanuma, H. *Chem. Lett.* **2006**, *35*, 934. (d) Kashida, H.; Takatsu, T.; Asanuma, H. *Tetrahedron Lett*. **2007**, *48*, 6759.

39. Tanaka, J. *Bull. Chem. Soc. Jpn.* **1963**, *36*, 1237.

40. Wilson, J. N.; Gao, J.; Kool, E. T.; *Tetrahedron*, **2007**, *63*, 3427.

41. Trkulja, I.; Haner, R. *Bioconjugate Chem.* **2007**, *18*, 289.

42. (a) Langenegger, S. M.; Haner, R. *ChemBioChem* **2005**, *6*, 2149. (b) Malinovskii, V. L.; Samain, F.; Haner, R. *Angew. Chem., Int. Ed.* **2007**, *46*, 4464. (c) Hariharan, M.; Zheng, Y.; Long, H.; Zeidan, T. A.; Schatz, G. C.;Vura-Weis, J.; Wasielewski, M. R.; Zuo, X. B.; Tiede, D. M.; Lewis, F. D. *J. Am. Chem. Soc.* **2009**, *131*, 5920. (d) Haner, R.; Garo, F.; Wenger,

D.; Malinovskii, V. L. *J. Am. Chem. Soc.* **2010**, *132*, 7466. (e) Nussbaumer, A. L.; Studer, D.; Malinovskii, V. L.; Haner, R. *Angew. Chem., Int. Ed.* **2011**, *50*, 5490. (f) Wenger, D.; Malinovskii, V. L.; Haner, R. *Chem. Commun.* **2011**, *47*, 3168.

43. (a) Probst, M.; Wenger, D.; Biner, S. M.; Haner, R. *Org. Biomol. Chem.* **2012**, *10*, 755. (b) Malinovskii, V. L.; Nussbaumer, A. L.; Haner, R. *Angew. Chem., Int. Ed.* **2012**, *51*, 4905. (c) Garo, F.; Haner, R. *Eur. J. Org. Chem.* **2012**, 2801. (d) Asanuma, H.; Osawa, T.; Kashida, H.; Fujii, T.; Liang, X.; Niwa, K.; Yoshida, Y.; Shimadad, N.; Maruyama, A. *Chem. Commun.* **2012**, *48*, 1760.

44. Garo, F.; Haner, R. *Angew. Chem., Int. Ed.* **2012**, *51*, 916.

45. Garo, F.; Haner, R. *Bioconjugate Chem.* **2012**, *23*, 2105.

46. (a) Wilson, J. N.; Cho, Y. J.; Tan, S.; Cuppoletti, A.; Kool, E. T. *ChemBioChem* **2008**, *9*, 279. (b) Kashida, H.; Sekiguchi, K.; Higashiyama, N.; Kato, T.; Asanuma, H. *Org. Biomol. Chem.* **2011**, *9*, 8313.

47. Tanaka, M.; Oguma, K.; Saito, Y.; Saito, I. *Bioorg. Med. Chem. Lett.* **2012**, *22*, 4103.

48. (a) Lee, I. J.; Kim, B. H. *Chem. Commun.* **2012**, *48*, 2074. (b) Park, J. W.; Seo, Y. J.; Kim, B. H. *Chem. Commun.* **2014**, *50*, 52. (c) Nagatoishi, S.; Nojima, T.; Juskowiak, B.; Takenaka, S. *Angew. Chem., Int. Ed.* **2005**, *44*, 5067.

49. Gueron, M.; Leroy, J. L. *Curr. Opin. Struct. Biol.* 2000, *10*, 326.

50. (a) Lee, I. J.; Kim, B. H. *Chem. Commun.* **2012**, *48*, 2074. (b) Park, J. W.; Seo, Y. J.; Kim, B. H. *Chem. Commun.* **2014**, *50*, 52. (c) Nagatoishi, S.; Nojima, T.; Juskowiak, B.; Takenaka, S. *Angew. Chem., Int. Ed.* **2005**, *44*, 5067.

51. (a) Xu, B.; Wu, X.; Yeow, E. K. L.; Shao. F. *Chem. Commun.* **2012**, 1. (b) Xu, B.; Wu, X.; Yeow, E. K. L.; Shao. F. *Chem. Commun.* **2014**, *50*, 6402.

52. (a) Bag, S. S.; Talukdar, S.; Matsumoto, K.; Kundu, R. *J. Org. Chem.* **2013**, *78*, 278. (b) Bag, S. S.; Kundu, R.; Talukdar, S. *RSC Advances* **2013**, *3*, 21352.

53. (a) Trawick, B. N.; Osiek, T. A.; Bashkin, J. K. *Biocon. Chem.* **2001**, *12*, 900. (b) Asanuma, H.; Toda, T.; Murayama, K.; Liang, X.; Kashida, H. *J. Am. Chem. Soc.* **2010**, *132*, 14702. (c) Kashida, H.; Murayama, K.; Toda T.; Asanuma, H. *Angew. Chem. Int. Ed.* **2011**, *50*, 1285.

54. (a) Dougherty, G.; Pilbrow, J. R. *Int. J. Biochem.* **1984**, *16*, 1179. (b) Nakamura, M.; Fukunaga, Y.; Sasa, K.; Ohtoshi, Y.; Kanaori, K.; Hayashi, H.; Nakano H.; Yamana, K. *Nucleic Acids Res.* **2005**, *33*, 5887.

55. (a) A. Iqbal, S. Arslan, B. Okumus, T. J. Wilson, G. Giraud, D. G. Norman, T. Ha and D. M. J. Lilley, *Proc. Natl. Acad. Soc. U.S.A.* 2008, **105**, 11176. (b) B. Juskowiak, *Anal. Bioanal. Chem.* 2011, **399**, 3157. (c) S. Preus and L. M. Wilhelmsson, *ChemBioChem.* 2012, **13**, 1990. (d) T. Kato, H. Kashida, H. Kishida, H. Yada, H. Okamoto and H. Asanuma *J. Am. Chem. Soc.* 2013, **135**, 741. (e) R. J. Nedumparaa, P. J. Manua, C.P.G. Vallabhanb, V.P.N. Nampooria and P. Radhakrishnana, *Opt. Laser Tech.* 2008, **40**, 953.

56. Maestro, version 9.0, Schrödinger, LLC, New York, NY, **2009**.

SUMMARY AND OUTLOOK

Summary and Outlook

Major findings and the future outlook of the present investigations described in this dissertation have been summarized below:

This dissertation has a total of six chapters out which two chapters are devoted to the synthesis of unnatural donor-acceptor triazolyl nucleosides and tetrazolyl nucleosides *via* "Click" reaction and Nucleophilic substitution reaction, respectively. Other chapters describe the applications of triazolyl unnatural nucleoside(s) in DNA duplex stabilisation, targeting abasic DNA and in establishing dual pathways of formation of exciplex in a chimeric DNA duplex.

Thus, in **Chapter 2**, we have described the synthesis of few new triazolyl nucleosides *via* azide-alkyne cycloaddition reaction ("Click") as a key step of the synthesis and studies on their photophysical properties in various organic solvents. Our design concept based on the hypothesis that a pair of such donor/acceptor nucleoside might involve in π-stacking as well as in photophysical interaction leading to stabilization of DNA duplex if such nucleosides can be incorporated into short oligonucleotide sequences. Therefore, the designed bases may find application in the biophysical study in the context of DNA. A ground-state charge transfer complexation phenomenon was observed in case of nucleoside pair $^{TPhen}\mathbf{B}_{Do}$: $^{TNB}\mathbf{B}_{Ac}$ in both the non-polar and polar media. This force of attraction was exploited in stabilizing a duplex DNA which is elaborated in **Chapter 4**. The biophysical studies in the context of synthetic DNA with the unexplored bases and the possibility of recognition by polymerase enzyme are the future scope of this chapter. The noncovalent interactions of pyrenyl and butylpyrenyl triazole nucleosides, in particular, with proteins can be studied.

Based on the same concept we have also synthesized few new tetrazolyl β-nucleosides *via* stereospecific substitution reaction as a key step of the synthesis which is documented in **Chapter 3**. The only β-anomers of the tetrazolyl nucleosides are obtained from the α-chloro sugar with aromatic tetrazoles *via* substitution reaction in presence of K_2CO_3 as base under mild reaction conditions. These tetrazolyl nucleosides constitute a new class of nucleoside base surrogates. Two of the tetrazolyl

aromatic nucleosides showed interesting solvatochromic photophysical property. As for example, the trimethoxyphenyl tetrazolyl nucleoside showed an intramolecular charge transfer (ICT) emission with large (38 nm) solvatochromicity. Therefore, a combination of donor-acceptor pair tetrazolyl nucleosides might form suitable base pair of unnatural DNA and are expected to stabilize a duplex DNA via π-π stacking/charge transfer interaction. Therefore, the tetrazolyl unnatural nucleosides might find application in decorating unnatural DNA usable for various biotechnological and DNA based material science applications.

In **Chapter 4** we have shown that ground state charge transfer complexation force among triazolyl unnatural donor-acceptor nucleobase pair ($^{TPhen}\mathbf{B}_{Do}$: $^{TNB}\mathbf{B}_{Ac}$) is good enough to stabilize a DNA duplex. These two nucleosides paired against each other with very good pairing selectivity. The $^{TPhen}\mathbf{B}_{Do}$ self-pair was also found to be highly stable and was comparable to that of a natural A:T pair. The stabilization of the self-pair duplex and the pairing selectivity was explained on the basis of possible involvement of π-stacking interactions. Both the theoretical and spectroscopic evidences supported the role of charge transfer interaction force and the π-π-stacking interaction in stabilizing hetero-pair and self-pair duplexes. We have also shown that electrostatic/dipolar repulsion among the $^{TNB}\mathbf{B}_{Ac}$ self pair lead to the duplex destabilization. This is the first direct evidence of charge transfer complexation mediated DNA hetero-duplex stabilization. Therefore, our results might shed light to design such type of donor-acceptor base pair and to further elaborate this new force of duplex stabilization in the context of recognition by polymerase enzymes. The static quenching of fluorescence of $^{TPhen}\mathbf{B}_{Do}$ by $^{TNB}\mathbf{B}_{Ac}$ in any sequence context clearly shows that our unnatural DNA might find applications in studying charge transfer process in DNA.

Chapter 5 described the high stabilization of $^{TPhen}\mathbf{B}_{Do}$**:Φ** duplex that is comparable to that of a natural **A:T** pair which represents a remarkable improvement in stability and selectivity over previously reported stabilization of abasic site with non-hydrogen-bonded base. The large surface area, polarizability and strong stacking propensity play a major role to offer high duplex stabilization *via* strong intercalative

stacking interaction which is evident from high duplex stability, UV-visible spectroscopy, increased fluorescence anisotropy and negative induced CD signal.

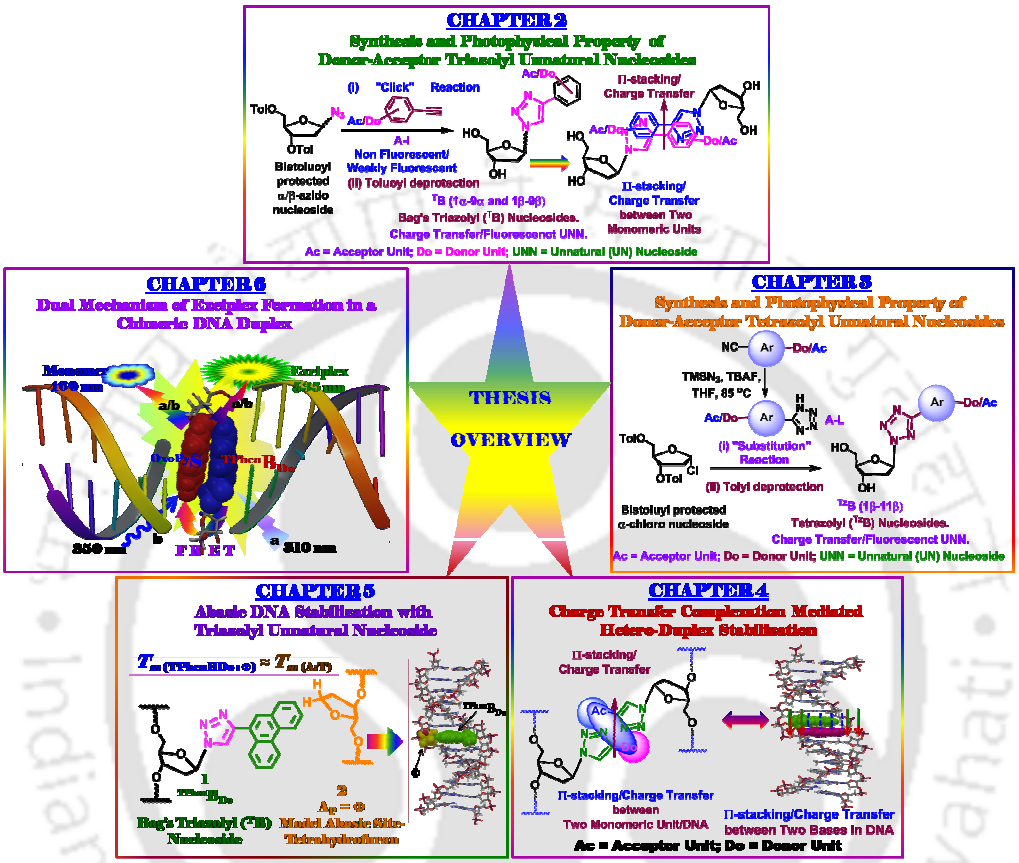

Finally, **Chapter 6** introduced a novel chemeric DNA duplex, wherein a non-nucleosidic base surrogate ^{OxoPy}**S** selectively paired against an unnatural triazolylphenanthrene nucleoside (^{TPhen}**B**$_{Do}$), which represents a very interesting dual door entry system for exciplex emission. All the spectroscopic evidences suggested that both the process of excitation of oxopyrene chromophore of ^{OxoPy}**S**-either energy transfer from excited triazolylphenanthrene to oxopyrene *via* FRET or direct excitation of ^{OxoPy}**S** at its absorbance maximum-led to the exciplex emission. The mechanism of exciplex formation *via* FRET which we have shown would become possible further by judicious designing and proper positioning the donor/acceptor pair in a probe wherein the pair involves in strong intercalative π-π stacking interaction. To the best of our knowledge this is the start of a new generation of probes which

could find wide applications in the field of chemical biology and in designing light harvesting DNA materials. We also hope that the design of such systems would have great impact in devising optoelectronics and might find application in chemistry, biology, material sciences and in diagnostic technology.

Therefore, this novel and important findings presented in this dissertation are expected to further define research to establish and to create more of such conceptually designed DNA system for future applications in chemistry, biology and material sciences. Our result is sufficient enough to advance the on-going examination of such related systems and thus, attract the interest of broad scientific community. The concept of designing fluorescent triazolyl- and tetrazolyl-nucleoside base analogues and the oligonucleotide probes might find special attention in future in the field of chemical genomics. The rapidly growing research towards the expansion of genetic alphabet as well as growing demand of nucleic acid based diagnostics and sensing materials necessitates the design and incorporation of unnatural base pairs with high duplex stability as well as tuned charge transfer/photophysical properties. In this connection, the concept of charge transfer complexation force of nucleobase pairing might knock the future chemical biologists to uncover and utilize such type of force of attraction in creating new and novel expanded genetic alphabets with diverse and potential functionality. Many more advancements in the field of expanding the genetic alphabet and the application of same to drive the synthesis of unnatural proteins are expected in near future with a hope to translate an expanded genetic alphabet into an expanded genetic code creating a synthetic organism one day with ability to encode proteins with new physicochemical properties.